



# Synthesis of original PHAs by ROP of functional $\beta$ -lactones : Mechanistic insights and stereoselectives catalysis

Rama Shakaroun

## ► To cite this version:

Rama Shakaroun. Synthesis of original PHAs by ROP of functional  $\beta$ -lactones : Mechanistic insights and stereoselectives catalysis. Catalysis. Université Rennes 1, 2021. English. NNT : 2021REN1S134 . tel-03847885

**HAL Id: tel-03847885**

**<https://theses.hal.science/tel-03847885>**

Submitted on 10 Nov 2022

**HAL** is a multi-disciplinary open access archive for the deposit and dissemination of scientific research documents, whether they are published or not. The documents may come from teaching and research institutions in France or abroad, or from public or private research centers.

L'archive ouverte pluridisciplinaire **HAL**, est destinée au dépôt et à la diffusion de documents scientifiques de niveau recherche, publiés ou non, émanant des établissements d'enseignement et de recherche français ou étrangers, des laboratoires publics ou privés.

# THESE DE DOCTORAT DE

L'UNIVERSITE DE RENNES 1

ECOLE DOCTORALE N° 596

*Matière, Molécules, Matériaux*

Spécialité : « *Chimie Moléculaire et Macromoléculaire* »

Par

« **Rama Shakaroun** »

« **Synthesis of functional PHAs by ROP of  $\beta$ -lactones : Mechanistic insights and stereoselective catalysis** »

Thèse présentée et soutenue à « **Rennes** », le « **05/11/2021** »

Unité de recherche : **UMR 6226 CNRS Institut des Sciences Chimique de Rennes**

**UFR Sciences et Proprietes de la Matiere**

## **Rapporteurs avant soutenance:**

Véronique Bennevault    Maître de conférences, Université d'Evry Val d'Essonne  
Antoine Bucharid        Reader, Université de Bath - UK

## **Composition du Jury:**

Président :	Gilles Alcaraz	Directeur de recherche, CNRS, Université de Rennes1, examinateur
Examineurs :	Julien Pinaud	Maître de conférences, Université de Montpellier, examinateur
Dir. de thèse :	Sophie Guillaume	Directrice de recherche, CNRS, Université de Rennes1
	Ali Alaaeddine	Professeur, Université de Beyrouth - Liban
Co-dir. de thèse :	Jean-François Carpentier	Professeur, Université de Rennes1



In memory of my father “Mohammad Shakaroun”

Passed away on 22/10/2020





# Résumé

Les stratégies actuelles de gestion des déchets plastiques se concentrent principalement sur la prévention et la réduction des déchets, et sur l'utilisation de polymères biodégradables tels que les poly(hydroxyalcanoates) (PHAs). Les PHAs sont biosourcés, biodégradables, biocompatibles et non toxiques, ce qui leur confère un rôle important dans l'emballage et dans une moindre mesure dans les applications médicales. Ils peuvent être naturels dérivés de bactéries, ou synthétisés par polymérisation par ouverture de cycle (ROP) catalysée de  $\beta$ -lactones. Les PHAs naturels présentent une microstructure stéréorégulière isotactique principalement cristalline (configuration *R*) ce qui les rend cassants. Ils ont également des masses molaires limitées et une fonctionnalité restreinte sur le groupe exocylique - principalement une chaîne alkyle-, ce qui limite leurs propriétés mécaniques et donc leur domaine d'application. Aussi, afin de palier ces limitations, les chimistes des polymères ont recouru à la synthèse chimique par ROP. La ROP des  $\beta$ -lactones conduit à des PHAs bien définis d'une manière stéréocontrôlée (PHAs isotactiques ou syndiotactiques).

La synthèse de  $\beta$ -lactones fonctionnelles, nommément BPL<sup>FG</sup>s (FG = OAlI, O<sup>n</sup>Bu, OBn, OTBDMS, OPh, SPh, O<sup>i</sup>Pr, O<sup>t</sup>Bu, OP(O)Ph<sub>2</sub>), a été réalisée par carbonylation des époxydes correspondants. Certains de ces derniers BPL<sup>FG</sup>s ont été polymérisés par ROP selon une approche exempte de solvant et de métal (par des activateurs organiques : BEMP, TBD et DBU), où les mécanismes mis en jeu pour produire les PHAs ont été examinés. D'autres BPL<sup>FG</sup>s ont été polymérisés par ROP par des catalyseurs stéréosélectifs achiraux diamino-bis(phénolate) de yttrium pour produire des PHAs fonctionnels présentant un enrichissement syndiotactique élevé et des masses molaires élevées. Les efforts ont été focalisés sur la compréhension de la relation entre la fonctionnalité du monomère et les substituants des catalyseurs.

**Mots clés :** Poly(hydroxyalkanoate) (PHA), polymérisation par ouverture de cycle (ROP),  $\beta$ -lactones, catalyse organique, catalyseur d'yttrium, stéréochimie.



# **Abstract**

The recent plastic waste management strategies focus mainly on the prevention and reduction of waste, and on the use of biodegradable counterparts such as poly(hydroxyalkanoates) (PHAs). PHAs are biobased, biodegradable, biocompatible, and non-toxic which endowed them a significant role in packaging and to a lesser extent in medical applications. They can be either natural derived from bacteria or synthetically produced through catalysed ring-opening polymerization (ROP) of  $\beta$ -lactones. Natural PHAs are only found as stereoregular isotactic mainly crystalline (*R* configuration) which makes them brittle. They also have limited molar masses and restricted functionality on the exocyclic group mainly alkyl chain, which limit their mechanical properties and hence their range of application. Therefore, in order to exceed these drawbacks, polymer chemists tend to resort to chemical synthesis via ROP. ROP of  $\beta$ -lactones can provide well-defined PHAs in a stereocontrol manner (isotactic or syndiotactic).

The synthesis of assorted functional  $\beta$ -lactones, namely BPL<sup>FG</sup>s (FG = OAl, O<sup>n</sup>Bu, OBn, OTBDMS, OPh, SPh, O<sup>i</sup>Pr, O<sup>t</sup>Bu, OP(O)Ph<sub>2</sub>), was achieved successfully by carbonylation of their corresponding epoxides. Some of the latter BPL<sup>FG</sup>s were ring-open polymerized by solvent- and metal-free approach (by organic activators: BEMP, TBD and DBU neat), where the mechanisms at play to produce PHAs were investigated. Other BPL<sup>FG</sup>s were ring-open polymerized by stereoselective achiral diamino-bis(phenolate) yttrium catalysts to produce functional PHAs with high syndiotactic enrichment and high molar masses. An emphasis was placed on the relation between the monomer functionality and the catalysts substituents.

**Keywords :** Poly(hydroxyalkanoate) (PHA), ring-opening polymerization (ROP), functional  $\beta$ -lactones, organocatalyst, yttrium catalyst, stereochemistry.



# Acknowledgments

This thesis is the output of a series of efforts from a life-changing experience, called PhD. In these years, I could have never climbed this mountain without the help and support of special people to whom I am extremely grateful.

First, I would like to thank the Brittany region, **Rennes Institute of Chemical Sciences** and the **Lebanese University Faculty of Science** for funding this thesis.

I would like to express my deepest appreciation to my advisors for their consistent supervision, patience, and for making my PhD meaningful,

**Dr. Sophie Guillaume**, my second mother, who has always been very supportive for me from the beginning of the 3 years, in my first oral presentation at the GFP conference, for my first publication, during my physical health problems, and her sympathy when my father passed away. Sophie is one-of-a-kind scientists and I am very honored to work with.

**Professor Ali Alaaeddine**, who was the reason I left Lebanon and went to France, without him I will not have reached France in the first place. Not to mention his supportiveness intellectually and kindness all the way long.

**Professor Jean-François Carpentier**, who inspired me to love my research project and move forward with it. I never forget when he called me a “bright student”, that encouraged me a lot. We faced many challenges, but because of his firm determination, foresight, and wisdom, we surpassed them.

I would essentially like to thank my committee members, **Dr. Véronique Bennevault**, **Dr. Antoine Buchard**, **Dr. Julien Pinaud**, **Dr. Gilles Alcaraz** for accepting our invitation and evaluating my manuscript and research. It will be a great honour for me to present them my PhD work and acquire their feedback.

I am grateful to the CSID committee members, **Dr. Bruno Beche** and **Dr. Françoise Le Guen** for their time in reading my reports for the past years and for giving encouragement feedbacks and important advices.

Of course, I would like to thank our group members and my colleagues, **Dr. Valerie Hardouin Duparc**, **Dr. Abdallah Zeineddine**, **Dr. Thierry Chavagnan**, **Dr. Orlando Santoro**, **Dr. Romain Ligny**, **Dr. Xavier Desert**, **Dr. Erwann Le Coz**, **Dr. Peter Chapple**, **Dr. Quentin Beuguel**, **Dr. Albert Soran**, **Dr. Hanieh Roueindeji**, **Dimitra theodosopoulou**, **Weiheng Huang**,

**Jenani Louis, Liye Qu, Corina Stoian, Vishal Chugh, Vyshakh Panakkal, and Ali Dhaini** for their presence, company, help and wisdom.

Special thanks to the permanent staff from our laboratory and neighbouring laboratories for their help in different ways, **Dr. Evgueni Kirillov** and **Dr. Yann Sarazin** for their involvement in attending my group meetings. **Pr. Ali Hachem, Dr. Cedric Fischmeister, Dr. Pierre-Antoine Bouit, Pr. Stéphane Rigaut, Dr. Marc Devillard, Dr. Gilles Alcaraz, Dr. Lucie Norel, and Dr. Olivier Galangau**, for their cooperation when I asked for help.

I am very grateful to the Centre Régional de Mesures Physiques de l'Ouest, Rennes (CRMPO) team for the mass spectrometry analyses, especially **Philippe Jéhan** for all his efforts and hard work, I really appreciate his intelligence. A special thanks also for **Jerome Ollivier** for taking care for our laboratory instruments, and **Marielle Blot** for the chiral GC and HPLC analysis. **Elsa Caytan** and **Clement Orione** for looking after the NMR instruments and educating us on how to operate them. **Theirry Roisnel** for XRD analysis.

Many thanks to **Cathrine Jolivet, Corinne Perier, Karine Robin, Sandrine Nogues, Beéatrice Mahi**, for managing administrative work and being very helpful and kind.

A great thanks to all my friends throughout my PhD, especially the future **Dr. Kana Kunihiro, Dr. Joanna Hammoud, Nour El Beyrouti, Shaymaa Shehimi, Bassima Hoteit, Nour Nouredine**, and **Khalil Youssef**, for being there for me in my pleasant and harsh days. They have believed in me, motivated me, and offered a lot of help.

My best friends in Lebanon, **Maha Macki, Zainab Mhanna, Hasan Cheaito, Fatima Awada, Alaa Khalil, Hiba Fadel, Yasser Mukdad, Fatima Hakim**, and **Hiba Nahhas**.

I dedicate this thesis manuscript very sincerely to my gone father the **Electric engineer Mohammad Shakaroun**, my lovely and precious mother **Mona Sbeity**, and my big awesome family of sisters and brother, **Pharmacist Sahar Shakaroun, Dr. Noura Shakaroun, Journalist Amani Shakaroun, Programmer Dana Shakaroun, Mechanical engineer Ahmad Shakaroun**, and **Tala Shakaroun**. My Brothers-in-law, **Dr. Ali Dakik** and **Mohammad Hraybi**. All of them support, encourage, and inspire me all over my life to achieve this.

Most sincerely, I am utterly thankful to the person who has always been an inspiration and helped me through my difficult days. A deep thank to my friend for more than 8 years and my Partner **Dr. Ali Soulieman**, who gave me hope and encouragement.

In the end I am completely grateful to the **Almighty God** for making science one of the interesting ways to reach and acknowledge Him better.

*“What we know is a drop, what we don't know is an ocean.”*

**– Isaac Newton**





# Table of Content

<b>General Introduction.....</b>	<b>1</b>
1. Conventional plastics: impact on the environment .....	3
2. Bioplastics: a potential solution for the plastics crisis? .....	5
3. My research input to bioplastics.....	7
4. References .....	10
<b>Chapter 1. Poly(hydroxyalkanoate)s (PHAs) : from bacterial to synthetic polyesters.....</b>	<b>15</b>
1. Introduction .....	19
2. Poly(hydroxyalkanoate)s “PHAs”: biodegradability matters .....	19
3. Natural PHAs: discovery, biosynthesis, and significance.....	21
4. Synthetic PHAs: biotechnology & chemical synthesis.....	28
4.1. Advanced biotechnological studies .....	28
4.2. Chemical polymerization.....	30
4.2.1. Polycondensation of $\alpha$ - and $\beta$ -hydroxy-acids .....	30
4.2.2. Ring-opening polymerization (ROP) of $\beta$ -lactones.....	32
5. Conclusion on natural and synthetic PHAs.....	56
6. References .....	59
<b>Chapter 2. From epoxide to <math>\beta</math>-lactones: carbonylation stage .....</b>	<b>69</b>
1. Introduction .....	73
1.1. Significance of $\beta$ -lactones .....	73
1.2. Prevailing synthesis of $\beta$ -lactones .....	74
1.3. Stand and outlooks on the synthesis of $\beta$ -lactones .....	81
2. Results and discussion.....	81

2.1. Synthesis and characterization of <i>racemic</i> and enantiopure functional epoxides “G <sup>FG</sup> s” .....	82
2.2. Synthesis and characterization of <i>racemic</i> and enantiopure functional $\beta$ -lactones “BPL <sup>FG</sup> s” .....	86
3. Conclusion: achievements and blueprints .....	97
4. Experimental section .....	98
5. References .....	109

### **Chapter 3. Organocatalyzed ROP of substituted $\beta$ -lactones towards functional PHAs: Macromolecular structure analysis and new insights into the ROP mechanism ..... 113**

1. Objectives .....	117
2. Pioneering ROP of cyclic esters mediated by organic activators: Mechanistic aspects .....	118
2.1. 2- <i>tert</i> -Butylimino-2-diethylamino-1,3dimethylperhydro-1,3,2-diazaphosphorine (BEMP) .....	119
2.2. 1,5,7-Triazabicyclo[4.4.0]dec-5-ene (TBD) .....	123
2.3. 1,8-Diazabicyclo[5.4.0]-undec-7-ene (DBU) .....	127
2.4. Overall considerations on the BEMP, TBD, and DBU-mediated ROP of LA, $\delta$ -VL and $\epsilon$ -CL .....	132
3. State-of-the-art: BEMP, TBD and DBU as organic activators for ROP of $\beta$ -lactones .....	134
4. Results and discussion .....	137
4.1. ROP of BPL <sup>FG</sup> s promoted by BEMP .....	138
4.1.1. Molecular characterization of PBPL <sup>FG</sup> s obtained from BEMP .....	139
4.1.2. Macromolecular structure of BEMP-synthesized PBPL <sup>FG</sup> s assessed by NMR spectroscopy and MALDI-ToF mass spectrometry .....	141
4.1.3. Mechanistic pathway for the BEMP-mediated ROP of BPL <sup>FG</sup> s .....	152
4.2. ROP of BPL <sup>FG</sup> s promoted by TBD .....	153

4.2.1.	Molecular characterization of PBPL <sup>FG</sup> s obtained from TBD .....	154
4.2.2.	Macromolecular structure of TBD-synthesized PBPL <sup>FG</sup> s assessed by NMR spectroscopy and MALDI-ToF mass spectrometry .....	155
4.2.3.	Mechanistic pathway for the TBD-mediated ROP of BPL <sup>FG</sup> s .....	162
4.3.	ROP of BPL <sup>FG</sup> s promoted by DBU .....	163
4.3.1.	Molecular characterization of PBPL <sup>FG</sup> s obtained from DBU .....	164
4.3.2.	Macromolecular structure of DBU-synthesized PBPL <sup>FG</sup> s assessed by NMR spectroscopy and MALDI-ToF mass spectrometry .....	165
4.3.3.	Mechanistic pathway for the DBU-catalyzed ROP of BPL <sup>FG</sup> s .....	170
4.4.	PBPL <sup>FG</sup> s : stereochemistry, kinetics and thermal properties.....	171
5.	Conclusion: better understanding of the BEMP, TBD, and DBU-promoted ROP mechanism of $\beta$ -lactones- Perspectives.....	174
6.	Experimental Section .....	177
7.	References .....	180

## **Chapter 4. Stereoselective ROP of functional chiral $\beta$ -lactones mediated by achiral yttrium-bis(phenolate) complexes..... 187**

1.	Introduction .....	191
1.1.	Preliminary general considerations .....	191
1.1.1.	Coordination-insertion ROP mechanism.....	191
1.1.2.	Tacticity and stereoselective ROP mechanism.....	192
1.2.	State-of-the-art stereoselective ROP of racemic $\beta$ -lactones mediated by Y{ONXO <sup>R1,R2</sup> } .....	195
1.2.1.	Stereoselective ROP of MLA <sup>FG</sup> s (FG = All, Bn, Me).....	196
1.2.2.	Stereoselective ROP of BPL <sup>FG</sup> s (FG = OAll, OBn, OMe).....	198
1.3.	Summary.....	200
2.	Results and discussion: Stereoselective ROP of new <i>racemic</i> $\beta$ -lactones mediated by Y{ONXO <sup>R1,R2</sup> } .....	201
2.1.	ROP of BPL <sup>FG</sup> s with different alkoxide chain length .....	202

2.1.1.	ROP of <i>rac</i> -BPL <sup>O<sup>Ph</sup></sup> .....	203
2.1.2.	ROP of <i>rac</i> -BPL <sup>CH<sub>2</sub>OBn</sup> .....	209
2.1.3.	ROP of <i>rac</i> -BPL <sup>S<sup>Ph</sup></sup> .....	211
2.1.4.	Insights into the kinetics and the catalyst activity .....	217
2.1.5.	Summery on the ROP of <i>rac</i> -BPL <sup>O<sup>Ph</sup>/CH<sub>2</sub>OBn/S<sup>Ph</sup></sup> .....	218
2.2.	ROP of BPL <sup>FG</sup> s with bulky exocyclic chains .....	219
2.2.1.	ROP of <i>rac</i> -BPL <sup>O<sup>i</sup>Pr</sup> .....	220
2.2.2.	ROP of <i>rac</i> -BPL <sup>O<sup>t</sup>Bu</sup> .....	225
2.2.3.	ROP of <i>rac</i> -BPL <sup>OTBDMS</sup> .....	230
2.2.1.	Summary of the kinetics and the activity of the catalyst .....	233
2.2.2.	Recapitulation on PBPL <sup>O<sup>i</sup>Pr/O<sup>t</sup>Bn/OTBDMS</sup> .....	234
2.3.	Preliminary investigations of the ROP of <i>rac</i> -BPL <sup>OP(O)Ph<sub>2</sub></sup> .....	235
3.	Conclusion : achievements and perspectives .....	243
4.	Experimental section .....	244
5.	References .....	249
	<b>General Conclusion .....</b>	<b>253</b>
	<b>Appendices.....</b>	<b>259</b>

# List of abbreviations

<b>3HA</b>	3-Hydroxyalkanoate
<b>3HP</b>	3-Hydroxypropanoic acid
<b>ε-CL</b>	ε-Caprolactone
<b>δ-VL</b>	δ-Valerolactone
<b>AROP</b>	Anionic ring-opening polymerization
<b>BEMP</b>	2- <i>tert</i> -Butylimino-2-diethylamino-1,3-dimethylperhydro-1,3,2-diazaphosphorine
<b>BL<sup>Me</sup></b>	β-Butyrolactone
<b>BnOH</b>	Benzyl alcohol
<b>BNPP</b>	Bis(4-nitrophenyl) phosphate
<b>COSY</b>	Correlation spectroscopy
<b>CROP</b>	Catanionic ring-opening polymerization
<b>DABCO</b>	1,4-Diazabicyclo[2.2.2]octane
<b>DBU</b>	1,8-Diazabicyclo[5.4.0]-undec-7-ene
<b>DCC</b>	Dicyclohexylcarbodiimide
<b>DCM</b>	Dichloromethane
<b>DCTB</b>	<i>trans</i> -2-(3-(4- <i>tert</i> -Butylphenyl)-2-methyl-2-propenylidene)malononitrile
<b>DFT</b>	Density functional theory
<b>DL</b>	Diolide
<b><i>D</i><sub>M</sub></b>	Dispersity
<b>DMAP</b>	4-Dimethylaminopyridine
<b>DME</b>	1,2-Dimethoxyethane
<b>DMF</b>	<i>N,N</i> -Dimethylformamide
<b>dMMLA<sup>Bn</sup></b>	α,α'-Dimethyl benzyl malolactonate

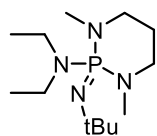
<b>DMSO</b>	Dimethyl sulfoxide
<b>DNA</b>	Deoxyribonucleic acid
<b>DP</b>	Degree of polymerization
<b>DPP</b>	Diphenyl phosphate
<i>ee</i>	Enantiomeric excess
<b>EROP</b>	Enzymatic ring-opening polymerization
<b>ESI MS</b>	Electrospray ionization mass spectrometry
<b>HKR</b>	Hydrokinetic resolution
<b>HPLC</b>	High performance liquid chromatography
<b>IAA</b>	<i>trans</i> -3-Indoleacrylic acid
<b>IMes</b>	1,3-Bis-(2,4,6-trimethylphenyl)imidazole-2-ylidene
<b>J-MOD</b>	J-Modulated Spin-Echo
$k_i$	Rate constant of initiation
$k_p$	Rate constant of propagation
$k_t$	Rate constant of termination
$k_{tr}$	Rate constant of transfer
<b>LA</b>	Lactide
<b>MALDI-ToF MS</b>	Matrix assisted laser desorption ionization - time of flight mass spectrometry
<b>MeCN</b>	Acetonitrile
<b>MLA<sup>Bn</sup></b>	Benzyl malolactonate
<b>MPL</b>	$\alpha$ -Methyl- $\beta$ -propiolactone
<b>MTBD</b>	7-Methyl-1,5,7-triazabicyclo[4.4.0]dec-5-ene
<b>NHC</b>	<i>N</i> -Heterocyclic carbene
<b>NMR</b>	Nuclear magnetic resonance
<b>P1-<i>t</i>-Bu</b>	<i>tert</i> -Butylimino-tris(dimethylamino)phosphorane

<b>P<sub>2</sub>-<i>t</i>-Bu</b>	1- <i>tert</i> -Butyl-2,2,4,4,4 -pentakis(dimethylamino)-2 $\Delta$ 5,4 $\Delta$ 5-catenadi(phosphazene)
<b>P<sub>4</sub>-<i>t</i>-Bu</b>	1- <i>tert</i> -Butyl-4,4,4-tris(dimethylamino)-2,2-bis[tris(dimethylamino)phosphoranyl-idenamino]-2 $\Delta$ 5,4 $\Delta$ 5-catenadi(phosphazene)
<b>PA</b>	Polyamide
<b>PBAT</b>	Poly(butylene adipate terephthalate)
<b>PBL<sup>Me</sup></b>	Poly( $\beta$ -butyrolactone)
<b>PBS</b>	Poly(butylene succinate)
<b>PCL</b>	Poly( $\epsilon$ -caprolactone)
<b>PdMMLA<sup>Bn</sup></b>	Poly(dimethylbenzyl malolactonate)
<b>PE</b>	Polyethylene
<b>PEF</b>	Poly(ethylene 2,5-furandicarboxylate)
<b>PET</b>	Poly(ethylene terephthalate)
<b>PGA</b>	Poly(glycolic acid)
<b>PHA</b>	Poly(hydroxy alkanoate)
<b>PHB</b>	Poly(3-hydroxybutyrate)
<b>PHBV</b>	Poly(3-hydroxybutyrate- <i>co</i> -3-hydroxyvalerate)
<b>PHH</b>	Poly(3-hydroxyhexanoate)
<b>PHP</b>	Poly(3-hydroxypropylate)
<b>PL</b>	$\beta$ -Propiolactone
<b>PLA</b>	Poly(lactic acid)
<b>PLGA</b>	Poly(lactic- <i>co</i> -glycolic acid)
<b>P<sub>m</sub></b>	Probability of isotactic enchainment
<b>PMLA</b>	Poly(malic acid)
<b>PMLA<sup>Bn</sup></b>	Poly(benzyl malolactonate)
<b>PMPL</b>	Poly( $\alpha$ -methyl- $\beta$ -propiolactone)

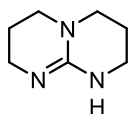


<b>PP</b>	Polypropylene
<b>ppm</b>	Part per million
<b><math>P_r</math></b>	Probability of syndiotactic enchainment
<b>PS</b>	Polystyrene
<b>PTT</b>	Poly(trimethylene terephthalate)
<b>PVC</b>	Poly(vinyl chloride)
<b>PVL</b>	Poly( $\delta$ -valerolactone)
<b>ROP</b>	Ring-opening polymerization
<b>SCL</b>	Short-chain-length
<b>SEC</b>	Size exclusion chromatography
<b>TBD</b>	1,5,7-Triazabicyclo[4.4.0]dec-5-ene
<b>TBDMS</b>	<i>tert</i> -Butyldimethylsilyl
<b><math>T_g</math></b>	Glass transition temperature
<b><math>T_m</math></b>	Melting temperature
<b>TOF</b>	Turnover frequency
<b>THF</b>	Tetrahydrofuran
<b>TU</b>	Thiourea

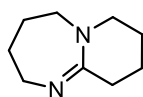
## Organic Activators



**BEMP**

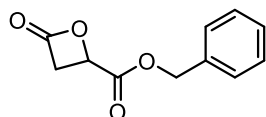


**TBD**

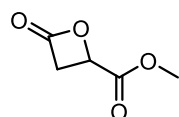


**DBU**

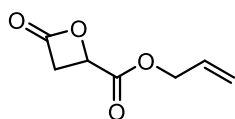
## MLA<sup>FG</sup>s



**MLA<sup>Bn</sup>**

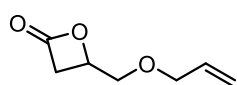


**MLA<sup>Me</sup>**

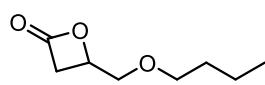


**MLA<sup>All</sup>**

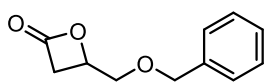
## BPL<sup>FG</sup>s



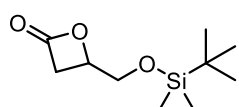
**BPL<sup>OAII</sup>**



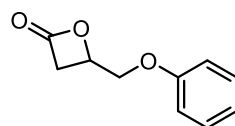
**BPL<sup>OnBu</sup>**



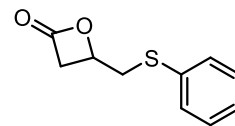
**BPL<sup>OBn</sup>**



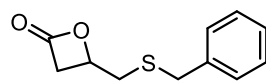
**BPL<sup>OTBDMS</sup>**



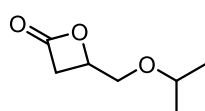
**BPL<sup>OPh</sup>**



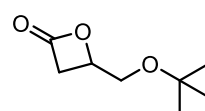
**BPL<sup>SPh</sup>**



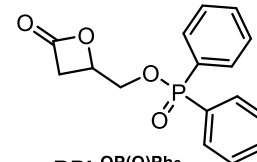
**BPL<sup>SBn</sup>**



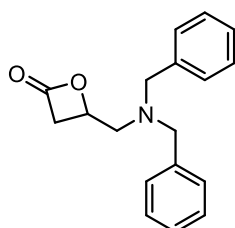
**BPL<sup>O<sup>i</sup>Pr</sup>**



**BPL<sup>O<sup>t</sup>Bu</sup>**

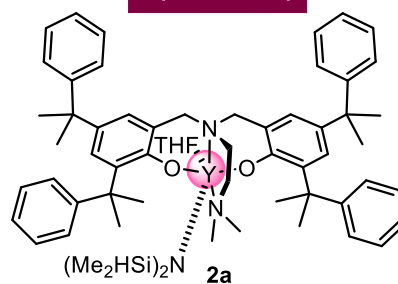


**BPL<sup>OP(O)Ph2</sup>**

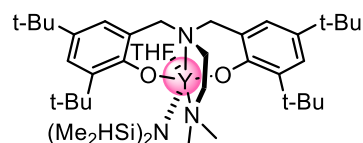


**BPL<sup>NBn2</sup>**

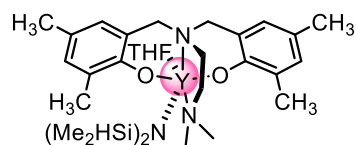
## Y{ONNO<sup>R1,R2</sup>}



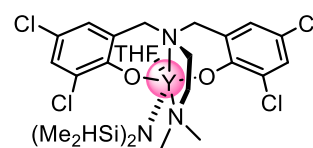
**2a**



**2b**

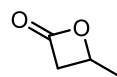


**2c**

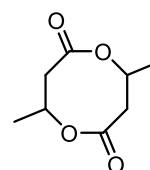


**2d**

## Others



**BL<sup>Me</sup>**



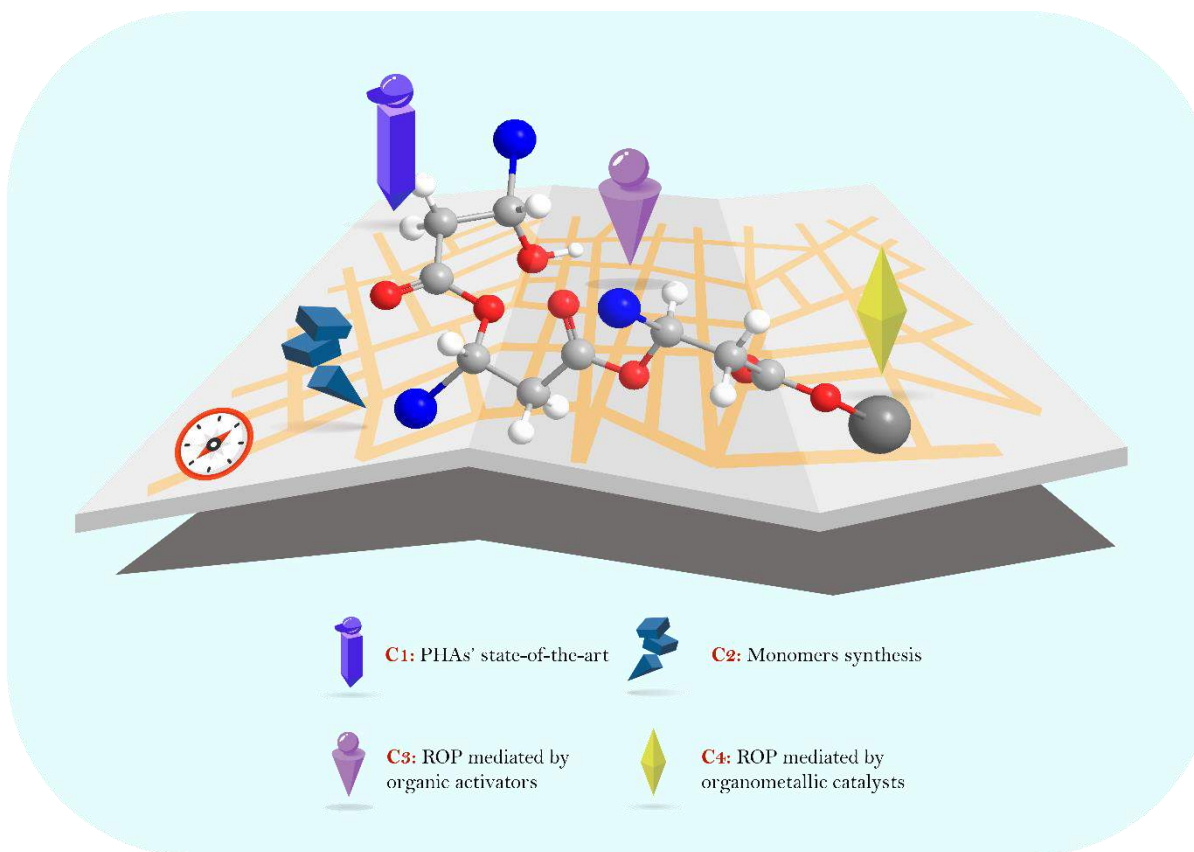
**DL<sup>Me</sup>**







# General Introduction





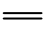
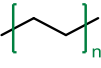
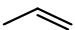
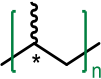
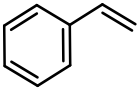
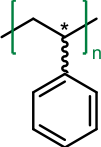
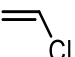
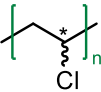
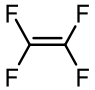
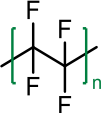
## 1. Conventional plastics: impact on the environment

"Only we humans make waste that nature can't digest", these are the words uttered by an oceanographer, *Capt. Charles Moore*, who was referring in his speech to plastics.<sup>[1]</sup> The term "plastic" is derived from the Greek word "*plastikos*", meaning fit for moulding, since plastics often cover a wide range of heterogeneous materials made up of polymer chains that are processed in a variety of ways and mixed with various additives, antioxidants, foaming agents, plasticizers, flame retardants, etc.<sup>[2]</sup> The physical/mechanical properties (flexibility, malleability strength, melting point...) of plastics enable them to fulfil a variety of niche functions that make them so versatile in household, pharmaceutical, and commercial sectors.<sup>[3]</sup> Accordingly, plastics are ubiquitous materials and an essential commodity in modern society, that drove research interests to improve the sustainability of its industry. In fact, the annual production of conventional plastics worldwide was reported as more than 360 million tons, still in permanent growth every year, and roughly half of that is intended for single use.<sup>[3-4]</sup>

Conventional plastics are made from raw materials that are derived from fossil-based petroleum/gas (Table 1). The most popular and highly demanded are polyolefins, especially polyethylene (PE) and polypropylene "PP" that are produced from crude oil and natural gas, and have become very common and widely produced polymers (Table 1, entries 1, 2). PE's tailoring allows it to be used to make plastics of different densities and mechanical behaviours, meaning it can be flimsy and pliable or sturdy and tough. Meanwhile, PP is particularly flexible and resilient, other than being resistant to degradation and light.<sup>[5]</sup> Thus, their applications are extremely diverse in everyday use, predominantly in single-use items such as milk carton, plastic wrappers, straws, water bottles, shopping bags, shampoo containers, bottle caps and so on. Yet, these are just two varieties of synthetic plastics out of many dozen hydrocarbons that may come from different sources of fossil fuel other than crude oil such as natural gas or coal and that are essentially non-biodegradable (Table 1, entries 3-5).<sup>[6]</sup>



**Table 1** – (from left to right) Molecular structure of fossil-based monomers and corresponding polymers; polymers' main properties and applications (\* indicates the chiral center).

Entry	Fossil-based monomers	Non-biodegradable polymers	Main properties <sup>[7]</sup>	Main applications <sup>[8]</sup>
1	 Ethylene	 Polyethylene (PE)	Excellent chemical resistance, stable in cryogenic environments and zero water absorption	Plastic bags, wire insulation, packaging films, squeeze bottles, housewares, toys and medical equipment
2	 Propylene	 Polypropylene (PP)	Semi-rigid, good chemical resistance and good heat resistance	Textiles, bottles, indoor-outdoor carpets, automotive industry
3	 Styrene	 Polystyrene (PS)	Very good electrical insulator, excellent optical clarity, and good chemical resistance	Styrofoam cups, disposable cutlery (forks, knives, and spoons), trays, videocassette cases, containers, lids, bottles, trays, tumblers, foams and films
4	 Vinyl chloride	 Poly(vinyl chloride) (PVC)	Good insulators, high durability, excellent flame retardation and abrasion resistant	Clear food wrap, bottles, water & drain pipes, floor covering, synthetic leather and building materials
5	 Tetrafluoroethylene	 Polytetrafluoroethylene / Teflon	Chemical, thermal, electrical resistance, high flexibility and non-stickable	Non-stick surfaces, plumbing tape, chemical-resistant containers and films

The fact that the demands for conventional plastics have been increasing continuously due to modernization and population boom is a risky reality that one cannot elude. Despite their fascinating properties and applications, environment has been adversely affected by commercialized fossil fuel-based/nonbiodegradable polymers.<sup>[9]</sup> PE, PP, and alike hydrocarbon polymers can take centuries to decompose or mineralize in landfill sites, which means that much polymers that have been produced still remain in their near original form.<sup>[4b, 10]</sup> Polyolefins may gradually break apart under the influence of sunshine, water and wind, releasing greenhouse gas emissions contained within, as well as resulting in the leaching into the environment of chemicals/additives added during production.<sup>[11]</sup> Some of this waste makes its way into rivers and ultimately into the seas, with around 7.2 million metric tons of plastic pollution entering the oceans every year, a detrimental effect on the oceanic ecosystem.<sup>[3, 12]</sup> The sheer volume of single-use plastic pollution, especially combined with its persistence and an ongoing environmental impact that can last for centuries, has created the environmental catastrophe we

see today. Noteworthy, the problem has now been further exacerbated by the coronavirus pandemic as “a new wave of plastic pollution” is littering beaches and public spaces in the form of disposable masks and gloves.<sup>[13]</sup> As the marine biologist *Daniel Pauly* expressed sadly “I’m convinced that plastics will cause some species to go extinct and it breaks my heart just to think about that”.<sup>[14]</sup> From the green and sustainable chemistry standpoint, one of the current challenges of polymer chemistry/industry is to switch from petroleum-based/non-biodegradable polymers (Table 1) to biobased and/or biodegradable polymers, termed as “bioplastics” (Figure 1),<sup>[15]</sup> that are preferred to be sustainable in both production and use and that can be recycled or disposed of in ways that are environmentally innocuous.<sup>[16]</sup>

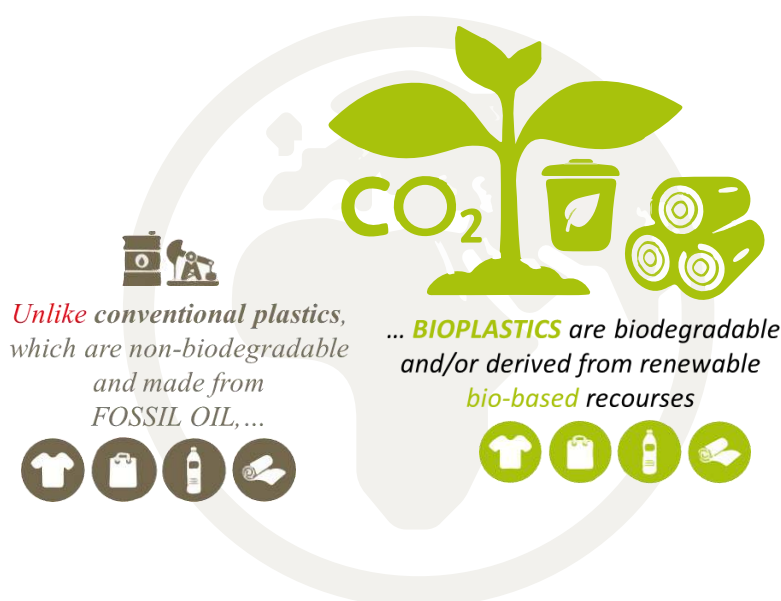


**Figure 1** – Diagram displays the difference between conventional plastics and bioplastics; bioplastics may help decrease hazardous environmental impact.<sup>[17]</sup>

## 2. Bioplastics: a potential solution for the plastics crisis?

In the process of creating plastics, humans have managed to take raw materials from nature and transform them so thoroughly that nature no longer recognizes them. Humans’ ingenuity is what got earth in this plastics crisis nowadays, and hopefully, their ingenuity could remove this mess. Indeed, “bioplastics” are an important innovation and it would offer sustainable and eco-friendly alternatives to avoid the plastic pollution.<sup>[18]</sup>

Similar to conventional plastics (*vide supra*), bioplastics can be used in several ways under ordinary conditions. Unlike conventional plastics that are fossil-based and non-biodegradable (Figure 2 – (D)), bioplastics can be bio-based and non-biodegradable (Figure 2 – (A)), or biodegradable and fossil-based (Figure 2 – (C)), or biobased and biodegradable at

once (Figure 2 – (B)).<sup>[17, 19]</sup> Biodegradable polymers can replace non-biodegradable ones and at the same time provide properties like strength and flexibility that make conventional polymers so desirable.<sup>[19]</sup>

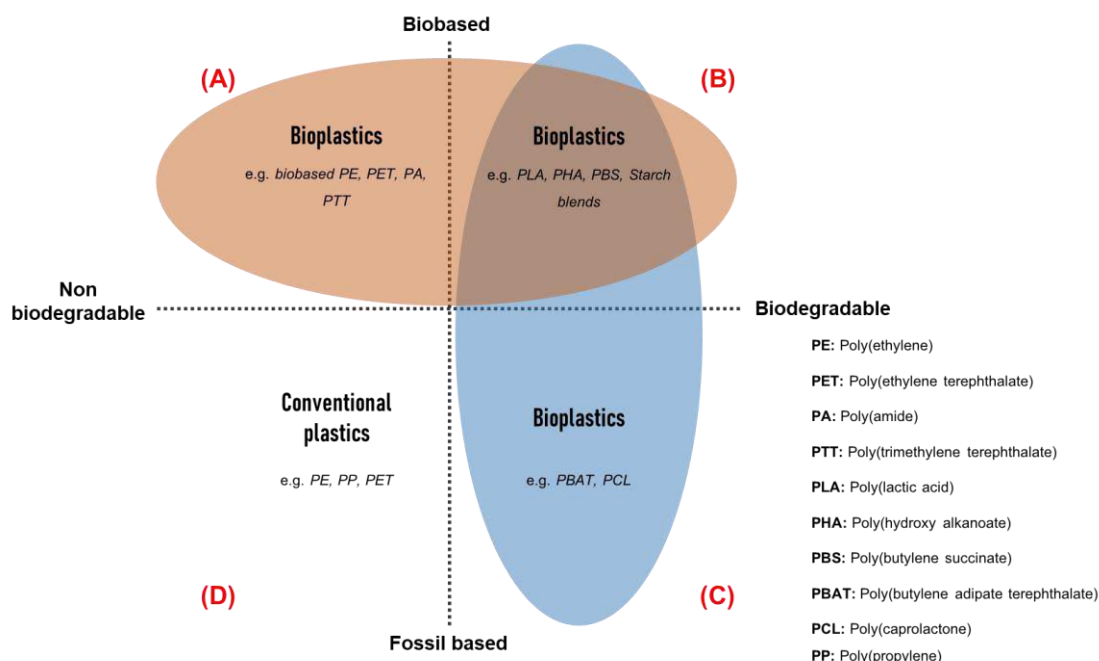


**Figure 2** – Classification of plastics according to their origin and biodegradation.<sup>[17]</sup>

The continuous research and developmental activities towards bioplastics and growing awareness towards environmental preservation have led to a remarkable growth of the overall bioplastics market.<sup>[20]</sup> Presently, bioplastics represent about one percent of plastic produced annually,<sup>[17]</sup> however their market is rising dynamically due to the increase in their demand (increasing eco-awareness among consumers) and due to the sophisticated materials, applications, and products they afford. The 2020 report of European Bioplastics/Nova Institute, estimates the current bioplastics production at 2.11 million tonnes per year and projects that it will increase up to 2.87 million tonnes by 2025.<sup>[17, 21]</sup>

Bioplastics have a wide range of applications such as packaging, catering products, consumer electronics, automotive, agriculture/horticulture, toys, textiles and several other sections.<sup>[22]</sup> Their main application in 2020 is packaging with 47% (0.99 million tonnes) of the total bioplastics market, followed by textiles.<sup>[17]</sup> On the other hand, some field of applications such as automotive, transport, building, construction, electric and electronics may still grow thanks to the production of functional polymers (Figure 3).<sup>[21b, 22-23]</sup> The major disadvantage of bioplastics is their high production cost (could be 2-4 times depending on product) compared to conventional plastics.<sup>[24]</sup>

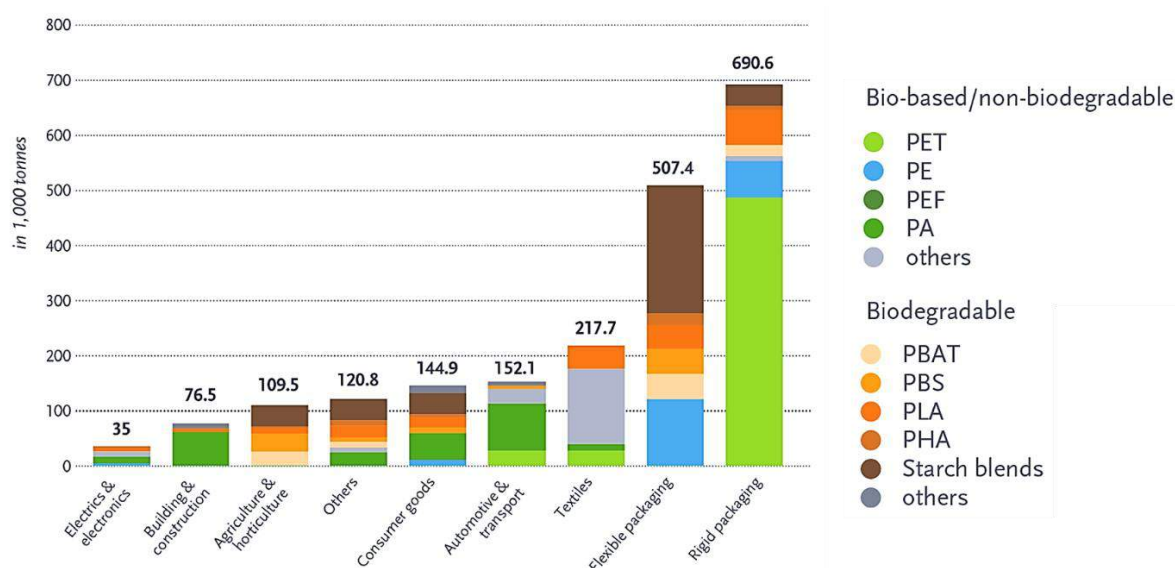


**Figure 3** – Global production capacities of different bioplastics by market applications, in 2020.<sup>[17]</sup>

### 3. My research input to bioplastics

The recent plastic waste management strategies focus mainly on the prevention and reduction of waste, and on the use of biodegradable counterparts. Our research group at the Rennes Institute of Chemical Science (ISCR) in cooperation with Laboratoire de Chimie Médicinale et de Produits Naturels (LCMPN) laboratory in Lebanon, has been investigating over the past decades the synthesis of functional poly(hydroxyalkanoates) (PHAs) as an alternative to plastics due to their eco-friendly character. PHAs are biobased, biodegradable (Figure 2), biocompatible, and non-toxic which endowed them a significant role in packaging and to a lesser extent in medical applications. While PHA represent less than 2% of the global production capacities of bioplastics in 2019, their production is anticipated to increase significantly going from ca. 1.17 to 1.33 million tonnes from 2019 to 2024 (Figure 4).<sup>[17]</sup>



**Figure 4** – Global production capacities of PHAs were set to more than triple in the next years, in 2019 (left), 2024 (right).<sup>[17]</sup>

In Chapter 1, we introduce the benefits of biobased and biodegradable polymers and the impact of biodegradability on the environment, followed by the discovery of natural or bacterial PHAs, including their biosynthetic pathways, applications, qualifications and limitations. The motivations towards synthetic PHAs are discussed, counting a brief view on chemical pathways such as polycondensation vs. catalysed ring-opening polymerization “ROP” of  $\beta$ -lactones, the latter being our on-going approach.

Chapter 2 presents a bibliographic summary – highlighting pros and cons – of the most common approaches for the synthesis of various  $\beta$ -lactones, focussing on our endorsed strategy through the catalysed carbonylation reaction of functional epoxides to alternative  $\beta$ -lactones (known or novel functional  $\beta$ -lactones), along with a presentation of the catalysts used. The synthesis of racemic *rac*-BPL<sup>FG</sup>s or enantiopure (*S*)-BPL<sup>FG</sup>s (FG = OAll, O<sup>n</sup>Bu, OBn, OTBDMS, OPh, SPh, SBn, O<sup>i</sup>Pr, O<sup>t</sup>Bu, OP(O)Ph<sub>2</sub>, NBn<sub>2</sub>) (Figure 5), with the yields and spectroscopic characterizations are reported.

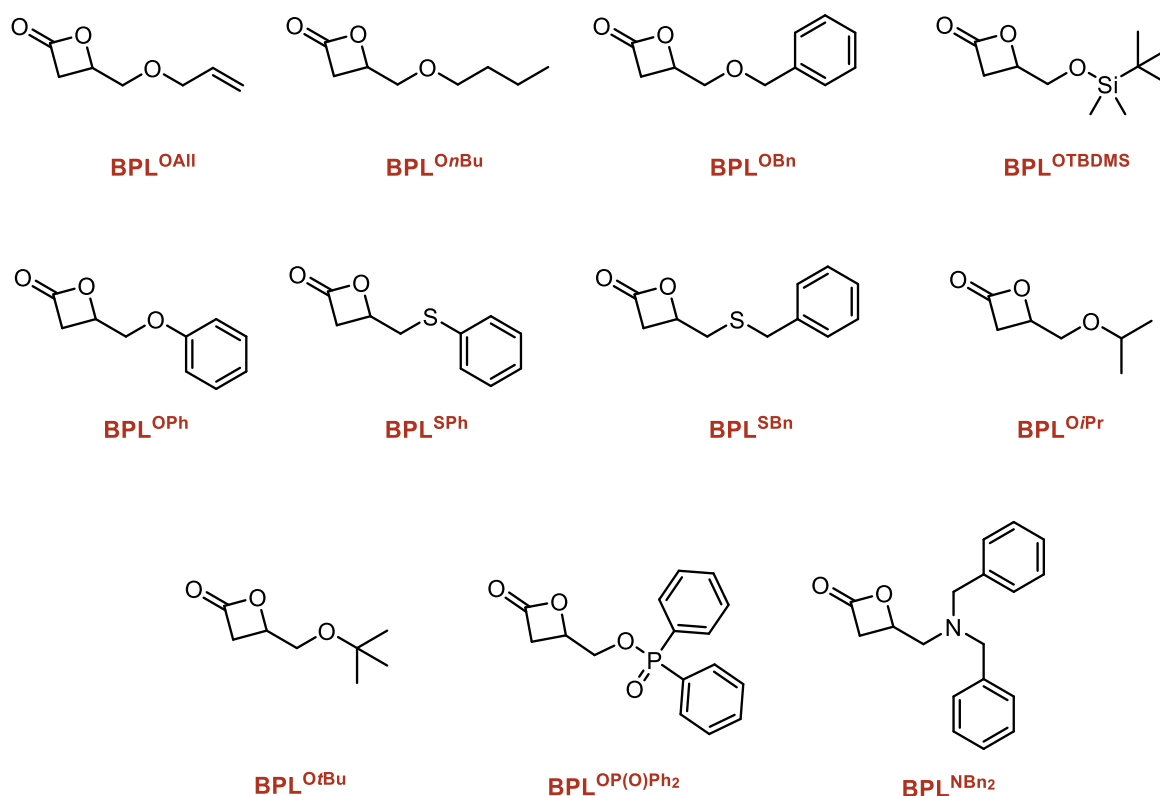


**Figure 5** – Scope of our targeted substituted  $\beta$ -lactone monomers BPL<sup>FG</sup>s.

In virtue of increasing environmental concerns and rapidly growing demands for polymeric materials free of metallic residues to meet the requirements of applications in medicine, microelectronics, food packaging, *etc.*, studies on organic activators (initiators and catalysts) to mediate polymerization, have gained special attention. Chapter 3 thus first reviews the ROP of different ring size cyclic esters ( $\beta$ -lactones, lactides “LA”,  $\delta$ -valerolactone “ $\delta$ -VL”, and  $\epsilon$ -caprolactone “ $\epsilon$ -CL”) through the most common organic activators. Then, my research work, including the synthesis of diverse alkoxy substituted PHAs, PBPL<sup>FG</sup>s (R = OAll, O<sup>t</sup>Bu, OBn, OTBDMS), by organocatalyzed ring-opening polymerization (ROP) of the corresponding *racemic*  $\beta$ -lactones (*rac*-BPL<sup>FG</sup>s), and the thorough characterization of the thus prepared PBPL<sup>FG</sup>s, is described. Focus is placed on the reactivity and efficiency of the organic activators, and mechanistic studies to provide a better understanding of organic-mediated ROP of  $\beta$ -lactones.

On the other hand, the homogeneous single-site metal catalysed ROP of cyclic esters reaches high performances in terms of control and efficiency, i.e. activity, chain-end fidelity, low dispersities, stereocontrol. As explained in Chapter 4, it remains to date the best strategy toward the synthesis of well-defined stereoregular side-chain functionalized polyesters, as reviewed with the ROP of a large variety of cyclic esters via metal centred catalysts. Our work described in this last chapter focuses on amino-alkoxybis(phenolate) yttrium catalysts mediated stereoselective ROP of known and/or novel functional *racemic*  $\beta$ -lactones, emphasizing on the relationship between the pendent functional group on the  $\beta$ -lactone and the tacticity of the PHA.

Finally, the general conclusion summarises the most significant results and suggests some possible outcomes on functional PHAs.

## 4. References

- [1] Charles Moore, [https://www.ted.com/speakers/charles\\_moore](https://www.ted.com/speakers/charles_moore), **2009**.
- [2] a) S. Guilbert, B. Cuq, N. Gontard, *Food Addit. Contam.* **1997**, *14*, 741-751; b) G. W. Halek, **1988**.
- [3] G. Scott, *Polymers and the Environment*, Royal Society of Chemistry, **1999**.
- [4] a) M. Anjum, R. Miandad, M. Waqas, I. Ahmad, Z. Alafif, A. Aburizaiza, M. Barakst, T. Akhtar, *Applied Agriculture and Biotechnology* **2016**, *1*, 13-26; b) M. Marichelvam, M. Jawaid, M. Asim, *Fibers* **2019**, *7*, 32.
- [5] a) M. Avella, E. Bonadies, E. Martuscelli, R. Rimedio, *Polym. Test.* **2001**, *20*, 517-521; b) Y. Zheng, E. K. Yanful, A. S. Bassi, *Crit. Rev. Biotechnol.* **2005**, *25*, 243-250.
- [6] A. Kumar, R. Priyadarshinee, A. Roy, D. Dasgupta, T. Mandal, *Chemosphere* **2016**, *164*, 404-412.
- [7] a) S. K. Gulrez, M. Ali Mohsin, H. Shaikh, A. Anis, A. M. Pulose, M. K. Yadav, E. H. P. Qua, S. Al-Zahrani, *Polym. Compos.* **2014**, *35*, 900-914; b) J. R. Wünsch, **2000**; c) R. Hsissou, R. Seghiri, Z. Benzekri, M. Hilali, M. Rafik, A. Elharfi, *Compos. Struct.* **2021**, *262*, 113640; d) E. Dhanumalayan, G. M. Joshi, *Advanced Composites and Hybrid Materials* **2018**, *1*, 247-268.
- [8] Y. Yamaguchi, *Tribology of plastic materials: their characteristics and applications to sliding components*, Vol. 16, Elsevier, **1990**.
- [9] M. Kishna, E. Niesten, S. Negro, M. P. Hekkert, *Journal of Cleaner Production* **2017**, *155*, 7-16.
- [10] M. J. Kirwan, J. W. Strawbridge, *Food packaging technology* **2003**, *1*, 174-240.
- [11] A. Chadha, *Journal of commercial biotechnology* **2010**, *16*, 159-167.
- [12] a) L. Neufeld, F. Stassen, R. Sheppard, T. Gilman, in *World Economic Forum*, Vol. 7, **2016**; b) H. Ritchie, M. Roser, *Our World in Data* **2018**; c) J. Boucher, G. Billard, *Field Actions Science Reports. The journal of field actions* **2019**, 68-75.
- [13] K. R. Vanapalli, H. B. Sharma, V. P. Ranjan, B. Samal, J. Bhattacharya, B. K. Dubey, S. Goel, *Sci. Total Environ.* **2020**, *750*, 141514.
- [14] Daniel Pauly, [https://www.ted.com/speakers/daniel\\_pauly](https://www.ted.com/speakers/daniel_pauly), **2012**.
- [15] Y. Zhu, C. Romain, C. K. Williams, *Nature* **2016**, *540*, 354-362.
- [16] a) D. K. Schneiderman, M. A. Hillmyer, *Macromolecules* **2017**, *50*, 3733-3749; b) X. Zhang, M. Fevre, G. O. Jones, R. M. Waymouth, *Chem. Rev.* **2018**, *118*, 839-885; c) X. B. Lu, Y. Liu, H. Zhou, *Chem. Eur. J.* **2018**, *24*, 11255-11266; d) Z. Ghayour-Kelly, **2019**; e) M. Hong, E. Y.-X. Chen, *Trends in Chemistry* **2019**, *1*, 148-151.
- [17] <https://www.european-bioplastics.org/bioplastics/>, **2019**.
- [18] M. S. Muthusamy, S. Pramasivam, *Current World Environment* **2019**, *14*, 49.
- [19] Y. Tokiwa, B. P. Calabia, C. U. Ugwu, S. Aiba, *Int. J. Mol. Sci.* **2009**, *10*, 3722-3742.
- [20] A. Iles, A. N. Martin, *Journal of Cleaner Production* **2013**, *45*, 38-49.
- [21] a) N. Escobar, S. Haddad, J. Börner, W. Britz, *Environmental Research Letters* **2018**, *13*, 125005; b) M. Van den Oever, K. Molenveld, M. van der Zee, H. Bos, *Bio-based and biodegradable plastics: facts and figures: focus on food packaging in the Netherlands*, Wageningen Food & Biobased Research, **2017**.
- [22] R. Bhattacharya, K. Chandrasekhar, P. Roy, A. Khan, **2018**.

- [23] J. Hopewell, R. Dvorak, E. Kosior, *Philosophical Transactions of the Royal Society B: Biological Sciences* **2009**, 364, 2115-2126.
- [24] a) K. Petersen, P. V. Nielsen, G. Bertelsen, M. Lawther, M. B. Olsen, N. H. Nilsson, G. Mortensen, *Trends Food Sci. Technol.* **1999**, 10, 52-68; b) R. Miller, *Miller-Klein Associates report. Summary and Full Report available from The National Non-Food Crops Centre, Heslington, York, UK www.nnfcc.co.uk* **2005**.



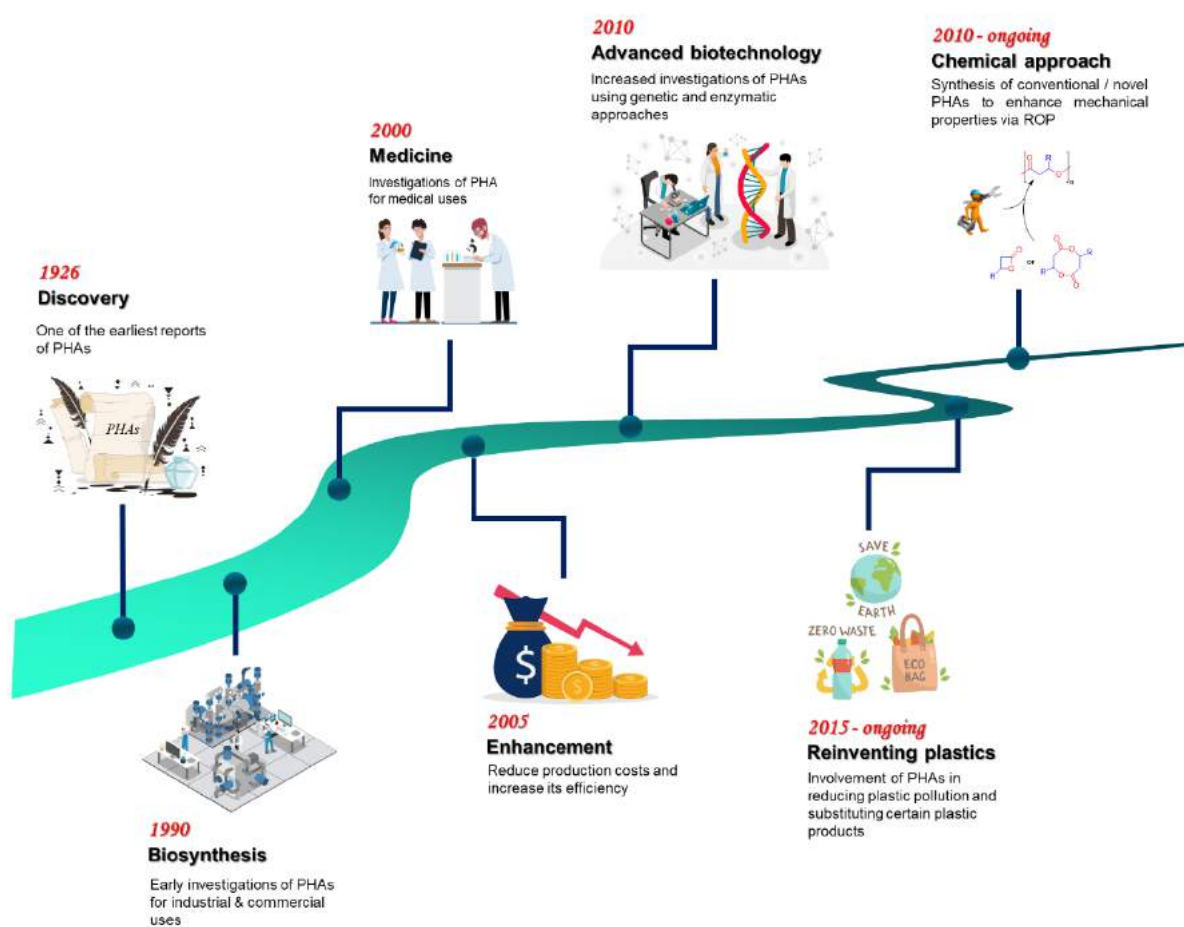






# Chapter 1.

## Poly(hydroxyalkanoate)s (PHAs) : from bacterial to synthetic polyesters





<b>1. Introduction .....</b>	<b>19</b>
<b>2. Poly(hydroxyalkanoate)s “PHAs”: biodegradability matters .....</b>	<b>19</b>
<b>3. Natural PHAs: discovery, biosynthesis, and significance.....</b>	<b>21</b>
<b>4. Synthetic PHAs: biotechnology &amp; chemical synthesis.....</b>	<b>28</b>
4.1.    Advanced biotechnological studies .....	28
4.2.    Chemical polymerization .....	30
4.2.1.    Polycondensation of $\alpha$ - and $\beta$ -hydroxy-acids .....	30
4.2.2.    Ring-opening polymerization (ROP) of $\beta$ -lactones .....	32
<b>5. Conclusion on natural and synthetic PHAs .....</b>	<b>56</b>
<b>6. References.....</b>	<b>59</b>



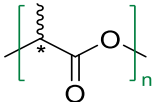
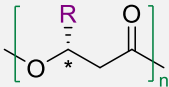
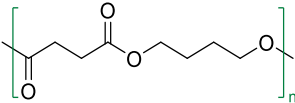
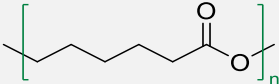
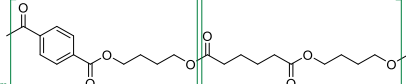
## 1. Introduction

The first chapter presents the general interest of biobased and biodegradable poly(hydroxyalkanoate)s “PHAs” bioplastics. The differences between natural and synthetic PHAs, their synthesis, industrial production, physico-chemical properties, applications, and restrictions, are first presented. The success of synthesizing PHAs from four-membered ring cyclic esters through ring-opening polymerization (ROP) mediated by either organic activators or organometallic catalysts relative to other polymerization methods (polycondensation), is next discussed.

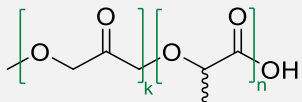
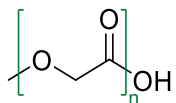
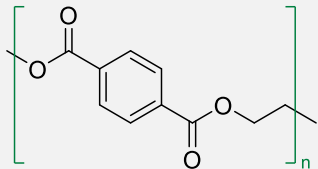
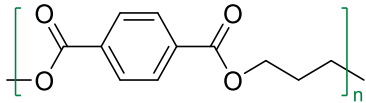
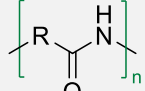
## 2. Poly(hydroxyalkanoate)s “PHAs”: biodegradability matters

Biodegradable bioplastics are considered by many as a promising solution to reinvent and replace conventional plastics. Bioplastics with only biobased feature (Table 1. 1 – entries 8-10) have the unique advantage over conventional plastics to reduce the dependency on limited fossil resources, to decrease greenhouse gas emissions or even to reduce polymers’ carbon footprint.<sup>[1]</sup> On the other hand, biodegradable bioplastics (Table 1. 1 – entries 1-7) offer a lot of advantages such as increased soil fertility, low accumulation of bulky plastic materials in the environment (which invariably will minimize injuries to wild animals), and reduction in the cost of waste management.<sup>[2]</sup> Therefore, biodegradable bioplastics are considered to provide a better potential solution for the plastic wastes.

**Table 1. 1** – Chemical structure of the most common bioplastics (\* indicates the chiral center).

Entry	Name	Structure	Reference
1	Poly(lactic acid) “PLA”		Figure 2 – (B)
2	Poly(hydroxyalkanoate)s “PHA”		Figure 2 – (B)
3	Poly(butylene) succinate “PBS”		Figure 2 – (B)
4	Poly(ε-caprolactone) “PCL”		Figure 2 – (C)
5	Poly(butylene) adipate terephthalate “PBAT”		Figure 2 – (C)



6	PLGA		-
7	PGA		-
8	Poly(ethylene) terephthalate “PET”		Figure 2 – (A)
9	Poly(trimethylene) terephthalate “PTT”		Figure 2 – (A)
10	Poly(amide) “PA”		Figure 2 – (A)

Biodegradation is the property of a material that can be completely converted into CO<sub>2</sub>, water, and biomass, through the action of microorganisms present in the environment such as fungi and bacteria, in aerobic or anaerobic process.<sup>[3]</sup> It is highly controlled by numerous factors, both endogenous (e.g. molar mass, crystallinity, flexibility of the macromolecule) and exogenous (e.g. temperature, humidity, pH, availability of oxygen, enzymatic activity).<sup>[4]</sup> Consequently, biodegradation is directly linked to the chemical structure of the polymer but does not depend on the resource type (fossil-based vs. bio-based). In particular, the type of chemical functions present throughout the polymer defines whether and in which time the microorganisms or water can biodegrade the material; such polymers include a heteroatom in their main chain, and the most important ones are polyesters (Table 1. 1 – entries 1-5). Polyesters are susceptible to break down reasonably efficiently by many enzymatic cleavages in water and soil, in a reasonable period.<sup>[5]</sup> The rate of biodegradation depends on temperature (50-70 °C), humidity, number and type of microorganisms. The degradation is fast only if all three requirements are gathered. Generally, at home or in a supermarket, biodegradation occurs very slowly in comparison to composting. In industrial composting, polyesters are converted into biomass, water and CO<sub>2</sub> in about 6-12 weeks.<sup>[3]</sup> The degradation products of the biodegradable polyesters are typically hydroxy acids, such as β-hydroxy acids, glycolic acid and lactic acid obtained from PHA, PGA and PLA, respectively, that are generally recognized as being non-toxic.<sup>[5]</sup>

Among the different biodegradable polyesters, poly(hydroxyalkanoate)s “PHAs” (Table 1. 1 – entry 2) attracted considerable attention due to their efficient and fast biodegradation in

different environments, combined to their highest sensitivity to microorganisms in comparison to PCL, PBS, and PLA (Table 1. 1 – entries 1 to 4).<sup>[6]</sup> Moreover, PHAs are gaining special attention for having a wide range of applications imparted by, in particular, the chiral carbon that may provide diverse stereochemistry from atactic (no stereoregularity) to isotactic (same relative configuration) to syndiotactic (alternated relative configuration) (Figure 1. 1), along with various functionalities “FG” on the repeating unit.

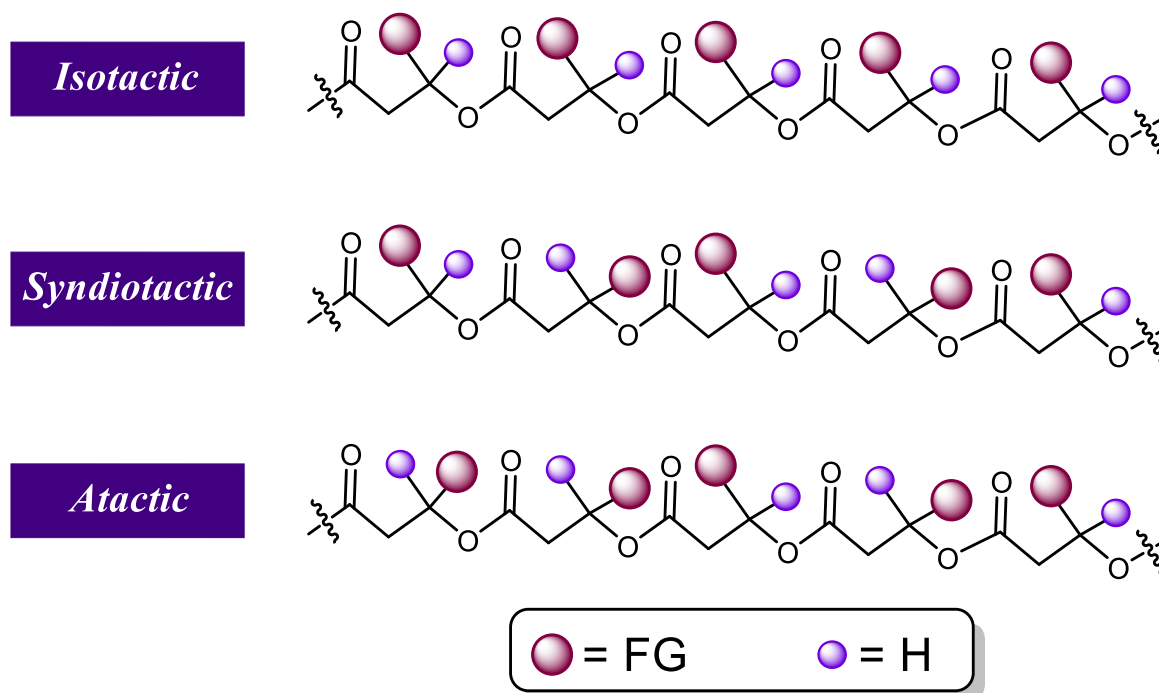


**Figure 1. 1** – PHAs stereochemistry; (a) isotactic; (b) syndiotactic; (c) atactic.

In summary, bioplastics based on biodegradable aliphatic polyesters such as PHAs offer a broad range of functionalities and stereochemistry that can be optimised for each type of application. In addition, they can reduce the impact on the environment, when compared to conventional plastics. It is however important to glimpse on natural and synthetic PHAs, their functionalities, stereochemistry, and limitations.

### 3. Natural PHAs: discovery, biosynthesis, and significance

Natural PHAs are a family of linear aliphatic biopolyesters that are produced from renewable resources, mostly via microorganism’s fermentation. The world came to know about natural PHAs in 1925-1926 with the discovery by the French chemist and bacteriologist Maurice Lemoigne while working at the Lille branch of the Pasteur Institute (Figure 1. 2). Maurice Lemoigne was studying the Gram-positive *Bacillus megaterium*, when he noticed that the latter produced an intracellular biopolyester, a PHA named poly(3-hydroxybutyrate) “PHB” (Table

1. 1 – entry 2; with  $R = CH_3$ ) which is accumulated as insoluble granules in the cytoplasm of the bacteria as a carbon reserve under nutrient limitation.<sup>[7]</sup> In 1968, Griebel investigated the composition of PHB granules of *Bacillus megaterium* for the first time, concluding that they consisted of 97.7% polyesters, 1.87% protein, and 0.46% lipids or phospholipids.<sup>[8]</sup>

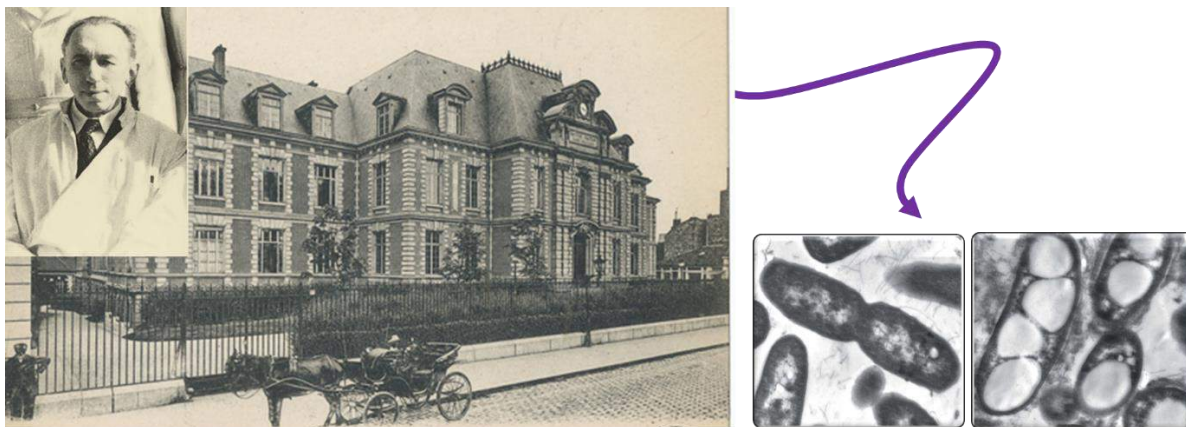


**Figure 1. 2** – Photo of the French chemist and bacteriologist Maurice Lemoigne, Pasteur Institute, and Gram-positive *Bacillus megaterium* under the microscope.

Later on, PHB was found to be part of a large family of natural PHAs that differ only in their substituent located on the  $\beta$ -carbon. More than 150 different forms of PHAs consisting of 3-hydroxy fatty acids monomers (3-hydroxyalkanoates, 3HAs) have been investigated (Figure 1. 3). Natural PHAs may be divided into three main classes depending on the length of the group at the  $\beta$ -position of the monomers: (i) short-chain-length PHAs, which consist of monomers with chain lengths of 3–5 carbon units, of which the most popular are “PHB”, poly(3-hydroxypropylate) “PHP”, poly(3-hydroxyvalerate) “PHV”, poly(3-hydroxyhexanoate) “PHH”, and even copolymer poly(3-hydroxybutyrate-*co*-valerate) “PHBV”;<sup>[9]</sup> (ii) medium chain-length PHAs, which include monomers with lateral chain lengths between 6 and 14 carbon units;<sup>[10]</sup> and (iii) long-chain-length PHAs, which are composed of monomers with carbon chain lengths greater than 14 units. Interestingly, due to their fermentation synthesis, natural PHAs are strictly isotactic, featuring exclusively (*R*)-configuration (Figure 1. 1, (a)). Anyhow, the most prominent, thus the most extensively studied PHA is PHB, in which bacterial poly[(*R*)-3-hydroxybutyrate], P[(*R*)-3HB], is a perfectly stereoregular, purely isotactic crystalline thermoplastic material.<sup>[11]</sup>

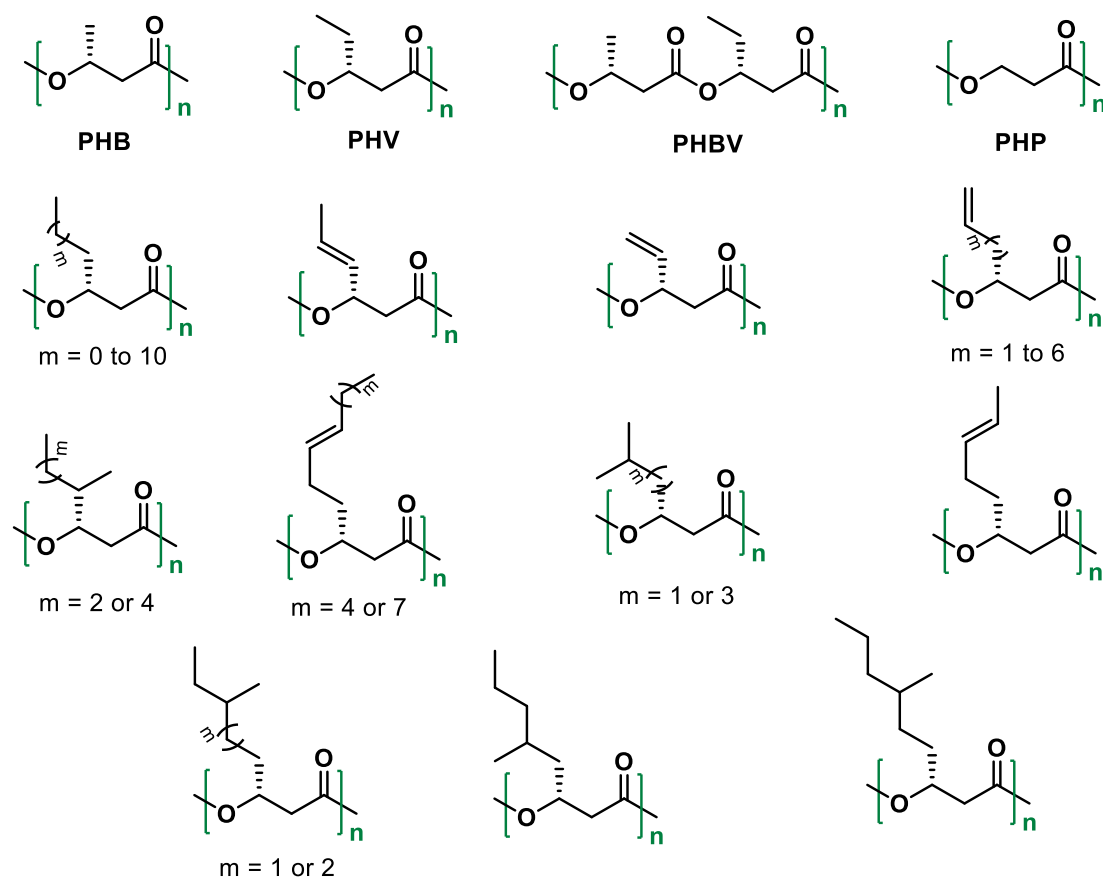


**Figure 1. 3** – Chemical structure of various types of isotactic natural (*R*)-PHAs, extracted from microorganisms.

This diversity of side groups leads to various physio-chemical properties that can be tailored over a wide range, hence leading to various applications.<sup>[12]</sup> For example, polymers composed solely of short chain-length monomer units generally have thermoplastic properties, while polymers composed of medium chain-length subunits generally have elastomeric properties. PHA copolymers with a relatively high mol% of short chain-length monomers (typically PHB) and low mol% of medium chain-length monomers have properties similar to the bulk commodity plastic polypropylene “PP”, although they have much lower elongation to break and are more brittle.<sup>[13]</sup> The glass transition temperature and melting temperature of natural PHAs are in the range of  $-50$  to  $4$  °C and  $40$ – $180$  °C, respectively.<sup>[14]</sup> It is therefore estimated that most of PP applications can be covered to a large extent by PHAs, such as preparation of films, bottles and paper, disposal items such as razors, utensils, and diapers.<sup>[15]</sup>

PHAs were found to be synthesized and accumulated by a wide range of prokaryotic microorganisms’ generally found in the environment i.e. gram-negative, gram-positive bacteria, cyanobacteria and archaea or plants.<sup>[16]</sup> Stanier and Wilkinson and their co-workers were responsible for some of the initial fundamental research into the mechanisms of PHA

biosynthesis, beginning in 1975.<sup>[17]</sup> Commonly, the main substrates used by microorganisms to produce PHAs are sugars (glucose, fructose, sucrose, lactose, maltose, xylose)<sup>[18]</sup> and fatty acids.<sup>[19]</sup> The PHB metabolic pathway inside a bacterium as an example for PHAs is illustrated in Figure 1. 4 – route 1. Bacteria produce acetyl-coenzyme-A (acetyl-CoA, such as hydroxyacyl-CoA thioesters) starting from sugars, where the latter is converted into PHB by three biosynthetic enzymes. In the first step, 3-ketothiolase (PhaA) condenses two molecules of acetyl-CoA to form acetoacetyl-CoA. (*R*)-specific acetoacetyl-CoA reductase (PhaB) allows the reduction of acetoacetyl-CoA to (*R*)-3-hydroxybutyryl-CoA with simultaneous oxidation of nicotinamide adenine dinucleotide phosphate (NADPH) to NADP<sup>+</sup>. Finally, PHB synthase (PhaC) polymerizes 3-hydroxybutyryl-CoA to PHB upon forming an ester bond between the carboxyl group of one monomer and the hydroxyl group of the neighbouring monomer, coenzyme-A being liberated. Only (*R*)-isomers are accepted as substrates for the biosynthetic polymerizing enzyme (PhaC) due to its stereo-specific nature.<sup>[20]</sup> During normal bacterial growth, the 3-ketothiolase is inhibited by free coenzyme-A coming out of the Krebs cycle. But when entry of acetyl-CoA into the Krebs cycle is restricted (during noncarbon nutrient limitation), the surplus acetyl-CoA is channelled into PHB biosynthesis.<sup>[21]</sup> Noteworthy, there are similar pathways starting from fatty acids to produce PHAs of medium chain-length through the  $\beta$ -oxidation of alkanolic acids by producing hydroxyalkanoyl-CoA as a substrate.<sup>[22]</sup> Fascinatingly, intracellular degradation or mobilization of natural PHAs takes place when the bacterium is stressed under carbon limitation conditions, generally carried out by secretion of intra- or extracellular PHA hydrolases and PHA depolymerases (PHaZ).<sup>[23]</sup> PHaZ are granule-associated proteins that hydrolyze water-insoluble PHAs into water-soluble forms so that it can be utilized by the microorganisms as energy source.<sup>[24]</sup> From there, PHAs are broken down to 3-hydroxyalkanoic acids (in case of PHB, it is 3-hydroxybutyric acid) which is then oxidized by a dehydrogenase to acetoacetyl-CoA, which is finally converted into acetyl-CoA by  $\beta$ -ketothiolase (Figure 1. 4 – route 2).<sup>[25]</sup>

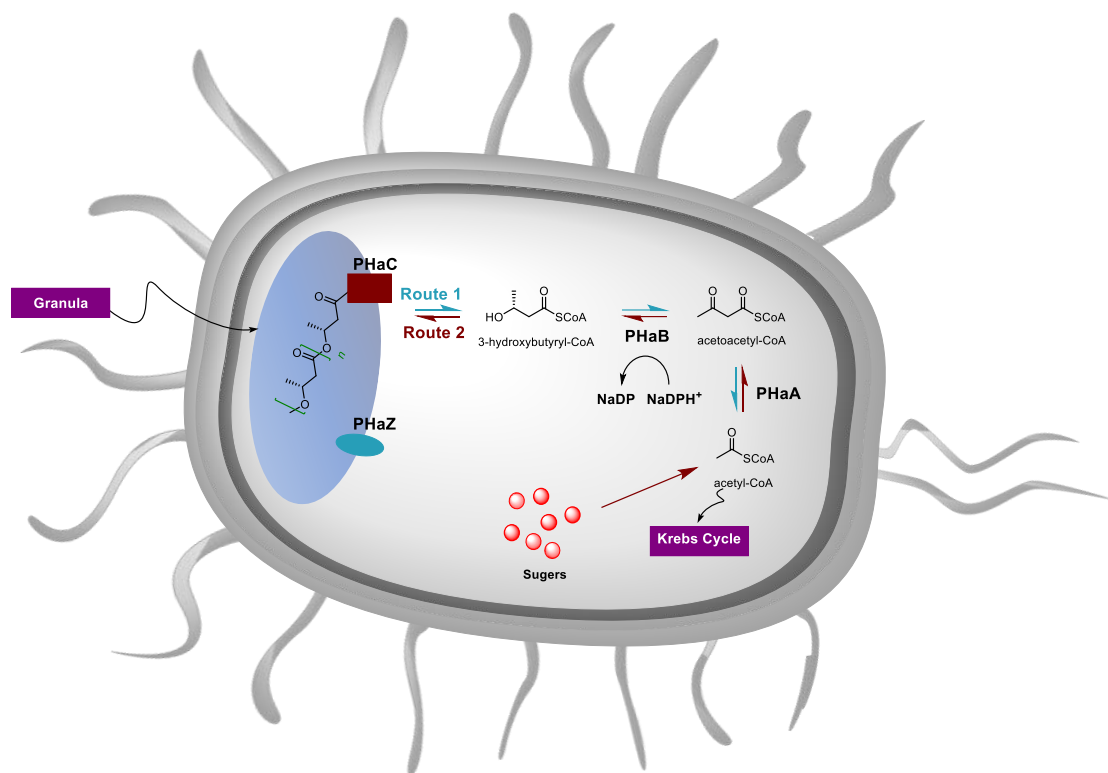


**Figure 1. 4** – Metabolic pathway to natural PHB inside a bacteria starting from sugars.

Bacterial PHAs have gained enormous interests in scientific research and commercial uses worldwide (Figure 1. 5).<sup>[26]</sup> The first commercialization attempted, was done in 1959, when W.R. Grace patented a PHB production process using bacteria.<sup>[27]</sup> In 1970, Imperial Chemical Industries Ltd. commercialized the production of P(3HB-*co*-3HV) under the trade name of Biopol<sup>TM</sup>, with the technology being sold to Monsanto and then to Metabolix.<sup>[28]</sup> Then the synthesis of alternative copolymers such as P(3HB-*co*-3HHx) was marketed as Nodax<sup>TM</sup>.<sup>[29]</sup> Nowadays the major producers of PHAs are Danimer Scientific<sup>[30]</sup> and Kaneka corporation.<sup>[31]</sup> There have been a range of new technologies developed, and recent focus within industrial manufacture to use optimum culture conditions in order to maximize PHA production, termed as “1<sup>st</sup> generation”. Researchers in industry are also working on valorisation of municipal wastewater as non-food competing sources for cultivating a range of bacteria with the purpose of obtaining PHA biopolymers with improved sustainability. Different research efforts also deal with transgenic crops that express PHA synthesis routes from bacteria to produce PHA as energy storage in their tissues.<sup>[32]</sup> Potential utilization of agricultural feedstocks, industrial by-products, waste oils, wastewater, and sewage sludge is gaining attention for the production of PHAs while simultaneously solving the problem of waste disposal, which is referred to as 2<sup>nd</sup> generation.<sup>[33]</sup> Anyhow, after accumulation, PHAs are extracted and further purified in tedious and costly processes as they are intracellular storage materials. Broadly applied methods for the



extraction and recovery of PHAs from biomass are via solvent extraction, floatation, and supercritical fluid extraction.<sup>[10b, 34]</sup>

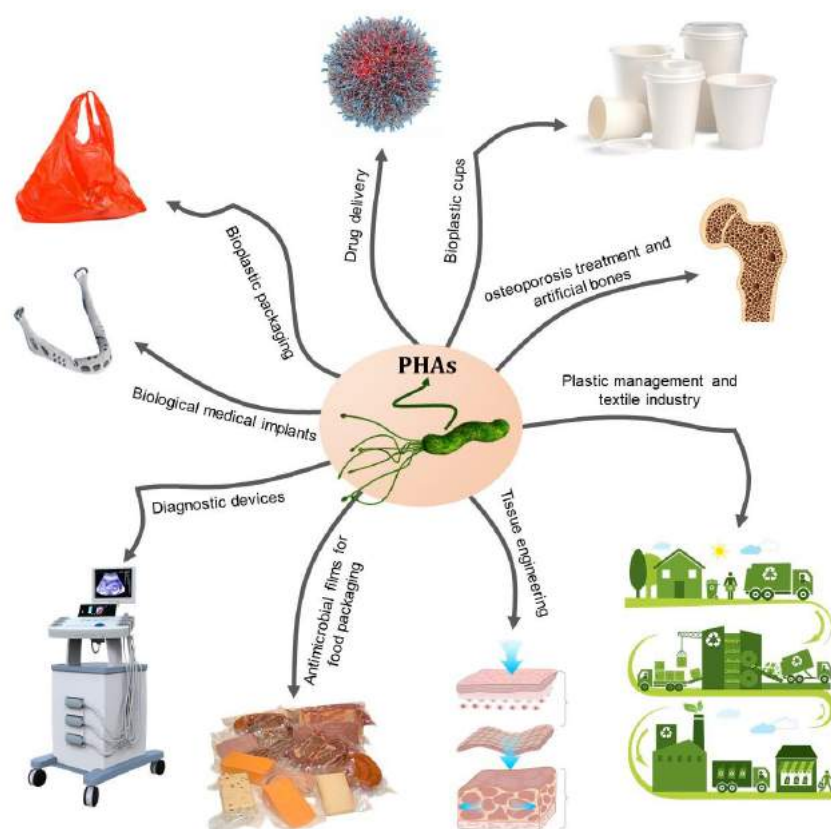


**Figure 1. 5** – Wide-ranging applications of natural PHAs.

The extracted bacterial PHAs are biodegradable in both aerobic and anaerobic environments, without forming any toxic products. Furthermore, their biodegradation in living cells revealed to breakdown into products that are naturally found in animals, therefore PHAs were also categorized as a biocompatible material.<sup>[35]</sup> Thanks to their biodegradability and biocompatibility, PHAs can be used in medical field (Figure 1. 6). Micro- and nanospheric PHA-based compartments were used as drug delivery carriers, in which the used drugs were automatically released from the vector after degradation of PHA.<sup>[36]</sup> Moreover, PHAs as drug delivery or vaccine carrier vehicle have been used in several animals such as cattle, mice, dogs, and in humans to cure gingivitis.<sup>[37]</sup> For the cure of chronic and implant osteomyelitis, drugs such as sulbactam cefoperazone have been loaded to rods of PHBV.<sup>[38]</sup> PHB polymers have also been used as a vehicles in transdermal tissues along with poly(amidoamine) dendrimers to increase the transdermal permeability of tamsulosin drug.<sup>[39]</sup> The piezoelectric property of PHAs has been applied to repair the damaged nerves.<sup>[12, 40]</sup> PHAs are also applied in the dressing of wounds as well as for the preparation of scaffolds.<sup>[41]</sup> PHA such as PHB and PHBV are used

as matrices in *in vitro* proliferation of human cells. The various human cells, such as endothelium cells, liver cells, and fibroblasts exhibit comparable adhesive property as PHAs when these polymers are applied as matrices.<sup>[35a]</sup>

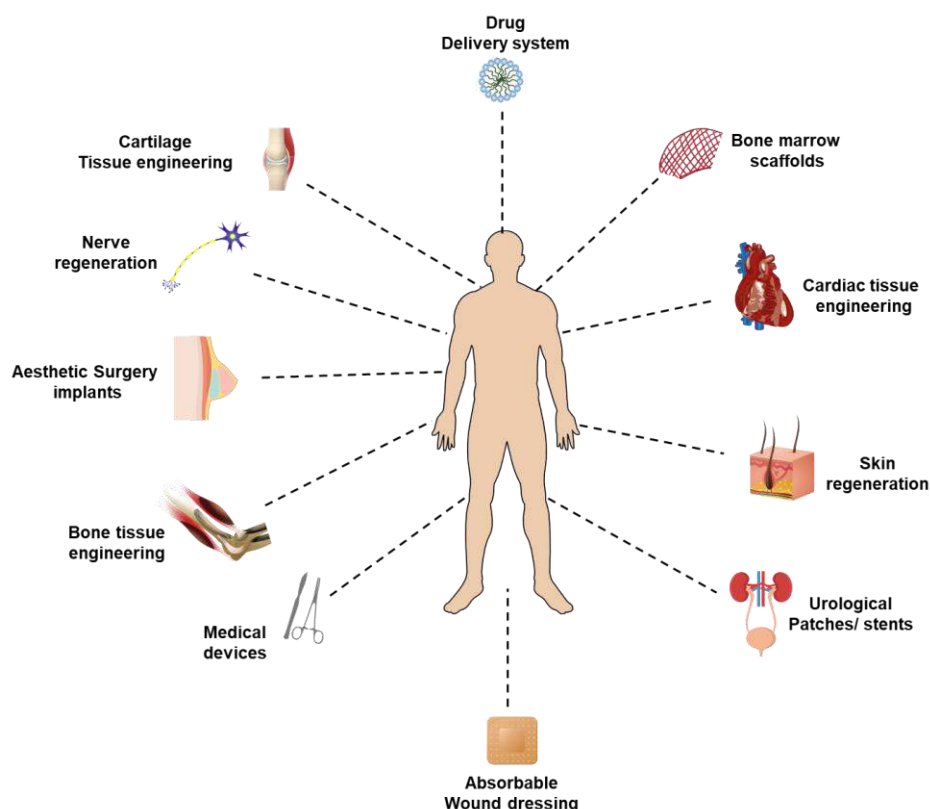


**Figure 1. 6** – Medical applications of natural PHAs.

Nevertheless, natural isotactic PHAs still show some limitations in terms of performance like thermal resistance, barrier and mechanical properties, such as mediocre mechanical stability, unfavourable biodegradation rate, or either too high or too low degree of crystallinity. Another main limitation in the application of natural PHAs for the production of single use items, is its relatively high cost when compared to other polymers. The main cost absorbing factor being carbon feedstock and the PHAs extraction methods.<sup>[42]</sup> Further investigations and efforts are undertaken by scientists in order to reduce the production costs of PHAs and to increase the industrial sustainability and commercialisation of PHAs via *3<sup>rd</sup> generation* biotechnology. Otherwise, another approach is to plainly chemically synthesize functional PHAs, that are expected to have better mechanical properties, and also to be biodegradable and biocompatible.



## 4. Synthetic PHAs: biotechnology & chemical synthesis

Different synthetic procedures enable to access to PHAs. Synthetic methods such as the advanced biotechnology can provide new monomer compositions and are able to control the chain lengths and molar masses of the produced PHAs; or above all that could as well tune the tacticity (Figure 1. 1) in case of some synthetic chemical polymerization approaches. By this, one can increase PHAs' versatility, their properties can vary over a broader range, possibly comparable to that of conventional plastics. Hence, such synthetic procedures can help improving the usage of PHAs in medical field and packaging or even expanding its application to other domains that natural PHAs can't provide, such as automotive, transport, building, construction, or electronics (Figure 3).

### 4.1. Advanced biotechnological studies

After biosynthesis pathways of PHAs have been elucidated (Figure 1. 4), they have been optimized. Biotechnological studies towards the biosynthesis of PHAs have extensively progressed through the development of various metabolic engineering strategies. Efficient PHA production (*1<sup>st</sup> generation*) has been achieved using fermentation technology of naturally occurring PHA-producing bacteria based on external substrate manipulation (*vide supra*), and by means of utilization of agricultural feedstocks, wastewater, and sewage sludge (*2<sup>nd</sup> generation*). More recently, subsequent reinforcement with recombinant gene technology and “enzyme evolution” is considered and referred to as the *3<sup>rd</sup> generation* approach for PHAs production (Figure 1. 7).<sup>[43]</sup>

Nowadays, the current scenario to improve PHA production efficiency involved a deoxyribonucleic acid (DNA) reprogramming tool such as regulating gene expression; this has been successfully applied to manipulate PHA synthetic pathways. They have proven to be efficient in adjusting the transcription levels by completely studying the sequence design, binding strength, chromosomal regulation, and library construction for enhancing its contribution to PHA synthesis. These strategies have boosted PHA accumulation in large cellular spaces of bacteria, and have enabled the selective synthesis of PHAs instead of a mixture of copolymers.<sup>[44]</sup>

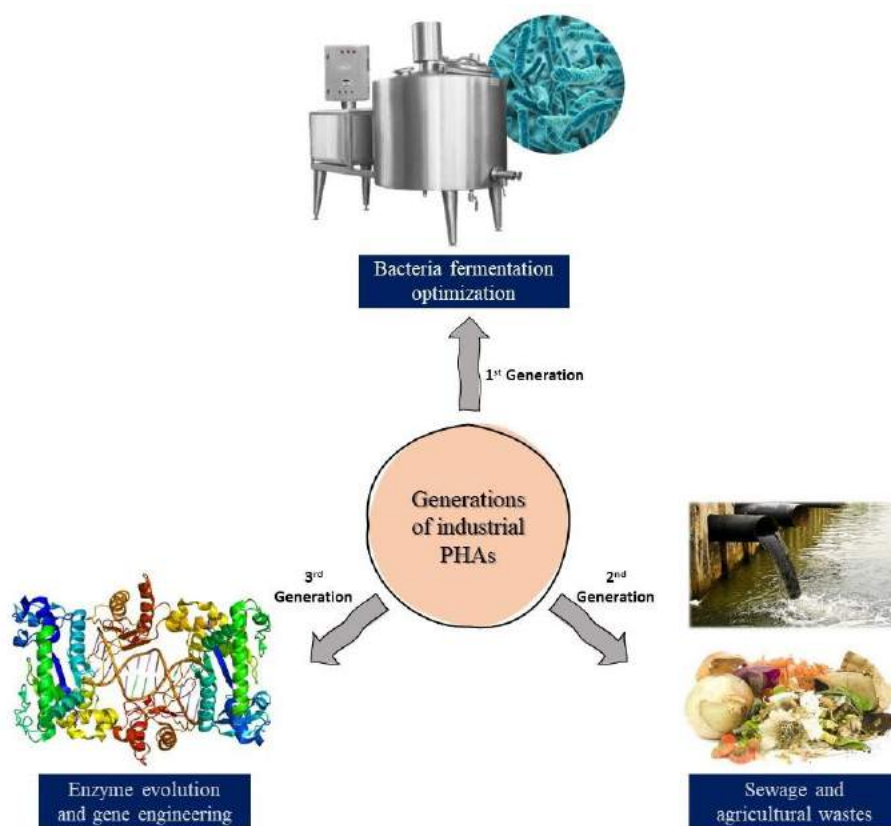


**Figure 1. 7** – Different generations of the enhancement in PHAs accumulation and extraction in and from the bacteria (*1<sup>st</sup>* & *2<sup>nd</sup>* generations) and their synthesis via advanced biotechnology (*3<sup>rd</sup>* generation).<sup>[43]</sup>

On the other hand, “enzyme evolution” is a very versatile approach to optimize PHAs production systems.<sup>[45]</sup> Artificial evolution techniques (*in vitro*) have been successfully used to generate enzymes (by mutation) with enhanced activity and substrate specificity capable of producing a wide range of variation in monomeric compositions or molar mass of PHA copolymers products.<sup>[46]</sup> For example, an alteration of the key enzyme for PHA synthesis (PhaC) has been demonstrated to provide various custom-made enzymes applicable for extending the capacity for enhanced accumulation and changed the monomer composition of PHA copolyester by using a catalytic function not available from a natural source.<sup>[47]</sup> It is worth to mention that, in 1995, Gerngross and Martin first achieved and demonstrated the *in vitro* synthesis of PHB in aqueous solution. The resulting PHB had higher molar mass than that of *in vivo* synthesized PHB.<sup>[48]</sup>

Genetic engineering combined with enzyme and synthetic biological tools can lead to the production of novel tailor-made PHA biopolymers. In fact, this way is also a significant reduction of non-renewable energy consumption. However, extracted PHAs require post-

cleaning actions, especially if targeted to be used in the medical field, that makes the PHAs production costlier and proved economically nonviable.<sup>[49]</sup>

## 4.2. Chemical polymerization

Synthesis of aliphatic polyesters such as PHAs (Figure 1. 3) via chemical polymerization methods are applicable for various practical demands. Two polymerization approaches have been implemented to date: (a) polycondensation of  $\beta$ -hydroxy-acids, and (b) ring-opening polymerization (ROP) of 4 membered ring cyclic esters ( $\beta$ -lactones).<sup>[50]</sup> The latter being our adopted method due to its better efficiency and control in terms of macromolecular parameters (molar masses, dispersity) and stereochemistry that are discussed below (Figure 1. 8).

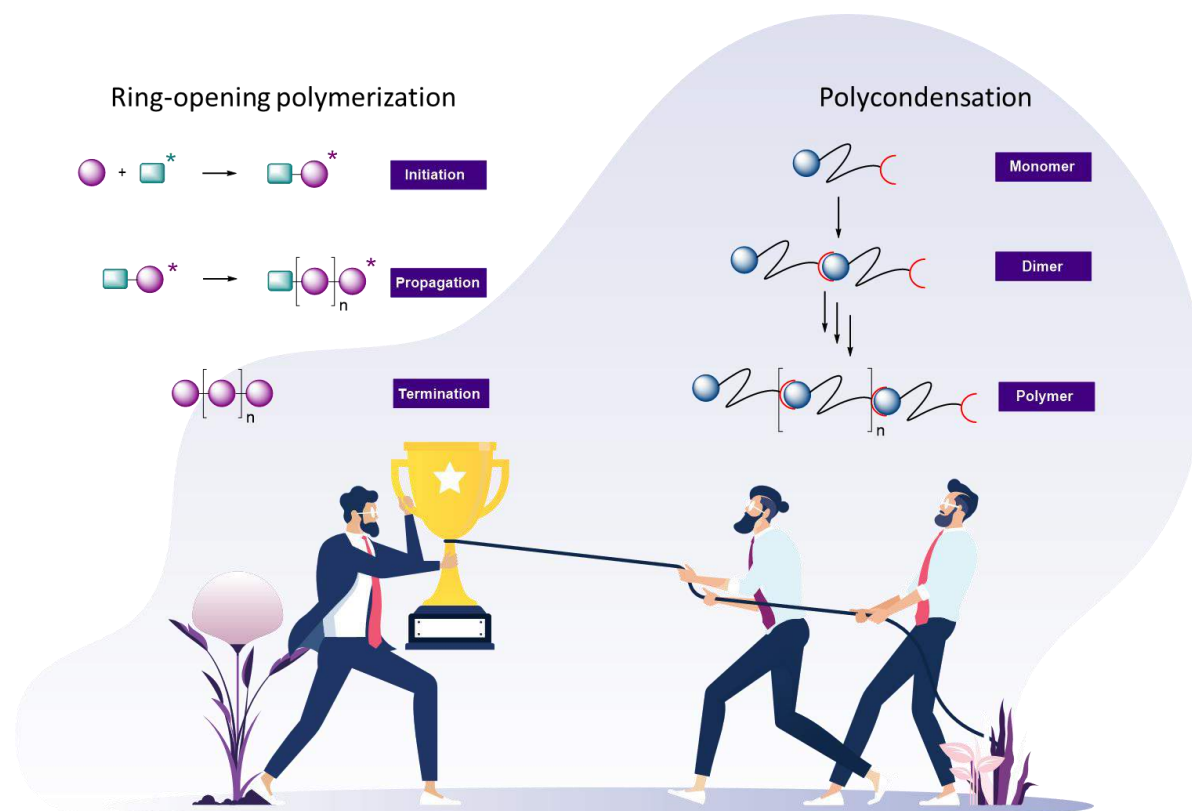
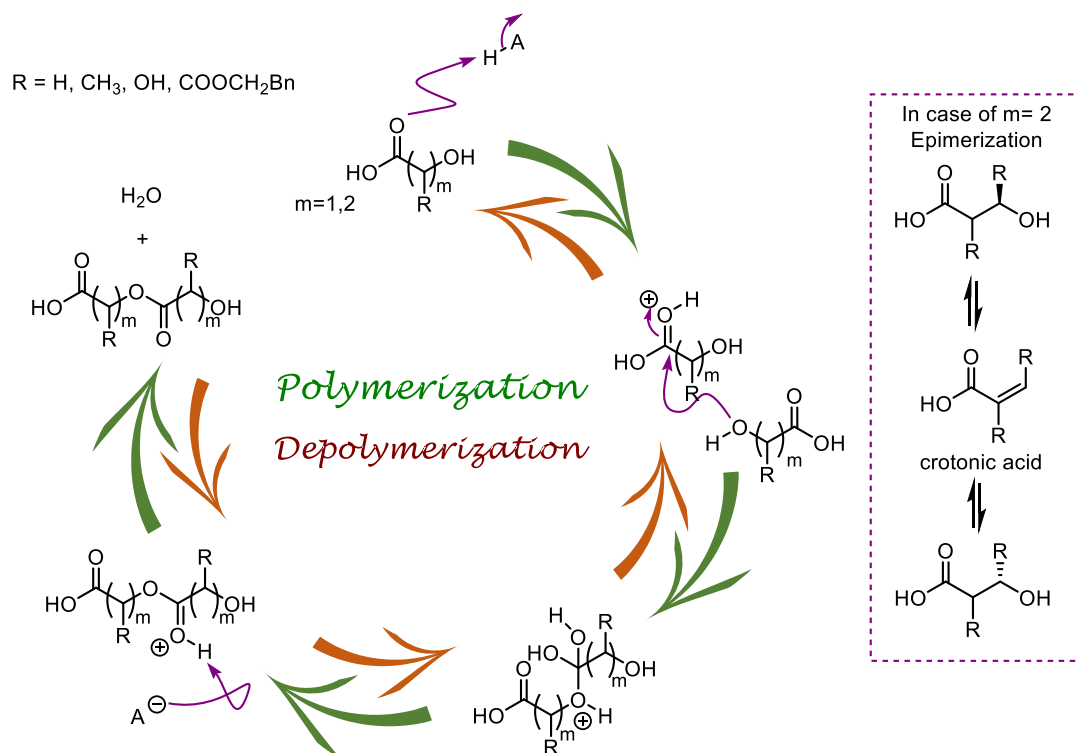


**Figure 1. 8** – Illustration of (left) ring-opening polymerization (ROP) vs. (right) polycondensation processes.

### 4.2.1. Polycondensation of $\alpha$ - and $\beta$ -hydroxy-acids

Polycondensation is a step-growth polymerization that relies on the Fischer self-esterification reaction of  $\alpha$ - or  $\beta$ -hydroxy-acids in the presence of acid catalyst (Scheme 1. 1 – right). In this case, the polymerization process is reversible and the polymers formed (e.g., PLA

or PHA, respectively; Table 1. 1 – entries 1, 2) have the potential to depolymerize, enabling the recovery of the initial monomers by properly guiding the polymer-monomer equilibrium (Scheme 1. 1 – right).<sup>[51]</sup> The principal benefit of this technique is the easy availability of a wide range of substituted  $\alpha$ - or  $\beta$ -hydroxy-acid monomers, that for most of them occur naturally (biobased) in plants, microorganisms as well as in animal tissues (produced in the liver via the metabolism of fatty acids).<sup>[52]</sup> Whereas polycondensation of  $\alpha$ -hydroxy acids is common, the polycondensation of  $\beta$ -hydroxy acids is not because of their tendency to undergo epimerization and formation of crotonic acid  $\alpha,\beta$ -unsaturated species (Scheme 1. 1 – right). It has been, to our knowledge, only successfully reported for a derivative of malic acid or unsubstituted 3-hydroxypropanoic acid (3HP). In 1976, Wise *et al.* synthesized  $\alpha,\beta$ -poly(malic acid) “PMLA” with low molecular weight ( $1900 \text{ g mol}^{-1}$ ) by direct Polycondensation of L-malic acid.<sup>[53]</sup> In 1994, poly(3HP) was synthesized by condensation of the corresponding 3HP in the presence of a transesterification catalyst at  $70^\circ\text{C}$ .<sup>[54]</sup> In 2014, the optimum Polycondensation conditions to obtain  $\alpha,\beta$ -PMLA ( $5300 \text{ g mol}^{-1}$ ) were using tin(II) chloride as a catalyst at  $110^\circ\text{C}$  after 45 h.<sup>[55]</sup> Subsequently, Polycondensation of benzyl malolactonate “MLA<sup>Bn</sup>” was attempted by using dicyclohexylcarbodiimide (DCC) as a coupling reagent; but only oligomers were obtained.<sup>[56]</sup>



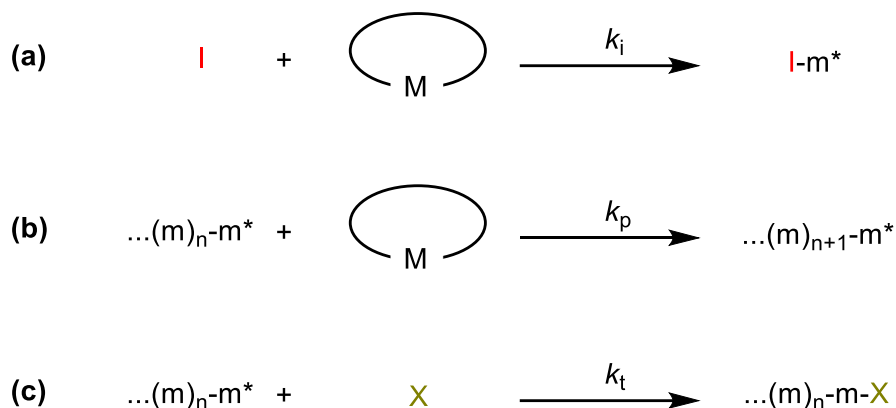
**Scheme 1.1** – Fisher self-esterification mechanism (left) for the polymerization of  $\alpha$ -hydroxy-acids ( $m = 1$ ) or  $\beta$ -hydroxy-acids ( $m = 2$ ) and depolymerization of PLA ( $m = 1$ ) or PHAs ( $m = 2$ ); (right) epimerization of  $\beta$ -hydroxy-acids ( $m = 2$ ) that hampers the polymerization.<sup>[51, 57]</sup>

Anyway, Polycondensation of  $\beta$ -hydroxy-acids suffers from severe limitations. The esterification reaction generates H<sub>2</sub>O in the medium that requires removal for the sake of achieving higher molar mass polymers. Hence, high-energy cost (high temperatures > 100 °C) is required to eliminate water and to reduce the viscosity. Moreover, it is almost impossible to achieve controlled polymerization with predetermined molar masses, defined chain-end groups, and narrow dispersities ( $\bar{D}_M > 2$ ). Also, stereo-controlled polymers of either *rac*- $\alpha$  or  $\beta$ -hydroxy-acids cannot be achieved through polycondensation. More importantly,  $\beta$ -hydroxy-acids are susceptible to an elimination reaction that obstructs the polymerization.<sup>[58]</sup> Consequently, it seems that preparing PHAs from polycondensation of  $\beta$ -hydroxy-acids is elusive, and thus another approach should be adopted.

#### 4.2.2. Ring-opening polymerization (ROP) of $\beta$ -lactones

Ring-opening polymerization (ROP) is a chain-growth polymerization, and unlike polycondensation, it has three distinctive steps: (a) initiation, (b) propagation, and (c) termination and/or transfer, the latter step (c) is not taking place in case of a living ROP (Scheme 1. 2). In ROP, the monomers react with the active species at the end of the growing polymer

chain until their concentration decreases with time. This type of polymerization has great interest in both academic and industrial areas. It is considered more efficient than polycondensation to prepare linear aliphatic polyesters with controlled macromolecular parameters, dispersities ( $\mathcal{D}_M < 2$ ), and stereochemistry.<sup>[59]</sup> ROP is performed under mild reaction conditions (minimum amount of solvent, low temperatures) and the formation of small molecule by-products is avoided (greener approach).<sup>[60]</sup> The monomers include a range of simple cyclic compounds that contain heteroatoms in their ring structure, of which the polarized character facilitates the heterolytic cleavage of the bond. Although the monomers generally come from non-renewable petroleum sources, the biodegradability of the resulting polyester may be maintained. The exclusive disadvantage of ROP compared to polycondensation is the limited availability of cyclic ester monomers, even though varying ring size and strain have been investigated over the past decades in ROP.<sup>[60]</sup>

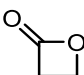
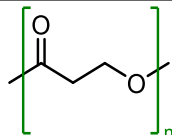
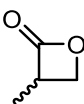
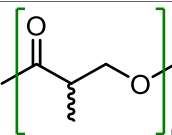
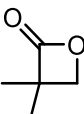
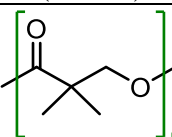
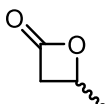
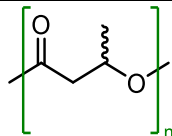
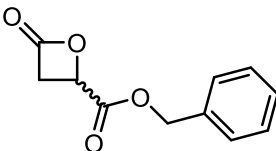
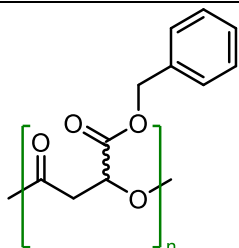


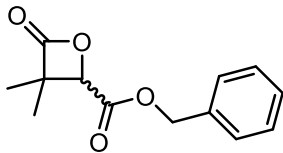
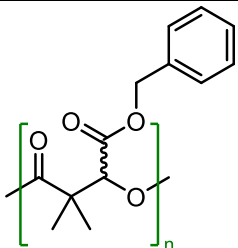
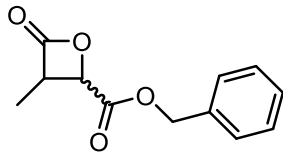
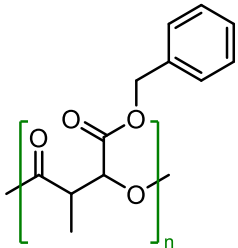
**Scheme 1. 2** – General mechanistic steps for ROP of cyclic monomers; (a) initiation; (b) propagation, (c) termination;  $k_i$ ,  $k_p$ , and  $k_t$  are the rate constants of initiation, propagation, and termination, respectively; where  $k_i \gg k_p$  and  $k_t = 0$  in a living polymerization.

The thermodynamic peculiarities of ROPs will not be addressed in details. Yet, it is important to understand that these polymerizations are particularly governed by the cycle tension (ring strain) as well as different steric considerations when the polymer chain grows. Indeed, the enthalpy loss associated with the opening of the ring may or may not allow the polymerization reaction. The monomer concentration is sometimes a critical parameter to allow polymerization of a little constrained lactone. The thermodynamic driving force for ROP processes is the relief of ring strain, which increases the entropy, thus enabling small rings (three- or four-membered) to polymerize more easily than larger rings. This increase in entropy is based on the increase in the degrees of freedom of rotation gained when rings are transformed into open chains.<sup>[61]</sup>

Among the various monomers, the literature presented hitherto focuses on the polymerization of assorted functional  $\beta$ -lactones through diverse types of ROP including enzymatic, cationic, and anionic to reach synthetic PHAs.<sup>[60]</sup>  $\beta$ -lactones are anticipated to be more reactive towards ROP due to their high ring strain, however their ROP is considered challenging.<sup>[62]</sup> The most significant  $\beta$ -lactones studied beforehand in ROP are represented in Table 1. 2. It is noteworthy to mention that only few  $\beta$ -lactones are commercially available and most of them need to be synthesized by different methods that are discussed in Chapter 2.

**Table 1. 2** – Some examples of common non-substituted or substituted  $\beta$ -lactones used in ROP process and their corresponding polyesters.

Entry	$\beta$ -Lactones	Polyester (PHA)
1	 $\beta$ -Propiolactone (PL)	 Poly(propiolactone) (PPL)
2	 $\alpha$ -Methyl- $\beta$ -propiolactone (MPL)	 Poly( $\alpha$ -methyl- $\beta$ -propiolactone) (PMPL)
3	 Pivalolactone	 Poly(pivalolactone)
4	 $\beta$ -Butyrolactone (BL <sup>Me</sup> )	 Poly( $\beta$ -butyrolactone) (PBL <sup>Me</sup> )
5	 Benzyl malolactonate (MLA <sup>Bn</sup> )	 Poly(benzyl malolactonates) (PMLA <sup>Bn</sup> )

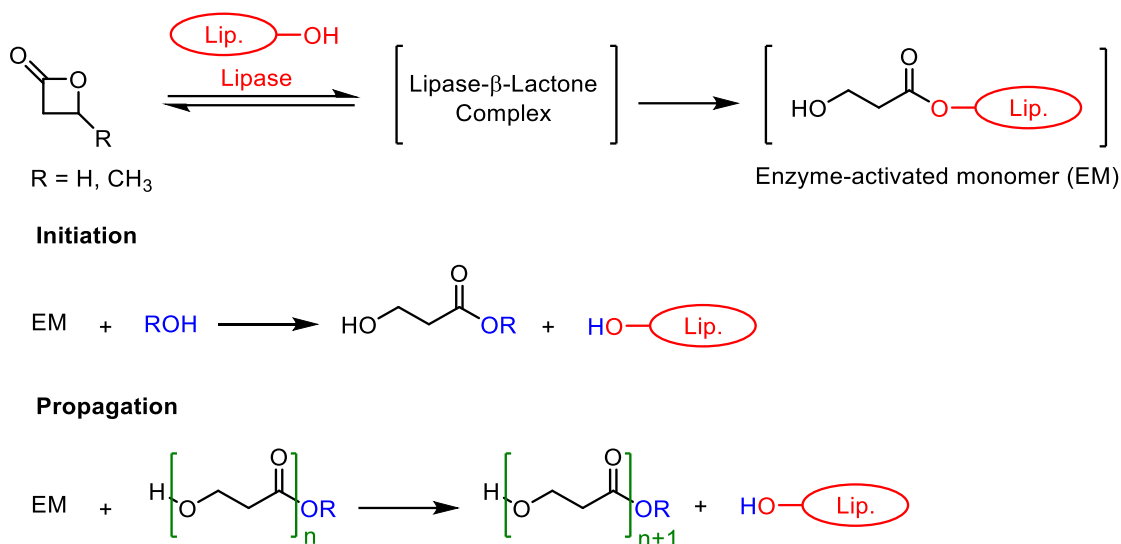
6	 <p><math>\alpha, \alpha'</math>-Dimethyl benzyl malolactonate (dMMLA<sup>Bn</sup>)</p>	 <p>Poly(<math>\alpha, \alpha'</math>-Dimethyl benzyl malolactonates) (PdMMLA<sup>Bn</sup>)</p>
7	 <p><math>\alpha, 3</math>-Methyl-4-benzylloxycarbonyl-2-oxetanone</p>	 <p>Poly(<math>\alpha, 3</math>-methyl-4-benzylloxycarbonyl-2-oxetanone)</p>

#### 4.2.2.a Enzymatic ring-opening polymerization (EROP) of $\beta$ -lactones

Enzymatic ring-opening polymerization (EROP) was established decades ago. It is a ROP mediated by enzyme (Lipase) as a catalyst that is usually accompanied with nucleophilic initiator (alcohols).<sup>[63]</sup> The first EROPs of  $\beta$ -lactones, reported in 1996 on PL (degree of polymerization, DP = 50) and *rac*-BL<sup>Me</sup> (DP = 5–200) (Table 1. 2 – entries 1,4), were performed in different solvents or in the absence of solvents at a temperature ranging from 23 °C to 60 °C, to produce PPL ( $M_{n,Exp(max)} = 2300 \text{ g mol}^{-1}$ ) and PBL<sup>Me</sup> ( $M_{n,Exp(max)} = 1050 \text{ g mol}^{-1}$ ) (Table 1. 2 – entries 1,4), respectively.<sup>[64]</sup> Kobayashi *et al.* suggested the formation of a mixture of linear and cyclic PPL after EROP of PL in bulk at 60 °C, due to the high gap between theoretical and experimental molar masses ( $M_{n,theo}$  vs.  $M_{n,SEC}$ ) and broad dispersities ( $\mathcal{D}_M = 1.6\text{--}2.8$ ).<sup>[65]</sup> In 1997, EROP of *rac*-BL<sup>Me</sup> was performed in bulk at 75 °C using thermophilic lipase to produce isotactic-enriched (*R*)-PBL<sup>Me</sup> ( $M_{n,SEC} = 2400 \text{ g mol}^{-1}$ ,  $\mathcal{D}_M = 2.3$ ,  $P_m = 0.67$ ) after 4–5 days.<sup>[66]</sup> On the other hand, isotactic-enriched poly( $\alpha$ -methyl- $\beta$ -propiolactone) ((*S*)-PMPL) ( $M_{n,SEC} = 2900 \text{ g mol}^{-1}$ ,  $\mathcal{D}_M = 1.7\text{--}1.8$ ,  $P_m = 0.75$ ) (Table 1. 2 – entry 2) was produced after 3–4 days from the lipase catalysed EROP of *rac*-MPL (Table 1. 2 – entry 2) in toluene.<sup>[67]</sup> Interestingly, in 2007, EROP of PL (DP = 170) and *rac*-BL<sup>Me</sup> (DP = 50) was carried out in ionic liquid (as a replacement of volatile organic solvents) at 60 °C to generate after 1 day high molar mass PPL ( $M_{n,SEC} = 11,900 \text{ g mol}^{-1}$ ) relative to that of (*R*)-PBL<sup>Me</sup>, where only oligomers were obtained (reached DP = 5 out of 50). The authors alluded that this is due to the poor fit of *rac*-BL<sup>Me</sup>



moiety in the active site of the enzyme used, unlike PL moiety.<sup>[68]</sup> Lipases are known to catalyse EROP according to an “activated monomer” mechanism (transesterification reactions). The key step is the reaction of the lipase with  $\beta$ -lactones to form an acyl–enzyme intermediate, which further reacts with water, alcohols, or hydroxyl end-capped chains during either the initiation or the propagation step (Scheme 1. 3).<sup>[69]</sup>



**Scheme 1. 3** – Activated monomer mechanism proposed for EROP of  $\beta$ -lactones (PL, *rac*-BL<sup>Me</sup>).

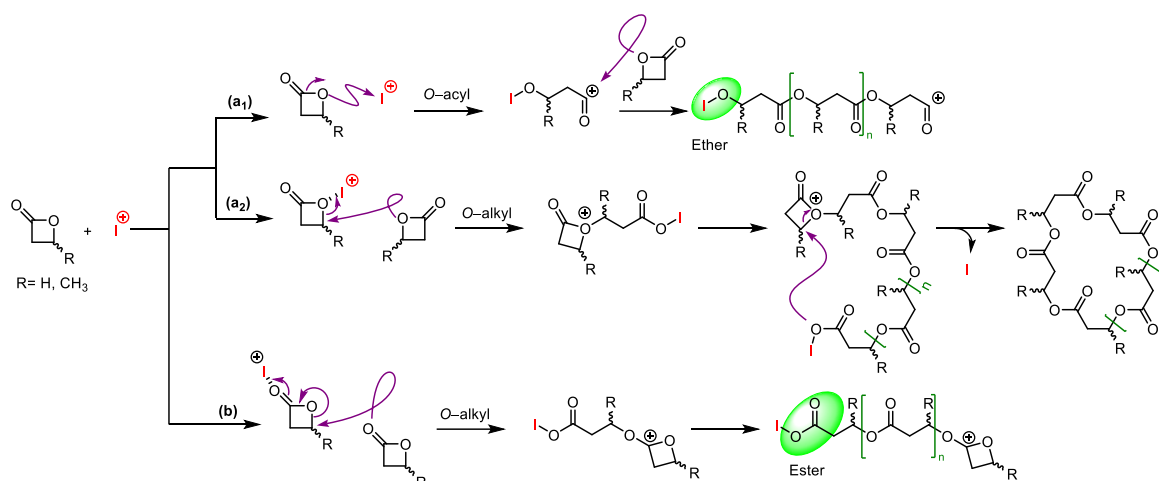
Advantageously, EROPs can be handled with no special precautions (no need for dry or oxygen-free medium), there is no need for solvent, PHA is easy to isolate (by filtration), and it is well-suited for PHAs designed for biomedical applications (non-toxic enzymes). Moreover, the stereospecificity of lipases can open up a new route to stereoselective ROP.<sup>[69b]</sup> Nevertheless, EROP outcomes largely depend on the reaction conditions (water content and temperature). A mixture of linear and cyclic polymers can be formed, and the polymer produced tends to solidify from the reaction mixture thus limiting further polymer chain-growth and leading to heterogeneity and eventually large dispersities. Furthermore, polymerization may require days without always achieving full monomer conversion. Notably, the  $\beta$ -lactone used should also fit into the enzyme active site, in a way that high monomer concentration or polar and hydrophilic functional substituted  $\beta$ -lactones can fail to polymerize and thus limiting the formation of high molar mass PHAs or PHAs with specific and diverse functionalities.<sup>[70]</sup>

#### 4.2.2.b Cationic ring-opening polymerization (CROP) of $\beta$ -lactones

Cationic ring-opening polymerization (CROP) of  $\beta$ -lactones (the most studied are PL and *rac*-BL<sup>Me</sup>) has been known for a long time (since the mid-1940s) but it is not very popular

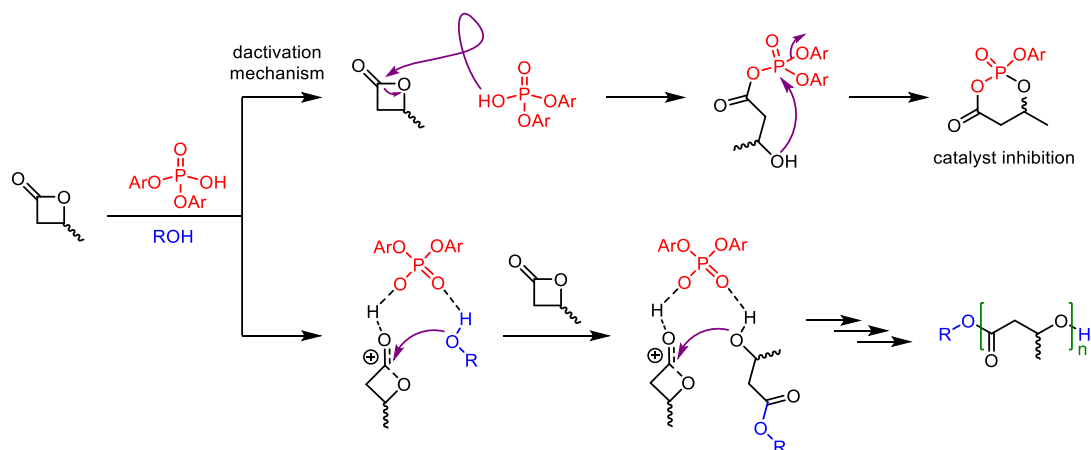
due to its general poor control of the macromolecular parameters and high dispersities ( $M_{n,SEC} < 10,000 \text{ g mol}^{-1}$ ;  $\bar{D}_M < 2.5$ ); this is probably due to undesired side reactions and the formation of a mixture of cyclic and linear polymers.<sup>[58a, 71]</sup> CROP can be promoted by cationic catalysts such as Lewis acids and protonic/Bronsted acids, accompanied with a protic initiator (typically alcohols) or mainly by a cationic initiator only (alkylating agent, acylating agent, Lewis acid, and protonic/Brønsted acid).<sup>[72]</sup> CROP has a distinct advantage in its simplicity and in the wide range of diverse acids or cationic initiators (organic or inorganic) available. The mechanistic pathway of CROP of  $\beta$ -lactones depends much on the catalyst or initiator used, and on the presence or absence of the accompanying alcohols.

In the case of the absence of alcohol, CROP polymerizations proceed via an electrophilic activation of the monomer by the cationic initiator, through a cationic or pseudo-cationic mechanism. Two distinctive sites of monomer activation leading to different pathways were evidenced, depending on the cationic initiator used. Monomer activation can occur through the cationic initiator interacting with the endocyclic oxygen (*O*-CO) to allow an *O*-acyl cleavage and polymers with ether functionality at the  $\alpha$ -chain end; this is the case with Brønsted acids (e.g. triflic acid “TfOH”<sup>[73]</sup>, sulfuric acid<sup>[74]</sup>, or  $[(\text{CH}_3\text{CH}_2)_3\text{O}^+][\text{Cl}^-]$ ,  $[(\text{Et}_3\text{O}^+)[\text{BF}_4]^-]$ <sup>[75]</sup> as initiators (Scheme 1. 4 – a<sub>1</sub>). When Lewis acids are used instead (i.e.  $\text{FeCl}_3$ <sup>[76]</sup>,  $\text{BF}_3$ ,  $\text{TiCl}_4$ <sup>[74]</sup>, an *O*-alkyl cleavage usually takes place by the endocyclic oxygen to produce cyclic PHAs (Scheme 1. 4 – a<sub>2</sub>).<sup>[74]</sup> Otherwise, monomer activation can happen via the interaction between the cationic initiator and exocyclic oxygen (carbonyl activation) followed by *O*-alkyl cleavage leading to esters groups at the  $\alpha$ -chain end; this is the case with alkylation initiators (e.g.,  $[(\text{CH}_3\text{CH}_2)_3\text{O}^+][\text{Cl}^-]$ ,  $[(\text{Et}_3\text{O}^+)[\text{BF}_4]^-]$ <sup>[75]</sup> (Scheme 1. 4 – b).<sup>[77]</sup> Interestingly, when acylating initiators (e.g.,  $[\text{CH}_3\text{CO}^+][\text{SbF}_6]^-$ ,  $[\text{CH}_3\text{CH}_2\text{CO}^+][\text{SbF}_6]^-$ )<sup>[77a, 78]</sup> are employed, two mechanistic pathways can be observed at the same time, with concurrence between the two monomer activation courses (Scheme 1. 4 – a<sub>1</sub> and b).



**Scheme 1. 4** – Effect of the cationic initiator used on the mechanistic pathways and  $\beta$ -lactones monomer activation in CROP in the absence of alcohol; Brønsted acids follow route (a<sub>1</sub>), Lewis acids route (a<sub>2</sub>), alkylating agents route (a<sub>1</sub>) or (b), acylating agents route (a<sub>1</sub>) and (b).

CROP of  $rac$ -BL<sup>Me</sup> using phosphoric acid derivatives (Brønsted acids) such as diphenyl phosphate “DPP”, bis(4-nitrophenyl) phosphate “BNPP”, and trifluoromethanesulfonic acid were recently studied in the presence of a protic initiator (alcohol). PBL<sup>Me</sup> was formed with relatively high molar masses and rather narrow dispersities ( $M_{n,SEC} = 10,000 \text{ g mol}^{-1}$ ;  $D_M = 1.23$ ). The mechanism of initiation is based on the activation of  $rac$ -BL<sup>Me</sup> by protonation of the exocyclic oxygen, followed by nucleophilic attack of the alcohol and scission of the *O*-acyl bond selectively. However, an undesired deactivated pathway was also noticed that can be suppressed according to the phosphoric catalyst used (Scheme 1. 5).<sup>[79]</sup> Noteworthy, the deactivation mechanism of CROP mediated by phosphoric acids derivatives was only observed in case of  $\beta$ -lactones vs. other cyclic esters.



**Scheme 1. 5** – CROP mechanism of *rac*-BL<sup>Me</sup> mediated by phosphoric acid derivatives in the presence of alcohol with the deactivation catalyst mechanism.<sup>[79]</sup>

Eventually, CROP is highly dependent on temperature and solvent because cationic initiators and cationic intermediates are very reactive, thus the polymerization is difficult to control. Customarily, CROP is favoured by increasing carbocation stability, and regarding  $\beta$ -lactones the carbocations intermediates ( $C=O^+$  or  $-O-C^+$ -ring, Scheme 1. 4 & Scheme 1. 5) are considered not stable. The low molar masses and high dispersities of PHAs (PPL or PBL<sup>Me</sup>) obtained from CROP of  $\beta$ -lactones, caused from the presence of several mechanistic pathways and adverse side reactions, have decreased the interest in investigating CROP on other  $\beta$ -lactones functionality.<sup>[60]</sup>

#### 4.2.2.c Anionic ring-opening polymerization (AROP) of $\beta$ -lactones

Anionic ring-opening polymerization (AROP) of  $\beta$ -lactones is definitely not less intricate than CROP, yet it showed more appealing results in terms of controlling the polymerization (molar masses and dispersities) through time which makes it an elected method. AROP can be promoted by organic activators or metal/organometallic catalysts, both classes are discussed generally beneath.

- **Organic activators or metal-free activators**

Metal-free initiating systems have been applied to  $\beta$ -lactones well before the beginning of the current century; they can be initiator or catalyst, nucleophiles or bases (Figure 1. 9). Polymerization based on simple organic molecules to promote AROP has revealed an appealing approach, especially for polyesters designed for electronics and biomedical applications. The topical interest of organic activators is their high chemical stability and long shelf live, low cost,

easy availability, ease of handling and high performances.<sup>[50b, 57, 71, 80]</sup> Moreover, they are well suited to a broad range of reaction conditions, solvents, and monomers. Existing as simple nucleophilic or basic compounds, their removal from the resultant polymers is simplified by washing or trapping into resin beads.<sup>[81]</sup>

## Organic, metal-free activators

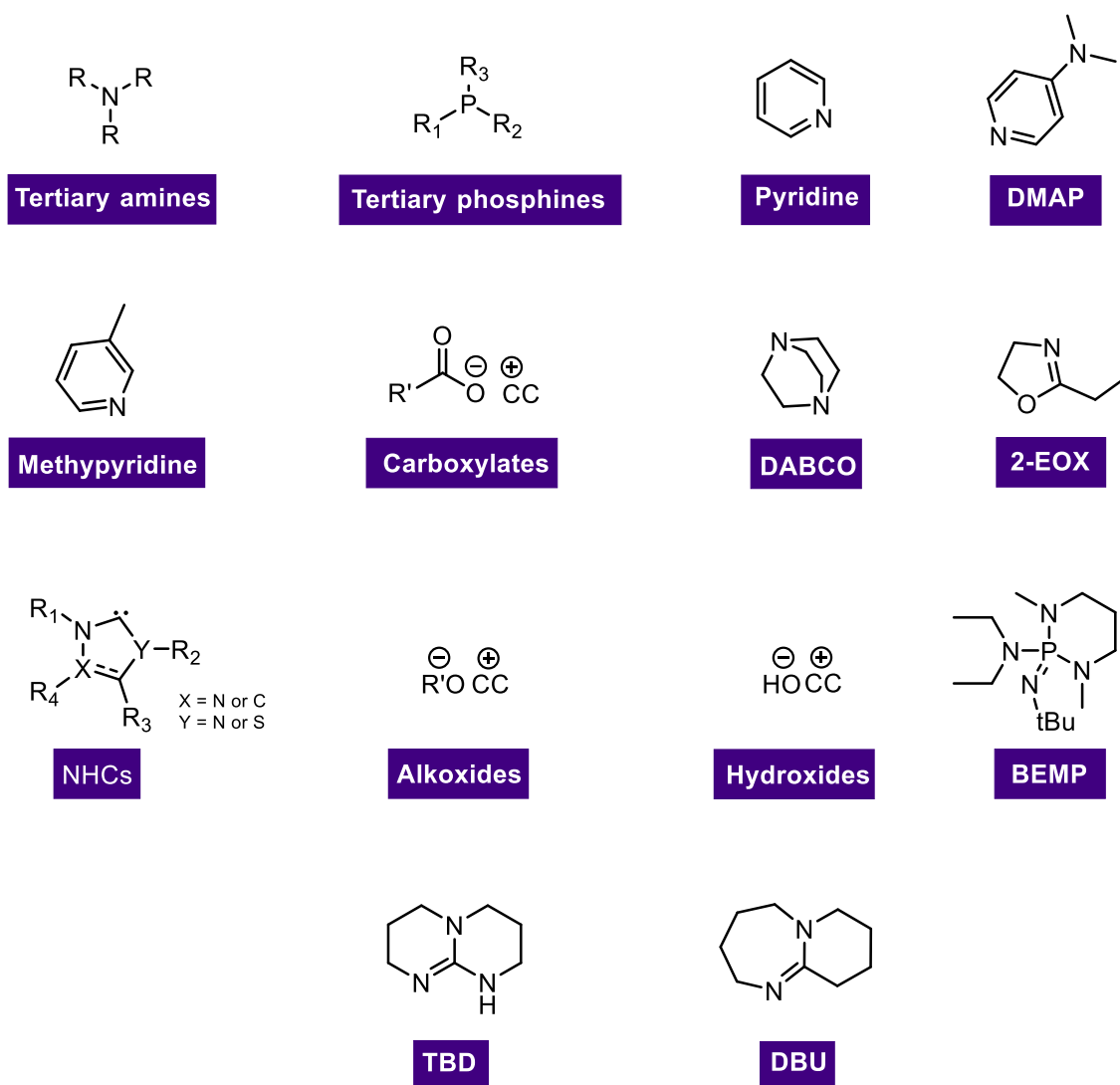
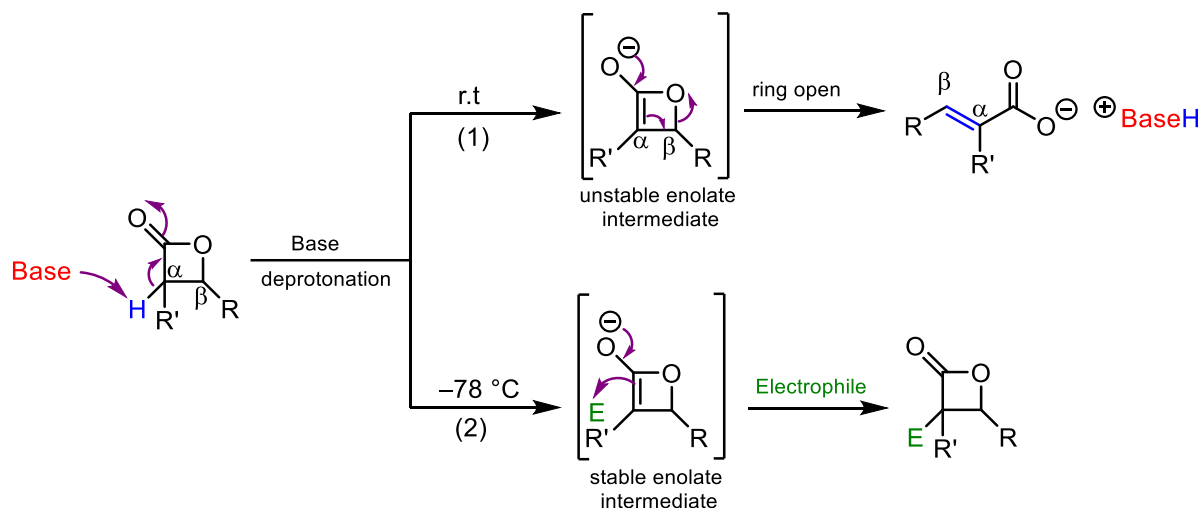


**Figure 1. 9** – Examples of different organic activators (initiator or catalyst, nucleophiles or bases) used for the ROP of  $\beta$ -lactones; with  $CC^+$  is organic counter cation, usually a substituted ammonium or Brønsted phosphazene bases or  $NHCH^+$ .

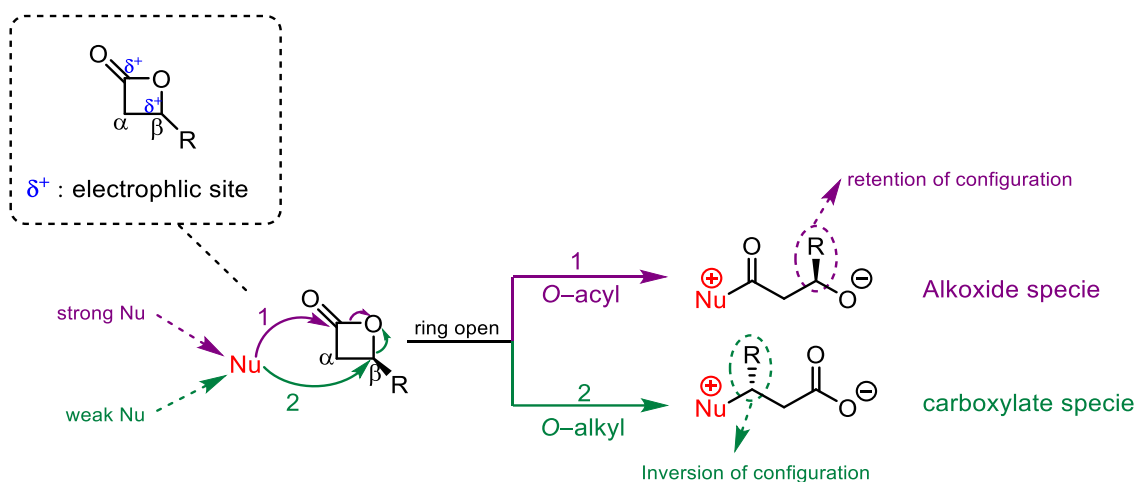
It is important to consider the general reactivity of  $\beta$ -lactones towards organic activators before viewing examples in AROP. To begin with, in the presence of a base,  $\beta$ -lactones act as a good proton donor on the  $\alpha$ -position to form an unstable enolate at room temperature, leading to the opening of the ring through  $\beta$ -elimination (Scheme 1. 6, (1)).<sup>[82]</sup> The stereochemistry of  $\beta$ -elimination has been extensively studied and states that  $\beta$ -elimination, of any type, proceeds

if the electron donating and accepting orbitals adopt a *syn* or *trans* arrangement.<sup>[83]</sup> Paradoxically, this enolate is stable at low temperature ( $-78\text{ }^{\circ}\text{C}$ ) and can be exposed to electrophile afterwards in the case of  $\text{R}' = \text{CH}_3$  (Scheme 1. 6, (2)).<sup>[84]</sup>



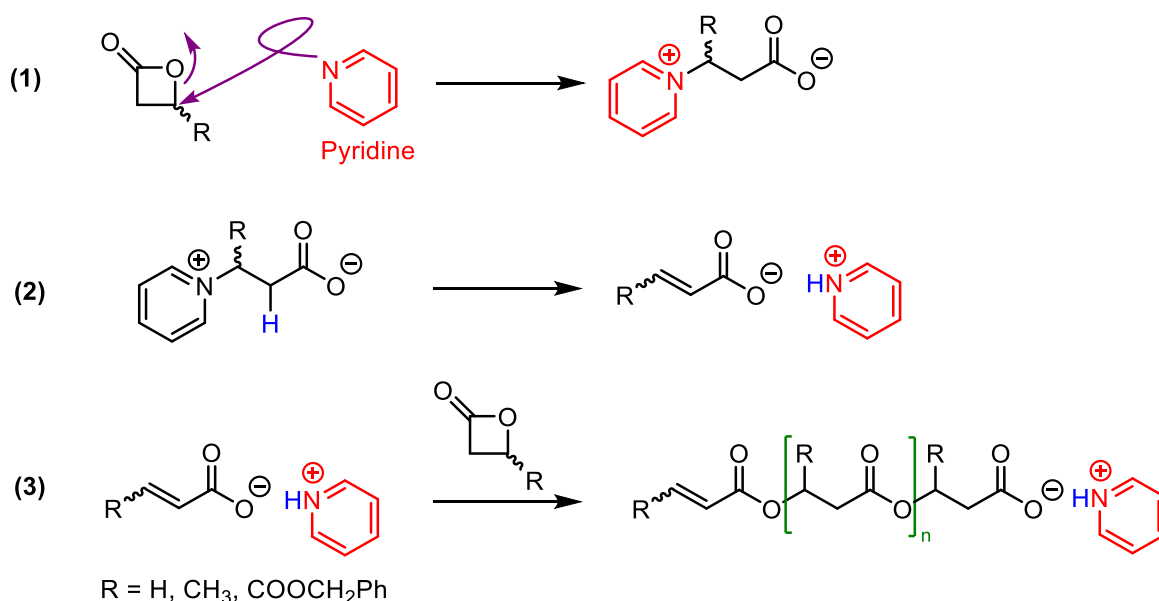
**Scheme 1. 6** –  $\beta$ -lactones, with a good proton donor on the  $\alpha$ -position, in the presence of basic organic activator; (1) at room temperature; (2) at  $-78\text{ }^{\circ}\text{C}$ .

Moreover, in the presence of a nucleophile,  $\beta$ -lactones act as an electrophile where they have two distinct electrophilic sites, the acyl carbonyl and the  $\beta$ -carbon (Scheme 1. 7 – (top-left)). Thus, when it is exposed to a nucleophile, two possible attacks are present depending on the nucleophile (strong vs. weak) leading to two types of bond cleavage. An  $O$ -acyl one followed by the formation of alkoxide-type active species with retention of configuration (Scheme 1. 7 – 1), or an  $O$ -alkyl cleavage leading to carboxylate active species and inversion of configuration (Scheme 1. 7 – 2), respectively.<sup>[85]</sup>



**Scheme 1. 7** –  $\beta$ -Lactones' reactivity in the presence of a nucleophilic organic activator; (top-left) two distinct electrophilic sites (represented as blue  $\delta^+$ ); (1–purple)  $O$ -acyl cleavage by a strong nucleophile, followed by retention of configuration and alkoxide active species; (2–green)  $O$ -alkyl cleavage by weak nucleophile and its relative carboxylate species with inversion of configuration (if  $\text{R} \neq \text{H}$ ).

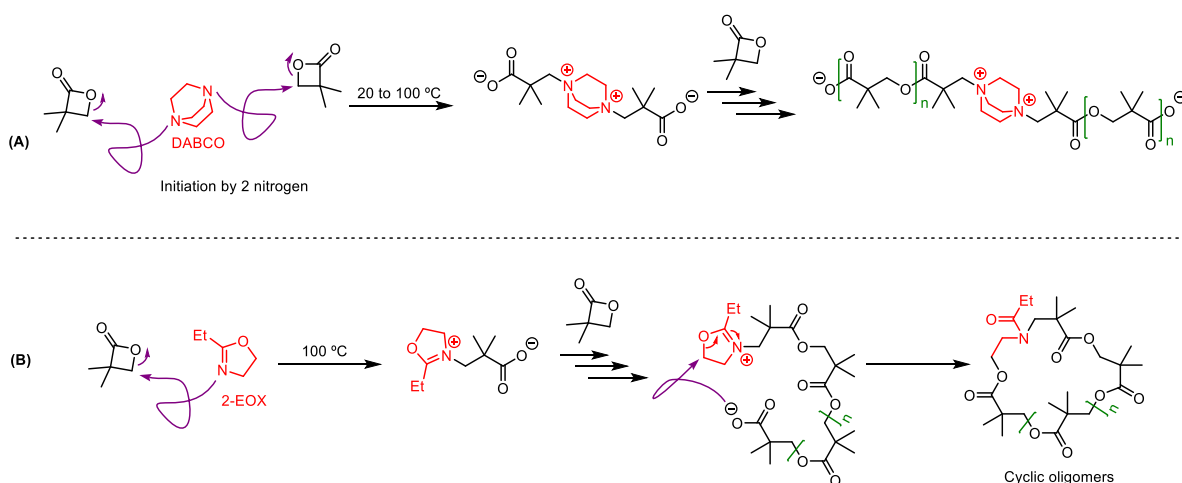
The AROP of  $\beta$ -lactones may advance using weak nucleophiles as organic activators.<sup>[86]</sup> In 1969, tertiary amines ( $R_3N$ ) and pyridines were applied in AROP of PL to produce PPL of low molar masses ( $DP = 6$ ).  $R_3N$  and pyridines appear to initiate the ROP through  $O$ -alkyl cleavage to produce zwitterionic species with ammonium or pyridinium cation and carboxylate anions (Scheme 1. 8 – (1)). Complete elimination reactions then happen and propagation proceeds through the later carboxylate anions to generate linear chains with the total absence of cyclic structures (Scheme 1. 8 – (2)).<sup>[87]</sup> At the same time the AROP of pivolactone<sup>[88]</sup> and *rac*-BL<sup>Me</sup><sup>[89]</sup> (Table 1. 2 – entries 3,4) in the presence of carboxylate salts initiators ( $[RCOO]^- [NR_4]^+$ ) was done and it was suggested that initiation proceeds similarly as with  $R_3N$  and pyridines (Scheme 1. 8 – (3)). In 1981, tertiary phosphines were used as organic activators for AROP of PL, and they also appeared to ring-open PL via  $O$ -alkyl cleavage to propagate as zwitterionic species (Scheme 1. 8 – (1)).<sup>[90]</sup> After that, attempts to mediate AROP of *rac*-MLA<sup>Bn</sup> via triethylamine ( $Et_3N$ ) and tetraethylammonium benzoate ( $[PhCOO]^- [NEt_4]^+$ ) were performed in bulk at 40 and 60 °C, respectively. PMLA<sup>Bn</sup> with molar masses as high as  $M_{n,SEC} = 50,000$  and  $27,000 \text{ g mol}^{-1}$ , respectively, were produced after 30 or 17 days, but with a large gap relative to the expected ones ( $M_{n,theo} = 200,000$  and  $150,000 \text{ g mol}^{-1}$ ;  $D_M = 1.3\text{--}1.4$ ). However, AROP of *rac*-MLA<sup>Bn</sup> under the same conditions ( $[PhCOO]^- [NEt_4]^+$ , bulk, 40 °C) with prior extensive purification of *rac*-MLA<sup>Bn</sup> led to the production of PMLA<sup>Bn</sup> with high molar masses ( $M_{n,SEC} = 174,000 \text{ g mol}^{-1}$  with  $M_{n,theo} = 200,000 \text{ g mol}^{-1}$ ).<sup>[91]</sup> The discrepancies between theoretical and measured molar masses in the former examples was proposed to arise from the presence of transfer reactions as illustrated in Scheme 1. 10 (top), resulting from the  $\alpha$ -hydrogen acidity of the monomer (Scheme 1. 6 – (1)).<sup>[92]</sup>



**Scheme 1. 8** – Proposed mechanism for AROP of  $\beta$ -lactones mediated by tertiary amines and pyridines, showing initiation (1) & (2) and propagation (3) steps; initiation with tertiary phosphines follows path (1) while quaternary ammonium carboxylate salts follow path (3).

Plenty of research confirmed the presence of undesired deprotonation transfer reactions along with the *O*-alkyl propagation route, when weak nucleophiles such as triphenylphosphines, pyridine, 4-methylpyridine, 4-dimethylaminopyridine (DMAP), triethylamine, carboxylate ammonium salts  $[\text{RCOO}]^- [\text{NR}_4]^+$ , 2-ethyloxazoline (2-EOX) and 1,4-diazabicyclo[2.2.2]octane (DABCO) (Figure 1. 9), were used in AROP of PL, pivalactone, *rac*-BL<sup>Me</sup>, and *rac*-MLA<sup>Bn</sup> at temperatures from 20 °C to 100 °C.<sup>[93]</sup> Among them, in 2005, DABCO and 2-EOX showed interesting features that are worth to mention. ROP of pivalactone with DABCO was quantitative whatever the temperature used (20 °C – 100 °C), and the poly(pivalactone) obtained was linear and propagated through both nitrogen atoms of DABCO (propagation in both directions, Scheme 1. 9 – (A)). On the other hand, the propagation via 2-EOX was hampered by the formation of cyclic oligomers resulting from end-to-end reaction between the nucleophilic carboxylate and the electrophilic methylene group of 2-EOX (Scheme 1. 9 – (B)).<sup>[93c]</sup>

Regarding the stereocontrol via organic activation, atactic PBL<sup>Me</sup> and PMLA<sup>FG</sup> (FG = linear or branched alkyl chains) or isotactic (*R*)-PBL<sup>Me</sup> and (*S*)-poly(MLA<sup>FG</sup>) ( $M_{n,\text{SEC}} = 73,000$  g mol<sup>-1</sup>;  $D_M = 2.2$ ), were obtained after 5-7 days from the bulk AROP at 40 °C–60 °C of *rac*-BL<sup>Me</sup> and *rac*-MLA<sup>FG</sup> or (*S*)-BL<sup>Me</sup> and (*R*)-MLA<sup>FG</sup>, respectively, promoted by  $[\text{RCOO}]^- [\text{NR}_4]^+$  (Scheme 1. 7 – 2, where Nu = carboxylate).<sup>[93b, 94]</sup>

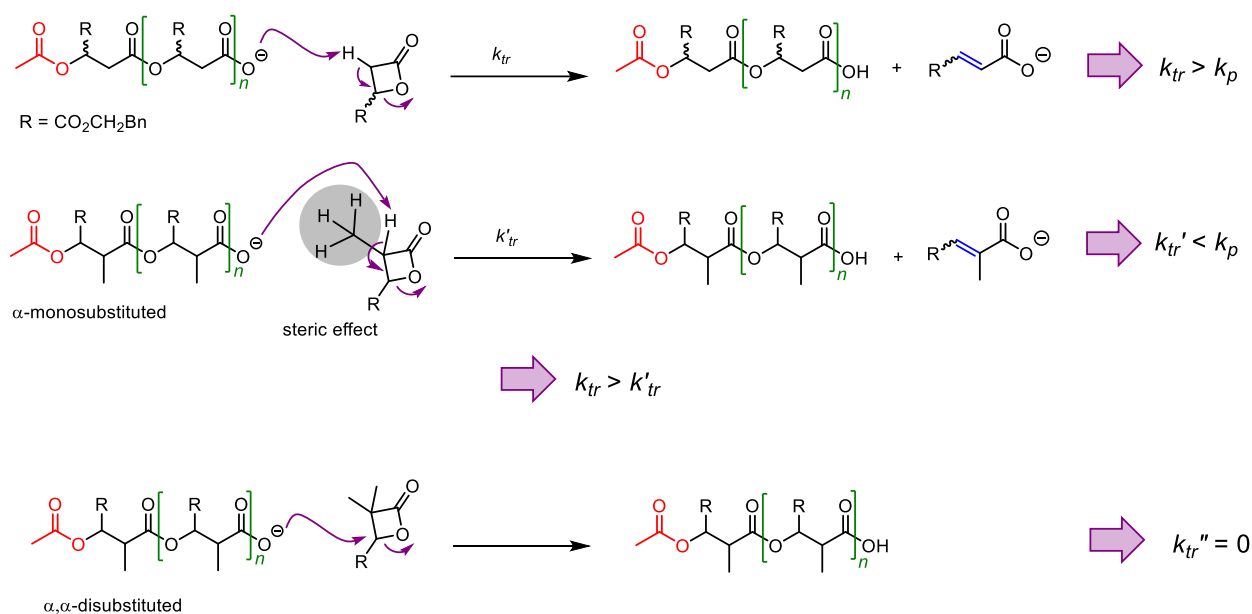


**Scheme 1. 9** – AROP of pivalactone in the presence of (A) DABCO, initiation and propagation occur on both nitrogen atoms; (B) 2-EOX, competitive cyclization reaction.

Noteworthy, in AROP mediated by weak nucleophiles, higher polymerization rate and less transfer reactions (lower dispersities) were observed in bulk conditions than in solution and



at lower temperatures (20 °C–40 °C) than higher ones (> 40 °C).<sup>[87a, 92a]</sup> Also, the rate of transfer reactions was found to be higher than that of propagation ( $k_{tr} > k_p$ , Scheme 1. 10 – top).<sup>[93]</sup> Researchers tend to mask the acidic  $\alpha$ -H by  $\alpha$ -monosubstituted or  $\alpha,\alpha'$ -disubstituted  $\beta$ -lactones known as protected  $\beta$ -lactones (replace  $\alpha$ -H by  $\text{CH}_3$ ), especially in the case of  $\text{MLA}^{\text{FG}}$ s. The first attempt was done on 1994, where  $\alpha$ -monosubstituted (3*S*,4*R*)-(3*R*,4*S*)-3-methyl-4-benzyloxycarbonyl-2-oxetanone (Table 1. 2 – entry 7) was synthesized and polymerized via  $[\text{PhCOO}]^-[\text{NEt}_4]^+$  in bulk at 40 °C to obtain poly((3*S*,4*S*)-(3*R*,4*R*)-3-methyl-4-benzyloxycarbonyl-2-oxetanone) after 3 days; and a decrease in rate constant of transfer reactions ( $k_{tr}$ ;  $k_{tr} < k_p$ ) was successfully managed (Scheme 1. 10 – middle).<sup>[95]</sup> Again in 2003–2012,  $[\text{PhCOO}]^-[\text{NEt}_4]^+$  was used in bulk at 37 °C to polymerize  $\alpha$ -disubstituted  $\alpha,\alpha',\beta$ -trisubstituted  $\beta$ -lactones (Table 1. 2 – entry 6) and produced polymers after 5 days having  $M_{n,\text{SEC}} = 180,000 \text{ g mol}^{-1}$  (vs.  $M_{n,\text{theo}} = 234,000 \text{ g mol}^{-1}$ ), with total absence of crotonate chain-ends ( $D_M = 1.1$ ) (Scheme 1. 10 – bottom).<sup>[96]</sup>

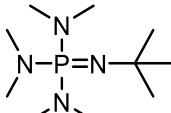
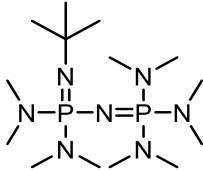
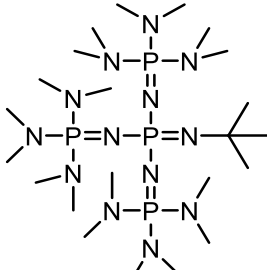


**Scheme 1. 10** – Elimination transfer reaction ( $k_{tr}$ ) in bulk AROP mediated by  $[\text{PhCOO}]^-[\text{NEt}_4]^+$ ; (top)  $\alpha$ ,unsubstituted  $\text{rac-MLA}^{\text{Bn}}$  having  $k_{tr} > k_p$ ; (middle)  $\alpha$ ,monosubstituted  $\text{MLA}^{\text{Bn}}$  having  $k_{tr}' < k_p$  due to steric effect; (bottom)  $\alpha$ ,disubstituted  $\text{MLA}^{\text{Bn}}$  having  $k_{tr}'' = 0$  due to the absence of acidic  $\alpha$ -H.

Other than ammonium-based carboxylate salts, Brønsted phosphazene bases, specifically *tert*-butylimino-tris(dimethylamino)phosphorane ( $\text{P}_1$ -*t*-Bu), 1-*tert*-butyl-2,2,4,4,4-pentakis(dimethylamino)-2 $\Lambda$ 5,4 $\Lambda$ 5-catenadi(phosphazene) ( $\text{P}_2$ -*t*-Bu) 1-*tert*-butyl-4,4,4-tris(dimethylamino)-2,2-bis[tris(dimethylamino)phosphoranyl-idenamino]-2 $\Lambda$ 5,4 $\Lambda$ 5-catenadi(phosphazene) ( $\text{P}_4$ -*t*-Bu), have been investigated in combination with 1-pyrene acetic acid as well (Table 1. 3).  $\text{P}_1$ -*t*-Bu,  $\text{P}_2$ -*t*-Bu, and  $\text{P}_4$ -*t*-Bu were first mixed with 1-pyrene acetic acid to

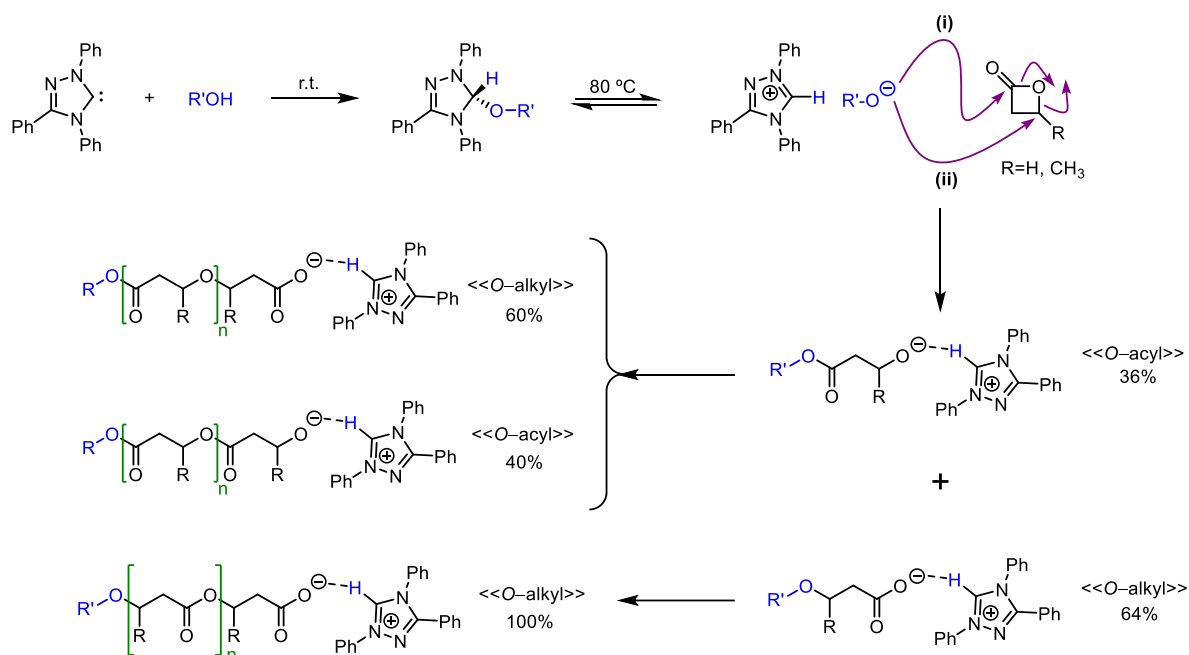
form the corresponding 1-pyrene carboxylate phosphazene salts ( $[P_1-t-BuH]^+[RCOO]^-$ ,  $[P_2-t-BuH]^+[RCOO]^-$ ,  $[P_4-t-BuH]^+[RCOO]^-$ ), and then the latter salts were investigated in AROP of *rac*-BL<sup>Me</sup> and *rac*- $\alpha,\alpha'$ -4-benzylcarbonyl-3,3-dimethyl-2-oxetanone (*rac*-dMMLA<sup>Bn</sup>) (Table 1. 2 – entries 4,6). In both cases, the polymerization proceeded via *O*-alkyl cleavage, and the  $[P_4-t-BuH]^+[RCOO]^-$  salt revealed to have the uppermost activity, likely due to the higher basicity of  $P_4-t-Bu$  relative to  $P_1-t-Bu$  and  $P_2-t-Bu$  (by more than 10 p*Ka* units, Table 1. 3) that loosens the ionic pair.<sup>[97]</sup> Anyhow, applying  $[P_4-t-BuH]^+[RCOO]^-$  in the AROP of *rac*-BL<sup>Me</sup> in bulk at room temperature, produced PBL<sup>Me</sup> (87% monomer conversion after 1 h) with molar mass  $M_{n,SEC} = 14,500 \text{ g mol}^{-1}$  and fair dispersity ( $\mathcal{D}_M = 1.16$ ). However, attempting to further increase the conversion (99%) led to a decrease in the molar mass and increase of the dispersity ( $M_{n,SEC} = 12,600 \text{ g mol}^{-1}$ ;  $\mathcal{D}_M = 1.31$ ), reasoning that the transfer reactions are the same as those with ammonium-based carboxylate salts (Scheme 1. 10).<sup>[97a]</sup> Moreover, when  $[P_4-t-BuH]^+[RCOO]^-$  was used to promote the AROP of *rac*-dMMLA<sup>Bn</sup> in THF at 21 °C, it gave PdMMLA<sup>Bn</sup> after 3 days with the highest molar mass ever obtained from a  $\beta$ -lactone with organic activators ( $M_{n,SEC} = 1,650,000 \text{ g mol}^{-1}$  vs.  $M_{n,theo} = 2,100,000 \text{ g mol}^{-1}$ ). The gap between the molar masses and the dispersities higher than 1.55 were ascribed to the observed high viscosity of the medium in the onset of the polymerization and that may prevent reaching complete conversions.<sup>[97b]</sup>

**Table 1. 3** – Acetonitrile (MeCN) basicity data of phosphazene bases applied in ROP of  $\beta$ -lactones with carboxylic acids.<sup>[98]</sup>

Phosphazene base	p <i>Ka</i> in MeCN
 <p>P<sub>1</sub>-<i>t</i>-Bu</p>	27
 <p>P<sub>2</sub>-<i>t</i>-Bu</p>	33.5
 <p>P<sub>4</sub>-<i>t</i>-Bu</p>	43

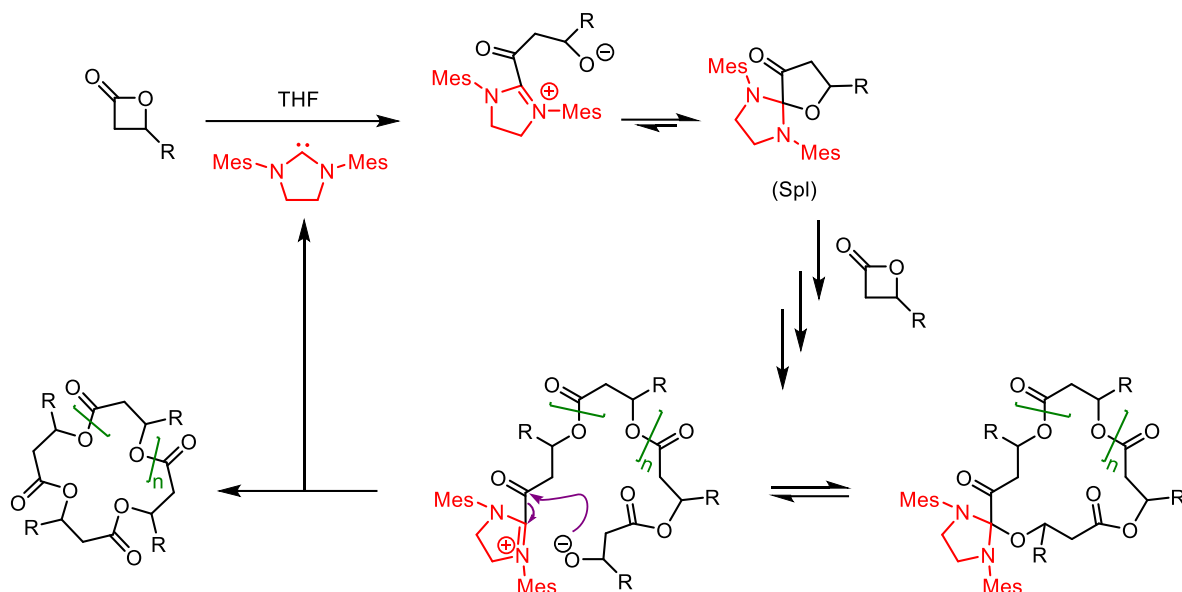


On the other hand, strong nucleophiles were also used as organic activators in the ROP of  $\beta$ -lactones. Starting with *N*-heterocyclic carbenes (NHCs),<sup>[99]</sup> 1,3-bis-(2,4,6-trimethylphenyl)imidazole-2-ylidene (IMes) was applied for the first time in 2002 by James Hedrick *et. al.* to catalyse the ROP of *rac*-BL<sup>Me</sup> in the presence of pyrene butanol in THF at 25 °C.<sup>[100]</sup> For a [IMes]<sub>0</sub>/[ROH]<sub>0</sub> = 1.5, the obtained PBL<sup>Me</sup> molar mass closely matched the monomer-to-initiator ratio, with  $\bar{D}_M = 1.15$ . The authors proposed two possible mechanisms based either on an anionic/basic “chain-end” mechanism, where the carbene activates the initiating/propagating alcohol by H-bonding, or on a monomer activated “encompassing nucleophilic” mechanism, involving a zwitterionic intermediate through *O*-acyl cleavage (Scheme 1. 7 – 2). It was presumed that the nucleophilic pathway overcomes the basic pathway due to the fact the IMes has a lower pK<sub>a</sub> than that of pyrene butanol (<sup>DMSO</sup>pK<sub>a</sub>, 24 < 29). In 2006-2007, another type of NHC, namely 1,3,4-triphenyl-4,5-dihydro-1H-1,2,4-triazol-5-ylidene carbene, referred to as triazole, was investigated in the ROP of *rac*-BL<sup>Me</sup> in the presence of protic agent (methanol) in toluene at 80 °C (this temperature was needed to activate this triazole NHC (Scheme 1. 11)).<sup>[101]</sup> <sup>1</sup>H NMR analyses revealed an uncontrolled process in which PBL<sup>Me</sup> chains are end-capped by either an  $\alpha$ -methoxy group or a crotonate moiety; the basicity of the triazole carbene might lead to undesired elimination reactions, generating crotonate initiators (Scheme 1. 6 – 1). *Tert*-butyl alcohol was used as a co-solvent to enhance propagation over detrimental deprotonation side reactions by minimizing the concentration of free triazole, leading to decrease in crotonate formation to produce PBL<sup>Me</sup> oligomers ( $M_{n,SEC} < 200 \text{ g mol}^{-1}$ ). Both “*O*-acyl” and “*O*-alkyl” pathways were observed and the corresponding alkoxide and carboxylate groups were found at the early stages of the reaction, whereas the relative number of carboxylate end-groups increased during polymerization to finally represent the only propagating center (Scheme 1. 11).<sup>[101b]</sup>



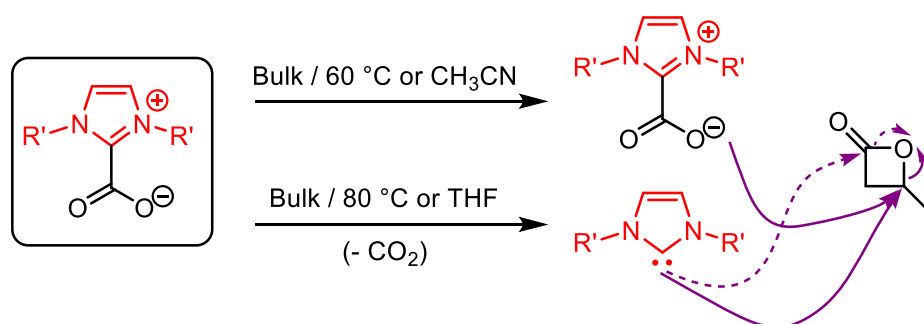
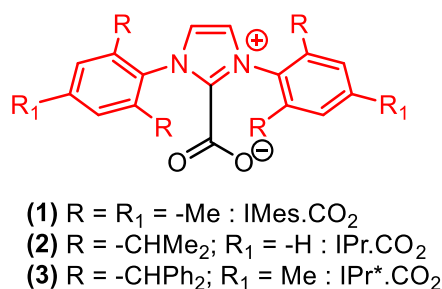
**Scheme 1.11** – ROP of PL or  $rac$ -BL<sup>Me</sup> at 80 °C in *t*BuOH revealing an “O-alkyl” (ii) and “O-acyl” (i) cleavage contest.

On the other hand, the ROP of  $\beta$ -lactones, such as PL,  $rac$ -BL<sup>Me</sup> and  $rac$ -dMMLA<sup>Bn</sup>, was investigated in the absence of a protic initiator (alcohol), with saturated IMes (SIMes) carbene or IMes, eventually affording cyclic polymers.<sup>[102]</sup> Once using the NHC alone in THF at 21 °C, the authors proposed a mechanism of ring-expansion reaction involving a reversible collapse of the zwitterionic species to macrocyclic spirocycles (SpI) all along the propagation (Scheme 1.12). The mechanism was supported by DFT calculations and by performing the ROP of enantiopure (*R*)-BL<sup>Me</sup> to produce (*R*)-PBL<sup>Me</sup> (retention of the configuration), thus confirming the O-acyl cleavage (Scheme 1.7 – route 1).<sup>[102a]</sup> A remarkable degree of control of the polymerization, presumably due to the generation of a small amount of reactive zwitterionic intermediates by the reversible formation of SpI, was reported. The low concentration of reactive alkoxides during polymerization suppresses side reactions such as termination and elimination reactions analogous to modern controlled polymerization. In case of  $rac$ -dMMLA<sup>Bn</sup>, a degree of polymerization (DP = 116) was targeted to reach 60 % conversion after 28 min ( $M_{n,SEC} = 13,800 \text{ g mol}^{-1}$  vs.  $M_{n,theo} = 16,200 \text{ g mol}^{-1}$ ) with a rather narrow dispersity ( $D_M = 1.34$ ). The structure of the cyclic polymer was evidenced by Matrix Assisted Laser Desorption ionization - Time of Flight mass spectrometry (MALDI-ToF MS).<sup>[102b]</sup>



**Scheme 1.12** – ROP of a  $\beta$ -lactone promoted by SIMes (in the absence of an alcohol) giving a cyclic polymer.<sup>[102a]</sup>

Inspired by the above considerations represented in Scheme 1.11, Thomas *et al.* reported in 2013 the use of various  $\text{NHC} \cdot \text{CO}_2$  as potent initiating systems for the ROP of  $\text{rac-BL}^{\text{Me}}$  (Scheme 1.13 – top).<sup>[103]</sup> Polymerizations were carried out in bulk or in solution (MeCN, THF) at 60 or 80 °C. At 60 °C, in the case of bulk ROP ( $\text{DP}_{(\text{rac-BPL}(\text{Me}))} = 100$ ),  $\text{PBL}^{\text{Me}}$  was produced in 10 min (80% conversion;  $\bar{D}_M = 1.41$ ) upon using the less hindered catalyst (Scheme 1.13 – top (1), (2)). In solution, the polymerization appeared faster in the more polar solvent (MeCN) than in the less polar one (THF). An increase of macromolecular parameters was observed in a control manner ( $\bar{D}_M = 1.22\text{--}1.28$ ) for the bulk polymerization at 60 °C, with the increase in the monomer loadings from 100 to 2000, yet without reaching complete or high conversions (e.g., for  $\text{DP} = 1000$  and 2000, ROP was stopped at 47% and 28% monomer consumption, respectively). Moreover, this control was hampered upon increasing the temperature to 80 °C ( $\bar{D}_M > 1.4$ ). Mechanistic studies, mainly based on MALDI-Tof MS analyses and DFT calculations, suggested that the ROP of  $\text{rac-BL}^{\text{Me}}$  from  $\text{NHCs} \cdot \text{CO}_2$  adducts at 60 °C is initiated and propagated by an “O–alkyl” bond cleavage. In contrast, a higher temperature (80 °C) leads to decarboxylation of the  $\text{NHCs} \cdot \text{CO}_2$  adducts to produce the reactive NHC. The latter will act as an initiator to proceed the polymerization through “O–alkyl” (major route) and “O–acyl” (minor route) cleavages (Scheme 1.13 – bottom).<sup>[103]</sup>



**Scheme 1. 13** – (top) Different NHC.CO<sub>2</sub> catalysts; (bottom) NHC.CO<sub>2</sub> initiated ROP of *rac*-BL<sup>Me</sup> under various conditions; the dashed arrow represents a minor pathway.<sup>[103]</sup>

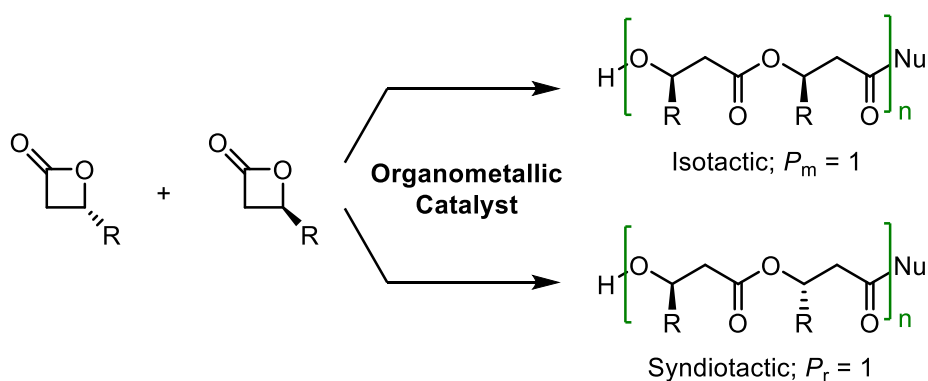
Despite that most phosphazene bases (Table 1. 3) and NHCs have been explored in the AROP of  $\beta$ -lactones and their mechanistic pathways were revealed, other types of phosphazene bases and heterocyclic organic activators were also probed in ROP of *rac*-BL<sup>Me</sup> and *rac*-MLA<sup>Bn</sup>.<sup>[102b, 104]</sup> Those are 2-*tert*-butylimino-2-diethylamino-1,3-dimethylperhydro-1,3,2-diazaphosphorine (BEMP), 1,5,7-triazabicyclo[4.4.0]dec-5-ene (TBD), and 1,8-diazabicyclo[5.4.0]-undec-7-ene (DBU) (Figure 1. 9), which proved to be effective. Yet, their mechanistic pathways are controversial and still under investigation, leaving the door open for further examinations to possibly unveil unprecedented performances. Resumption of bibliography on the mode of action of BEMP, TBD and DBU is done in Chapter 3, with investigations on their activity towards specific  $\beta$ -lactones that have not yet been examined with any organic activators.

#### • Metal-based activators and organometallic catalysts

Herein, we briefly describe metal activators that have been quite exhaustively detailed within recent publications and reviews.<sup>[58a, 59a, 86, 93a, 94c, 105]</sup> Metal-based activators are like organic activators but with a metallic cation ( $\text{CC} = \text{K}^+, \text{Mg}^{2+}, \text{Na}^+$ ) (Figure 1. 9). They can be weak nucleophiles such as carboxylates or strong nucleophiles such as alkoxides and hydroxides. Their mode of action depends on the nucleophilicity and the basicity of each; for example, carboxylates promote *O*-alkyl cleavage, while nucleophilic non-bulky alkoxides

(methoxide, ethoxide) and hydroxides favour *O*-acyl cleavage (Scheme 1. 7), while basic bulky alkoxides (*tert*-butoxide) or basic compounds (naphthalenide)<sup>[106]</sup> abstract the acidic  $\alpha$ -H of the  $\beta$ -lactone to produce carboxylate initiators *in situ* (Scheme 1. 8).<sup>[85]</sup> The difference between organic and inorganic CCs was examined to reveal that the rate of polymerization is proportional to the size of the CC. Hence, bigger size CCs such as phosphazene bases and ammonium CC showed higher reactivity than metal-based activators.<sup>[89, 92a, 105a, 107]</sup>

On the other hand, organometallic catalytic systems are types of specific metal-alkoxide species supported by ancillary ligands. They are arguably among the most efficient systems to tackle the *O*-acyl vs. *O*-alkyl bond cleavage chemo-regioselectivity issues, (*vide supra*). More interestingly, ROP promoted by organometallic catalyst systems are the only ones to date to effect significant stereocontrol in ROP starting from chiral racemic  $\beta$ -lactones, besides their good-to-high activity (Scheme 1. 14).<sup>[108]</sup>



**Scheme 1. 14** – Stereoselective and regioselective ROP of racemic  $\beta$ -lactone to isotactic or syndiotactic PHAs;  $P_m$  and  $P_r$  are the probability of isotactic and syndiotactic enrichment, respectively.

In this Chapter, some recent examples on efficient and/or stereoselective ROP of  $\text{BL}^{\text{Me}}$  to afford  $\text{PBL}^{\text{Me}}$  are addressed. Starting from Rieger *et al.* in 2008, achiral chromium(III) salophenes complexes ( $R = \text{H, F, Cl, Br}$ ; Figure 1. 10 – **1a-d**,) were used in ROP experiments of *rac*- $\text{BL}^{\text{Me}}$ , in bulk at 100 °C. These catalysts provide  $\text{PBL}^{\text{Me}}$  slightly enriched in isotactic sequences ( $P_m = 0.63\text{--}0.66$ ) resulting from the creation of chromium carboxylate initiator species. The polymerizations show modest activity (turnover frequency (TOF)  $< 162 \text{ h}^{-1}$ ) with high yet uncontrolled molar masses and extremely broad dispersities ( $190,000 \text{ g mol}^{-1} < M_{n,\text{SEC}} < 780,000 \text{ g mol}^{-1}$ ;  $5.2 < D_M < 8.5$ ).<sup>[109]</sup> In 2011, Jones and Davidson designated the ROP of *rac*- $\text{BL}^{\text{Me}}$ , in solution in toluene ( $[\text{BL}^{\text{Me}}]_0 = 10 \text{ M}$ ) at 80°C, initiated by complexes of group 4 metals (Figure 1. 10 – **2a-d, 3a-d, 4a-d**). Subsequently, titanium alcoholates have been shown to be non-stereoselective (atactic  $\text{PBL}^{\text{Me}}$  were obtained;  $P_r = 0.50$ ), zirconium and hafnium



alcoholates offer syndiotactic enriched PBL<sup>Me</sup> ( $P_r = 0.58$ – $0.76$ ). The better enrichments were observed with hafnium-based complexes. In all the experiments reported, the catalysts show modest activities ( $\text{TOF} = 2$ – $50 \text{ h}^{-1}$ ), but a good molar mass control during the polymerization, leading to PBL<sup>Me</sup> of predictable molar masses and narrow dispersities ( $\mathcal{D}_M < 1.29$ ).<sup>[110]</sup> After that, Shaver's group has attempted to synthesize PBL<sup>Me</sup> by ROP of *rac*-BL<sup>Me</sup> catalyzed by achiral aluminum complexes bridged bisphenoxiimines, salen and salophen (Figure 1. 10 – **5**, **6**, **7a-c**), in the presence of 1 to 5 eq. of BnOH, dissolved in toluene ( $[\text{BL}^{\text{Me}}]_0 = 1.5 \text{ M}$ ) at  $100^\circ\text{C}$ . However, these catalysts exhibit poor isotactic enrichments of **5**, **6** (almost atactic;  $P_m = 0.54$ – $0.55$ ) and poor syndio-enrichment of **7a-c** ( $P_r = 0.53$ – $0.55$ ) with modest activities ( $\text{TOF} = 2$ – $33 \text{ h}^{-1}$ ).<sup>[111]</sup>

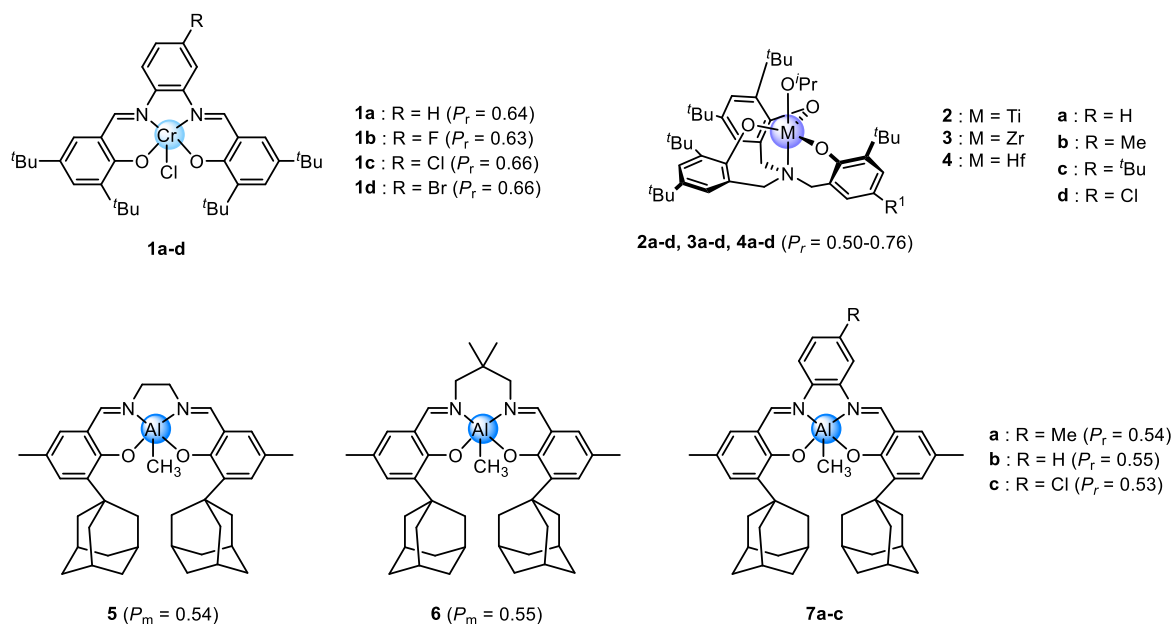


**Figure 1. 10** – Chromium Salophen complexes described by Rieger *et al.*;<sup>[109]</sup> Group 4 metal complexes studied by Jones and Davidson;<sup>[110]</sup> Salophen and aluminum salen complexes described by Shaver *et al.*; in stereoselective ROP of *rac*-BL<sup>Me</sup>.<sup>[111]</sup>

Furthermore, rare earth-based complexes were mostly studied by our group, such as 2,6-bis(naphtholate)yttrium/scandium/lanthanum amido catalytic systems that produce syndio-enriched PBL<sup>Me</sup> ( $P_r$  up to 0.87) from ROP of *rac*-BL<sup>Me</sup> in toluene at  $20$ – $50^\circ\text{C}$  (Figure 1. 11 – **8** to **13**) with molar masses ranging from  $2,600$  to  $40,700 \text{ g mol}^{-1}$ , narrow dispersities ( $1.12 < \mathcal{D}_M < 1.69$ ) and TOF up to  $720 \text{ h}^{-1}$ .<sup>[112]</sup> Other series of complexes based on bis(guanidinate) yttrium and lutetium isopropoxide (Figure 1. 11 – **14,15**) proved able to control the ROP of *rac*-BL<sup>Me</sup>, giving syndio-enriched PBL<sup>Me</sup> ( $P_r = 0.80$ – $0.84$ ), with molar masses ranging from  $2000$  to  $28,200 \text{ g mol}^{-1}$ , narrow dispersities ( $1.09 < \mathcal{D}_M < 1.69$ ) and TOF up to  $50 \text{ h}^{-1}$ .<sup>[113]</sup> Otherwise, more active and highly stereospecific controlled ROP was achieved through achiral yttrium

complexes having tetradentate ( $\{ONXO^{R^1R^2}\}$ ; X = OMe or NMe<sub>2</sub>) ligands (Figure 1. 11 – **16a-f**). Initially, ROP experiments of *rac*-BL<sup>Me</sup>, in solution in toluene ( $[BL^{Me}]_0 = 1.0$  M) at 20°C, were carried out with the different substituted (R<sup>1</sup> & R<sup>2</sup>) ligand complexes **16a-f**, leading to PBL<sup>Me</sup> with predictable molar masses, and dispersities range  $1.03 < \bar{D}_M < 1.80$  with high activity (TOF = 12–24,000 h<sup>-1</sup>). Analysis of the produced PBL<sup>Me</sup> microstructure shows that the R<sup>1</sup> substituents of the ligands have a strong impact on the syndioselectivity of the polymerization reaction. The bulkier and the less electronic substituent affords the highest selectivity with the trend, R<sup>1</sup> = Cl (**16c**) ( $P_r = 0.42\text{--}0.45$ )  $\ll$  CMe<sub>2</sub>*t*Bu (**16a**) ( $P_r = 0.62\text{--}0.70$ ) < CMe<sub>3</sub> (**16fc**) ( $P_r = 0.80$ ) < CMe<sub>2</sub> (4-CF<sub>3</sub>-Ph) (**16e**) ( $P_r = 0.82\text{--}0.84$ ) < CMe<sub>2</sub>Ph (**16d**) ( $P_r = 0.94\text{--}0.95$ ) < CPh<sub>3</sub> (**16b**) ( $P_r = 0.94$ ).<sup>[114]</sup> Details on the effect of the interactions between the ligand substituents and the β-lactones on the polymerization mechanism are discussed in Chapter 4. Noteworthy, none of the scandium analogous complexes of **16** proved active for the ROP of *rac*-BL<sup>Me</sup> under the conditions investigated (toluene, 60 °C, 24 h;  $[BL^{Me}]_0:[Sc]:[iPrOH]_0 = 100:1:0$  or 100:1:1).<sup>[114d]</sup> Meanwhile, under the same conditions as with catalysts **16** (in toluene at 20 °C), but with a higher catalyst loading of bridged bisphenoxyamine yttrium complexes of salan or salen types, Pappalardo and Pellecchia reported the ROP of *rac*-BL<sup>Me</sup> ( $[BL^{Me}]_0 = 5.8\text{--}11.5$  M) (Figure 1. 11 – **17a-b**, **18a-b**). Nonetheless, the syndioselectivity, the activity, and molar mass control of these catalysts remain inferior to those reported by Carpentier *et al.* (**16**), and allow the production of PBL<sup>Me</sup> with  $P_r$  varying from 0.68 to 0.81, TOF = 30–70 h<sup>-1</sup>, and fairly wide dispersities ( $1.35 < \bar{D}_M < 1.84$ ).<sup>[115]</sup> Thomas and Maron *et al.* also studied the use of yttrium complexes coordinated by salan-like ligands with a mixture of bimetallic alcoholate complexes (Figure 1. 11 – **19a-b**). These complexes revealed active towards the ROP of *rac*-BL<sup>Me</sup> in a solution of C<sub>6</sub>D<sub>6</sub> or THF ( $[BL^{Me}]_0 = 2.4\text{--}3.4$  M; *i*PrOH 1–5 eq) at 20°C. They lead to the formation of highly enriched PBL<sup>Me</sup> with syndiotactic sequences ( $P_r = 0.90$ ), exhibiting molar masses close to those expected ones with relatively narrow dispersities ( $1.06 < \bar{D}_M < 1.37$ ). These catalysts also exhibit good ROP activities of *rac*-BL<sup>Me</sup> (TOF = 30–400 h<sup>-1</sup>).<sup>[116]</sup> Finally, the rare earth (Y, La) amido-pyridyl-phenolate complexes (Figure 1. 11 – **20,21**) developed by Carpentier *et al.* allow the synthesis of only very slightly iso-enriched PBL<sup>Me</sup> ( $P_m = 0.58$ ) in the case of yttrium, and moderately syndio-enriched ( $P_r = 0.66$ ) in the case of lanthanum, from *rac*-BL<sup>Me</sup>.<sup>[117]</sup>

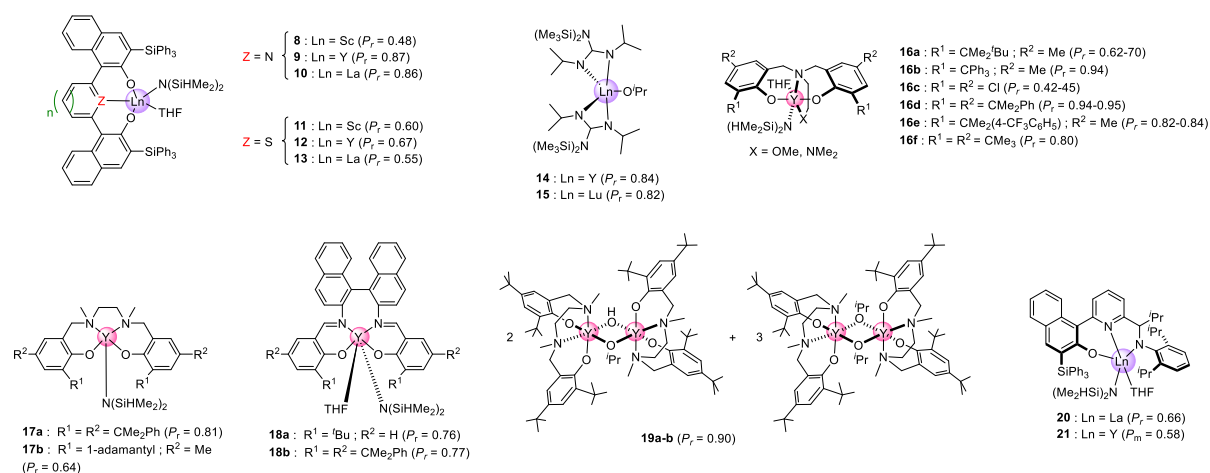


**Figure 1. 11** – Rare earth metals-based complexes used to promote stereoselective ROP of *rac*-BL<sup>Me</sup>, described by Carpentier *et al.* or Pappalardo *et al.* or Thomas *et al.* [112-117]

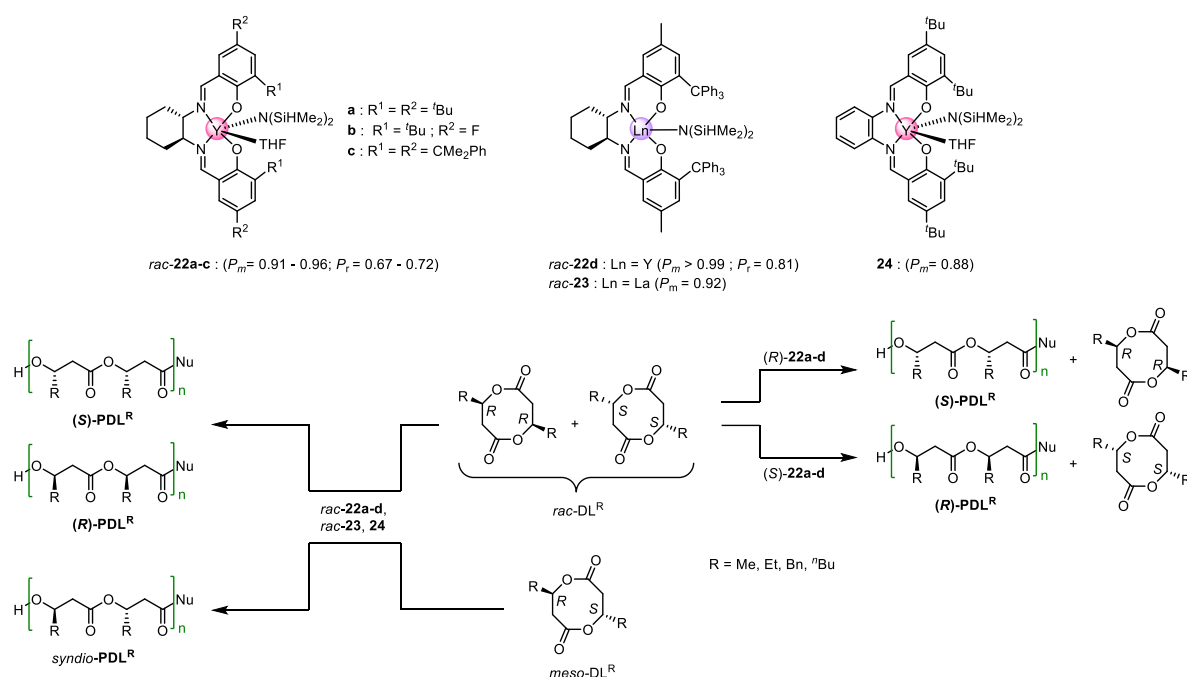
From all the above-mentioned catalysts, complex series **16** (Figure 1. 11) afforded the most active ROP catalysts and the highest syndioenriched PBL<sup>Me</sup>. Correspondingly, Rieger *et al.* rationalized the stereoselectivity of this complex (having R<sup>1</sup> = R<sup>2</sup> = <sup>t</sup>Bu) with yttrium and other rare earths such as samarium (Sm), terbium (Tb), lutetium (Lu), in the ROP of *rac*-BL<sup>Me</sup> by theoretical modeling DFT. This study confirms the influence of the ionic radius of the metal center on the activity and selectivity of the catalytic system. The smaller the metal, the better the activity and syndioselectivity of the complex. Thus, the best performance is observed in ROP of *rac*-BL<sup>Me</sup> with the yttrium and lutetium-based complexes (Table 1. 4). [118]

**Table 1. 4** – Influence of the rare earth metal-based tetradentate ligand complexes (Figure 1. 11 – **16**, R<sup>1</sup> = R<sup>2</sup> = <sup>t</sup>Bu) on the activity and syndioselectivity of the produced PBL<sup>Me</sup>.

Entry	Metal	Ionic radius (Å)	T (min)	Conv.(%)	TOF (h <sup>-1</sup> )	P <sub>r</sub>
1	Sm	1,219	165	50	1 800	0.56
2	Tb	1,180	20	40	2 200	0.77
3	Y	1,159	60	89	4 900	0.82
4	Lu	1,117	20	73	6 900	0.88

A very significant breakthrough was recently brought by Chen's group. They have presented the ROP of an eight membered ring diester, namely *rac*-diolide (*rac*-DL<sup>R</sup>; R : Me = CH<sub>3</sub>, Et = CH<sub>2</sub>CH<sub>3</sub>, Bn = CH<sub>2</sub>Ph, <sup>n</sup>Bu = CH<sub>2</sub>CH<sub>2</sub>CH<sub>2</sub>CH<sub>3</sub>), a cyclic dimer of substituted 3-hydroxybutyric acid (3-HB<sup>R</sup>) as an alternative to the ROP of racemic β-lactones to generate highly stereoregular PHAs (PDL<sup>R</sup>, e.g. R = Me afford mimic of bacterial PHB; Figure 1. 3). [119] Starting from *rac*-DL<sup>Me</sup> (*R,R* and *S,S*) accompanied with achiral yttrium silylamido complexes supported by *N,N*-bis(salicylidene) cyclohexanediimine (salcy) ligands (R<sup>1</sup> = R<sup>2</sup> = <sup>t</sup>Bu; Scheme 1. 15 – **24**), highly isotactic (*R*)-PDL<sup>Me</sup> and (*S*)-PDL<sup>Me</sup> of  $P_m = 0.88$  were obtained; noteworthy when catalyst **16d** (Figure 1. 11) was applied,  $P_m$  was 0.76. When the *rac*-analogues of the

achiral catalyst **24** were used instead of **22a-d** ( $R^1 = R^2 = t\text{Bu}$  or  $\text{CMe}_2\text{Ph}$ ;  $R^1 = t\text{Bu}$  and  $R^2 = \text{F}$ ;  $R^1 = \text{Me}$  and  $R^2 = \text{CPh}_3$ ; Scheme 1. 15), highly-to-perfectly isotactic (*R*)-PDL<sup>Me</sup> and (*S*)-PDL<sup>Me</sup> were produced ( $P_m = 0.91\text{--}0.99$ ). When enantiopure catalysts analogues ((*R*)-**22a-d** or (*S*)-**22a-d**) were used, they lead to the production of (*S*)-PDL<sup>Me</sup> and (*R*)-PDL<sup>Me</sup>, respectively, with a high kinetic resolution (with enantiomeric excess,  $ee > 99\%$ ). The ROP *rac*-DL<sup>Me</sup> was done under mild conditions (DCM at room temperature) and the produced isotactic PDL<sup>Me</sup> have high molar masses and narrow dispersities ( $4770 \text{ g mol}^{-1} < M_{n,\text{SEC}} < 154,000 \text{ g mol}^{-1}$ ;  $1.01 < \bar{D}_M < 1.24$ ), and thermal properties similar to natural iso-PHB ( $T_m = 170^\circ\text{C}$ ).<sup>[119a]</sup> On the other hand, starting from *meso*-DL<sup>Me</sup> (*R,S*) (or *meso*-DL<sup>Et/Bn/*n*Bu</sup>) with the racemic catalysts **22a-d** and **23** ( $M = \text{Y}$  or  $\text{La}$ ; Scheme 1. 15), moderate to high syndiotactic PDL<sup>R</sup> were obtained ( $P_r = 0.67\text{--}0.92$ ).<sup>[119b, 119d]</sup> This study opens a new path for the synthesis of PHAs, especially PHB and its derivatives, besides, it promotes the examination of other efficient catalytic systems in stereoselective ROP.



**Scheme 1. 15** – ROP of *rac*-DL<sup>R</sup> and *meso*-DL<sup>R</sup> ( $R = \text{Me, Et, Bn, }^n\text{Bu}$ ) reported by Chen *et al.* using rare-earth metal-based catalysts **22a-d**, **23**, and **24** to afford highly isotactic and syndiotactic PDL<sup>R</sup>, respectively.

The intriguing results of the stereospecific ROP promoted by the catalysts series **16** (Figure 1. 11) of racemic  $\beta$ -lactones having original functionalities (esters and ethers) exceeding those in Table 1. 2, are described in Chapter 4.

## 5. Conclusion on natural and synthetic PHAs

Eventually, one can easily accept the concept that PHAs are important candidates that can diminish environmental concerns of plastics due to their intrinsic features such as biodegradability and biocompatibility. A special emphasize was put on PHB and its related PHAs derivatives, because bacterial PHB is a perfectly isotactic, crystalline material possessing properties suitable for substituting conventional plastics, yet it has some restriction in performance. PHAs can be produced naturally or synthetically (bio- or chemical). Natural or bacterial PHAs requires specific growth substrates or metabolic engineering to extract them from bacteria, while they suffer from high costs relative to conventional fossil-resourced polymers, and low production volumes makes them impractical for commodity applications. Biosynthetic PHAs through mutating enzymes and/or DNA that are responsible for the polymer formation, can help in enhancing or boosting the production volume and offer access to already existing PHAs in nature with restricted molar masses and stereochemistry, un-optimized functionality and still encountering high production cost.<sup>[22a, 120]</sup>

In order to overcome these drawbacks, polymer chemists tend to resort to chemical synthetic procedures to produce PHAs through polycondensation of  $\beta$ -hydroxy acids or ring-opening polymerization (ROP) of  $\beta$ -lactones or most recently dilactones diolide (DL). Polycondensation of  $\beta$ -hydroxy acids is granted by the availability of the biosourced monomers, however, it is conducted in harsh experimental conditions and produce PHAs with high dispersity ( $\bar{D}_M > 2$ ) and low molar masses (maximum  $M_{n,SEC} = 5,300 \text{ g mol}^{-1}$ ), because  $\beta$ -hydroxy acid monomers tend to dehydrate and prevent their own polymerization. On the other hand, in ROP of  $\beta$ -lactones or DL, the monomer should usually be synthesized previously (details in Chapter 2), nevertheless ROP may be more receptive, responsive and scalable than polycondensation depending on its type, namely enzymatic (EROP), cationic (CROP), and anionic (AROP). EROP is an interesting choice because it can be operated under mild conditions (solvent free, unsensitive to water and oxygen) and the enzymes are non-toxic, hence the produced PHAs can have biomedical applications. However, the polymerization is slow (days), cannot reach full conversion and generally a mixture of linear and cyclic PHAs are obtained with dispersities range  $1.6 < \bar{D}_M < 2.3$ . Its main challenge is the compatibility of the enzyme active site with the  $\beta$ -lactone. It can reach molar masses up to  $12,000 \text{ g mol}^{-1}$  in the case of unsubstituted monomers (PL), and maximum of  $3000 \text{ g mol}^{-1}$  in the case of substituted ones ( $BL^{Me}$  and MPL) so far, yet with moderate isotactic stereocontrol ( $P_m = 0.67\text{-}0.75$ ). CROP of  $\beta$ -lactones (PL,  $rac\text{-}BL^{Me}$ ) lacks stereocontrol and faces regioselectivity issues (endocyclic

vs. exocyclic monomer activation; *O*-alkyl vs. *O*-acyl bond cleavage) with low maximum experimental molar mass ( $M_{n,SEC} < 10,100 \text{ g mol}^{-1}$ ) and dispersities up to 2.5; despite of owning a wide range of simple and available cationic activators. Similar to EROP, AROP promoted by organic activators is conducted in moderate conditions (solvent free, unsensitive to water and oxygen) and the used metal free activators are mainly non-toxic giving an indisputable advantage for the produced PHAs in both microelectronic and biomedical applications. Alike CROP, the organic activators whether nucleophilic or basic are easily available in diversity and are practical, however the presence of undesirable side-reactions and complicated mechanistic aspects with regioselectivity problems (*O*-alkyl vs. *O*-acyl bond cleavage) (Figure 1. 12) is also encountered. The extent of the latter obstacles depends on the nature of the initiating organic system engaged (basicity vs. weak or strong nucleophiles; Figure 1. 12) and the choice of the  $\beta$ -lactone used, therefore it was revealed that when it is done judiciously, it can afford high molar mass PHAs with fair dispersities ( $M_{n,SEC} < 1,650,000 \text{ g mol}^{-1}$ ;  $\bar{D}_M > 1.55$ ). Moreover, three organic activators BEMP, TBD, and DBU were noticed to have unclear mechanistic pathways and their mode of action is not yet proposed, unlike for the other extensively studied organic activators (Figure 1. 12). Fortunately, the mechanistic insights of BEMP, TBD and DBU are presented later in our work (Chapter 3). Finally, AROP mediated by organometallic catalytic systems is often advantageous compared to other ROPs, thanks to its fast kinetics and tunability of catalysts and monomers. Intelligent organometallic catalyst design framework depending on the metal and the ligand can avoid regioselectivity obstacles and enhance stereoselectivity. It was shown that in the ROP of *rac*-BL<sup>Me</sup> and *rac*-DL<sup>Me</sup> or *meso*-DL<sup>Me</sup>, the highest activity and stereoselectivity ( $P_m$  up to 0.99;  $P_r$  up to 0.95) were obtained from rare-earth metals, especially yttrium, with sterically hindered substituted ligands (more inputs are presented in Chapter 4). Noteworthy, exclusively AROP, regardless of the organic activators (initiators or catalysts) or organometallic complexes catalysts systems used, is so far the most feasible among the other ROPs in extending the monomer functionality scope of  $\beta$ -lactones.

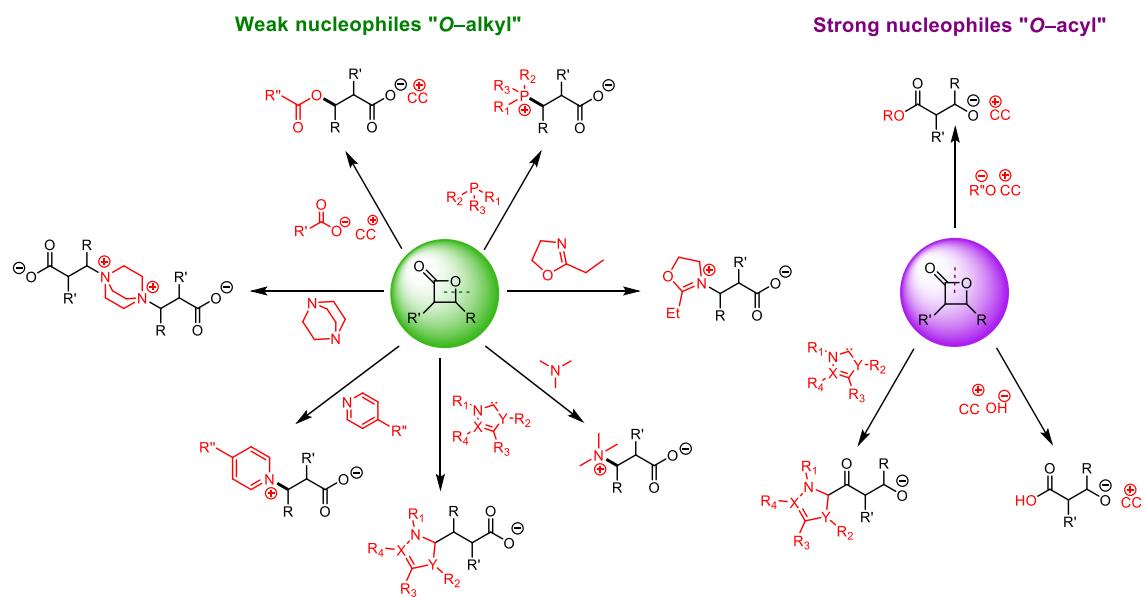


**Figure 1. 12** – Regioselectivity of the ring opening of  $\beta$ -lactones depends on the nucleophile nature of the organic activators.



## 6. References

- [1] a) R. A. Gross, B. Kalra, *Science* **2002**, 297, 803-807; b) E. B. ARIKAN, H. D. OZSOY, in *International Congress on “Green Infrastructure and Sustainable Societies/Cities” GreInSus’ 14*, **2014**, p. 66.
- [2] T. Ishigaki, W. Sugano, A. Nakanishi, M. Tateda, M. Ike, M. Fujita, *Chemosphere* **2004**, 54, 225-233.
- [3] Y. Tokiwa, B. P. Calabia, C. U. Ugwu, S. Aiba, *Int. J. Mol. Sci.* **2009**, 10, 3722-3742.
- [4] G. Kale, T. Kijchavengkul, R. Auras, M. Rubino, S. E. Selke, S. P. Singh, *Macromol. Biosci.* **2007**, 7, 255-277.
- [5] a) M. Asgher, S. A. Qamar, M. Bilal, H. M. N. Iqbal, *Food Res. Int.* **2020**, 137, 109625; b) Y. Tokiwa, **1976**; c) Y. Tokiwa, T. Suzuki, *Nature* **1977**, 270, 76-78; d) Y. Tokiwa, T. Suzuki, *Agric. Biol. Chem.* **1977**, 41, 265-274.
- [6] a) H. Nishida, Y. Tokiwa, *J. Environ. Polymer Degradation* **1993**, 1, 227-233; b) J. Mergaert, J. Swings, *J. Ind. Microbiol.* **1996**, 17, 463-469; c) T. Suyama, Y. Tokiwa, P. Ouichanpagdee, T. Kanagawa, Y. Kamagata, *Appl. Environ. Microbiol.* **1998**, 64, 5008-5011; d) H. Pranamuda, Y. Tokiwa, H. Tanaka, *Appl. Environ. Microbiol.* **1997**, 63, 1637-1640; e) D. H. Vu, D. Åkesson, M. J. Taherzadeh, J. A. Ferreira, *Bioresour. Technol.* **2020**, 298, 122393; f) J. Myung, N. I. Strong, W. M. Galega, E. R. Sundstrom, J. C. Flanagan, S.-G. Woo, R. M. Waymouth, C. S. Criddle, *Bioresour. Technol.* **2014**, 170, 167-174; g) K. Changwichan, T. Silalertruksa, S. H. Gheewala, *Sustainability* **2018**, 10, 952; h) A. Soroudi, I. Jakubowicz, *Eur. Polym. J.* **2013**, 49, 2839-2858; i) B.-Y. Chen, T.-J. Shiau, Y.-H. Wei, W.-M. Chen, B.-H. Yu, C.-Y. Yen, C.-C. Hsueh, *Journal of the Taiwan Institute of Chemical Engineers* **2012**, 43, 455-458; j) S. Kaihara, Y. Osanai, K. Nishikawa, K. Toshima, Y. Doi, S. Matsumura, *Macromol. Biosci.* **2005**, 5, 644-652.
- [7] a) M. Lemoigne, *CR Acad Sci* **1925**, 180, 1539-1541; b) M. Lemoigne, *Bull. Soc. Chim. Biol.* **1926**, 8, 770-782; c) S. Obruca, P. Sedlacek, M. Koller, D. Kucera, I. Pernicova, *Biotechnol. Adv.* **2018**, 36, 856-870.
- [8] R. Griebel, Z. Smith, J. Merrick, *Biochemistry* **1968**, 7, 3676-3681.
- [9] L. L. Wallen, W. K. Rohwedder, *Environ. Sci. Technol.* **1974**, 8, 576-579.
- [10] a) C. Kourmentza, J. Plácido, N. Venetsaneas, A. Burniol-Figols, C. Varrone, H. N. Gavala, M. A. Reis, *Bioengineering* **2017**, 4, 55; b) B. Kunasundari, K. Sudesh, *Express Polymer Letters* **2011**, 5.
- [11] M. Winnacker, *Eur. J. Lipid Sci. Technol.* **2019**, 121, 1900101.
- [12] E. Bugnicourt, P. Cinelli, A. Lazzeri, V. A. Alvarez, **2014**.
- [13] a) S. Balaji, K. Gopi, B. Muthuvelan, *Algal Research* **2013**, 2, 278-285; b) T. Tsuge, *J. Biosci. Bioeng.* **2002**, 94, 579-584; c) B. Laycock, P. Halley, S. Pratt, A. Werker, P. Lant, *Prog. Polym. Sci.* **2013**, 38, 536-583; d) F. Luzi, L. Torre, J. M. Kenny, D. Puglia, *Materials* **2019**, 12, 471.
- [14] A. Czerniecka-Kubicka, W. Frącz, M. Jasiorski, W. Błażejowski, B. Pilch-Pitera, M. Pyda, I. Zarzyka, *J. Therm. Anal. Calorim.* **2017**, 128, 1513-1526.
- [15] a) D. L. Kaplan, in *Biopolymers from renewable resources*, Springer, **1998**, pp. 1-29; b) R. A. Sequeira, S. Dubey, M. M. Pereira, T. K. Maity, S. Singh, S. Mishra, K. Prasad,



- ACS Sustainable Chemistry & Engineering* **2020**, 8, 12005-12013; c) J. Możejko-Ciesielska, R. Kiewisz, *Microbiol. Res.* **2016**, 192, 271-282.
- [16] S. Ansari, D. Yasin, T. Fatma, *Am J PharmTech Res* **2016**.
- [17] a) D. Williamson, J. Wilkinson, *Microbiology* **1958**, 19, 198-209; b) M. Doudoroff, R. Stanier, *Nature* **1959**, 183, 1440-1442.
- [18] a) Z. N. Yüksekdağ, B. Aslim, Y. Beyatli, N. Mercan, *African Journal of Biotechnology* **2004**, 3, 63-66; b) F. K. Young, J. R. Kastner, S. W. May, *Appl. Environ. Microbiol.* **1994**, 60, 4195-4198; c) C.-C. Chien, C.-C. Chen, M.-H. Choi, S.-S. Kung, Y.-H. Wei, *J. Biotechnol.* **2007**, 132, 259-263.
- [19] a) S. P. Valappil, A. R. Boccaccini, C. Bucke, I. Roy, *Antonie Van Leeuwenhoek* **2007**, 91, 1-17; b) E. Z. Gomaa, *Brazilian Archives of Biology and Technology* **2014**, 57, 145-154.
- [20] C.-Y. Loo, W.-H. Lee, T. Tsuge, Y. Doi, K. Sudesh, *Biotechnol. Lett* **2005**, 27, 1405-1410.
- [21] a) C. Ratledge, *Basic Biotechnology*, C Ratledge, B Kristiansen, Editors **2001**; b) R. A. Verlinden, D. J. Hill, M. Kenward, C. D. Williams, I. Radecka, *J. Appl. Microbiol.* **2007**, 102, 1437-1449; c) C. Ratledge, B. Kristiansen, *Basic biotechnology*, Cambridge University Press, **2001**.
- [22] a) A. Anjum, M. Zuber, K. M. Zia, A. Noreen, M. N. Anjum, S. Tabasum, *Int. J. Biol. Macromol.* **2016**, 89, 161-174; b) S. Riaz, K. Y. Rhee, S. J. Park, *Polymers* **2021**, 13, 253.
- [23] D. Jendrossek, R. Handrick, *Annu. Rev. Microbiol.* **2002**, 56, 403-432.
- [24] a) K. Sudesh, H. Abe, Y. Doi, *Prog. Polym. Sci.* **2000**, 25, 1503-1555; b) Á. Sandoval, E. Arias-Barrau, F. Bermejo, L. Cañedo, G. Naharro, E. R. Olivera, J. M. Luengo, *Appl. Microbiol. Biotechnol.* **2005**, 67, 97-105.
- [25] J. Eggers, A. Steinbüchel, *J. Bacteriol.* **2013**, 195, 3213-3223.
- [26] H. M. Müller, D. Seebach, *Angew. Chem. Int. Ed.* **1993**, 32, 477-502.
- [27] J. N. Baptist, J. B. Ziegler, Google Patents, **1965**.
- [28] P. Holmes, *Physics in technology* **1985**, 16, 32.
- [29] I. Noda, P. R. Green, M. M. Satkowski, L. A. Schechtman, *Biomacromolecules* **2005**, 6, 580-586.
- [30] <https://danimerscientific.com/>.
- [31] <https://www.kaneka.co.jp/en/>.
- [32] Y. Doi, K. Mukai, K. Kasuya, K. Yamada, in *Studies in Polymer Science*, Vol. 12, Elsevier, **1994**, pp. 39-51.
- [33] a) D. Van-Thuoc, J. Quillaguaman, G. Mamo, B. Mattiasson, *J. Appl. Microbiol.* **2008**, 104, 420-428; b) E. Haba, J. Vidal-Mas, M. Bassas, M. Espuny, J. Llorens, A. Manresa, *Biochem. Eng. J.* **2007**, 35, 99-106; c) E. Akaraonye, T. Keshavarz, I. Roy, *J. Chem. Technol. Biotechnol.* **2010**, 85, 732-743; d) G. Pagliano, V. Ventorino, A. Panico, O. Pepe, *Biotechnology for Biofuels* **2017**, 10, 1-24.
- [34] M. H. Ibrahim, A. Steinbüchel, *Appl. Environ. Microbiol.* **2009**, 75, 6222-6231.
- [35] a) T. Volova, E. Shishatskaya, V. Sevastianov, S. Efremov, O. Mogilnaya, *Biochem. Eng. J.* **2003**, 16, 125-133; b) P. Suriyamongkol, R. Weselake, S. Narine, M. Moloney, S. Shah, *Biotechnol. Adv.* **2007**, 25, 148-175; c) J. M. Chai, T. S. M. Amelia, G. K.

- Mouriya, K. Bhubalan, A.-A. A. Amirul, S. Vigneswari, S. Ramakrishna, *Polymers* **2021**, *13*, 51.
- [36] a) I. Ali, N. Jamil, *Frontiers in biology* **2016**, *11*, 19-27; b) S. Ray, V. C. Kalia, *Indian J. Microbiol.* **2017**, *57*, 261-269.
- [37] a) S. K. Misra, S. P. Valappil, I. Roy, A. R. Boccaccini, *Biomacromolecules* **2006**, *7*, 2249-2258; b) S. P. Valappil, S. K. Misra, A. R. Boccaccini, I. Roy, *Expert Rev. Med. Devices* **2006**, *3*, 853-868.
- [38] M. F. Yagmurlu, F. Korkusuz, I. Gürsel, P. Korkusuz, Ü. Örs, V. Hasirci, *Journal of Biomedical Materials Research: An Official Journal of The Society for Biomaterials, The Japanese Society for Biomaterials, and The Australian Society for Biomaterials and the Korean Society for Biomaterials* **1999**, *46*, 494-503.
- [39] I. Gursel, F. Yagmurlu, F. Korkusuz, V. Hasirci, *J. Microencaps.* **2002**, *19*, 153-164.
- [40] A. Hazari, M. Wiberg, G. Johansson-Ruden, C. Green, G. Terenghi, *Br. J. Plast. Surg.* **1999**, *52*, 653-657.
- [41] a) E. Shishatskaya, T. Volova, A. Puzyr, O. Mogilnaya, S. Efremov, *J. Mater. Sci. Mater. Med.* **2004**, *15*, 719-728; b) E. I. Shishatskaya, E. D. Nikolaeva, O. N. Vinogradova, T. G. Volova, *J. Mater. Sci. Mater. Med.* **2016**, *27*, 1-16.
- [42] a) M. Koller, G. Braunegg, *The EuroBiotech Journal* **2018**, *2*, 89-103; b) M. Koller, K. Shahzad, G. Braunegg, *Applied Food Biotechnology* **2018**, *5*, 193-203; c) G.-Q. Chen, X.-R. Jiang, *Curr. Opin. Biotechnol.* **2018**, *50*, 94-100.
- [43] a) Y. Wang, J. Yin, G.-Q. Chen, *Curr. Opin. Biotechnol.* **2014**, *30*, 59-65; b) S. Nakkeeran, W. D. Fernando, Z. A. Siddiqui, in *PGPR: Biocontrol and biofertilization*, Springer, **2005**, pp. 257-296; c) R. Turco, G. Santagata, I. Corrado, C. Pezzella, M. Di Serio, *Frontiers in Bioengineering and Biotechnology* **2021**, *8*, 1454.
- [44] D. Elhadi, L. Lv, X.-R. Jiang, H. Wu, G.-Q. Chen, *Metab. Eng.* **2016**, *38*, 358-369.
- [45] K. Tajima, X. Han, Y. Satoh, A. Ishii, Y. Araki, M. Munekata, S. Taguchi, *Appl. Microbiol. Biotechnol.* **2012**, *94*, 365-376.
- [46] S. Taguchi, M. Yamada, K. i. Matsumoto, K. Tajima, Y. Satoh, M. Munekata, K. Ohno, K. Kohda, T. Shimamura, H. Kambe, *Proceedings of the National Academy of Sciences* **2008**, *105*, 17323-17327.
- [47] a) K. Takase, S. Taguchi, Y. Doi, *J. Biochem.* **2003**, *133*, 139-145; b) T. Kichise, S. Taguchi, Y. Doi, *Appl. Environ. Microbiol.* **2002**, *68*, 2411-2419.
- [48] L. Su, R. W. Lenz, Y. Takagi, S. Zhang, S. Goodwin, L. Zhong, D. P. Martin, *Macromolecules* **2000**, *33*, 229-231.
- [49] T. U. Gerngross, S. C. Slater, *Sci. Am.* **2000**, *283*, 36-41.
- [50] a) W. Amass, A. Amass, B. Tighe, *Polym. Int.* **1998**, *47*, 89-144; b) A. Bossion, K. V. Heifferon, L. Meabe, N. Zivic, D. Taton, J. L. Hedrick, T. E. Long, H. Sardon, *Progress in Polymer Science* **2019**, *90*, 164-210; c) C. K. Williams, *Chem. Soc. Rev.* **2007**, *36*, 1573-1580.
- [51] a) E. Gabirondo, A. Sangroniz, A. Etxeberria, S. Torres-Giner, H. Sardon, *Poly. Chem.* **2020**, *11*, 5548-5548; b) D. Bandelli, J. Alex, C. Weber, U. S. Schubert, *Macromol. Rapid Commun.* **2020**, *41*, 1900560.
- [52] T. Bhalla, V. Kumar, S. Bhatia, *Advances in industrial biotechnology. IK International Publishing House Pvt Ltd, India* **2013**, 56-76.
- [53] D. L. Wise, Google Patents, **1976**.

- [54] T. Nanba, H. Ito, H. Kobayashi, T. Hayashi, *JP patent* **1994**, 6329774.
- [55] T. Kajiyama, H. Kobayashi, T. Taguchi, K. Kataoka, J. Tanaka, *Biomacromolecules* **2004**, 5, 169-174.
- [56] R. Nakashima, T. Okuda, M. Okazaki, T. Ouchi, *Rep Fac Eng Tottori Univ* **1977**, 8, 124-127.
- [57] A. Khalil, S. Cammas-Marion, O. Coulembier, *J. Polym. Sci., Part A: Polym. Chem.* **2019**, 57, 657-672.
- [58] a) P. Lecomte, C. Jérôme, *Synthetic biodegradable polymers* **2011**, 173-217; b) G. Odian, *Principles of polymerization*, John Wiley & Sons, **2004**.
- [59] a) P. Dubois, O. Coulembier, J.-M. Raquez, *Handbook of ring-opening polymerization*, John Wiley & Sons, **2009**; b) M. Okada, *Prog. Polym. Sci.* **2002**, 27, 87-133.
- [60] O. Nuyken, S. D. Pask, *Polymers* **2013**, 5, 361-403.
- [61] W. Saiyasombat, R. Molloy, T. Nicholson, A. Johnson, I. Ward, S. Poshychinda, *Polymer* **1998**, 39, 5581-5585.
- [62] a) A. Duda, A. Kowalski, *Handbook of ring-opening polymerization* **2009**, 1-51; b) P. Olsén, K. Odellius, A.-C. Albertsson, *Biomacromolecules* **2016**, 17, 699-709.
- [63] S. Matsumura, *Enzyme-catalyzed synthesis of polymers* **2006**, 95-132.
- [64] G. A. Nobes, R. J. Kazlauskas, R. H. Marchessault, *Macromolecules* **1996**, 29, 4829-4833.
- [65] S. Namekawa, H. Uyama, S. Kobayashi, *Polym. J.* **1996**, 28, 730-731.
- [66] W. Xie, J. Li, D. Chen, P. G. Wang, *Macromolecules* **1997**, 30, 6997-6998.
- [67] Y. Y. Svirkin, J. Xu, R. A. Gross, D. L. Kaplan, G. Swift, *Macromolecules* **1996**, 29, 4591-4597.
- [68] J. T. Gorke, K. Okrasa, A. Louwagie, R. J. Kazlauskas, F. Srienc, *J. Biotechnol.* **2007**, 132, 306-313.
- [69] a) S. Kobayashi, in *Macromolecular symposia*, Vol. 240, Wiley Online Library, **2006**, pp. 178-185; b) C. Jérôme, P. Lecomte, *Adv. Drug Del. Rev.* **2008**, 60, 1056-1076.
- [70] H. Zhao, *Methods Enzymol.* **2019**, 627, 1-21.
- [71] W. N. Ottou, H. Sardon, D. Mecerreyes, J. Vignolle, D. Taton, *Prog. Polym. Sci.* **2016**, 56, 64-115.
- [72] E. Ludvig, A. Khomyakov, G. Sanina, in *Journal of Polymer Science: Polymer Symposia*, Vol. 42, Wiley Online Library, **1973**, pp. 289-302.
- [73] M. Basko, A. Duda, S. Kazmierski, P. Kubisa, *J. Polym. Sci., Part A: Polym. Chem.* **2013**, 51, 4873-4884.
- [74] J. Dale, J.-E. Schwartz, *Acta Chem. Scand. B.* **1986**, 40, 559-567.
- [75] K. Ito, T. Inoue, Y. Yamashita, *Macromol. Chem. Phys.* **1968**, 117, 279-282.
- [76] T. Gresham, J. Jansen, F. Shaver, *J. Am. Chem. Soc.* **1948**, 70, 998-999.
- [77] a) A. Hofman, R. Szymański, S. Słomkowski, S. Penczek, *Macromol. Chem. Phys.* **1984**, 185, 655-667; b) H. R. Kricheldorf, J. M. Jonté, R. Dunsing, *Macromol. Chem. Phys.* **1986**, 187, 771-785.
- [78] S. Słomkowski, R. Szymański, A. Hofman, *Macromol. Chem. Phys.* **1985**, 186, 2283-2290.
- [79] a) K. Makiguchi, Hokkaido University **2014**; b) K. Makiguchi, T. Saito, T. Satoh, T. Kakuchi, *J. Polym. Sci., Part A: Polym. Chem.* **2014**, 52, 2032-2039; c) F. A. Jaipuri, B. D. Bower, N. L. Pohl, *Tetrahedron: Asymmetry* **2003**, 14, 3249-3252; d) A. Couffin,

- B. Martín-Vaca, D. Bourissou, C. Navarro, *Poly. Chem.* **2014**, 5, 161-168; e) E. K. Macdonald, M. P. Shaver, *Eur. Polym. J.* **2017**, 95, 702-710.
- [80] a) A. Dove, H. Sardon, S. Naumann, *Organic catalysis for polymerisation*, Vol. 31, Royal Society of Chemistry, **2018**; b) M. K. Kiesewetter, E. J. Shin, J. L. Hedrick, R. M. Waymouth, *Macromolecules* **2010**, 43, 2093-2107.
- [81] A. P. Dove, *ACS Macro Letters* **2012**, 1, 1409-1412.
- [82] A. Duda, *J. Polym. Sci., Part A: Polym. Chem.* **1992**, 30, 21-29.
- [83] a) D. V. Banthorpe, *Elimination reactions*, Vol. 2, Elsevier Publishing Company, **1963**; b) A. Cockerill, in *Comprehensive chemical kinetics*, Vol. 9, Elsevier, **1973**, pp. 163-372.
- [84] A. Pommier, J.-M. Pons, *Synthesis* **1993**, 1993, 441-459.
- [85] A. Hofman, S. Słomkowski, S. Penczek, *Macromol. Chem. Phys.* **1984**, 185, 91-101.
- [86] E. Dunn, **2012**.
- [87] a) Y. Yamashita, K. Ito, F. Nakakita, *Macromol. Chem. Phys.* **1969**, 127, 292-295; b) H. R. Kricheldorf, G. Schwarz, *Macromol. Rapid Commun.* **2003**, 24, 359-381.
- [88] H. Hall Jr, *Macromolecules* **1969**, 2, 488-497.
- [89] M. Iida, T. Araki, K. Teranishi, H. Tani, *Macromolecules* **1977**, 10, 275-284.
- [90] L. S. Corley, O. Vogl, T. Biela, S. Penczek, S. Słomkowski, *Die Makromolekulare Chemie, Rapid Communications* **1981**, 2, 47-50.
- [91] S. Cammas, I. Renard, V. Langlois, P. Guéri, *Polymer* **1996**, 37, 4215-4220.
- [92] a) D. B. Johns, R. W. Lenz, M. Vert, *J. Bioact. Compatible Polym.* **1986**, 1, 47-60; b) J.-P. Caruelle, D. Barritault, V. Jeanbat-Mimaud, S. Cammas-Marion, V. Langlois, P. Guerin, C. Barbaud, *J. Biomater. Sci. Polym. Ed.* **2000**, 11, 979-991.
- [93] a) H. R. Kricheldorf, N. Scharnagl, Z. Jedlinski, *Polymer* **1996**, 37, 1405-1411; b) P. Kurcok, M. Śmiga, Z. Jedliński, *J. Polym. Sci., Part A: Polym. Chem.* **2002**, 40, 2184-2189; c) H. R. Kricheldorf, M. Garaleh, G. Schwarz, *J. Macromol. Sci. A* **2005**, 42, 139-148; d) I. TABLEAU, in *Journal of Polymer Science: Polymer symposia. Part C*, Interscience Publishers., **1963**, p. 1061; e) Y. Etienne, R. Soulas, in *Journal of Polymer Science Part C: Polymer Symposia*, Vol. 4, Wiley Online Library, **1963**, pp. 1061-1074; f) R. Bizzarri, F. Chiellini, R. Solaro, E. Chiellini, S. Cammas-Marion, P. Guerin, *Macromolecules* **2002**, 35, 1215-1223.
- [94] a) S. C. Arnold, R. W. Lenz, in *Makromolekulare Chemie. Macromolecular Symposia*, Vol. 6, Wiley Online Library, **1986**, pp. 285-303; b) S. Cammas, K. Boutault, F. Huet, P. Guérin, *Tetrahedron: Asymmetry* **1994**, 5, 1589-1597; c) Y. Zhang, R. A. Gross, R. W. Lenz, *Macromolecules* **1990**, 23, 3206-3212.
- [95] S. Cammas, I. Renard, J. P. Girault, P. Guérin, *Polym. Bull.* **1994**, 33, 149-158.
- [96] a) C. Barbaud, F. Faÿ, F. Abdillah, S. Randriamahefa, P. Guérin, *Macromol. Chem. Phys.* **2004**, 205, 199-207; b) F. Ouhib, S. Randriamahefa, P. Guérin, C. Barbaud, *Designed monomers and polymers* **2005**, 8, 25-35.
- [97] a) M. Kawalec, O. Coulembier, P. Gerbaux, M. Sobota, J. De Winter, P. Dubois, M. Kowalczyk, P. Kurcok, *React. Funct. Polym.* **2012**, 72, 509-520; b) J. De Winter, O. Coulembier, P. Gerbaux, P. Dubois, *Macromolecules* **2010**, 43, 10291-10296.
- [98] I. Binkowska, W. Gałęzowski, A. Jarczewski, *Open Chemistry* **2010**, 8, 582-586.
- [99] a) M. Fèvre, J. Pinaud, Y. Gnanou, J. Vignolle, D. Taton, *Chem. Soc. Rev.* **2013**, 42, 2142-2172; b) D. Bourissou, O. Guerret, F. P. Gabbai, G. Bertrand, *Chem. Rev.* **2000**,



- 100, 39-92; c) D. Enders, O. Niemeier, A. Henseler, *Chem. Rev.* **2007**, *107*, 5606-5655; d) S. Naumann, A. P. Dove, *Poly. Chem.* **2015**, *6*, 3185-3200.
- [100] E. F. Connor, G. W. Nyce, M. Myers, A. Möck, J. L. Hedrick, *J. Am. Chem. Soc.* **2002**, *124*, 914-915.
- [101] a) O. Coulembier, B. G. Lohmeijer, A. P. Dove, R. C. Pratt, L. Mespouille, D. A. Culkin, S. J. Benight, P. Dubois, R. M. Waymouth, J. L. Hedrick, *Macromolecules* **2006**, *39*, 5617-5628; b) O. Coulembier, X. Delva, J. L. Hedrick, R. M. Waymouth, P. Dubois, *Macromolecules* **2007**, *40*, 8560-8567.
- [102] a) W. Jeong, J. L. Hedrick, R. M. Waymouth, *J. Am. Chem. Soc.* **2007**, *129*, 8414-8415; b) S. Moins, C. Henoumont, J. De Winter, A. Khalil, S. Laurent, S. Cammas-Marion, O. Coulembier, *Poly. Chem.* **2018**, *9*, 1840-1847.
- [103] E. Brulé, V. Guérineau, P. Vermaut, F. Prima, J. Balogh, L. Maron, A. M. Slawin, S. P. Nolan, C. M. Thomas, *Poly. Chem.* **2013**, *4*, 2414-2423.
- [104] a) C. G. Jaffredo, J. F. Carpentier, S. M. Guillaume, *Macromol. Rapid Commun.* **2012**, *33*, 1938-1944; b) C. G. Jaffredo, J.-F. Carpentier, S. M. Guillaume, *Poly. Chem.* **2013**, *4*, 3837-3850; c) B. G. Lohmeijer, R. C. Pratt, F. Leibfarth, J. W. Logan, D. A. Long, A. P. Dove, F. Nederberg, J. Choi, C. Wade, R. M. Waymouth, *Macromolecules* **2006**, *39*, 8574-8583.
- [105] a) M. Kawalec, M. Śmiga-Matuszowicz, P. Kurcok, *Eur. Polym. J.* **2008**, *44*, 3556-3563; b) O. Coulembier, P. Degée, J. L. Hedrick, P. Dubois, *Prog. Polym. Sci.* **2006**, *31*, 723-747; c) Z. Jedliński, M. Kowalczyk, Z. Grobelny, A. Stolarzewicz, *Die Makromolekulare Chemie, Rapid Communications* **1983**, *4*, 355-358; d) N. Tanahashi, Y. Doi, *Macromolecules* **1991**, *24*, 5732-5733.
- [106] Z. Jedlinski, M. Kowalczyk, W. Glowkowski, J. Grobelny, M. Szwarc, *Macromolecules* **1991**, *24*, 349-352.
- [107] G. Adamus, M. Kowalczyk, *Biomacromolecules* **2008**, *9*, 696-703.
- [108] a) C. M. Thomas, *Chem. Soc. Rev.* **2010**, *39*, 165-173; b) J. F. Carpentier, *Macromol. Rapid Commun.* **2010**, *31*, 1696-1705; c) J.-F. Carpentier, *Organometallics* **2015**, *34*, 4175-4189; d) R. M. Shakaroun, H. Li, S. M. Guillaume, J. F. Carpentier, *Chem. Eur. J.* **2020**, *26*, 128-138.
- [109] M. Zintl, F. Molnar, T. Urban, V. Bernhart, P. Preishuber-Pflügl, B. Rieger, *Angew. Chem. Int. Ed.* **2008**, *47*, 3458-3460.
- [110] B. J. Jeffery, E. L. Whitelaw, D. Garcia-Vivo, J. A. Stewart, M. F. Mahon, M. G. Davidson, M. D. Jones, *Chem. Commun.* **2011**, *47*, 12328-12330.
- [111] C. Agatemor, A. E. Arnold, E. D. Cross, A. Decken, M. P. Shaver, *J. Organomet. Chem.* **2013**, *745*, 335-340.
- [112] E. Grunova, E. Kirillov, T. Roisnel, J.-F. Carpentier, *Dalton Transactions* **2010**, *39*, 6739-6752.
- [113] N. Ajellal, D. M. Lyubov, M. A. Sinenkov, G. K. Fukin, A. V. Cherkasov, C. M. Thomas, J. F. Carpentier, A. A. Trifonov, *Chem. Eur. J.* **2008**, *14*, 5440-5448.
- [114] a) A. Amgoune, C. M. Thomas, S. Ilinca, T. Roisnel, J. F. Carpentier, *Angew. Chem. Int. Ed.* **2006**, *45*, 2782-2784; b) N. Ajellal, M. Bouyahyi, A. Amgoune, C. M. Thomas, A. Bondon, I. Pillin, Y. Grohens, J.-F. Carpentier, *Macromolecules* **2009**, *42*, 987-993; c) M. Bouyahyi, N. Ajellal, E. Kirillov, C. M. Thomas, J. F. Carpentier, *Chem. Eur. J.*

- 2011**, 17, 1872-1883; d) Y. Chapurina, J. Klitzke, O. d. L. Casagrande Jr, M. Awada, V. Dorcet, E. Kirillov, J.-F. Carpentier, *Dalton Transactions* **2014**, 43, 14322-14333.
- [115] D. Pappalardo, M. Bruno, M. Lamberti, C. Pellecchia, *Macromol. Chem. Phys.* **2013**, 214, 1965-1972.
- [116] J. Fang, M. J.-L. Tschan, T. Roisnel, X. Trivelli, R. M. Gauvin, C. M. Thomas, L. Maron, *Poly. Chem.* **2013**, 4, 360-367.
- [117] Y. Chapurina, T. Roisnel, J.-F. Carpentier, E. Kirillov, *Inorg. Chim. Acta* **2015**, 431, 161-175.
- [118] P. T. Altenbuchner, A. Kronast, S. Kissling, S. I. Vagin, E. Herdtweck, A. Pöthig, P. Deglmann, R. Loos, B. Rieger, *Chem. Eur. J.* **2015**, 21, 13609-13617.
- [119] a) X. Tang, E. Y.-X. Chen, *Nat. comm.* **2018**, 9, 1-11; b) X. Tang, A. H. Westlie, E. M. Watson, E. Y.-X. Chen, *Science* **2019**, 366, 754-758; c) X. Tang, A. H. Westlie, L. Caporaso, L. Cavallo, L. Falivene, E. Y. X. Chen, *Angew. Chem.* **2020**, 132, 7955-7964; d) A. H. Westlie, E. Y.-X. Chen, *Macromolecules* **2020**, 53, 9906-9915.
- [120] a) P. C. Sabapathy, S. Devaraj, K. Meixner, P. Anburajan, P. Kathirvel, Y. Ravikumar, H. M. Zabed, X. Qi, *Bioresour. Technol.* **2020**, 306, 123132; b) G. Mannina, D. Presti, G. Montiel-Jarillo, J. Carrera, M. E. Suárez-Ojeda, *Bioresour. Technol.* **2020**, 297, 122478.









## Chapter 2.

### From epoxide to $\beta$ -lactones: carbonylation stage





<b>1.Introduction.....</b>	<b>73</b>
1.1.    Significance of $\beta$ -lactones .....	73
1.2.    Prevailing $\beta$ -lactones' synthesis .....	74
1.3.    Stand and outlooks on $\beta$ -lactones' synthesis.....	81
<b>2.Results and discussion .....</b>	<b>81</b>
2.1.    Synthesis and characterization of <i>racemic</i> and enantiopure functional epoxides " $G^{FGs}$ " .....	82
2.2.    Synthesis and characterization of <i>racemic</i> and enantiopure functional $\beta$ -lactones " $BPL^{FGs}$ " .....	86
<b>3.Conclusion: achievements and blueprints.....</b>	<b>97</b>
<b>4.Experimental section .....</b>	<b>98</b>
<b>5.References.....</b>	<b>109</b>



## 1. Introduction

Herein, the prominence of  $\beta$ -lactones for various industrial compounds among them our targeted PHAs is discussed. An assessment of the most used methods to synthesize  $\beta$ -lactones is briefly reviewed with focus on our elected approach known as, the carbonylation of epoxides.

### 1.1. Significance of $\beta$ -lactones

$\beta$ -Lactones, that is, four-membered strained ester rings, also named 2-oxetanones, represent a very well-known class of heterocyclic monomers. They have attracted a lot of interest over the past four decades, being recognized as useful organic synthons and pharmaceutical radix group. They have received an important attention for their antimicrobial, anticancer, and antiobesity properties.<sup>[1]</sup> Over 30 core scaffolds of  $\beta$ -lactone have been described as key structures in various natural products to date, many with potent bioactivity against bacteria, fungi, or human cancer cell lines, such as Lipstatin, Obafluorin, and Salinosporamide A (Figure 2. 1).<sup>[2]</sup> The intrinsic reactivity of  $\beta$ -lactones as highly electrophilic scaffolds has also prompted researchers to investigate such cyclic esters as intermediates in the formation of some important classes of molecules, such as the total synthesis of some natural compounds used in medicinal chemistry,<sup>[3]</sup>  $\alpha$ -amino acids,<sup>[4]</sup> propionic acid,<sup>[5]</sup> tetrahydrofuran derivatives<sup>[6]</sup> or polymers.<sup>[7]</sup>

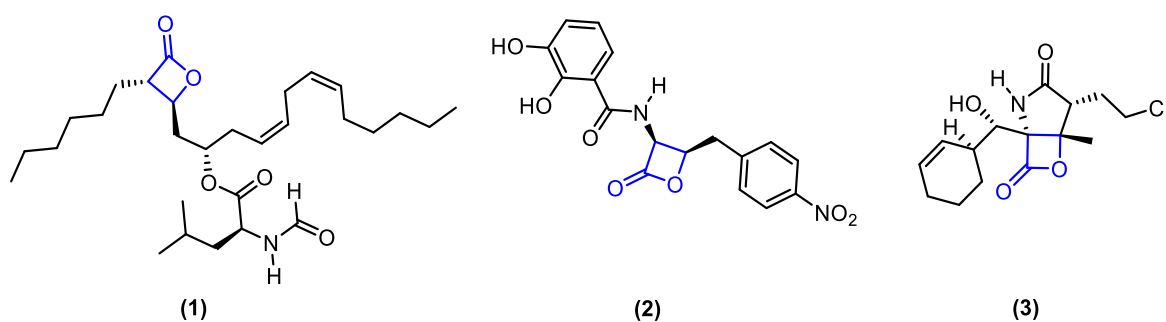


**Figure 2. 1** – Some natural products containing  $\beta$ -lactone as the core of the structure: Lipstatin (1), Obafluorin (2), and Salinosporamide A (3).

In a riveting fashion, despite than readily undergoing acidic or basic hydrolysis,  $\beta$ -lactones are relevant precursors for diverse reactions (Figure 2. 2).  $\beta$ -lactones can alter between attacking an electrophile (Figure 2. 2 – (a))<sup>[8]</sup> or being attacked by a nucleophile (Figure 1.14; Figure 2. 2 – (b)),<sup>[4, 8a]</sup> decarboxylation that can be caused from thermal degradation<sup>[9]</sup> or enzymatic biocatalysts (Figure 2. 2 – (c)).<sup>[10]</sup> Ring expansion catalysed rearrangement through Lewis acids are also possible (Figure 2. 2 – (d)),<sup>[11]</sup> besides direct

conversion to  $\beta$ -lactam or  $\gamma$ -lactam (Figure 2. 2 – (e)).<sup>[12]</sup> Last and most valuable to our interests is the ability of  $\beta$ -lactones to ring-open polymerize to form polyesters and more precisely PHAs (Figure 2. 2 – (f)).<sup>[13]</sup> Hence, all of this has subjected  $\beta$ -lactones to extensive studies on their synthesis that are described below.

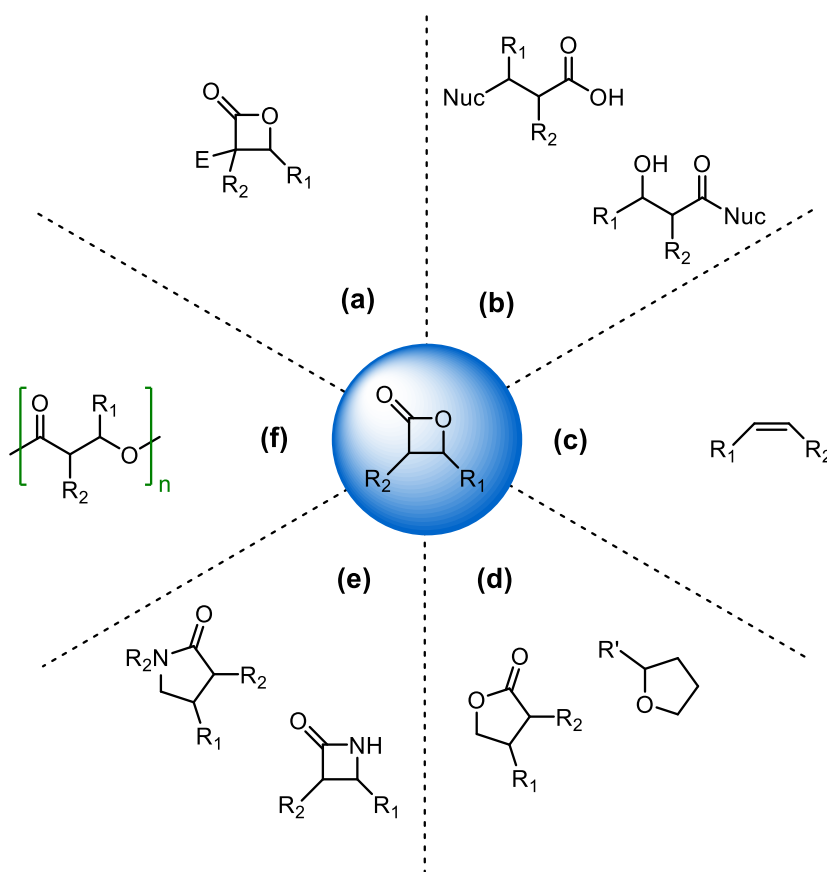
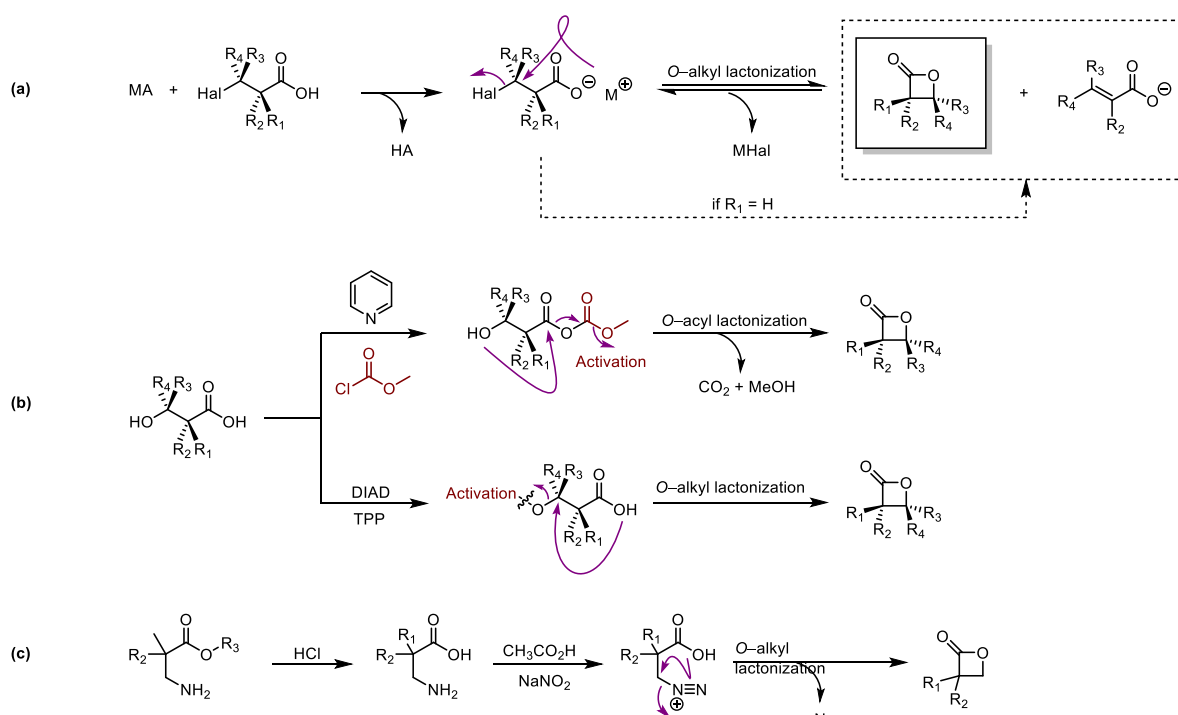


**Figure 2. 2** – Possible  $\beta$ -lactone transformations; (a) addition of an electrophile “E”; (b) nucleophilic “Nuc” attack; (c) decarboxylation; (d) Lewis acid catalysed rearrangement; (e) direct conversion to  $\beta$ -lactams; (f) ring-opening polymerization “ROP” towards PHAs.

## 1.2. Prevailing synthesis of $\beta$ -lactones

The first synthesis of a  $\beta$ -lactone was described by Einhorn in 1883,<sup>[14]</sup> while the first natural  $\beta$ -lactone extracted from a Japanese fruit was reported in the mid of 1950’s,<sup>[15]</sup> and the first chiral synthesis was established in 1982.<sup>[16]</sup> The first reported synthesis generally involved cyclization or lactonization<sup>[17]</sup> of  $\beta$ -halocarboxylate salts through a Knoevenagel reaction (Scheme 2. 1 – (a); *O*-alkyl ring closing),<sup>[18]</sup> or of  $\beta$ -hydroxy acids mainly in the presence of alkyl chloroformate and pyridine (or other similar reagents) to activate the carboxyl group and deliver *O*-acyl lactonization (Scheme 2. 1 – (b)),<sup>[18b]</sup> or under Mitsunobu conditions in order to

activate the hydroxyl group and afford *O*-alkyl lactonization (Scheme 2. 1 – (b)).<sup>[19]</sup> Otherwise, cyclization of  $\beta$ -amino acids was reported in diazotation medium (Scheme 2. 1 – (c); *O*-alkyl ring closing).<sup>[4, 20]</sup> It should be noted that in case of *O*-alkyl lactonization, an inversion of configuration at the  $\beta$ -position was noticed, in contrast to that of *O*-acyl lactonization where configuration retention was observed; and choosing between *O*-alkyl and *O*-acyl lactonization was the common way to tune the stereochemistry of the produced  $\beta$ -lactone. Concerning the drawbacks, upon using  $\beta$ -halocarboxylate salts, the lactonization is often limited mostly by  $\beta$ -elimination ( $E_1$ ) from the starting metal salt (MA), and scarcely from decarboxylative elimination of the produced  $\beta$ -lactone ( $E_2$ ; Figure 2. 2 – (c)). Also,  $E_1$  undesired reactions are highly dependent on the  $\alpha$ -substituents, so that they increase when  $R_1 = R_2 = H$ , or with bulky substituents that require high temperatures ( $> 50^\circ\text{C}$ ) during lactonization which promote both  $E_1$  and  $E_2$ . In the end, this method affords 9 to 12% yield of the produced  $\beta$ -lactone, since the latter is also reversible in the presence of metal halides (MHal) (Scheme 2. 1 – (a)).<sup>[8a, 21]</sup> On the other hand, regarding utilizing  $\beta$ -hydroxy acids or  $\beta$ -amino acids, the elimination reactions were less pronounced and the reaction yields range between 8 to 90% due to the reaction reliance on the starting material substituents, the total steps in the synthesis (starting material are not commercially available) and the catalyst used.<sup>[22]</sup>



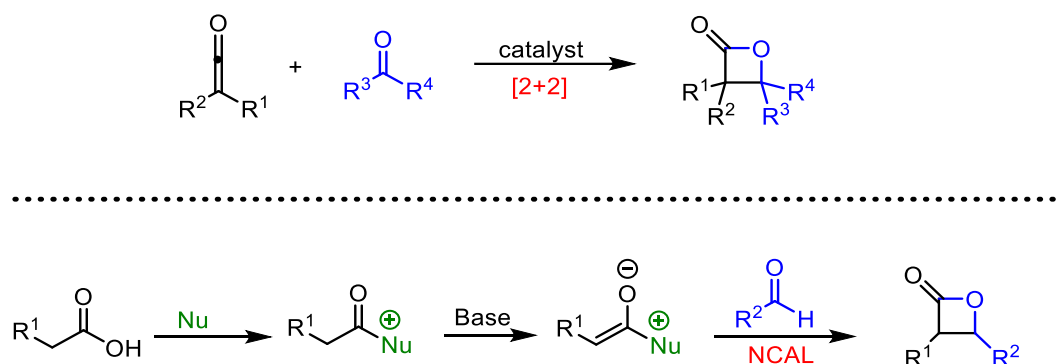
**Scheme 2. 1** – Intramolecular lactonization of (a)  $\beta$ -halocarboxylate,<sup>[18]</sup> (b)  $\beta$ -hydroxy acids,<sup>[19]</sup> (c)  $\beta$ -amino acids,<sup>[4, 20]</sup> to produce  $\beta$ -lactones.



In addition, C-C bond formation reactions based on catalysed [2+2] cycloadditions or aldol condensation were also applied to produce  $\beta$ -lactones, especially bicyclic ones.<sup>[23]</sup> Catalysed [2+2] cycloadditions of ketenes and carbonyl compounds (aldehydes or ketones) has been first realized by Staudinger and Bareza to next become convenient and popular.<sup>[24]</sup> This reaction includes the formation of  $\beta$ -lactones directly, usually in the presence of (chiral) organic or metal catalyst and sometimes with good stereoselectivity (Scheme 2. 2 – top). However, both ketenes and carbonyl compounds need to be synthesized separately, thus the total yield will be altered and it will consume time to reach the needed  $\beta$ -lactone. In addition, it is difficult to produce stable and storable ketenes. Hence, sometimes the latter are produced *in situ* and this can affect the stoichiometric ratio leading to troublesome purification.<sup>[17, 25]</sup>

The aldol condensation type reactions are essentially followed by intramolecular lactonization, they are known as nucleophilic catalysed aldol-lactonization (NACL). Concomitantly, they can provide two contiguous stereocenters leading to stereocontrolled products (Scheme 2. 2 – bottom).<sup>[6b, 26]</sup> Similarly to lactonization reactions discussed above, the yield for the final step (only  $\beta$ -lactone formation) varies from 8 to 90% depending on the substituent's functional groups.

A common deficiency of C-C methods, is the use of stoichiometric amounts of an activating agent, e.g. a base, thus a careful control of the reaction parameters is essential. Furthermore, strict control of reaction conditions and additional auxiliaries or catalysts are often needed to induce high levels of relative and absolute stereocontrol since they suffer chronically from low enantiomeric excess (*ee*'s). Hence, these attributes can be disadvantageous in terms of cost and operational simplicity.<sup>[17, 21, 23]</sup>



**Scheme 2. 2** – C-C bond formation approaches toward  $\beta$ -lactone synthesis; (top) catalyzed [2+2] cycloadditions of ketenes and aldehydes/ketones; (bottom) nucleophilic catalysed aldol-lactonization “NCAL” of aldehydes and enolates, Nu = nucleophile.<sup>[23]</sup>

Realizing the industrial importance of  $\beta$ -lactones, a simple, atom economical, and one-step ring-expansion carbonylation of epoxides to  $\beta$ -lactones has been developed in the early 2000s, as an alternative to lactonization and C-C bond formation reactions (Scheme 2. 1; Scheme 2. 2). The insertion of carbon monoxide (CO) into an epoxide, has important advantages, not only because of the nature of the reaction but also because the starting materials are typically inexpensive and are abundant feedstocks (CO and epoxides). This path has mainly become viable through the work of Alper *et al.*<sup>[27]</sup> and Coates *et al.*<sup>[28]</sup>, who have demonstrated efficient carbonylation of epoxides by a series of homogeneous catalysts constituted of a [Lewis acid]<sup>+</sup> and [Co(CO)<sub>4</sub>]<sup>-</sup>. In 2001, Alper and co-workers were the first to improve the already reported carbonylation catalyst systems such as Co<sub>2</sub>(CO)<sub>8</sub>, Co<sub>2</sub>(CO)<sub>8</sub>/pyridine, Co<sub>2</sub>(CO)<sub>8</sub>/3-hydroxypyridine, and RhCl(CO)(PPh<sub>3</sub>)<sub>2</sub>,<sup>[27, 29]</sup> that initially gave low yields of alkyl substituted  $\beta$ -lactones (15%). Practically, Alper *et al.* demonstrated an effective system based on bis(triphenylphosphine)iminium [PPN]<sup>+</sup>[Co(CO)<sub>4</sub>]<sup>-</sup>/BF<sub>3</sub>.Et<sub>2</sub>O (Figure 2. 3 – (4)) in dimethoxyethane (DME) for the preparation of simple and functionalized epoxides such as alkenyl, halide, hydroxy, and alkyl ether ones, in good-to-high yields (63–86%). The carbonylation occurred regioselectively at the unsubstituted C–O bond of the epoxide ring (less sterically encumbered).<sup>[27]</sup> It is true that [PPN]<sup>+</sup>[Co(CO)<sub>4</sub>]<sup>-</sup>/BF<sub>3</sub>.Et<sub>2</sub>O system advanced the field substantially, providing  $\beta$ -lactones with good turnover frequencies (TOF = 3.2 h<sup>-1</sup>); yet, this catalyst required a high temperature (80 °C), a high catalytic loading (2 mol %), and external additives (BF<sub>3</sub>).

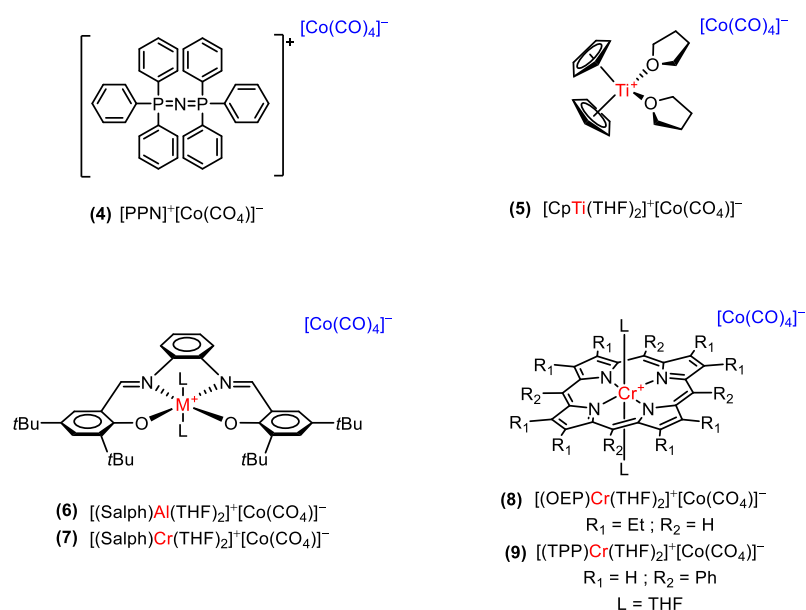
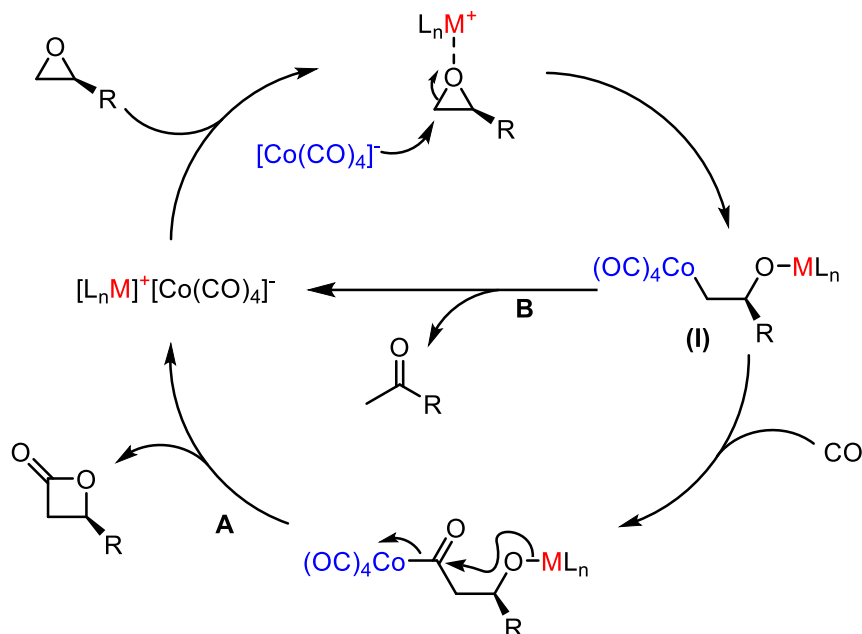


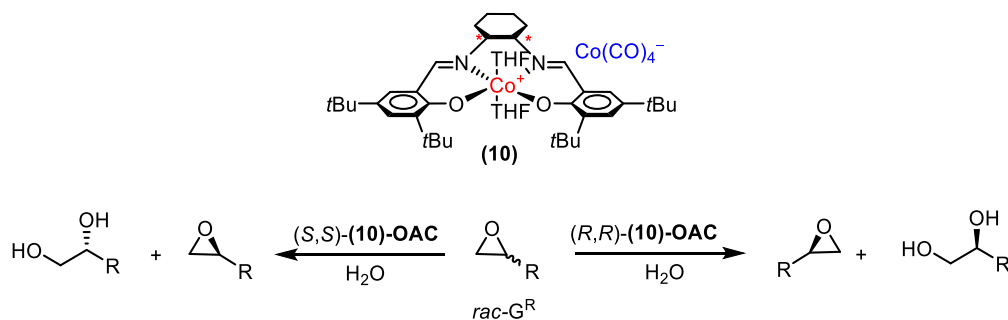
**Figure 2. 3** – Different catalyst systems reported for the carbonylation of epoxides into  $\beta$ -lactones by Alper *et al.*<sup>[27]</sup> & Coates *et al.*<sup>[28]</sup>

Later on, from 2001 to 2008, Coates *et al.* worked on improving the catalyst system into a single component, addressing a variety of epoxide substrates under milder conditions and resulting in higher yields of  $\beta$ -lactones. Taking into consideration that the active ion pair is essential in the efficiency of the epoxide carbonylation and that the carbonyl is an effective nucleophilic ligand, thus it is about modifying the cation to ultimately establish a well-defined homogeneous bimetallic complex, namely  $[(L)_nM]^+[Co(CO)_4]^-$  (Figure 2. 3 – (5)-(9)). Indeed, the efficiency of carbonylation was found to dependent on the catalyst used, with complexes (5) and (6) (Figure 2. 3) being the least efficient. They required a high temperature of 50–60 °C and a pressure of 42 bars, with reaction times within 10 h, with moderate regioselectivity regarding the attack of  $Co(CO)_4^-$  especially for sterically hindered functionalities leading to a mixture of  $\alpha$  and  $\beta$ -substituted lactones.<sup>[28a, 28b]</sup> Complexes (8) and (9) (Figure 2. 3) under the same conditions (60 °C, 42 bar) exhibited a substantially increased activity providing a TOF value of  $1670\text{ h}^{-1}$ <sup>[28c, 28d]</sup>. Ultimately, catalyst (7) revealed to be the most active and selective carbonylation catalyst reported to date for a wide range of epoxides, with excellent yields (typically > 70%). It has good functional group tolerance along with a unique efficiency even under very mild condition such as, a CO pressure as low as 1 atm, a low temperature (22 °C), a minimal catalyst loading, hence enabling a simplified product isolation and removal of trace metals.<sup>[28e, 28f]</sup> A mechanism consisting in several steps was proposed, involving: (1) the epoxide activation by the  $[Lewis\ acid]^+$  species; (2) the epoxide ring opening by  $Co(CO)_4^-$  at the less substituted carbon of the epoxide with inversion of configuration to form (I); (3) CO insertion; and (4) ring closure with configuration retention at the  $\beta$ -position, and finally the regeneration of the catalyst (Scheme 2. 3, pathway A). However, in some cases, the intermediate (I) can undergo a  $\beta$ -hydride elimination followed by the enolate protonation and tautomerization, to afford a ketone as a by-product (Scheme 2. 3, pathway B).<sup>[28]</sup> The retention of configuration at the  $\beta$ -position encouraged the synthesis of enantiopure  $\beta$ -substituted  $\beta$ -lactones through this carbonylation starting from the enantiopure related epoxide.<sup>[28]</sup>



**Scheme 2. 3** – Mechanism proposed by Coates *et al.* for the carbonylation of epoxides to β-lactone mediated by  $[(\text{L})_n\text{M}]^+[\text{Co}(\text{CO})_4]^-$  catalyst.<sup>[28]</sup>

In fact, carbonylation of enantiopure epoxides proceeds with high yields depending on the substituents (> 65%). The remaining encounter of this approach was the synthesis of the enantiopure epoxides and this can fortunately be done via the hydrokinetic resolution (HKR) reported by Jacobsen *et al.* using the chiral (salen)Co<sup>(III)</sup> complex. OAc catalyst ((*S,S*)- or (*R,R*)-(-)-*N,N*-bis (3,5-di-*tert*-butylsalicylidene)-, 2-cyclohexanediaminocobalt(II), (**10**); Scheme 2. 4). The HKR reaction has several appealing features from a practical standpoint, including the use of H<sub>2</sub>O as a reactant and low loadings (0.2–2.0 mol %) of a recyclable, commercially available catalyst. In addition, the HKR displays extraordinary scope, as a wide assortment of sterically and electronically varied epoxides can be resolved to get 99% *ee* while the minimal yield is around 35%.<sup>[30]</sup>



**Scheme 2. 4** – Hydrokinetic resolution (HKR) reaction for *rac*-epoxides to enantiopure epoxides using Jacobsen chiral catalyst (**10**).<sup>[30]</sup>

Notably, in 2013-2018, due to the effectiveness of the epoxide carbonylation method (*vide supra*), the research efforts improved the carbonylation reaction up to an industrial applicability. Hence, heterogenous catalysts based on the homogenous catalyst  $[\text{Lewis acid}]^+[\text{Co}(\text{CO})_4]^-$ , were developed. These catalysts have shown the same reactivity as the homogenous ones along with a high stability; in addition, they enable the facile product separation, reusability, and recyclability. Examples of the heterogenous catalysts include, a solid porous network based on  $\text{Al}^{\text{(III)}}$  picket fence phthalocyanine complex  $[\text{AlPc}']\text{-based porous network}^+[\text{Co}(\text{CO})_4]^-$ , polymerized tetraphenylporphyrin “TPP” chromium cobaltate complex porous organic polymer (POP $[\text{TPPCr}]^+[\text{Co}(\text{CO})_4]^-$ ), and  $\text{Co}(\text{CO})_4\text{-Cr-MIL-101}$  matrix (Figure 2. 4).<sup>[31]</sup>

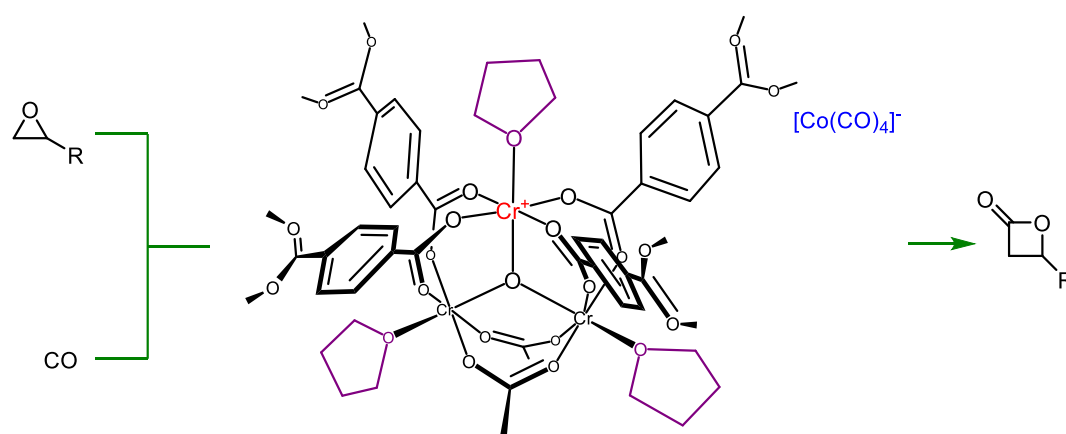


**Figure 2. 4** – Illustration of the metal cluster structure of  $\text{Co}(\text{CO})_4\text{-Cr-MIL-101}$  with coordinated THF molecules, a heterogeneous catalyst for epoxide carbonylation to β-lactones.

It is worth mentioning the newly discovered synthesis, in 2016, of β-lactones via a biochemical method in the presence of a specific enzyme named lactone synthetase or OleC. OleC was found to transform specific long ( $\text{C}_8$  and  $\text{C}_9$ ) disubstituted β-hydroxy acids with 90% conversion to β-lactones.<sup>[10]</sup> However, the exclusively long substituted compatibility to OleC leads to solubility problems. Moreover, an enzyme engineering development should be done so that the enzyme can accept a new range of short or bulky substituted chains on the β-lactones.<sup>[1c]</sup>

### 1.3. Stand and outlooks on the synthesis of $\beta$ -lactones

$\beta$ -lactones were noticed to be versatile, resourceful, and flexible precursors for multiple privileged classes of industrial compounds, especially in medicine (anti-cancer, anti-obesity, anti-inflammatory ...) and in the synthesis of bioplastics (PHAs). This prominence has stimulated the effort on their synthesis. Almost all  $\beta$ -lactones are prepared through four main routes: intramolecular lactonization, [2+2] cycloaddition, NACL, or carbonylation of epoxides. Among them, the latter requires the milder conditions, provides better yields and higher stereocontrol, offering a viable, efficient, and economical approach that is of high importance for the industry. Furthermore, carbonylation is characterized by cheap, stable and readily available diverse epoxide substrates, in contrast to the other methods for which the synthesis of the starting materials should be done and sometimes through multistep processes. Anyway, one cannot deny the importance of all the methods depending on the targeted  $\beta$ -lactone and its subsequent use. Finally, since the carbonylation of epoxides is the most practical method to produce assorted functional  $\beta$ -lactones on a multigram scale, it was the nominated approach in our work as portrayed hereafter.

## 2. Results and discussion

At this point, our interests to produce functional  $\beta$ -lactones rely on their ability in affording substituted or functional PHAs (Figure 2. 2 – (f)), through ROP. Thus, previously known and innovative *racemic* and enantiopure  $\beta$ -lactone monomers carrying various exocyclic (thio)ether functionalities, represented by  $\text{BPL}^{\text{FGs}}$  ( $\text{FG} = \text{OAlI}$ ,  $\text{O}^n\text{Bu}$ ,  $\text{OBn}$ ,  $\text{OTBDMS}$ ,  $\text{OPh}$ ,  $\text{SPh}$ ,  $\text{SBn}$ ,  $\text{O}^i\text{Pr}$ ,  $\text{O}^t\text{Bu}$ ,  $\text{OP}(\text{O})\text{Ph}_2$ ,  $\text{NBn}_2$ ), are synthesized from their related racemic and enantiopure epoxides ( $\text{G}^{\text{FGs}}$ ), respectively. The choice of these specific functional groups “FGs” is discussed in each of Chapter 3 and 4. The targeted substituted  $\beta$ -lactones investigated in my work as monomers are abbreviated or represented as shown in Figure 2. 5.

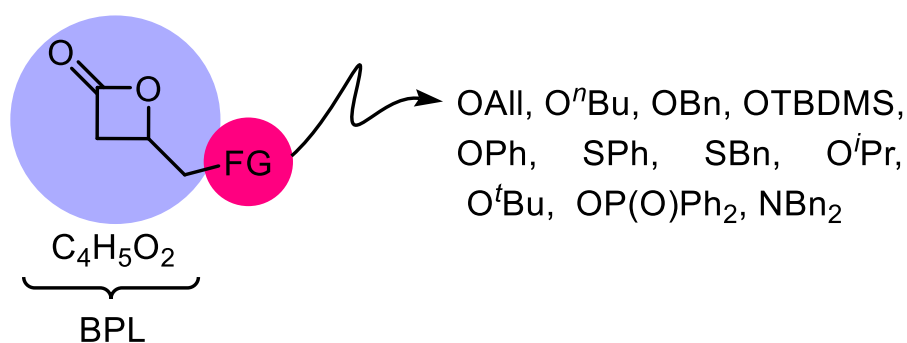
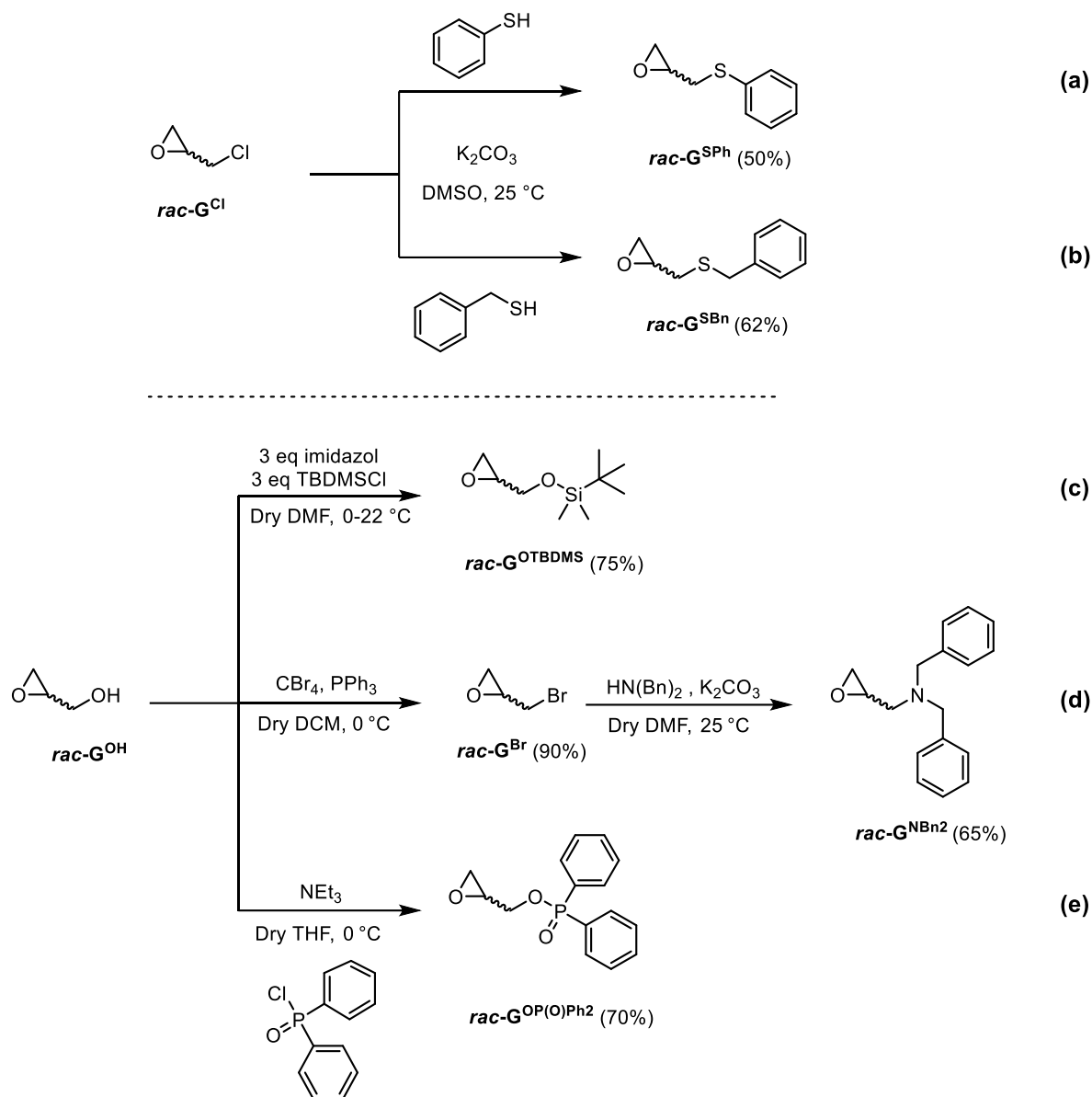


**Figure 2. 5** – Abbreviations of the targeted substituted  $\beta$ -lactones investigated in my work.

## 2.1. Synthesis and characterization of *racemic* and enantiopure functional epoxides “G<sup>FGs</sup>”

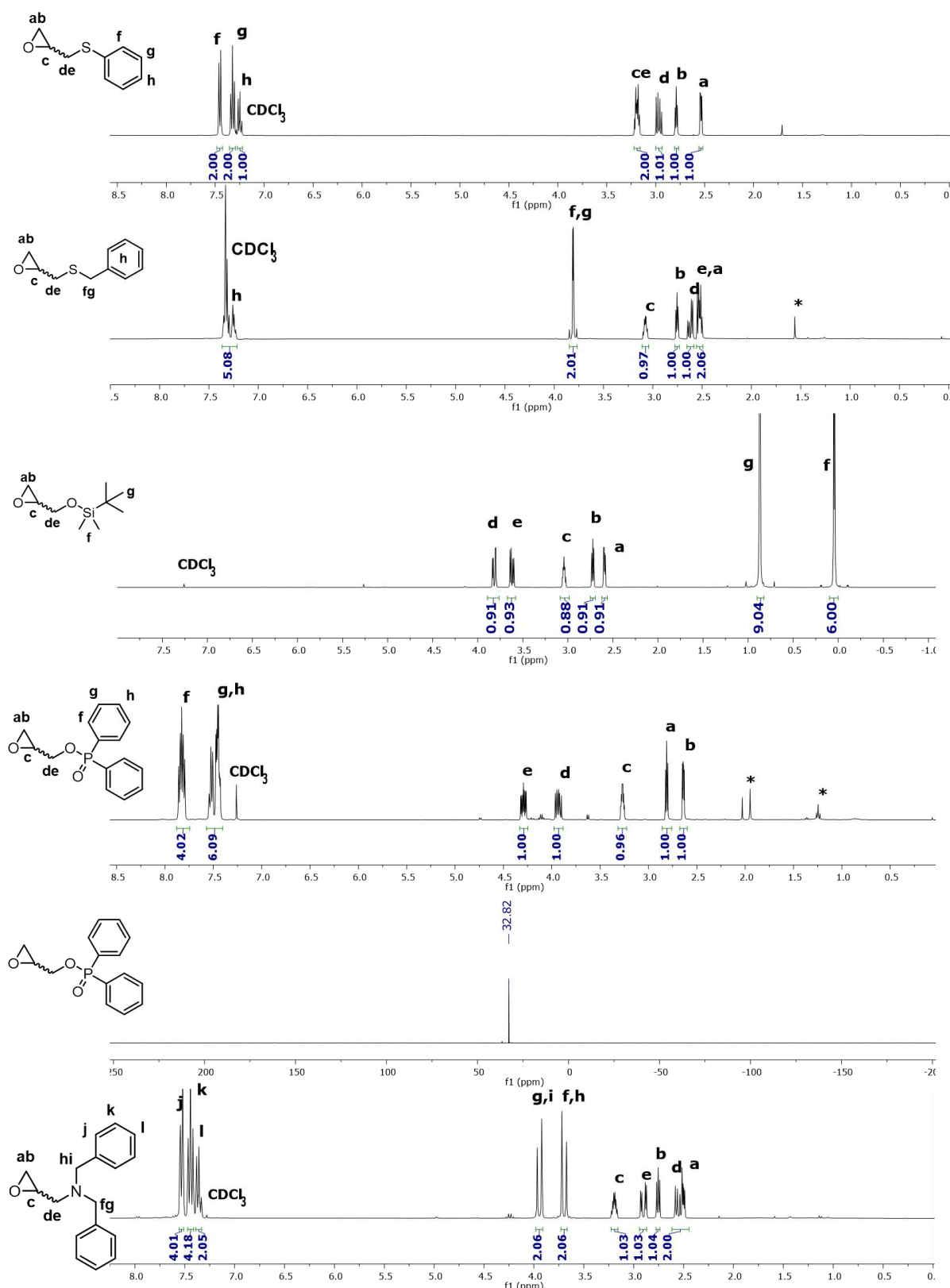
As previously mentioned, most racemic epoxides are commercially accessible. However, for our chosen functionalities, some (*i.e.*, *rac*-G<sup>FGs</sup>; FG = SPh, SBn, OTBDMS, OP(O)Ph<sub>2</sub>, NBn<sub>2</sub>) were not available and their synthesis was established. Epoxides carrying thiol moieties, namely *rac*-G<sup>SPh</sup> and *rac*-G<sup>SBn</sup>, were synthesised in DMSO at room temperature, using an electrophilic *racemic* epoxide (1.2 equivalent of epichlorohydrin; *rac*-G<sup>Cl</sup>) in the presence of excess base (K<sub>2</sub>CO<sub>3</sub>) and phenylthiol or benzyl thiol, respectively (Scheme 2. 5 – (a) & (b)). Both *rac*-G<sup>OTBDMS</sup> and *rac*-G<sup>OP(O)Ph<sub>2</sub></sup> were synthesized through a S<sub>N</sub>2 reaction type, starting from *racemic* glycidol (*rac*-G<sup>OH</sup>) and 3 equivalents of *tert*-butylchlorodimethylsilane (ClTBDMS) or 1.2 equivalent of diphenylphosphinic chloride (ClP(O)Ph<sub>2</sub>), respectively (Scheme 2. 5 – (c) & (e)). *rac*-G<sup>NBn<sub>2</sub></sup> was also synthesized starting from *rac*-G<sup>OH</sup>, that was converted to the more reactive epibromohydrin (*rac*-G<sup>Br</sup>) through Apple reaction. Then 1.4 equivalent of *rac*-G<sup>Br</sup> was mixed with dibenzylamine and K<sub>2</sub>CO<sub>3</sub> to end with *rac*-G<sup>NBn<sub>2</sub></sup> through the ring opening of *rac*-G<sup>Br</sup> followed by S<sub>N</sub>2 reaction type (Scheme 2. 5 – (d)).



**Scheme 2. 5** – Synthesis of  $\text{rac-G}^{\text{FGs}}$  (FG = SPh, SBn, OTBDMS, OP(O)Ph<sub>2</sub>, NBn<sub>2</sub>) from commercially available epoxides; the final isolated yields are given in parentheses (%).

The produced  $\text{rac-G}^{\text{FGs}}$  (FG = SPh, SBn, OTBDMS, OP(O)Ph<sub>2</sub>, NBn<sub>2</sub>) were analysed by <sup>1</sup>H and <sup>31</sup>P (in the case of FG = OP(O)Ph<sub>2</sub>) nuclear magnetic resonance “NMR”, after being purified by column chromatography and before being used in the subsequent carbonylation reaction (Figure 2. 6). The <sup>1</sup>H NMR clearly display the methine (ranged from  $\delta$  3–3.27 ppm) and methylene (ranged from  $\delta$  2.4–4.27 ppm) for each of the  $\text{rac-G}^{\text{FGs}}$  (refer to experimental section; *vide infra*).

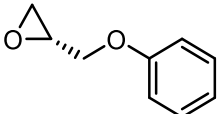
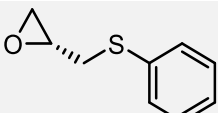
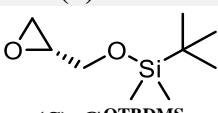
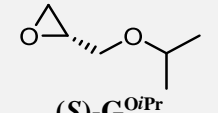
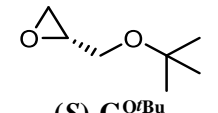




**Figure 2. 6** –  $^1\text{H}$  NMR and  $^{31}\text{P}$  NMR spectra (400 MHz,  $\text{CDCl}_3$ , 23  $^\circ\text{C}$ ) of *rac*- $\text{G}^{\text{FG}}$ s; FG = SPh, SBn, OTBDMS,  $\text{OP}(\text{O})\text{Ph}_2$ ,  $\text{NBN}_2$  (\*: residual solvents (ethyl acetate) or water and acetone from the deuterated solvent).

The synthesis of enantiopure (*S*)-G<sup>FG</sup>s (FG = OPh, SPh, OTBDMS, O<sup>i</sup>Pr, O<sup>t</sup>Bu) was performed through HKR reaction starting from their related *racemic* epoxides (*rac*-G<sup>FG</sup>s (FG = OPh, SPh, OTBDMS, O<sup>i</sup>Pr, O<sup>t</sup>Bu)). HKR was performed using 5% Jacobsen chiral catalyst ((*R,R*)-(10)) in the presence of 2% acetic acid (HOAc) and 50% water (**Scheme 2. 4**). The produced (*S*)-G<sup>FG</sup> were separated by distillation from their associated formed diols, and then characterized by NMR (Appendix 1), chiral high performance liquid chromatography (HPLC) or chiral gas chromatography (GC) depending on the pendent substituent (Table 2. 1).

**Table 2. 1** – Yield and enantiopurity of the isolated (*S*)-G<sup>FG</sup>s (FG = OPh, SPh, OTBDMS, O<sup>i</sup>Pr, O<sup>t</sup>Bu).

( <i>S</i> )-G <sup>FG</sup> s	Yield (%)	Enantiopurity (%)
 ( <i>S</i> )-G <sup>OPh</sup>	43.33	99.97 by HPLC
 ( <i>S</i> )-G <sup>SPh</sup>	42	99.87 by HPLC
 ( <i>S</i> )-G <sup>OTBDMS</sup>	39.8	97.53 by GC
 ( <i>S</i> )-G <sup>O<sup>i</sup>Pr</sup>	42.4	97.6 by GC
 ( <i>S</i> )-G <sup>O<sup>t</sup>Bu</sup>	41.7	99.43 by GC

The illustrative HPLC spectra for 99.97% (*S*)-G<sup>OPh</sup> and 99.87% (*S*)-G<sup>SPh</sup> are given in Figure 2. 7, while GC spectra for 99.97% (*S*)-G<sup>OTBDMS</sup>, 97.6% (*S*)-G<sup>O<sup>i</sup>Pr</sup> and 99.43% (*S*)-G<sup>O<sup>t</sup>Bu</sup> are gathered in appendices (Appendix 2,3).

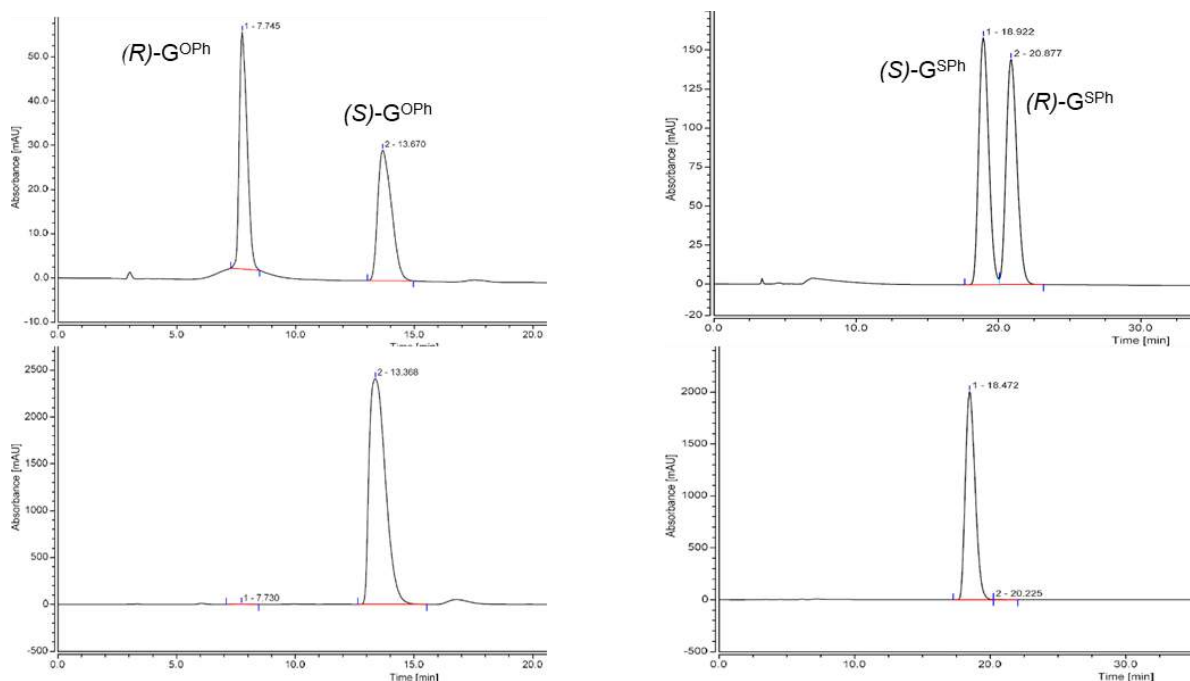
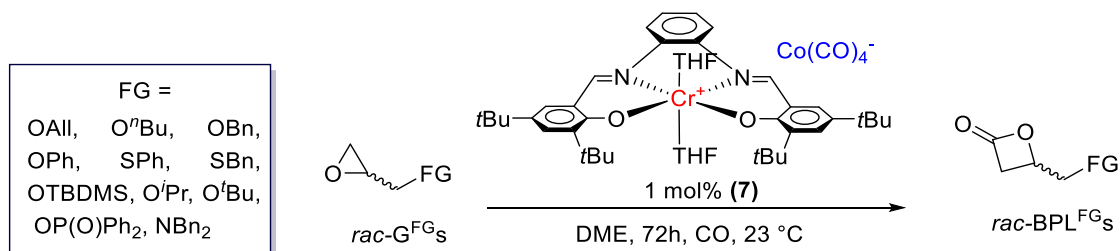


**Figure 2. 7** – Chiral HPLC chromatogram (column Chiralcel-OD DAICEL; 250 mm  $\times$  4.6 mm, 5  $\mu$ m; 20  $^{\circ}$ C with a UV detector at 214 nm) of: (left-top) *racemic* phenyl glycidyl ether (*rac*-G<sup>OPh</sup>); (left-bottom) 99.97 % enantiopure (*S*)-phenyl glycidyl ether ((*S*)-G<sup>OPh</sup>); (right-top) *racemic* 2-((phenylthio)methyl)oxirane (*rac*-G<sup>SPh</sup>), and (right-bottom) 99.87% enantiopure (*S*)-2-((phenylthio)methyl)oxirane ((*S*)-G<sup>SPh</sup>)).

## 2.2. Synthesis and characterization of *racemic* and enantiopure functional $\beta$ -lactones “BPL<sup>FG</sup>s”

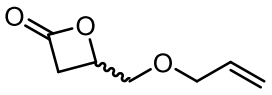
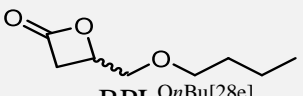
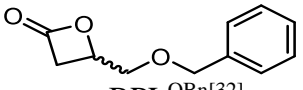
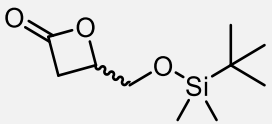
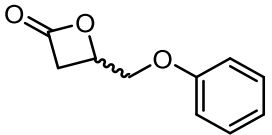
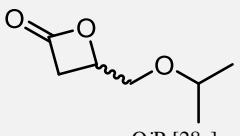
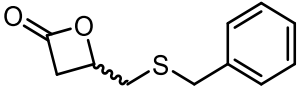
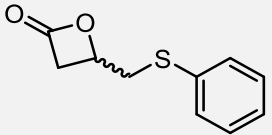
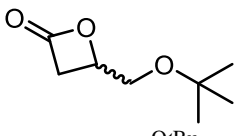
As aforementioned, the carbonylation reaction of *racemic* epoxide to *racemic*  $\beta$ -lactone is an efficient and simple approach, and catalyst (**7**) showed to be the most effective (Figure 2. 3). Therefore, the first attempt to synthesize our targeted *rac*-BPL<sup>FG</sup>s (FG = OAll, O<sup>*n*</sup>Bu, OBn, O<sup>*n*</sup>Ph, SPh, SBn, O<sup>*i*</sup>Pr, O<sup>*t*</sup>Bu, OP(O)Ph<sub>2</sub>, NBn<sub>2</sub>), was done by means of 1 mol% (**7**) in dry DME at room temperature in the presence of 40 bar CO (**Scheme 2. 6**).

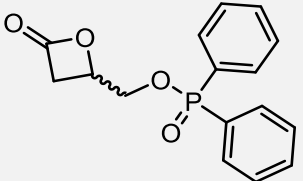
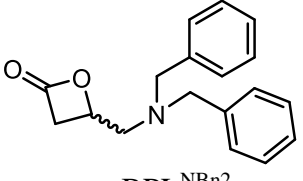


**Scheme 2. 6** – Synthesis of *rac*-BPL<sup>FG</sup>s (FG = OAll, O<sup>*n*</sup>Bu, OBn, OTBDMS, OPh, SPh, SBn, O<sup>*i*</sup>Pr, O<sup>*t*</sup>Bu, OP(O)Ph<sub>2</sub>, NBn<sub>2</sub>) by carbonylation of *rac*-G<sup>FG</sup>s promoted by catalyst (**7**).

Remarkably, some of the synthesised *rac*-BPL<sup>FGs</sup> are novel (never synthesized before) and other are known. Conversions of *rac*-G<sup>FGs</sup> during carbonylation manipulation and *rac*-BPL<sup>FGs</sup> final isolated yields after purification are gathered in Table 2. 2.

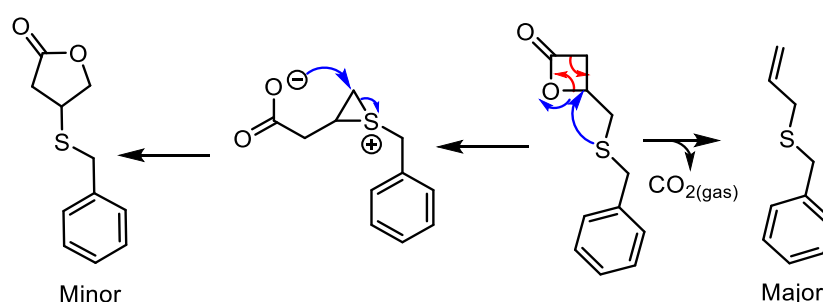
**Table 2. 2** – Conversion of *rac*-G<sup>FGs</sup> and final isolated yields for each synthesized *rac*-BPL<sup>FGs</sup> through carbonylation reaction catalysed by (7).

	$\beta$ -Lactone (BPL <sup>FGs</sup> )	Conversion (%)	Yield (%)
KNOWN BPL <sup>FGs</sup>	 <i>rac</i> -BPL <sup>OAl[28e]</sup>	100	79
	 <i>rac</i> -BPL <sup>OnBu[28e]</sup>	100	82
	 <i>rac</i> -BPL <sup>OBn[32]</sup>	100	62
	 <i>rac</i> -BPL <sup>OTBDMS[28e]</sup>	100	60
	 <i>rac</i> -BPL <sup>OPh[32]</sup>	100	75
	 <i>rac</i> -BPL <sup>OiPr[28e]</sup>	100	65
NOVEL BPL <sup>FGs</sup>	 <i>rac</i> -BPL <sup>SBn</sup>	100	86 to 0
	 * <i>rac</i> -BPL <sup>SPh</sup>	100	51
	 <i>rac</i> -BPL <sup>OrBu</sup>	100	64

	0	0
<i>rac</i> -BPL <sup>OPOPh<sub>2</sub></sup>		
	0	0
<i>rac</i> -BPL <sup>NBn<sub>2</sub></sup>		

\**rac*-BPL<sup>SPh</sup> was synthesized by radical reaction in the 1980s as an intermediate *in situ*, but never been isolated and characterized.<sup>[33]</sup>

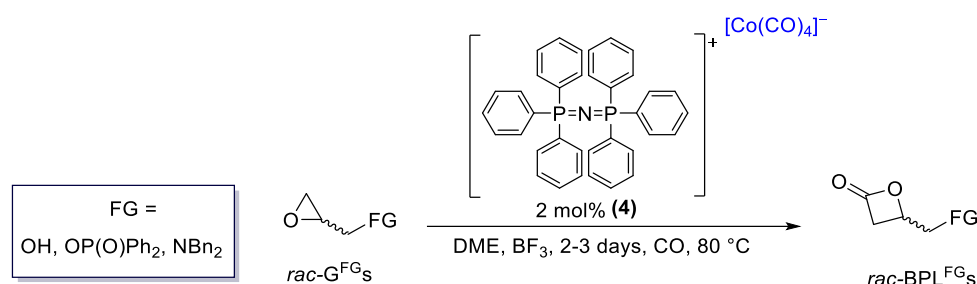
As seen from Table 2. 2, known *rac*-BPL<sup>FG</sup>s were successfully synthesized with good isolated yields (50-82%; similar to those reported), however for the novel ones, only *rac*-BPL<sup>SPh</sup> and *rac*-BPL<sup>OrBu</sup> were successfully obtained with 100% *rac*-G<sup>SPh</sup> and *rac*-G<sup>OrBu</sup> conversions and good isolated yields (51, 64%, respectively). On the other hand, *rac*-G<sup>SBn</sup> was completely consumed (100%) given yet a good *rac*-BPL<sup>SBn</sup> yield (86%); however, upon purification (column and distillation at 120 °C) all the product was converted to other unsought side products. It was deduced that *rac*-BPL<sup>SBn</sup> is unstable, as it undergoes elimination and rearrangement reactions as soon as it is formed during carbonylation and purification processes (Scheme 2. 7; refer to the NMR, Appendix 4). No further attempt was made to synthesise *rac*-BPL<sup>SBn</sup>.



**Scheme 2. 7** – Major and minor side-products detected by <sup>1</sup>H NMR resulting from (right-red) decarboxylation and (left-blue) rearrangement of *rac*-BPL<sup>SBn</sup> that appears during the carbonylation and distillation.

Finally, and unexpectedly, neither of *rac*-G<sup>OP(O)Ph<sub>2</sub></sup> or *rac*-G<sup>NBn<sub>2</sub></sup> was able to be converted into the corresponding *rac*-BPL<sup>OP(O)Ph<sub>2</sub></sup> or *rac*-BPL<sup>NBn<sub>2</sub></sup> in the presence of (7) (Table 2. 2). Consequently, other approaches were studied for the synthesis of *rac*-BPL<sup>OP(O)Ph<sub>2</sub></sup> and *rac*-BPL<sup>NBn<sub>2</sub></sup>. For instance, reactions of *rac*-BPL<sup>OH</sup> (Table 2. 3 – entry 1) with ClP(O)Ph<sub>2</sub> (mimicking that of Scheme 2. 5 – (e)) in different conditions (in dry THF; absence or presence

of base such as  $\text{NEt}_3$  or  $\text{K}_2\text{CO}_3$ ; different temperature 23,  $-72\text{ }^\circ\text{C}$ ) were performed, expecting to obtain  $\text{rac-BPL}^{\text{OP(O)Ph}_2}$ . Yet, all attempts failed, leading instead to the opening of  $\text{rac-BPL}^{\text{OH}}$  or to no reaction. Note that  $\text{rac-BPL}^{\text{OH}}$  was produced successfully by carbonylation of  $\text{rac-G}^{\text{OH}}$  only in the presence of 2mol%  $[\text{PPN}]^+[\text{Co}(\text{CO})_4]^-/\text{BF}_3\cdot\text{Et}_2\text{O}$  (Figure 2. 3 – (4)) at  $80\text{ }^\circ\text{C}$  and 60 bar  $\text{CO}_{(\text{g})}$  while it failed in the presence of catalyst (7).<sup>[27]</sup> In this manner, under the same latter conditions (2mol%  $[\text{PPN}]^+[\text{Co}(\text{CO})_4]^-/\text{BF}_3\cdot\text{Et}_2\text{O}$ , at  $80\text{ }^\circ\text{C}$  and 60 bar CO), the carbonylation of  $\text{rac-G}^{\text{OP(O)Ph}_2}$  and  $\text{rac-G}^{\text{NBn}_2}$  were performed (Scheme 2. 8).



**Scheme 2. 8** – Synthesis of  $\text{rac-BPL}^{\text{FGs}}$  (FG = OH, OP(O)Ph<sub>2</sub>, NBn<sub>2</sub>) by carbonylation of the corresponding  $\text{rac-G}^{\text{FGs}}$  promoted by catalyst (4).

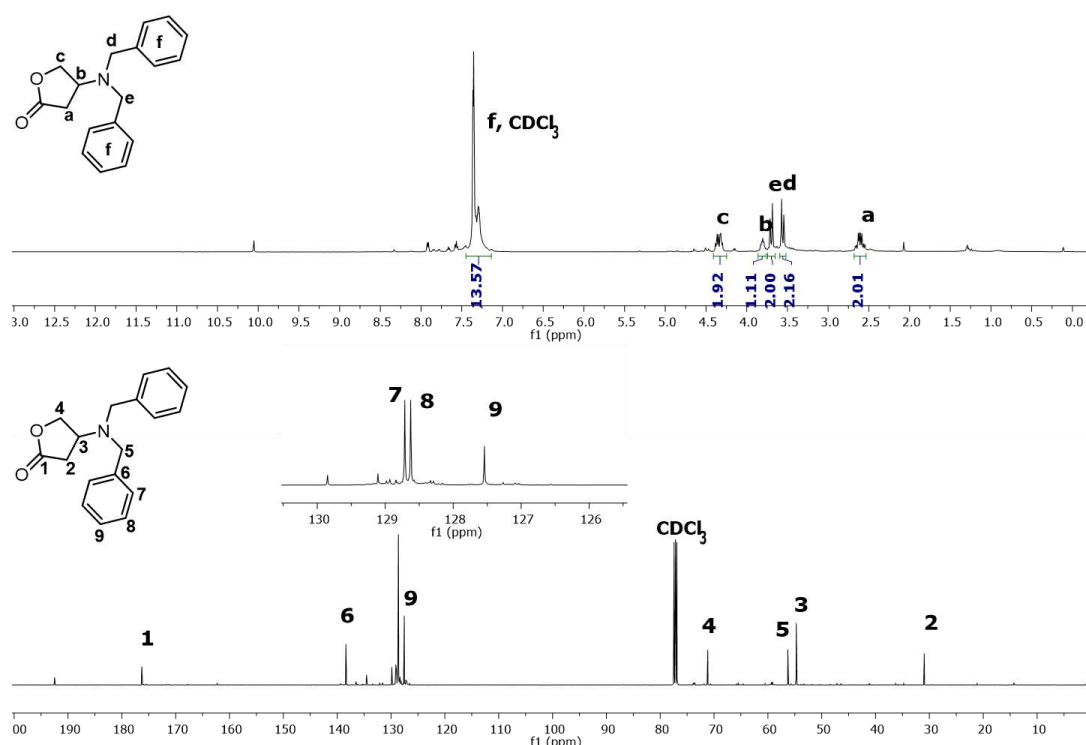
Interestingly,  $\text{rac-BPL}^{\text{OP(O)Ph}_2}$  was obtained effectively with 60% isolated yield (Table 2. 3 – entry 2), while  $\text{rac-BPL}^{\text{NBn}_2}$  revealed to be a little trickier. Despite that, using (4), all the  $\text{rac-G}^{\text{NBn}_2}$  was consumed unlike the reaction with (7), yet still, it afforded the corresponding five membered  $\gamma$ -lactone, namely 4-(dibenzylamino)dihydrofuran-2(3H)-one ( $\text{rac-GPL}^{\text{NBn}_2}$ ), instead of the targeted  $\text{rac-BPL}^{\text{NBn}_2}$  (Table 2. 3 – entry 3).

**Table 2. 3** –  $\text{rac-G}^{\text{FGs}}$  conversions and isolated yields for each of the synthesized  $\text{rac-BPL}^{\text{FGs}}$  through carbonylation reaction promoted by (4).<sup>[27]</sup>

Entry	$\beta$ -Lactone (BPL <sup>FGs</sup> )	Conversion (%)	Yield (%)
1*	 $\text{rac-BPL}^{\text{OH}}$	100	76
2	 $\text{rac-BPL}^{\text{OP(O)Ph}_2}$	100	60
3	 $\text{rac-BPL}^{\text{NBn}_2}$	100	0

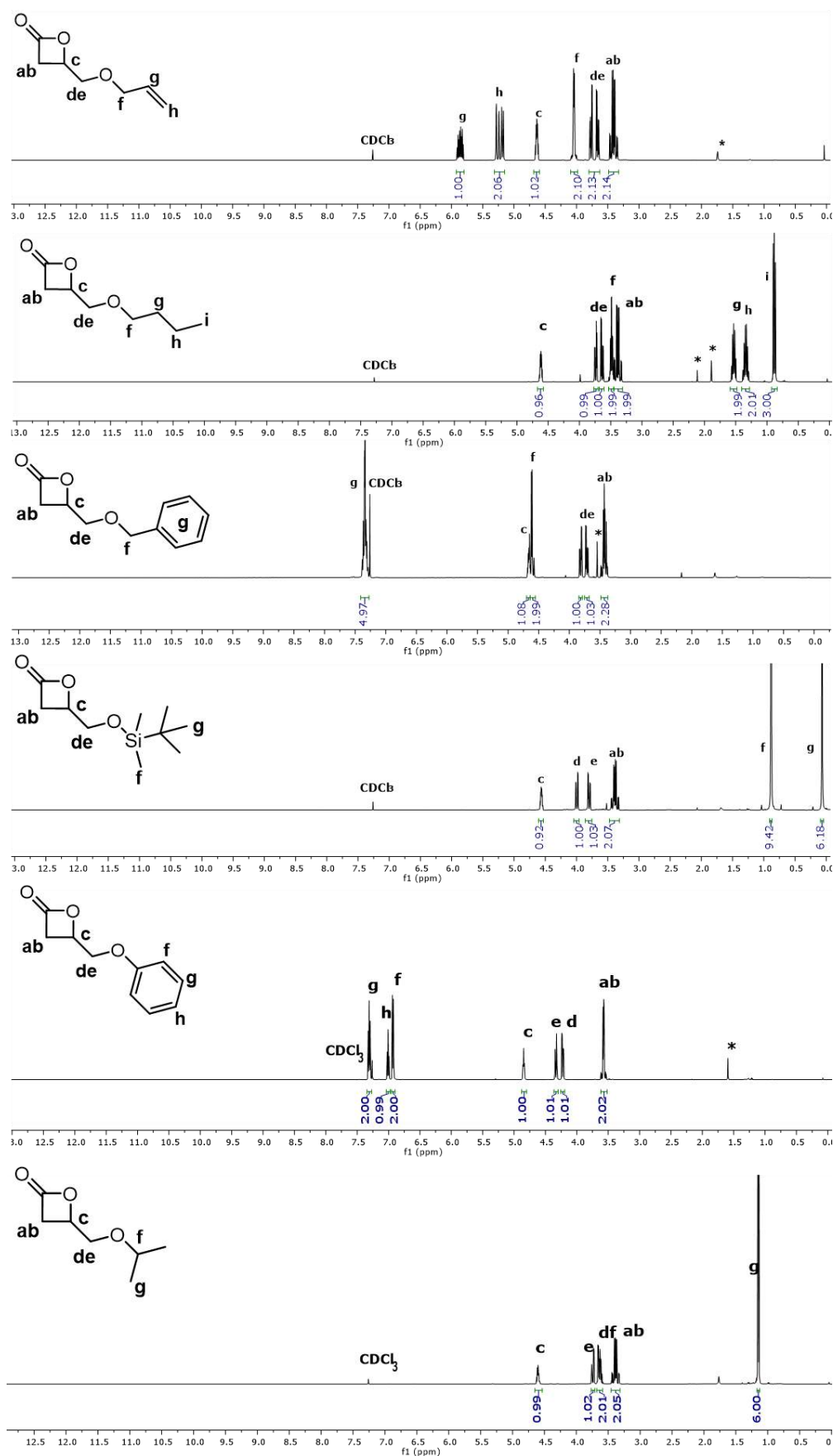
\*For  $^1\text{H}$  and  $^{13}\text{C}$  NMR of  $\text{rac-BPL}^{\text{OH}}$  refer to appendices (Appendix 5).

The observed *rac*-GPL<sup>NBn2</sup> may result from either the presence of the Lewis acid BF<sub>3</sub> that can catalyse this rearrangement (Figure 2. 2 – (d)), the high temperature in the reaction medium (80 °C), long reaction time (2-3 days), and/or the high nucleophilicity of the nitrogen atom (in *rac*-BPL<sup>NBn2</sup>), all possibly inducing the expansion of the ring (Scheme 2. 7 – left). Anyhow, only two attempts to prepare *rac*-BPL<sup>NBn2</sup> were made, and further experimentation will be carried out in our laboratory. The <sup>1</sup>H and <sup>13</sup>C NMR data of the produced *rac*-GPL<sup>NBn2</sup> are depicted in Figure 2. 8.



**Figure 2. 8** – <sup>1</sup>H NMR (400 MHz, CDCl<sub>3</sub>, 25 °C) (top) and <sup>13</sup>C (100 MHz, CDCl<sub>3</sub>, 25 °C) (bottom) spectra of *racemic* 4-(dibenzylamino)dihydrofuran-2(3H)-one (*rac*-GPL<sup>NBn2</sup>) formed from the carbonylation of *rac*-G<sup>NBn2</sup> in the presence of (**4**).

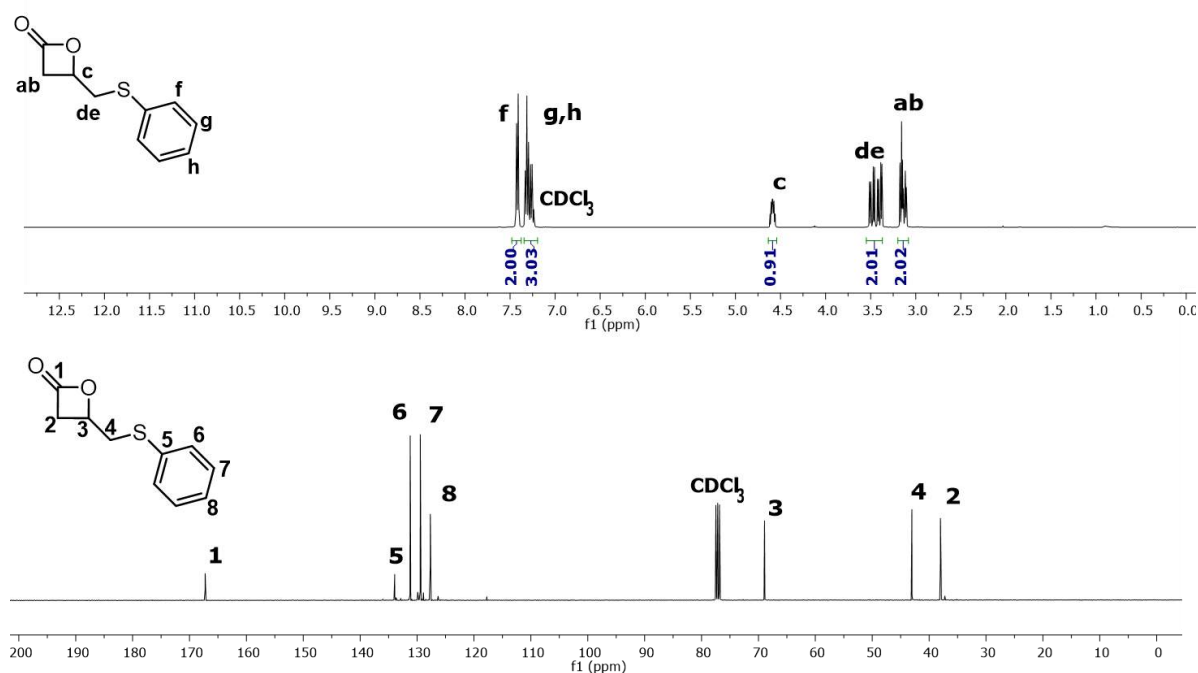
The successful preparation of all the isolated known and original *rac*-BPL<sup>FG</sup>s (FG = OAll, O<sup>n</sup>Bu, OBn, OTBDMS, OPh, O<sup>i</sup>Pr) were supported by <sup>1</sup>H NMR analyses which agreed with literature reports (Figure 2. 9). The <sup>1</sup>H NMR demonstrated methine signals of the latter *rac*-BPL<sup>FG</sup>s (δ 4.61–4.85 ppm; refer to experimental section – *vide infra*), that are more deshielded than their corresponding epoxides (*rac*-G<sup>FG</sup>s).



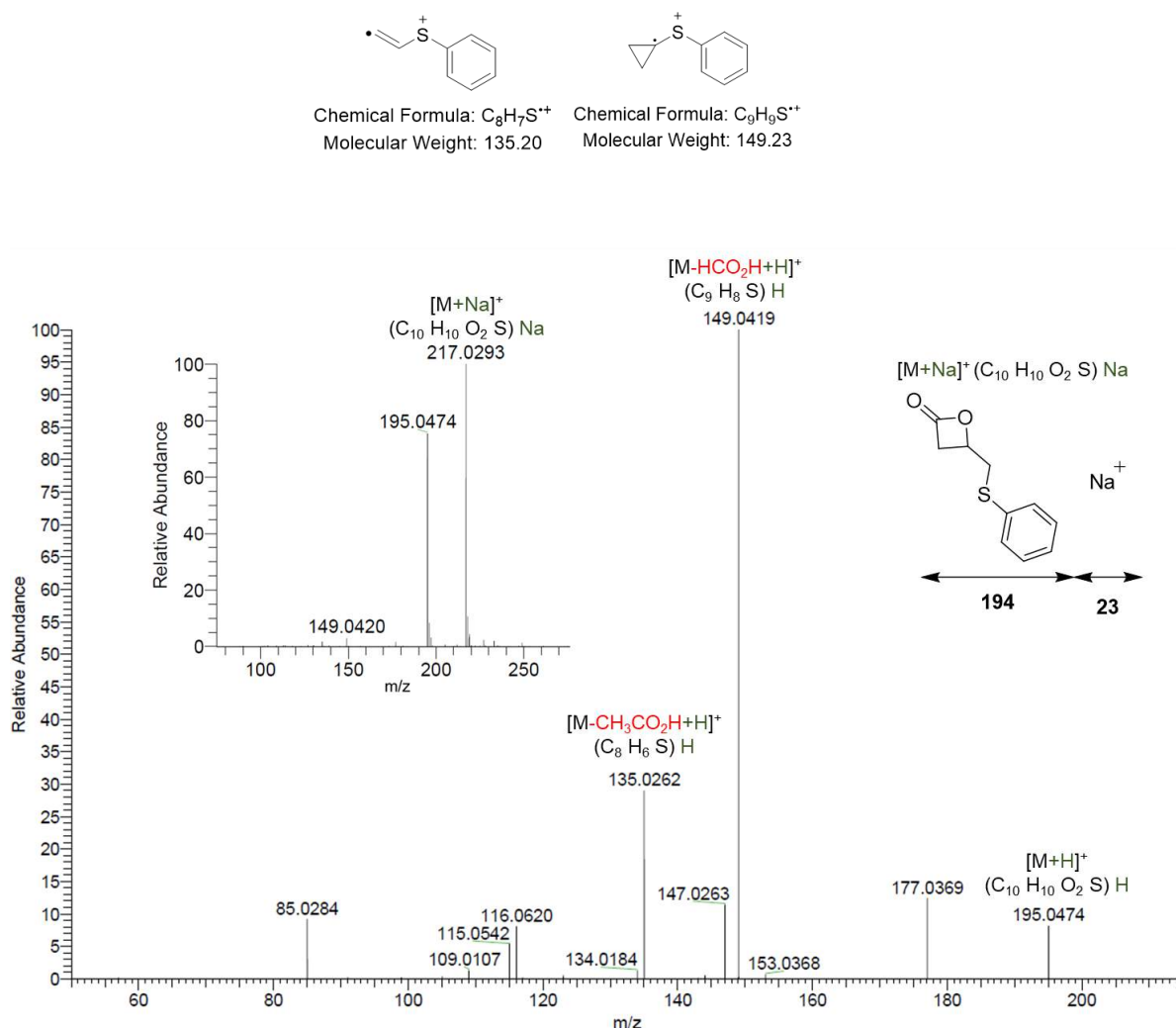
**Figure 2. 9** –  $^1\text{H}$  (500 MHz,  $\text{CDCl}_3$ , 23  $^\circ\text{C}$ ) NMR of isolated *rac*-BPL<sup>FG</sup>s; (from top to bottom): *rac*-BPL<sup>OAll</sup>, *rac*-BPL<sup>nBu</sup>, *rac*-BPL<sup>OBn</sup>, *rac*-BPL<sup>OTBDM</sup>, *rac*-BPL<sup>O<sup>Ph</sup></sup>, *rac*-BPL<sup>O<sup>iPr</sup></sup>; \* residual DME solvent or water from the  $\text{CDCl}_3$ .



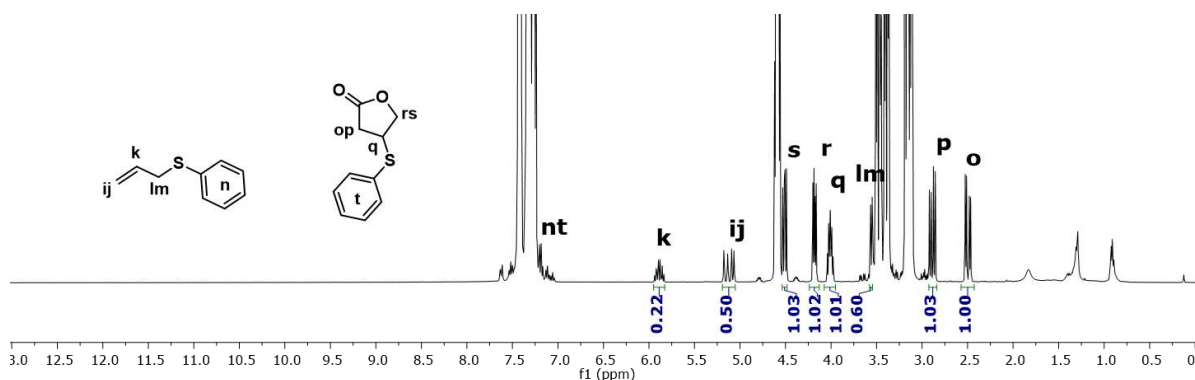
Additional characterization was done for the novel *rac*-BPL<sup>FG</sup>s (FG = SPh, O<sup>t</sup>Bu, OP(O)Ph<sub>2</sub>) to confirm their structure. Both *rac*-BPL<sup>SPh</sup> and *rac*-BPL<sup>O<sup>t</sup>Bu</sup> were characterized by <sup>1</sup>H/<sup>13</sup>C NMR (Figure 2. 10 & Figure 2. 13, respectively), 2D COSY/HMBC and Electrospray Ionization Mass Spectrometry “ESI-MS” (Figure 2. 11 & Figure 2. 14, respectively). Moreover, a stability study was done for *rac*-BPL<sup>SPh</sup> in particular, due to its structure similarity with the unstable *rac*-BPL<sup>SBn</sup> (*vide supra*). Indeed, *rac*-BPL<sup>SPh</sup> was found to act similarly to *rac*-BPL<sup>SBn</sup> (Scheme 2. 7) after storage at – 30 °C for a couple of days (Figure 2. 12), yet with a higher stability than that of *rac*-BPL<sup>SBn</sup>. Consequently, *rac*-BPL<sup>SPh</sup> was handled carefully during its purification (refer to the experimental section, *vide infra*) and used directly after its synthesis. Analysis of *rac*-BPL<sup>OP(O)Ph<sub>2</sub></sup> by <sup>1</sup>H/<sup>13</sup>C/<sup>31</sup>P NMR, 2D COSY/HMBC (Appendix 7,8), ESI, and X-ray crystallography (XRC) (Figure 2. 15 to Figure 2. 17) confirmed its structure and purity.



**Figure 2. 10** – <sup>1</sup>H NMR (400 MHz, CDCl<sub>3</sub>, 25 °C) (top) and <sup>13</sup>C (100 MHz, CDCl<sub>3</sub>, 25 °C) (bottom) spectra of *racemic* 4-(phenylthio)methylene-β-propiolactone (*rac*-BPL<sup>SPh</sup>).



**Figure 2. 11** – ESI-MS (ionized by  $Na^+$ , solvent  $CH_2Cl_2/CH_3OH$  (95/5 v:v)) of freshly synthesized *racemic* 4-(phenylthio)methylene- $\beta$ -propiolactone, *rac*-BPL<sup>SPh</sup> and ESI-MS/MS of  $[M+H]^+$   $m/z$  195 with a collision energy of 10 eV. The zoomed region shows the peak corresponding to  $[(COCH_2CH(CH_2SC_6H_5)O)H] \cdot Na^+$  ( $m/z = 217.0293$ ). The two other fragmentation products depicted in red correspond to the loss of  $CH_2CO$  ( $m/z$  149), and to the subsequent loss of  $CH_2$  from the latter ( $m/z$  135), or to the loss of  $CH_2CH_2CO$  from the monomer during the analysis, respectively.



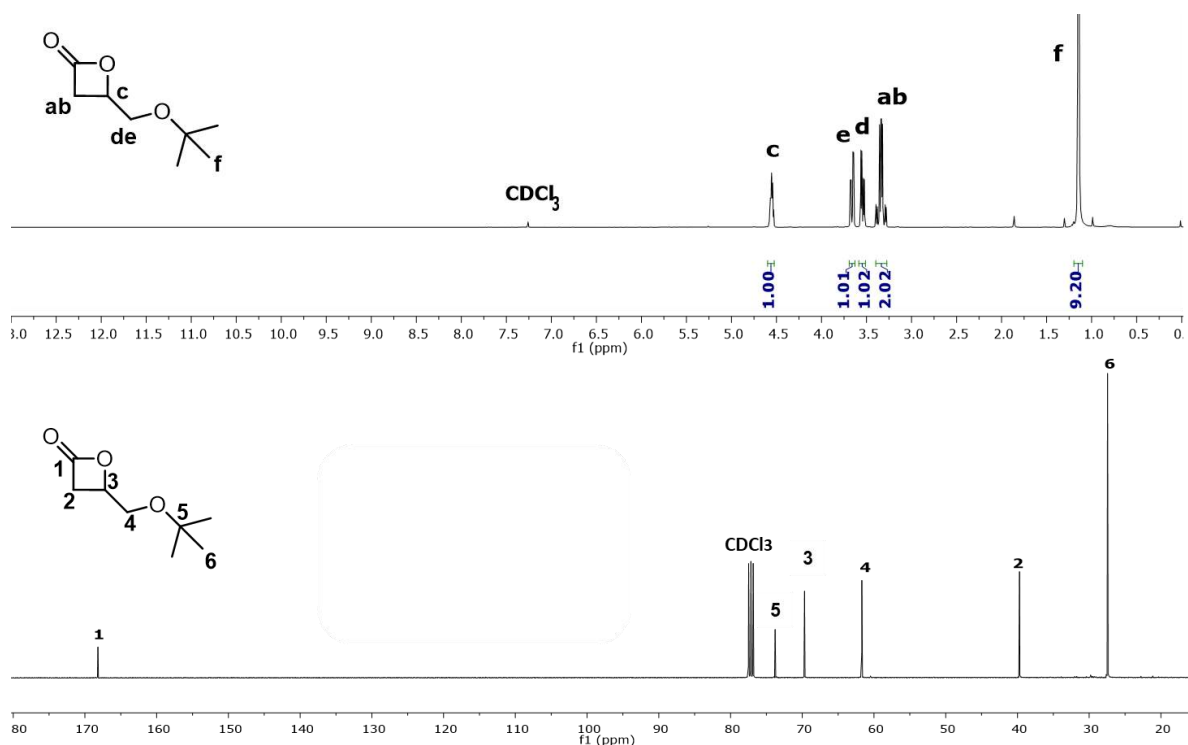


**Figure 2.13** –  $^1\text{H}$  NMR (400 MHz,  $\text{CDCl}_3$ , 25 °C) (top) and  $^{13}\text{C}$  (100 MHz,  $\text{CDCl}_3$ , 25 °C) (bottom) spectra of *racemic* 4-(*tert*-butoxymethyl)oxetan-2-one (*rac*-BPL<sup>OrBu</sup>).

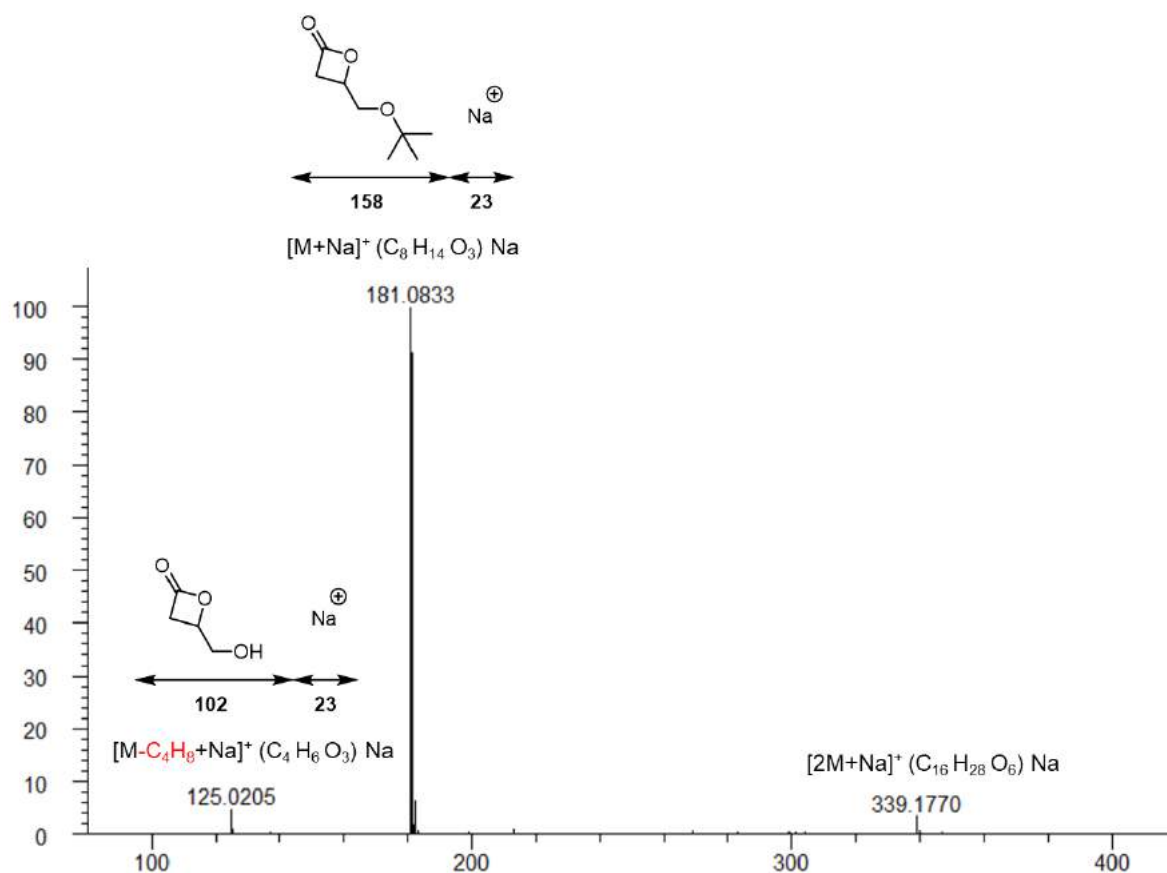


**Figure 2.14** – ESI-MS (ionized by  $\text{Na}^+$ , solvent  $\text{CH}_3\text{OH}$ ) of freshly synthesized *racemic* 4-(*tert*-butoxymethyl)oxetan-2-one (*rac*-BPL<sup>OrBu</sup>) showing the peak corresponding to

$[(\text{COCH}_2\text{CH}(\text{CH}_2\text{OC}_4\text{H}_9)\text{O})]\text{Na}^+$  ( $m/z = 181.0833$ ). The fragmentation product depicted in the bottom left corresponds to the loss of  $\text{C}_4\text{H}_9$  ( $m/z = 125.0205$ ) during the analysis.

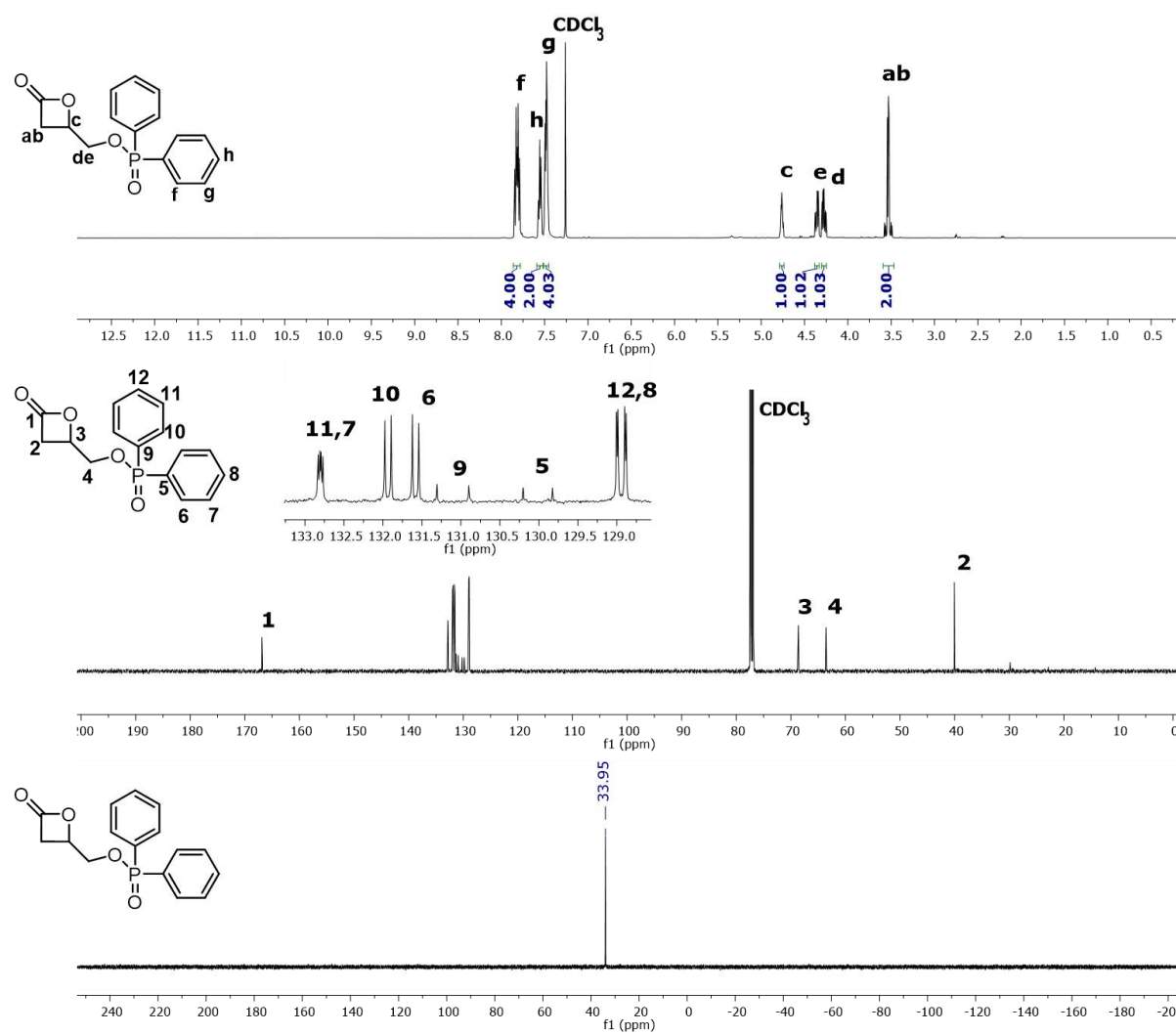


**Figure 2. 15** – <sup>1</sup>H NMR (500 MHz, CDCl<sub>3</sub>, 25 °C) (top), <sup>13</sup>C (125 MHz, CDCl<sub>3</sub>, 25 °C) (middle), and <sup>31</sup>P (125 MHz, CDCl<sub>3</sub>, 25 °C) (bottom) spectra of *racemic* (4-oxooxetan-2-yl) methyl diphenylphosphinate (*rac*-BPL<sup>OP(O)Ph<sub>2</sub></sup>).

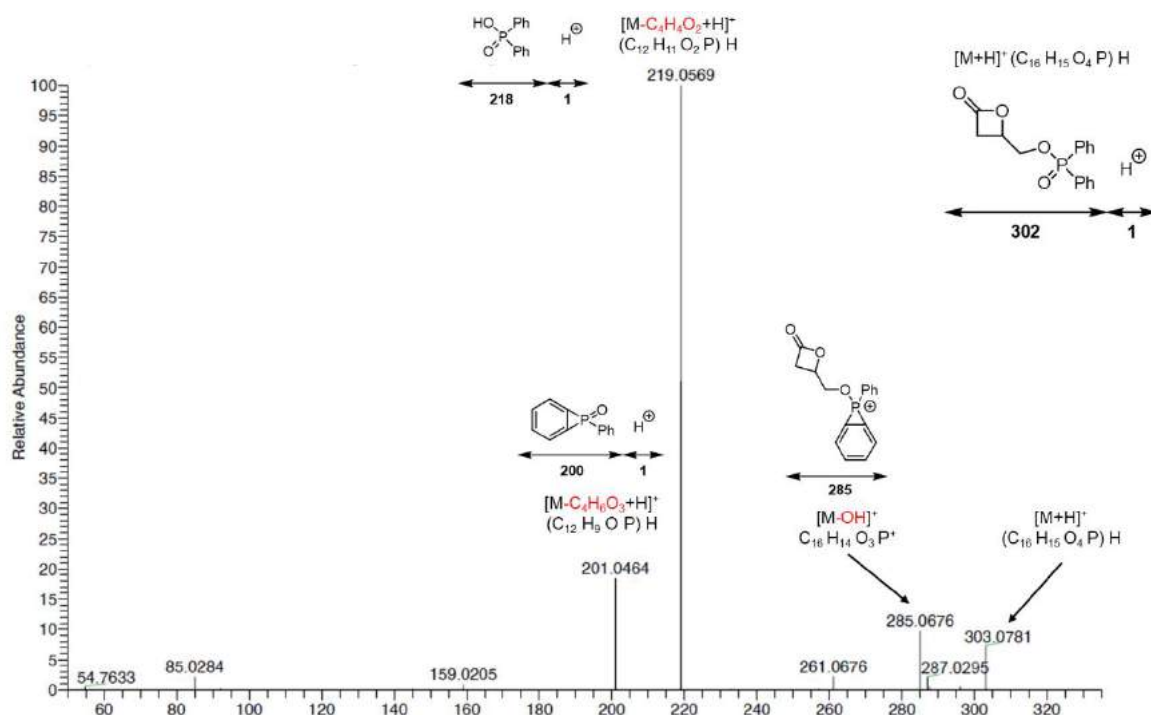


**Figure 2. 16** – ESI-MS/MS of  $[M+H]^+$  (solvent  $\text{CH}_2\text{Cl}_2/\text{CH}_3\text{OH}$  (95/5 v:v)) of freshly synthesized *racemic* (4-oxooxetan-2-yl)methyl diphenylphosphinate (*rac*-BPL<sup>OP(O)Ph<sub>2</sub></sup>) displaying the peak on the right corresponding to  $[(\text{COCH}_2\text{CH}(\text{CH}_2\text{O}_2\text{PC}_{12}\text{H}_{10}\text{O}))\text{H}]^+$  ( $m/z = 303.0781$ ). The three fragmentation products are described from right to left and correspond to the loss of OH to form another benzene–P bond ( $m/z = 285.0676$ ), or the loss of  $\text{C}_4\text{H}_4$  ring ( $m/z = 219.0569$ ), and the subsequent loss of  $\text{H}_2\text{O}$  ( $m/z = 219.0464$ ), respectively. Refer to the literature for details on the fragmented products.<sup>[34]</sup>

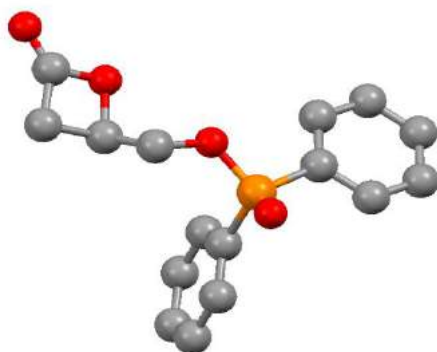
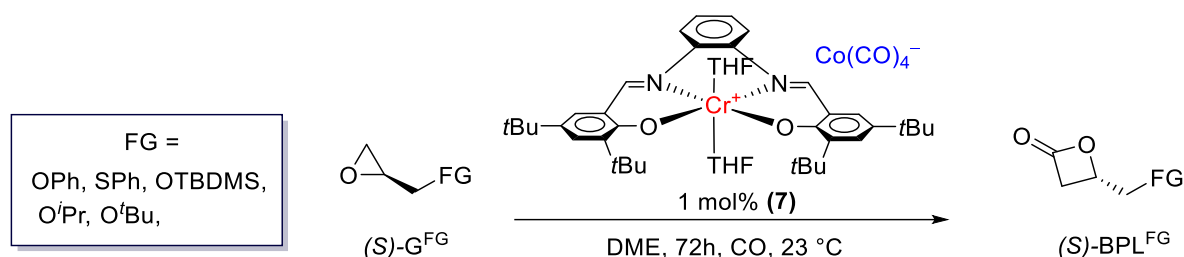


**Figure 2. 17** – ORTEP representation of the molecular structure of *rac*-BPL<sup>OP(O)Ph<sub>2</sub></sup>, hydrogen atoms are omitted for clarity.

Lastly, the synthesis of the required enantiopure BPL<sup>FG</sup>s (FG = OTBDMS, OPh, SPh, O<sup>*i*</sup>Pr, O<sup>*t*</sup>Bu) was performed according to the same approach as for the preparation of *rac*-BPL<sup>FG</sup>s. Hence carbonylation was achieved starting from the synthesized (*S*)-G<sup>FG</sup>s (FG = OTBDMS, OPh, SPh, O<sup>*i*</sup>Pr, O<sup>*t*</sup>Bu; Table 2. 1) mediated by 1% of (**7**) in dry DME at room temperature to directly afford the corresponding (*S*)-BPL<sup>FG</sup>s (Scheme 2. 9), since carbonylation is able to retain the configuration at the  $\beta$ -position (Scheme 2. 3). The obtained yields and

conversions are very similar to those of *rac*-BPL<sup>FG</sup>s, respectively (Table 2. 2), as the <sup>1</sup>H and <sup>13</sup>C NMR spectra.



**Scheme 2. 9** – Synthesis of enantiopure (*S*)-BPL<sup>FG</sup>s through carbonylation of (*S*)-G<sup>FG</sup>s mediated by achiral catalyst (**7**).

### 3. Conclusion: achievements and blueprints

The synthesis of *racemic* and enantiopure epoxides precursors (*rac*-G<sup>FG</sup>s and (*S*)-G<sup>FG</sup>s) prior to their subsequent carbonylation, was successfully performed in fair-to-high yields (50–75% and 39.8–43.33%; respectively) through the nucleophilic substitution and HKR mediated by chiral catalyst (**10**) reactions, respectively. Then, the production of a collection of known and innovative functional *racemic* and enantiopure β-lactones abbreviated as *rac*-BPL<sup>FG</sup>s and (*S*)-BPL<sup>FG</sup>s (FG = OAll, O<sup>n</sup>Bu, OBn, OTBDMS, OPh, SPh, SBn, O<sup>i</sup>Pr, O<sup>t</sup>Bu, OP(O)Ph<sub>2</sub>) through carbonylation mediated by [Lewis acid]<sup>+</sup>[Co(CO)<sub>4</sub>]<sup>−</sup> type achiral catalyst, was achieved. Fortunately, all the desired BPL<sup>FG</sup>s were synthesized under mild conditions (room temperature, low catalyst loading and no additive) in fair-to-high yields (51–82%) in the presence of [(Salph)Cr(THF)<sub>2</sub>]<sup>+</sup>[Co(CO)<sub>4</sub>]<sup>−</sup> (**7**), except for BPL<sup>SBn</sup>, BPL<sup>OP(O)Ph<sub>2</sub></sup> and BPL<sup>NBn<sub>2</sub></sup>. BPL<sup>SBn</sup> appeared to be unstable, rapidly undergoing decomposition and ring expansion rearrangements. On the other hand, BPL<sup>OP(O)Ph<sub>2</sub></sup> revealed to be a highly stable solid compound, but it was necessary to be synthesized using a different catalyst than (**7**), namely [PPN]<sup>+</sup>[Co(CO)<sub>4</sub>]<sup>−</sup> (**4**), under less mild conditions (high temperature (80 °C), high CO pressure (60 bars), and with Lewis acid additive (BF<sub>3</sub>)) in comparison to other BPL<sup>FG</sup>s. Nevertheless, BPL<sup>OP(O)Ph<sub>2</sub></sup> was synthesized herein, for the first time, in high isolated yield (60%), and fully characterized. Optimization toward a higher yield under milder operating conditions (*e.g.* lower temperature, pressure, and time) could still be sought for. The synthesis of *rac*-BPL<sup>NBn<sub>2</sub></sup> revealed the most challenging, for which two carbonylation routes were evaluated, namely using (**7**) under mild conditions or using (**4**) under harsher conditions. Whereas the epoxide corresponding to *rac*-BPL<sup>NBn<sub>2</sub></sup>, that is *rac*-G<sup>NBn<sub>2</sub></sup> remained unreacted in the presence of (**7**), it was quantitatively converted in the presence of (**4**), yet into the corresponding five membered ring γ-lactone instead. Anyhow, further investigations of the operating conditions using catalyst

(4) could be carried out, such as decreasing the temperature ( $< 80\text{ }^{\circ}\text{C}$ ) and the  $\text{BF}_3$  loading ( $< 2\text{mol}\%$ ) while increasing the catalyst loading and monitoring the reaction to detect the degradation of  $\text{rac-BPL}^{\text{NBn}_2}$ . Otherwise, replacing  $\text{rac-BPL}^{\text{NBn}_2}$  by  $\text{rac-BPL}^{\text{NPh}_2}$  may prevent or reduce its rearrangement driving force and at the same time it may maintain the nitrogen functionality, similarly to the behavior of  $\text{rac-BPL}^{\text{SBn}}$  vs.  $\text{rac-BPL}^{\text{SPh}}$ . Fortunately, all the  $\text{BPL}^{\text{FG}}$ s were synthesized in significant amount, way sufficient to be subsequently investigated in ring-opening polymerization (ROP) by organic activators (Chapter 3) or organometallic catalyst systems (Chapter 4).

## 4. Experimental section

### Material and methods

All manipulations involving organometallic catalysts were performed under inert atmosphere (argon,  $< 3\text{ ppm O}_2$ ) using standard Schlenk, vacuum line, and glovebox techniques. Solvents were freshly distilled from Na/benzophenone under argon and degassed thoroughly by freeze-thaw-vacuum cycles prior to use. *Racemic* glycidol ( $\text{rac-G}^{\text{OH}}$ ), glycidyl allyl ether ( $\text{rac-G}^{\text{OAll}}$ ), glycidyl *n*-butyl ether ( $\text{rac-G}^{\text{O}^n\text{Bu}}$ ), glycidyl benzyl ether ( $\text{rac-G}^{\text{OBn}}$ ), glycidyl phenyl ether ( $\text{rac-G}^{\text{OPh}}$ ), glycidyl *iso*-propyl ether ( $\text{rac-G}^{\text{O}^i\text{Pr}}$ ), and glycidyl *tert*-butyl ether ( $\text{rac-G}^{\text{O}^t\text{Bu}}$ ) were dried onto and distilled from  $\text{CaH}_2$  and then stored over 3–4 Å activated molecular sieves (Sigma) in the fridge ( $-27\text{ }^{\circ}\text{C}$ ). *Racemic* glycidyl *tert*-butyldimethylsilyl ether ( $\text{rac-G}^{\text{OTBDMS}}$ ),<sup>[35]</sup> 2-((benzylthio)methyl)oxirane ( $\text{rac-G}^{\text{SBn}}$ ),<sup>[36]</sup> 2-((phenylthio)methyl)oxirane ( $\text{rac-G}^{\text{SPh}}$ ),<sup>[36]</sup> oxiran-2-ylmethyl diphenylphosphinate ( $\text{rac-G}^{\text{OP(O)Ph}_2}$ ),<sup>[37]</sup> epibromohydrin ( $\text{rac-G}^{\text{Br}}$ ),<sup>[38]</sup> and *N,N*-dibenzyl-1-(oxiran-2-yl)methanamine ( $\text{rac-G}^{\text{NBn}_2}$ )<sup>[39]</sup> were synthesized according or similar to literature reports, dried onto and distilled from  $\text{CaH}_2$  and then stored over 3–4 Å activated molecular sieves in the fridge ( $-27\text{ }^{\circ}\text{C}$ ). Enantiopure (*S*)-phenyl glycidyl ether ((*S*)- $\text{G}^{\text{OPh}}$ ), (*S*)-2-((phenylthio)methyl)oxirane ((*S*)- $\text{G}^{\text{SPh}}$ ), (*S*)-glycidyl *tert*-butyldimethylsilyl ether ((*S*)- $\text{G}^{\text{OTBDMS}}$ ), (*S*)-glycidyl *iso*-propyl ether ((*S*)- $\text{G}^{\text{O}^i\text{Pr}}$ ), and (*S*)-glycidyl *tert*-butyl ether ((*S*)- $\text{G}^{\text{O}^t\text{Bu}}$ ) were prepared by hydrolytic kinetic resolution (HKR) of the corresponding *racemic* compound following the reported procedure.<sup>[30]</sup>  $[\text{Salph}(\text{Cr}(\text{THF})_2)][\text{Co}(\text{CO})_4]$ ,<sup>[28e, 40]</sup>  $[\text{PPN}][\text{Co}(\text{CO})_4]$ ,<sup>[40a, 41]</sup>  $\text{rac-BPL}^{\text{FG}}$ s (FG = OAll, O<sup>*n*</sup>Bu, OBn, OPh, SPh, SBn, OTBDMS, O<sup>*i*</sup>Pr, O<sup>*t*</sup>Bu, OH, OP(O)Ph<sub>2</sub>, NBn<sub>2</sub>) and (*R*)- $\text{BPL}^{\text{FG}}$ s (FG = SPh, SBn, OTBDMS, O<sup>*i*</sup>Pr, O<sup>*t*</sup>Bu) were synthesized according to the literature procedures.<sup>[27, 42]</sup> *Racemic* epichlorohydrin ( $\text{rac-G}^{\text{Cl}}$ ), (*R,R*)-(-)-*N,N*-bis(3,5-di-*tert*-butylsalicylidene)-2-

cyclohexanediaminocobalt(II), and all other reagents were purchased from Aldrich, Sigma or Acros and used as received.

Reactions were monitored by thin layer chromatography (Merck TLC silica gel 60 F254 on aluminium sheets) and visualized under UV irradiation at 254 nm, KMnO<sub>4</sub> and anisaldehyde staining solution. Compounds were purified by column chromatography using Geduran® silica gel 60 (0.040–0.063 nm). Retardation factor ( $R_f$ ) calculations as based on the experimental TLC and the eluent, is indicated in brackets.

## Instrumentation and measurements

<sup>1</sup>H (500 and 400 MHz), <sup>13</sup>C{<sup>1</sup>H} (125 MHz and 100 MHz) and <sup>31</sup>P (162 MHz and 202 MHz) NMR spectra were recorded on Bruker Avance AM 500 and Ascend 400 spectrometers at 25 °C. <sup>1</sup>H, <sup>13</sup>C{<sup>1</sup>H} and <sup>31</sup>P NMR spectra were referenced internally relative to SiMe<sub>4</sub> ( $\delta$  = 0 ppm) using the residual solvent resonances.

Chiral HPLC analysis of (*S*)-G<sup>FG</sup> (FG = OPh, SPh) was performed on a Thermofisher Scientific chromatograph equipped with a Chiralcel-OD DAICEL column (250 mm × 4.6 mm, 5  $\mu$ m) and a UV detector at 214 nm at 20 °C, using for (*S*)-G<sup>OPh</sup>: hexane/isopropanol 90:10 v/v (1 mL.min<sup>-1</sup>, 22 bar) and (*S*)-G<sup>SPh</sup>: hexane/isopropanol 99.5:0.5 v/v (0.9 mL.min<sup>-1</sup>, 23 bar).

Chiral GC analysis (*S*)-G<sup>FG</sup> (FG = OTBDMS, O<sup>i</sup>Pr and O<sup>t</sup>Bu) was performed on a Shimadzu chromatograph, injecting 1  $\mu$ L sample for 25 min. For (*S*)-G<sup>OTBDMS</sup>, a capillary Chiralcel-OD (25 m × 0.2 mm) column at 135 °C (constant temperature), using helium as carrier gas (0.94 mL.min<sup>-1</sup>, pressure: 101 kPa). For (*S*)-G<sup>O<sup>i</sup>Pr/O<sup>t</sup>Bu</sup>, Chirasil DEX CB Varian CP7502 (25 m × 0.25 mm) column inject temperature 50 °C, then ascending to 135 °C to 200–220 °C, using helium as carrier gas (0.94 mL.min<sup>-1</sup>, pressure: 101 kPa).

Mass spectra were recorded at “Centre de Mesures Physiques de l’Ouest” CRMPO-ScanMAT (Rennes, France). ESI mass spectra were recorded on an orbitrap type Thermofisher Scientific Q-Exactive instrument with an ESI source in positive mode by direct introduction with a flow rate of 5–10  $\mu$ L min<sup>-1</sup>. Samples were prepared in CH<sub>2</sub>Cl<sub>2</sub>/MeOH at 10  $\mu$ g mL<sup>-1</sup>.



## Synthesis of *rac*-G<sup>FGs</sup>

### Synthesis of *rac*-G<sup>SPh</sup> from *rac*-G<sup>Cl</sup>

A Schlenk flask was put in an ice bath (0 °C) and charged with K<sub>2</sub>CO<sub>3</sub> (22 g, 159 mmol), thiophenol HSPH (5.85 g, 53.14 mmol) and solubilized in DMSO, under argon. Then dry epichlorohydrin *rac*-G<sup>Cl</sup> (5.9 g, 63.77 mmol) was added dropwise using a degassed syringe at 0 °C. The reaction was left to run overnight at room temperature. On completion, the reaction mixture was extracted with dichloromethane (25 mL × 3) and the combined organic layers were washed with water (205 mL × 2) then dried over anhydrous Na<sub>2</sub>SO<sub>4</sub> before the solvent was removed under reduced pressure. Purification by flash column chromatography on silica gel (8.5:1.5 *n*-hexane/ethyl acetate) gave *rac*-G<sup>SPh</sup> (50% yield, 4.48 g) as yellow viscous liquid. Its spectral data were consistent with data reported in the literature.<sup>[43]</sup>

<sup>1</sup>H NMR (400 MHz, CDCl<sub>3</sub>, 25 °C) δ (ppm): δ 7.49 – 7.40 (m, 2H), 7.36 – 7.29 (m, 2H), 7.27 – 7.20 (m, 1H), 3.25 – 3.12 (m, 2H), 2.97 (dd, <sup>2</sup>J<sub>H-H</sub> = 15 Hz, <sup>3</sup>J<sub>H-H</sub> = 7.3 Hz, 1H), 2.79 (ddd, <sup>2</sup>J<sub>H-H</sub> = 5 Hz, <sup>3</sup>J<sub>H-H</sub> = 4 Hz, <sup>4</sup>J<sub>H-H</sub> = 1 Hz, 1H), 2.54 (dd, <sup>2</sup>J<sub>H-H</sub> = 5 Hz, <sup>3</sup>J<sub>H-H</sub> = 2 Hz, 1H) (Figure 2. 6).

### Synthesis of *rac*-G<sup>SBn</sup> from *rac*-G<sup>Cl</sup>

A Schlenk flask was placed in an ice bath (0 °C) and charged with K<sub>2</sub>CO<sub>3</sub> (18.65 g, 135 mmol), and benzyl mercaptan HSBn (5.58 g, 45 mmol), and solubilized in DMSO under argon. Then, dry epichlorohydrin *rac*-G<sup>Cl</sup> (5 g, 54 mmol) was added dropwise using a degassed syringe at 0 °C. The reaction was stirred overnight at room temperature. On completion, the reaction mixture was extracted with dichloromethane (25 mL × 3) and the combined organic layers were washed with water (205 mL × 2), then dried over anhydrous Na<sub>2</sub>SO<sub>4</sub> before the solvent was removed under reduced pressure. Purification by flash column chromatography on silica gel (9:1 *n*-hexane/ethyl acetate) gave *rac*-G<sup>SBn</sup> (62% yield, 5 g) as a yellow viscous liquid. Its spectroscopic data were consistent with data reported in the literature.<sup>[36]</sup>

<sup>1</sup>H NMR (400 MHz, CDCl<sub>3</sub>, 25 °C) δ (ppm): δ 7.37 – 7.16 (m, 5H), 3.81 (d, <sup>4</sup>J<sub>H-H</sub> = 3 Hz, 2H), 3.12 – 3.03 (m, 1H), 2.76 (dd, <sup>3</sup>J<sub>H-H</sub> = 4 Hz, <sup>3</sup>J<sub>H-H</sub> = 4.4 Hz, 1H), 2.62 (dd, <sup>2</sup>J<sub>H-H</sub> = 14 Hz, <sup>3</sup>J<sub>H-H</sub> = 6 Hz, 1H), 2.55 – 2.48 (m, 2H) (Figure 2. 6).

### Synthesis of *rac*-G<sup>OTBDMS</sup> from *rac*-G<sup>OH</sup>

In a round bottom flask, glycidol (5.36 g, 72.4 mmol), TBMSCl (16.8 g, 111 mmol) and imidazole (7.59 g, 111 mmol) were dissolved in dry DMF (100 mL). The reaction mixture was

stirred at room temperature overnight. The resulting precipitate was filtered off over a thick layer of celite, and the solution was concentrated. The resulting residue was purified by flash column chromatography on silica gel (9:1 *n*-hexane/ethyl acetate) to give *rac*-G<sup>OTBDMS</sup> (75% yield, 10 g) as colourless viscous liquid. Its spectroscopic data were consistent with those reported in the literature.<sup>[35]</sup>

**<sup>1</sup>H NMR** (400 MHz, CDCl<sub>3</sub>, 25 °C) δ (ppm): δ 3.82 (dd, <sup>2</sup>*J*<sub>H-H</sub> = 12 Hz, <sup>3</sup>*J*<sub>H-H</sub> = 3 Hz, 1H), 3.62 (dd, <sup>2</sup>*J*<sub>H-H</sub> = 12 Hz, <sup>3</sup>*J*<sub>H-H</sub> = 5 Hz, 1H), 3.04 (tt, <sup>3</sup>*J*<sub>H-H</sub> = 5 Hz, <sup>3</sup>*J*<sub>H-H</sub> = 3 Hz, 1H), 2.72 (dd, <sup>3</sup>*J*<sub>H-H</sub> = 5 Hz, <sup>3</sup>*J*<sub>H-H</sub> = 4 Hz, 1H), 2.59 (dd, <sup>3</sup>*J*<sub>H-H</sub> = 5 Hz, <sup>3</sup>*J*<sub>H-H</sub> = 3 Hz, 1H), 0.87 (s, 9H), 0.05 (s, 3H), 0.04 (s, 3H) (Figure 2. 6).

### Synthesis of *rac*-G<sup>OP(O)Ph<sub>2</sub></sup> from *rac*-G<sup>OH</sup>

In a Schlenk flask, glycidol *rac*-G<sup>OH</sup> (2 g, 27.30 mmol) in THF (15 mL) was added to a solution of ClP(O)Ph<sub>2</sub> (7.73 g, 32.76 mmol) in THF (15 mL) at 0 °C. NEt<sub>3</sub> (3.32 g, 32.76 mmol) was then added dropwise to the reaction mixture at 0 °C. A white precipitate (NEt<sub>3</sub>HCl) was formed directly. The reaction was stirred overnight at room temperature. Purification was done firstly by filtration of NEt<sub>3</sub>HCl and then by flash column chromatography on silica gel (3:7 *n*-hexane/ethyl acetate) to give *rac*-G<sup>OP(O)Ph<sub>2</sub></sup> (70% yield, 5.25 g) as yellow viscous oil. Its spectroscopic data were consistent with those reported in the literature.<sup>[37]</sup>

**<sup>1</sup>H NMR** (400 MHz, CDCl<sub>3</sub>, 25 °C) δ (ppm): δ 7.89 – 7.74 (m, 4H), 7.58 – 7.39 (m, 6H), 4.29 (ddd, <sup>2</sup>*J*<sub>H-H</sub> = 12 Hz, <sup>3</sup>*J*<sub>H-H</sub> = 8 Hz, <sup>3</sup>*J*<sub>H-P</sub> = 3 Hz, 1H), 3.93 (ddd, <sup>2</sup>*J*<sub>H-H</sub> = 12 Hz, <sup>3</sup>*J*<sub>H-H</sub> = 8 Hz, <sup>3</sup>*J*<sub>H-P</sub> = 6 Hz, 1H), 3.27 (ddt, <sup>3</sup>*J*<sub>H-H</sub> = 6 Hz, <sup>3</sup>*J*<sub>H-H</sub> = 4 Hz, <sup>3</sup>*J*<sub>H-H</sub> = 3 Hz, 1H), 2.81 (dd, <sup>3</sup>*J*<sub>H-H</sub> = 5 Hz, <sup>3</sup>*J*<sub>H-H</sub> = 5 Hz, 1H), 2.64 (dd, <sup>3</sup>*J*<sub>H-H</sub> = 5 Hz, <sup>3</sup>*J*<sub>H-H</sub> = 2.6 Hz, 1H) (Figure 2. 6).

**<sup>31</sup>P NMR** (162 MHz, CDCl<sub>3</sub>, 25 °C) δ (ppm): δ 32.82 (Figure 2. 6).

### Synthesis of *rac*-G<sup>NBn<sub>2</sub></sup> from *rac*-G<sup>OH</sup>

In a round bottom flask, epibromohydrin (1 g, 7.35 mmol), HNBn<sub>2</sub> (1.04 g, 5.25 mmol) and potassium carbonate (8.71 g, 6.30 mmol) were dissolved in DMF (10 mL). Then, the mixture was stirred at room temperature overnight, and the reaction was quenched with NH<sub>4</sub>Cl (20 mL) and diluted with water (80 mL). After that, the reaction mixture was extracted with dichloromethane (100 mL x 2) and washed with a solution of 1:1 brine and water. The combined organic layers were dried over Na<sub>2</sub>SO<sub>4</sub> and concentrated over vacuum. Purification was accomplished using silica column flash chromatography (7:3 *n*-hexane/ethyl acetate) to yield *rac*-G<sup>NBn<sub>2</sub></sup> (65% yield, 0.87 g) as colourless oil. Its spectroscopic data were consistent with those reported in the literature.<sup>[39]</sup>

**$^1\text{H}$  NMR** (400 MHz,  $\text{CDCl}_3$ , 25 °C)  $\delta$  (ppm):  $\delta$  7.57 – 7.50 (m, 4H), 7.48 – 7.40 (m, 4H), 7.39 – 7.32 (m, 2H), 3.94 (d,  $^2J_{\text{H-H}} = 14$  Hz, 2H), 3.70 (d,  $^2J_{\text{H-H}} = 14$  Hz, 2H), 3.25 – 3.13 (m, 1H), 2.90 (dd,  $^2J_{\text{H-H}} = 14$  Hz,  $^3J_{\text{H-H}} = 4$  Hz, 1H), 2.75 (dd,  $^3J_{\text{H-H}} = 5$  Hz,  $^3J_{\text{H-H}} = 4$  Hz, 1H), 2.60 – 2.43 (m, 2H) (Figure 2. 6).

## Synthesis of enantiopure (S)-G<sup>FGs</sup>

### Synthesis of (S)-G<sup>O<sup>Ph</sup></sup>

The catalyst (*R,R*)-**10** (80.5 mg, 130  $\mu\text{mol}$ ) was dissolved in *racemic* phenyl glycidyl ether, *rac*-G<sup>O<sup>Ph</sup></sup> (4 g, 26.67 mmol), AcOH (0.032 g, 0.53 mmol) and THF (0.3 mL) when using a solid diol. The solution was cooled to 0 °C and treated with H<sub>2</sub>O (0.26 g, 14.67 mmol). After 18 h, (S)-phenyl glycidyl ether (1.73 g, 43.33% yield) was isolated by vacuum distillation using a Kugelrohr oven (150 °C, 0.15 torr) as a colourless viscous liquid. Its spectroscopic data were consistent with those of the commercially available *rac*-G<sup>O<sup>Ph</sup></sup>.

### Synthesis of (S)-G<sup>S<sup>Ph</sup></sup>

The catalyst (*R,R*)-**10** (54.5 mg, 90  $\mu\text{mol}$ ) was dissolved in *rac*-G<sup>S<sup>Ph</sup></sup> (3 g, 18.07 mmol), AcOH (0.022 g, 0.36 mmol) and THF (0.2 mL). The solution was cooled to 0 °C and treated with H<sub>2</sub>O (0.18 g, 9.94 mmol). After 18 h, (S)-G<sup>S<sup>Ph</sup></sup> (1.26 g, 42% yield) was isolated by vacuum distillation using a Kugelrohr oven (40 °C, 0.15 torr) as a yellow viscous liquid. Its spectroscopic data were consistent with those of the synthesized *rac*-G<sup>O<sup>Ph</sup></sup> (*vide supra*).

### Synthesis of (S)-G<sup>OTBDMS</sup>

The catalyst (*R,R*)-**10** (48.17 mg, 80  $\mu\text{mol}$ ) was dissolved in *rac*-G<sup>OTBDMS</sup> (3 g, 15.96 mmol), AcOH (0.019 g, 0.32 mmol) and THF (0.2 mL). The solution was cooled to 0 °C and treated with H<sub>2</sub>O (0.16 g, 8.78 mmol). After 18 h, (S)-G<sup>OTBDMS</sup> (1.19 g, 39.8% yield) was isolated by vacuum distillation using a Kugelrohr oven (120 °C, 0.15 torr) as a colourless viscous liquid. Its spectroscopic data were consistent with those of the synthesized *rac*-G<sup>OTBDMS</sup> (*vide supra*).

### Synthesis of (S)-G<sup>O<sup>i</sup>Pr</sup>

The catalyst (*R,R*)-**10** (143 mg, 240  $\mu\text{mol}$ ) was dissolved in *rac*-G<sup>O<sup>i</sup>Pr</sup> (5.5 g, 15.96 mmol), AcOH (0.057 g, 0.95 mmol). The solution was cooled to 0 °C and treated with H<sub>2</sub>O (0.47 g, 26.08 mmol). After 18 h, (S)-G<sup>O<sup>i</sup>Pr</sup> (2.33 g, 42.4% yield) was isolated by vacuum

distillation using a Kugelrohr oven (50-60 C, 0.15 torr) as a colourless viscous liquid. Its spectroscopic data were consistent with those of the commercially available *rac*-G<sup>OiPr</sup>.

### Synthesis of (*S*)-G<sup>O*t*Bu</sup>

The catalyst (*R,R*)-**10** (128 mg, 210 mol) was dissolved in *rac*-G<sup>O*r*Bu</sup> (5.5 g, 42.31 mmol), AcOH (0.051 g, 0.85 mmol). The solution was cooled to 0 C and treated with H<sub>2</sub>O (0.42 g, 23.27 mmol). After 18 h, (*S*)-G<sup>O*r*Bu</sup> (2.29 g, 41.7% yield) was isolated by vacuum distillation using a Kugelrohr oven (50 C, 0.15 torr) as a colourless viscous liquid. Its spectroscopic data were consistent with those of the commercially available *rac*-G<sup>O*r*Bu</sup>.

## Typical carbonylation procedure via (**7**)

### Carbonylation of *rac*-G<sup>OAll</sup> to *rac*-BPL<sup>OAll</sup>

In a typical experiment, in the glovebox, a Schlenk flask was charged with [Salph(Cr(THF)<sub>2</sub>)] [Co(CO)<sub>4</sub>] (**7**) (320 mg, 0.35 mmol). On a vacuum line, dry DME (15 mL) was syringed in and the resulting solution was cannulated into a degassed high-pressure reactor which was pressurized with carbon monoxide to 20 bars, and stirred for 15 min before depressurization. A solution of *racemic* allyl glycidyl ether (*rac*-G<sup>OAll</sup>) (3.93 g, 34.5 mmol, 100 equiv.) in dry DME (15 mL) was transferred into the reactor which was then pressurized with CO to 40 bars. The reaction mixture was stirred for 2 days at 20 C. Then, the reactor was vented to atmospheric pressure, volatiles were removed under vacuum and the crude product was purified through a short alumina column (CHCl<sub>3</sub>, 2  200 mL). After evaporation of volatiles, *rac*-BPL<sup>OAll</sup> was obtained by double distillation using a Kugelrohr oven (110 C–130 C, 0.1 torr) to afford a colourless viscous liquid (79% yield, 3.87 g). *rac*-BPL<sup>OAll</sup> was stored under argon in the fridge at –27 C.

**<sup>1</sup>H NMR** (500 MHz, CDCl<sub>3</sub>, 25 C)  (ppm): 5.86 (ddt, <sup>3</sup>*J*<sub>H-H</sub> = 17 Hz, <sup>3</sup>*J*<sub>H-H</sub> = 10 Hz, <sup>3</sup>*J*<sub>H-H</sub> = 5 Hz, 1H), 5.31 – 5.21 (m, 1H), 5.23 – 5.14 (m, 1H), 4.63 (dtd, <sup>3</sup>*J*<sub>H-H</sub> = 6 Hz, <sup>3</sup>*J*<sub>H-H</sub> = 5 Hz, <sup>3</sup>*J*<sub>H-H</sub> = 3 Hz, 1H), 4.19 – 3.90 (m, 2H), 3.77 (dd, <sup>2</sup>*J*<sub>H-H</sub> = 12 Hz, <sup>3</sup>*J*<sub>H-H</sub> = 3.0 Hz, 1H), 3.66 (dd, <sup>2</sup>*J*<sub>H-H</sub> = 12 Hz, <sup>3</sup>*J*<sub>H-H</sub> = 4.5 Hz, 1H), 3.44 (dd, <sup>2</sup>*J*<sub>H-H</sub> = 16 Hz, <sup>3</sup>*J*<sub>H-H</sub> = 6 Hz, 1H), 3.37 (dd, <sup>2</sup>*J*<sub>H-H</sub> = 16 Hz, <sup>3</sup>*J*<sub>H-H</sub> = 4.5 Hz, 1H) (Figure 2. 9).

**<sup>13</sup>C NMR** (125 MHz, CDCl<sub>3</sub>, 25 C)  (ppm): 167.9 (C=O), 134.1 (OCH<sub>2</sub>CH=CH<sub>2</sub>), 117.7 (OCH<sub>2</sub>CH=CH<sub>2</sub>), 72.7 (CH<sub>2</sub>OAllyl), 69.5 (CHOC(O)), 69.3 (OCH<sub>2</sub>CH=CH<sub>2</sub>), 39.7 (CH<sub>2</sub>C(O)O).

### Carbonylation of *rac*-G<sup>nBu</sup> to *rac*-BPL<sup>nBu</sup>

Following the aforementioned typical procedure, starting from [Salph(Cr(THF)<sub>2</sub>)] [Co(CO)<sub>4</sub>] (316 mg, 0.35 mmol) and *rac*-G<sup>OnBu</sup> (4.54 g, 43.9 mmol, 100 equiv), *rac*-BPL<sup>OnBu</sup> was isolated after double distillation using a Kugelrohr oven (130 C–160 C, 0.1 torr) as a colourless viscous liquid (82% yield, 4.52 g). *rac*-BPL<sup>nBu</sup> was stored under argon in the fridge at –27 C.

**<sup>1</sup>H NMR** (500 MHz, CDCl<sub>3</sub>, 25 C)  $\delta$  (ppm): 4.64 (dtd, <sup>3</sup>*J*<sub>H-H</sub> = 6 Hz, <sup>3</sup>*J*<sub>H-H</sub> = 4 Hz, <sup>3</sup>*J*<sub>H-H</sub> = 3 Hz, 1H), 3.76 (dd, <sup>2</sup>*J*<sub>H-H</sub> = 12 Hz, <sup>3</sup>*J*<sub>H-H</sub> = 3 Hz, 1H), 3.68 (dd, <sup>2</sup>*J*<sub>H-H</sub> = 12 Hz, <sup>3</sup>*J*<sub>H-H</sub> = 4 Hz, 1H), 3.57 – 3.48 (m, 2H), 3.48 – 3.36 (m, 2H), 1.61 – 1.51 (m, 2H), 1.37 (h, *J* = 7 Hz, 2H), 0.92 (t, *J* = 7 Hz, 3H) (Figure 2. 9).

**<sup>13</sup>C NMR** (125 MHz, CDCl<sub>3</sub>, 25 C)  $\delta$  (ppm): 169.7 (C=O), 72.4 (CH<sub>2</sub>O<sup>n</sup>Butyl), 70.7 (CHOC(O)), 70.7 (OCH<sub>2</sub>CH<sub>2</sub>CH<sub>2</sub>CH<sub>3</sub>), 38.0 (CH<sub>2</sub>C(O)O) 31.4 (OCH<sub>2</sub>CH<sub>2</sub>CH<sub>2</sub>CH<sub>3</sub>), 19.1 (OCH<sub>2</sub>CH<sub>2</sub>CH<sub>2</sub>CH<sub>3</sub>), 14.0 (OCH<sub>2</sub>CH<sub>2</sub>CH<sub>2</sub> guanidines H<sub>3</sub>).

### Carbonylation of *rac*-G<sup>OBn</sup> to *rac*-BPL<sup>OBn</sup>

Following the typical experiment reported above, using [Salph(Cr(THF)<sub>2</sub>)] [Co(CO)<sub>4</sub>] (246 mg, 0.27 mmol) and *rac*-G<sup>OBn</sup> (4.43 g, 27.0 mmol, 100 equiv), *rac*-BPL<sup>OBn</sup> was isolated after double distillation using a Kugelrohr oven (180 C, 0.1 torr) as a colorless viscous liquid (62% yield, 3.2 g). *rac*-BPL<sup>OBn</sup> was stored under argon in the fridge at –27 C.

**<sup>1</sup>H NMR** (500 MHz, CDCl<sub>3</sub>, 25 C)  $\delta$  (ppm): 7.41 – 7.26 (m, 5H), 4.69 – 4.63 (m, 1H), 4.64 – 4.56 (m, 2H), 3.82 (dd, <sup>2</sup>*J*<sub>H-H</sub> = 12 Hz, <sup>3</sup>*J*<sub>H-H</sub> = 3 Hz, 1H), 3.71 (dd, <sup>2</sup>*J*<sub>H-H</sub> = 12 Hz, <sup>3</sup>*J*<sub>H-H</sub> = 4 Hz, 1H), 3.50 – 3.36 (m, 2H) (Figure 2. 9).

**<sup>13</sup>C NMR** (125 MHz, CDCl<sub>3</sub>, 25 C)  $\delta$  (ppm): 167.6 (C=O), 137.3 (*ipso*-C aro), 128.5 (*m*-CH aro), 127.9 *p*-CH aro, 127.7 (*o*-CH aro), 73.6 (CH<sub>2</sub>OCH<sub>2</sub>Ph), 69.3 (CHOC(O)), 69.2 (CH<sub>2</sub>Ph), 39.7 (CH<sub>2</sub>C(O)O).

### Carbonylation of *rac*-/(*S*)-G<sup>OTBDMS</sup> to *rac*-/(*S*)-BPL<sup>OTBDMS</sup>

Following the typical experiment previously reported, using [Salph(Cr(THF)<sub>2</sub>)] [Co(CO)<sub>4</sub>] (246.4 mg, 0.27 mmol) and *rac*-G<sup>OTBDMS</sup> (5.57g, 29.64 mmol, 100 equiv.) afforded *rac*-BPL<sup>OTBDMS</sup> isolated following a double distillation using a Kugelrohr oven (140C under vacuum of 0.1 torr) as a colourless viscous liquid (60% yield, 3.8 g).

**$^1\text{H}$  NMR** (500 MHz,  $\text{CDCl}_3$ , 25 °C)  $\delta$  (ppm): 4.65 – 4.46 (m, 1H), 4.02 (dd,  $^2J_{\text{H-H}} = 12$  Hz,  $^2J_{\text{H-H}} = 3$  Hz, 1H), 3.82 (dd,  $^3J_{\text{H-H}} = 12$  Hz,  $^3J_{\text{H-H}} = 3$  Hz, 1H), 3.53 – 3.28 (m, 2H), 0.91 (s, 9H), 0.09 (s, 6H) (Figure 2. 9).

**$^{13}\text{C}$  NMR** (125 MHz,  $\text{CDCl}_3$ , 25 °C)  $\delta$  (ppm): 171.7 (C=O), 74.8 (CHOC(O)), 63.9 ( $\text{CH}_2\text{OTBDMS}$ ), 37.4 ( $\text{CH}_2\text{C}(\text{O})\text{O}$ ), 25.7  $\text{Si}(\text{CH}_3)_2\text{C}(\text{CH}_3)_3$ , 15.7  $\text{Si}(\text{CH}_3)_2\text{C}(\text{CH}_3)_3$ , –4.9  $\text{Si}(\text{CH}_3)_2\text{C}(\text{CH}_3)_3$ .

The carbonylation of (*S*)-BPL<sup>OTBDMS</sup> was performed similarly but starting from (*S*)-G<sup>OTBDMS</sup> and gave (*S*)-BPL<sup>OTBDMS</sup> as a colourless viscous liquid (3.65 g, 58% yield) that displayed NMR spectra identical to those of *rac*-BPL<sup>OTBDMS</sup> (*vide supra*). Both *rac*-BPL<sup>OTBDMS</sup> and (*S*)-BPL<sup>CH<sub>2</sub>OTBDMS</sup> were stored under argon in the fridge at –27 °C.

### Carbonylation of *rac*-/(*S*)-G<sup>O<sup>Ph</sup></sup> to *rac*-/(*S*)-BPL<sup>O<sup>Ph</sup></sup>

Following the typical experiment previously reported, using [Salph(Cr(THF)<sub>2</sub>)] [Co(CO)<sub>4</sub>] (235 mg, 0.26 mmol) and *rac*-G<sup>O<sup>Ph</sup></sup> (3.88 g, 25.9 mmol, 100 equiv.) afforded *rac*-BPL<sup>O<sup>Ph</sup></sup> as a white solid., that was next crystallized from diethyl ether to give pure white crystals of 4-phenoxyethylene-β-propiolactone (*rac*-BPL<sup>O<sup>Ph</sup></sup>) (75% yield, 3.5 g).

**$^1\text{H}$  NMR** (500 MHz,  $\text{CDCl}_3$ , 25 °C)  $\delta$  (ppm):  $\delta$  7.34–7.28 (m, 2H), 7.03–6.98 (m, 1H), 6.95–6.91 (m, 2H), 4.88–4.81 (m, 1H), 4.33 (dd,  $J = 11$ , 3 Hz, 1H), 4.23 (dd,  $J = 11$ , 4 Hz, 1H), 3.62–3.53 (m, 2H) (Figure 2. 9).

**$^{13}\text{C}$  NMR** (125 MHz,  $\text{CDCl}_3$ , 25 °C)  $\delta$  (ppm): 167.3 (C=O), 158.1 (*ipso*-C<sub>5</sub>), 129.8 (*m*-CH), 121.9 (*p*-CH), 114.8 (*o*-CH), 68.4 (CHOC(O)), 67.4 ( $\text{CH}_2\text{O}^{\text{Ph}}$ ), 40.2 ( $\text{CH}_2\text{C}(\text{O})\text{O}$ ).

The carbonylation of (*S*)-phenyl glycidyl ether was performed similarly but starting from (*S*)-G<sup>O<sup>Ph</sup></sup> and gave (*S*)-BPL<sup>O<sup>Ph</sup></sup> as an off-white solid (3.45 g, 74% yield) that displayed NMR spectra identical to those of *rac*-BPL<sup>O<sup>Ph</sup></sup> (*vide supra*). Both *rac*-BPL<sup>O<sup>Ph</sup></sup> and (*S*)-BPL<sup>CH<sub>2</sub>O<sup>Ph</sup></sup> were stored under argon in the fridge at –27 °C.

### Carbonylation of *rac*-/(*S*)-G<sup>S<sup>Ph</sup></sup> to *rac*-/(*S*)-BPL<sup>S<sup>Ph</sup></sup>

Following the typical experiment previously reported, using [Salph(Cr(THF)<sub>2</sub>)] [Co(CO)<sub>4</sub>] (218 mg, 0.24 mmol) and *rac*-G<sup>S<sup>Ph</sup></sup> (4 g, 24 mmol, 100 equiv.) afforded *rac*-BPL<sup>S<sup>Ph</sup></sup> as a pale yellow viscous liquid. Purification was done through a silica column using  $\text{CHCl}_3$  as eluent followed by drying over 3–4 Å molecular sieves (thus avoiding

distillation due to *rac*-BPL<sup>SPh</sup> unstability). Also, drying solvent residues was under reduced pressure at 0 °C to finally afford *rac*-BPL<sup>SPh</sup> (51% yield, 2.4 g) as yellow viscous oil.

**<sup>1</sup>H NMR** (500 MHz, CDCl<sub>3</sub>, 25 °C)  $\delta$  (ppm):  $\delta$  7.45–7.40 (m, 2H), 7.36–7.24 (m, 3H), 4.63–4.55 (m, 1H), 3.50 (dd,  $J$  = 17, 6 Hz, 1H), 3.43 (dd,  $J$  = 14, 5 Hz, 1H), 3.17–3.11 (m, 2H) (Figure 2. 10).

**<sup>13</sup>C NMR** (125 MHz, CDCl<sub>3</sub>, 25 °C)  $\delta$  (ppm): 167.3 (C=O), 133.9 (*ipso*-C), 131.2 (*o*-CH), 129.4 (*m*-CH), 127.7 (*p*-CH), 68.9 (CHOC(O)), 43.0 (CH<sub>2</sub>SPh), 38.0 (CH<sub>2</sub>C(O)O) (Figure 2. 10).

**ESI-MS**  $m/z$  observed = 217.0293 vs  $m/z$  calculated = 217.0299 (Figure 2. 11).

The carbonylation of (*S*)-BPL<sup>SPh</sup> was performed similarly but starting from (*S*)-G<sup>SPh</sup> and gave (*S*)-BPL<sup>SPh</sup> as a yellow viscous liquid (2.2 g, 47% yield) that displayed NMR spectra identical to those of *rac*-BPL<sup>SPh</sup> (*vide supra*). To prevent the degradation of *rac*-BPL<sup>SPh</sup> and (*S*)-BPL<sup>SPh</sup>, they were both freshly prepared prior to use.

### Carbonylation of *rac*-/(*S*)-G<sup>OiPr</sup> to *rac*-/(*S*)-BPL<sup>OiPr</sup>

Following the typical experiment previously reported, using [Salph(Cr(THF)<sub>2</sub>)] [Co(CO)<sub>4</sub>] (431 mg, 0.47 mmol) and *rac*-G<sup>OiPr</sup> (5.51 g, 47.51 mmol, 100 equiv.) afforded *rac*-BP<sup>OiPr</sup> isolated following a double distillation using a Kugelroth oven (180°C under vacuum of 0.1 torr) as a colourless viscous liquid (65% yield, 4.45 g).

**<sup>1</sup>H NMR** (500 MHz, CDCl<sub>3</sub>, 25 °C)  $\delta$  (ppm):  $\delta$  4.60 (dtd,  $^3J_{H-H}$  = 6 Hz,  $^3J_{H-H}$  = 4 Hz,  $^3J_{H-H}$  = 3 Hz, 1H), 3.74 (dd,  $^2J_{H-H}$  = 12 Hz,  $^3J_{H-H}$  = 3 Hz, 1H), 3.68 – 3.58 (m, 2H), 3.42 (dd,  $^2J_{H-H}$  = 16 Hz,  $^3J_{H-H}$  = 6 Hz, 1H), 3.35 (dd,  $^2J_{H-H}$  = 16 Hz,  $^3J_{H-H}$  = 4 Hz, 1H), 1.15 (d,  $J$  = 6 Hz, 6H) (Figure 2. 9).

**<sup>13</sup>C NMR** (125 MHz, CDCl<sub>3</sub>, 25 °C)  $\delta$  (ppm): 72.6 (OCH(CH<sub>3</sub>)<sub>2</sub>), 69.6 (CHOC(O)), 67.4 (CH<sub>2</sub>OCH), 39.4 (CH<sub>2</sub>C(O)O), 21.8 (CH(CH<sub>3</sub>)<sub>2</sub>), 21.8 (CH(CH<sub>3</sub>)<sub>2</sub>) (Figure 2. 9).

The carbonylation of (*S*)-BPL<sup>OiPr</sup> was performed similarly but starting from (*S*)-G<sup>OiPr</sup> and gave (*S*)-BPL<sup>OiPr</sup> as colourless viscous liquid (4.3 g, 62.8% yield) that displayed NMR spectra identical to those of *rac*-BPL<sup>OiPr</sup> (*vide supra*). Both *rac*-BPL<sup>OiPr</sup> and (*S*)-BPL<sup>OiPr</sup> were stored under argon in the fridge at –27 °C.

### Carbonylation of *rac*-/(*S*)-G<sup>OtBu</sup> to *rac*-/(*S*)-BPL<sup>OtBu</sup>

Following the typical experiment previously reported, using [Salph(Cr(THF)<sub>2</sub>)] [Co(CO)<sub>4</sub>] (281.1 mg, 0.31 mmol) and *rac*-G<sup>OtBu</sup> (4.03 g, 30.99 mmol, 100



equiv.) afforded *rac*-BPL<sup>OrBu</sup> isolated following a double distillation using a Kugelrohr oven (190-200 C under vacuum of 0.1 torr) as a colourless viscous liquid (64% yield, 3.13 g).

**<sup>1</sup>H NMR** (500 MHz, CDCl<sub>3</sub>, 25 C)  $\delta$  (ppm):  $\delta$  4.55 (dtd, <sup>3</sup>*J*<sub>H-H</sub> = 6 Hz, <sup>3</sup>*J*<sub>H-H</sub> = 4 Hz, <sup>3</sup>*J*<sub>H-H</sub> = 3 Hz, 1H), 3.66 (dd, <sup>2</sup>*J*<sub>H-H</sub> = 11 Hz, <sup>3</sup>*J*<sub>H-H</sub> = 3 Hz, 1H), 3.54 (dd, <sup>2</sup>*J*<sub>H-H</sub> = 11 Hz, <sup>3</sup>*J*<sub>H-H</sub> = 4 Hz, 1H), 3.37 (dd, <sup>2</sup>*J*<sub>H-H</sub> = 16 Hz, <sup>3</sup>*J*<sub>H-H</sub> = 6 Hz, 1H), 3.31 (dd, <sup>2</sup>*J*<sub>H-H</sub> = 16 Hz, <sup>3</sup>*J*<sub>H-H</sub> = 5 Hz, 1H), 1.15 (s, 9H) (Figure 2. 13).

**<sup>13</sup>C NMR** (125 MHz, CDCl<sub>3</sub>, 25 C)  $\delta$  (ppm):  $\delta$  167.9 (C=O), 74.3 (OC(CH<sub>3</sub>)<sub>3</sub>), 69.6 (CHOC(O)), 63.6 (CH<sub>2</sub>OC), 39.4 (CH<sub>2</sub>C(O)O), 27.2 (C(CH<sub>3</sub>)<sub>3</sub>) (Figure 2. 13).

**ESI-MS** *m/z* observed = 181.0833 vs *m/z* calculated = 181.0835 (Figure 2. 14).

The carbonylation of (*S*)-BPL<sup>OrBu</sup> was performed similarly but starting from (*S*)-G<sup>OrBu</sup> and gave (*S*)-BPL<sup>OrBu</sup> as colourless viscous liquid (3 g, 61.3% yield) that displayed NMR spectra identical to those of *rac*-BPL<sup>OrBu</sup> (*vide supra*). Both *rac*-BPL<sup>OrBu</sup> and (*S*)-BPL<sup>OrBu</sup> were stored under argon in the fridge at -27 C.

## Typical carbonylation procedure via (4)

### Carbonylation of *rac*-G<sup>OP(O)Ph<sub>2</sub></sup> to *rac*-BPL<sup>OP(O)Ph<sub>2</sub></sup>

In a typical experiment, in the glovebox, a Schlenk flask was charged with [PPN][Co(CO)<sub>4</sub>] (**4**) (155.48 mg, 218.98  $\mu$ mol). On a vacuum line, dry DME (15 mL) was syringed in the flask containing (**4**) in order to solubilize it. The resulting solution was cannulated into a degassed high-pressure reactor under argon. In another Schlenk flask, dry DME (15 mL) was added to *racemic* oxiran-2-ylmethyl diphenylphosphinate *rac*-G<sup>OP(O)Ph<sub>2</sub></sup> (3 g, 10.95 mmol, 50 equiv.) under argon. Using a degassed microsyringe, dry BF<sub>3</sub>·Et<sub>2</sub>O (30.88 mg, 218.98  $\mu$ mol) was also added to the autoclave reactor. The reactor was pressurized with carbon monoxide to 60 bars, and was put in an oil bath at 80 C. The reaction mixture was stirred for 2 days at 80 C. Then, the reactor was vented to atmospheric pressure, volatiles were removed under vacuum to obtain a green-blue viscous oil product. The green-blue viscous oil product was solubilized in minimum amount of ethyl acetate and then diluted with diethyl ether (150-200 mL) to give a precipitate (residual catalyst (**4**)). The precipitate was filtered off and the remaining organic solution was dried under vacuum from the residual solvents to obtain yellow viscous oily crude product. The crude product was purified as solid deposit with flash column chromatography (gradient eluent of 2:8 to 1:9 *n*-hexane/ethyl acetate) to obtain *rac*-



BPL<sup>OP(O)Ph<sub>2</sub></sup> as white solid after drying the volatiles. Crystallisation was done in ethyl acetate at room temperature to give *rac*-BPL<sup>OP(O)Ph<sub>2</sub></sup> as crystals, that was then stored under argon.

**<sup>1</sup>H NMR** (500 MHz, CDCl<sub>3</sub>, 25 °C) δ (ppm): δ 7.88 – 7.77 (m, 4H), 7.59 – 7.52 (m, 2H), 7.52 – 7.42 (m, 4H), 4.80 – 4.72 (m, 1H), 4.36 (ddd, <sup>2</sup>*J*<sub>H-H</sub> = 12 Hz, <sup>3</sup>*J*<sub>H-H</sub> = 7 Hz, <sup>3</sup>*J*<sub>H-P</sub> = 2.9 Hz, 1H), 4.27 (ddd, <sup>2</sup>*J*<sub>H-H</sub> = 12 Hz, <sup>3</sup>*J*<sub>H-H</sub> = 7 Hz, <sup>3</sup>*J*<sub>H-P</sub> = 3.9 Hz, 1H), 3.58 – 3.49 (m, 2H) (Figure 2. 15).

**<sup>13</sup>C NMR** (125 MHz, CDCl<sub>3</sub>, 25 °C) δ (ppm): δ 166.9 (C=O), 132.8 (d, <sup>3</sup>*J*<sub>C-P</sub> = 4 Hz, *m*-CH), 132.8 (d, <sup>3</sup>*J*<sub>C-P</sub> = 3 Hz, *m*-CH), 131.9 (d, <sup>2</sup>*J*<sub>C-P</sub> = 10 Hz, *o*-CH), 131.6 (d, <sup>2</sup>*J*<sub>C-P</sub> = 10 Hz, *o*-CH), 131.1 (d, <sup>1</sup>*J*<sub>C-P</sub> = 52 Hz, *ipso*-C), 130.0 (d, <sup>1</sup>*J*<sub>C-P</sub> = 48 Hz, *ipso*-C), 129.0 (d, <sup>4</sup>*J*<sub>C-P</sub> = 2 Hz, *p*-CH), 128.9 (d, <sup>4</sup>*J*<sub>C-P</sub> = 2 Hz, *p*-CH), 68.6 (d, <sup>2</sup>*J*<sub>C-P</sub> = 7 Hz, CH<sub>2</sub>OP), 63.5 (d, <sup>3</sup>*J*<sub>C-P</sub> = 5 Hz, CHOC(O)), 40.1 (CH<sub>2</sub>C(O)O) (Figure 2. 15).

**<sup>31</sup>P NMR** (162 MHz, CDCl<sub>3</sub>, 25 °C) δ (ppm): δ 33.95 (Figure 2. 15).

**ESI-MS** *m/z* observed = 303.0781 vs *m/z* calculated = 303.0781 (Figure 2. 16).

### Carbonylation of *rac*-G<sup>OH</sup> to *rac*-BPL<sup>OH</sup>

Following the typical experiment previously reported, using [PPN][Co(CO)<sub>4</sub>] (642 mg, 904 μmol), dry BF<sub>3</sub>·Et<sub>2</sub>O (127.5 mg, 218.98 μmol) and *rac*-G<sup>OH</sup> (3.35 g, 45.20 mmol, 50 equiv.) afforded *rac*-BPL<sup>OH</sup> isolated, following precipitation in diethyl ether, as a pale yellow viscous liquid (76% yield, 3.5 g).

**<sup>1</sup>H NMR** (500 MHz, CDCl<sub>3</sub>, 25 °C) δ (ppm): δ 4.67 – 4.59 (m, 1H), 4.39 (dd, <sup>2</sup>*J*<sub>H-H</sub> = 10 Hz, <sup>3</sup>*J*<sub>H-H</sub> = 4 Hz, 1H), 4.27 (dd, <sup>2</sup>*J*<sub>H-H</sub> = 10 Hz, <sup>3</sup>*J*<sub>H-H</sub> = 1 Hz, 1H), 3.56 (s, 1H), 2.72 (dd, <sup>2</sup>*J*<sub>H-H</sub> = 18 Hz, <sup>3</sup>*J*<sub>H-H</sub> = 6 Hz, 1H), 2.48 (dd, <sup>2</sup>*J*<sub>H-H</sub> = 18 Hz, <sup>2</sup>*J*<sub>H-H</sub> = 1 Hz, 1H) (Appendix 5 – top).

**<sup>13</sup>C NMR** (125 MHz, CDCl<sub>3</sub>, 25 °C) δ (ppm): δ 177.2 (C=O), 76.5 (CHOC(O)), 67.5 (CH<sub>2</sub>OH), 37.9 (CH<sub>2</sub>C(O)O) (Appendix 5 – bottom).

## 5. References

- [1] a) J. Wang, Y. Shi, D. Jiang, *Curr. Top. Med. Chem.* **2021**; b) J. Bińczak, K. Dziuba, A. Chrobok, *Materials* **2021**, *14*, 2881; c) S. L. Robinson, J. K. Christenson, L. P. Wackett, *Nat. Prod. Rep.* **2019**, *36*, 458-475.
- [2] a) T. Böttcher, S. A. Sieber, *MedChemComm* **2012**, *3*, 408-417; b) C. Lowe, J. C. Vederas, *Org. Prep. Proced. Int.* **1995**, *27*, 305-346.
- [3] a) N. Wang, Z. Wu, J. Wang, N. Ullah, Y. Lu, *Chem. Soc. Rev.* **2021**; b) Y. Wang, R. L. Tennyson, D. Romo, *Heterocycles* **2004**, *64*, 605-658.
- [4] L. D. Arnold, J. C. Drover, J. C. Vederas, *J. Am. Chem. Soc.* **1987**, *109*, 4649-4659.
- [5] M. Kawashima, T. Sato, T. Fujisawa, *Tetrahedron* **1989**, *45*, 403-412.
- [6] a) K. T. Mead, H.-L. Yang, *Tetrahedron Lett.* **1989**, *30*, 6829-6832; b) T. A. Mitchell, D. Romo, *J. Org. Chem.* **2007**, *72*, 9053-9059.
- [7] L. R. Rieth, D. R. Moore, E. B. Lobkovsky, G. W. Coates, *J. Am. Chem. Soc.* **2002**, *124*, 15239-15248.
- [8] a) A. Pommier, J.-M. Pons, *Synthesis* **1993**, *1993*, 441-459; b) J. Mulzer, T. Kerkmann, *J. Am. Chem. Soc.* **1980**, *102*, 3620-3622; c) J. Mulzer, A. Chucholowski, *Angew. Chem. Int. Ed.* **1982**, *21*, 777-778.
- [9] J. Mulzer, M. Zippel, *J. Chem. Soc., Chem. Commun.* **1981**, 891-892.
- [10] a) J. K. Christenson, J. E. Richman, M. R. Jensen, J. Y. Neufeld, C. M. Wilmot, L. P. Wackett, *Biochemistry* **2017**, *56*, 348-351; b) J. K. Christenson, S. L. Robinson, T. A. Engel, J. E. Richman, A. N. Kim, L. P. Wackett, *Biochemistry* **2017**, *56*, 5278-5287.
- [11] a) J. Mulzer, K. Hoyer, A. Müller-Fahrnow, *Angew. Chem. Int. Ed.* **1997**, *36*, 1476-1478; b) R. Zemribo, M. S. Champ, D. Romo, *Synlett* **1996**, *1996*, 278-280; c) L. Fournier, A. Gaudel-Siri, P. J. Kociński, J.-M. Pons, *Synlett* **2003**, *2003*, 0107-0111; d) W. Ren, Y. Bian, Z. Zhang, H. Shang, P. Zhang, Y. Chen, Z. Yang, T. Luo, Y. Tang, *Angew. Chem.* **2012**, *124*, 7090-7094; e) C. A. Leverett, V. C. Purohit, A. G. Johnson, R. L. Davis, D. J. Tantillo, D. Romo, *J. Am. Chem. Soc.* **2012**, *134*, 13348-13356; f) X. Lei, Y. Li, Y. Lai, S. Hu, C. Qi, G. Wang, Y. Tang, *Angew. Chem. Int. Ed.* **2021**, *60*, 4221-4230.
- [12] F. Machrouhi, J.-L. Namy, *Tetrahedron* **1998**, *54*, 11111-11122.
- [13] P. Dubois, O. Coulembier, J.-M. Raquez, *Handbook of ring-opening polymerization*, John Wiley & Sons, **2009**.
- [14] T. Curtius, *Ber. Dtsch. Chem. Ges.* **1883**, *16*, 2230-2231.
- [15] J. F. Lane, W. T. Koch, N. S. Leeds, G. Gorin, *J. Am. Chem. Soc.* **1952**, *74*, 3211-3215.
- [16] H. Wynberg, E. G. Staring, *J. Am. Chem. Soc.* **1982**, *104*, 166-168.
- [17] H. W. Yang, D. Romo, *Tetrahedron* **1999**, *55*, 6403-6434.
- [18] a) E. Knoevenagel, *Ber. Dtsch. Chem. Ges.* **1898**, *31*, 2585-2595; b) R. R. Gupta, M. Kumar, V. Gupta, in *Heterocyclic Chemistry*, Springer, **1998**, pp. 357-410.
- [19] O. Mitsunobu, *Synthesis* **1981**, *1981*, 1-28.
- [20] E. Testa, L. Fontanella, G. F. Cristiani, L. Mariani, *Justus Liebigs Ann. Chem.* **1961**, *639*, 166-180.
- [21] H. E. Zaugg, *Organic Reactions* **2004**, *8*, 305-363.
- [22] A. Pommier, J.-M. Pons, *Synthesis* **1995**, *1995*, 729-744.

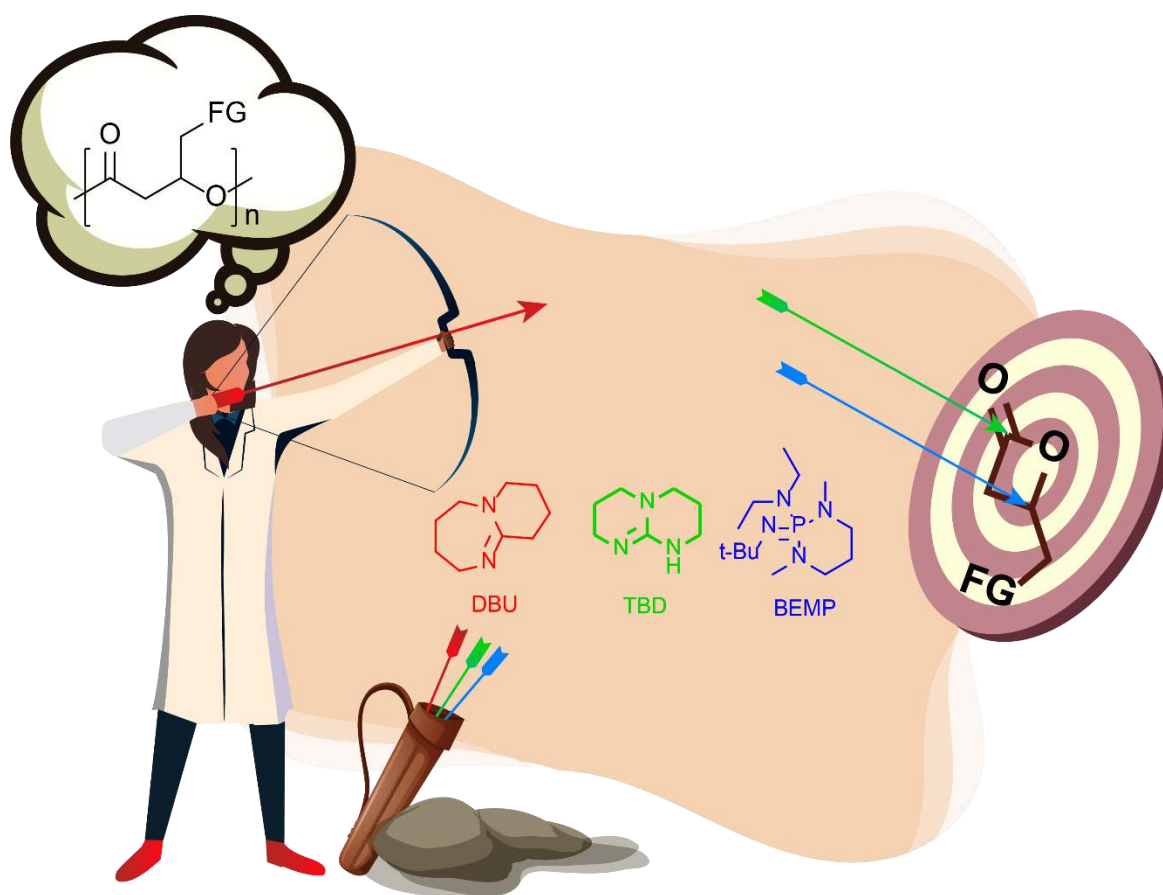
- [23] S. Mukherjee, A. T. Biju, *Chem. Asian J.* **2018**, *13*, 2333-2349.
- [24] H. Staudinger, S. Bereza, *Justus Liebigs Ann. Chem.* **1911**, *380*, 243-277.
- [25] a) M. J. Gaunt, C. C. Johansson, *Chem. Rev.* **2007**, *107*, 5596-5605; b) C. Schneider, *Angew. Chem. Int. Ed.* **2002**, *41*, 744-746; c) A. B. Concepcion, K. Maruoka, H. Yamamoto, *Tetrahedron* **1995**, *51*, 4011-4020; d) I. Hoppe, U. Schöllkopf, *Liebigs Ann. Chem.* **1979**, *1979*, 219-226.
- [26] a) J. Li, D. Menche, *Synthesis* **2009**, *2009*, 2293-2315; b) R. Mahrwald, *Chem. Rev.* **1999**, *99*, 1095-1120; c) R. Mahrwald, *Modern methods in stereoselective aldol reactions*, John Wiley & Sons, **2013**; d) S. G. Nelson, Z. Wan, T. J. Peelen, K. L. Spencer, *Tetrahedron Lett.* **1999**, *40*, 6535-6539.
- [27] J. T. Lee, P. Thomas, H. Alper, *J. Org. Chem.* **2001**, *66*, 5424-5426.
- [28] a) Y. D. Getzler, V. Mahadevan, E. B. Lobkovsky, G. W. Coates, *J. Am. Chem. Soc.* **2002**, *124*, 1174-1175; b) V. Mahadevan, Y. D. Getzler, G. W. Coates, *Angew. Chem.* **2002**, *114*, 2905-2908; c) J. A. Schmidt, V. Mahadevan, Y. D. Getzler, G. W. Coates, *Org. Lett.* **2004**, *6*, 373-376; d) J. A. Schmidt, E. B. Lobkovsky, G. W. Coates, *J. Am. Chem. Soc.* **2005**, *127*, 11426-11435; e) J. W. Kramer, E. B. Lobkovsky, G. W. Coates, *Org. Lett.* **2006**, *8*, 3709-3712; f) J. W. Kramer, G. W. Coates, *Tetrahedron* **2008**, *64*, 6973-6978.
- [29] K. Okuro, T. Dang, K. Khumtaveeporn, H. Alper, *Tetrahedron Lett.* **1996**, *37*, 2713-2716.
- [30] S. E. Schaus, B. D. Brandes, J. F. Larrow, M. Tokunaga, K. B. Hansen, A. E. Gould, M. E. Furrow, E. N. Jacobsen, *J. Am. Chem. Soc.* **2002**, *124*, 1307-1315.
- [31] a) J. Jiang, S. Yoon, *J. Mater. Chem.* **2019**, *7*, 6120-6125; b) H. D. Park, M. Dincă, Y. Román-Leshkov, *ACS central science* **2017**, *3*, 444-448; c) S. Rajendiran, V. Ganesan, S. Yoon, *Inorg. Chem.* **2019**, *58*, 3283-3289.
- [32] J. W. Kramer, D. S. Treitler, G. W. Coates, S. E. Denmark, A. J. Hoover, *Organic Syntheses* **2009**, *86*, 287-297.
- [33] J. G. Dingwall, B. Tuck, *J. Chem. Soc., Perkin Trans. 1* **1986**, 2081-2090.
- [34] R. Qian, Y.-X. Liao, Y.-L. Guo, H. Guo, *J. Am. Soc. Mass. Spectrom.* **2006**, *17*, 1582-1589.
- [35] F. Löbermann, L. Weisheit, D. Trauner, *Org. Lett.* **2013**, *15*, 4324-4326.
- [36] H.-J. Zhong, B. R. Lee, J. W. Boyle, W. Wang, D.-L. Ma, P. W. H. Chan, C.-H. Leung, *Chem. Commun.* **2016**, *52*, 5788-5791.
- [37] H. V. Babu, K. Muralidharan, *Polymer* **2014**, *55*, 83-94.
- [38] A. Soulieman, R. Ibrahim, Z. Barakat, N. Gouault, T. Roisnel, J. Boustie, R. Grée, A. Hachem, *Eur. J. Org. Chem.* **2020**, *2020*, 5741-5751.
- [39] A. B. Kumar, J. M. Anderson, A. L. Melendez, R. Manetsch, *Bioorg. Med. Chem. Lett.* **2012**, *22*, 4740-4744.
- [40] a) W. F. Edgell, J. Lyford IV, *Inorg. Chem.* **1970**, *9*, 1932-1933; b) J. Wöltinger, J. E. Bäckvall, Á. Zsigmond, *Chem. Eur. J.* **1999**, *5*, 1460-1467.
- [41] a) P. C. Steinhardt, W. L. Gladfelter, A. D. Harley, J. R. Fox, G. L. Geoffroy, *Inorg. Chem.* **1980**, *19*, 332-339; b) F. Joó, H. Alper, *Can. J. Chem.* **1985**, *63*, 1157-1160.
- [42] J. W. Kramer, D. S. Treitler, G. W. Coates, *Organic Syntheses* **2003**, *86*, 287-297.
- [43] X.-P. Gu, I. Ikeda, M. Okahara, *Bull. Chem. Soc. Jpn.* **1987**, *60*, 667-672.





## Chapter 3.

# Organocatalyzed ROP of substituted $\beta$ -lactones towards functional PHAs: Macromolecular structure analysis and new insights into the ROP mechanism





<b>1. Objectives .....</b>	<b>117</b>
<b>2. Pioneering ROP of cyclic esters mediated by organic activators: Mechanistic aspects .....</b>	<b>118</b>
2.1. 2- <i>tert</i> -Butylimino-2-diethylamino-1,3dimethylperhydro-1,3,2- diazaphosphorine (BEMP).....	119
2.2. 1,5,7-triazabicyclo[4.4.0]dec-5-ene (TBD).....	123
2.3. 1,8-Diazabicyclo[5.4.0]-undec-7-ene (DBU) .....	127
2.4. Overall considerations on the BEMP, TBD, and DBU-mediated ROP of LA, $\delta$ -VL and $\epsilon$ -CL.....	132
<b>3. State-of-the-art: BEMP, TBD, and DBU as organic activators for ROP of functional <math>\beta</math>-lactones.....</b>	<b>134</b>
<b>4. Results and discussion .....</b>	<b>137</b>
4.1. ROP of BPL <sup>FG</sup> s promoted by BEMP .....	138
4.1.1. Molecular characterization of PBPL <sup>FG</sup> s from BEMP .....	139
4.1.2. BEMP-synthesized PBPL <sup>FG</sup> s macromolecular structure assessed by NMR spectroscopy and MALDI-ToF mass spectrometry .....	141
4.1.3. Mechanistic pathway for the BEMP-mediated ROP of BPL <sup>FG</sup> s.....	152
4.2. ROP of BPL <sup>FG</sup> s promoted by TBD .....	153
4.2.1. Molecular characterization of PBPL <sup>FG</sup> s from TBD .....	154
4.2.2. TBD-synthesized PBPL <sup>FG</sup> s macromolecular structure assessed by NMR spectroscopy and MALDI-ToF mass spectrometry .....	155
4.2.3. Mechanistic pathway for the TBD-mediated ROP of BPL <sup>FG</sup> s.....	162
4.3. ROP of BPL <sup>FG</sup> s promoted by DBU .....	163
4.3.1. Molecular characterization of PBPL <sup>FG</sup> s from DBU.....	164
4.3.2. DBU-synthesized PBPL <sup>FG</sup> s macromolecular structure assessed by NMR spectroscopy and MALDI-ToF mass spectrometry .....	165



4.3.3. Mechanistic pathway for the DBU-catalyzed ROP of BPL <sup>FG</sup> s.....	170
4.4. PBPL <sup>FG</sup> s : stereochemistry, kinetics and thermal properties .....	171
<b>5. Conclusion: Better understanding of the BEMP, TBD, and DBU promoted ROP mechanism of <math>\beta</math>-lactones, and perspectives .....</b>	<b>174</b>
<b>6. Experimental Section .....</b>	<b>177</b>
<b>7. References.....</b>	<b>180</b>

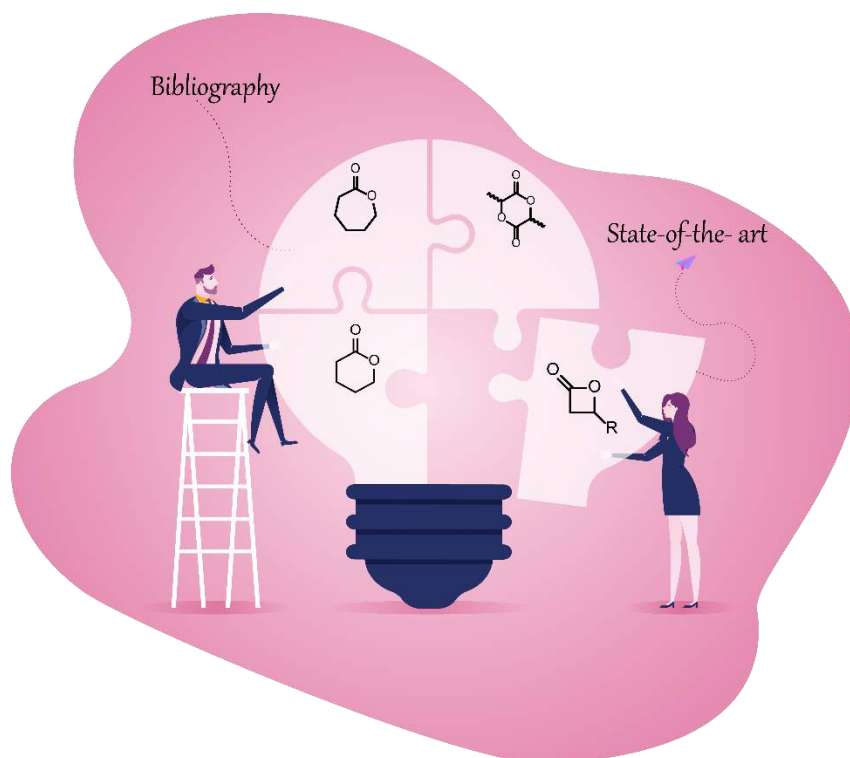
Part of the results gathered in this chapter have been the object of a paper published in [\*Polymer Chemistry\* 2020, 11, 2640-2652](#), entitled "Organocatalyzed ring-opening polymerization (ROP) of functional  $\beta$ -lactones: New insights into the ROP mechanism and poly(hydroxyalkanoate)s (PHAs) macromolecular structure" by R. M. Shakaroun, A. Alaaeddine, P. Jéhan, J.-F. Carpentier, S. M. Guillaume.<sup>1</sup>

---

<sup>1</sup> <https://pubs.rsc.org/en/content/articlelanding/2020/py/d0py00125b#!divAbstract>  
<https://pubs.rsc.org/en/content/articlelanding/2020/py/d0py90062a#!divAbstract>

## 1. Objectives

The ring-opening polymerization (ROP) of  $\beta$ -lactones promoted by organic activators provides a practical, environmentally friendly synthetic process towards the preparation of functional poly(hydroxyalkanoate)s “PHAs” that have not yet been found in nature. While diverse organic activators have been reviewed in Chapter 1, the focus of this Chapter will be on the most common commercially available organic activators, typically phosphazenes, guanidines and amidines such as 2-*tert*-butylimino-2-diethylamino-1,3-dimethylperhydro-1,3,2-diazaphosphorine (BEMP), 1,5,7-triazabicyclo[4.4.0]dec-5-ene (TBD), or 1,8-diazabicyclo[5.4.0]undec-7-ene (DBU),<sup>[1]</sup> that were recently used in the ROP of prevalent  $\beta$ -lactones (BL<sup>Me</sup>, MLA<sup>Bn</sup>), and their mechanistic aspects are still not fully understood to date. In this regard, the ROP of a specific family of  $\beta$ -lactones, namely, 4-alkoxymethylene- $\beta$ -propiolactones (BPL<sup>FG</sup>s, FG = OBn, OAll, O<sup>n</sup>Bu, OTBDMS, OP(O)Ph<sub>2</sub>), mediated by BEMP, TBD, or DBU towards the formation of the corresponding non-bacterial functional PHAs (poly(BPL<sup>FG</sup>)s or (PBPL<sup>FG</sup>)s, FG = (OBn, OAll, O<sup>n</sup>Bu, OTBDMS, OP(O)Ph<sub>2</sub>), was herein investigated for the first time. Analysis of the newly produced polymers microstructures PBPL<sup>FG</sup>s, and reinvestigation of that of the previously synthesized ones PBL<sup>Me</sup> and PMLA<sup>Bn</sup>, were performed on the basis of literature insights to ultimately propose some mechanistic pathways for each of the organic activator used with BPL<sup>FG</sup>s. This then further extends the mechanistic knowledge on  $\beta$ -lactones ROP mediated by the latter organic activators, and contributes forward on disclosing original mechanisms at play. At the outset of this chapter, a brief review of the mode of action of BEMP, TBD, and DBU in ROP of larger cyclic esters (vs.  $\beta$ -lactones) is highlighted for a better perception on their characteristic behavior and general features (Figure 3. 1).

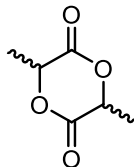
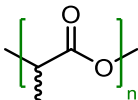
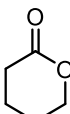
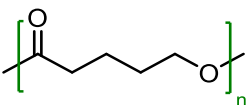
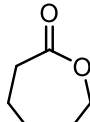
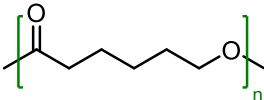


**Figure 3. 1** – Illustration of the work described in Chapter. 3 on ROP mediated by the organic activators BEMP, TBD, or DBU; starting from bibliography of Lactide,  $\delta$ -valerolactone, and  $\epsilon$ -caprolactone to the state-of-the-art on  $\beta$ -lactones.

## 2. Pioneering ROP of cyclic esters mediated by organic activators: Mechanistic aspects

One particular interest of our work being the comprehension of the mechanistic pathway of BEMP, TBD, and DBU-promoted ROP of  $\beta$ -lactones, it is essential to relate our studies to the modes of action of these catalysts in the ROP of related cyclic ester monomers that similarly feature an ester group ( $\text{OC=O}$ ) and  $\alpha$ -hydrogen; this is notably the case of the previously investigated larger cyclic esters that are lactide “LA”,  $\delta$ -valerolactone “ $\delta$ -VL”, and  $\epsilon$ -caprolactone “ $\epsilon$ -CL”. Within the past two decades, extensive studies were done on the ROP mediated by BEMP, TBD, and DBU of these latter commercially available cyclic esters, to obtain poly(lactide) (PLA), poly( $\delta$ -valerolactone) (PVL) and poly( $\epsilon$ -caprolactone) (PCL), respectively (Table 3. 1).<sup>[2]</sup> Generally, polymerizations were performed using distinct reaction conditions such as different reaction temperature, solvent or absence of solvent, and most notably the presence or absence of alcohol co-initiator and/or organic cocatalyst accompanying BEMP, TBD or DBU. The characteristics and the activity of BEMP, TBD, and DBU towards these cyclic esters is demonstrated separately thereafter.

**Table 3. 1** – Significant polyesters and their associated cyclic ester monomer that can be prepared from the ROP mediated by organic activators “BEMP, TBD, and DBU”.

Cyclic ester	Polyester
 lactide (LA)	 Polylactide - PLA
 $\delta$ -valerolactone ( $\delta$ -VL)	 poly( $\delta$ -valerolactone) - PVL
 $\epsilon$ -caprolactone ( $\epsilon$ -CL)	 poly( $\epsilon$ -caprolactone) - PCL

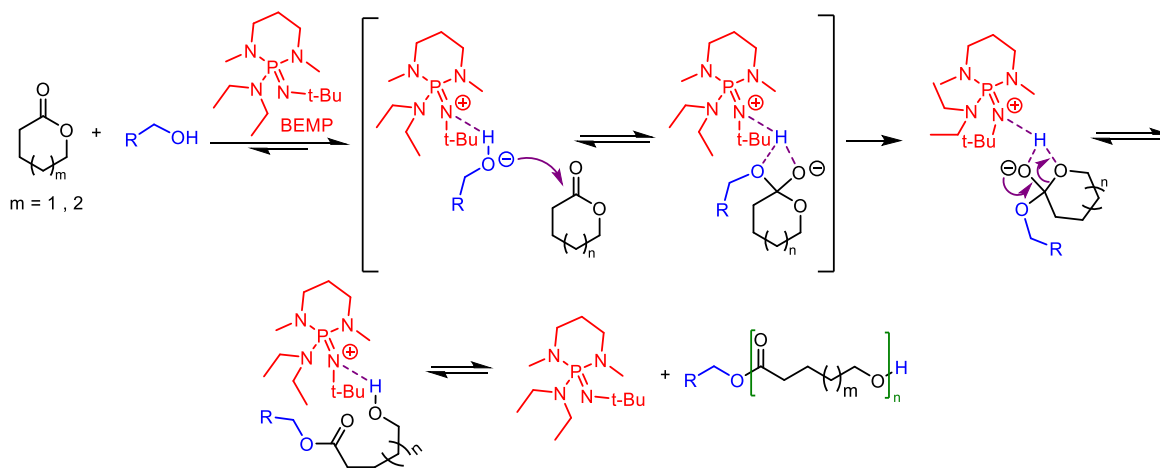
### 2.1. 2-*tert*-Butylimino-2-diethylamino-1,3dimethylperhydro-1,3,2-diazaphosphorine (BEMP)

2-*tert*-Butylimino-2-diethylamino-1,3-dimethylperhydro-1,3,2-diazaphosphorine (BEMP) is the most common phosphazene base. Phosphazene bases are well known to possess a remarkable basicity (in acetonitrile, their pK<sub>a</sub> values range within 26–47) and weak nucleophilicity,<sup>[3]</sup> and thus they have found various usages in the organic synthesis domain. Most phosphazene bases have been synthesized and characterized by Schwesinger.<sup>[4]</sup> They are extremely strong, uncharged Brönsted bases, which contain at least one phosphorus atom bonded to four nitrogen atoms of three amines and one imine substituents. Besides their high basicity, they combine many interesting features such as their high solubility in apolar-to-moderately polar solvents, remarkable stability towards electrophilic attacks, oxidation, and hydrolysis, as well as good thermal stability, easy handling and work up.<sup>[5]</sup> Phosphazene bases have attracted interest in the field of anionic ring-opening polymerization (AROP) of heterocyclic monomers, since these non-ionic superbases generate highly reactive anionic species by deprotonation of acids, thereby becoming the counter cation themselves.<sup>[5-6]</sup>

BEMP was basically used as a base (<sup>MeCN</sup>pK<sub>a</sub> = 27.6)<sup>[4]</sup> for assorted organic reactions such as Michaël addition and alkylation.<sup>[7]</sup> In 2007, its first exploitation as a polymerization organocatalyst was accompanied by an alcohol co-initiator (RCH<sub>2</sub>OH, mainly benzyl alcohol “BnOH” or 1-pyrene butanol ) for the ROP of LA,  $\delta$ -VL and  $\epsilon$ -CL. BEMP was found to be an

active organocatalyst in the ROP of *rac*-LA and *L*-LA (with monomer loading ca. DP = 100) in toluene at room temperature when accompanied with BnOH and 1-pyrene butanol, respectively. Isotactic-enriched PLA (probability of isotactic enchainment of adjacent monomer units;  $P_m = 0.70$ ;  $M_{n,SEC} = 15,000 \text{ g mol}^{-1}$ ;  $D_M = 1.05$ ), and pure isotactic PLA ( $P_m = 0.98$ ;  $M_{n,SEC} = 13,000 \text{ g mol}^{-1}$ ;  $D_M = 1.08$ ), were afforded after 66 h (97% conversion of *rac*-LA) and 23 h (76% conversion of *L*-LA), respectively. Whereas PVL was produced in bulk from BEMP/1-pyrene butanol system from  $\delta$ -VL, with 70% conversion off 100 equivalents, after 73 h, reaching a molar mass of  $9200 \text{ g mol}^{-1}$  and  $D_M$  1.12. On the other hand, the ROP of  $\epsilon$ -CL was sluggish (14% conversion of 100 equivalents after 10 days) even at elevated temperatures ( $80^\circ\text{C}$ ).<sup>[8]</sup>

Under such circumstances, BEMP was estimated to catalyse the ROP of LA,  $\delta$ -VL and  $\epsilon$ -CL by activating the alcohol co-initiator via a proton transfer mechanism. In this type of mechanisms, BEMP facilitate the alcohol attack (increase its nucleophilicity) on the monomer carbonyl group to ring-open the monomer via *O*-acyl cleavage, and then to continue propagation through pseudo-anionic active specie (Scheme 3. 1). This proposal was based on  $^1\text{H}$  NMR analyses that showed the presence of an intermolecular hydrogen bond between BEMP and the acidic hydrogen of the alcohol, and the absence of BEMP-LA/VL/CL adduct (*N*-CO bond) in solution.<sup>[8]</sup>

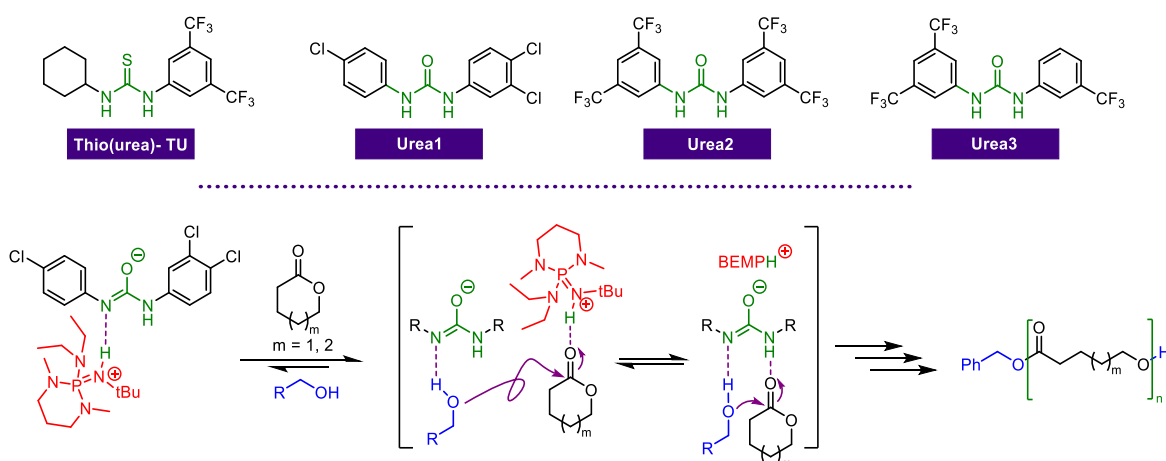


**Scheme 3. 1** – Proposed mechanism of the ROP of cyclic esters (LA,  $\delta$ -VL,  $\epsilon$ -CL) promoted by a BEMP-ROH catalytic system, revealing the catalytic activity of BEMP via H-transfer and its regeneration.<sup>[8]</sup>

Further studies successfully enhanced the activity of BEMP by associating it with a H-bond donating cocatalyst to increase the ring-strain of the monomer, such as with thiourea (TU) or Urea (Urea1-3) (Scheme 3. 2 – top), resulting in bifunctional phosphazene-thiourea/urea

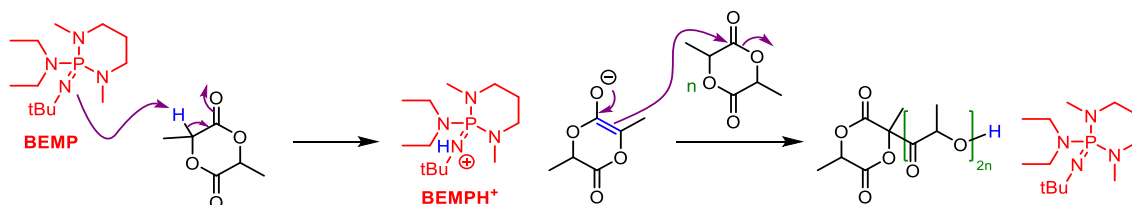
catalytic systems.<sup>[9]</sup> The ROP process was found to be depended on the cocatalyst and on the solvent used. For example, upon using a 5%mol TU – 5%mol BEMP catalytic system with ROH in toluene for the ROP of  $\delta$ -VL (DP = 500) and  $\epsilon$ -CL (DP = 100) at room temperature, PVL was obtained in good yield after 5 h (98% conversion,  $\bar{D}_M = 1.01$ ) and PCL was recovered after 75 h (94% conversion,  $\bar{D}_M = 1.02$ ).<sup>[10]</sup> However, 5%mol Urea**1** – 5%mol BEMP and ROH catalytic system was shown to be more effective, where PVL (DP = 500) and PCL (DP = 100) were produced in C<sub>6</sub>D<sub>6</sub> in good yields and narrow dispersities only in 10 min (90% conversion,  $\bar{D}_M = 1.05$ ) and 6 min (90% conversion,  $\bar{D}_M = 1.04$ ), respectively. Nevertheless, the same ROPs failed to reach full conversion in more polar solvents, e.g. THF or acetone-*d*<sub>6</sub>, within 30 min.<sup>[11]</sup> Interestingly, when performing the ROP of  $\delta$ -VL (DP = 500) in the absence of any solvent at room temperature, PVL with high molar masses and narrow dispersities (95% conversion,  $M_{n,SEC} = 108,000 \text{ g mol}^{-1}$ ,  $\bar{D}_M = 1.04$ ) were obtained with higher rates than in C<sub>6</sub>D<sub>6</sub> (3 min vs. 10 min) even with lower catalyst/cocatalyst loadings (0.5%mol Urea**1** – 0.5%mol BEMP and ROH); the only drawback was the solidification of the reaction medium at high conversions > 60%, yet living polymerization was achieved.<sup>[12]</sup> Another attempt on the ROP of  $\delta$ -VL (DP = 100) fostered by 2.5%mol Urea**2-3** – 2.5%mol BEMP and ROH catalytic system in toluene to reach 94% and 95% conversion in 45 sec and 20 sec at room temperature with Urea**2** and Urea**3**, respectively. It was noted that the activity of cocatalyst Urea**3** was higher than that of Urea**2** as the result of the acidity of Urea**3** ( $pK_a^{DMSO} = 16.1$ ) which is closer to the acidity of BEMPH<sup>+</sup> ( $pK_a^{DMSO} = 16.5$ ) than Urea**2** ( $pK_a^{DMSO} = 13.8$ ).<sup>[13]</sup> The authors suggested that the TU/Urea–BEMP–ROH catalytic system mediates the ROP of  $\delta$ -VL and  $\epsilon$ -CL through an imidate-mediated mechanism due the high basicity of BEMP, where the TU/Urea is protonated first by BEMP, and then TU/Urea activates the alcohol co-initiator while BEMP activates the monomer, as illustrated in Scheme 3. 2.

## Cocatalysts



**Scheme 3. 2** – (Top) TU and Urea**1-3** structures used as cocatalysts; (bottom) plausible mechanism for the ROP of  $\delta$ -VL and  $\epsilon$ -CL promoted by Urea/TU–BEMP–ROH catalytic system, that shows higher efficiency than BEMP–ROH catalytic system (Scheme 3. 1), where BEMP acts as an organocatalyst, Urea behaves as an organic cocatalyst and ROH as an organic initiator.<sup>[11]</sup>

The role of BEMP in the absence of an alcohol co-initiator was examined in 2015-2017 for the ROP of *rac*-LA in dichloromethane<sup>[14]</sup> and of  $\delta$ -VL in a solvent free medium,<sup>[12]</sup> affording PLA after 8 min (65% conversion of 100 equivalences at room temperature,  $M_{n,SEC} = 8300 \text{ g mol}^{-1}$ ,  $D_M = 1.24$ ) and PVL after 21 days (17% conversion of 200 equivalence room temperature), respectively. Depending on the matrix assisted laser desorption ionization - time of flight mass spectrometry (MALDI-ToF MS) analysis, the authors detected an enolate chain end-group on the produced PLA and PVL. Accordingly, they presumed that BEMP initiates the polymerization by forming an enolate active species ready to undergo anionic propagation with  $BEMPH^+$  as counter cation, that would be regenerated after H-transfer to the polymer chain (Scheme 3. 3).



**Scheme 3. 3** – Proposed ROP mechanism of LA (or  $\delta$ -VL) in the presence of BEMP only via enolate formation, where BEMP act as a H-transfer catalyst to produce PLA and PVL end-capped with their relative cyclic enolate.<sup>[14]</sup>

Overall, one can perceive that the ROP of LA,  $\delta$ -VL and  $\epsilon$ -CL (Table 3. 1) performed by BEMP is efficient and controlled in terms of molar masses, dispersities, and chain-ends. The efficiency of BEMP was found to depend on the polymerization medium (reagents, solvents).

BEMP act as an organocatalyst when accompanied with a ROH co-initiator to ring-open cyclic esters with the rate trend of monomer activity is: LA >  $\delta$ -VL >  $\epsilon$ -CL, by means of hydrogen transfer mechanism. Interestingly, in the absence of any protic co-reagents (ROH), BEMP mediates the polymerization via an anionic process through a H-transfer mechanism to form *in situ* enolate by abstracting the  $\alpha$ -acidic hydrogen of the monomers. When accompanied with a hydrogen bonding cocatalyst (TU or Urea**1-3**), BEMP revealed more active. BEMP appeared to best mediate the ROP in bulk medium rather than in non-polar solvents, and to be poorly efficient in polar solvents when accompanied with an alcohol. This may raise some questionings on the 1,5,7-triazabicyclo[4.4.0]dec-5-ene (TBD) performance in ROP of LA,  $\delta$ -VL,  $\epsilon$ -CL, that will be addressed below.

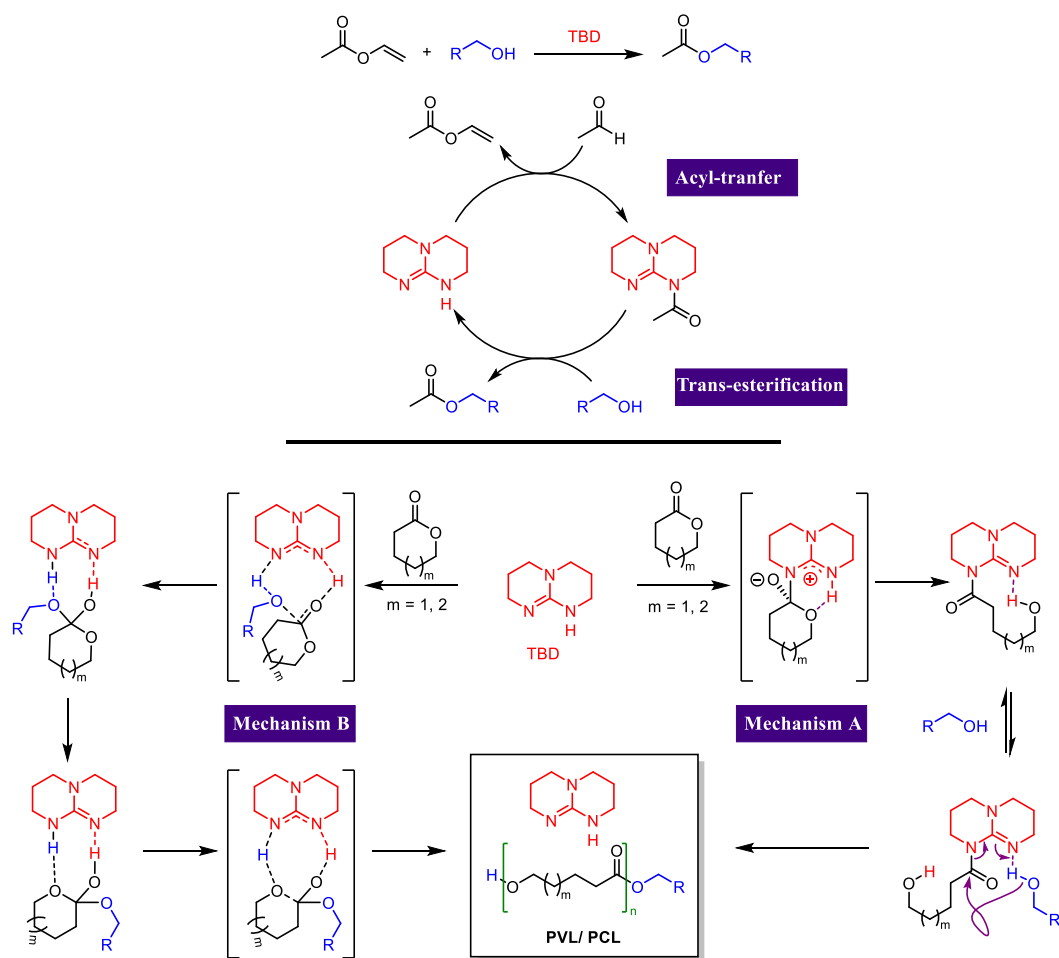
## 2.2. 1,5,7-Triazabicyclo[4.4.0]dec-5-ene (TBD)

1,5,7-Triazabicyclo[4.4.0]dec-5-ene (TBD) is a commercially available organic soluble bicyclic strong guanidine base ( $^{\text{MeCN}}\text{pK}_a = 26.0$ ).<sup>[4]</sup> TBD received considerable attention due to its multifunctional organocatalyst role,<sup>[15]</sup> acting as a base<sup>[16]</sup> proton transfer agent<sup>[17]</sup>, nucleophile<sup>[18]</sup> or even bifunctional<sup>[19]</sup> catalyst for different types of reactions.<sup>[20]</sup> More importantly, TBD was found to be the strongest nucleophile in the guanidine series,<sup>[21]</sup> and was shown to react with malonate esters via nucleophilic attack of both disubstituted nitrogen atoms at the carbonyl groups to form betaine-like structures.<sup>[22]</sup>

Over the last decades, TBD was shown to be an efficient organocatalyst for the ROP of LA,  $\delta$ -VL and  $\epsilon$ -CL initiated by alcohols in solution ( $\text{CH}_2\text{Cl}_2$  or  $\text{C}_6\text{D}_6$ ). In 2006, their polymerization was successfully carried out by Hedrick and co-workers, mediated with TBD–1-pyrene butanol catalytic system, and the corresponding PLA, PVL, and PCL were obtained with narrow dispersities and predictable degrees of polymerization (DPs). At room temperature, 95% conversion of 500 equivalence *rac*-LA in 1 min from 0.1% TBD, and 77% conversion of 200 equivalence  $\delta$ -VL in 30 min from 0.3% TBD, and 72% conversion of 200 equivalence  $\epsilon$ -CL in 8 h from 0.5% TBD, were afforded to produce the corresponding polyesters with  $\bar{D}_M = 1.11$ –1.16.<sup>[23]</sup> However, this high activity of TBD is impeded by its ability to catalyse transesterification side-reactions, resulting in the loss of the control of the molecular parameters observed at extended reaction times.<sup>[23a]</sup> Such a behavior was more pronounced in the case of PVL and PCL than PLA.<sup>[23b]</sup>

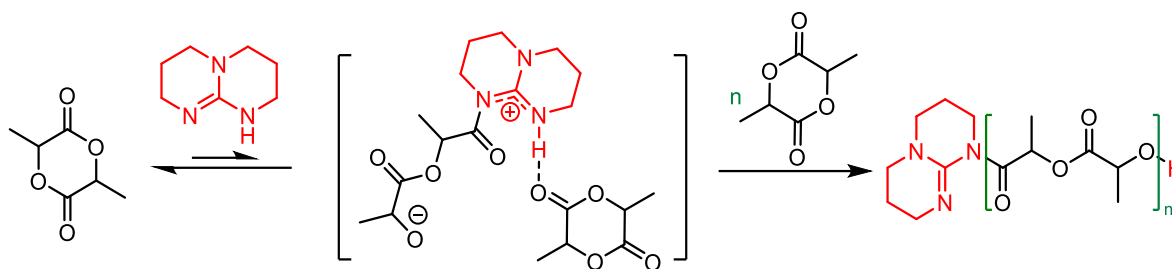


Regarding the mechanistic pathway, the authors suggested a bifunctional role of TBD in the ROP of LA,  $\delta$ -VL and  $\epsilon$ -CL, acting both as a nucleophile to activate the acyl group of the monomer permitting afterward a transesterification reaction via ROH initiator, and then to continue as a hydrogen bonding agent (Scheme 3. 4 – bottom; mechanism A).<sup>[23]</sup> This mechanism was established relying on TBD's reactivity when mixed with vinyl acetate. TBD was revealed as an efficient acyl-transfer catalyst since a TBD-*N*-acyl adduct was detected by <sup>1</sup>H NMR spectroscopy. TBD also behaves as a transesterification catalyst as evidenced by the quantitative formation of benzyl acetate after addition of benzyl alcohol to the TBD-*N*-acyl adduct, thus eliminating its role as a base catalyst, according to the authors.<sup>[23]</sup> Further studies were conducted to reveal a remarkable ability of TBD to catalyse acylation reactions due to its stereoelectronic properties based on spectroscopic mechanistic and theoretical studies.<sup>[24]</sup> Even though, they hinted that an alternative pseudo-anionic mechanism attributed entirely on H-bonding is also plausible (Scheme 3. 4 – bottom; mechanism B). In the first step of this pathway, the hydrogen attached to the nitrogen of TBD activates the carbonyl group of the cyclic ester, and the imine nitrogen simultaneously activates the alcohol by attracting the hydrogen of its hydroxyl group through a lone pair interaction. This results in an intermediate with a tetrahedral center at the carbon of this carbonyl group. TBD then affects the subsequent ring-opening by continuing to hydrogen-bond the oxygen of the carbonyl group, but then transferring the hydrogen (originally from the alcohol) to the ring-oxygen adjacent to the carbonyl group.<sup>[23a]</sup> In any case, they assured the bifunctionality of TBD by its two nitrogen atoms, reasoning this by the much lower activity (90 times slower) obtained from the methyl substituted TBD “MTBD” in the ROP of LA. However, in 2007-2010, additional investigation was done with the aid of density functional theory (DFT computations) by Goodman *et al.*<sup>[25]</sup> and by Hedrick/Waymouth *et al.*,<sup>[26]</sup> confirming that mechanism A is feasible, but has a considerably higher barrier than mechanism B (Scheme 3. 4 – bottom). Although experimental evidences were lacking, they lean toward mechanism B, strengthened it by the fact that the polymerization rates in less polar solvents (benzene and dichloromethane) are higher than that in more polar solvents (THF and DMF), thereby suggesting pseudo-anionic mechanisms instead of complete anionic polymerization. Moreover, mechanism B was further corroborated in 2016 by advanced DFT studies.<sup>[27]</sup> Decisively, TBD is currently recognized as a H-bonding bifunctional catalyst behaving as TU and Urea cocatalysts (Scheme 3. 2), a great advantage for utilization in the ROP of heterocycles.<sup>[28]</sup>



**Scheme 3. 4** – Postulated mechanisms (top) reaction of TBD with vinyl acetate; (bottom) bifunctionality of TBD in the ROP of cyclic esters (LA,  $\delta$ -VL and  $\epsilon$ -CL) in the presence of alcohol; (right) Mechanism A: TBD catalyses the ROP acting as a nucleophile and a H-bond donor; (left) Mechanism B: TBD catalyses the ROP via H-bond donor and acceptor solely.

In 2015, an attempt to ring-open polymerise *L*-LA in DCM using TBD in the absence of an alcohol or of any protic co-initiator/co-catalyst generated PLA (11% conversion of 500 equivalence in 8 sec at room temperature,  $M_{n,SEC} = 19,000 \text{ g mol}^{-1}$ ,  $\bar{D}_M = 1.39$ ). Concerning the mechanism, the authors reported that TBD exhibits a mixed behaviour, involving nucleophilic initiation to produce a covalent acylated TBD zwitterion active species that apparently propagates via a H-bond mechanism with the same TBD molecule (Scheme 3. 5). This mechanism was supported by the identification of the microstructure of the produced PLA by  $^1\text{H}$  NMR spectroscopy and MALDI-ToF MS spectrometry analyses, the latter revealing PLA chains end-capped with TBD and hydroxy moieties at both termini.<sup>[14]</sup> This result emphasizes the impact of the polymerisation medium on the activity of TBD to behave either as a catalyst or as an initiator, or both.



**Scheme 3. 5** – Proposed mechanism for the ROP of LA in solution in the presence of TBD only, displaying the nucleophilic tendency of TBD in the absence of an alcohol and maintaining its H-bonding catalytic activity.

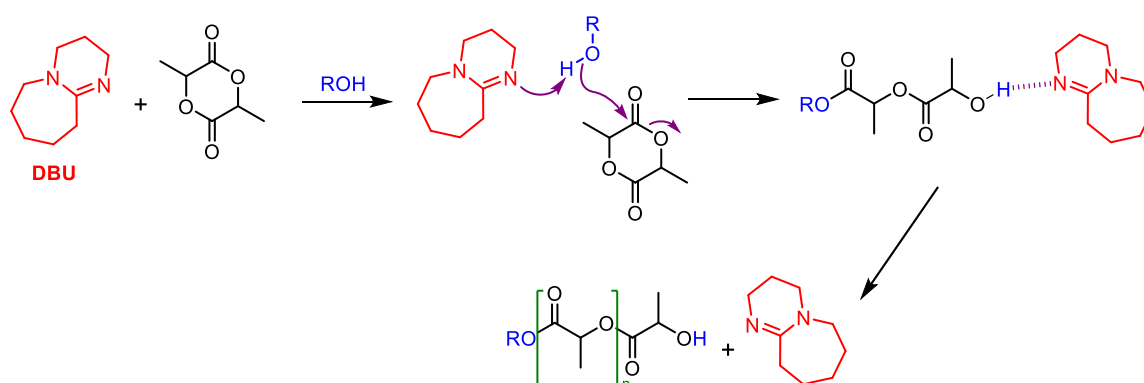
In 2017, the ROP of  $\delta$ -VL (DP = 500) was performed under neat conditions (solvent-free) in the presence of TBD and BnOH, to produce PVL with high molar mass ( $M_{n,SEC} = 115,500 \text{ g mol}^{-1}$ ) in 27 min at room temperature  $^{\circ}\text{C}$ . It was stated that the rate trends in neat VL is nearly similar to that in solution but with broadened dispersities ( $\mathcal{D}_M = 1.21$  vs. 1.12).<sup>[12]</sup> Recently, in 2020, TBD proved to be efficient in the ROP of *rac*-LA and *meso*-LA in toluene ( $[\text{LA}]/[\text{BnOH}]/[\text{TBD}] = 100:1:1$ ) at low temperatures ( $-75^{\circ}\text{C}$ ) to obtain highly isotactic ( $P_m = 0.85$ ) and heterotactic ( $P_m = 0.80$ ) PLA with 77% and 82% conversion after 30 min and  $\mathcal{D}_M$  of 1.25 and 1.24, respectively. Alternatively, the polymerization was done in DCM rather than toluene at a lower catalytic ratio ( $[\text{rac-LA}]/[\text{BnOH}]/[\text{TBD}] = 100:1:0.1$ ) to barely increase the tacticity control of PLA ( $P_m = 0.88$ ) and improve the conversion (90% in 1 h,  $\mathcal{D}_M = 1.09$ ). The authors then postulated that stereoselectivity (0.85 vs. 0.88) is independent of the solvent (toluene vs. DCM) but that it is dependent on the secondary intermolecular interactions between TBD, polymer chain-end, and the LA monomer. Hence, they once again suggested the H-bonding mechanism illustrated in Scheme 3. 4 (bottom, mechanism B) further supporting it by DFT studies, while, the higher conversion was justified by the higher solubility of *rac*-LA in DCM than in toluene.<sup>[29]</sup>

In spite of that, TBDs' basicity is slightly lower than that of BEMP ( $^{\text{MeCN}}\text{pK}_a = 26$  vs. 27.6),<sup>[4]</sup> it revealed to be more active in mediating controlled ROP of LA,  $\delta$ -VL and  $\epsilon$ -CL (Table 3. 1) in terms of molar masses, dispersities, chain-ends and tacticity, albeit the presence of more pronounced transesterification side-reactions (in the case of  $\delta$ -VL and  $\epsilon$ -CL). The high activity of TBD is reasonable since the basicity of the organic activator during the polymerization was noticed not to be the sole criterion. What essential is its ability to undertake intermolecular hydrogen bonding interactions through TBD's two active nitrogen atoms (H-bond donor and acceptor). Thus, unlike BEMP, TBD did not need to be accompanied by any H-bonding cocatalysts (TU or Urea), and it was even active for the ROP of lactides at  $-75^{\circ}\text{C}$ . TBD showed

to have the same reactivity trend as BEMP towards the monomers, that is  $LA > \delta\text{-VL} > \varepsilon\text{-CL}$ . Besides, its mode of action also relied on the polymerization medium as further confirmed by DFT studies. When TBD is accompanied with a ROH co-initiator, it behaves as an organocatalyst promoting the ROP through H-bonding. However, in the absence of co-initiator or of any other reagents, TBD acts as both an initiator (nucleophile) and as a catalyst (H-bonding). TBD is more active in bulk than in less polar solvents, and even less active in polar solvents.

### 2.3. 1,8-Diazabicyclo[5.4.0]-undec-7-ene (DBU)

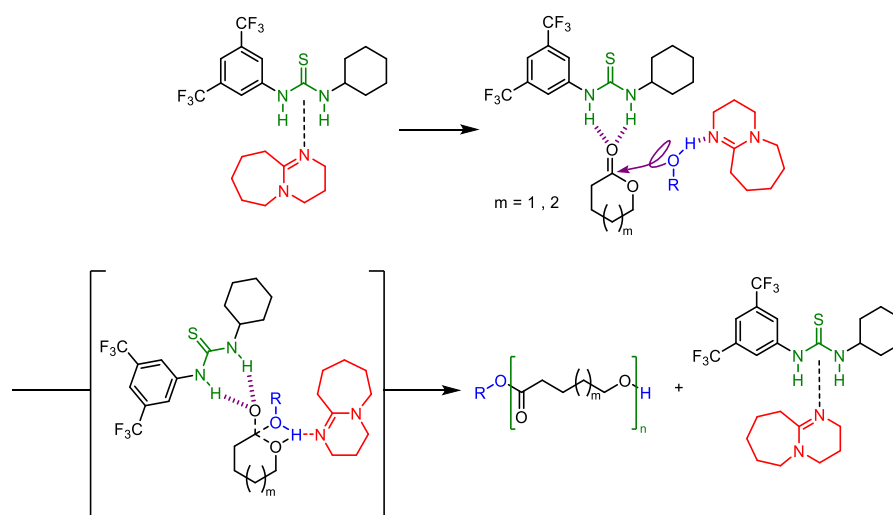
1,8-Diazabicyclo[5.4.0]undec-7-ene (DBU) is a commercially available organic compound which belongs to the amidine family. DBU has been established as a super base ( $^{\text{MeCN}}\text{pK}_a = 24.3$ )<sup>[4]</sup> in the sixties<sup>[30]</sup>, and later identified as a nucleophile,<sup>[31]</sup> while being recently showed to display a significant dual activity as a base and a nucleophile in some organic reactions.<sup>[32]</sup> Currently, DBU has proven to be a valuable ROP organocatalyst and has been largely applied to the ROP of LA,  $\delta\text{-VL}$  and  $\varepsilon\text{-CL}$ . In 2006, assessing DBU with an initiator (1-pyrene butanol) in solution ( $\text{CH}_2\text{Cl}_2$  or  $\text{C}_6\text{D}_6$ ) revealed successful for the ROP of *L*-LA ( $\text{DP} = 500$ ), affording 98% conversion after 2 h at 21 °C and PLA with narrow dispersities ( $\text{D}_M = 1.08$ ). Under these conditions, DBU was postulated to stimulate the ROP of LA by means of H-transfer mechanism (Scheme 3. 6) similarly to that mediated by BEMP (Scheme 3. 1, *vide supra*).<sup>[23b]</sup>



**Scheme 3. 6** – Postulated mechanism for ROP of LA by a DBU-ROH catalytic system, where DBU acts as an organocatalyst promoting H-transfer mechanism and then regenerates.

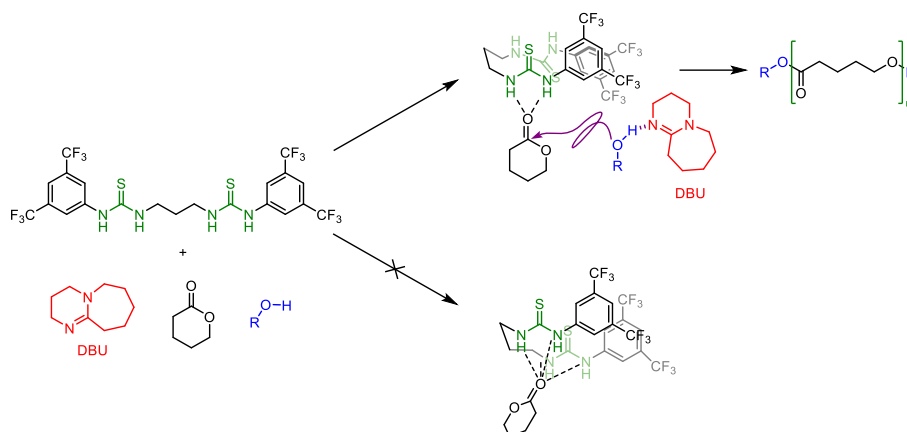
On the other hand, the ROP of  $\delta\text{-VL}$  and  $\varepsilon\text{-CL}$  ( $\text{DP} = 100$ ) remained unsuccessful (0% conversion after days at 21 °C), even after increasing the DBU loading (1 to 5%).<sup>[23b]</sup> Hinted by the high activity of TBD caused by its bifunctionality as a H-bond donor and acceptor at the

same time, it was conceded to accompany DBU (which is a H-bond acceptor only) with a H-bond donor cocatalyst such as TU or Urea. Indeed, the addition of 5mol% TU (Scheme 3. 2 – top) DBU in the polymerization medium enabled to ring-open polymerize  $\delta$ -VL (DP = 200) and  $\varepsilon$ -CL (DP = 100) in a control manner to give PVL (95% conversion in 6 h at 21 °C,  $\bar{D}_M$  = 1.05) and PCL (78% conversion in 120 h at 21 °C,  $\bar{D}_M$  = 1.05), respectively. The surmised mechanism in this case involves neutral H-bonding, where TU activates the monomer (carbonyl) and DBU increases the nucleophilicity of the alcohol (Scheme 3. 7). The TU/urea–DBU–ROH mechanism is different to that suggested for TU/urea–BEMP–ROH catalytic system (Scheme 3. 2, *vide supra*). This is due to the higher basicity of BEMP relative to DBU ( $^{\text{MeCN}}\text{pK}_a = 27.6 > 24.3^{[4]}$ ), making TU act as a counter-anion in case of BEMP and as an activator for the monomer in case of DBU.<sup>[10a, 23b]</sup>



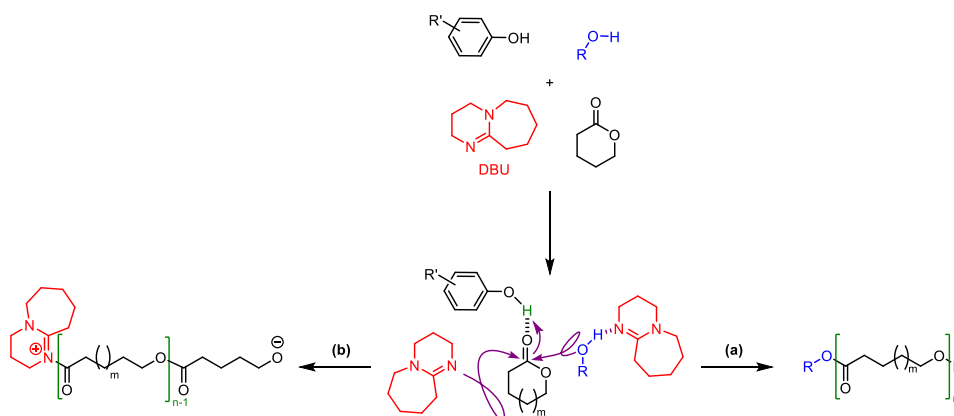
**Scheme 3. 7** – Surmised mechanism of the ROP of  $\delta$ -VL and  $\varepsilon$ -CL through neutral H-bonding interplay, activation of alcohol by DBU (H-acceptor) and of the monomers by TU (H-donor).

In 2016-2018, bisTU or Urea1 or Urea2 (2.5/5/2.5 mol%) (Scheme 3. 2 – top) was used as the cocatalyst with DBU (2.5/5/2.5 mol%) for the ROP of  $\delta$ -VL (DP = 100) in  $\text{C}_6\text{D}_6$  or toluene at room temperature to obtain PVL more effectively (86/90/92% conversion in 90/81/7 min,  $\bar{D}_M$  = 1.05/1.06/1.02), respectively. The mechanism reported for Urea1-2–DBU–ROH catalytic system is the same as that with TU (Scheme 3. 7),<sup>[11, 13]</sup> while that of the bisTU–DBU–ROH catalytic system was suggested to proceed through an activated-TU mechanism, whereby one TU moiety activates the other instead of a dual activation mechanism (Scheme 3. 8), as asserted by computational studies.<sup>[10b]</sup> Furthermore, even better enhanced activity was obtained in bulk upon using Urea1 (0.5 mol%) for the ROP of  $\delta$ -VL (DP = 500), allowing the production of PVL (97% conversion in 65 min at room temperature,  $\bar{D}_M$  = 1.12).<sup>[12]</sup>



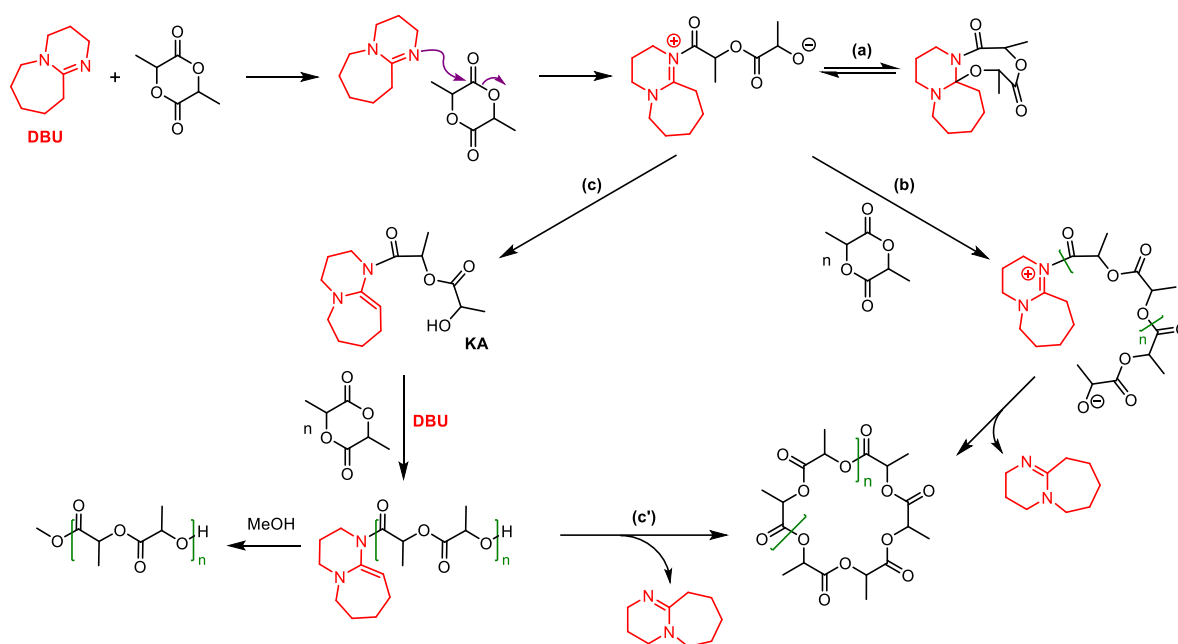
**Scheme 3. 8** – Anticipated mechanism for the ROP of  $\delta$ -VL activated by TU, as promoted by the bisTU–DBU–ROH catalytic system.

Phenols are another cocatalysts that were investigated in 2012 along with DBU for the ROP of  $\delta$ -VL (DP = 25) and of  $\epsilon$ -CL (DP = 25) at room temperature. It is true that phenols were less active than TU, reaching 80% conversion after 24 h and 120 h, respectively, yet they are advantageously commercially available reagents (unlike TU) and the polymerizations can be performed under mild experimental conditions (over the bench, no pre-drying of reactants). An unprecedented mechanistic pathway was suggested after the detection of DBU as a chain-end of PVL by MALDI-ToF MS, which involves a nucleophilic activation of the monomer by DBU via *O*-acyl cleavage as a concomitant pathway to that of the neutral H-bonding (Scheme 3. 9).<sup>[33]</sup>



**Scheme 3. 9** – Expected two concomitant mechanistic pathways for the ROP of  $\delta$ -VL (m =1) and  $\epsilon$ -CL (m=2) mediated by phenol–DBU–ROH catalytic systems via neutral H-bonding and initiation by either (a) ROH or (b) free DBU.

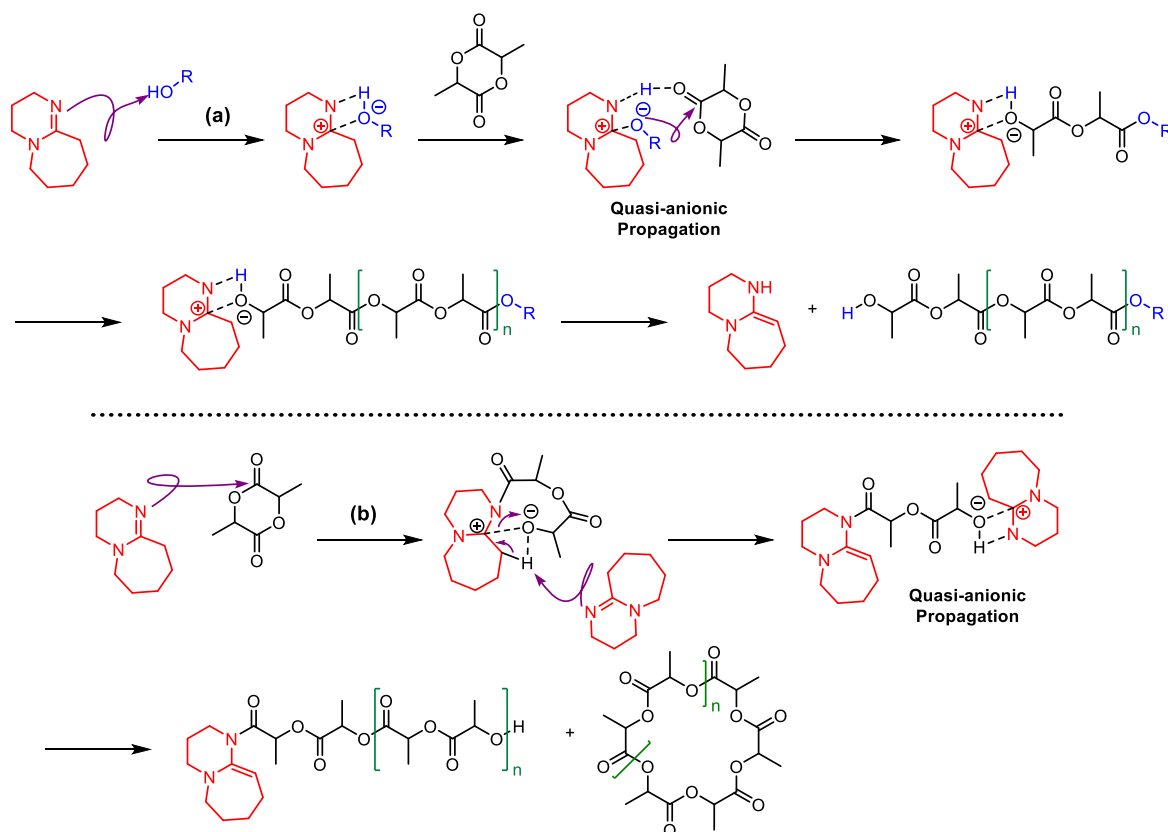
On the other hand, DBU acted specifically as a nucleophile in the absence of alcohol or of any other proton-containing activators, in the ROP of *L*-LA in DCM. In this work, Waymouth *et al.* detected the formation of macrocyclic PLA mixed with minor amounts of linear PLA ( $56,000 \text{ g mol}^{-1}$ ,  $D_M = 1.63$ ) that were end-capped with MeO groups after treatment of the reaction mixtures with MeOH, as assessed by MALDI-ToF MS. It was proposed that DBU initiates the zwitterionic ROP by forming a zwitterionic acyl-amidinium intermediate that may undergo several pathways. The first one was the reversible ring closure to the neutral tricycle, which would likely be a dormant species (Scheme 3. 10 – (a)), or ionic nucleophilic chain growth propagation to larger zwitterions followed by cyclization with a release a cyclic PLA and DBU (Scheme 3. 10 – (b)). Otherwise, intramolecular deprotonation of the zwitterion could generate the neutral ketene-aminal (KA), that can propagate to form linear PLA (Scheme 3. 10 – (c)), with the possibility to also cyclize and generate cyclic PLA (Scheme 3. 10 – (c')). This mechanism was further supported by DFT calculations.<sup>[34]</sup>



**Scheme 3. 10** – Mechanistic proposal for the ROP of *L*-LA mediated by the nucleophilic DBU in the absence of alcohol; (a) reversible dormant neutral tricyclic species; (b) ionic propagation of the zwitterionic intermediate to produce cyclic PLA; (c) propagation via neutral ketene-aminal (KA) intermediate producing linear and (c') cyclic PLA.

In 2016, Won and co-workers considered the effect of the  $[\text{ROH}]/[\text{DBU}]$  ratio on the mechanistic pathway for the ROP of *rac*-LA. In the presence of excess ROH ( $[\text{ROH}] \gg \gg [\text{DBU}]$ ), DBU was found to act as a base to activate ROH and then to continue via a quasi-anionic propagation, ultimately terminated by traces of acids (**Scheme 3. 11** – (a)). An excellent agreement between theoretical and experimental molar masses was obtained along with narrow

dispersities ( $M_{n,theo} = 9824 \text{ g mol}^{-1}$  vs.  $M_{n,SEC} = 8800 \text{ g mol}^{-1}$ ;  $\bar{D}_M = 1.12$ ). On the other hand, with excess DBU ( $[ROH] \ll [DBU]$ ), DBU interplayed between two polymerization routes to most likely behave as a nucleophile and initiate the ROP via the KA intermediate similar to that of Scheme 3. 11 – ((c),(c')), and less likely as a base to activate ROH (Scheme 3. 11- (a)) to finally give a mixture of cyclic and linear PLA (Scheme 3. 11). In such conditions, a loss of agreement between theoretical and experimental molar masses was observed with somehow broadened dispersities ( $M_{n,theo} = 31,028 \text{ g mol}^{-1}$  vs.  $M_{n,SEC} = 14,700 \text{ g mol}^{-1}$ ;  $\bar{D}_M = 1.30$ ). Hence, Won and co-workers provided new insights on the mechanism of the ROP of *rac*-LA mediated by DBU, in which the anionic propagation initially suggested by Waymouth/Hedrick and co-workers has been replaced by the quasi-anionic propagation.<sup>[35]</sup>



**Scheme 3. 11** – Quasi-anionic mechanism suggested for ROP of *rac*-LA in the presence of DBU and ROH in different ratios; (a) ROH excess, activated alcohol pathway by DBU basicity; (b) DBU excess, mainly nucleophilic attack pathway accompanied with less pronounced basic pathway (a).

In 2020, it was shown that DBU failed to catalyse the ROP of *rac*-LA/*meso*-LA in toluene ( $[LA]/[BnOH]/[DBU] = 100:1:1$ ) at low temperature ( $-75^\circ \text{C}$ ), after attempting to prepare stereocontrolled PLA.<sup>[29]</sup> However, in 2021, when this ROP was evaluated at room temperature ( $[rac\text{-LA}]/[BnOH]/[TBD] = 100:1:1$ ), PLA was produced after 1 h (90% conversion,  $\bar{D}_M = 1.27$ ), yet with a poor stereocontrol ( $P_m = 0.68$ ). Taking into consideration



that DBU is an efficient catalyst when accompanied with a cocatalyst (TU, BisTU, urea, phenols), Li *et al.* tested the same polymerization again at room temperature, but in the presence of specific family of cocatalysts bearing different steric and chiral substituents, namely squaramides (SQ). Hence, a polymerization with a similar efficiency as in the absence of SQ was achieved, but this time with a higher tacticity control ( $P_m = 0.79\text{--}0.88$ ).<sup>[36]</sup>

While DBU is an excellent catalyst for the polymerization of LA, the addition of a cocatalyst is required to polymerize  $\delta$ -VL or  $\epsilon$ -CL. The bulk ROP seemed to be more effective than that in solution upon using a cocatalyst–DBU–alcohol system. The mechanism at play for DBU along with a cocatalyst, involved neutral H-bonding and is less active than that of BEMP with a cocatalyst. Also, DBU proved to be less active than TBD, especially at low temperatures ( $-75^\circ\text{C}$ ) where no polymerization was observed. Similar to the ROP of LA mediated by BEMP and TBD, mechanistic pathways with DBU revealed to be dependent on the reagents present in the medium. In presence of a protic agent (ROH), DBU mediates the ROP as a base and with H-bonding through a quasi-anionic propagation. Whereas the absence or limited protic agents leads DBU to initiate ROP by nucleophilic attack and quasi-anionic propagation, to produce a mixture of linear and cyclic PLA.

## 2.4. Overall considerations on the BEMP, TBD, and DBU-mediated ROP of LA, $\delta$ -VL and $\epsilon$ -CL

Foremost, the monomer activity trend in the ROP of LA,  $\delta$ -VL,  $\epsilon$ -CL promoted by BEMP, TBD, or DBU was always the same, namely  $\text{LA} > \delta\text{-VL} > \epsilon\text{-CL}$ . Also, the organic activator efficiency trend regardless of the monomer was  $\text{TBD} > \text{BEMP} > \text{DBU}$ , with several factors governing this tendency such as nucleophilicity, basicity, and capability of H-bonding. It was demonstrated that the BEMP, TBD and DBU role (as initiator and/or as catalyst) and their mechanistic pathways essentially change according to the polymerization conditions and in particular according to the presence or the absence of a protic agent (alcohol). The BEMP/DBU–ROH catalytic system promotes the ROP through a H-transfer mechanism acting as a basic organocatalyst, while TBD–ROH mediates the ROP via H-bonding. TU/Urea–BEMP/DBU–ROH catalytic systems favour ROP through H-bonding (neutral or imidate). In the absence of ROH, BEMP catalyses anionic ROP by deprotonating the cyclic ester and propagates as a counter cation, while TBD and DBU initiate ROP by a nucleophilic attack and propagate (zwitterionic or quasi anionic) as H-bond catalyst, each in its own way

(bifunctionality of TBD and monofunctionality of DBU). The results of the above-mentioned investigations are summarized in Table 3. 2. Noteworthy, the same organic activator trends were obtained in solvent-free conditions (TBD > BEMP > DBU), and also provide a higher efficiency than in solution.

**Table 3. 2** – Comparative summary on the activity of BEMP, TBD and DBU in mediating the ROP of large lactones.

	Presence of alcohol “ROH”	Absence of alcohol “ROH”
 BEMP		
 TBD		
 DBU		

This overview of the state-of-the-art on the ROP of cyclic esters promoted by BEMP, TBD or DBU highlights the superior basicity of BEMP (that abstracts the  $\alpha$ -H of the cyclic esters) and its inability to promote *O*-acyl scission of the cyclic ester, that is traced back to BEMP steric bulkiness (Figure 3. 2).<sup>[37]</sup> Moreover, it draws attention to the bifunctionality of TBD as both a nucleophile and a H-bonding agent (donor and acceptor), and lastly to the dual functionality of DBU as both a nucleophile or base.

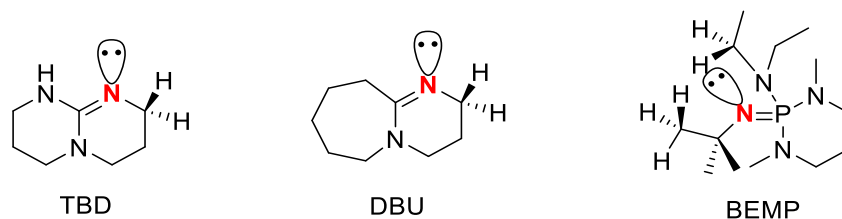
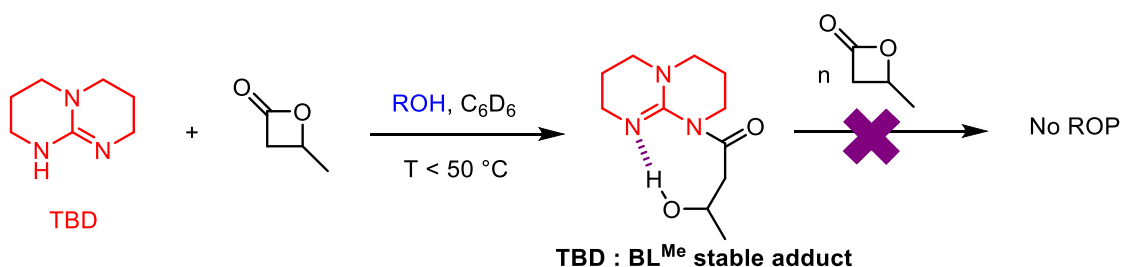


**Figure 3. 2** – Illustration of the steric bulkiness of BEMP that weakens its nucleophilicity, unlike TBD and DBU.

After covering the activity and the mode of action of BEMP, TBD, and DBU in the ROP of several ubiquitous cyclic esters (LA,  $\delta$ -VL,  $\epsilon$ -CL), the same literature overview will be addressed thereafter for the ROP of  $\beta$ -lactones into synthetic functional PHAs.

### 3. State-of-the-art: BEMP, TBD and DBU as organic activators for ROP of $\beta$ -lactones

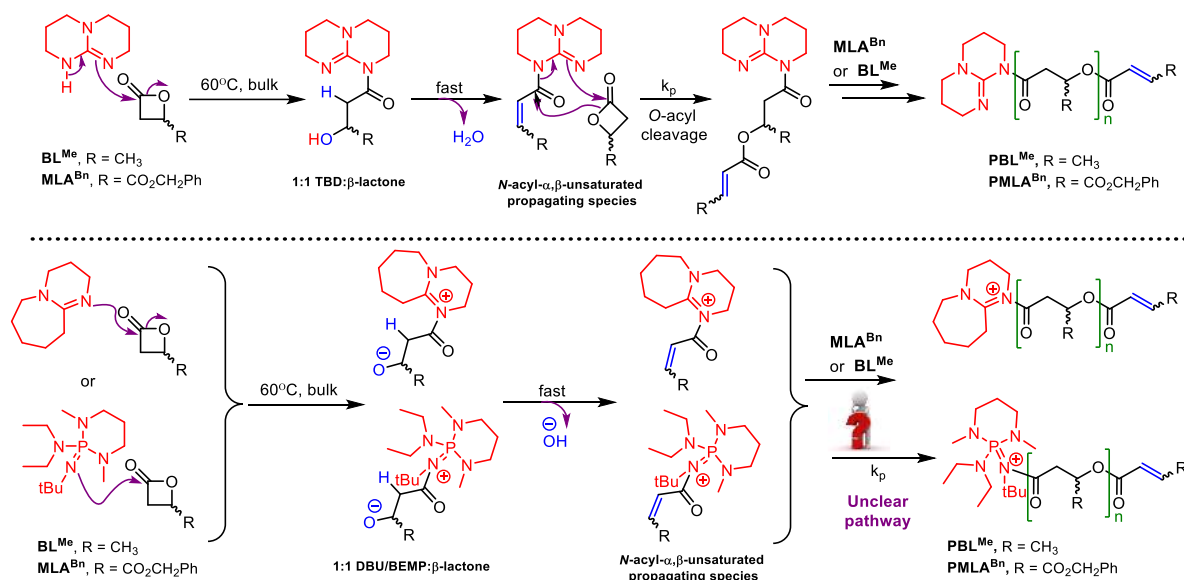
Less documented efforts have been made in ROP of  $\beta$ -lactones mediated by BEMP, TBD or DBU compared to the larger cyclic esters (LA,  $\delta$ -VL,  $\epsilon$ -CL); this is likely because  $\beta$ -lactones are more reluctant to ring open and thus are more challenging. In accordance with investigations of TBD in the ROP of large lactones revealing its unique efficiency and capability (Scheme 3. 4), Hedrick *et al.* were the first to trigger the ROP of  $\beta$ -lactones ( $\text{BL}^{\text{Me}}$ ) using TBD in 2006.<sup>[23b]</sup> However, their attempt to ring-open polymerize  $\text{BL}^{\text{Me}}$  using the TBD–ROH catalytic system in  $\text{C}_6\text{D}_6$  at room temperature surprisingly failed. The authors demonstrated the formation of an acyl intermediate (1:1,  $\text{BL}^{\text{Me}}$ –TBD) adduct which is stabilized by strong hydrogen bonding of the eight-membered ring, resulting in precluding the propagation (Scheme 3. 12). Upon heating to 50 °C, only oligomers with crotonate by-products were observed in an uncontrolled manner. Theoretical calculations from Simon and Goodman effectively confirmed that the adduct intermediate is indeed too stabilized, presenting an energy barrier “insurmountable” for propagation.<sup>[25]</sup> Nearly the same results were obtained upon using DBU instead of TBD under the same conditions (DP = 100, ROH, in  $\text{C}_6\text{D}_6$ , at room temperature) accompanied with TU cocatalyst (Scheme 3. 2 – top), with unexpectedly 0% conversion of  $\text{BL}^{\text{Me}}$  observed after 72 h and an uncontrolled oligomerization was obtained at high temperature (> 50 °C).<sup>[23b]</sup> This contrasts with the high conversions observed at room temperature for the ROP of LA,  $\delta$ -VL or  $\epsilon$ -CL, upon using TBD–ROH or TU–DBU–ROH catalytic systems (*vide supra*). Noteworthy, before 2012, BEMP had not been investigated as an organic catalyst for the ROP of any type of  $\beta$ -lactones, albeit its use in the ROP of larger lactones.<sup>[8, 11]</sup>



**Scheme 3. 12** – First attempt of the ROP of BL<sup>Me</sup> using TBD in the presence of an alcohol in solution at < 50 °C, unsuccessful due to the formation of the stable eight-membered TBD–BL<sup>Me</sup> adduct.<sup>[23b, 25]</sup>

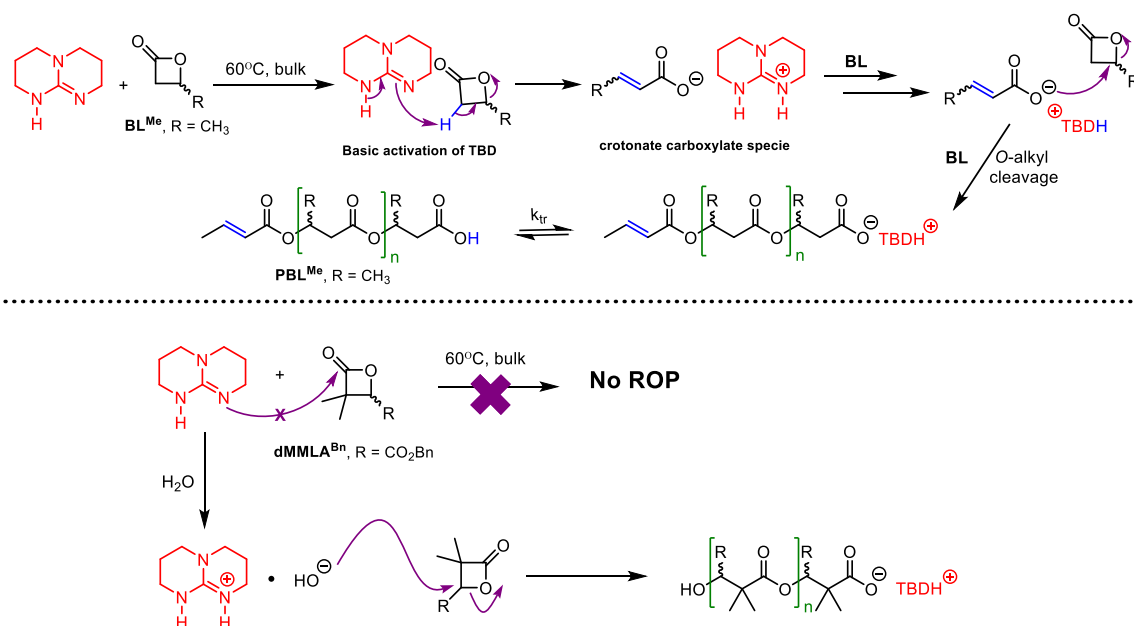
Later on, in 2012-2013, our group successfully performed the ROP of  $\beta$ -lactones such as *rac*-BL<sup>Me</sup> and *rac*-MLA<sup>Bn</sup> promoted by BEMP, TBD or DBU under mild conditions (bulk, 60 °C, without using any exogenous protic initiator), highlighting the importance of both the monomer concentration and the reaction temperature.<sup>[38]</sup> The PBL<sup>Me</sup> produced featured moderately narrow dispersities ( $1.05 < \bar{D}_M < 1.52$ ) and a fair control over molar masses for DPs  $\leq 100$ . This control was generally attenuated when targeting higher DPs (250-500), where a clear gap was obtained between theoretical molar masses ( $M_{n,theo}$ ) and experimental molar masses obtained from size exclusion chromatography ( $M_{n,SEC}$ ). For example, PBL<sup>Me</sup>s produced from BEMP have  $M_{n,theo} = 34,000 \text{ g mol}^{-1}$  vs.  $M_{n,SEC} = 24,700 \text{ g mol}^{-1}$ , while those produced from TBD have  $M_{n,theo} = 35,400 \text{ g mol}^{-1}$  vs.  $M_{n,SEC} = 22,700 \text{ g mol}^{-1}$ , and those formed from DBU have  $M_{n,theo} = 38,800 \text{ g mol}^{-1}$  vs.  $M_{n,SEC} = 6050 \text{ g mol}^{-1}$ .<sup>[38a]</sup> Similarly, PMLA<sup>Bn</sup> obtained had narrow dispersities ranging from  $1.12 < \bar{D}_M < 1.39$ , while the gap between theoretical and experimental molar masses was more pronounced when targeting high DPs (250–500). PMLA<sup>Bn</sup> formed from BEMP have  $M_{n,theo} = 48,200 \text{ g mol}^{-1}$  vs.  $M_{n,SEC} = 7550 \text{ g mol}^{-1}$ , while those promoted by TBD have  $M_{n,theo} = 39,900 \text{ g mol}^{-1}$  vs.  $M_{n,SEC} = 9300 \text{ g mol}^{-1}$ , and those from DBU have  $M_{n,theo} = 42,900 \text{ g mol}^{-1}$  vs.  $M_{n,SEC} = 7450 \text{ g mol}^{-1}$ .<sup>[38b]</sup> Our group rationalized this difference by the presence of side reactions that are usually known for polyesters such as back-biting and/or transesterification reactions. Anyhow, the PBL<sup>Me</sup> and PMLA<sup>Bn</sup> produced from bulk ROP promoted by either BEMP, TBD or DBU were noticed, as based on 1D and 2D NMR spectroscopy and MALDI-ToF spectrometry analyses, to have an end-group featuring the catalyst bound by their N atoms to the acyl group to form *N*-acyl, and another one at the other terminus being an  $\alpha,\beta$ -unsaturated group. The  $\alpha,\beta$ -unsaturated group was formed from the onset of the polymerization as deduced from the <sup>1</sup>H NMR analyses.<sup>[38]</sup> Hence, it was suggested that an *N*-acyl- $\alpha,\beta$ -unsaturated propagating species might originate from 1:1 BEMP/TBD/DBU: $\beta$ -lactone adducts via a nucleophilic pathway, leading to an *O*-acyl cleavage. In fact, the latter proposition and the propagation mechanism were established primarily for TBD (Scheme 3. 13

– top). However, the initiation/propagation for BEMP and DBU (Scheme 3. 13 – bottom) were not fully clarified, demanding further investigations as the authors conveyed.<sup>[38b]</sup> Notably, in 2014-2017, attempts to ring open *rac*-BL<sup>Me</sup> (100 equivalence, in C<sub>6</sub>D<sub>6</sub>) in the presence of the TU/Urea1–BEMP–ROH catalytic system were unsuccessful (0% conversion after 72 h at room temperature).<sup>[10a, 11]</sup>



**Scheme 3. 13** – (top) Proposed ROP mechanism of *rac*-BL<sup>Me</sup> and *rac*-MLA<sup>Bn</sup> promoted by TBD via O-acyl cleavage; (bottom) Possible ROP mechanism of *rac*-BL<sup>Me</sup> and *rac*-MLA<sup>Bn</sup> mediated by DBU and BEMP that still requires investigation, by Guillaume *et al.*<sup>[38]</sup>

A recent reinvestigation was done in 2018 by Coulembier and co-workers, on the ROP of *rac*-BL<sup>Me</sup> promoted by TBD following the same operating procedure of Guillaume *et al.* (neat, 60 °C, absence of protic agent).<sup>[39]</sup> By means of <sup>1</sup>H/DOSY NMR and MALDI/ESI-MS techniques, the authors reported that PBL<sup>Me</sup> is actually mainly obtained from the basic activation of TBD involving the *in situ* generation of crotonate carboxylate species leading to propagation via an O-alkyl cleavage process (Scheme 3. 14 – top). Correspondingly, the authors indicated that the N-acyl-α,β-unsaturated moiety previously reported by our group is the minor propagating species (Scheme 3. 13 – top). Coulembier *et al.* then claimed that the TBD nucleophilicity is not sufficient to initiate ROP of *rac*-BL<sup>Me</sup> via O-acyl cleavage, in view of the fact that TBD (unlike NHC) failed to ring-open *rac*-α,α'-benzylcarbonyl-3,3-dimethyl-2-oxetanone (*rac*-dMMLA<sup>Bn</sup>), attributing that to the absence of α-acidic hydrogen in case of *rac*-dMMLA<sup>Bn</sup> and to the poor nucleophilicity of TBD. Yet, the authors detected through ESI MS, the presence of oligomers end-capped with hydroxy and carboxylate species; suggesting that ROP of dMMLA<sup>Bn</sup> is initiated by undesired traces of water that formed hydroxide anion in the presence of TBD to propagate via O-alkyl bond session (Scheme 3. 14 – bottom).<sup>[39]</sup>



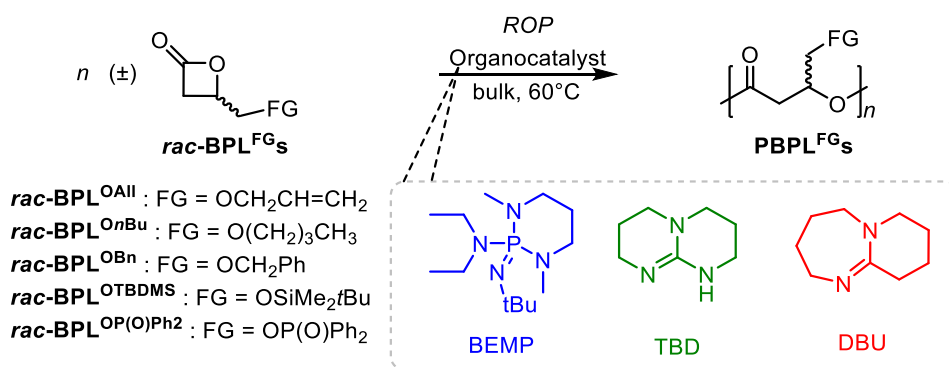
**Scheme 3. 14** –ROP of *rac*-BL<sup>Me</sup> in bulk at 60 °C; (top) proposed mechanism presenting *O*-alkyl cleavage as the major mechanistic pathway, the minor pathway is not shown (*O*-acyl cleavage; Scheme 3. 13); (bottom) failure to polymerize dMMLA<sup>Bn</sup> due to the weak nucleophilicity of TBD and formation of oligomers via water; as proposed by Coulembier *et al.*<sup>[39]</sup>

Ultimately, the organocatalyzed ROP of cyclic esters revealed to be quite complex and also apparently very dependent on reaction conditions. Studies have emphasized on many factors that may influence the course of the polymerization, including the lactone ring-size and the reaction parameters (catalyst/initiator ratio, solvent, monomer concentration, temperature, cocatalyst, protic agent, transfer reactions). Special attention is paid to the effect of the ring size, where BEMP, TBD, and DBU were efficient in the ROP of large cyclic lactones (LA,  $\delta$ -VL,  $\epsilon$ -CL) to precisely control the synthesis of the corresponding polyesters, yet that of smaller ring size ( $\beta$ -lactones) is still challenging and rather obscure, subsequently requiring further examination.

## 4. Results and discussion

Taking into account that BEMP, TBD and DBU are effective to promote the ROP of  $\beta$ -lactones (BL<sup>Me</sup> and MLA<sup>Bn</sup>) in bulk conditions but that their mechanistic pathways are blurred and puzzling, we extended the study to a specific family of  $\beta$ -lactones, namely the 4-alkoxymethylene- $\beta$ -propiolactones, BPL<sup>FGs</sup> (R = OAlI, O<sup>n</sup>Bu, OBn, OTBDMS, OP(O)Ph<sub>2</sub>), under the previously reported conditions (bulk, 60 °C) (Scheme 3. 15). Focus was placed on the macromolecular structure (especially the chain-ends) analysis of the produced poly(4-alkoxymethylene- $\beta$ -propiolactones) “PBPL<sup>FGs</sup>” and on the mechanisms at play. In addition, a new analysis of the previously reported PBL<sup>Me</sup> and PMLA<sup>Bn</sup> microstructural data and

mechanistic pathways was undertaken. This study also afforded an important series of non-bacterial functional PHAs (PBPL<sup>FGs</sup>) with diverse properties depending on the pendent group along the polymer main chain. For instance, OAll and O<sup>n</sup>Bu functionalities can provide hydrophobic chains, while OP(O)Ph<sub>2</sub> can be hydrophilic and “metallophilic”. The OBn and TBDMS functionalities may supply hydrophilic hydroxy segment upon subsequent hydrogenolysis or deprotection, respectively. This can be next exploited in the design of self-assemblies derived from amphiphilic copolymers.<sup>[40]</sup> Also, the highly reactive allyl function in OAll may be valorized upon exposure to further post-polymerization chemical modifications (epoxidation, hydroboration, olefin cross-metathesis...<sup>[41]</sup> Valuably, chains of polyesters incorporating phosphorus “OP(O)Ph<sub>2</sub>” as pendant group can bring improved flame retardancy, thermal oxidative stability, good adhesion on metallic surfaces and low birefringence.<sup>[42]</sup> Furthermore, one cannot avoid the fact that this bulk ROP mediated by organic activators is a step forward towards “Green Chemistry,” since it embraces most of the latter principles as defined by Anastas and Warner.<sup>[43]</sup> Principles such as, atom economy, catalytic amounts, biodegradation, accident prevention (absence of hazardous chemicals),<sup>[43]</sup> or running the polymerization neat in the substrate to reduce waste (waste minimisation) and to facilitate the purification.<sup>[44]</sup>



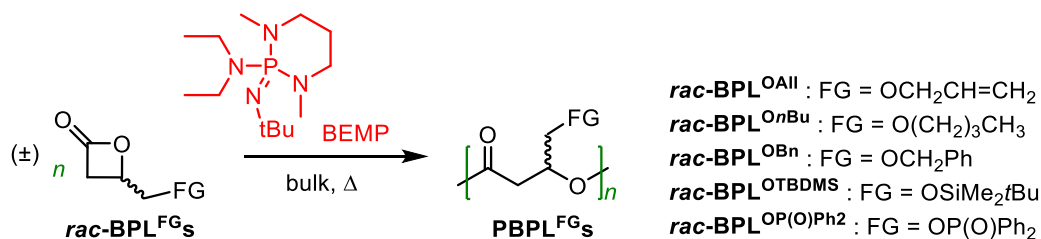
**Scheme 3. 15** – Bulk ROP of BPL<sup>FGs</sup> promoted by BEMP, TBD, or DBU to afford PBPL<sup>FGs</sup> (FG = OAll, O<sup>n</sup>Bu, OBn, OTBDMS, OP(O)Ph<sub>2</sub>).

#### 4.1. ROP of BPL<sup>FGs</sup> promoted by BEMP

As previously mentioned, the use of BEMP as a neutral organic activator for the ROP of four-membered ring lactones was reported only once by our group.<sup>[38]</sup> Despite the successful accomplishment in obtaining PBL<sup>Me</sup> and PMLA<sup>Bn</sup> in bulk at 60 °C, the mechanistic fingerprint was yet not clearly established (Scheme 3. 13 – bottom). Herein, we thus report for the first



time the bulk ROP of  $rac$ -BPL<sup>FG</sup>s promoted by BEMP (Scheme 3. 16) along with PBPL<sup>FG</sup>s characterization and mechanistic investigations of the polymerization.



**Scheme 3. 16** – Bulk ROP of  $rac$ -BPL<sup>FG</sup>s promoted by BEMP.

#### 4.1.1. Molecular characterization of PBPL<sup>FG</sup>s obtained from BEMP

Representative experimental results of the neat (i.e., reaction performed in bulk) ROP of  $rac$ -BPL<sup>FG</sup>s (FG = OAll, OBn, O<sup>n</sup>Bu, OTBDMS, OP(O)Ph<sub>2</sub>) using BEMP at different temperatures (ranging from 25 °C to 60 °C) and [BPL<sup>FG</sup>]<sub>0</sub>/[BEMP]<sub>0</sub> ratios (ranging from 15 to 60) are gathered in Table 3. 3. Regarding the ether functional moiety, BPL<sup>FG</sup>s polymerized by BEMP proceeded significantly more slowly (typical turnover frequency (TOF) < 13 h<sup>-1</sup>; Table 3. 3 – entry 3) than BL<sup>Me</sup> and  $rac$ -MLA<sup>Bn</sup> (typical TOF = 100 h<sup>-1</sup>, and 150 h<sup>-1</sup>, respectively) under the same conditions.<sup>[38]</sup> Interestingly, the ROP of BPL<sup>OAll/nBu/Bn</sup> (40 equiv) was found effective at room temperature (Table 3. 3 – entries 1, 4, 7), reaching conversions of 91% (in 21 h), 72% (in 19 h) and 60% (in 12 h), respectively, with narrow dispersities (1.09 ≤  $\bar{D}_M$  ≤ 1.23). As expected, ROP of BPL<sup>OAll/nBu/Bn/TBDMS</sup> (40 equiv) proceeded faster at higher temperatures 60 °C (or 40 °C) (Table 3. 3 – entries 3,6,12,15) reaching higher conversion (97/98/82/88%, respectively) in shorter reaction time (3,4,3,8 h, respectively), but with broader dispersities (1.20 ≤  $\bar{D}_M$  ≤ 1.32). Unexpectedly, this evidences that the temperature does not only impact the rate of propagation, but also the occurrence of undesirable side-reactions that may occur during the polymerization.

The molar masses were evaluated by <sup>1</sup>H NMR analysis ( $M_{n,NMR}$ ) from the relative intensities of the signals of the PBPL<sup>FG</sup>s main-chain methine hydrogen and of the crotonate chain-end hydrogens (*vide infra*). These values are in fair agreement with the molar mass values calculated from the monomer conversion ( $M_{n,theo}$ ; not taking into account end-capping groups). The number-average molar mass values as determined by the size exclusion chromatography “SEC” ( $M_{n,SEC}$ ) were also generally in fair agreement with the  $M_{n,NMR}$  data, when addressing low ratios [BPL<sup>FG</sup>]<sub>0</sub>/[BEMP]<sub>0</sub> ≤ 40 (DP ≤ 40). However, targeting higher loading of



$[\text{BPL}^{\text{FG}}]_0/[\text{BEMP}]_0 = 60$  (Table 3. 3, entry 10) and elevated temperature 60 °C (Table 3. 3, entry 13) led to a larger gap between the molar masses ( $M_{n,\text{NMR}}$  vs.  $M_{n,\text{theo}}$  vs.  $M_{n,\text{SEC}}$ ), and higher dispersities ( $\mathcal{D}_M = 1.38, 1.53$ , respectively).

$\text{BPL}^{\text{OP(O)Ph}_2}$ , a novel monomer, and its ROP has never been investigated before using any initiating system. In this work, we only report a preliminary study. The ROP of *rac*- $\text{BPL}^{\text{OP(O)Ph}_2}$  through BEMP at 60 °C in dry THF (Table 3. 3, entries 16, 17) was sluggish compared to other  $\text{PBL}^{\text{FG}}$ s, even for low monomer loadings (20–40 equiv), possibly due to the steric hindrance of the monomer, or to the highly viscous polymerization medium. The monomer conversions (20–40 equiv) were 78% and 50% after 8 and 36 h, respectively, and the produced  $\text{PBPL}^{\text{OP(O)Ph}_2}$  had molar mass up to 6400 g mol<sup>-1</sup> ( $M_{n,\text{SEC}}$ ) and fairly narrow dispersities ( $\mathcal{D}_M = 1.15$ –1.33).

**Table 3. 3** – Characteristics of the  $\text{PBPL}^{\text{FG}}$ s synthesized by ROP of *rac*- $\text{BPL}^{\text{FG}}$ s mediated by BEMP<sup>a</sup>.

Entry	$\text{BPL}^{\text{FG}}$ (FG =)	$[\text{BPL}^{\text{FG}}]_0/[\text{BEMP}]_0$	Temp. (°C)	time <sup>b</sup> (h)	Conv. <sup>c</sup> (%)	$\overline{M}_{n,\text{theo}}$ <sup>d</sup> (g mol <sup>-1</sup> )	$\overline{M}_{n,\text{NMR}}$ <sup>e</sup> (g mol <sup>-1</sup> )	$\overline{M}_{n,\text{SEC}}$ <sup>f</sup> (g mol <sup>-1</sup> )	$\mathcal{D}_M$ <sup>f</sup>
1	OAll	40	25	21	91	5150	4100	4600	1.09
2	OAll	40	40	7	50	2850	1800	1300	1.17
3	OAll	40	60	3	97	5500	4800	3900	1.26
4	OnBu	40	25	19	72	4550	4850	6200	1.18
5	OnBu	44	40	8	78	5400	5650	7700	1.16
6	OnBu	40	60	4	98	6200	3800	4900	1.32
7	OBn	43	25	12	60	4950	3300	2800	1.23
8	OBn	15	40	3	94	2700	3100	2500	1.32
9	OBn	40	40	9	84	6450	5500	5000	1.15
10	OBn	60	40	10	32	3700	1700	1500	1.38
11	OBn	15	60	4	100	2900	2500	2400	1.21
12	OBn	40	60	3	82	6300	4200	3100	1.27
13	OBn	60	60	2	50	5750	3000	2800	1.53
14	OTBDMS	40	40	6	34	2950	2000	1900	1.18
15	OTBDMS	35	60	8	88	6650	3600	3300	1.20
16 <sup>g</sup>	OP(O)Ph <sub>2</sub>	20	60	8	78	4750	5200	5000	1.15
17 <sup>g</sup>	OP(O)Ph <sub>2</sub>	40	60	36	50	6050	6300	6400	1.33

<sup>a</sup> Results are representative of at least duplicated experiments performed neat. <sup>b</sup> The reaction time was not necessarily optimized. <sup>c</sup>  $\text{BPL}^{\text{FG}}$  conversion as determined by <sup>1</sup>H NMR analysis of the crude reaction mixture (refer to the Experimental Section). <sup>d</sup> Theoretical molar mass calculated from the relation:  $[\text{BPL}^{\text{FG}}]_0/[\text{BEMP}]_0 \times \text{Conv. BPLFG} \times M_{\text{BPLFG}}$ , i.e. without considering end-capping groups, with  $M_{\text{BPLOAll}} = 142$  g mol<sup>-1</sup>,  $M_{\text{BPLOnBu}} = 158$  g mol<sup>-1</sup>,  $M_{\text{BPLOBn}} = 192$  g mol<sup>-1</sup>,  $M_{\text{BPLOTBDMS}} = 216$  g mol<sup>-1</sup> and  $M_{\text{BPLOP(O)Ph}_2} = 302$  g mol<sup>-1</sup>. <sup>e</sup> Experimental molar mass value determined by <sup>1</sup>H NMR analysis of the isolated polymer, from the resonances of the crotonate end-group (refer to the Experimental Section). <sup>f</sup> Experimental molar mass and dispersity values as determined by SEC in THF using a RI detector at 30 °C vs polystyrene standards. <sup>g</sup> ROP was performed in a few drops of dehydrated THF used to pre-solubilize the monomer.

In a nutshell, these outputs most likely evidenced the occurring of some undesirable side reactions, typically known in polyesters synthesis, namely intra- and inter-molecular transesterification reactions and/or transfer reactions (to polymer and/or monomer). It was correspondingly assumed that the rate of initiation ( $k_i$ ) and/or transfer ( $k_{tr}$ ) is competitive with

that of propagation ( $k_p$ ). Thus, efforts to control molar mass values, to limit side-reactions, and/or to enhance the catalytic activity and productivity, were not taken into consideration. The focus of the present work was rather placed on elucidating the mechanism at play to grasp the activity of BEMP in the ROP of  $\beta$ -lactones, that can pave the way for unprecedented approaches.

#### 4.1.2. Macromolecular structure of BEMP-synthesized PBPL<sup>FG</sup>s assessed by NMR spectroscopy and MALDI-ToF mass spectrometry

BPL<sup>FG</sup>  $\beta$ -lactones have two possible mechanistic opening pathways, either through an *O*-acyl cleavage to generate alkoxide moieties and eventually an alcohol end-group, or via an *O*-alkyl cleavage to produce carboxylate moieties and eventually a carboxylic acid end-group (Scheme 1. 7). We thus carefully investigated the end-capping groups of PBPL<sup>FG</sup>s and therefrom suggested the possible corresponding ROP mechanism. All the purified PBPL<sup>FG</sup>s samples isolated from the ROP of *rac*-BPL<sup>FG</sup>s mediated by BEMP were characterized by <sup>1</sup>H, J-MOD and 2D (COSY) NMR spectroscopy and MALDI-ToF and ESI MS (*vide infra*).

The typical <sup>1</sup>H and J-MOD NMR spectra of PBPL<sup>FG</sup>s recovered from the ROP of *rac*-BPL<sup>FG</sup>s mediated by BEMP are depicted in Figure 3. 3 to Figure 3. 7. Regardless of the monomer/polymer ether functional group (OAll, O<sup>n</sup>Bu, OBn, OTBDMS, OP(O)Ph<sub>2</sub>), as exemplified with PBPL<sup>OBn</sup>, besides the main chain repeating unit typical methine and methylene backbone hydrogens' signals ( $\delta_{1H}$  ppm 5.39 (OCH<sup>c</sup>CH<sub>2</sub>) and 2.67 (CH<sub>2</sub><sup>a,b</sup>C(O))), resonances for both crotonate ( $\delta_{1H}$  ppm 6.99 (CH<sup>h</sup>=CHCH<sub>2</sub>O), 6.14 (CH=CH<sup>s</sup>C(O)O)) and BEMP (especially methyl signals:  $\delta_{1H}$  ppm 1.36 (NC(CH<sub>3</sub>)<sub>3</sub>) and 1.15 (NCH<sub>2</sub>CH<sub>3</sub>)) moieties were clearly observed in a 1:1 ratio (Figure 3. 5 – top). The corresponding carbon signals of these two moieties were assigned from the J-MOD spectrum (Figure 3. 5 – bottom).

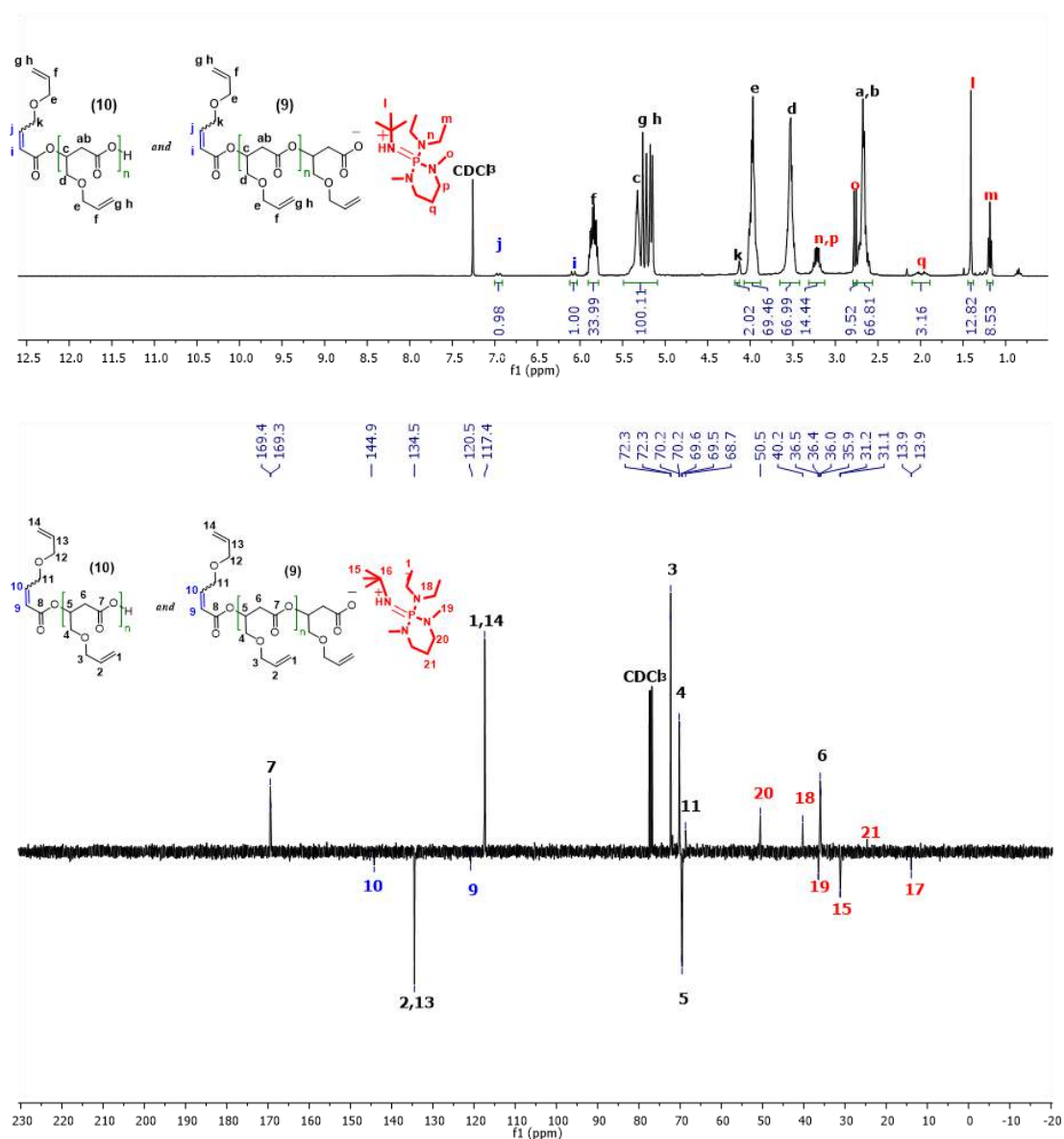


**Figure 3. 3** –  $^1\text{H}$  (500 MHz,  $\text{CDCl}_3$ , 25  $^\circ\text{C}$ ) (top) and J-MOD (125 MHz,  $\text{CDCl}_3$ , 25  $^\circ\text{C}$ ) (bottom) NMR spectra of  $\text{PBPL}^{\text{OAll}}$  with  $[\text{AlloCH}_2\text{CH}=\text{CHCOO}(\text{PBL}^{\text{OAll}})]^-[\text{BEMPH}]^+$  (Scheme 3. 17 – 9) and  $\text{AlloCH}_2\text{CH}=\text{CHCOO}(\text{PBL}^{\text{OAll}})\text{H}$  (Scheme 3. 17 – 10) (note that the possible  $[\text{AlloCH}_2\text{CH}=\text{CHCOO}]^-[\text{BEMPH}]^+$  species (Scheme 3. 17 – 8) is not depicted) recovered from the ROP of  $\text{rac-BPL}^{\text{OAll}}$  mediated by BEMP (Table 3. 3 – entry 3).

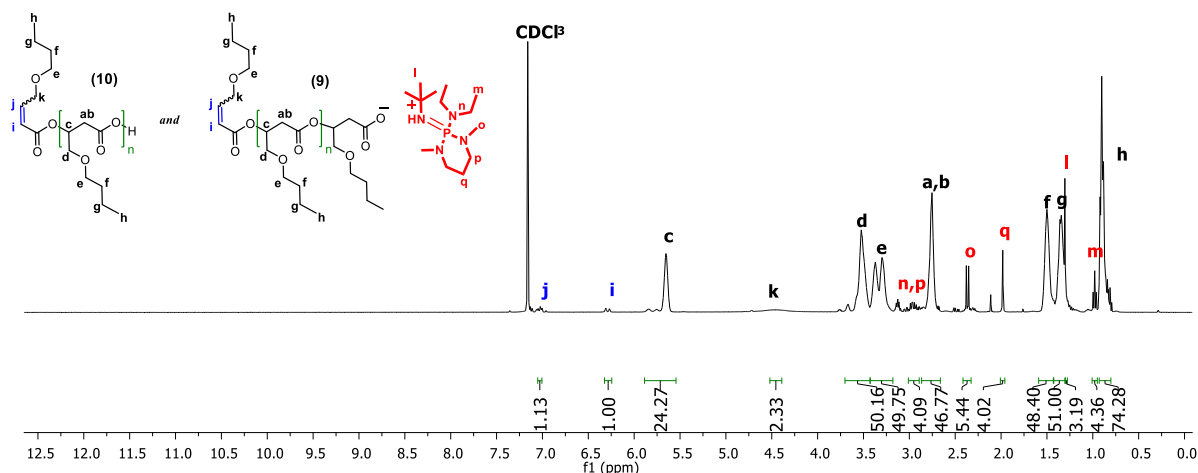


**Figure 3. 4** –  $^1\text{H}$  (500 MHz,  $\text{CDCl}_3$ , 25 °C) NMR spectra of  $\text{PBPL}^{n\text{Bu}}$  with  $[\text{}^n\text{BuOCH}_2\text{CH}=\text{CHCOO}(\text{PBL}^{n\text{Bu}})]^-[\text{BEMPH}]^+$  (Scheme 3. 17 – 9) and  $^n\text{BuOCH}_2\text{CH}=\text{CHCOO}(\text{PBL}^{n\text{Bu}})\text{H}$  (Scheme 3. 17 – 10) (note that the possible  $[\text{}^n\text{BuOCH}_2\text{CH}=\text{CHCOO}]^-[\text{BEMPH}]^+$  species (Scheme 3. 17 – 8) is not depicted) recovered from the ROP of  $\text{rac-BPL}^{n\text{Bu}}$  mediated by BEMP (Table 3. 3 – entry 6).

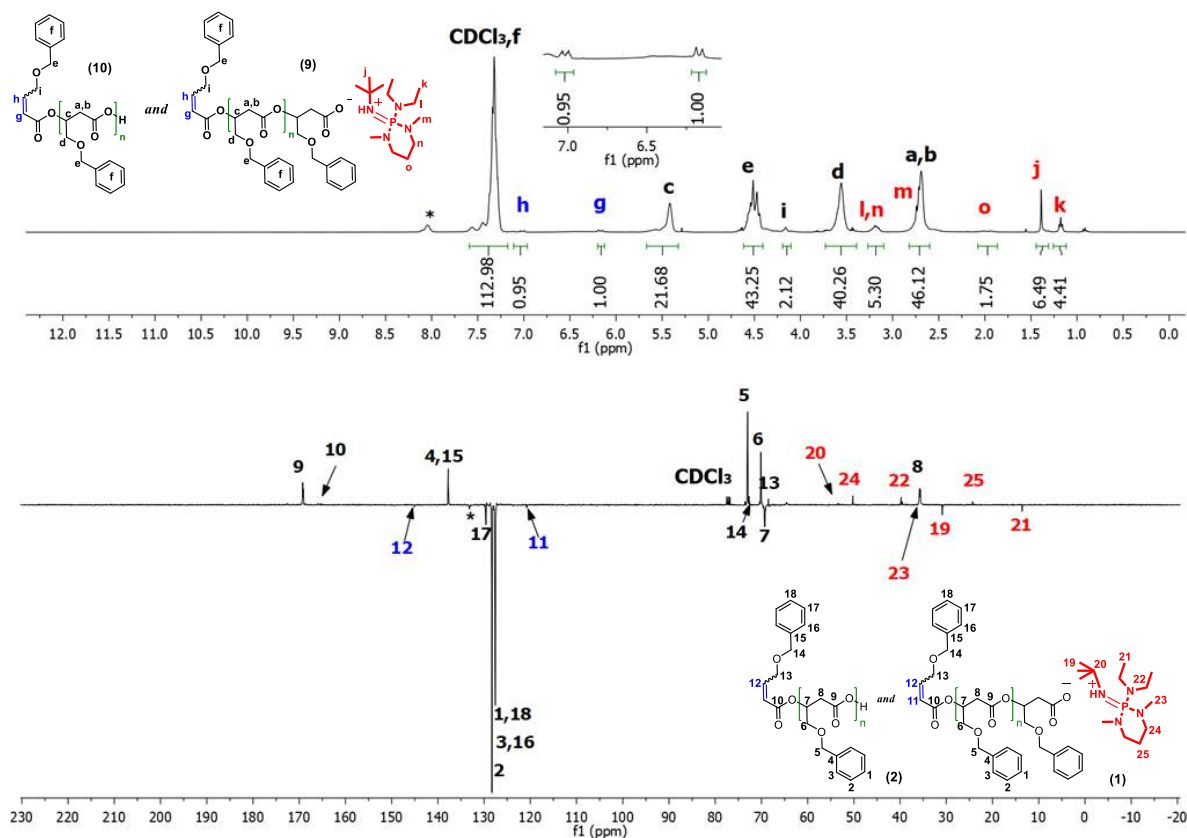


**Figure 3. 5** –  $^1\text{H}$  (500 MHz,  $\text{CDCl}_3$ , 25 °C) (top) and J-MOD (125 MHz,  $\text{CDCl}_3$ , 25 °C) (bottom) NMR spectra of  $\text{PBPL}^{\text{OBn}}$  with  $[\text{BnOCH}_2\text{CH}=\text{CHCOO}(\text{PBL}^{\text{OBn}})]^-[\text{BEMPH}]^+$  (Scheme 3. 17 – 9) and  $\text{BnOCH}_2\text{CH}=\text{CHCOO}(\text{PBL}^{\text{OBn}})\text{H}$  (Scheme 3. 17 – 10) (note that the possible  $[\text{BnOCH}_2\text{CH}=\text{CHCOO}]^-[\text{BEMPH}]^+$  species (Scheme 3. 17 – 8) is not depicted) recovered from the ROP of  $\text{rac-BPL}^{\text{OBn}}$  mediated by BEMP (Table 3. 3 – entry 12); \* unidentified minor impurity not observed in other spectra of  $\text{PBPL}^{\text{FGs}}$  obtained from BEMP.

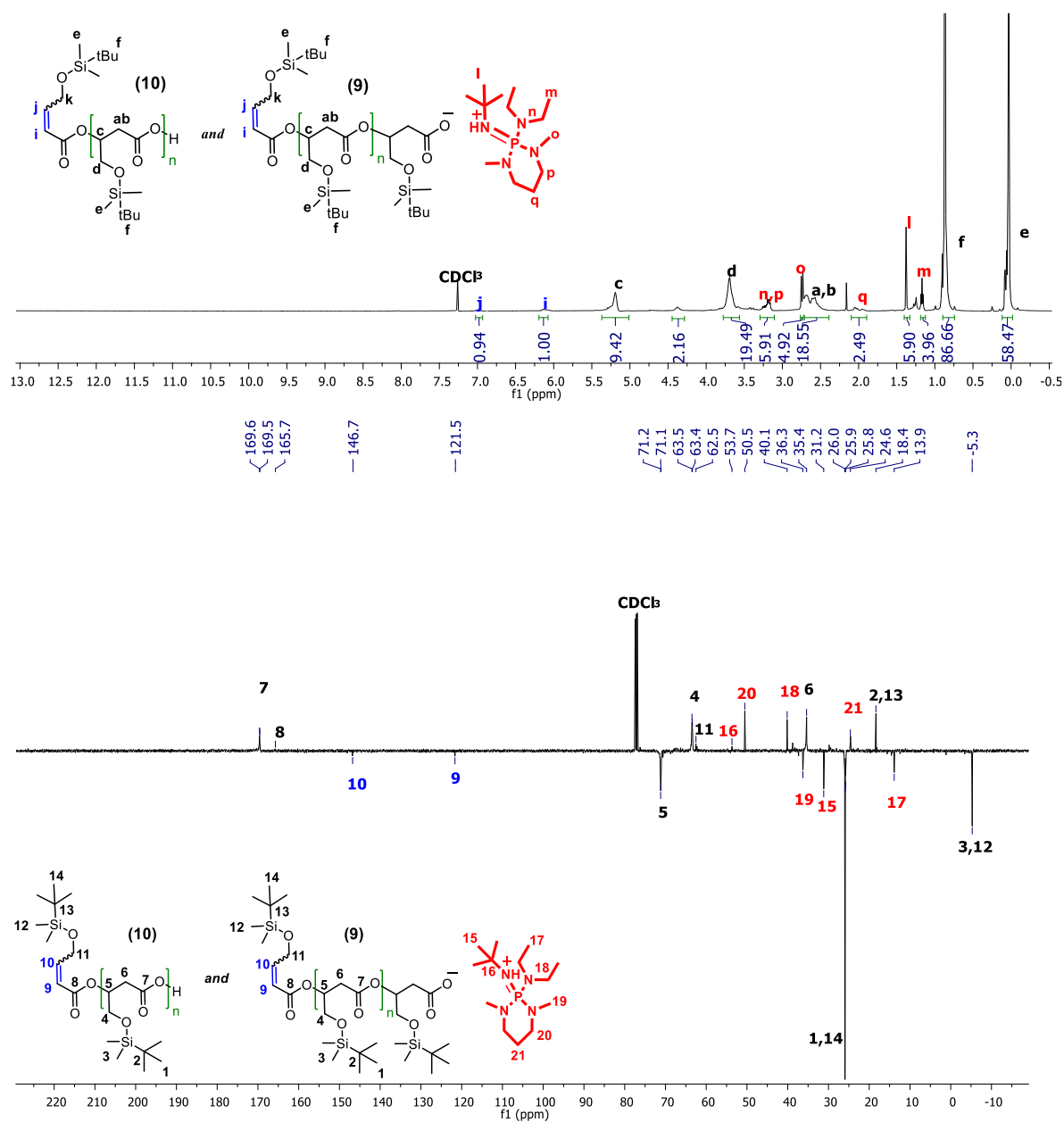


**Figure 3. 6** – <sup>1</sup>H (500 MHz, CDCl<sub>3</sub>, 25 °C) (top) and J-MOD (125 MHz, CDCl<sub>3</sub>, 25 °C) (bottom) NMR spectra of PBPL<sup>OTBDMS</sup> with [TBDMSOCH<sub>2</sub>CH=CHCOO(PBL<sup>OTBDMS</sup>)]<sup>-</sup>[BEMPH]<sup>+</sup> (Scheme 3. 17 – 9) and TBDMSOCH<sub>2</sub>CH=CHCOO(PBL<sup>OTBDMS</sup>)H (Scheme 3. 17 – 10) (note that the possible [TBDMSOCH<sub>2</sub>CH=CHCOO]<sup>-</sup>[BEMPH]<sup>+</sup> species (Scheme 3. 17 – 8) is not depicted) recovered from the ROP of *rac*-BPL<sup>OTBDMS</sup> mediated by BEMP (Table 3. 3 – entry 14).

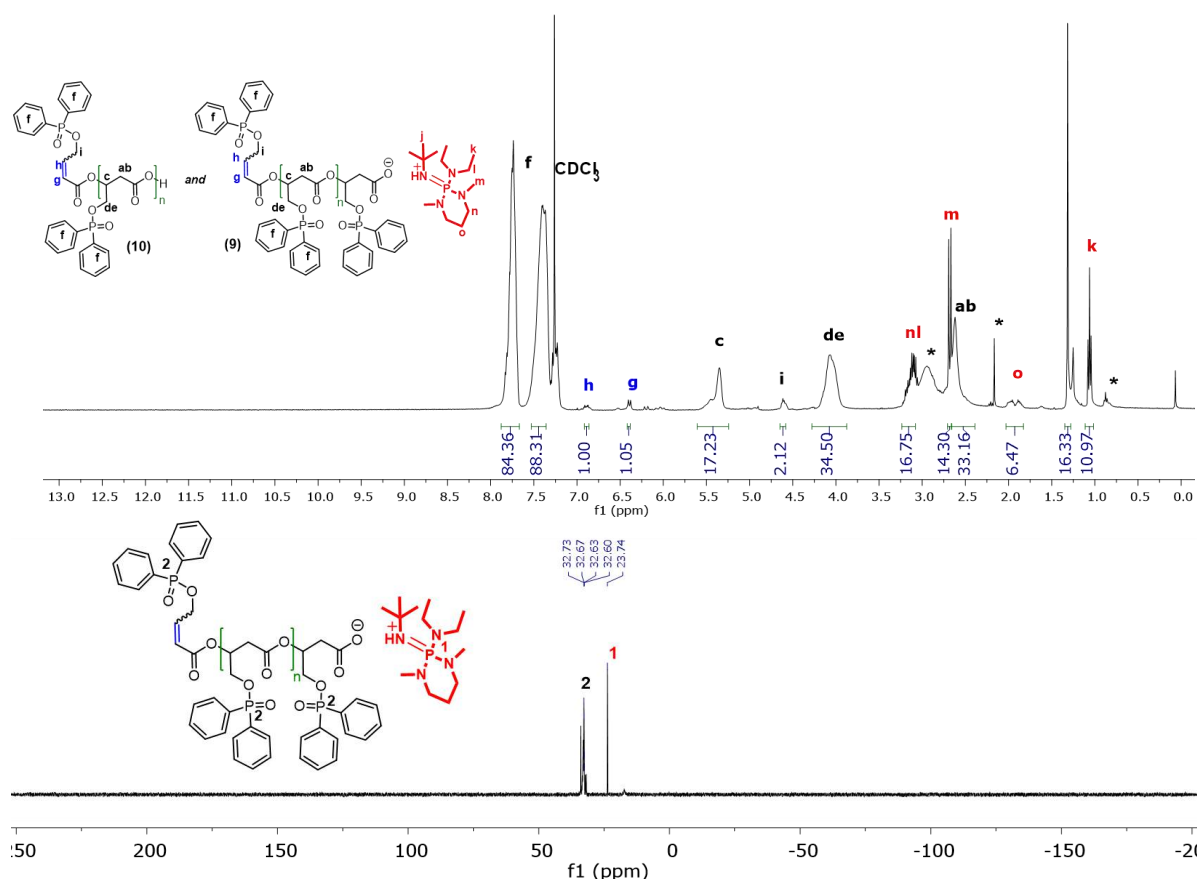


**Figure 3. 7** – <sup>1</sup>H (500 MHz, CDCl<sub>3</sub>, 25 °C) (top) and <sup>31</sup>P (125 MHz, CDCl<sub>3</sub>, 25 °C) (bottom) NMR spectra of PBPL<sup>OP(O)Ph<sub>2</sub></sup> with [P(O)Ph<sub>2</sub>OCH<sub>2</sub>CH=CHCOO(PBL<sup>OP(O)Ph<sub>2</sub></sup>)]<sup>−</sup>[BEMPH]<sup>+</sup> (Scheme 3. 17 – 9) and P(O)Ph<sub>2</sub>OCH<sub>2</sub>CH=CHCOO(PBL<sup>OP(O)Ph<sub>2</sub></sup>)H (Scheme 3. 17 – 10) (note that the possible [POPh<sub>2</sub>OCH<sub>2</sub>CH=CHCOO]<sup>−</sup>[BEMPH]<sup>+</sup> species (Scheme 3. 17 – 8) is not depicted) recovered from the ROP of *rac*-BPL<sup>OP(O)Ph<sub>2</sub></sup> mediated by BEMP (Table 3. 3 – entry 16); \* H-grease, acetone and water from the deuterated solvent (CDCl<sub>3</sub>).

All signals' assignments were supported by 2D COSY NMR analyses; in particular, the correlation between the vinylic hydrogens and the end-group methylene hydrogens supports a crotonate “α,β-unsaturated group” chain-end (Figure 3. 8).

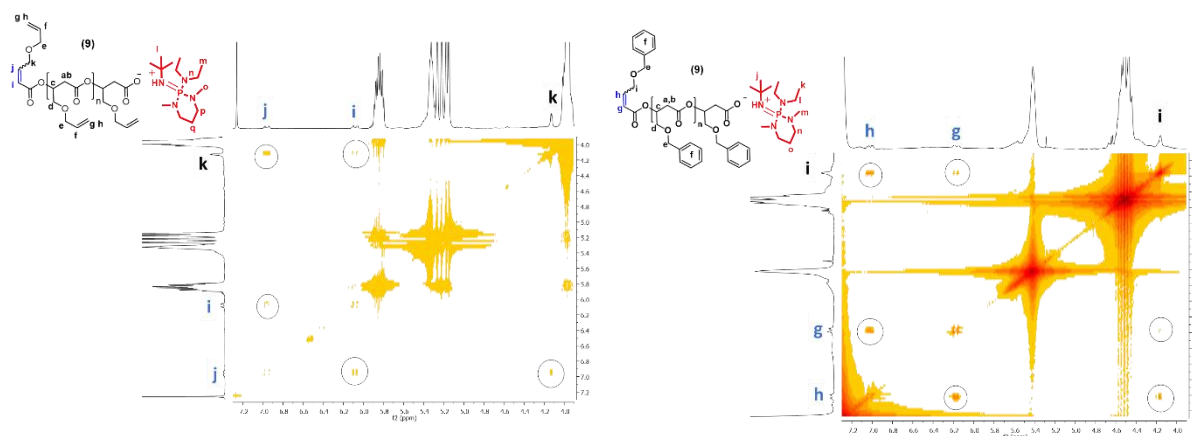


**Figure 3. 8** –  $^1\text{H}$ - $^1\text{H}$  COSY (500 MHz,  $\text{CDCl}_3$ , 25 °C) NMR zoomed spectra; (left) for  $\text{PBPL}^{\text{OAll}}$  (Table 3. 3, entry 3); (right) for  $\text{PBPL}^{\text{OBn}}$  (Table 3. 3 – entry 12) recovered from the ROP of  $\text{rac-BPL}^{\text{OAll}}$  and  $\text{rac-BPL}^{\text{OBn}}$ , respectively; mediated by BEMP supporting the  $\alpha$ -crotonate end-capping group.

To further assess the nature of the  $\alpha,\beta$ -unsaturated group,  $^1\text{H}$  NMR monitoring of the  $\alpha,\beta$ -unsaturation-to-BEMP molar ratio was examined. The crotonate group was observed to be generated from the very beginning of the polymerization and an increase of its content during the course of the reaction was revealed, especially at high temperature (60 °C) and/or at a larger initial monomer loading (40 vs. 60 equiv.) (Table 3. 3 – entries 9,10,12,13; Figure 3. 9). Hence, it was deduced that the crotonate group may be related to the initiation as depicted in Scheme 1. 6 – route (1), and to the transfer reactions as depicted in Scheme 1. 10 (refer to Chapter 1).

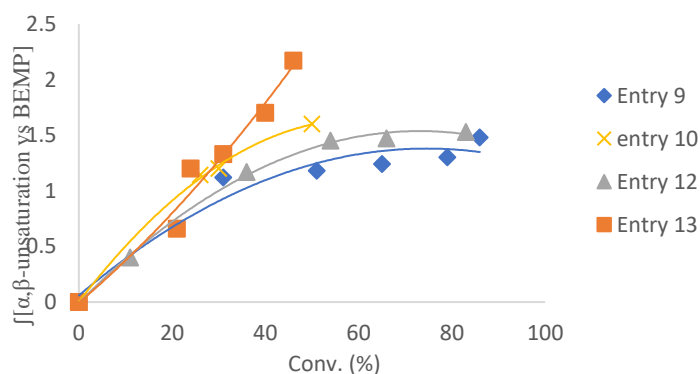


**Figure 3. 9** –  $^1\text{H}$  NMR monitoring of the molar content of the crotonate with respect to BEMP as a function of  $\text{rac-BPL}^{\text{OBn}}$  consumption for the ROP of  $\text{rac-BPL}^{\text{OBn}}$  mediated by BEMP, using the methine ( $\delta_{\text{CHC(O)O}}$  6.17 ppm) and methyl ( $\delta_{\text{NC(CH}_3)_3}$  1.39 ppm) resonances, respectively (Table 3. 3 – entries 9,10,12,13).

Closer examination of the  $^1\text{H}$  NMR signals of the BEMP moiety, and as further corroborated by  $^{31}\text{P}$  NMR analysis, showed that the resonances correspond to the protonated base  $[\text{BEMPH}]^+$ ; this was demonstrated by the significant shift of the  $\text{NC}(\text{CH}_2)_3$   $^1\text{H}$  ( $\Delta\delta -0.25$  ppm) and  $^{31}\text{P}$  ( $\Delta\delta 27.18$  ppm) resonances, relative to the free BEMP signals, respectively, and comparison with a genuine sample of  $[\text{BEMPH}]^+[\text{OAc}]^-$  (Figure 3. 10).  $[\text{BEMPH}]^+[\text{OAc}]^-$  was prepared from the 1:1 reaction of BEMP and glacial acetic acid in dry toluene at room temperature. Hence, the  $^1\text{H}$  NMR signals indicate that BEMP is present in its protonated form  $[\text{BEMPH}]^+$  during the polymerization process, which is in agreement with the suggested *O*-alkyl cleavage initiation Scheme 1. 6 – route (1); Chapter 1). It excludes the possibility of BEMP behaving as a nucleophile that would ring-open the monomer via an *O*-acyl cleavage (Figure 3. 15 – bottom). Obviously, this is a similar behavior of BEMP to that initiating the larger lactones (LA,  $\delta$ -VL,  $\epsilon$ -CL) in the absence of alcohols (Table 3. 2).

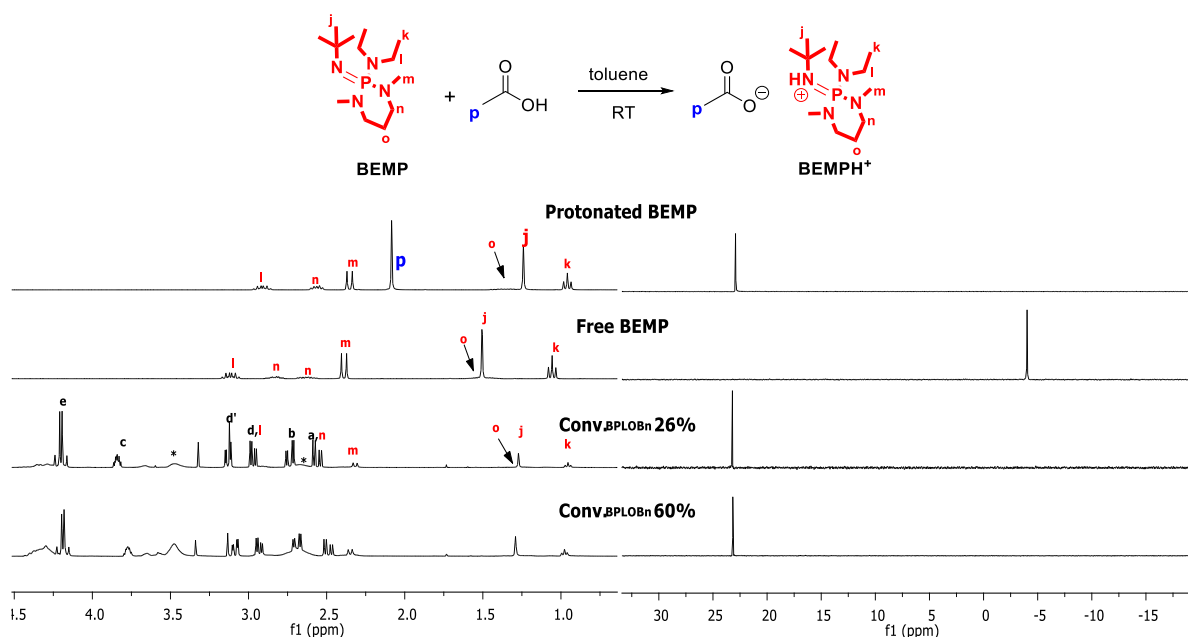
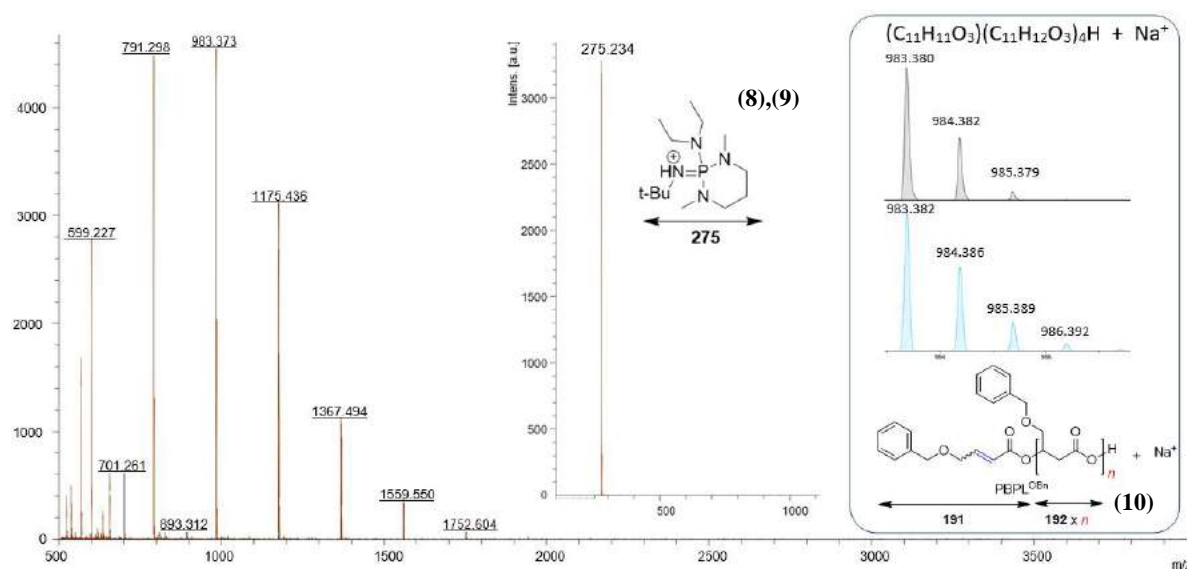


**Figure 3. 10** –  $^1\text{H}$  (left, 400 MHz,  $\text{C}_6\text{D}_6$ , 25  $^\circ\text{C}$ ) and  $^{31}\text{P}$  (right) (121 MHz,  $\text{C}_6\text{D}_6$ , 25  $^\circ\text{C}$ ) NMR monitoring of the ROP of  $\text{rac-BPL}^{\text{OBn}}$  mediated by BEMP in dry  $\text{C}_6\text{D}_6$  (to avoid adventitious protonation by  $\text{H}_2\text{O}$ ) (Table 3. 3 – entry 12) as compared to free and protonated BEMP ( $[\text{BEMPH}]^+[\text{CH}_3\text{COO}]^-$ ; prepared from the equimolar reaction of BEMP with acetic acid in dry toluene under inert conditions).

The MALDI-ToF (Figure 3. 11) and ESI (Appendix 9) mass spectra of  $\text{PBPL}^{\text{OBn}}$  samples prepared by the BEMP-mediated ROP are both consistent with the above-mentioned  $\alpha$ -crotonate,  $\omega$ -carboxylic acid terminated polymer. The spectra showed a major population of  $\text{PBPL}^{\text{OBn}}$  with a repeating unit of 192  $\text{g mol}^{-1}$  end-capped with a benzyloxycrotonate and a carboxylic acid group (the latter which was not observed in the  $^1\text{H}$ ,  $^{13}\text{C}$  or HMBC NMR spectra,



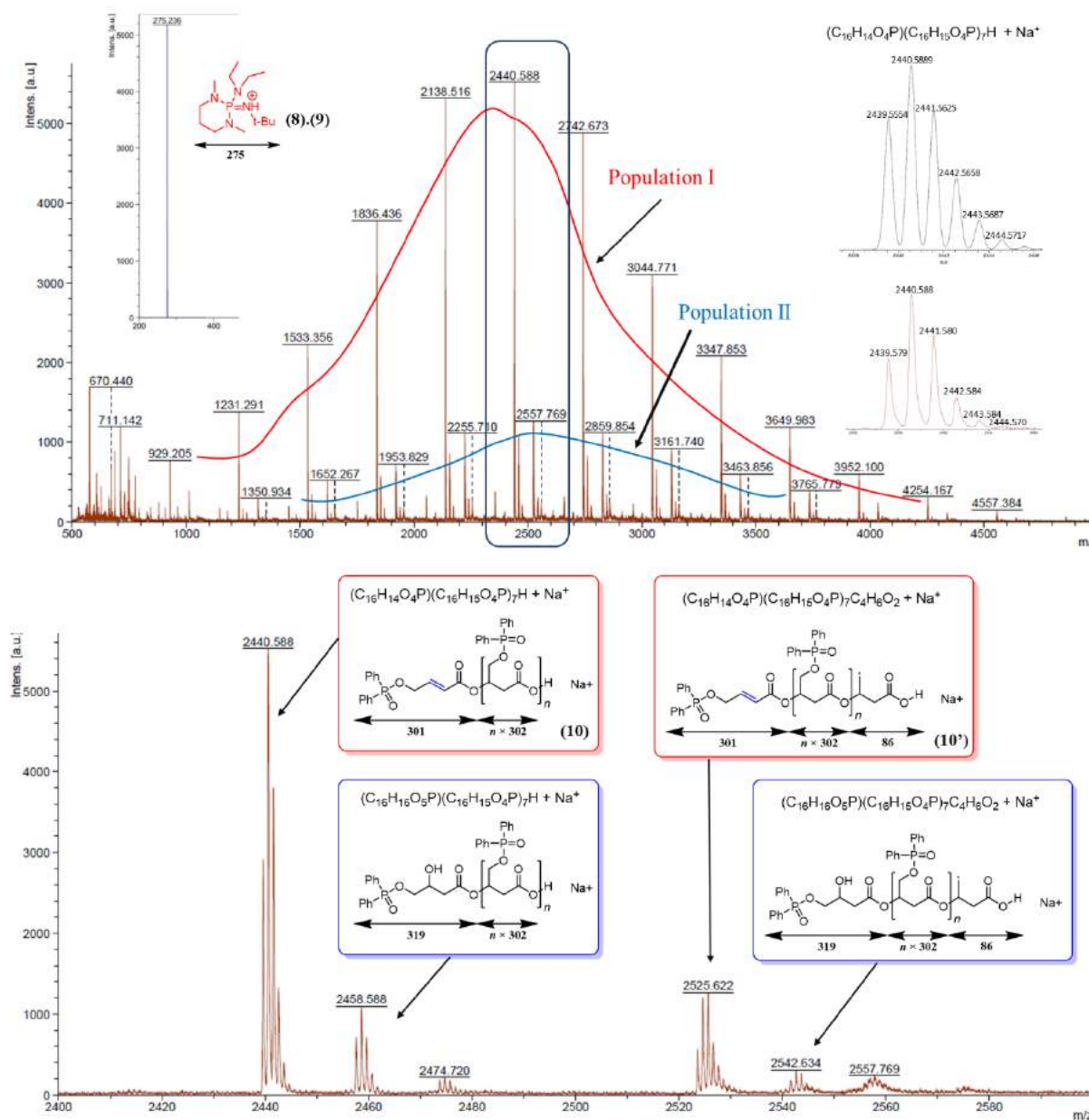
a labile proton; refer to Appendix 10-12), as unequivocally supported by the close match of the simulated isotopic distribution with e.g.,  $m/z_{\text{exp}} = 983.380$  vs.  $m/z_{\text{simul}} = 983.382$  for  $n = 4$  (see left zoomed region).  $[\text{BEMPH}]^+$  was also clearly observed at  $m/z_{\text{exp}} = 275.234$  (top zoomed region) vs.  $m/z_{\text{simul}} = 275.236$ . However, its counter anion, the carboxylate end-capped (macro)molecule(s) (Scheme 3. 17 – (8),(10)) could not be observed under the positive MALDI-ToF MS conditions while analysis under the negative mode did not reveal sensitive enough. No cyclic polymer was observed therein. Moreover, MALDI-ToF MS analysis done in the absence of cationizing agent ( $\text{Na}^+$ ) showed only  $\text{BEMPH}^+$  without any polymeric chains, emphasizing the significance of the MALDI-ToF MS conditions on the characterization (Appendix 13).



**Figure 3. 11** – MALDI-ToF mass spectrum (positive mode, DCTB matrix,  $\text{Na}^+$  cationizing salt) of a sample freshly synthesized from the ROP of  $\text{rac-BPL}^{\text{OBn}}$  mediated by BEMP (Table 3. 3 – entry 11) showing populations corresponding to  $\text{PBPL}^{\text{OBn}}$  macromolecules end-capped with both an  $\alpha$ -crotonate and an  $\omega$ -carboxylic acid end-groups (Scheme 3. 17 – (10)); the right zoomed regions correspond to the simulated (blue, bottom) and experimental (black, top) spectra, and  $[\text{BEMPH}]^+$  (Scheme 3. 17 – (8),(9)); the top middle zoomed region shows the  $[\text{BEMPH}]^+$  fragment recorded.

The MALDI-ToF mass spectrum of a  $\text{PBPL}^{\text{OP(O)Ph}_2}$  sample depicted in Figure 3. 12 supports also the BEMP-mediated production of this innovative aromatic phosphorus containing PHA. The spectrum showed a major population (population I) of  $\text{PBPL}^{\text{OP(O)Ph}_2}$  with a repeating unit of  $302 \text{ g mol}^{-1}$  end-capped with a crotonate and a carboxylic acid group ( $m/z_{\text{exp}} = 2440.588$  vs.  $m/z_{\text{simul}} = 2440.589$ ; for  $n = 7$ ), similarly to the aforementioned  $\text{PBPL}^{\text{OBn}}$  population. As well,  $[\text{BEMPH}]^+$  was observed with  $m/z_{\text{exp}} = 275$ . The minor population (population II) of  $\text{PBPL}^{\text{OP(O)Ph}_2}$  is end-capped with hydroxy and carboxylic acid groups having  $m/z_{\text{exp}} = 2458.588$  for  $n = 7$ . The latter population is only observed in  $\text{rac-BPL}^{\text{OP(O)Ph}_2}$

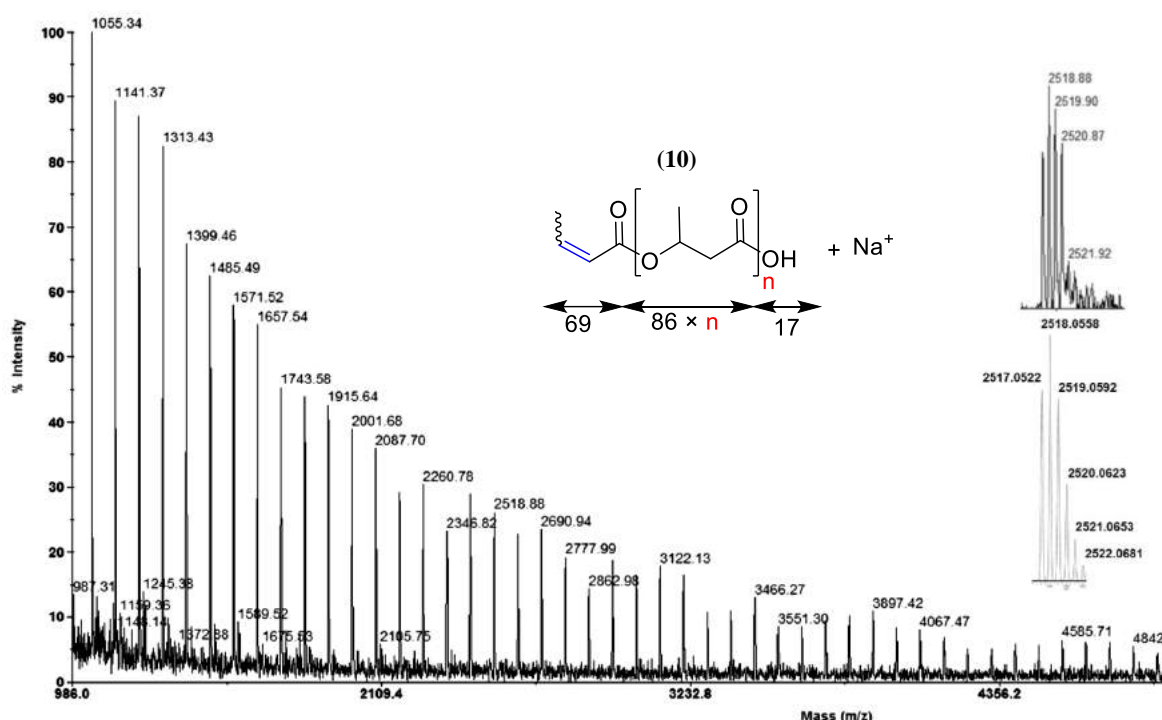
polymerization, probably due to the presence of traces of water in the THF used to solubilize the monomer. Moreover, two populations derived from both populations I and II (Figure 3. 12 – (10')) were also observed resulting from partial fragmentation upon abstraction of the phosphorus group (OP(O)Ph<sub>2</sub>). Once again MALDI-ToF MS analysis performed in the absence of a cationizing agent (Na<sup>+</sup>) in DCTB or in  $\alpha$ -cyano-4-hydroxycinnamic acid (CHCA) showed only BEMPH<sup>+</sup> without any polymeric chains (Appendix 14).

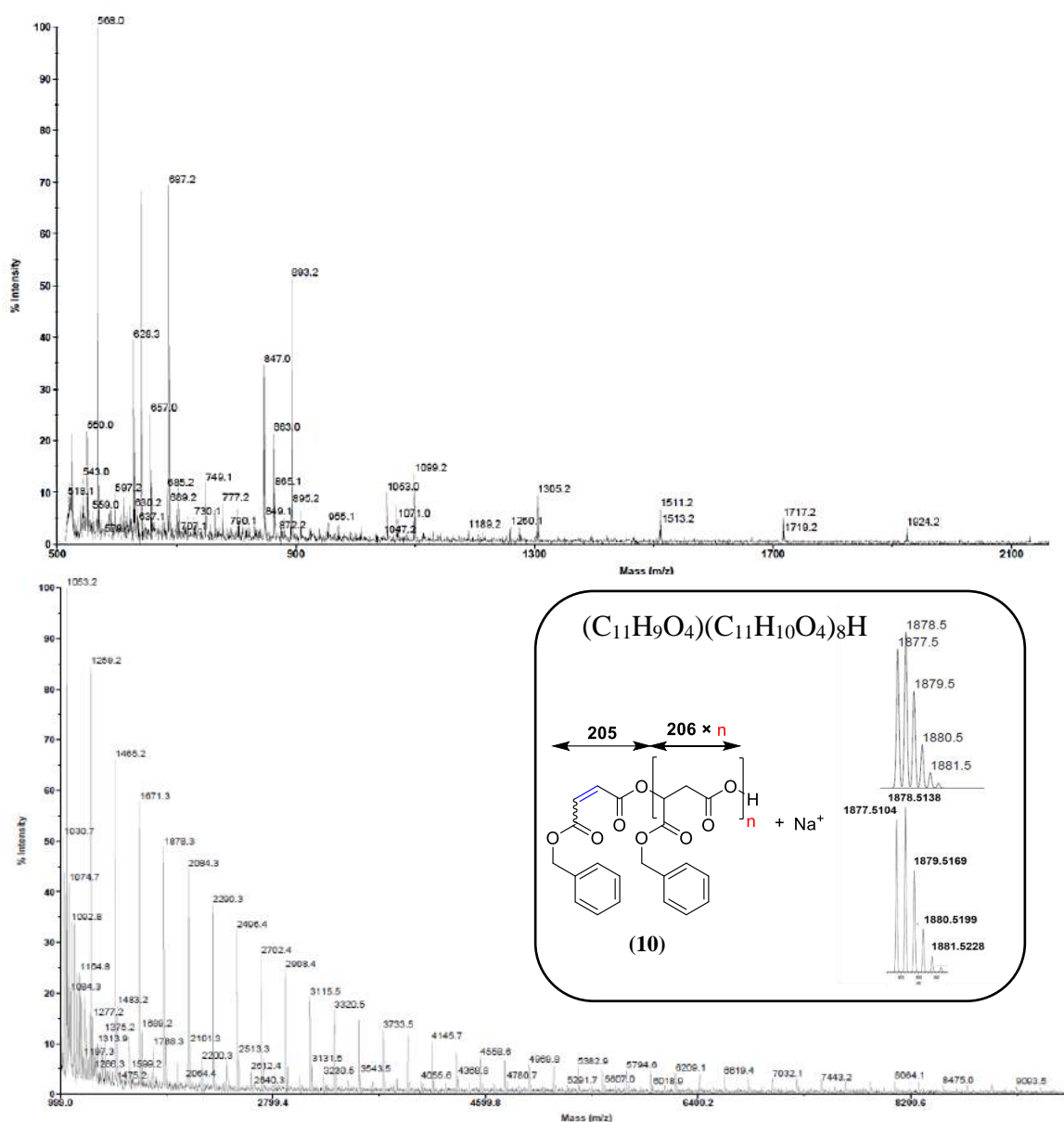


**Figure 3. 12** – MALDI-ToF mass spectrum (positive mode, DCTB matrix, Na<sup>+</sup> cationizing salt) of a sample freshly synthesized from the ROP of *rac*-BPL<sup>OP(O)Ph<sub>2</sub></sup> mediated by BEMP (Table 3. 3 – entry 16) showing population I (in red top boxes) corresponding to PBPL<sup>OP(O)Ph<sub>2</sub></sup> macromolecules end-capped with both an  $\alpha$ -crotonate and an  $\omega$ -carboxylic acid end-groups (Scheme 3. 17 – (10)) and its fragmented product (10'), with the right top zoomed region in the top spectrum are the simulated (black top) and experimental (red bottom); and population II (in blue bottom boxes) of PBPL<sup>OP(O)Ph<sub>2</sub></sup>

macromolecules end-capped with hydroxy and an  $\omega$ -carboxylic acid end-groups and its fragmented product; and [BEMPH]<sup>+</sup> (Scheme 3. 17 – (8),(9)) in the top left side.

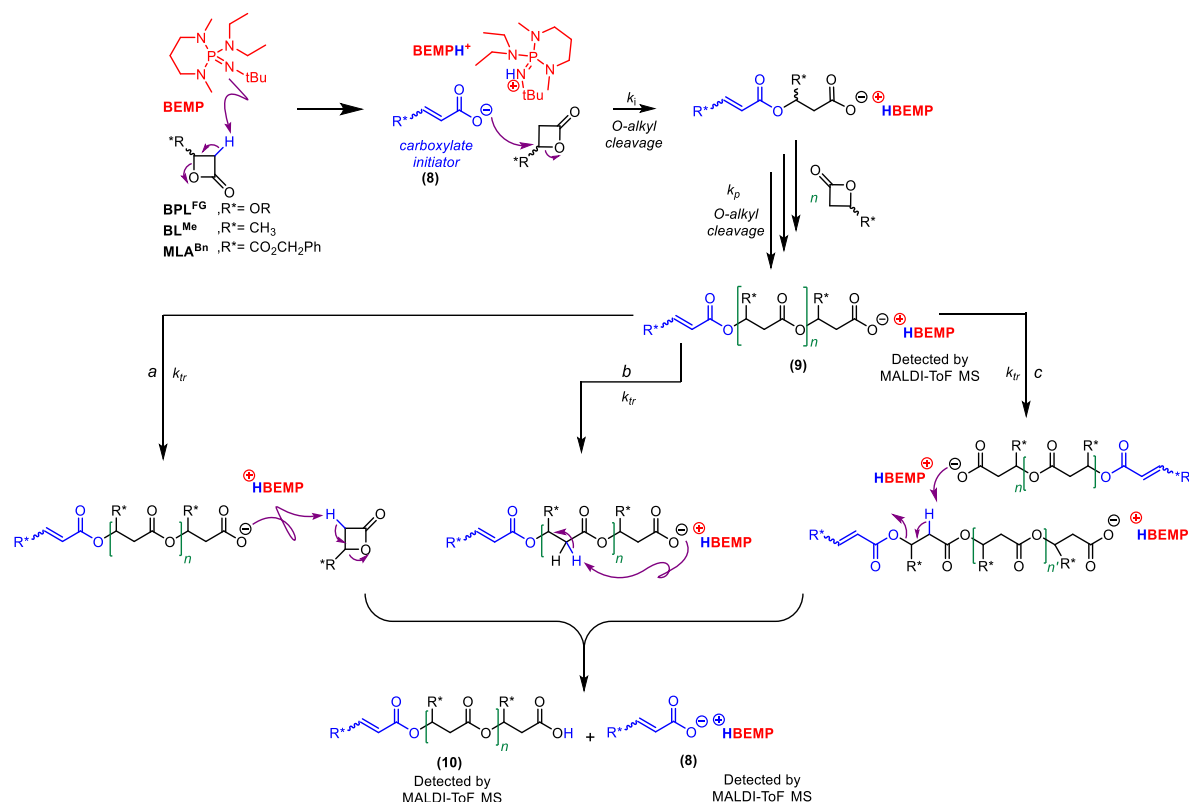
Note that the MALDI-ToF mass spectra previously recorded for PBL<sup>Me</sup> and PMLA<sup>Bn</sup> samples prepared from the alike BEMP-mediated ROP of *rac*-BL<sup>Me</sup> and *rac*-MLA<sup>Bn</sup>, respectively, could not evidence the possible presence of –COOH end-capping group because the matrix/cationizing agent used did not enable it.<sup>[38]</sup> A revised analysis of these MALDI-ToF mass spectra is presented (Figure 3. 13, Figure 3. 14) and shows that the ROP of *rac*-BL<sup>Me</sup> and *rac*-MLA<sup>Bn</sup> mediated by BEMP proceeds in the same way as the ROP of *rac*-BPL<sup>FGs</sup>.





### 4.1.3. Mechanistic pathway for the BEMP-mediated ROP of BPL<sup>FG</sup>s

Considering these spectroscopic and spectrometric evidences of the formation of a mixture of  $\alpha$ -benzyloxy crotonate,  $\omega$ -COOH PBPL<sup>OBn</sup> and [BEMPH]<sup>+</sup>, we may propose the ROP mechanism depicted in Scheme 3. 17. Thus, BEMP would act as a basic pre-initiator (similar to Scheme 3. 3) that abstracts one of the methylene hydrogen in  $\alpha$ -position of the BPL<sup>FG</sup> monomer, thereby generating *in situ* an  $\alpha,\beta$ -unsaturated carboxylate species as the real initiator (Scheme 3. 17 – (8)), which in turn would propagate the polymerization via *O*-alkyl cleavage of further incoming monomer units. Carboxylate initiators with metals or crown ethers,<sup>[45]</sup> or even phosphazene base<sup>[46]</sup> counter cations have previously been reported to promote the ROP of *rac*-BL<sup>Me</sup> and *rac*-MLA<sup>Bn</sup> through such *O*-alkyl opening, a behavior specific to  $\beta$ -lactones (Chapter 1; Scheme 1. 8; Table 1. 3; *vide supra*). Ultimately, (ROCH<sub>2</sub>CH=CHC(O)O)-PBPL<sup>OBn</sup>-H chains would form upon termination/transfer reactions. Transfer reactions may a) involve the monomer ( $k_{tr,a}$ ) (Chapter 1; Scheme 1. 6; *vide supra*), b) take place intramolecularly ( $k_{tr,b}$ ), and/or c) intermolecularly ( $k_{tr,c}$ ), eventually generating a shorter active macromolecular chain ready to propagate (similar to (9)), a dormant chain with a carboxylic acid end-group (10), and/or the carboxylate initiator [BnOCH<sub>2</sub>CH=CHC(O)O]<sup>−</sup>[BEMPH]<sup>+</sup> (8). As a consequence, this could account for the slight discrepancies between molar mass values ( $M_{n,SEC}$ ,  $M_{n,NMR}$ , and  $M_{n,theo}$ ) as well as for the slightly broad dispersities (Table 3. 3). Reinterpretation of the previously reported MALDI-ToF mass spectra of PBL<sup>Me</sup> and PMLA<sup>Bn</sup>, similarly synthesized by ROP of *rac*-BL<sup>Me</sup> and *rac*-MLA<sup>Bn</sup>, respectively, mediated by BEMP (Figure 3. 13, Figure 3. 14) further supports this suggested mechanism. Thereby, the BEMP mode of action is proposed and thus it can be added to the left of Figure 1. 12 (Chapter 1).

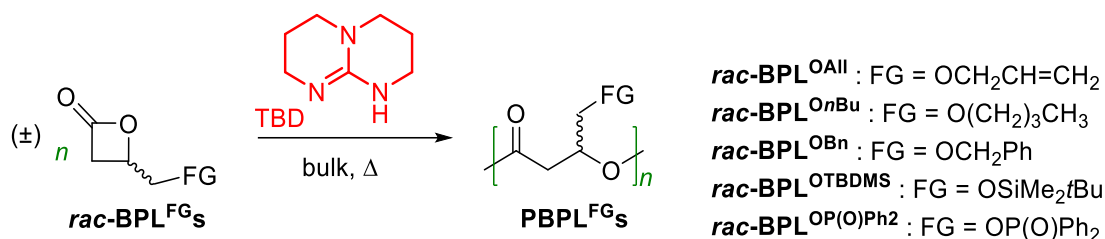


**Scheme 3. 17** – Proposed mechanism for the ROP of *rac*-BPL<sup>FG</sup>s (FG = OAll, *On*Bu, *OB*n, OTBDMS, OP(O)Ph<sub>2</sub> and *rac*-BL<sup>Me</sup>, *rac*-MLA<sup>Bn</sup>) mediated by BEMP proceeding via a proton transfer reaction to generate *in situ* the carboxylate initiating moiety (**8**); (*k<sub>i</sub>*, *k<sub>p</sub>*, *k<sub>tr</sub>*, refer to the rate constant of initiation, propagation, and transfer reactions, respectively), showing the various macromolecular species (**9**) and (**10**).

## 4.2. ROP of BPL<sup>FG</sup>s promoted by TBD

Earlier research on the ROP of large lactones promoted by TBD in the absence of any protic initiators (alcohols) suggested a nucleophilic behavior of TBD (Scheme 3. 5; Table 3. 2). On the other hand, the TBD-promoted ROP of  $\beta$ -lactones (*rac*-BL<sup>Me</sup> and *rac*-MLA<sup>Bn</sup>) was more puzzling, with both Hedrick *et al.* and our group reporting a nucleophilic behavior of TBD via a 1:1 adduct (Scheme 3. 12, Scheme 3. 13 – top), while Coulembier *et al.* stated a major basic contribution of TBD and a minor nucleophilic one (Scheme 3. 14), under the same conditions (bulk medium, 60 °C). Therefore, an extended reinvestigation was undertaken to better understand the behavior of TBD towards the ROP of  $\beta$ -lactones. Hence, in this work, the ROP of BPL<sup>FG</sup>s (R = All, <sup>n</sup>Bu, Bn, TBDMS, OP(O)Ph<sub>2</sub>) via TBD in bulk conditions was investigated (Scheme 3. 18).





**Scheme 3. 18** – Bulk ROP of  $rac-BPL^{FGs}$  promoted by TBD.

#### 4.2.1. Molecular characterization of $PBPL^{FGs}$ obtained from TBD

Representative experimental results of the neat (i.e., performed in bulk) ROP of  $rac-BPL^{FGs}$  using TBD at different temperatures and  $[BPL^{FG}]_0/[BEMP]_0$  ratios ranging from 20 to 75, are gathered in Table 3. 4. TBD proved significantly less active than BEMP (Table 3. 3), a general tendency also reported for the alike ROP of  $rac-BL^{Me}$  and  $rac-MLA^{Bn}$ ,<sup>[38]</sup> though with a reverse trend for LA,  $\delta$ -VL, or  $\epsilon$ -CL, towards which TBD was highly more active than BEMP (*vide supra*). Most of the polymerizations were performed at 60 °C, since those at lower temperature (25–40 °C) were very sluggish (Table 3. 4, entries 2,3). The experimental and theoretical molar masses were generally in good agreement ( $M_{n,theo}$  vs.  $M_{n,NMR}$  vs.  $M_{n,SEC}$ ) with fairly narrow dispersities ranging from  $1.14 < \bar{D}_M < 1.41$ , in the case of  $[BPL^{FG}]_0/[BEMP]_0 \leq 40$ . This would imply that not all growing chains are initiated at the same time when the initiator is added/formed or that TBD is not fully consumed at an early stage.<sup>[47]</sup> Also, it may account for the presence of detrimental side-reactions such as possible intra- and inter-molecular transesterifications, which can be promoted by TBD, presumably by direct transfer of the acyl group between alcohols (similarly to the ROP of LA,  $\delta$ -VL or  $\epsilon$ -CL by TBD; *vide supra*). Alike BEMP, TBD seemed to polymerize  $rac-BPL^{FGs}$  less rapidly ((TOF) = 8.7 h<sup>-1</sup>; Table 3. 4, entry 1) than  $rac-BL^{Me}$  and  $rac-MLA^{Bn}$  ((TOF) = 19.5 h<sup>-1</sup> and 39.5 h<sup>-1</sup>, respectively) under the same conditions.<sup>[38]</sup> Finally, an attempt to ring-open polymerize  $BPL^{OP(O)Ph_2}$  (DP = 40) by TBD was carried out at 60 °C, in THF solution since both TBD and the monomer are solids. The polymerization under these conditions was very slow and afforded only 15% monomer conversion after 3 days, presumably due to the bulkiness of the phosphorous group and the more diluted operated medium compared to other  $BPL^{FGs}$ . Thus, no more experimentation was done for the ROP of  $rac-BPL^{OP(O)Ph_2}$  promoted by TBD.

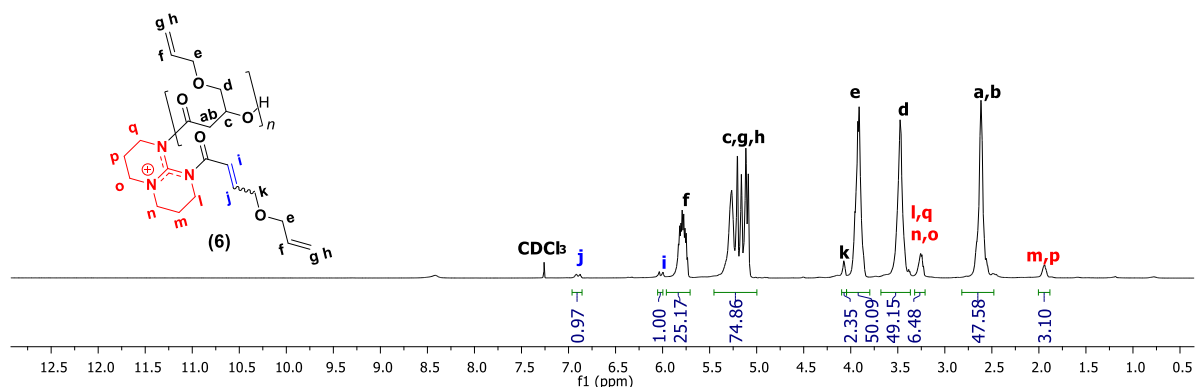
**Table 3. 4** – Characteristics of the PBPL<sup>FG</sup>s synthesized by ROP of *rac*-BPL<sup>FG</sup>s mediated by TBD<sup>a</sup>.

Entry	BPL <sup>FG</sup> (FG=)	[BPL <sup>FG</sup> ] <sub>0</sub> / [TBD] <sub>0</sub>	Temp. (°C)	Time <sup>b</sup> (h)	Conv. <sup>c</sup> (%)	$\bar{M}_{n,theo}^d$ (g mol <sup>-1</sup> )	$\bar{M}_{n,NMR}^e$ (g mol <sup>-1</sup> )	$\bar{M}_{n,SEC}^f$ (g mol <sup>-1</sup> )	$\bar{D}_M^f$
1	OAll	43	60	4	81	4950	3600	3100	1.41
2	O <sup>n</sup> Bu	40	25	19	21	1350	1000	1000	1.14
3	O <sup>n</sup> Bu	42	40	9	44	2900	2800	2100	1.14
4	O <sup>n</sup> Bu	40	60	7	68	4300	3300	3200	1.29
5	O <sup>n</sup> Bu	75	60	16	88	10450	11850	7000	1.15
6	OBn	20	60	3	61	2350	2100	1100	1.26
7	OBn	41	60	6	70	5500	4300	3900	1.32
8	OTBDMS	40	60	8	40	3450	1000	1100	1.34
9 <sup>g</sup>	OP(O)Ph <sub>2</sub>	40	60	72	15	1800	1200	1400	1.12

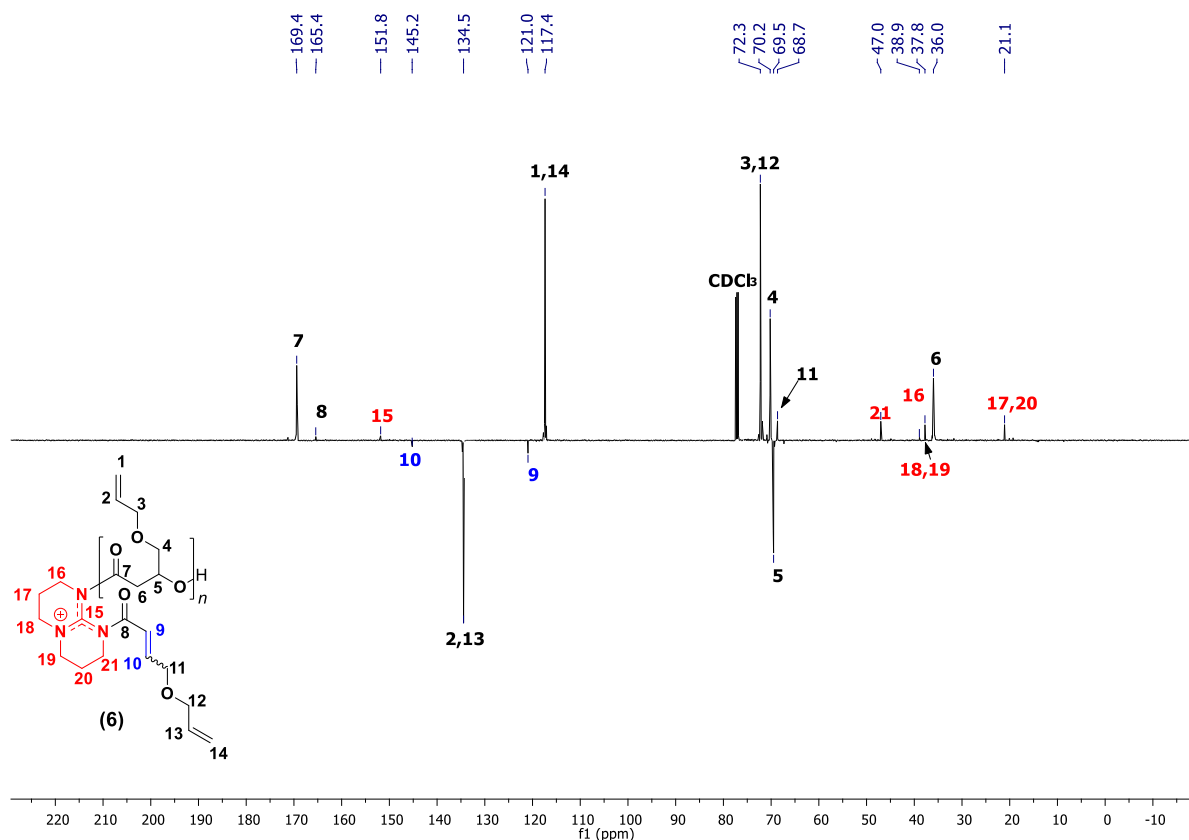
<sup>a</sup> Results are representative of at least duplicated experiments performed neat. <sup>b</sup> The reaction time was not necessarily optimized. <sup>c</sup> BPL<sup>FG</sup> conversion as determined by <sup>1</sup>H NMR analysis of the crude reaction mixture (refer to the Experimental Section). <sup>d</sup> Theoretical molar mass calculated from the relation: [BPL<sup>FG</sup>]<sub>0</sub>/[TBD]<sub>0</sub> × Conv.<sub>BPLOR</sub> ×  $\bar{M}_{BPLFG}$ , i.e. without considering end-capping groups, with  $\bar{M}_{BPLORAll}$  = 142 g mol<sup>-1</sup>,  $\bar{M}_{BPLORnBu}$  = 158 g mol<sup>-1</sup>,  $\bar{M}_{BPLORBn}$  = 192 g mol<sup>-1</sup>,  $\bar{M}_{BPLORTBDMS}$  = 216 g mol<sup>-1</sup> and  $\bar{M}_{BPLOROP(O)Ph_2}$  = 302 g mol<sup>-1</sup>. <sup>e</sup> Experimental molar mass value as determined by <sup>1</sup>H NMR analysis of the isolated polymer, from the resonances of the crotonate end-group (refer to the Experimental Section). <sup>f</sup> Experimental molar mass and dispersity values as determined by SEC in THF using a RI detector at 30 °C vs polystyrene standards. <sup>g</sup> ROP was done in a dry THF solution (0.1 mL) to solubilize the monomer and the catalyst.

#### 4.2.2. Macromolecular structure of TBD-synthesized PBPL<sup>FG</sup>s assessed by NMR spectroscopy and MALDI-ToF mass spectrometry

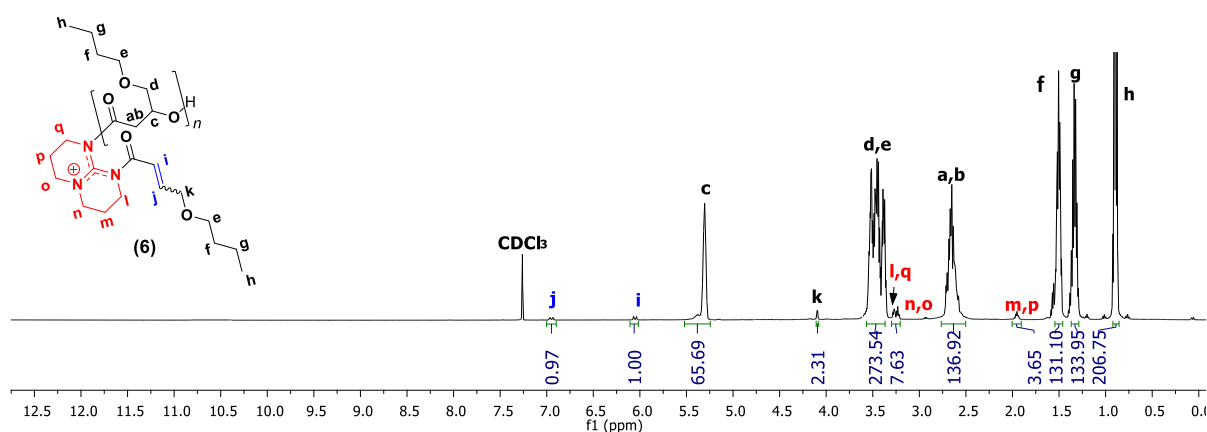
All the purified PBPL<sup>FG</sup>s isolated from the ROP of *rac*-BPL<sup>FG</sup>s mediated by TBD were characterized by <sup>1</sup>H, J-MOD and 2D (COSY) NMR spectroscopy and MALDI-ToF MS, with the aim to determine the nature of the end-capping groups. The typical <sup>1</sup>H and J-MOD NMR spectra exemplified in Figure 3. 15 to Figure 3. 17 unambiguously showed, alongside the characteristic backbone methine and methylene hydrogens' signals, the resonances of both crotonate and TBD moieties in a near 1:1 ratio ( $\delta_{1H}$  ppm 3.28 ( $CH^i_2N=C(N)NHCH^o_2$ ), 3.20 ( $CH^l_2N(C)CH^m_2$ ), and 1.93 ( $CH_2CH^k_{n_2}CH_2$ )). For the PBPL<sup>OP(O)Ph<sub>2</sub></sup> crude <sup>1</sup>H NMR with 15% monomer conversion (Table 3. 4 – entry 9; Appendix 15).







**Figure 3. 15** –  $^1\text{H}$  (500 MHz,  $\text{CDCl}_3$ , 25 °C) (top) and J-MOD (125 MHz,  $\text{CDCl}_3$ , 25 °C) (bottom) NMR spectra of PBPL<sup>OAll</sup> recovered from the ROP of *rac*-BPL<sup>OAll</sup> mediated by TBD (Table 3. 4 – entry 1); depicting only one (I, Scheme 3. 19 – (13)) out of the two populations (I and II, Scheme 3. 19 – (13),(15)) observed by MALDI-ToF MS (Figure 3. 19).



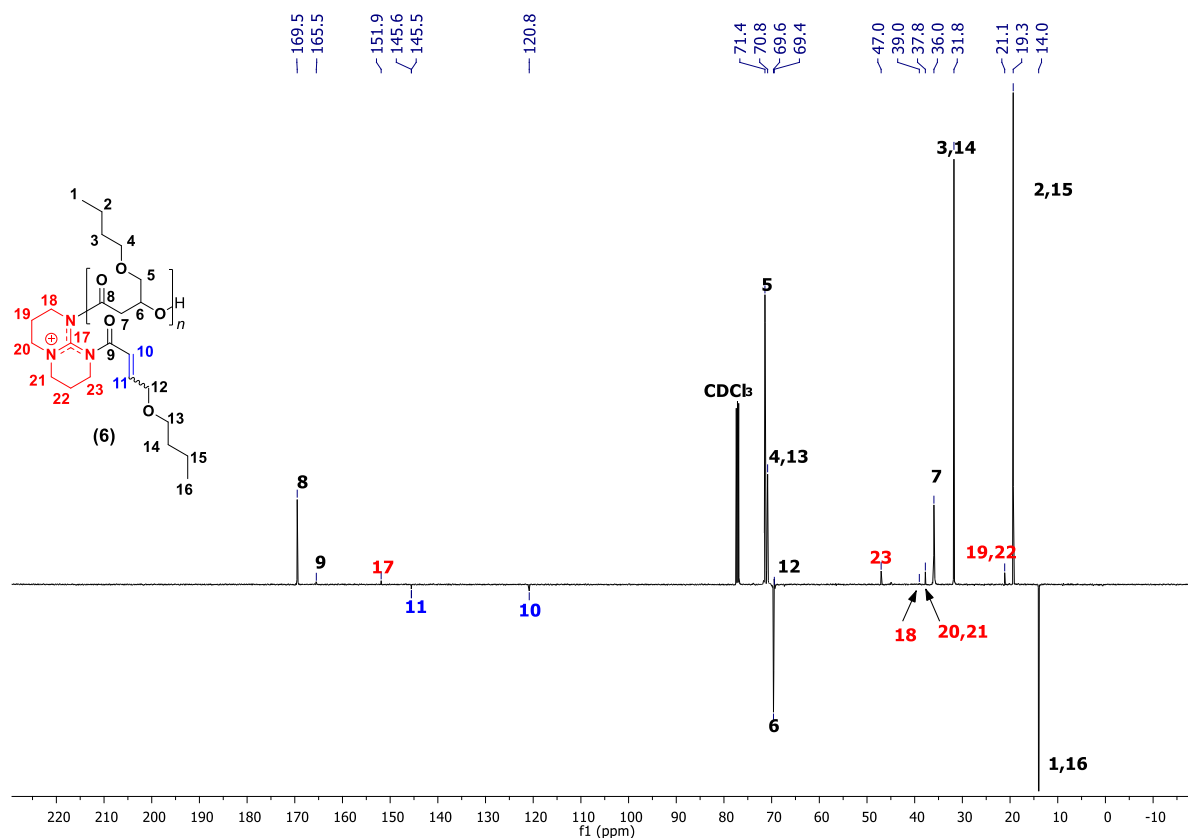


**Figure 3. 16** – <sup>1</sup>H (500 MHz, CDCl<sub>3</sub>, 25 °C) (top) and J-MOD (125 MHz, CDCl<sub>3</sub>, 25 °C) (bottom) NMR spectra of PBPL<sup>OnBu</sup> recovered from the ROP of *rac*-BPL<sup>OnBu</sup> mediated by TBD (Table 3. 4); depicting only one (I, Scheme 3. 19 – (13)) out of the two populations (I and II, Scheme 3. 19 – (13),(15)) observed by MALDI-ToF MS (Figure 3. 19).

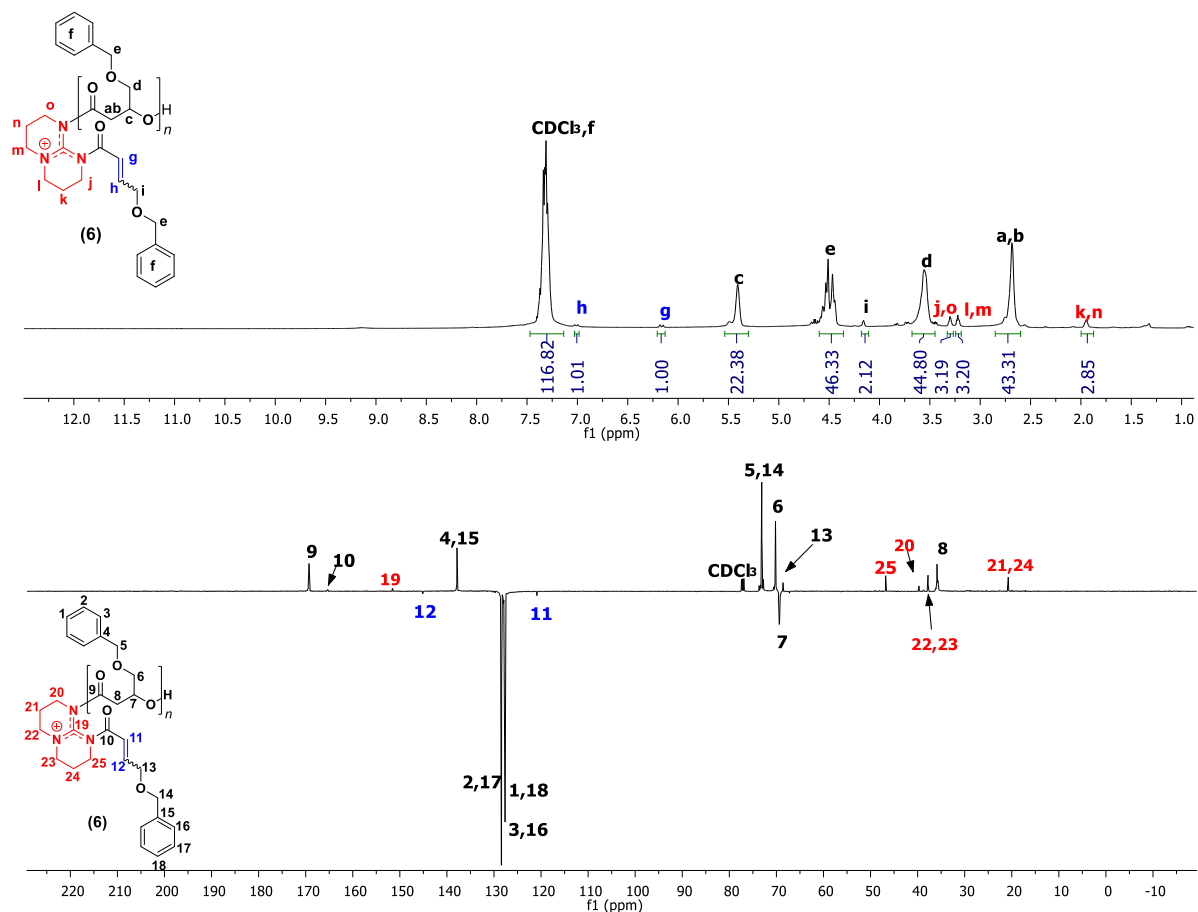


**Figure 3. 17** –  $^1\text{H}$  (500 MHz,  $\text{CDCl}_3$ , 25 °C) (top) and J-MOD (125 MHz,  $\text{CDCl}_3$ , 25 °C) (bottom) NMR spectra of a purified  $\text{PBPL}^{\text{OBn}}$  sample recovered from the ROP of  $\text{rac-BPL}^{\text{OBn}}$  mediated by TBD (Table 3. 4, entry 7), depicting only one (**I**, Scheme 3. 19 – (**13**)) out of the two populations (**I** and **II**, Scheme 3. 19 – (**13**), (**15**)) observed by MALDI-ToF MS (Figure 3. 19).

The 2D COSY NMR spectra evidenced, similarly as with BEMP, a correlation between the vinylic and methylene hydrogens of the crotonate end-group, supporting the crotonate chain-end (Figure 3. 18).

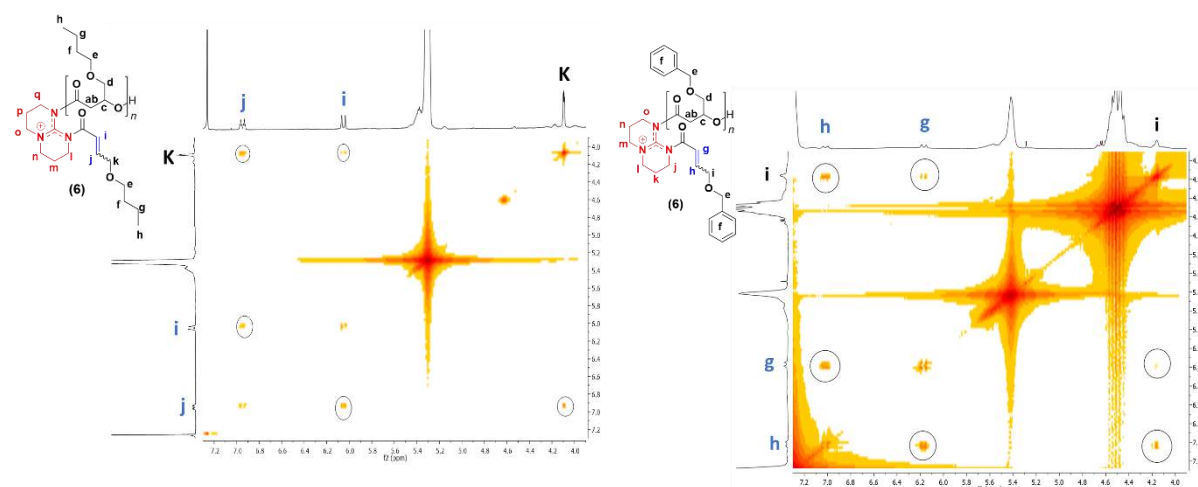


**Figure 3. 18** –  $^1\text{H}$ - $^1\text{H}$  COSY (500 MHz,  $\text{CDCl}_3$ , 25 °C) NMR zoomed spectrum; of  $\text{PBPL}^{\text{OBnBu}}$  (left) and of  $\text{PBPL}^{\text{OBn}}$  (right) recovered from the ROP of  $\text{rac-BPL}^{\text{OBnBu}}$  and  $\text{rac-BPL}^{\text{OBn}}$  mediated by TBD supporting the  $\alpha$ -crotonate end-capping group (Table 3. 4 – entries 5, 7).

Consequently, while a crotonate chain-end was definitively observed from the NMR analyses, further examination was required in order to reveal the nature of TBD (nucleophile vs. base) that was observed in the NMR spectra. More information was gained from MALDI-ToF MS analyses of the isolated PBPL<sup>FG</sup> samples, as exemplified with PBPL<sup>OBn</sup> depicted in Figure 3. 19. Two distinct populations of macromolecules were observed with a repeating unit of 192 g mol<sup>-1</sup>. A first population (**I**) corresponds to PBPL<sup>OBn</sup> flanked with a TBD-*N*-acyl- $\alpha,\beta$ -unsaturated species and hydroxy chain-ends (Figure 3. 21 – (**13**)), as unequivocally confirmed by the isotopic simulation (e.g.,  $m/z_{\text{exp}} = 1659.753$  vs  $m/z_{\text{simul}} = 1659.740$  for  $n = 7$ ; see right zoomed region (purple)). The second population (**II**) is the same as the former one featuring an additional TBD moiety (Figure 3. 21 – (**15**)), as supported by the isotopic simulation with e.g.,  $m/z_{\text{exp}} = 1221.611$  vs  $m/z_{\text{simul}} = 1221.612$  for  $n = 4$  (see left zoomed region (blue)). Interestingly, two TBD adducts were also revealed, namely the [TBD-crotonate]<sup>+</sup> ( $m/z_{\text{exp}} = 314.200$  g mol<sup>-1</sup>) species (Figure 3. 21 – (**11**)) and [TBDH]<sup>+</sup> ( $m/z_{\text{exp}} = 140.116$ ). Moreover, PBPL<sup>OBn</sup> end-capped with carboxylic acid, similarly to the one obtained by BEMP (Figure 3. 11 – (**10**)), was not observed. Note that MALDI-ToF MS analysis done in the absence of cationizing agent (Na<sup>+</sup>) revealed the same spectra as the one obtained with added Na<sup>+</sup> (Appendix 16).

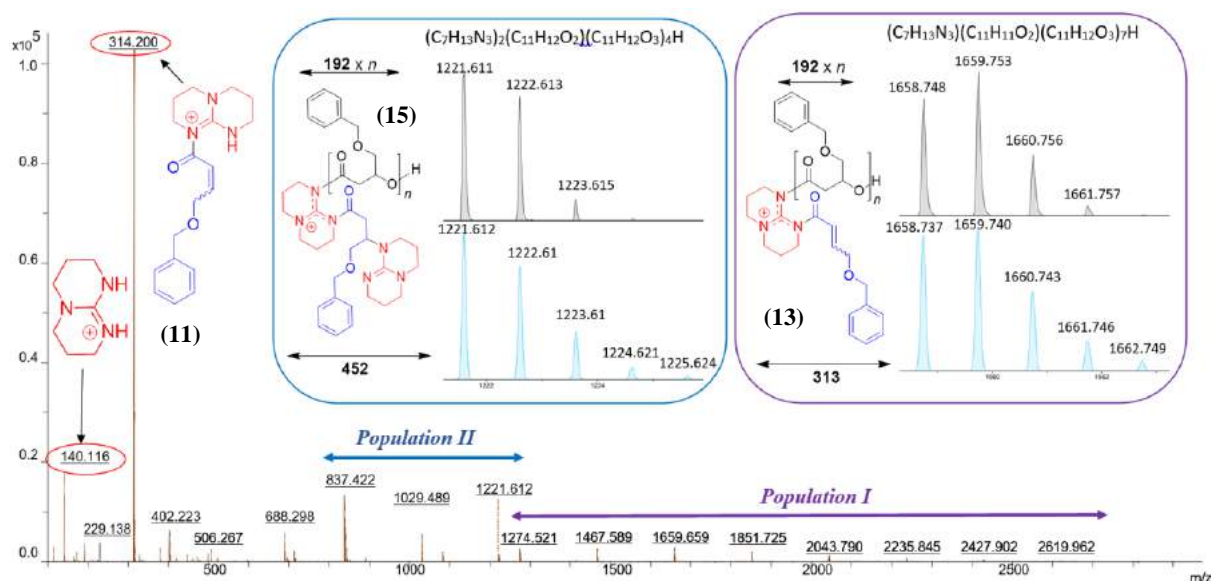


**Figure 3. 19** – MALDI-ToF mass spectrum (positive mode, DCTB matrix,  $\text{Na}^+$  cationizing salt) of a sample freshly synthesized from the ROP of *rac*-BPL<sup>OBn</sup> mediated by TBD (Table 3. 4 – entry 6) showing populations corresponding to PBPL<sup>OBn</sup> macromolecules end-capped with both an  $\alpha$ -benzyloxycrotonate-TBD and an  $\omega$ -hydroxy end-groups (population I; Scheme 3. 19 – (13)), and to a subsequently modified population I where a TBD molecule is added into the crotonate moiety to give population II (Scheme 3. 19 – (15)); the zoomed regions correspond to the simulated (blue, bottom) and experimental (grey, top) corresponding spectra, respectively. Species TBD:BPL<sup>FG</sup> adduct (Scheme 3. 19 – (11)) and [TBDH]<sup>+</sup> are also shown.

According to these analyses, a nucleophilic mode of TBD to promote the ROP of BPL<sup>FG</sup>s was revealed as in Scheme 3. 13 – top, for BL<sup>Me</sup> and MLA<sup>Bn</sup>. Nevertheless, a reinterpretation of the MALDI-ToF mass spectra of the previously synthesized PBL<sup>Me</sup> and PMLA<sup>Bn</sup> was done (Figure 3. 20 , Figure 3. 21), exposing that PBL<sup>Me</sup> and PMLA<sup>Bn</sup> macromolecular structures are analogous to population I (Figure 3. 21 – (13)), delineated with a TBD-*N*-acyl- $\alpha,\beta$ -unsaturated species and hydroxy chain-ends instead of TBD-*N*-acyl and an  $\alpha,\beta$ -unsaturated group as it was expressed previously (Scheme 3. 13 – top).<sup>[38]</sup> Remarkably, neither PBPL<sup>FG</sup>s (Figure 3. 19) nor PBL<sup>Me</sup> and PMLA<sup>Bn</sup> (Figure 3. 20) MALDI-ToF mass spectra showed carboxylic acid chain-ends, in contrast to what was reported by Coulembier *et al.* for PBL<sup>Me</sup> obtained from the same reaction (TBD, bulk, 60 °C) and MALDI- ToF MS (DCTB matrix,  $\text{Na}^+$ ) conditions (Scheme 3. 14 – top),<sup>[39]</sup> thus refuting the behavior of TBD as base to abstract  $\alpha$ -hydrogen of the  $\beta$ -lactones.

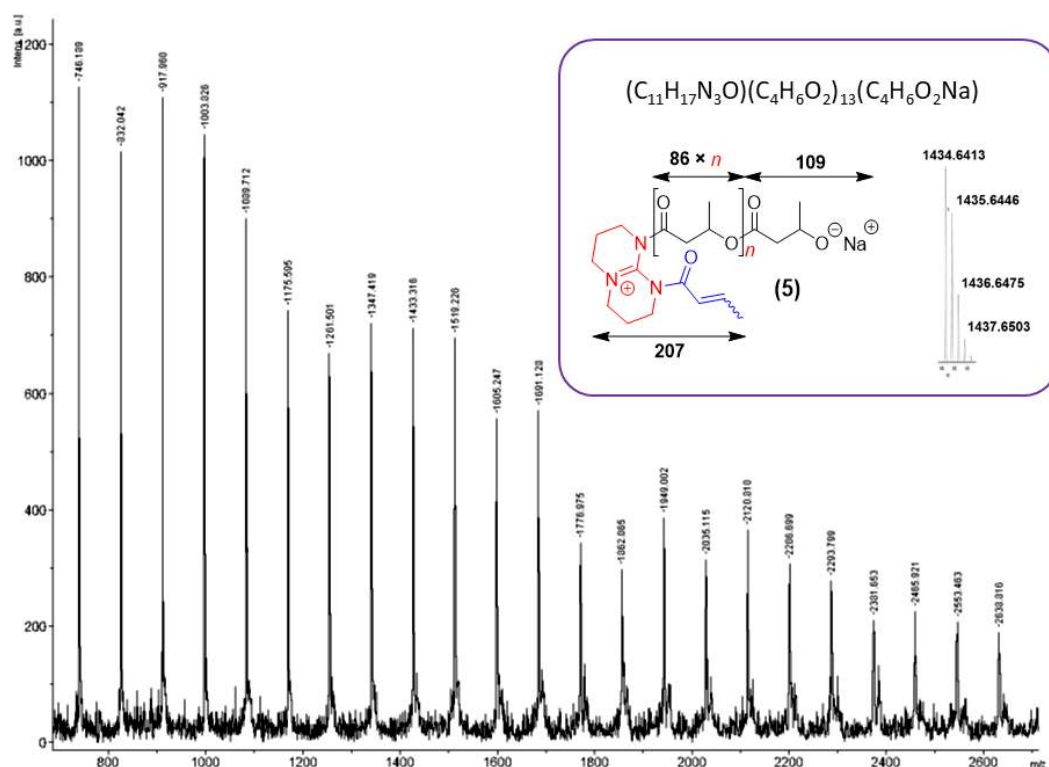


**Figure 3. 20** – MALDI–ToF mass spectrum (positive mode, DCTB matrix, Na<sup>+</sup> cationizing salt) of a PBL sample synthesized from the ROP of *rac*-BL mediated by TBD (as reproduced from Figure 4 in reference<sup>[38a]</sup>). Reinterpretation shows that the zoomed regions correspond to the simulated (bottom) and experimental (top) spectra of a zwitterionic species alike species Scheme 3. 19 – (13).

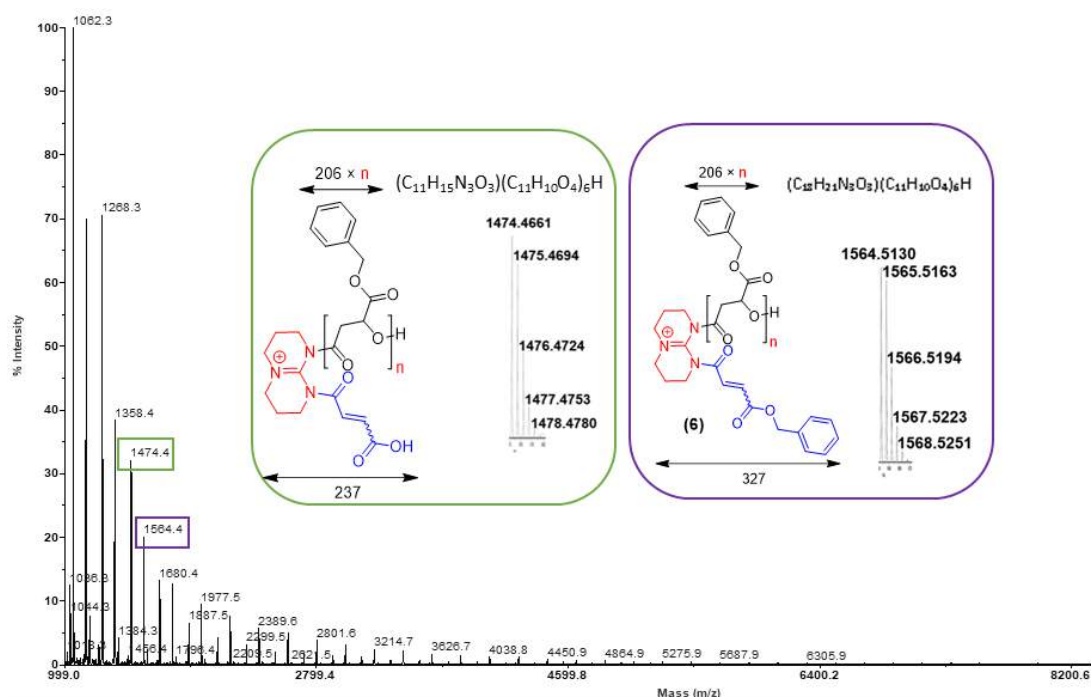
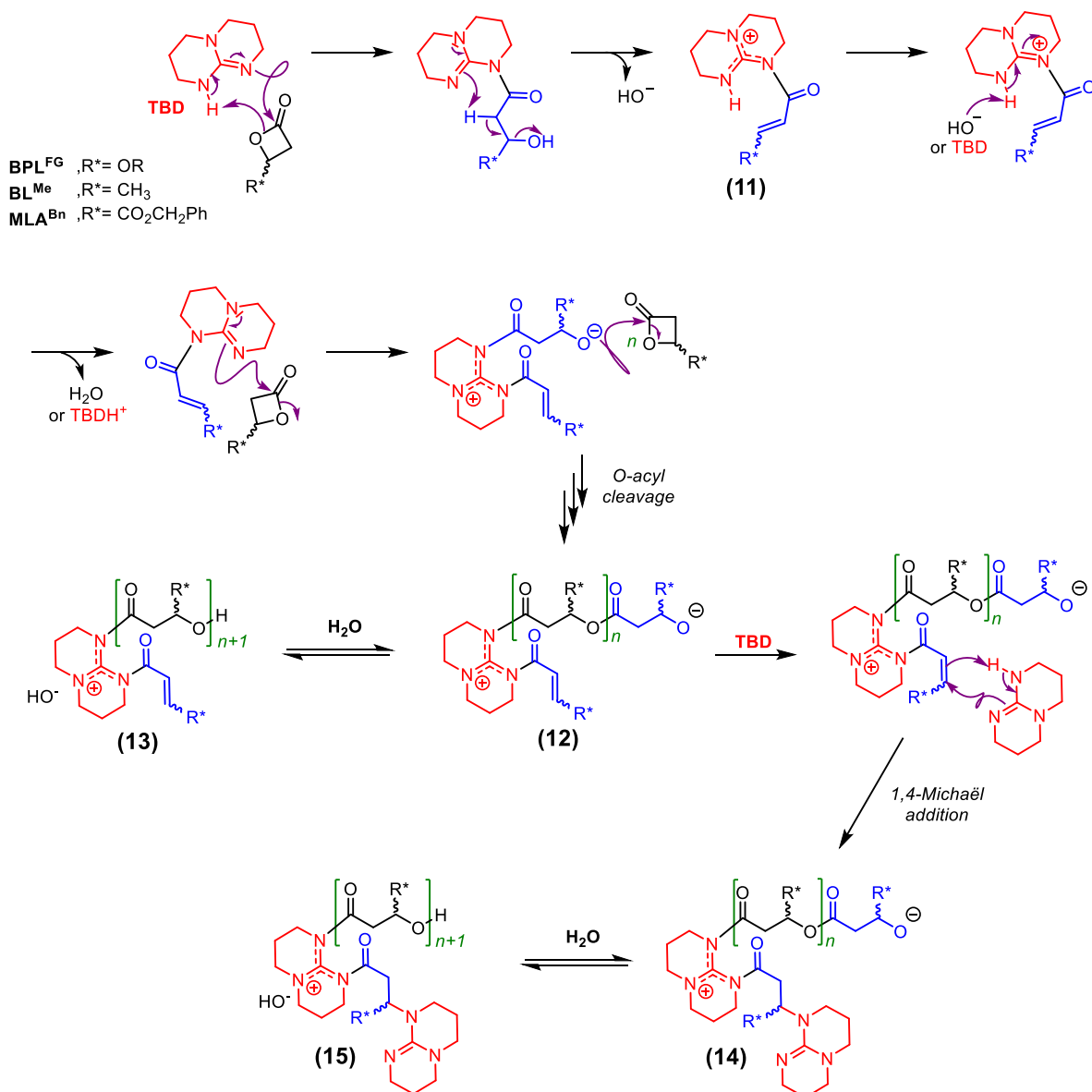


**Figure 3. 21** – MALDI–ToF mass spectrum (*trans*-3-indoleacrylic acid (IAA) matrix, no ionization agent) of a PMLA<sup>Bn</sup> sample freshly synthesized from the ROP of *rac*-MLA<sup>Bn</sup> mediated by TBD (as reproduced from Figure 7 from reference<sup>[38b]</sup>). Reinterpretation shows that the zoomed regions correspond to the simulated (bottom) and experimental (top) spectra of PMLA<sup>Bn</sup> macromolecules  $\alpha$ -benzyloxycrotonate-TBD and an  $\omega$ -hydroxy end-groups (Scheme 3. 19 – (13)), and of the same macromolecular species depleted of the benzylium ion [C<sub>6</sub>H<sub>5</sub>CH<sub>2</sub>]<sup>+</sup> depicted in green).

### 4.2.3. Mechanistic pathway for the TBD-mediated ROP of BPL<sup>FG</sup>s

From these results, it thus appears that TBD would follow a nucleophilic pathway to ring-open BPL<sup>FG</sup>s, rather than a basic one, as depicted in Scheme 3. 19. This is reminiscent of the mechanism reported for the ROP of larger lactones promoted by TBD under similar bulk operating conditions,<sup>[12]</sup> or in the absence of any protic reagents such as alcohols (Scheme 3. 5).<sup>[14]</sup> Further affirmation of this mechanism can be gained from the DFT studies reported previously by Goodman *et al.* on the ROP of BL<sup>Me</sup> in the presence of TBD, supporting the formation of a TBD-BL<sup>Me</sup> adduct and even its dehydrated product (TBD-*N*-acyl- $\alpha,\beta$ -unsaturated; (**11**)).<sup>[25, 48]</sup> Adventitiously, after the 1:1 TBD-BPL<sup>FG</sup> adduct is formed by ring-opening of the  $\beta$ -lactone via an *O*-acyl cleavage, a TBD-*N*-acyl- $\alpha,\beta$ -unsaturated species is generated (Scheme 3. 19 – (**11**), Figure 3. 19 – (**11**)), alike the intermediate reported previously by Hedrick *et al.* (Scheme 3. 12) and our group (Scheme 3. 13 – top) from which H<sub>2</sub>O or [TBDH]<sup>+</sup> is then eliminated. The adduct obtained would propagate the polymerization via an *O*-acyl cleavage operated by the second nucleophilic nitrogen of TBD, generating a zwitterionic propagating species (Scheme 3. 19 – (**12**)) ultimately giving population **I** (Figure 3. 19, Scheme 3. 19 – (**13**)) after protonation. This aspect of TBD, acting as double nucleophile due to its two nucleophilic nitrogen atoms, was previously revealed by Kappe *et al.*<sup>[22]</sup> Most likely, the  $\alpha,\beta$ -unsaturation from **12** or **13** acts as a Michaël acceptor towards TBD, a behavior common for bicyclic guanidine,<sup>[49]</sup> thereby generating macromolecules **14** or **15**, the latter being population **II** (Figure 3. 19, Scheme 3. 19 – (**15**)). This mechanism involves all the species detected in the MALDI-ToF mass spectra of PBPL<sup>FG</sup>s (Figure 3. 19), and it is in contrast with the TBD-mediated anionic ROP of *rac*-BL<sup>Me</sup> reported recently by Coulembier and co-workers, in which TBD is proposed to activate the  $\beta$ -lactone via its basic character (Scheme 3. 14 – top). Probably, in this latter case, TBD acted as a base due to the presence of adventitious H<sub>2</sub>O in the polymerization medium, which can act as an initiator itself by forming [HO]<sup>−</sup>[TBDH]<sup>+</sup> (Scheme 3. 14 – bottom), especially that the authors obtained a population of PBL<sup>Me</sup> end-capped with carboxylic acid and hydroxy chain-ends in the MALD-Tof mass spectrum.<sup>[39]</sup> Ostensibly, due to the strong nucleophilicity of TBD, its place should be on the right of Figure 1. 12 (Chapter 1).



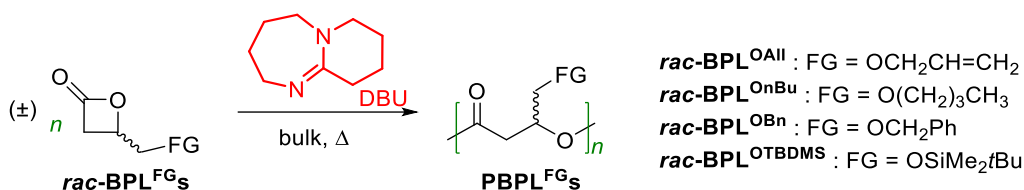
**Scheme 3. 19** – Proposed mechanism for the ROP of  $\text{rac-BPL}^{\text{FG}}$ s (FG = OAll, OnBu, OBn, OTBDMS, OP(O)Ph<sub>2</sub> and  $\text{rac-BL}^{\text{Me}}$ ,  $\text{rac-MLA}^{\text{Bn}}$ ) mediated by TBD, proceeding via an *O*-acyl cleavage of  $\text{BPL}^{\text{FG}}$  into species (12) mediated by (11) adduct, and the plausible side polymer species (14). Species (13) and (15) refer to the protonated form of (12) and (14), respectively, after quenching the polymerization by DCM.

### 4.3. ROP of $\text{BPL}^{\text{FG}}$ s promoted by DBU

DBU was the last organic activator investigated in our work. Whereas DBU associated with an alcohol failed to polymerize large lactones ( $\delta$ -VL,  $\epsilon$ -CL) unless a cocatalyst such as TU (*vide supra*, Scheme 3. 7) was added to the catalytic system<sup>[23b]</sup>, DBU was able to polymerize  $\beta$ -lactones ( $\text{BL}^{\text{Me}}$  and  $\text{MLA}^{\text{Bn}}$ ) without any alcohol or cocatalyst in bulk conditions.<sup>[38]</sup> Presuming that DBU may behave as a nucleophile to initiate the ROP via *O*-acyl cleavage is a pathway that needs further investigation (Scheme 3. 13 – bottom). Hereafter, we report the ROP



of BPL<sup>FG</sup>s (FG = OAll, O<sup>n</sup>Bu, OBn, OTBDMS) promoted by DBU at 60 °C in bulk conditions (Scheme 3. 21) alongside a mechanistic view.



**Scheme 3. 20** –ROP of *rac*-BPL<sup>FG</sup>s promoted by DBU in bulk conditions.

#### 4.3.1. Molecular characterization of PBPL<sup>FG</sup>s obtained from DBU

In light of the poor activity of DBU, all polymerizations were performed only at 60 °C, and the corresponding data are reported in Table 3. 5. In fact, the activity of DBU towards BPL<sup>FG</sup>s was lower than that of TBD and BEMP, similarly to what was reported previously concerning large lactones (LA, δ-VL, ε-CL; *vide supra*). However, the activity of DBU towards other β-lactones (BL<sup>Me</sup> and MLA<sup>Bn</sup>), was lower than that of BEMP, and higher than that of TBD.<sup>[38]</sup> Once more, similarly to what was observed with BEMP and TBD, DBU appeared to polymerize *rac*-BPL<sup>FG</sup>s (FG = OAll, O<sup>n</sup>Bu, OBn, OTBDMS) less efficiently (TOF = 2.9 h<sup>-1</sup>; Table 3. 5 – entry 1) than *rac*-BL<sup>Me</sup> and *rac*-MLA<sup>Bn</sup> (TOF = 11.75 h<sup>-1</sup> and 100 h<sup>-1</sup>, respectively) under the same conditions.<sup>[38]</sup> Targeting DPs of 40–50 resulted in a passable control of molar masses parameters ( $\bar{M}_{n,theo}$  vs.  $\bar{M}_{n,NMR}$  vs.  $\bar{M}_{n,SEC}$ ) and fairly narrow dispersities ( $1.12 \leq \bar{D}_M \leq 1.30$ ).

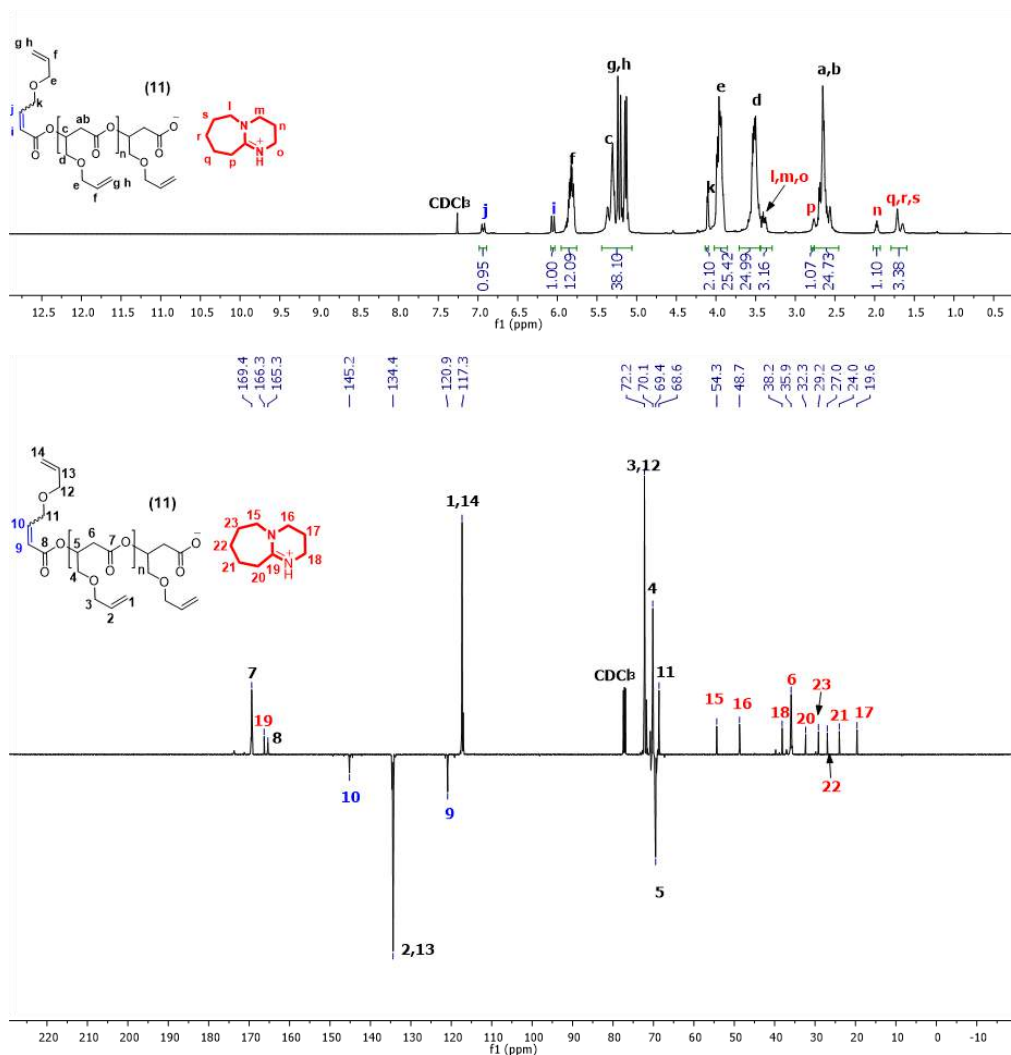
**Table 3. 5** – Characteristics of the PBPL<sup>FG</sup>s synthesized by ROP of *rac*-BPL<sup>FG</sup>s mediated by DBU<sup>a</sup>.

Entry	BPL <sup>FG</sup> (FG=)	[BPL <sup>FG</sup> ] <sub>0</sub> / [DBU] <sub>0</sub>	Time <sup>b</sup> (h)	Conv. <sup>c</sup> (%)	$\bar{M}_{n,theo}$ <sup>d</sup> (g mol <sup>-1</sup> )	$\bar{M}_{n,NMR}$ <sup>e</sup> (g mol <sup>-1</sup> )	$\bar{M}_{n,SEC}$ <sup>f</sup> (g mol <sup>-1</sup> )	$\bar{D}_M$ <sup>f</sup>
1	OAll	40	8	58	3300	1700	1300	1.18
2	OnBu	40	10	70	4400	2500	2500	1.30
3	OBn	50	5	51	4900	1650	1500	1.29
4	OTBDMS	40	8	25	2200	2600	1800	1.12

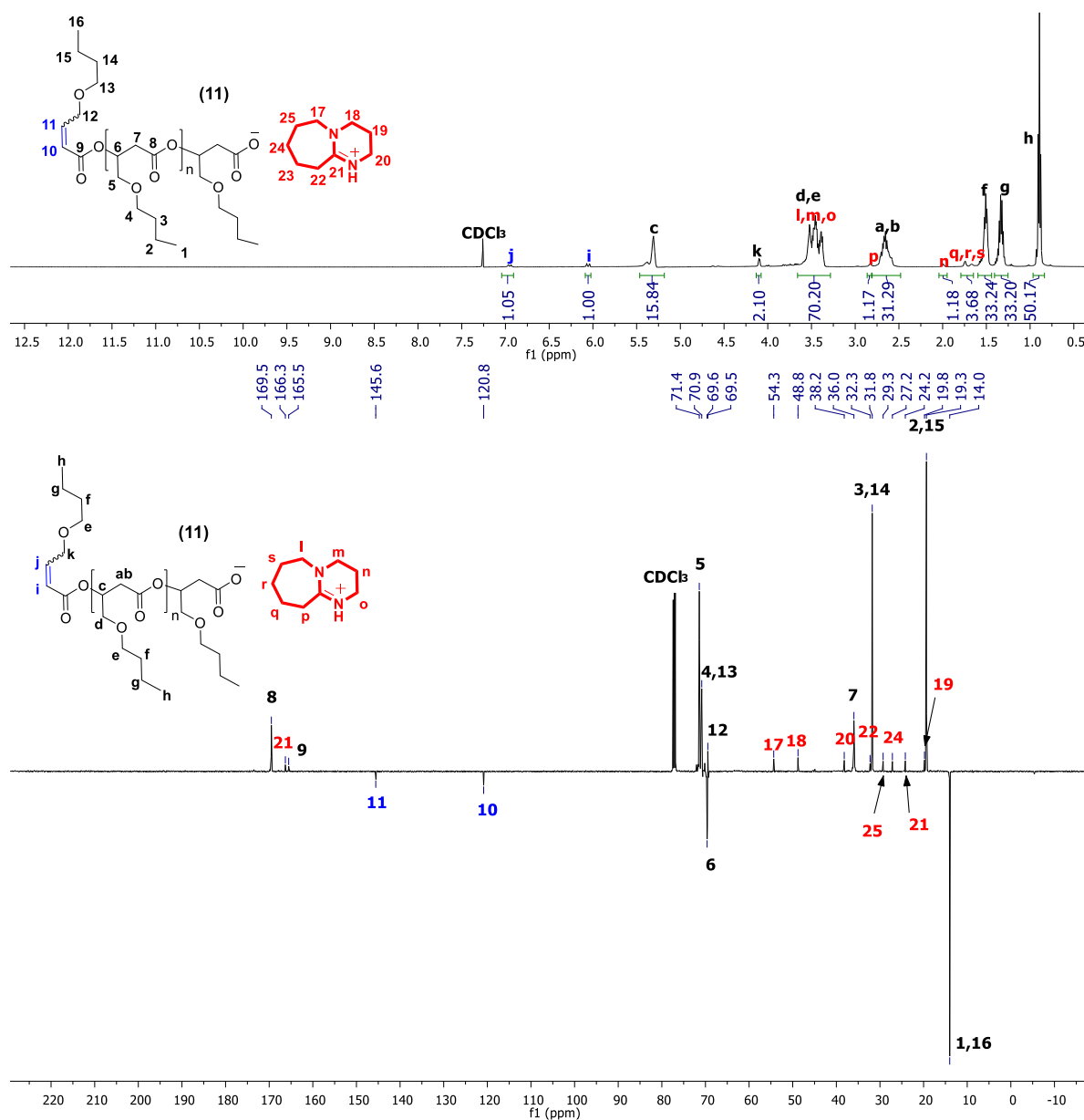
<sup>a</sup> Results are representative of at least duplicated experiments performed neat at 60 °C. <sup>b</sup> The reaction time was not necessarily optimized. <sup>c</sup> BPL<sup>FG</sup> conversion as determined by <sup>1</sup>H NMR analysis of the crude reaction mixture (refer to the Experimental Section). <sup>d</sup> Theoretical molar mass calculated from the relation: [BPL<sup>FG</sup>]<sub>0</sub>/[DBU]<sub>0</sub> × Conv.BPLFG ×  $M_{BPLFG}$ , i.e. without considering end-capping groups, with  $M_{BPLOAll} = 142$  g mol<sup>-1</sup>,  $M_{BPLOnBu} = 158$  g mol<sup>-1</sup>,  $M_{BPLOBn} = 192$  g mol<sup>-1</sup>, and  $M_{BPLOTBDMS} = 216$  g mol<sup>-1</sup>. <sup>e</sup> Experimental molar mass value as determined by <sup>1</sup>H NMR analysis of the isolated polymer, from the resonances of the crotonate end-group (refer to the Experimental Section). <sup>f</sup> Experimental molar mass and dispersity values as determined by SEC in THF using a RI detector at 30 °C vs polystyrene standards.

### 4.3.2. Macromolecular structure of DBU-synthesized PBPL<sup>FG</sup>s assessed by NMR spectroscopy and MALDI-ToF mass spectrometry

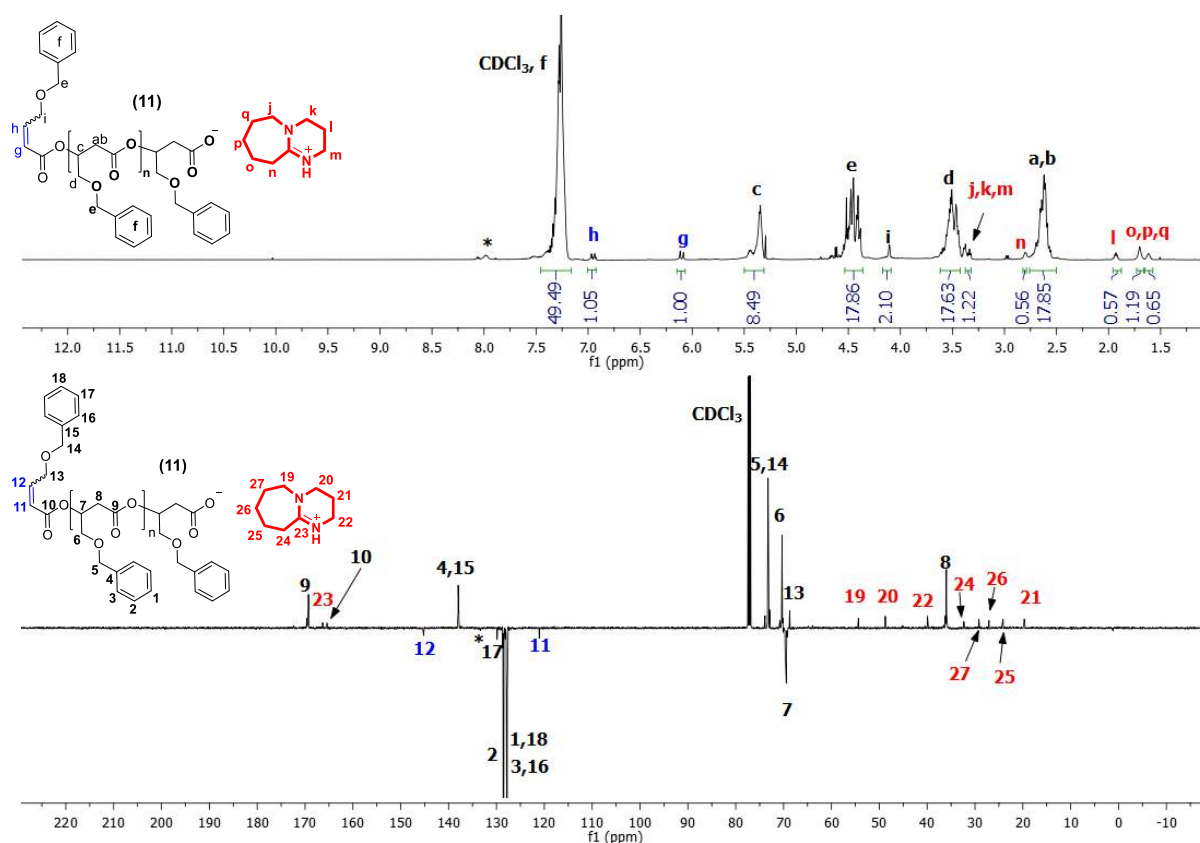
The microstructures of the purified PBL<sup>FG</sup>s isolated from the DBU mediated ROP of *rac*-BPL<sup>FG</sup>s were established by <sup>1</sup>H, J-MOD and 2D (COSY) NMR spectroscopy and MALDI-ToF MS, focusing on the end-capping groups. In accordance to the PBPL<sup>FG</sup>s synthesized using BEMP or TBD, <sup>1</sup>H NMR and J-MOD analyses (Figure 3. 22 to Figure 3. 24) of PBPL<sup>FG</sup>s unambiguously evidenced the presence of both  $\alpha,\beta$ -unsaturation and DBU moieties ( $\delta_{1H}$  ppm 3.37 ( $CH^i_2N(C)CH^k_2$ ), 3.34 ( $CNCH^m_2CH_2$ ), 2.80 ( $CH_2CH^n_2C(N)=N$ ), 1.93 ( $NCH_2CH^l_2CH_2$ ), 1.70 ( $CH_2CH_2CH^p_2CH^o_2CH_2$ ), 1.61 ( $CH_2CH^q_2CH_2CH_2CH_2$ ) for PBPL<sup>OBn</sup>.



**Figure 3. 22** – <sup>1</sup>H (500 MHz, CDCl<sub>3</sub>, 25 °C) (top) and J-MOD (125 MHz, CDCl<sub>3</sub>, 25 °C) (bottom) NMR spectra of PBPL<sup>OAll</sup> recovered from the ROP of *rac*-BPL<sup>OAll</sup> mediated by DBU (Table 3. 5 – entry 1); depicting only one species (Scheme 3. 21 – **18**) out of the two (Scheme 3. 21 – **16,18**).

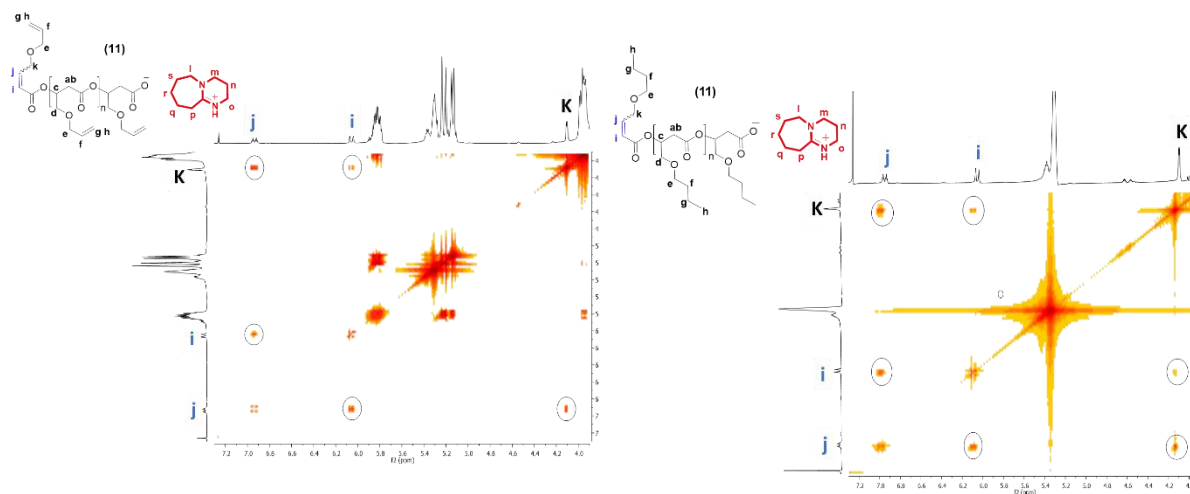


**Figure 3.23** –  $^1\text{H}$  (500 MHz,  $\text{CDCl}_3$ , 25  $^\circ\text{C}$ ) (top) and J-MOD (125 MHz,  $\text{CDCl}_3$ , 25  $^\circ\text{C}$ ) (bottom) NMR spectra of PBPL<sup>OnBu</sup> recovered from the ROP of *rac*-BPL<sup>OnBu</sup> mediated by DBU (Table 3. 5 – entry 3); depicting only one species (Scheme 3. 21 – (18)) out of the two (Scheme 3. 21 – (16),(18)).



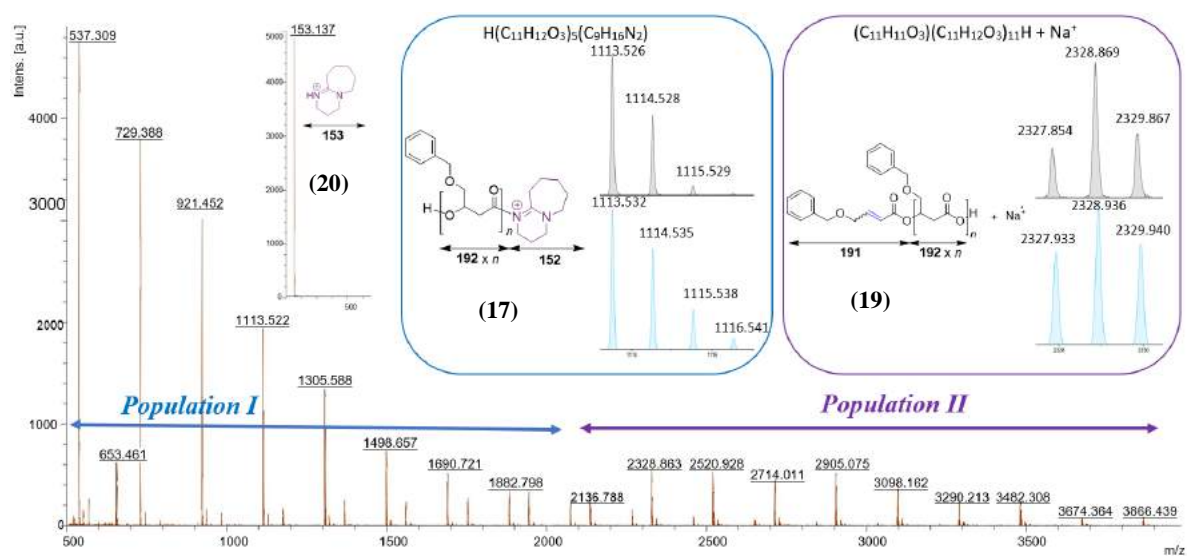
**Figure 3. 24** – <sup>1</sup>H (500 MHz, CDCl<sub>3</sub>, 25 °C) (top) and J-MOD (125 MHz, CDCl<sub>3</sub>, 25 °C) (bottom) NMR spectra of PBPL<sup>OBn</sup> recovered from the ROP of *rac*-BPL<sup>OBn</sup> mediated by DBU (Table 3. 5 – entry 3), depicting only one species (Scheme 3. 21 – (18)) out of the two (Scheme 3. 21 – (16),(18)); \* unidentified impurity.

The corresponding 2D correlations observed from COSY spectra evidence a correlation between the vinylic and methylene hydrogens of the crotonate end-group (Figure 3. 25), conforming an  $\alpha,\beta$ -unsaturation chain-end.

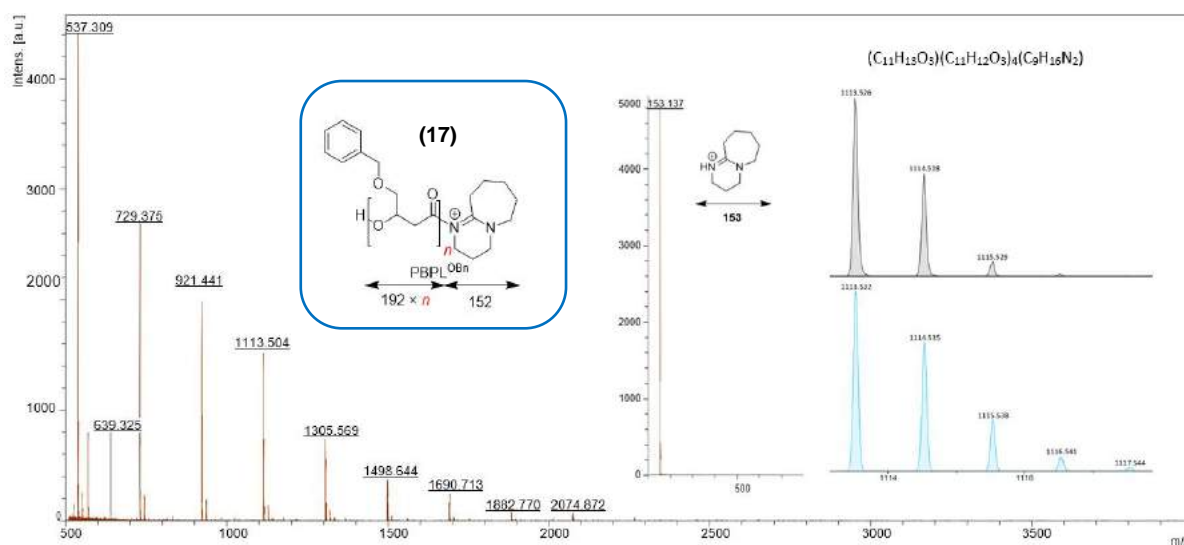


**Figure 3. 25** – Zoom of  $^1\text{H}$ - $^1\text{H}$  COSY (500 MHz,  $\text{CDCl}_3$ , 25 °C) NMR spectrum of  $\text{PBPL}^{\text{OAll}}$  and  $\text{PBPL}^{\text{OBu}}$  recovered from the ROP of  $\text{rac-BPL}^{\text{OAll}}$  and  $\text{rac-BPL}^{\text{OBu}}$  mediated by DBU supporting the presence of  $\alpha$ -crotonate end-capping group (Table 3. 5, entries 1, 2).

NMR spectroscopy revealed the presence of DBU onto the isolated polymer, however the exact nature of DBU (nucleophile or base) needed to be further established. To this end, MALDI-ToF MS of the thus prepared  $\text{PBPL}^{\text{FG}}$ s provided valuable information. Two macromolecular populations with a repeating unit of  $192 \text{ g mol}^{-1}$  was clearly observed in the mass spectrum of  $\text{PBPL}^{\text{OBn}}$  (Figure 3. 26). The first population (**I**) is consistent with  $\text{PBPL}^{\text{OBn}}$  chains end-capped with a  $\beta$ -hydroxyester and DBU moieties (e.g.,  $m/z_{\text{exp}} = 1113.526$  vs.  $m/z_{\text{simul}} = 1113.532$  for  $n = 5$ ) in agreement with the simulated isotopic spectrum (see left zoomed region (blue)). The other population (**II**) features a benzyloxy-crotonate and a carboxylic acid chain-end-groups, matching the isotopic simulation, with e.g.,  $m/z_{\text{exp}} = 2328.869$  vs.  $m/z_{\text{simul}} = 2328.936$  for  $n = 11$  (see right zoomed region (purple)). Remarkably, MALDI-ToF analysis done in the absence of cationizing agent ( $\text{Na}^+$ ) showed only population **I** (Figure 3. 27).

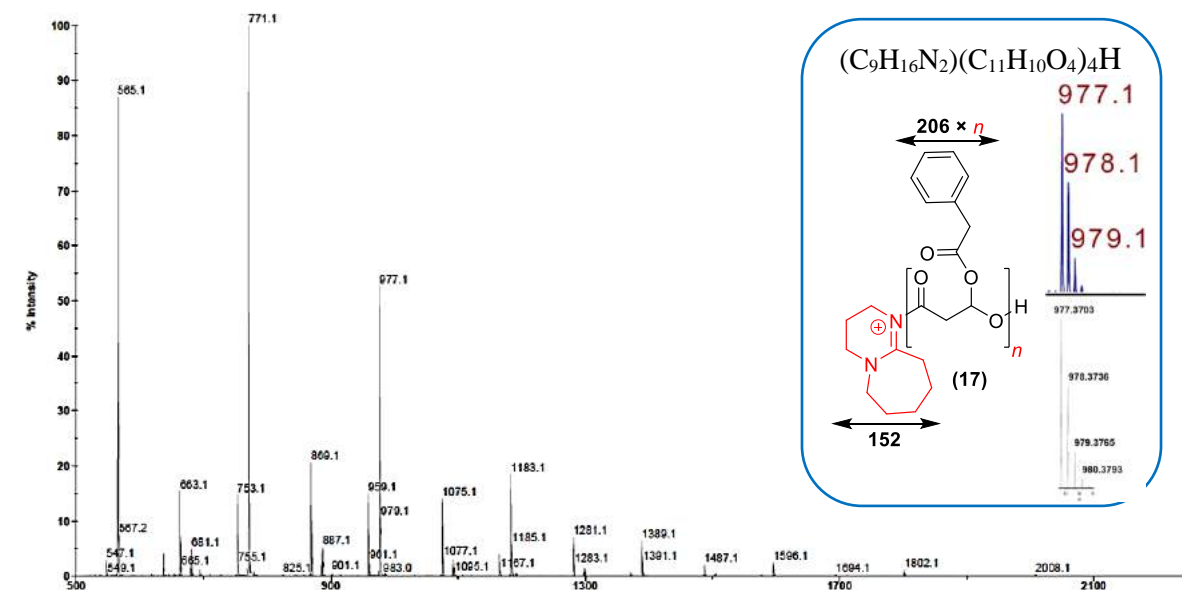


**Figure 3. 26** – MALDI-ToF mass spectrum (positive mode, DCTB matrix,  $\text{Na}^+$  cationizing agent) of a sample freshly synthesized from the ROP of  $\text{rac-BPL}^{\text{OBn}}$  mediated by DBU (Table 3. 5 – entry 3) showing populations corresponding to  $\text{PBPL}^{\text{OBn}}$  macromolecules end-capped with both an  $\alpha$ -hydroxy and  $\omega$ -DBU $^+$  groups (population **I**, Scheme 3. 21 – (17)), to  $\text{PBPL}^{\text{OBn}}$  macromolecules ionized with  $\text{Na}^+$  and end-capped with both an  $\alpha$ -crotonate and  $\omega$ -carboxylic acid (population **II**, Scheme 3. 21 – (19)), and to DBUH $^+$  (Scheme 3. 21 – (20)); the zoomed regions correspond to the simulated (blue, bottom) and experimental (grey, top) spectra, respectively.



**Figure 3. 27** – MALDI-ToF mass spectrum (DCTB matrix, absence of  $\text{Na}^+$  cationizing salt) of a sample freshly synthesized from the ROP of  $\text{rac-BPL}^{\text{OBn}}$  mediated by DBU (Table 3. 5 – entry 3); see the zoomed regions corresponding to the simulated (blue, bottom) and experimental (grey, top) spectra of  $\text{PBPL}^{\text{OBn}}$  macromolecules end-capped with both an  $\alpha$ -hydroxyester and  $\omega$ -DBU-groups (Figure 3. 26 – population **I**, Scheme 3. 21 – (17)).

Interestingly, the same results were obtained from the reinterpretation of  $\text{PMLA}^{\text{Bn}}$  microstructure produced previously.<sup>[38b]</sup> Population **I** was detected in the absence of  $\text{Na}^+$ , while both populations **I** and **II** were observed in the presence of  $\text{Na}^+$  for the same sample of  $\text{PMLA}^{\text{Bn}}$  (Figure 3. 28). This suggests that DBU reacts in the same way in the ROP of  $\text{rac-MLA}^{\text{Bn}}$  and of  $\text{rac-BPL}^{\text{FGs}}$  (*vide infra*).



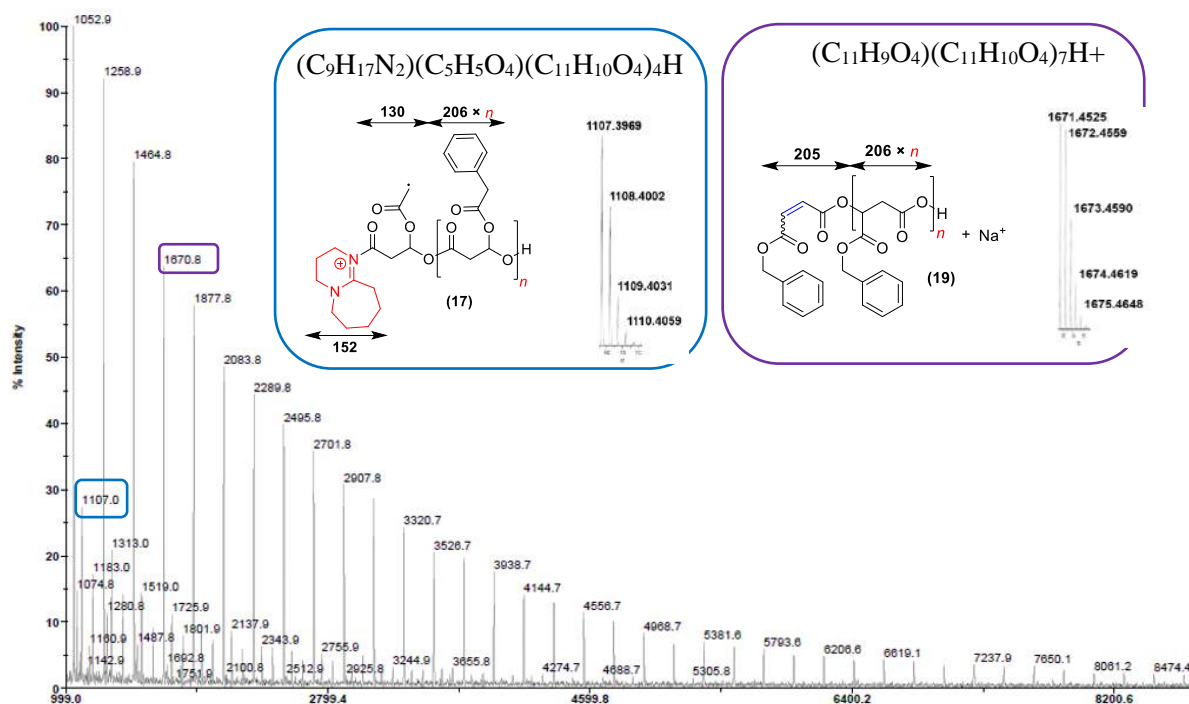


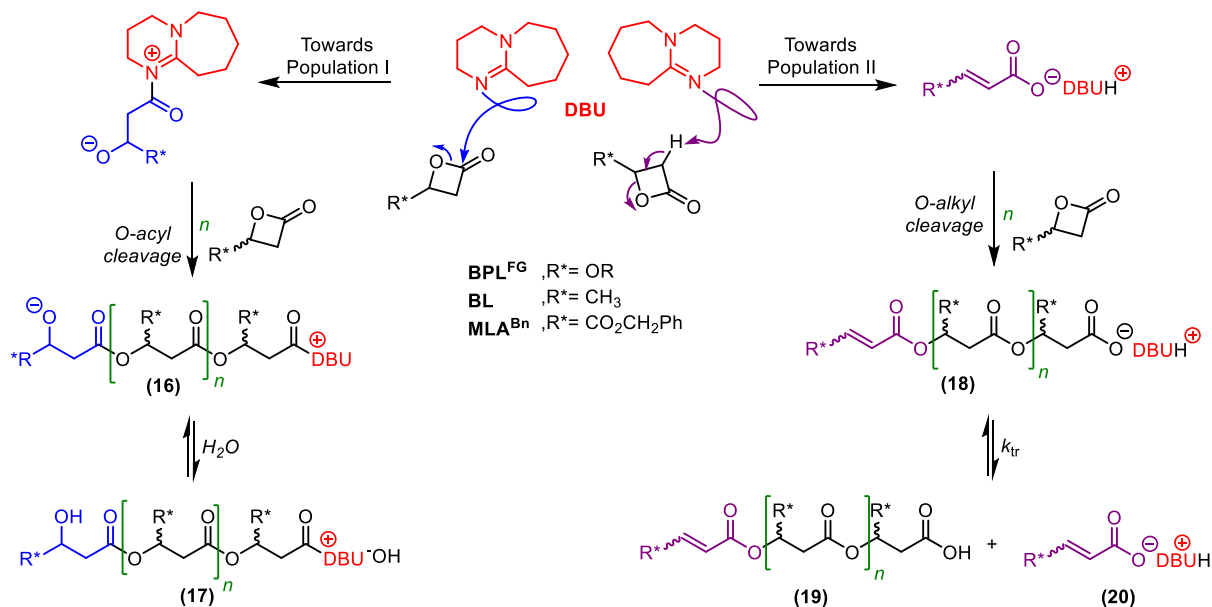
**Figure 3. 28** – MALDI-ToF mass spectra of a PMLA<sup>Bn</sup> sample freshly synthesized from the ROP of *rac*-MLA<sup>Bn</sup> mediated by DBU, using  $\alpha$ -cyano-4-hydroxycinnamic acid (CHCA) as matrix (no cationizing salt) (Top) (ESI, Figure S10 of reference<sup>[38b]</sup>), and of the same sample using *trans*-3-indoleacrylic acid (IAA) matrix in the presence of Na<sup>+</sup> cationizing salt (bottom) (ESI, Figure S12 of reference<sup>[38b]</sup>). Reinterpretation of the top spectrum shows the zoomed regions corresponding to the simulated (bottom) and experimental (top) spectra of PMLA<sup>Bn</sup> macromolecules end-capped with both an  $\alpha$ -hydroxy and  $\omega$ -DBU<sup>+</sup> groups (Figure 3. 26 – population I, Scheme 3. 21 – (17)). Also, the bottom spectrum shows a population corresponding to PMLA<sup>Bn</sup> which can only be observed in the presence of cationizing agent, of PMLA<sup>Bn</sup> macromolecules end-capped with both an  $\alpha$ -crotonate and an  $\omega$ -carboxylic acid end-groups, alike species Scheme 3. 21 – (19) (Figure 3. 26 – population II).

#### 4.3.3. Mechanistic pathway for the DBU-catalyzed ROP of BPL<sup>FGs</sup>

The identification of such end-capping groups suggests that DBU behaves as a dual catalyst, both basic and nucleophilic; apparently, DBU's dual activity prevails once again in polymerization as revealed previously in organic catalyzed reactions.<sup>[32]</sup> It would thus mediate the ROP of *rac*-BPL<sup>FGs</sup> through two competitive mechanistic pathways, in association with the acidic  $\alpha$ -H and electrophilic C=O reactivity of BPL<sup>FGs</sup> monomers. Hence, similarly to BEMP, DBU would act as a basic catalyst to form *in situ* the  $\alpha,\beta$ -unsaturated carboxylate-DBU real active species which propagates via *O*-alkyl cleavage of the  $\beta$ -lactone to ultimately generate macromolecules of population II (Figure 3. 26, Scheme 3. 21 – (19)). In addition, similarly to TBD, DBU can promote the nucleophilic ROP of *rac*-BPL<sup>FGs</sup> via its *O*-acyl cleavage, generating an alkoxy propagating species to eventually form PBPL<sup>OBn</sup> corresponding to population I (Figure 3. 26, Scheme 3. 21 – (20)). This latter approach was previously reported for the bulk ROP of lactide using DBU in excess or alone (Scheme 3. 10, Scheme 3. 11; route



(b)). Further evidence of the DBU's dual activity and of the above proposed mechanism was gained from the reinterpretation of the previously reported MALDI-ToF mass spectra of samples recovered from the ROP of *rac*-MLA<sup>Bn</sup> mediated by DBU (Figure 3. 28). The concomitant activation of DBU makes it similar to NHCs organic activators, hence it should be position on the right and left of Figure 1. 12 (Chapter 1).



**Scheme 3. 21** – Proposed mechanism for the ROP of *rac*-BPL<sup>FG</sup>s (FG = OAlI, OnBu, OBn, OTBDMS, OP(O)Ph<sub>2</sub> and *rac*-BL<sup>Me</sup>, *rac*-MLA<sup>Bn</sup>) mediated by the dual organocatalyst DBU proceeding either via an *O*-acyl cleavage when acting as a nucleophile (blue pathway; **(16)**), or via an *O*-alkyl cleavage when behaving as a base (purple pathway; **(18)**). Populations **I** and **II** observed in the MALDI-ToF mass spectra (Figure 3. 26) refer to the macromolecular species **(17)** and **(19)** obtained upon protonation and transfer reactions, respectively.

#### 4.4. PBPL<sup>FG</sup>s : stereochemistry, kinetics and thermal properties

Taking into consideration the chirality of BPL<sup>FG</sup>s, the stereochemistry of the produced PBPL<sup>FG</sup>s was investigated via <sup>13</sup>C NMR. Zoomed regions of typical <sup>13</sup>C NMR spectra of PBPL<sup>OBn</sup> obtained from BEMP, TBD and DBU are presented in Figure 3. 29 from bottom to top, respectively. Correspondingly, the organocatalyzed ROP via BEMP, TBD and DBU of *racemic*-BPL<sup>FG</sup>s did not show any stereoselectivity (*P<sub>r</sub>* around 0.5), hence the produced PBPL<sup>FG</sup>s are atactic. More details on the detection of *P<sub>r</sub>* are represented in Chapter 4.



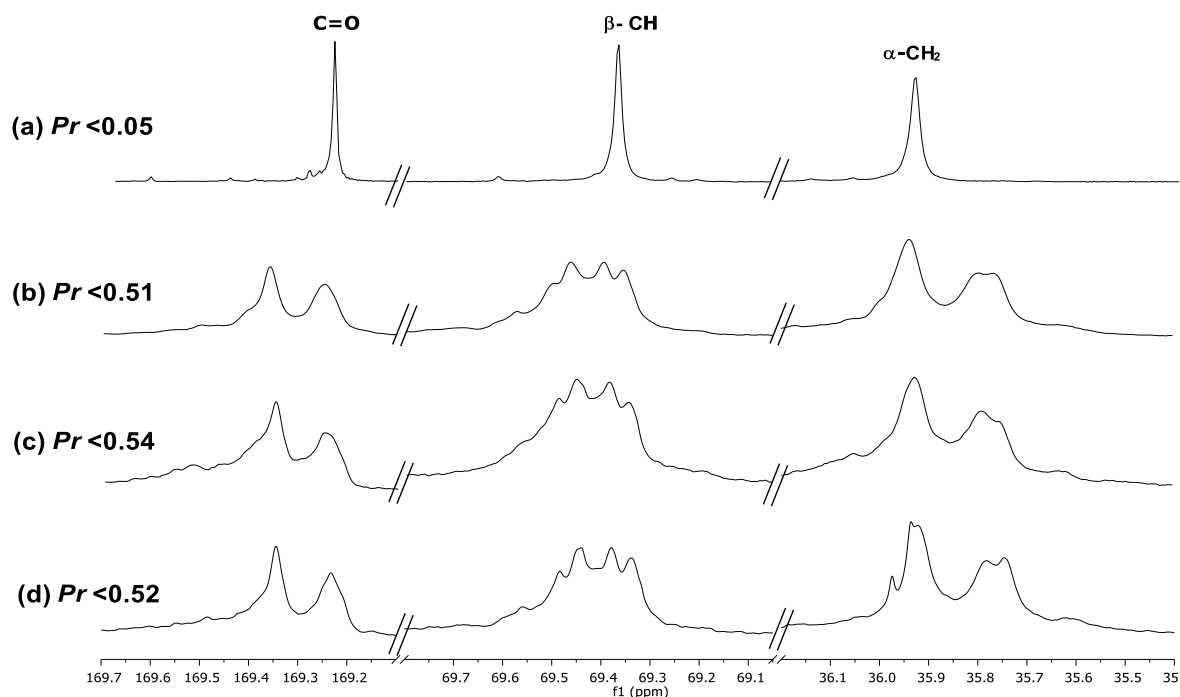


**Figure 3. 29** – Zoomed regions of the  $^{13}\text{C}\{^1\text{H}\}$  NMR spectra (125 MHz,  $\text{CDCl}_3$ , 23 °C) of  $\text{PBPL}^{\text{OBn}}$  prepared by the ROP of  $\text{rac-BPL}^{\text{OBn}}$  (except for the top spectrum (a): by the ROP of enantiopure (*S*)- $\text{BPL}^{\text{OBn}}$ ) in the presence of DBU-spectrum (b) (Figure 3. 26; Table 3. 5, entry 3), TBD-spectrum (c) (Figure 3. 19; Table 3. 4, entry 7), or BEMP-spectrum (d) (Figure 3. 11, Table 3. 3, entry 9), revealing atactic  $\text{PBPL}^{\text{OBn}}$ ;  $P_r$  is the probability of *racemic* linkages between  $\text{BPL}^{\text{OBn}}$  units as determined by  $^{13}\text{C}\{^1\text{H}\}$  NMR analysis of the isolated  $\text{PBPL}^{\text{OBn}}$ .

Kinetic monitoring by  $^1\text{H}$  NMR spectroscopy of the ROP of  $\text{rac-BPL}^{\text{FGs}}$  (FG = OAll,  $\text{O}^n\text{Bu}$ , OBn, OTBDMS) performed at 60 °C are shown in Figure 3. 30. The plots can be well-fitted by first-order kinetics at conversions below 70%, where viscosity and undesired side reactions are unlikely to have an impact (deceleration to semi-logarithmic in the plot detected for conversions higher than 70%). The nature of the ether moiety of the  $\text{CH}_2\text{OR}$  (FG) group appeared to similarly influence the rate of the polymerization from one organic activator to another. Using BEMP or TBD or DBU, while  $\text{BPL}^{\text{OBn}}$  exhibited a slightly faster rate of polymerization than  $\text{BPL}^{\text{OnBu}}$ , both monomers polymerized less rapidly than  $\text{BPL}^{\text{OAll}}$ , but much faster than  $\text{BPL}^{\text{OTBDMS}}$  (Figure 3. 30, Table 3. 3 to Table 3. 5), this is traced back to the steric and electronic factors of each of the pendent group.

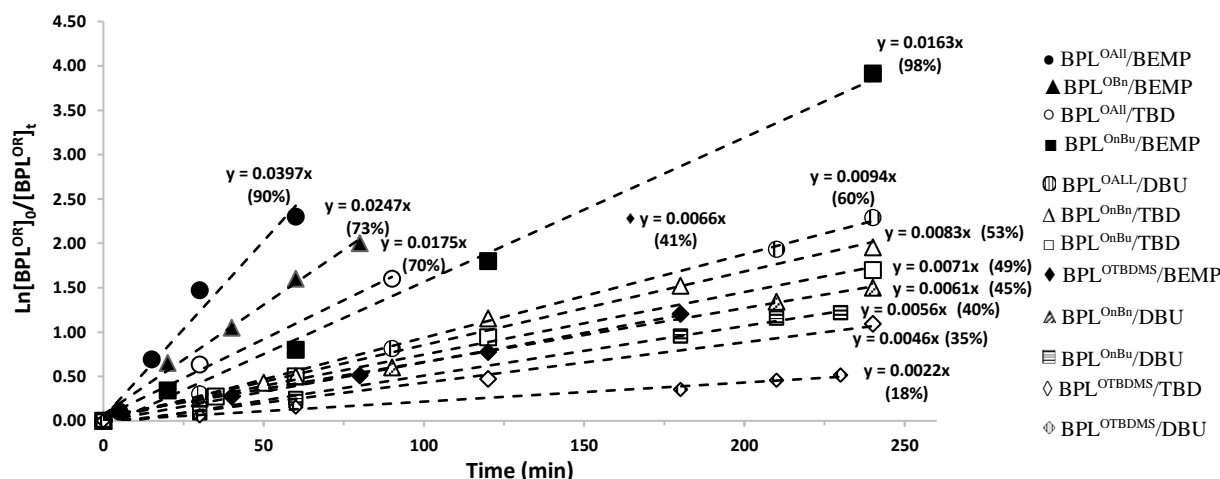


**Figure 3. 30** – Logarithmic plot of the kinetics of the ROP of *rac*-BPL<sup>FG</sup>s (40 equiv) mediated by BEMP (1 equiv) (Table 3. 3 – entries 3, 6, 12, 15), TBD (Table 3. 4 – entries 1, 4, 7, 8) and DBU (Table 3. 5 – entries 1, 2, 3, 4) at 60 °C in bulk; the data in parentheses are the final monomer conversions (before reaching a high viscosity and diffusion limits).

BEMP proved significantly more active than TBD and DBU (Figure 3. 30). This is probably because the *O*-alkyl cleavage is more favoured than that of *O*-acyl in case of  $\beta$ -lactones. As explained by Dunitz *et al.*, a nucleophilic approach to the carbonyl (acyl) is more hindered than that to  $\beta$ -carbon (alkyl), in the nearly flat  $\beta$ -lactones molecule (Figure 3. 31 – left). Besides, after the attack of nucleophile on the acyl site, an energetically unfavoured conformation happened due to the *syn*-periplanar interactions of the lone electron pairs of the endocyclic oxygen and the polar CO bond (Figure 3. 31 – right).<sup>[50]</sup>

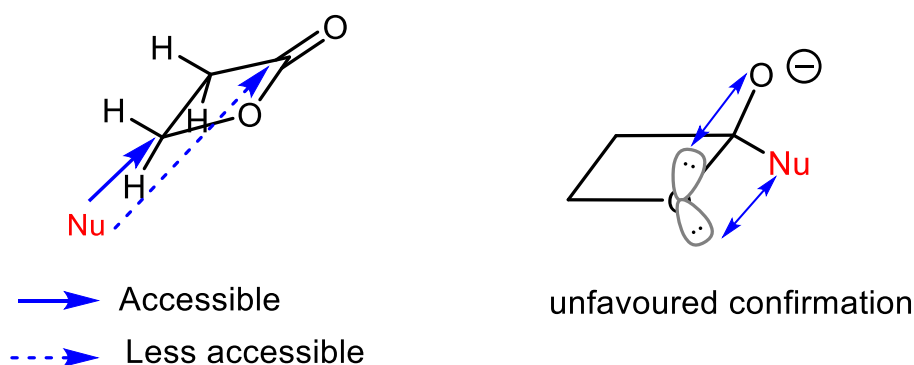


**Figure 3. 31** – Illustration on the reactivity of  $\beta$ -lactones toward nucleophiles; (left) permeability of a nucleophilic attack acyl vs. alkyl; (right) presence of *syn*-periplanar interactions leading to unfavoured electronic conformation  $\beta$ -lactones.

The thermal behavior of the synthesized PBPL<sup>FG</sup>s (excluding PBPL<sup>OP(O)Ph2</sup>) was probed by thermal gravimetry analysis (TGA). The degradation temperature for all atactic PBPL<sup>FG</sup>s studied are roughly in the same range, with that of PBPL<sup>OAll</sup> being the lowest and that of PBPL<sup>OBn</sup> the highest. The TGA thermograms are presented in Figure 3. 32, where

$T_d^{\text{onset}}_{\text{PBPL}(\text{OAll})} = 186\text{ }^{\circ}\text{C}$ ,  $T_d^{\text{onset}}_{\text{PBPL}(\text{OBn})} = 236\text{ }^{\circ}\text{C}$ ,  $T_d^{\text{onset}}_{\text{PBPL}(\text{OnBu})} = 224\text{ }^{\circ}\text{C}$  and  $T_d^{\text{onset}}_{\text{PBPL}(\text{OTBDMS})} = 228\text{ }^{\circ}\text{C}$ .

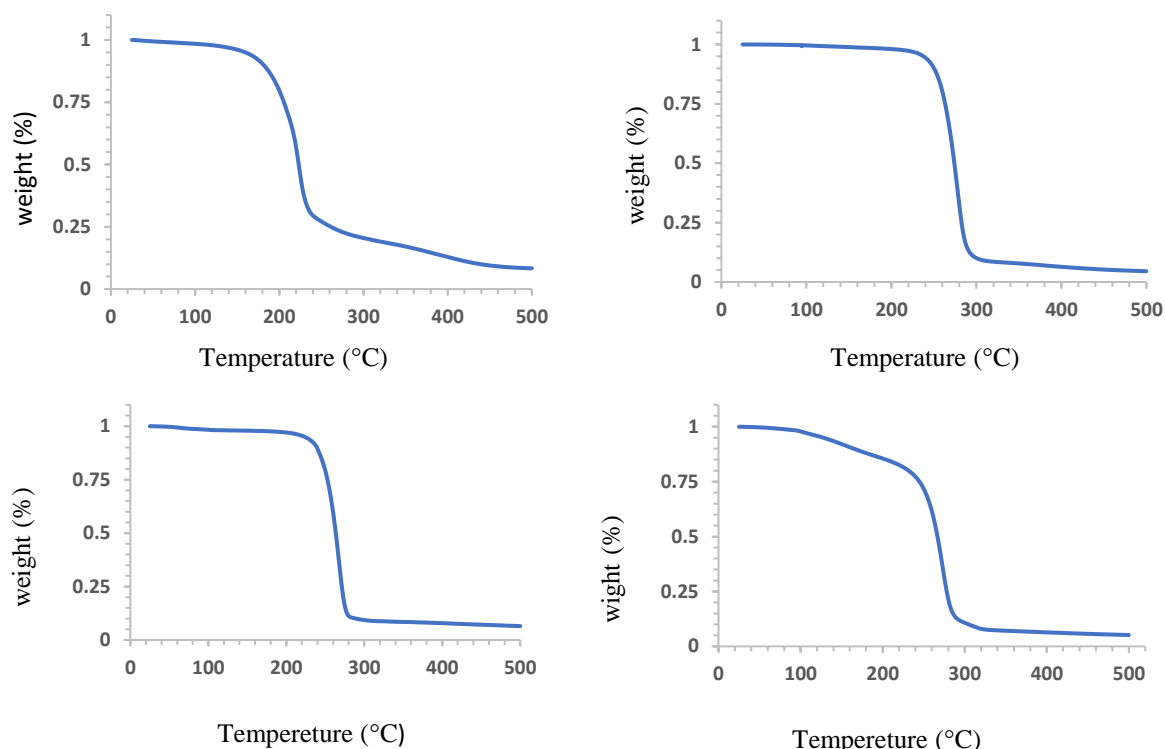


**Figure 3. 32** – TGA thermograms of atactic PBPL<sup>OAll</sup> (top-left); PBPL<sup>OBn</sup> (top-right); PBPL<sup>OnBu</sup> (bottom-left); PBPL<sup>OTBDMS</sup> (bottom-right).

## 5. Conclusion: better understanding of the BEMP, TBD, and DBU-promoted ROP mechanism of $\beta$ -lactones- Perspectives

Functional PHAs, namely PBPL<sup>FG</sup>s (FG = OAll, <sup>n</sup>Bu, OBn, OTBDMS, OP(O)Ph<sub>2</sub>), have been successfully synthesized from the bulk ROP of *rac*-BPL<sup>FG</sup>s monomers at 25–60 °C using BEMP, TBD, or DBU as organic catalysts/activators. The activity of the organic activators, under these operating conditions, is modest as typically encountered with four-membered ring  $\beta$ -lactones when compared to larger ones ( $\geq$  six-membered ring lactones). Also, their activity towards BPL<sup>FG</sup>s is lower than in the alkene ROP of the related *rac*-BL<sup>Me</sup> and *rac*-MLA<sup>Bn</sup>  $\beta$ -lactones. Moreover, *rac*-BPL<sup>OAll</sup>, *rac*-BPL<sup>OnBu</sup> and *rac*-BPL<sup>OBn</sup> seemed to polymerize faster than *rac*-BPL<sup>OTBDMS</sup> and *rac*-BPL<sup>OP(O)Ph<sub>2</sub></sup>, and this could be mainly due to the steric hindrance of the latter.

Inherent to their own intrinsic chemical features, each of the organic activators supports a unique mechanistic pathway (Figure 3. 32), as supported by detailed NMR and MALDI-ToF MS analyses of the produced PBPL<sup>FG</sup>s. ROP mechanisms at play dictate the nature of the macromolecules' chain-end-groups. BEMP, the most basic and bulky organic activator in that series, generates upon proton abstraction and *O*-alkyl cleavage of the *rac*-BPL<sup>FG</sup>s monomer, a [carboxylate]<sup>−</sup>/[BEMPH]<sup>+</sup> initiator. The latter initiator continues to propagate through the *O*-alkyl reaction, which is most likely accompanied by some transfer reactions, accounting for broadened dispersities if full conversions were targeted. On the contrary, the highly nucleophilic TBD forms, via an *O*-acyl cleavage of *rac*-BPL<sup>FG</sup>s, a 1:1 *N*-acyl- $\alpha,\beta$ -unsaturated adduct, that subsequently propagates in the same manner. Finally, the observed dual basic and nucleophilic activity of DBU favours the scission of both *O*-acyl and *O*-alkyl bonds of the *rac*-BPL<sup>FG</sup>s monomers, eventually forming alkoxy and carboxylate active species, respectively.

The mechanisms proposed herein for the ROP of BPL<sup>FG</sup>s mediated by BEMP, TBD or DBU, are fully compatible with those of the alike ROP of *rac*-BL<sup>Me</sup> and *rac*-MLA<sup>Bn</sup>. These results highlight that the mechanism operating in ROP of a  $\beta$ -lactone proceeded by organic activators is thus highly dependent on the chemical specificity of the organocatalyst used. Even more, ROP was found to be strongly affected by the operating conditions implemented to synthesize the polymers, in particular if the reactions are conducted neat or in solution, in the strict absence of water or of any other protic agent.<sup>[51]</sup>

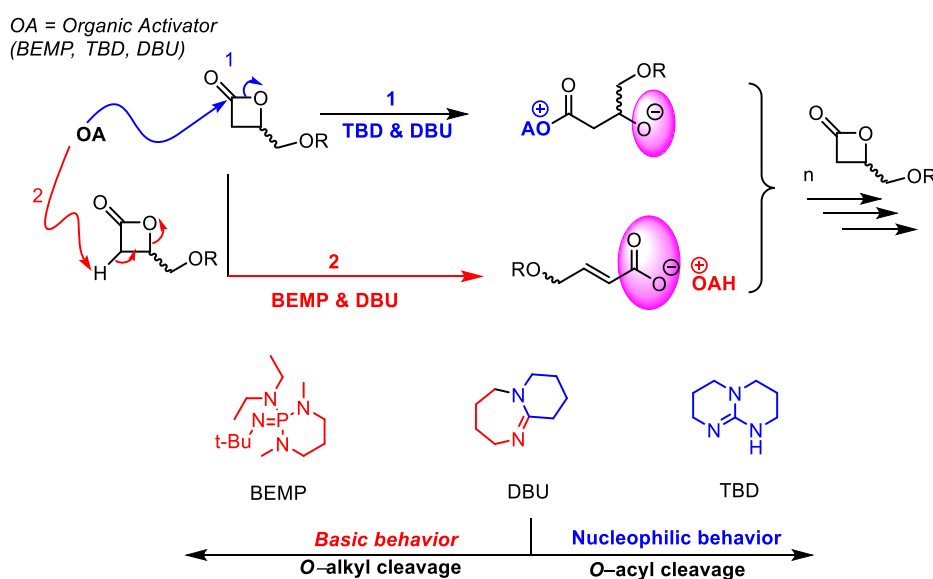


**Figure 3. 33** – Illustration on the mode of action of BEMP, TBD and DBU in ROP of *rac*-BPL<sup>FG</sup>s.

One way to further confirm our suggested mechanisms could be to ring-open enantiopure BPL<sup>FG</sup>s rather than *rac*-BPL<sup>FG</sup>s. For example, the ROP of (*S*)-BPL<sup>FG</sup> promoted by BEMP, should deliver dominant polymeric chains that are rich with (*R*)-PBPL<sup>FG</sup> (inversion of configuration). That mediated by TBD, ought to provide superior polymeric chains that are rich with (*S*)-PBPL<sup>FG</sup> (retention of configuration). That in the presence of DBU, is expected to afford a mixture of almost the same proportions of (*S*)-BPL<sup>FG</sup> and (*R*)-BPL<sup>FG</sup> (refer to Scheme 1. 7; Chapter 1). Acknowledging the activity of each of these organic activators, their polymerization mechanisms and kinetics may allow us to rationalize the design of new catalytic systems and may help us to better control polymerization to produce high molar mass functionalized PHAs in a metal-free approach. For instance, one could use  $\alpha,\alpha$ -fluorinated BPL<sup>FG</sup>s that are anticipated to prevent transfer reactions that originate from the  $\alpha$ -acidic hydrogen, or decrease the extent of transesterification reactions due to the steric and electronic effect provided by the two substituted fluorine atoms. Also, in the case of the ROP promoted by TBD, the lower concentration of TBD may decrease the extent of transesterification (enabling to target higher DPs). Moreover,  $\alpha,\alpha$ -fluorinated BPL<sup>FG</sup>s could increase the rate of the polymerization by increasing the electrophilicity of the active site in the  $\beta$ -lactone (acyl and  $\beta$ -carbon). Finally, it could provide regioselectivity favouring an *O*-acyl cleavage when nucleophilic addition competes with Brønsted base catalysis (Figure 3. 34 – left). Another approach can be to replace the  $\beta$ -lactone with eight-membered ring dilactone (diolide, DL) that upon ring-opening have also been shown to afford PHAs.<sup>[52]</sup> The reactivity of DL may be less challenging than that of a  $\beta$ -lactone, thus it is quite worth investigating its ROP via BEMP, TBD or DBU (Figure 3. 34 – right).

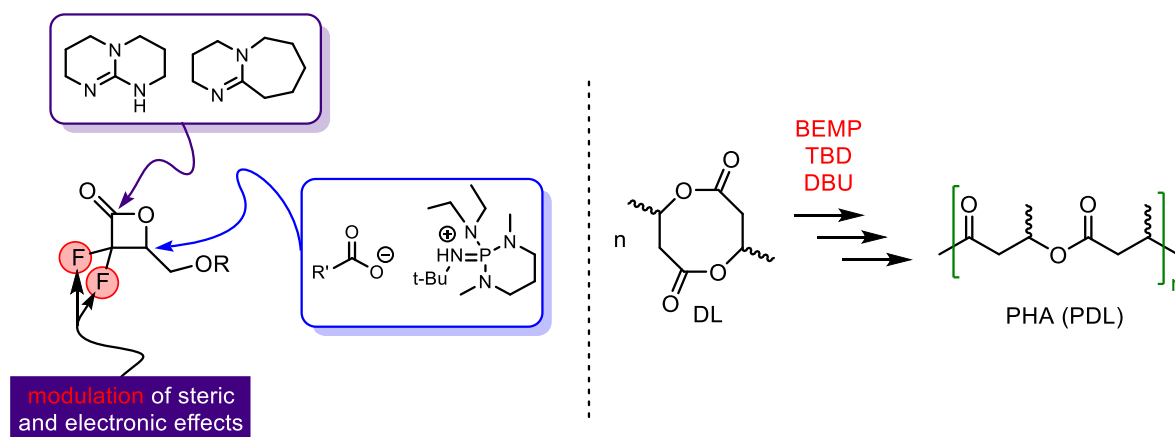


**Figure 3. 34** – Perspective; (left)  $\alpha,\alpha$ -fluorinated BPL<sup>FG</sup>s may prevent transfer reactions and enhance ROP activity/regioselectivity; (right) organocatalyzed ROP of DL to produce PHAs could be less challenging (regioselective) with less undesirable side reactions.

Finally, in the preliminary study of the ROP of *rac*-BPL<sup>OP(O)Ph<sub>2</sub></sup>, BEMP showed to be better choice to produce PBPL<sup>OP(O)Ph<sub>2</sub></sup> more effectively, than TBD. However, only low [*rac*-BPL<sup>OP(O)Ph<sub>2</sub></sup>]<sub>0</sub>/[BEMP]<sub>0</sub> ratios were targeted (ca. 20 or 40;  $M_{n,NMR(max)} 6300 = \text{g mol}^{-1}$ ). Hence, to proceed in this study, it is better to target higher monomer loadings (ca. 100-500 or higher) to produce PBPL<sup>OP(O)Ph<sub>2</sub></sup> with high molar masses. Nevertheless, it is suggested to use carboxylate initiators with phosphazene bases or NHCs as counter cation, since they provide the highest activity with  $\beta$ -lactones among all organic activators reported so far (check Chapter 1; Table 1.4 and scheme 1.13). Also, when targeting higher monomer loading, it is better to control the reaction by <sup>1</sup>H NMR and quench it after 60%–70% monomer consumption to decrease the intense of transfer reactions, and thus afford the narrowest dispersities as possible.

## 6. Experimental Section

### Material and methods

All catalytic experiments were performed under an inert argon atmosphere using standard Schlenk line and glovebox techniques. TBD (98%, Aldrich) was used as received after drying under vacuum. DBU (98%, Aldrich) and BEMP (> 98%, Aldrich) were distilled from CaH<sub>2</sub> prior to use.

### Instrumentation and measurements

<sup>1</sup>H (500 and 400 MHz), <sup>13</sup>C{<sup>1</sup>H} (125 MHz), <sup>31</sup>P{<sup>1</sup>H} (121 MHz) and COSY NMR spectra were recorded on Bruker Avance AM 500 and Ascend 400 spectrometers at 25 °C. <sup>1</sup>H and <sup>13</sup>C NMR spectra were referenced internally relative to SiMe<sub>4</sub> ( $\delta$  0 ppm) using the residual solvent resonances. <sup>31</sup>P NMR spectra were referenced externally relative to 85% H<sub>3</sub>PO<sub>4</sub> ( $\delta$  0 ppm).

Number-average molar mass ( $\bar{M}_{n,SEC}$ ) and dispersity ( $\bar{D}_M = \bar{M}_w/\bar{M}_n$ ) values of the PBPL<sup>FG</sup>s were determined by size exclusion chromatography (SEC) in THF at 30 °C (flow rate = 1.0 mL min<sup>-1</sup>) on a Polymer Laboratories PL50 apparatus equipped with a refractive index detector and a set of two ResiPore PLgel 3  $\mu\text{m}$  MIXED-D 300  $\times$  7.5 mm columns. The polymer samples were dissolved in THF (2 mg mL<sup>-1</sup>). All elution curves were calibrated with polystyrene standards; the reported  $\bar{M}_{n,SEC}$  values of the PBPL<sup>FG</sup>s are uncorrected for the difference in hydrodynamic radius vs. polystyrene.

The molar mass of PBPL<sup>FG</sup>s samples was determined also by <sup>1</sup>H NMR analysis ( $\bar{M}_{n,NMR}$ ) in CDCl<sub>3</sub> from the relative intensities of the signals of the PBPL<sup>FG</sup>s repeating unit methine hydrogen (OCH<sup>c</sup>(R)CH<sub>2</sub>,  $\delta_{Hc}$  5.76–5.19 ppm) and of the crotonate chain-end hydrogen (CH=CH<sup>g</sup>C(O),  $\delta_{Hg}$  6.99–6.08 ppm).

Monomer conversions were calculated from <sup>1</sup>H NMR spectra of the crude reaction mixtures in CDCl<sub>3</sub> or C<sub>6</sub>D<sub>6</sub> by using the integration (Int.) ratio  $\text{Int.}_{\text{polymer}} / [\text{Int.}_{\text{polymer}} + \text{Int.}_{\text{monomer}}]$  of the methine hydrogens of each polymer (as stated above) and of each residual monomer ( $\delta$  4.63 ppm for BPL<sup>OBn</sup>,  $\delta$  4.65 ppm for BPL<sup>OAll</sup>,  $\delta$  4.66 ppm for BPL<sup>OnBu</sup> and  $\delta$  4.54 ppm for BPL<sup>OTBDMS</sup>, in CDCl<sub>3</sub>).

Mass spectra were recorded at CRMPO-ScanMAT (Rennes, France). ESI mass spectra were recorded on an orbitrap type Thermo Fisher Scientific Q-Exactive instrument with an ESI source in positive or negative mode by direct introduction at 5–10  $\mu\text{g mL}^{-1}$ . Samples were prepared in CH<sub>2</sub>Cl<sub>2</sub> at 10  $\mu\text{g mL}^{-1}$ . High resolution MALDI-ToF mass spectra were recorded using an ULTRAFLEX III ToF / ToF spectrometer (Bruker Daltonik GmbH, Bremen, Germany) in positive and/or negative ionization mode. Spectra were recorded using reflectron mode and an accelerating voltage of 25 kV. A mixture of a freshly prepared solution of the polymer in THF or CH<sub>2</sub>Cl<sub>2</sub> (HPLC grade, 10  $\text{mg mL}^{-1}$ ) and DCTB (*trans*-2-(3-(4-*tert*-butylphenyl)-2methyl-2-propenylidene) malononitrile, and a MeOH solution of the cationizing agent (NaI, 10  $\text{mg mL}^{-1}$ ) were prepared. The solutions were combined in a 1:1:1 v/v/v ratio of matrix-to-sample-to-cationizing agent - if added. The resulting solution (0.25–0.5 mL) was deposited onto the sample target (Prespotted AnchorChip PAC II 384 / 96 HCCA) and air or vacuum dried.

Thermal gravimetry analyses (TGA) were performed on a Metler Toledo TGA/DSC1 by heating the polymer samples at a rate of 10  $^{\circ}\text{C min}^{-1}$  from +25 to +600  $^{\circ}\text{C}$  in a dynamic nitrogen atmosphere (flow rate = 50  $\text{mL min}^{-1}$ ).

## Typical polymerization procedure

In a typical experiment (Table 3. 4, entry 12), in a glovebox, BEMP (10  $\mu\text{L}$ , 34.6  $\mu\text{mol}$ ) was added using a microsyringe onto BPL<sup>OBn</sup> (0.28 g, 1.475 mmol, 42 equiv.) placed in Schlenk flask. The neat reaction mixture was then stirred in an oil bath at 60  $^{\circ}\text{C}$  over the appropriate reaction time (reaction times were not systematically optimized). The polymerization was quenched by addition of an excess of undried CH<sub>2</sub>Cl<sub>2</sub> (1 mL). The resulting mixture was concentrated to dryness under vacuum and the conversion was determined by <sup>1</sup>H NMR analysis

of the residue dissolved in  $\text{CDCl}_3$  or  $\text{C}_6\text{D}_6$ . The crude residue was then dissolved in  $\text{CH}_2\text{Cl}_2$  (1 mL) and precipitated in cold pentane (10 mL, 0 °C) (repeated twice, thus enabling the removal of potential unreacted/free base), filtered and dried overnight at 60 °C using a vacuum oven. All recovered polymers were yellow viscous and were analyzed by NMR, MALDI-ToF and ESI MS, SEC and TGA.  $\text{PBL}^{\text{FG}}$ s samples were stored under inert atmosphere at -27 °C.

### **Kinetic study procedure**

Following the typical polymerization procedure reported above, an aliquot of the reaction mixture was taken and quenched with excess DCM, at different reaction times. The resulting mixture was concentrated to dryness under vacuum and the conversion was determined by  $^1\text{H}$  NMR analysis.



## 7. References

- [1] T. Ishikawa, *Superbases for organic synthesis: guanidines, amidines, phosphazenes and related organocatalysts*, John Wiley & Sons, **2009**.
- [2] a) W. N. Ottou, H. Sardon, D. Mecerreyes, J. Vignolle, D. Taton, *Prog. Polym. Sci.* **2016**, *56*, 64-115; b) A. Bossion, K. V. Heifferon, L. Meabe, N. Zivic, D. Taton, J. L. Hedrick, T. E. Long, H. Sardon, *Prog. Polym. Sci.* **2019**, *90*, 164-210; c) C. Thomas, B. Bibal, *Green Chem.* **2014**, *16*, 1687-1699; d) D. Bourissou, S. Moebs-Sanchez, B. Martin-Vaca, *Chem. Rev.* **2007**, *107*, 5813-5840; e) M. K. Kiesewetter, E. J. Shin, J. L. Hedrick, R. M. Waymouth, *Macromolecules* **2010**, *43*, 2093-2107; f) J. M. Becker, R. J. Pounder, A. P. Dove, *Macromol. Rapid Commun.* **2010**, *31*, 1923-1937; g) R. T. Mathers, M. A. Meier, *Green polymerization methods: renewable starting materials, catalysis and waste reduction*, John Wiley & Sons, **2011**; h) M. Labet, W. Thielemans, *Chem. Soc. Rev.* **2009**, *38*, 3484-3504; i) A. P. Dove, *Chem. Commun.* **2008**, 6446-6470; j) N. E. Kamber, W. Jeong, R. M. Waymouth, R. C. Pratt, B. G. Lohmeijer, J. L. Hedrick, *Chem. Rev.* **2007**, *107*, 5813-5840; k) B. Guillermin, V. Lemaure, B. Ernould, J. Cornil, R. Lazzaroni, J.-F. Gohy, P. Dubois, O. Coulembier, *RSC Advances* **2014**, *4*, 10028-10038; l) P. P. Datta, M. K. Kiesewetter, *Macromolecules* **2016**, *49*, 774-780; m) Q.-l. Song, S.-y. Hu, J.-p. Zhao, G.-z. Zhang, *Chin. J. Polym. Sci.* **2017**, *35*, 581-601; n) D. N. Coderre, M. K. Kiesewetter, **2018**; o) C. Diaz, P. Mehrkhodavandi, *Poly. Chem.* **2021**, *12*, 783-806; p) P. Dubois, O. Coulembier, J.-M. Raquez, *Handbook of ring-opening polymerization*, John Wiley & Sons, **2009**; q) P. Lecomte, C. Jérôme, *Synthetic biodegradable polymers* **2011**, 173-217.
- [3] a) T. Rodima, V. Mäemets, I. Koppel, *J. Chem. Soc., Perkin Trans. 1* **2000**, 2637-2644; b) I. Binkowska, W. Gałęzowski, A. Jarczewski, *Open Chemistry* **2010**, *8*, 582-586.
- [4] R. Schwesinger, J. Willaredt, H. Schlemper, M. Keller, D. Schmitt, H. Fritz, *Chem. Ber.* **1994**, *127*, 2435-2454.
- [5] S. Boileau, N. Illy, *Prog. Polym. Sci.* **2011**, *36*, 1132-1151.
- [6] a) J. Zhao, N. Hadjichristidis, H. Schlaad, in *Anionic Polymerization*, Springer, **2015**, pp. 429-449; b) S. Liu, C. Ren, N. Zhao, Y. Shen, Z. Li, *Macromol. Rapid Commun.* **2018**, *39*, 1800485; c) D. Jardel, C. Davies, F. Peruch, S. Massip, B. Bibal, *Adv. Synth. Catal.* **2016**, *358*, 1110-1118.
- [7] a) Y.-J. Lee, J. Lee, M.-J. Kim, B.-S. Jeong, J.-H. Lee, T.-S. Kim, J. Lee, J.-M. Ku, S.-s. Jew, H.-g. Park, *Org. Lett.* **2005**, *7*, 3207-3209; b) J. Lee, Y.-I. Lee, M. J. Kang, Y.-J. Lee, B.-S. Jeong, J.-H. Lee, M.-J. Kim, J.-y. Choi, J.-M. Ku, H.-g. Park, *J. Org. Chem.* **2005**, *70*, 4158-4161.
- [8] L. Zhang, F. Nederberg, R. C. Pratt, R. M. Waymouth, J. L. Hedrick, C. G. Wade, *Macromolecules* **2007**, *40*, 4154-4158.
- [9] a) I. Jain, P. Malik, *Eur. Polym. J.* **2020**, 109791; b) R. Yuan, G. Xu, C. Lv, L. Zhou, R. Yang, Q. Wang, *Materials Today Communications* **2020**, *22*, 100747.
- [10] a) O. I. Kazakov, P. P. Datta, M. Isajani, E. T. Kiesewetter, M. K. Kiesewetter, *Macromolecules* **2014**, *47*, 7463-7468; b) K. V. Fastnacht, S. S. Spink, N. U. Dharmaratne, J. U. Pothupitiya, P. P. Datta, E. T. Kiesewetter, M. K. Kiesewetter, *ACS Macro Letters* **2016**, *5*, 982-986.

- [11] N. U. Dharmaratne, J. U. Pothupitiya, T. J. Bannin, O. I. Kazakov, M. K. Kiesewetter, *ACS Macro Letters* **2017**, *6*, 421-425.
- [12] J. U. Pothupitiya, N. U. Dharmaratne, T. M. M. Jouaneh, K. V. Fastnacht, D. N. Coderre, M. K. Kiesewetter, *Macromolecules* **2017**, *50*, 8948-8954.
- [13] B. Lin, R. M. Waymouth, *Macromolecules* **2018**, *51*, 2932-2938.
- [14] T. S. Stukenbroeker, J. S. Bandar, X. Zhang, T. H. Lambert, R. M. Waymouth, *ACS macro letters* **2015**, *4*, 853-856.
- [15] X. Fu, C.-H. Tan, *Chem. Commun.* **2011**, *47*, 8210-8222.
- [16] D. Simoni, M. Rossi, R. Rondanin, A. Mazzali, R. Baruchello, C. Malagutti, M. Roberti, F. P. Invidiata, *Org. Lett.* **2000**, *2*, 3765-3768.
- [17] P. Hammar, C. Ghobril, C. Antheaume, A. Wagner, R. Baati, F. Himo, *J. Org. Chem.* **2010**, *75*, 4728-4736.
- [18] a) R. Pierre, F. Gaigne, G. El-Bazbouz, G. Mouis, G. Ouvry, L. Tomas, C. S. Harris, *Synlett* **2018**, *29*, 1102-1106; b) J. Meimoun, A. Favrelle-Huret, M. Bria, N. Merle, G. Stoclet, J. De Winter, R. Mincheva, J.-M. Raquez, P. Zinck, *Polym. Degrad. Stab.* **2020**, 109188.
- [19] E. Corey, M. J. Grogan, *Org. Lett.* **1999**, *1*, 157-160.
- [20] A. Huczynski, B. Brzezinski, T. Furukawa, *Encyclopedia of Reagents for Organic Synthesis* **2001**, 1-8.
- [21] B. Maji, D. Stephenson, H. Mayr, *Reactivity Parameters for Understanding Nucleophilic Organocatalysis* **2012**, 85.
- [22] S. Kafka, B. Larissegger-Schnell, T. Kappe, *J. Heterocycl. Chem.* **2004**, *41*, 717-721.
- [23] a) R. C. Pratt, B. G. Lohmeijer, D. A. Long, R. M. Waymouth, J. L. Hedrick, *J. Am. Chem. Soc.* **2006**, *128*, 4556-4557; b) B. G. Lohmeijer, R. C. Pratt, F. Leibfarth, J. W. Logan, D. A. Long, A. P. Dove, F. Nederberg, J. Choi, C. Wade, R. M. Waymouth, *Macromolecules* **2006**, *39*, 8574-8583.
- [24] M. K. Kiesewetter, M. D. Scholten, N. Kirn, R. L. Weber, J. L. Hedrick, R. M. Waymouth, *J. Org. Chem.* **2009**, *74*, 9490-9496.
- [25] L. Simon, J. M. Goodman, *J. Org. Chem.* **2007**, *72*, 9656-9662.
- [26] a) A. Chuma, H. W. Horn, W. C. Swope, R. C. Pratt, L. Zhang, B. G. Lohmeijer, C. G. Wade, R. M. Waymouth, J. L. Hedrick, J. E. Rice, *J. Am. Chem. Soc.* **2008**, *130*, 6749-6754; b) L. Zhang, R. C. Pratt, F. Nederberg, H. W. Horn, J. E. Rice, R. M. Waymouth, C. G. Wade, J. L. Hedrick, *Macromolecules* **2010**, *43*, 1660-1664.
- [27] I. Nifant'ev, A. Shlyakhtin, V. Bagrov, B. Lozhkin, G. Zakirova, P. Ivchenko, O. Legon'kova, *Reaction Kinetics, Mechanisms and Catalysis* **2016**, *117*, 447-476.
- [28] Z.-L. Jiang, J.-P. Zhao, G.-Z. Zhang, *Chin. J. Polym. Sci.* **2019**, *37*, 1205-1214.
- [29] S. Moins, S. Hoyas, V. Lemaure, B. Orhan, K. Delle Chiaie, R. Lazzaroni, D. Taton, A. P. Dove, O. Coulembier, *Catalysts* **2020**, *10*, 620.
- [30] a) H. Oediger, F. Möller, *Angew. Chem. Int. Ed.* **1967**, *6*, 76-76; b) H. OEDIGER, F. MOELLER, K. EITER, *Synthesis* **1972**, 1972, 591-598.
- [31] a) X. Liu, S. Zhang, Q.-W. Song, X.-F. Liu, R. Ma, L.-N. He, *Green Chem.* **2016**, *18*, 2871-2876; b) J. Sun, W. Cheng, Z. Yang, J. Wang, T. Xu, J. Xin, S. Zhang, *Green Chem.* **2014**, *16*, 3071-3078; c) J. E. Taylor, S. D. Bull, J. M. Williams, *Chem. Soc. Rev.* **2012**, *41*, 2109-2121; d) R. Reed, R. Réau, F. Dahan, G. Bertrand, *Angew. Chem. Int.*

- Ed.* **1993**, 32, 399-401; e) N. De Rycke, F. Couty, O. R. David, *Chem. Eur. J.* **2011**, 17, 12852-12871; f) M. Baidya, H. Mayr, *Chem. Commun.* **2008**, 1792-1794.
- [32] a) C.-L. Zhang, Z.-F. Zhang, Z.-H. Xia, Y.-F. Han, S. Ye, *J. Org. Chem.* **2018**, 83, 12507-12513; b) A. K. Morri, Y. Thummala, V. R. Doddi, *Org. Lett.* **2015**, 17, 4640-4643; c) R. Singh, D. S. Raghuvanshi, K. N. Singh, *Org. Lett.* **2013**, 15, 4202-4205; d) Y. Thummala, G. V. Karunakar, V. R. Doddi, *Adv. Synth. Catal.* **2019**, 361, 611-616.
- [33] C. Thomas, F. Peruch, B. Bibal, *Rsc Advances* **2012**, 2, 12851-12856.
- [34] H. A. Brown, A. G. De Crisci, J. L. Hedrick, R. M. Waymouth, *Acs Macro Letters* **2012**, 1, 1113-1115.
- [35] N. J. Sherck, H. C. Kim, Y.-Y. Won, *Macromolecules* **2016**, 49, 4699-4713.
- [36] X. Jiang, N. Zhao, Z. Li, *Chin. J. Chem.*
- [37] U. Schuchardt, R. Sercheli, R. M. Vargas, *J. Braz. Chem. Soc.* **1998**, 9, 199-210.
- [38] a) C. G. Jaffredo, J. F. Carpentier, S. M. Guillaume, *Macromol. Rapid Commun.* **2012**, 33, 1938-1944; b) C. G. Jaffredo, J.-F. Carpentier, S. M. Guillaume, *Poly. Chem.* **2013**, 4, 3837-3850.
- [39] S. Moins, C. Henoumont, J. De Winter, A. Khalil, S. Laurent, S. Cammas-Marion, O. Coulembier, *Poly. Chem.* **2018**, 9, 1840-1847.
- [40] a) G. Barouti, K. Jarnouen, S. Cammas-Marion, P. Loyer, S. M. Guillaume, *Poly. Chem.* **2015**, 6, 5414-5429; b) G. Barouti, A. Khalil, C. Orione, K. Jarnouen, S. Cammas-Marion, P. Loyer, S. M. Guillaume, *Chem. Eur. J.* **2016**, 22, 2819-2830.
- [41] a) N. Ajellal, C. M. Thomas, J. F. Carpentier, *J. Polym. Sci., Part A: Polym. Chem.* **2009**, 47, 3177-3189; b) C. Guillaume, N. Ajellal, J. F. Carpentier, S. M. Guillaume, *J. Polym. Sci., Part A: Polym. Chem.* **2011**, 49, 907-917; c) F. Sinclair, L. Chen, B. W. Greenland, M. P. Shaver, *Macromolecules* **2016**, 49, 6826-6834.
- [42] a) S. V. Levchik, E. D. Weil, *Polym. Int.* **2005**, 54, 11-35; b) S. V. Levchik, E. D. Weil, *J. Fire Sci.* **2006**, 24, 345-364; c) O. Fischer, D. Pospiech, A. Korwitz, K. Sahre, L. Häußler, P. Friedel, D. Fischer, C. Harnisch, Y. Bykov, M. Döring, *Polym. Degrad. Stab.* **2011**, 96, 2198-2208; d) E. Aytan, T. A. Aytan, M. V. Kahraman, *ChemistrySelect* **2021**, 6, 6541-6547.
- [43] P. Anastas, N. Eghbali, *Chem. Soc. Rev.* **2012**, 39, 301.
- [44] G. Cave, C. Raston, J. Scott, C. Raston, J. Scott, K. Yoshizawa, S. Toyota, F. Toda, K. Tanaka, T. Sugino, *Tetrahedron Lett.* **2001**, 1, 2159-2169.
- [45] a) Z. Jedliński, P. Kurcok, M. Kowalczyk, J. Kasperczyk, *Macromol. Chem. Phys.* **1986**, 187, 1651-1656; b) Z. Jedliński, P. Kurcok, R. W. Lenz, *Macromolecules* **1998**, 31, 6718-6720; c) P. Kurcok, M. Śmiga, Z. Jedliński, *J. Polym. Sci., Part A: Polym. Chem.* **2002**, 40, 2184-2189; d) D. B. Johns, R. W. Lenz, M. Vert, *J. Bioact. Compatible Polym.* **1986**, 1, 47-60; e) S. C. Arnold, R. W. Lenz, in *Makromolekulare Chemie. Macromolecular Symposia, Vol. 6*, Wiley Online Library, **1986**, pp. 285-303; f) S. Cammas, K. Boutault, F. Huet, P. Guérin, *Tetrahedron: Asymmetry* **1994**, 5, 1589-1597; g) M. Kawalec, M. Śmiga-Matuszowicz, P. Kurcok, *Eur. Polym. J.* **2008**, 44, 3556-3563.
- [46] a) J. De Winter, O. Coulembier, P. Gerbaux, P. Dubois, *Macromolecules* **2010**, 43, 10291-10296; b) M. Kawalec, O. Coulembier, P. Gerbaux, M. Sobota, J. De Winter, P. Dubois, M. Kowalczyk, P. Kurcok, *React. Funct. Polym.* **2012**, 72, 509-520.

- [47] a) B. Lee, R. Quirk, *Polym. Int* **1992**, 27, 359; b) K. Matyjaszewski, *J. Phys. Org. Chem.* **1995**, 8, 197-207; c) A. H. Mueller, R. Zhuang, D. Yan, G. Litvinenko, *Macromolecules* **1995**, 28, 4326-4333.
- [48] I. Nifant'ev, P. Ivchenko, *Polymers* **2019**, 11, 2078.
- [49] a) A. Horvath, *Synthesis* **1995**, 1995, 1183-1189; b) Z. Yu, X. Liu, L. Zhou, L. Lin, X. Feng, *Angew. Chem. Int. Ed.* **2009**, 48, 5195-5198; c) M. W. Wong, A. M. E. Ng, *Aust. J. Chem.* **2014**, 67, 1100-1109.
- [50] a) J. Dunitz, J. Lehn, G. Wipff, *Tetrahedron* **1974**, 30, 1563-1572; b) C. J. Stirling, *Tetrahedron* **1985**, 41, 1613-1666.
- [51] R. M. Shakaroun, P. Jéhan, A. Alaaeddine, J.-F. Carpentier, S. M. Guillaume, *Poly. Chem.* **2020**, 11, 2640-2652.
- [52] a) X. Tang, A. H. Westlie, E. M. Watson, E. Y.-X. Chen, *Science* **2019**, 366, 754-758; b) X. Tang, E. Y.-X. Chen, *Nat. comm.* **2018**, 9, 1-11.

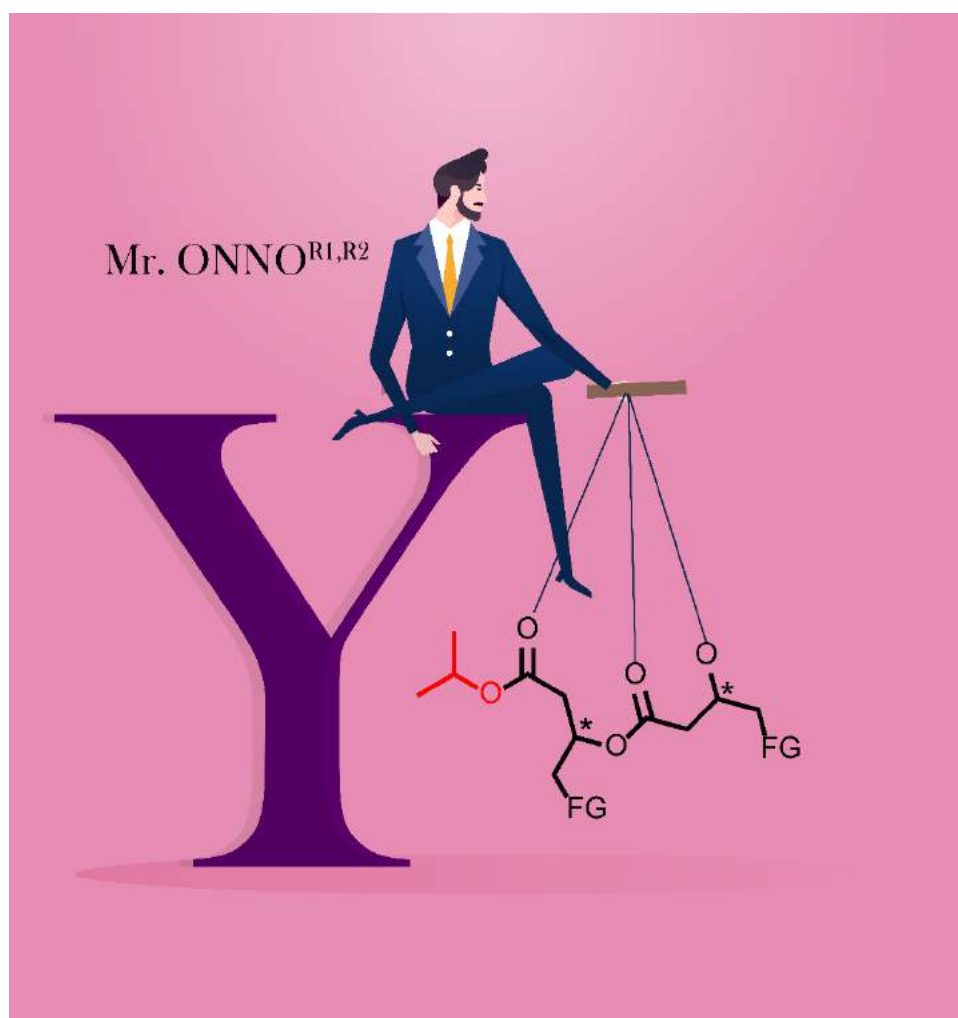






## Chapter 4

### Stereoselective ROP of functional chiral $\beta$ -lactones mediated by achiral yttrium-bis(phenolate) complexes







<b>1. Introduction .....</b>	<b>191</b>
1.1. Preliminary general considerations .....	191
1.1.1. Coordination-insertion ROP mechanism .....	191
1.1.2. Stereoselective ROP mechanism and polymer tacticity .....	192
1.2. State-of-the-art stereoselective ROP of racemic $\beta$ -lactones mediated by $Y\{ONXO^{R1,R2}\}$ .....	195
1.2.1. Stereoselective ROP of $MLA^{FGs}$ (FG = All, Bn, Me) .....	196
1.2.2. Stereoselective ROP of $BPL^{FGs}$ (FG = OAll, OBn, OMe) .....	198
1.3. Summary.....	200
<b>2. Results and discussion: Yttrium mediated stereocontrolled ROP of <math>BPL^{FGs}</math>.....</b>	<b>201</b>
2.1. ROP of $BPL^{FGs}$ with different alkoxide chain length .....	202
2.1.1. ROP of $rac-BPL^{OPh}$ .....	203
2.1.2. ROP of $rac-BPL^{CH_2OBn}$ .....	209
2.1.3. ROP of $rac-BPL^{SPh}$ .....	211
2.1.4. Insights into the kinetics and the activity of the catalyst .....	217
2.1.5. Summary on the ROP of $rac-BPL^{OPh/CH_2OBn/SPh}$ .....	218
2.2. ROP of $BPL^{FGs}$ with bulky exocyclic chains.....	219
2.2.1. ROP of $rac-BPL^{OiPr}$ .....	220
2.2.2. ROP of $rac-BPL^{OtBu}$ .....	225
2.2.3. ROP of $rac-BPL^{OTBDMS}$ .....	230
2.2.1. Kinetics and activity of the catalyst .....	233
2.2.2. Results summary on the stereochemistry of $PBPL^{OiPr/OtBu/OTBDMS}$ .....	234
2.3. Preliminary investigations on the ROP of $rac-BPL^{OP(O)Ph_2}$ .....	235
<b>3. Conclusion : achievements and perspectives .....</b>	<b>243</b>
<b>4. Experimental section .....</b>	<b>244</b>

**5. References ..... 249**

Part of the results gathered in this chapter have been the object of a paper published within the special issue on “Sustainable polymers” in *Polymer Chemistry* **2021**, *11*, 2640-2652, entitled "Stereoselective ring-opening polymerization of functional  $\beta$ -lactones: influence of the exocyclic side-group" by R. M. Shakaroun, H. Li, A. Alaaeddine, M. Blot, P. Jéhan, J.-F. Carpentier, S. M. Guillaume.<sup>2</sup>

---

<sup>2</sup> <https://pubs.rsc.org/en/content/articlelanding/2021/PY/D1PY00669J>

[https://www.rsc.org/suppdata/d1/py/d1py00669j/d1py00669j1.pdf?\\_ga=2.23812979.815582279.1630909216-1387992406.1630909216](https://www.rsc.org/suppdata/d1/py/d1py00669j/d1py00669j1.pdf?_ga=2.23812979.815582279.1630909216-1387992406.1630909216)

## 1. Introduction

Attaining PHAs with different functionalities and tacticity can enhance and tune their physio-chemical properties, thus widening their range of application.<sup>[1]</sup> While ROP promoted by organic activators (BEMP, TBD and DBU) have afforded atactic functional PHAs, stereoregular PHAs can be produced through the stereoselective rare-earth metal-mediated ring-opening polymerization (ROP) of chiral  $\beta$ -lactones.<sup>[2]</sup> Herein, ROP of some functional  $\beta$ -lactones, namely of  $\beta$ -malolactonates ( $\text{MLA}^{\text{FG}}$  (FG = All, Bn, Me)) and 4-alkoxymethylene- $\beta$ -butyrolactone ( $\text{BPL}^{\text{FG}}$ ; FG = OAll, OBn, OMe), promoted by yttrium-bis(phenolate) complexes ( $\text{Y}\{\text{ONXO}^{\text{R}^1, \text{R}^2}\}$ ,  $\text{R}^1 = \textit{ortho}$ -substituent), that were previously reported by our group, are reviewed. Emphasizing, in particular, on the impact of the substituents of the ancillary ligands ( $\text{R}^1$ ,  $\text{R}^2$ ) and of that of the  $\beta$ -lactones functional group (FG and R), on the stereochemistry of the produced  $\text{PMLA}^{\text{FG}}$  or  $\text{PBL}^{\text{FG}}$ . Subsequently, an outspread investigation to additional *rac*- $\text{BPL}^{\text{FG}}$ s (FG = OPh,  $\text{CH}_2\text{OBn}$ , SPh,  $\text{O}^i\text{Pr}$ ,  $\text{O}^t\text{Bu}$ , OTBDMS) were explored in this work. Moreover, a preparatory study on the ROP of *rac*- $\text{BPL}^{\text{OP}(\text{O})\text{Ph}_2}$  was commenced.

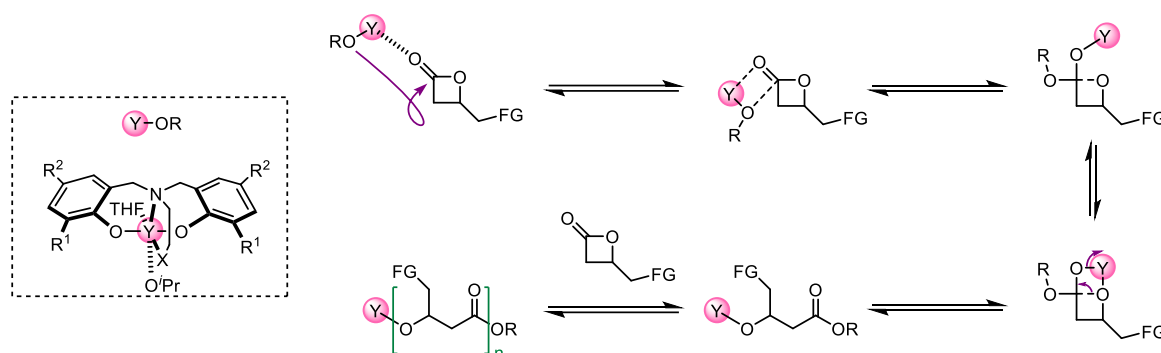
### 1.1. Preliminary general considerations

Prior to investigate the effectiveness, molecular control and stereocontrol of the ROP of  $\beta$ -lactones mediated by yttrium-bis(phenolate) complexes, it is important to understand the mode of action of these catalysts. The ROP mechanism and the stereoselective mechanism at play and tacticity detection are described beneath.

#### 1.1.1. Coordination-insertion ROP mechanism

Yttrium-bis(phenolate) complexes are Lewis acid metals supported by  $\{\text{ONNO}^{\text{R}^1, \text{R}^2}\}$  ancillary ligands and are usually accompanied by a nucleophile (typically an alcohol, usually isopropanol) during ROP. They are coordination complexes that operate through a coordination-insertion ROP mechanism. This mechanism involves the coordination of the carbonyl function of the monomer to the Lewis acid metal (yttrium) to next enable the addition of the nucleophile to the ester function. Then, the opening of the  $\beta$ -lactone is achieved – most often- by "oxygen–acyl" cleavage leading to the formation of an active alcoholate to ensure the propagation (Scheme 4. 1). The ROP of cyclic esters by coordination-insertion pathway has been an area of interest since the 1970s with the emergence of well-defined organometallic

complexes.<sup>[3]</sup> Its development has seen the appearance of many metal complexes supported by a wide variety of ligands.<sup>[4]</sup>



**Scheme 4. 1** – ROP of  $\beta$ -lactones through coordination-insertion mechanism mediated by yttrium-based catalysts ( $\text{Y}\{\text{ONXO}^{\text{R1,R2}}\}$ ).<sup>[3]</sup>

### 1.1.2. Tacticity and stereoselective ROP mechanism

The relation between the obtained tacticity of the polymers and the stereoselective ROP mechanism is briefly presented. Tacticity originates from the Greek word “*taktikos*” meaning arrangement or order. In polymer, it refers to the regularity of the relative configuration of stereocenters within the polymer chain. The consecutive insertion of two monomer units of the same configuration ((*R*)/(*R*) or (*S*)/(*S*)) will lead to the formation of a *meso* (*m*) sequence and that of two centers of opposite absolute configurations ((*R*)/(*S*) or (*S*)/(*R*)) will lead to the formation of a *racemo* (*r*) sequence. *Meso* sequence enrichment will lead to the formation of an isotactic polymer while that in *racemo* sequences will lead to a syndiotactic polymer.

NMR spectroscopy analysis provides (under suitable adjustment of the recording parameters) valuable information on the type of the sequence as well as its proportion within the polymer chain, to determine the enrichment of the polymer in regular sequences. The more precise the analysis the more resolved the NMR spectrum (by playing mainly on the intensity of the magnetic field). Thus, we can observe different sequences such as diads for two adjacent centers, triads for three adjacent centers, tetrads for four adjacent centers (Figure 4. 1).<sup>[5]</sup>

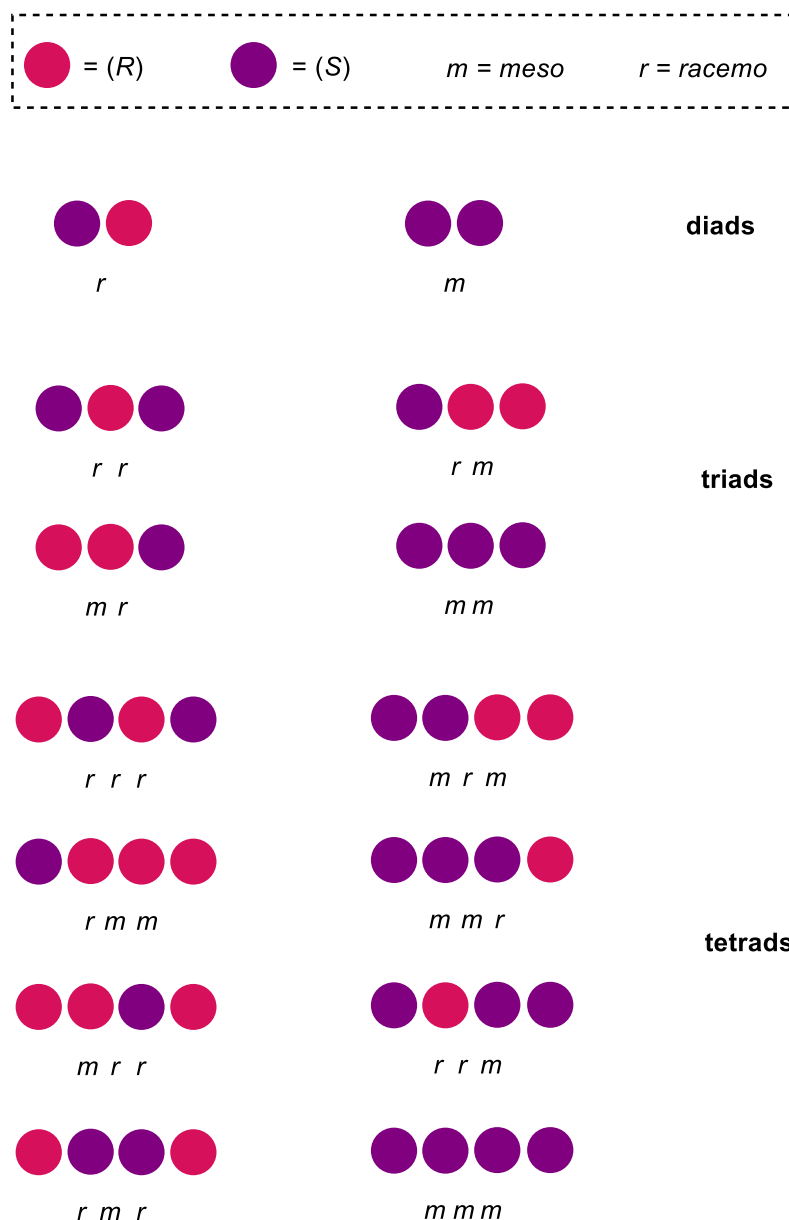


**Figure 4. 1** – Representation of the different sequences of repeating units, diads, triads and tetrads encountered in ROP of  $\beta$ -lactones.

Generally, isotactic polymers can be prepared by polymerizing enantio-pure monomers. In this case, the stereo-selectivity of the catalyst used has no impact on the tacticity of the polymer obtained, unless there is epimerization. Coates *et al.* thus used the zinc complex, (BDI)ZnO<sup>*i*</sup>Pr (BDI = 2-((2,6-diisopropylphenyl)amido)-4-((2,6-diisopropylphenyl)imino)-2-pentene), in the presence of (*R*)-BL<sup>Me</sup> to synthesize isotactic (*R*)-PBL<sup>Me</sup>.<sup>[6]</sup> This strategy is similar to the polycondensation of *L*-hydroxybutyryl-Coenzyme A by bacteria also leading to the formation of isotactic PHB.<sup>[7]</sup>

The real challenge is to polymerize a *racemic* monomer and end up with stereoregular polymers (isotactic or syndiotactic), which should be accomplished via stereoselective

catalysts. In this strategy, two types of stereocontrol mechanism are distinguished: enantiomorphic-site mechanism (ESM) and chain end mechanism (CEM). In the case of an ESM, the asymmetric environment of the catalyst causes the catalyst to react preferentially with one of the two enantiomers of the monomer. This asymmetric environment is very often related to the attached chiral ligand. Whereas, in the case of CEM, the insertion of a new unit into the growing chain is impacted by the last unit(s) inserted which contain(s) specific stereogenic center(s). The last unit(s) present at the active end of the growing chain then ensures propagation and thus imposes stereoselectivity.

Several statistical models make it possible to analyse the stereoselective control.<sup>[8]</sup> The three main ones are the Bernoulli model and the 1<sup>st</sup> and 2<sup>nd</sup> order Markov models, that allow the study of "end-of-line" stereoselective chain operating during ROP reactions.<sup>[8b]</sup> Bernoulli's model analyses the lack of control during the growth of the polymer chain (Figure 4. 2). Thus, the probability to insert a monomer unit of the same absolute configuration as the last inserted unit in the growing chain, is equal to the probability of insertion of a unit of opposite absolute configuration. More clearly, the probability of creating a *racemo* (*r*) diad is the same as the probability of creating a *meso* (*m*) diads, equation (I).

$$P_r = P_m \quad (\text{I})$$

According to this model, and therefore without control of tacticity, the set of probabilities of the formation of sequences of the same family (diads, triads or tetrads) must be equal to 1. Thus, in the case of diads, equations (II) and (III) are used,

$$\text{with, } P_r + P_m = 1 \quad (\text{II})$$

$$\text{Then, } P_r = P_m = 0.5 \quad (\text{III})$$

However, the models of 1<sup>st</sup> and 2<sup>nd</sup> order Markov's express the impact of the growing chain on the insertion of a new repeating unit. Thus, the insertion of a new unit of repetition will be defined by the last one (1<sup>st</sup> order Markov; Mk1) or the last two (2<sup>nd</sup> order Markov; Mk2) repeating units inserted in the polymer chain (Figure 4. 2). Both values are derived from the Bernoulli model. Thus, Equation (II) must be verified and applies directly in the case of the observation of diads. However, these models express an enrichment in regular sequence leading to the non-verification of Equation (I), wherefor ( $P_r \neq P_m \neq 0.5$ ). In the case of triads, the validity of the model is quantified by calculating the Bernoulli tuning factor (B), equation (IV). The

closer the value of this factor is to 1, the better the validity of the model. Finally, in the case of tetrads, no tuning factor is defined.

$$B = P_r + P_m = m^2 + r^2 = 4(mm)(rr)/[rm + mr]^2 \quad (\text{IV})$$

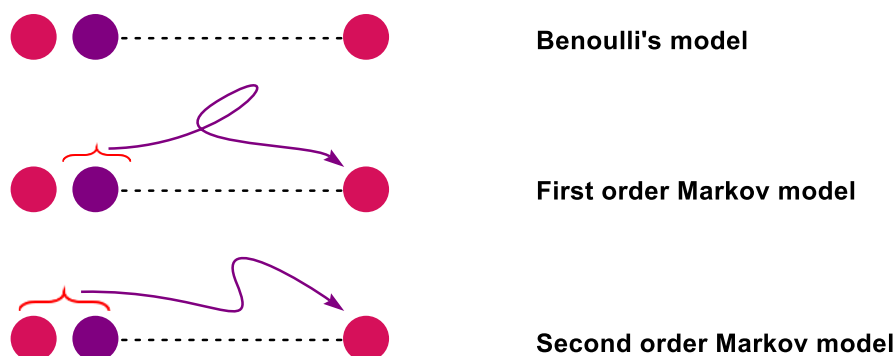


**Figure 4. 2** – Illustration of Bernoulli's and Markov's 1<sup>st</sup> and 2<sup>nd</sup> order models.

Finally, we can evaluate the tacticity of a polymer and therefore the selectivity of a catalyst by determination of the probability of *racemo* or *meso* concatenation of consecutive repeating units ( $P_r$  or  $P_m$ ).

## 1.2. State-of-the-art stereoselective ROP of racemic $\beta$ -lactones mediated by $Y\{ONXO^{R1,R2}\}$

$Y\{ONXO^{R1,R2}\}$  is an achiral stereoselective catalyst and normally undergoes CEM mechanism through coordination-insertion ROP. It has been already mentioned that the stereoselective ROP of *rac*-BL<sup>Me</sup> mediated by  $Y\{ONXO^{R1,R2}\}$  ( $X = \text{OMe}, \text{NMe}_2$ ) catalyst leads to highly syndiotactic PBL<sup>Me</sup> ( $P_r \leq 0.95$ ) depending on the nature of the *ortho*-substituent on the ligand ( $R^1$ ), which had better be bulky with electronic character (e.g.,  $R^1 = \text{cumyl} = \text{CMe}_2\text{Ph}$ ) and not only sterically encumbered (e.g.,  $R^1 = \text{CMe}_2\text{tBu}$ ; Figure 1. 11).<sup>[9]</sup> This was supported by the DFT studies, which suggest that the intermediate **II**-*trans*-alkoxy/amino is the most favourable intermediate in terms of energy as compared to **I**-*trans*-alkoxy/amino (Figure 4. 3). The presence of a significant steric component (red parentheses), along with an electronic contribution depicted by the weak  $\text{C-H} \cdots \pi$  bond (dashed blue), involving the methylene  $\alpha$ -hydrogens of the alkoxy-butyrates and the  $\pi$  ring of the aryl group of the *O*-phenolate substituent (cumyl), were noticed to be both responsible for stabilizing this conformation. Hence, it was suggested that in the case of *rac*-BL<sup>Me</sup>, the impact of the substituent on selectivity would be mainly steric (forcing the growing chain to adopt a conformation that minimizes steric



hindrance), accompanied with some electronic input.<sup>[9c, 9d]</sup> Moreover, statistical studies of the distributions of stereosequences in polyesters indicated that the control proceeded by chain end control of the 1<sup>st</sup> order Markov type.<sup>[9a-d]</sup>

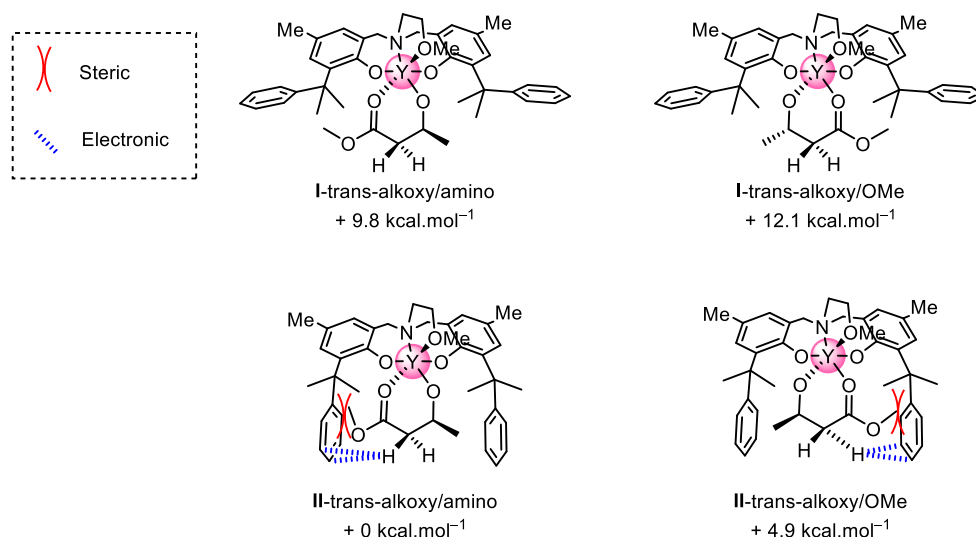


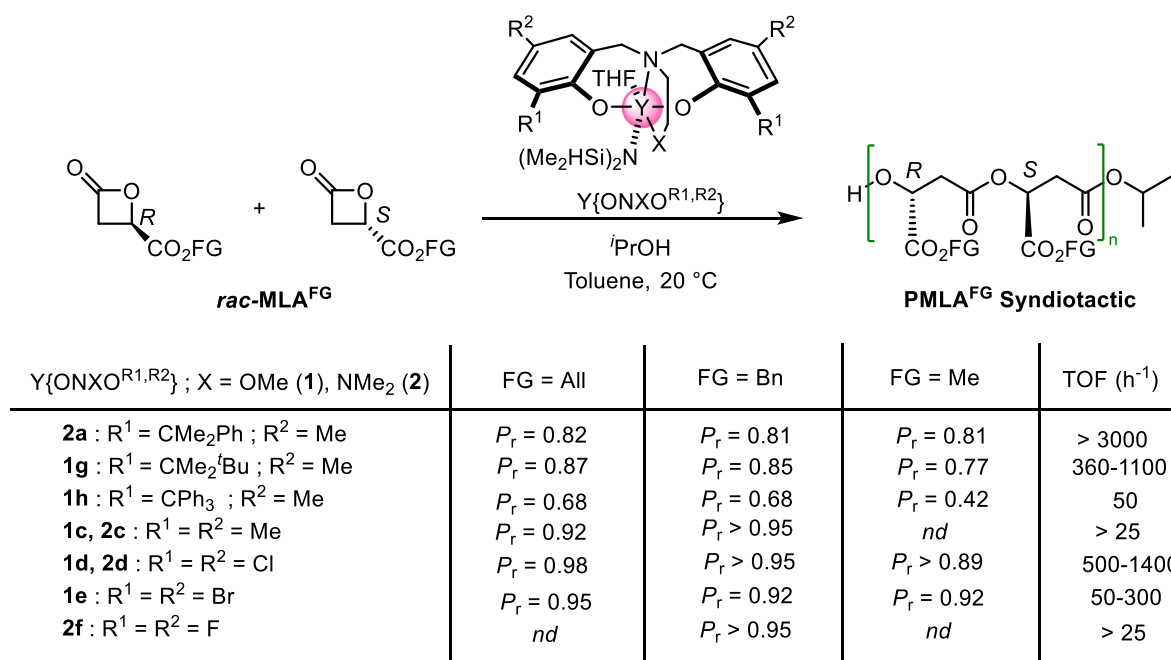
**Figure 4. 3** – Representation of modelled conformations for intermediates corresponding to the first coordination/insertion of *rac*-BL<sup>Me</sup> on Y{ONOO<sup>R1,R2</sup>} (R<sup>1</sup> = cumyl; R<sup>2</sup> = Me) as well as the computed energies related to these intermediaries.<sup>[9c]</sup>

Further investigations on the interactions between the ligand substituents and the monomer exocyclic substituent were accomplished by our group. The most recent examples address  $\beta$ -lactones functionalized with esters (MLA<sup>FG</sup>; FG = All, Bn, Me) or ethers (FG = OAll, OBn, OMe), that differ from *rac*-BL<sup>Me</sup> by the exocyclic group.

### 1.2.1. Stereoselective ROP of MLA<sup>FG</sup>s (FG = All, Bn, Me)

The stereocontrolled ROP of *racemic*  $\beta$ -malolactonates (*rac*-MLA<sup>FG</sup>s), was assessed using the Y{ONXO<sup>R1,R2</sup>} (X = OMe, NMe<sub>2</sub>) catalyst in the presence of isopropanol as co-initiator in toluene (Scheme 4. 2 – top).<sup>[10]</sup> Both yttrium complexes (**1**) and (**2**) showed a great activity, the highest activity being obtained with a highly sterically substituted complex **2a**/<sup>*i*</sup>PrOH (R<sup>1</sup> = cumyl) with TOF  $\geq 3000 \text{ h}^{-1}$  (at [monomer]<sub>0</sub>/[Catalyst]<sub>0</sub> = 100:1 equiv). Moreover, an excellent agreement was observed between the molar masses measured experimentally and the expected theoretical masses ( $M_{n,\text{SEC}}$  vs.  $M_{n,\text{NMR}}$  vs.  $M_{n,\text{theo}}$ ), and quite narrow dispersities were obtained with sterically crowded complexes **2a,1g,1h** ( $\mathcal{D}_M < 1.3$ ) as compared to the less bulky and halogenated ones (**1,2**)c-d ( $\mathcal{D}_M = 1.50\text{--}1.60$ ). The best syndioselectivity was obtained in the case of the (**1,2**)c-f/<sup>*i*</sup>PrOH catalytic system (R<sup>1</sup> = halogen or Me) in ROP of *rac*-MLA<sup>Bn</sup> and of *rac*-MLA<sup>All</sup> ( $P_r$  reaching 0.98, Scheme 4. 2 – bottom), and

the worst ( $P_r = 0.42$ ) in ROP of *rac*-MLA<sup>Me</sup> was measured with **1h**/<sup>i</sup>PrOH ( $R^1 = \text{CPh}_3$ ). This was in contrast to what was obtained in ROP of *rac*-BL<sup>Me</sup> with this catalytic system, where (**1,2**)**c-d**/<sup>i</sup>PrOH gave atactic PBL<sup>Me</sup> ( $R^1 = \text{halogen}$ ;  $P_r = 0.42$ – $0.45$  and  $R^1 = \text{Me}$ ;  $P_r = 0.56$ ).<sup>[10]</sup> These results highlighted the strong influence of the ancillary ligand substituents and of the  $\beta$ -lactone functionality on the syndioselectivity of the complexes.

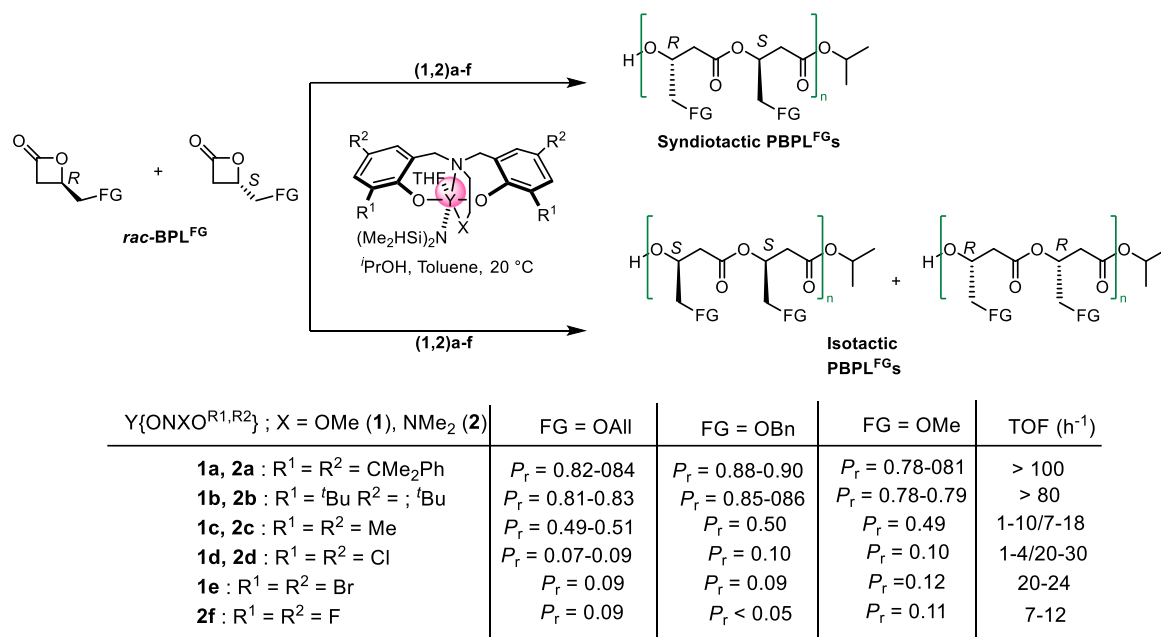


**Scheme 4. 2** – Stereoselective ROP of *rac*-MLA<sup>FG</sup> (FG: Bn = CH<sub>2</sub>C<sub>6</sub>H<sub>5</sub>; All = CH<sub>2</sub>CH<sub>2</sub>=CH<sub>2</sub>; Me = CH<sub>3</sub>) mediated by  $Y\{ONXO^{R1,R2}\}$  (top);  $P_r$  values (%) of PMLA<sup>FG</sup>S and TOF values (h<sup>-1</sup>) for the ROPs of *rac*-MLA<sup>Bn</sup> (bottom).<sup>[10]</sup>

Due to the results obtained from halides and methyl substituted ligands that both afforded highly to purely syndiotactic PMLA<sup>FG</sup>s, it was proposed that the halogen bonding is not at work in these polymerizations. Moreover, the studies on the intermediates and transition states of the ROP, suggested that the smaller ligand  $R^1$  substituents, such as halides or methyl, enable a sufficiently high coordination number ( $\kappa^2$ - or  $\kappa^3$ -) and also flexibility around the central metal, eventually leading to a good stereocontrol to syndiotactic PMLA<sup>FG</sup>s. Thus, the stereoselectivity control was considered to be affected by the size of the  $R^1$  substituents without an electronic effect interference, as reported for *rac*-BL<sup>Me</sup> (Figure 4. 3). Hence, the general trend of syndioselectivity (in ascending order) in the ROP of *rac*-MLA<sup>FG</sup>s is:  $R^1 = \text{purely aromatic bulky} < \text{bulky} < \text{purely aliphatic bulky} < \text{Me} \leq \text{Cl (or F and Br)}$ .

### 1.2.2. Stereoselective ROP of BPL<sup>FG</sup>s (FG = OAlI, OBn, OMe)

*Rac*-BPL<sup>FG</sup>s (FG = OAlI, OBn, OMe) simply differ from *rac*-MLA<sup>FG</sup>s (FG = AlI, Bn, Me) by replacement in the pendant (exocyclic) group of the carbonyl by a methylene moiety (C=O vs CH<sub>2</sub>). However, this proved to have major implications on stereochemistry. In fact, application of Y{ONXO<sup>R1,R2</sup>}/<sup>i</sup>PrOH complexes resulted in two very different outcomes: either a highly syndiotactic or an unexpected, highly isoselective ROP (Scheme 4. 3).<sup>[10c, 11]</sup>



**Scheme 4. 3** – Stereoselective ROP of *rac*-BPL<sup>FG</sup>s (FG: OBn = OCH<sub>2</sub>C<sub>6</sub>H<sub>5</sub>; OAlI = OCH<sub>2</sub>CH<sub>2</sub>=CH<sub>2</sub>; OMe = OCH<sub>3</sub>) mediated by Y{ONXO<sup>R1,R2</sup>} ((**1,2**)a-f) (top); *P<sub>r</sub>* values (%) of PBPL<sup>FG</sup>s and TOF values (h<sup>-1</sup>) (bottom).<sup>[10c, 11]</sup>

High syndiotacticity of *rac*-BPL<sup>FG</sup>s was achieved in the case of hindered R<sup>1</sup> substituents on the yttrium catalyst even with purely aliphatic bulky substituents. Similar to *rac*-MLA<sup>FG</sup>s, this indicated that the stereoselective ROP of *rac*-BPL<sup>FG</sup>s does not rely on the abovementioned aryl electronic effect suggested from *rac*-BL<sup>Me</sup> (Figure 4. 3). Moreover, the less steric methyl-substituted yttrium complex (R<sup>1</sup> = Me) afforded atactic PBPL<sup>FG</sup>s, demonstrating that syndiotactic ROP is under steric control, following the typical CEM model (Figure 4. 4 – grey). On the other hand, upon using yttrium complexes bearing ligands with halogen substituents, the formation of highly isotactic PBPL<sup>FG</sup>s (as a racemic mixture of iso-*R* and iso-*S* macromolecules) was induced (Figure 4. 4 – black).

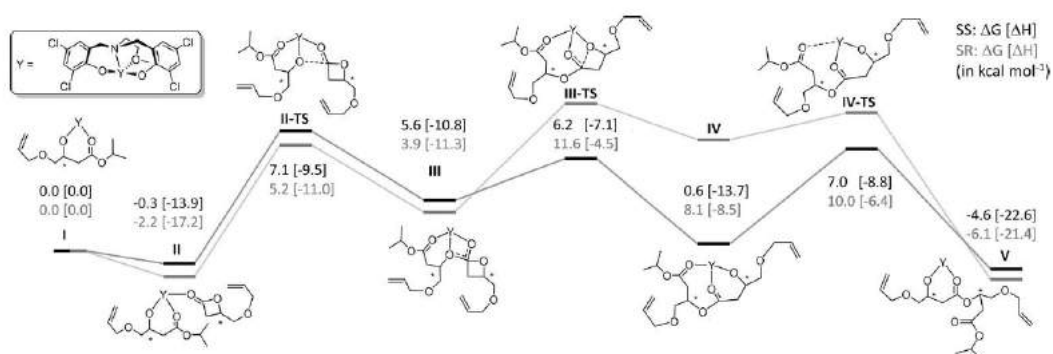


**Figure 4. 4** – Energy profile of the proposed ROP mechanism for isotactic (black) and syndiotactic (grey) PBPL<sup>OAll</sup> formation with **1d** as the initiator; taken from publication reference.<sup>[11]</sup>

Previous DFT investigations considered the first step of the reaction, which is the formation of the four-membered metallacycle prior to its ring opening with *rac*-BPL<sup>OAll</sup>, and both with chloro and methyl ligand substituents, to understand this unique isotactic control. Starting with modelling of the reaction with the chloro-substituted complex resulted in a transition state toward the formation of isotactic PBPL<sup>OAll</sup> lower in energy than that for the syndiotactic polymer. This was traced back to strong attractive C–H···Cl interactions between hydrogen from the alkoxymethylene group of the pendant chain (hydrogens of C<sub>A</sub> and C<sub>B</sub>) in the ring-opened monomer and the chloro substituents of the ligand (Figure 4. 5 – (a)), that stabilize the transition state leading to isotactic polymer and thus lowering the overall activation energy for the isotactic propagation. However, the modelling of the reaction with a methyl-substituted catalyst generated transition states on both iso- and syndio-propagation routes with virtually identical free energies, hence resulting into an atactic PBPL<sup>OAll</sup>. Moreover, the corresponding methyl substituents interaction (C–H···C and C–H···HC), although slightly weaker, are repulsive and thus destabilize the transition state (Figure 4. 5 – (b)). Overall, this indicated that electronic factors (and not steric ones) are the main feature governing the isoselective polymerization of *rac*-BPL<sup>FG</sup>s (FG = OAll, OBn, OMe).

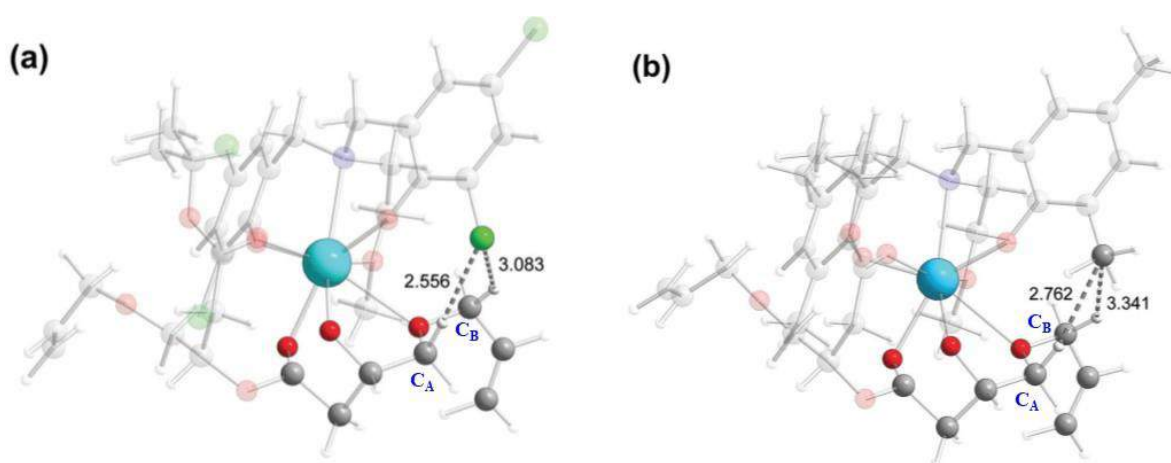


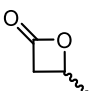
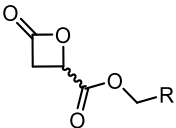
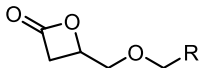
**Figure 4. 5** – Structures of the transition state at the ring-opening step of *rac*-BPL<sup>OAll</sup> leading toward isotactic or atactic PBPL<sup>OAll</sup>, showing the short contacts between the alkoxymethylene group (H of C<sub>A</sub> and C<sub>B</sub>) in the ring-opened monomer and the ligand chloro (**a**) or methyl (**b**) substituents; taken from publication reference.<sup>[11]</sup>

Noteworthy, the C–H···Cl attractive interactions can exist only because a methylene group (Figure 4. 5 – C<sub>A</sub>) in *rac*-BPL<sup>FGs</sup>/PBPL<sup>FGs</sup> (–CHCH<sub>2</sub>OR) has replaced a carbonyl group in *rac*-MLA<sup>FGs</sup>/PMLA<sup>FGs</sup> (–CHC(O)OR).

### 1.3. Summary

In this brief review of the state-of-the-art on the stereocontrolled ROP of  $\beta$ -lactones, it was shown that despite using the same cyclic ester ring size ( $\beta$ -lactones), the same yttrium-bis(phenolate) complexes (Y{ONXO<sup>R1,R2</sup>}) ROP catalytic systems afford different activity, efficiency and stereocontrol depending on the chemical nature of the exocyclic substituent. This was linked to the presence of repulsive or attractive secondary interactions between the ligand substituents of the yttrium-based complexes and the pendant substituents on the  $\beta$ -lactone, resulting from steric and electronic contributions. The previous results obtained in our group for the stereoselective ROP of *rac*-BL<sup>Me</sup>, *rac*-MLA<sup>FGs</sup>, and *rac*-BPL<sup>FGs</sup> mediated by Y{ONXO<sup>R1,R2</sup>} are summarized in Table 4. 1.

**Table 4. 1** –  $P_r$  values for PBL<sup>Me</sup>, PMLA<sup>FGs</sup>, PBPL<sup>FGs</sup> prepared from the stereoselective ROP of *rac*-BL<sup>Me</sup>, *rac*-MLA<sup>FGs</sup>, and *rac*-BPL<sup>FGs</sup> mediated by Y{ONXO<sup>R1,R2</sup>} catalytic systems.

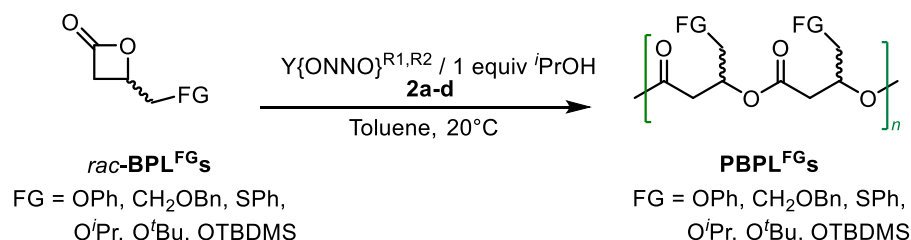
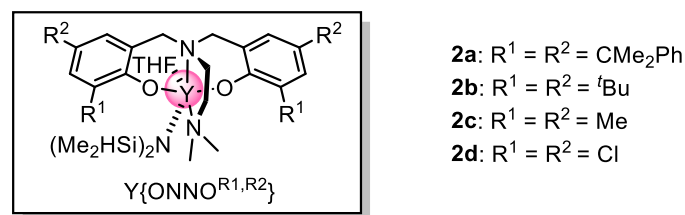
Monomers R <sup>1</sup> , R <sup>2</sup>	 <i>rac</i> -BPL <sup>Me</sup>	 <i>rac</i> -MLA <sup>All/Bn/Me</sup>	 <i>rac</i> -BPL <sup>OAll/Obn/OMe</sup>
<b>Crowded</b>	Syndiotactic $P_r = 0.70\text{--}0.96$	Syndiotactic $P_r = 0.68\text{--}0.87$	Syndiotactic $P_r = 0.78\text{--}0.90$
<b>Non-Crowded</b>	Atactic $P_r = 0.56$	Syndiotactic $P_r = 0.92\text{--}>0.95$	Atactic $P_r = 0.49\text{--}0.51$
<b>Halogenated</b>	Atactic	Syndiotactic	Isotactic
<b>Non-Crowded</b>	$P_r = 0.42\text{--}0.45$	$P_r = 0.91\text{--}>0.98$	$P_r = <0.05\text{--}0.12$

Investigating other functionalities of *rac*-BPL<sup>FGs</sup> (FG = OPh, CH<sub>2</sub>OBn, SPh, O<sup>i</sup>Pr, O<sup>t</sup>Bu, OTBDMS) is interesting to further explore their influence in ROP, especially after

obtaining different stereoregularity (high syndio- or high iso-) depending on the functionality of the  $\beta$ -lactone used (*rac*-MLA<sup>FG</sup>s (FG = All, Bn, Me) and *rac*-BPL<sup>FG</sup>s (FG = OAll, OBn, OMe).

## 2. Results and discussion: Stereoselective ROP of new *racemic* $\beta$ -lactones mediated by Y{ONXO<sup>R1,R2</sup>}

Essentially, to access to other functional PHAs displaying a regular tacticity, thereby expecting to widen the range of properties and applications of PHAs, we sought to ring-open polymerize new examples of *rac*-BPL<sup>FG</sup>s with FG = OPh, CH<sub>2</sub>OBn, SPh, O<sup>i</sup>Pr, O<sup>t</sup>Bu, OTBDMS, through Y{ONXO<sup>R1,R2</sup>} catalysis. Widening the range of PHA<sup>FG</sup>s would enable to further probe the influence of the pendant functional groups of the monomers and of the metal complexes, in order to better understand the factors that drive the stereoregularity of these ROPs. Meanwhile, as observed from the previous studies, since only the *ortho*-substituents on the ligand (R<sup>1</sup>) do influence the secondary interactions with the monomer and hence the resulting stereochemistry, *para*-substituents (R<sup>2</sup>) were thus not considered further in my studies. Moreover, no impact of the capping X substituent of the diamino- or amino-alkoxy-bis(phenolate) yttrium ((**1**) X = OMe or (**2**) X = NMe<sub>2</sub>) was generally observed on the stereochemistry of the polymer, yet complexes (**2**) showed higher TOF values. Therefore, the stereoselective ROP of *rac*-BPL<sup>FG</sup>s (FG = OPh, CH<sub>2</sub>OBn, SPh, O<sup>i</sup>Pr, O<sup>t</sup>Bu, OTBDMS) was investigated in the presence of (**2**) (Y{ONNO<sup>R1,R2</sup>}) with specific steric and electronic substituents (R<sup>1</sup> = R<sup>2</sup> = cumyl, <sup>t</sup>Bu, Me, Cl) (Scheme 4. 4).



**Scheme 4.4** – Stereoselective ROP of  $\text{rac-BPL}^{\text{FGs}}$  ( $\text{FG} = \text{OPh}, \text{CH}_2\text{OBn}, \text{SPh}, \text{O}^i\text{Pr}, \text{O}^t\text{Bu}, \text{OTBDMS}$ ) mediated by (**2a-d**).

As one can observe, the designed pendant group of  $\text{rac-BPL}^{\text{FGs}}$  have either shorter ( $\text{BPL}^{\text{OPh}}$ ) or longer ( $\text{BPL}^{\text{CH}_2\text{OBn}}$ ) chain from the previously studied  $\text{rac-BPL}^{\text{FGs}}$  ( $\text{FG} = \text{OAll}, \text{OBn}, \text{OMe}$ ); or shorter and bulkier substituents ( $\text{BPL}^{\text{O}^i\text{Pr}, \text{O}^t\text{Bu}, \text{OTBDMS}}$ ). These specific FGs were selected so as to examine the effect of these changes of the exocyclic chains, particularly on the electronic attractive interactions depicted in Figure 4. 5 that lead to the unanticipated isotactic polymers, or on the steric repulsive interactions that lead to syndiotactic polymers.

## 2.1. ROP of $\text{BPL}^{\text{FGs}}$ with different alkoxide chain length

The first category that was explored is the series of  $\text{rac-BPL}^{\text{FGs}}$  with  $\text{FG} = \text{OPh}$  and  $\text{CH}_2\text{OBn}$  that were compared with the similar formerly studied  $\text{rac-BPL}^{\text{FGs}}$  having  $\text{FG} = \text{OBn}$  (Figure 4. 6). Then, to understand if there is an impact of the exocyclic heteroatom (O vs. S) on the activity of the catalyst,  $\text{rac-BPL}^{\text{SPh}}$  (vs.  $\text{rac-BPL}^{\text{OPh}}$ ) was examined.

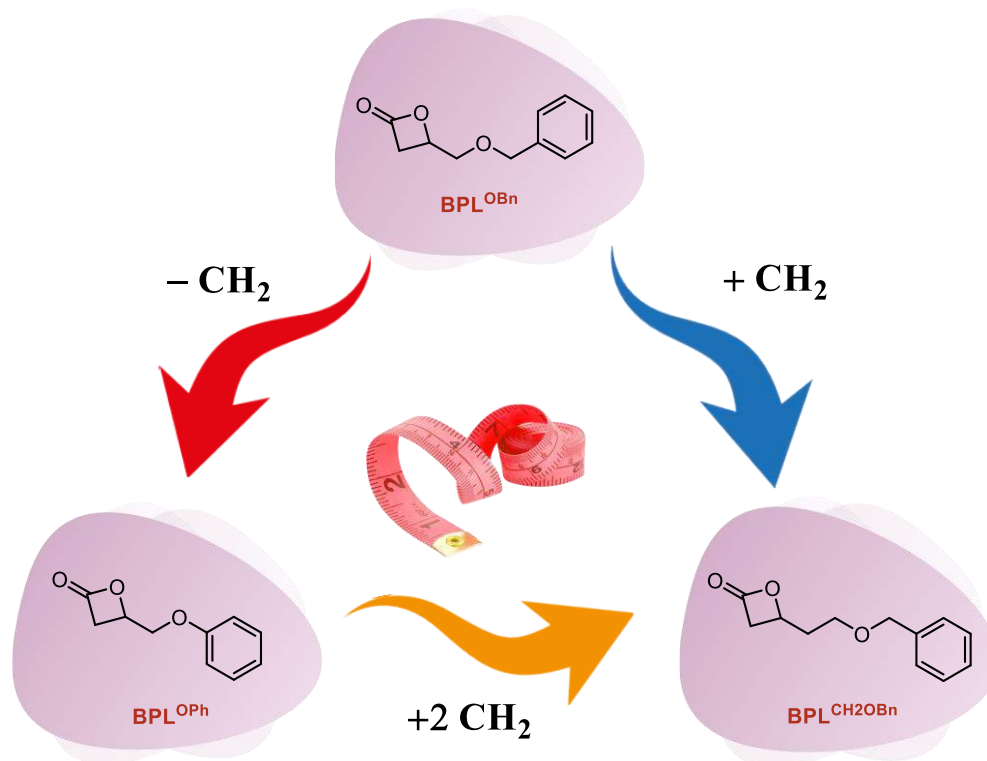


**Figure 4. 6** – Illustration of the difference in the chain length of the side chain of BPL<sup>OBn/OPh/CH<sub>2</sub>OBn</sup>.

### 2.1.1. ROP of *rac*-BPL<sup>OPh</sup>

To our knowledge, the ring-opening homopolymerization of *rac*-BPL<sup>OPh</sup> has never been described. Only the random copolymerization of *rac*-BPL<sup>OPh</sup> with *rac*-BPL<sup>Me</sup> via anionic simultaneous ring-opening copolymerization using the metal-free tetrabutylammonium acetate initiator was established, to next study the resulting oligomers ( $M_{n,\text{SEC}} = 1200 \text{ g mol}^{-1}$ ) by mass spectrometry.<sup>[12]</sup>

The ROP of *rac*-BPL<sup>OPh</sup> was investigated, at room temperature in toluene, using 1 mol% of the diamino-bis(phenolate)yttrium catalytic systems  $\text{Y}\{\text{ONNO}^{\text{R1,R2}}\}/(i\text{PrOH})$  (**2a-d**/(*i*PrOH)) (Scheme 4. 4). All the characteristic data of the obtained PBPL<sup>OPh</sup>s from the latter polymerization are gathered in Table 4. 2. Yttrium catalyst systems based on ligands with uncrowded methyl or chloro *ortho*-phenolate substituents (**2c-d**; Table 4. 2 – entries 1-4), in the presence of *i*PrOH, proved less active than the hindered cumyl and *tert*-butyl substituents (**2a-b**; Table 4. 2 – entries 5-12). The Me-substituted catalyst systems **2c**/(*i*PrOH) could achieve complete conversion of ca. 60 monomer equiv. in four hours with  $\text{TOF}_{2c} = 14.25 \text{ h}^{-1}$  (Table 4. 2 – entry 4), unlike the Cl-substituted **2d** which hardly proceeded to complete monomer consumption reaching only 45% conversion after 50 h with  $\text{TOF}_{2d} = 0.65 \text{ h}^{-1}$  (Table 4. 2 – entry



2). On the other hand, yttrium catalyst systems with ancillary ligands bearing bulky substituents ('Bu, cumyl, **2a-b**/(*i*PrOH)) revealed quite active for the ROP of *rac*-BPL<sup>OPh</sup>. Nearly quantitative conversion of ca. 100–120 equivalents of *rac*-BPL<sup>OPh</sup> by **2a-b** was reached within 5–15 min with TOF<sub>2b</sub> > 883 h<sup>-1</sup> and TOF<sub>2a</sub> > 1200 h<sup>-1</sup> (Table 4. 2 – entries 7,12). Furthermore, the highest TOF values obtained for the ROP of *rac*-BPL<sup>OPh</sup> (TOF<sub>2b(ca. 500)</sub> > 2000 h<sup>-1</sup>, Table 4. 2 – entry 9) is significantly higher than those reported for the closely related *rac*-BPL<sup>OBn/OAll/OMe</sup> (TOF<sub>(ca. 100)</sub> = 54–100 h<sup>-1</sup>)<sup>[10c, 11]</sup> and lower than *rac*-MLA<sup>Bn/All/Me</sup> (TOF<sub>(ca. 100)</sub> > 3000 h<sup>-1</sup>).<sup>[10]</sup>

**Table 4. 2** – Characteristics of the PBPL<sup>OPh</sup> synthesized by ROP of *rac*-BPL<sup>OPh</sup> mediated by **2a-d**/(*i*PrOH) catalytic systems in toluene at room temperature.

Entry	Cat.	[BPL <sup>OPh</sup> ] <sub>0</sub> / [2] <sub>0</sub> /[ <i>i</i> PrOH] <sub>0</sub> <sup>a</sup>	Time <sup>b</sup> (min)	Conv. <sup>c</sup> (%)	<i>M</i> <sub>n,theo</sub> <sup>d</sup> (g.mol <sup>-1</sup> )	<i>M</i> <sub>n,NMR</sub> <sup>e</sup> (g.mol <sup>-1</sup> )	<i>M</i> <sub>n,SEC</sub> <sup>f</sup> (g.mol <sup>-1</sup> )	<i>D</i> <sub>M</sub> <sup>f</sup>	<i>P</i> <sub>r</sub> <sup>g</sup>	<i>T</i> <sub>g</sub> <sup>h</sup> (°C)
1	<b>2d</b>	30:1:1	30 h	95	5100	5000	5200	1.14	0.77	22
2 <sup>i</sup>	<b>2d</b>	60:1:1	50 h	54	5800	5400	6200	1.15	0.75	21
3	<b>2c</b>	30:1:1	120	100	5400	5200	6200	1.18	0.76	<i>nd</i> <sup>j</sup>
4 <sup>i</sup>	<b>2c</b>	60:1:1	240	95	10 200	10 000	11 100	1.13	0.79	30
5	<b>2b</b>	20:1:1	120	100	3600	3200	4100	1.21	0.84	<i>nd</i> <sup>j</sup>
6 <sup>i</sup>	<b>2b</b>	60:1:1	8	100	10 700	10 600	12 200	1.14	0.86	37
7	<b>2b</b>	120:1:1	8	98	21 000	23 000	25 600	1.06	0.86	37
8	<b>2b</b>	250:1:1	15	100	44 600	44 100	51 200	1.16	0.87	38
9	<b>2b</b>	500:1:1	15	92	81 900	80 500	95 000	1.20	0.86	40
10	<b>2a</b>	28:1:1	120	100	5000	4700	5400	1.20	0.81	<i>nd</i> <sup>j</sup>
11 <sup>i</sup>	<b>2a</b>	60:1:1	30	100	10 700	10 000	12 200	1.15	0.84	38
12	<b>2a</b>	100:1:1	5	100	17 900	17 800	19 000	1.11	0.83	40
13 <sup>k</sup>	<b>2b</b>	60:1:1	60	100	10 700	10 500	11 700	1.10	<0.05	36

<sup>a</sup> Reactions performed with [BPL<sup>OPh</sup>]<sub>0</sub> = 1.0 M. <sup>b</sup> Reaction time was not necessarily optimized. <sup>c</sup> Conversion of BPL<sup>OPh</sup> as determined by <sup>1</sup>H NMR analysis of the crude reaction mixture. <sup>d</sup> Molar mass calculated according to *M*<sub>n,theo</sub> = ([BPL<sup>OPh</sup>]<sub>0</sub>/[2]<sub>0</sub> × conv.BPL<sup>OPh</sup>) × *M*<sub>BPL(OPh)</sub> + *M*<sub>*i*PrOH</sub>, with *M*<sub>BPL(OPh)</sub> = 178 g.mol<sup>-1</sup>, *M*<sub>*i*PrOH</sub> = 60 g.mol<sup>-1</sup>. <sup>e</sup> Molar mass determined by <sup>1</sup>H NMR analysis of the isolated polymer, from the resonances of the terminal O<sup>*i*</sup>Pr group (refer to Experimental section). <sup>f</sup> Number-average molar mass and dispersity (*M*<sub>w</sub>/*M*<sub>n</sub>) determined by SEC analysis in THF at 30 °C vs. polystyrene standards. <sup>g</sup> *P*<sub>r</sub> is the probability of *racemic* linkages between BPL<sup>OPh</sup> units as determined by <sup>13</sup>C{<sup>1</sup>H} NMR analysis of the isolated PBPL<sup>OPh</sup>s. <sup>h</sup> Glass transition temperature as determined by DSC. <sup>i</sup> Refer to the kinetic study (Figure 4. 20); <sup>j</sup> Not determined; <sup>k</sup> ROP of enantiopure (*S*)-BPL<sup>OPh</sup>.

The PBPL<sup>OPh</sup> isolated showed, regardless of the catalytic system used, a quite good agreement between the theoretical molar mass values (*M*<sub>n,theo</sub>) and the experimental values determined by NMR (*M*<sub>n,NMR</sub>) and by SEC (*M*<sub>n,SEC</sub>) analyses. The latter experimental molar mass values of the PBPL<sup>OPh</sup> increased linearly with the BPL<sup>OPh</sup> monomer loading up to a degree of polymerization of ca. 500, as illustrated for the ROP of *rac*-BPL<sup>OPh</sup> mediated by **2b**/(*i*PrOH) (1:1) catalytic system (Figure 4. 7). The dispersities of all PBPL<sup>OPh</sup> remained narrow (*D*<sub>M</sub> = 1.06–1.21), supporting a relatively fast initiation (compared to propagation) along with some limited undesirable side reactions (classically inter- and intra-molecular transesterification reactions (i.e. reshuffling and backbiting, respectively)). These characteristics highlighted the

controlled feature and to some extent the livingness of the ROP of the BPL<sup>OPh</sup> mediated by **2a–1d**/(*i*PrOH) catalytic systems.

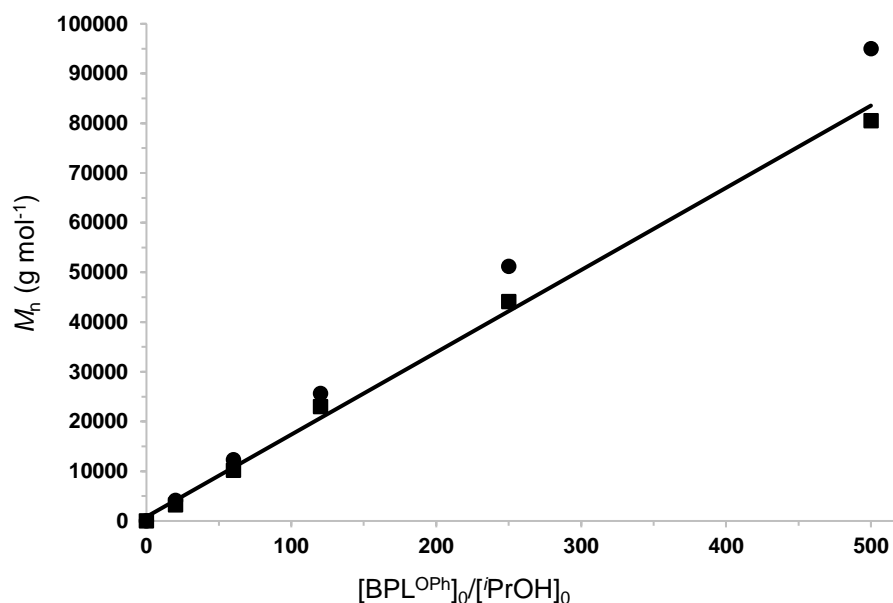


**Figure 4. 7** – Variation of  $M_{n,NMR}$  ■,  $M_{n,SEC}$  ●, and  $M_{n,theo}$  (solid line) values of PBPL<sup>OPh</sup> synthesized from the ROP of *rac*-BPL<sup>OPh</sup> mediated by **2b**/(*i*PrOH) (1:1) catalytic system as a function of the BPL<sup>OPh</sup> monomer loading (Table 4. 2 – entries 5–9).

The PBPL<sup>OPh</sup> were unambiguously characterized by 1D and 2D NMR spectroscopy (Figure 4. 8 and appendix 17,18). The <sup>1</sup>H and J-MOD NMR spectra (Figure 4. 8) clearly displayed the characteristic signals corresponding to both the BPL<sup>OPh</sup> repeating units, especially the backbone methine and methylene signals, and the typical pendant CH<sub>2</sub>OPh moieties, respectively. The distinctive isopropoxycarbonyl chain-end group resonances were also clearly observed ( $\delta$  (ppm): ca. 4.95 (CH<sub>3</sub>)<sub>2</sub>CHO–, ca. 1.19 (CH<sub>3</sub>)<sub>2</sub>CHO–).

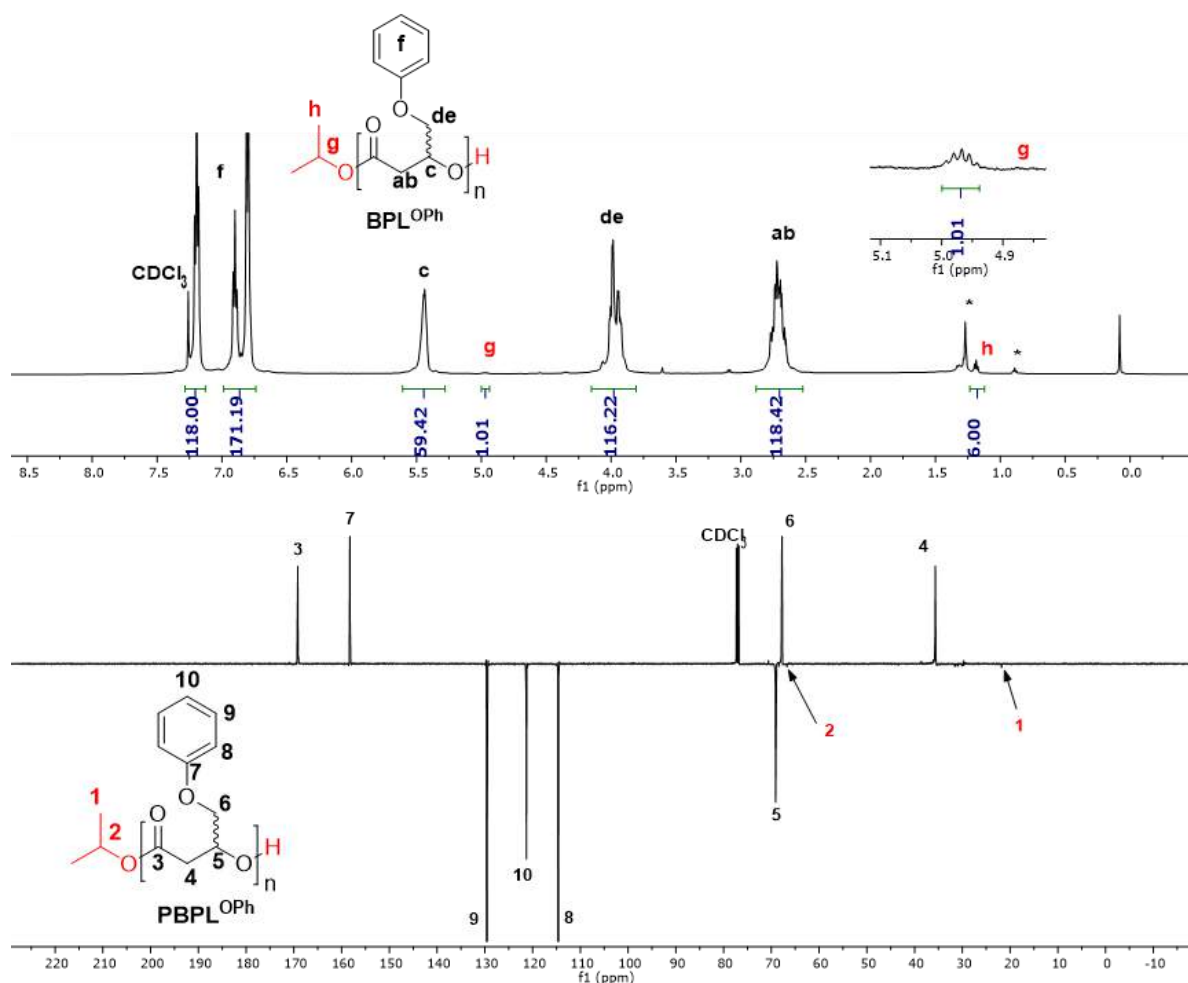


**Figure 4. 8** – <sup>1</sup>H NMR (500 MHz, CDCl<sub>3</sub>, 25 °C) (top) and J-MOD (125 MHz, CDCl<sub>3</sub>, 25 °C) (bottom) spectra of syndiotactic PBPL<sup>OPh</sup> prepared from the ROP of *rac*-BPL<sup>OPh</sup> mediated by complex **2b** in the presence of *i*PrOH and precipitated twice in cold pentane (Table 4. 2, entry 6) (\*: residual grease).

Further support of the macromolecular structure of the PBPL<sup>OPh</sup> was gained from MALDI-ToF mass spectrometry analyses (Figure 4. 9). The spectra recorded for low molar mass samples of PBPL<sup>OPh</sup> prepared from **2b**/*i*PrOH catalytic systems, showed a single population of macromolecules having a repeating unit of *m/z* 178, corresponding to  $\alpha$ -isopropoxy, $\omega$ -hydroxyl telechelic PBPL<sup>OPh</sup> chains ionized by Na<sup>+</sup>. This was unequivocally confirmed by the close match with the corresponding isotopic simulations, as illustrated for [(CH<sub>3</sub>)<sub>2</sub>CHO(COCH<sub>2</sub>CH(CH<sub>2</sub>OC<sub>6</sub>H<sub>5</sub>)O)<sub>*n*</sub>H]·Na<sup>+</sup> with, for example, calculated *m/z* 1507.551 versus found *m/z* 1507.548 for *n* = 8.

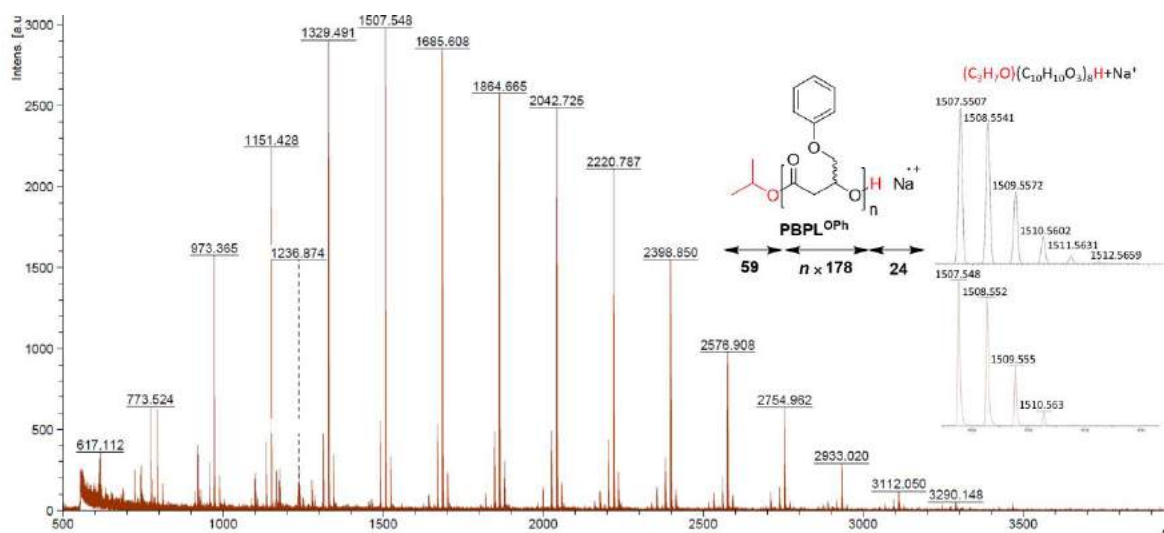


**Figure 4. 9** – MALDI-ToF MS (DCTB matrix, ionized by  $\text{Na}^+$ ) of  $\text{PBPL}^{\text{OPh}}$  precipitated twice in cold pentane (Table 4. 2, entry 5). Right zoomed regions correspond to the simulated (top) and experimental (bottom) spectra.

Regarding the tacticity of the recovered  $\text{PBPL}^{\text{OPh}}$ , it was assessed from  $^{13}\text{C}$  NMR spectra analyses upon comparison with the corresponding spectra of the isotactic  $\text{PBPL}^{\text{OPh}}$  synthesized from the enantiopure (*S*)- $\text{BPL}^{\text{OPh}}$  (Table 4. 2, entry 13). Interestingly, just by removing one of the methylene (Figure 4. 5 –  $\text{C}_\text{B}$ ) from the exocyclic side-chain of  $\text{BPL}^{\text{OBn}}$  to get  $\text{BPL}^{\text{OPh}}$ , the stereocontrol with the same catalysts framework **2a-d** (*i*PrOH) was altered (Scheme 4. 3). In the case of  $\text{BPL}^{\text{OPh}}$ , only syndiotactic enriched  $\text{PBPL}^{\text{OPh}}$  were produced whatever the  $\text{R}^1$  *ortho*-substituents on the ligands, in line with a CEM mechanism being at play (Figure 4. 10). Yet still higher syndio-enrichment was obtained from more crowded ligands **2a-b** ( $P_r = 0.84\text{--}0.86$ ) and less enrichment was from smaller ligand substituents **2c-d** ( $P_r = 0.75\text{--}0.79$ ). This is similar to what was previously obtained with  $\text{MLA}^{\text{FG}}$ s but with a different trend, where smaller substitutes (Me, Cl) lead to a higher syndio-enrichment (Scheme 4. 2). The results thus further highlight the strong dependence of the resulting PHA's stereocontrolled microstructure on the couple formed by the functional  $\beta$ -lactone and the yttrium catalyst, and more specifically on the chemical nature of the  $\beta$ -lactone side-arm and of the substituents on the metal surrounding ancillary.

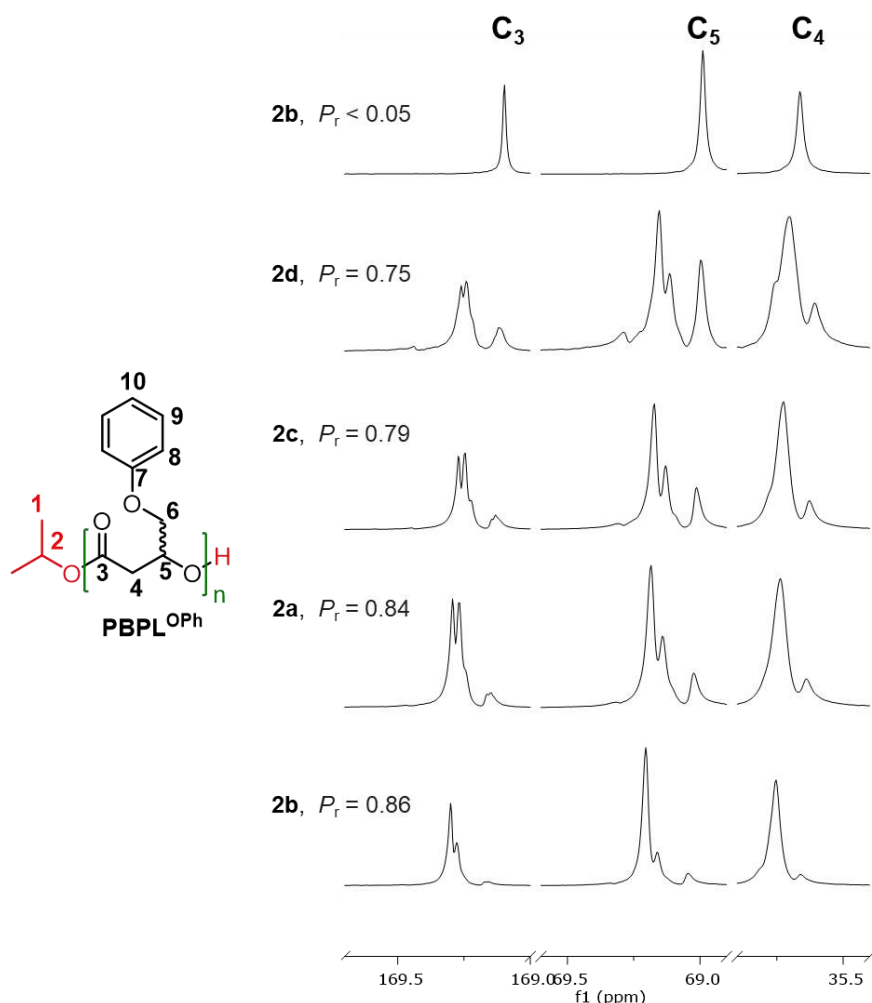


**Figure 4. 10** – Regions of the  $^{13}\text{C}\{^1\text{H}\}$  NMR spectra (125 MHz,  $\text{CDCl}_3$ , 23 °C) of PBPL<sup>OPh</sup> prepared by ROP of *rac*-BPL<sup>OPh</sup>, except for the top spectra: of enantiopure (*S*)-BPL<sup>OPh</sup> (Table 4. 2, entry 13), mediated by **2a**, **2b**, **2c**, or **2d**/*i*PrOH (Table 4. 2, entries 2,4,6,11); details for  $P_r$  calculations by  $^{13}\text{C}$  NMR check appendix 19.

The thermal behavior of the synthesized PBPL<sup>OPh</sup>s was analysed by differential scanning calorimetry (DSC). Thermograms only showed the presence of a glass transition temperature ( $T_g$ ); no melting temperature was observed below 200 °C, suggesting amorphous polyesters (Figure 4. 11, Appendix 20-22). This lack of crystallinity was similarly reported for the closely related syndiotactic or isotactic PBPL<sup>OBn</sup>,<sup>[11]</sup> PMLA<sup>Bn</sup>,<sup>[13]</sup> PDL<sup>Bn</sup> (refer to chapter 1).<sup>[14]</sup> The PBPL<sup>OPh</sup> displayed positive  $T_g$  values going from 21 to 40 °C (Table 4. 2). Typically, for PBPL<sup>OPh</sup>s with  $P_r = 0.75$ –0.79, the  $T_g$  values varied from 21 to 30 °C (Figure 4. 11 – left), while a higher syndio-enrichment with  $P_r = 0.83$ –0.87 or an almost purely isotactic sample ( $P_r < 0.05$ ) resulted in higher  $T_g$  values ranging from 36 to 40 °C (Figure 4. 11 – right). The latter high  $T_g$  values (36 to 40 °C) are, to our knowledge, considered to be the highest ones for functional PHAs, similarly to those observed in PMLA<sup>Bn</sup> ( $T_g = 45$  °C)<sup>[13]</sup> and PDL<sup>Bn</sup> ( $T_g =$

36–43 °C).<sup>[14]</sup> This can be explained by the stiffness of the aromatic group and the presence of  $\pi$ - $\pi$  stacking secondary interactions that lead to a better packing of the polymer.<sup>[15]</sup>

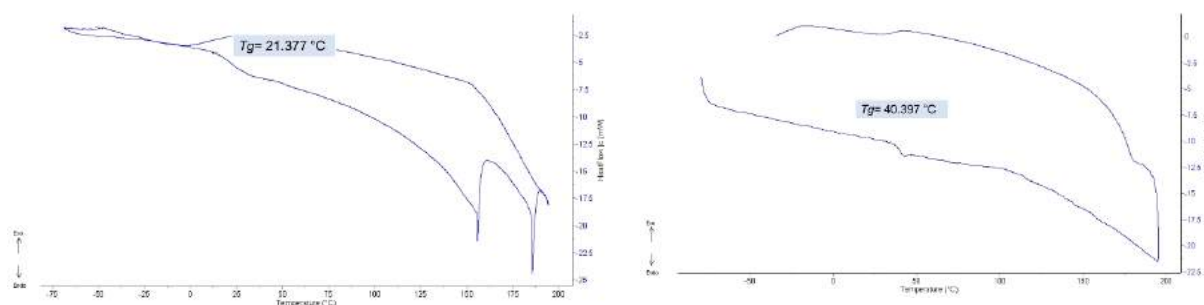


**Figure 4. 11** – DSC thermogram (heating rate of 10 °Cmin<sup>-1</sup>, second heating cycle, from –80 to 200 °C) of: (left) syndiotactic PBPL<sup>OPh</sup> ( $P_r = 0.75$ ) synthesized by ROP of *rac*-BPL<sup>OPh</sup> with **2d**/*i*PrOH) (Table 4. 2, entry 2) - The artefact observed (ca 160° C, 190° C) arise from the manual cooling; (right) syndiotactic PBPL<sup>OPh</sup> ( $P_r = 0.83$ ) synthesized by ROP of *rac*-BPL<sup>OPh</sup> with **2b**/*i*PrOH) (Table 4. 2, entry 12).

Thermal gravimetry analysis (TGA) was also performed for PBPL<sup>OPh</sup> samples, they were found to thermally degrade at  $T_{d\text{onset}}^{\text{PBPL(OPh)}} = 272.18$  °C (Figure 4. 12). To the best of our knowledge, this value represents one the highest decomposition temperature reported to date for homopolymers of PHAs family.

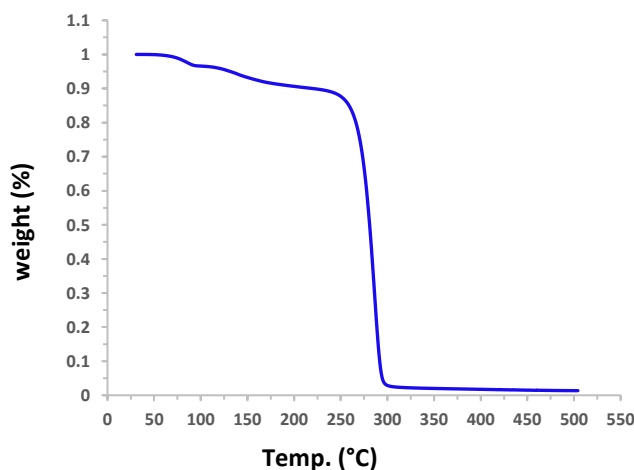


**Figure 4. 12** – TGA thermograms of syndiotactic PBPL<sup>OPh</sup> (Table 4. 2, entry 7).

### 2.1.2. ROP of *rac*-BPL<sup>CH2OBn</sup>

The ROP of BPL<sup>CH2OBn</sup> was achieved by my lab mate Hui LI; thus, the results are presented briefly just for the sake of comparison with BPL<sup>OBn</sup> and BPL<sup>OPh</sup>. The major results are depicted in Table 4. 3 and Figure 4. 13, which are reported in reference <sup>[16]</sup>.

**Table 4. 3** – Characteristics of the PBPL<sup>CH<sub>2</sub>OBn</sup> synthesized by ROP of *rac*-BPL<sup>CH<sub>2</sub>OBn</sup> mediated by **2a-d**/<sup>*i*</sup>PrOH catalytic systems in toluene at room temperature.

Entry	Cat.	[BPL <sup>CH<sub>2</sub>OBn</sup> ] <sub>0</sub> / [ <b>2</b> ] <sub>0</sub> / <sup><i>i</i></sup> PrOH] <sub>0</sub> <sup>a</sup>	Time <sup>b</sup> (min)	Conv. <sup>c</sup> (%)	<i>M</i> <sub>n,theo</sub> <sup>d</sup> (g.mol <sup>-1</sup> )	<i>M</i> <sub>n,NMR</sub> <sup>e</sup> (g.mol <sup>-1</sup> )	<i>M</i> <sub>n,SEC</sub> <sup>f</sup> (g.mol <sup>-1</sup> )	<i>D</i> <sub>M</sub> <sup>f</sup>	<i>P</i> <sub>r</sub> <sup>g</sup>	<i>T</i> <sub>g</sub> <sup>h</sup> (°C)
1	<b>2d</b>	25:1:1	14 h	78	4100	5200	4200	1.15	0.49	-13
2	<b>2c</b>	50:1:1	9 h	67	7000	8600	7000	1.23	0.49	-11
3	<b>2b</b>	25:1:1	5	99	5200	6400	6700	1.12	0.85	-11
4	<b>2a</b>	25:1:1	3	99	5200	5400	4400	1.09	0.77	-12
5 <sup>i</sup>	<b>2b</b>	50:1:1	10	99	10 300	9100	8400	1.15	<0.05	-13

<sup>a</sup> Reactions performed with [BPL<sup>CH<sub>2</sub>OBn</sup>]<sub>0</sub> = 1.0 M. <sup>b</sup> Reaction time was not necessarily optimized. <sup>c</sup> Conversion of BPL<sup>CH<sub>2</sub>OBn</sup> as determined by <sup>1</sup>H NMR analysis of the crude reaction mixture. <sup>d</sup> Molar mass calculated according to  $M_{n,theo} = ([BPL^{CH_2OBn}]_0/[2]_0 \times conv. BPL^{CH_2OBn}) \times M_{BPL^{CH_2OBn}} + M_{iPrOH}$ , with  $M_{BPL^{CH_2OBn}} = 206$  g.mol<sup>-1</sup>,  $M_{iPrOH} = 60$  g.mol<sup>-1</sup>. <sup>e</sup> Molar mass determined by <sup>1</sup>H NMR analysis of the isolated polymer, from the resonances of the terminal O<sup>*i*</sup>Pr group. <sup>f</sup> Number-average molar mass and dispersity (*M*<sub>w</sub>/*M*<sub>n</sub>) determined by SEC analysis in THF at 30 °C vs. polystyrene standards. <sup>g</sup> *P*<sub>r</sub> is the probability of *racemic* linkages between BPL<sup>CH<sub>2</sub>OBn</sup> units as determined by <sup>13</sup>C{<sup>1</sup>H} NMR analysis of the isolated PBPL<sup>CH<sub>2</sub>OBn</sup>s. <sup>h</sup> Glass transition temperature as determined by DSC; <sup>i</sup> ROP of enantiopure (*R*)-BPL<sup>CH<sub>2</sub>OBn</sup>.

Getting directly to the point, the recovered PBPL<sup>CH<sub>2</sub>OBn</sup> revealed to be either syndio-enriched or atactic, depending on the yttrium complex used (**2a-d**). Similar to BPL<sup>OBn</sup> and BPL<sup>OPh</sup> upon using crowded ligand substituents (cumyl and <sup>*t*</sup>Bu, **2a-b**), highly syndio-enriched polymers were obtained (*P*<sub>r</sub> = 0.77–0.85). As with BPL<sup>OBn</sup> but unlike with BPL<sup>OPh</sup>, when using non-crowded substituents (Me, **2c**), atactic PBPL<sup>CH<sub>2</sub>OBn</sup> (*P*<sub>r</sub> = 0.49) was observed. More strikingly, neither isotactic (as observed with BPL<sup>OBn</sup>) or syndiotactic (as obtained with BPL<sup>OPh</sup>) PBPL<sup>CH<sub>2</sub>OBn</sup> was produced from halogenated substituents (Cl, **2d**), where *P*<sub>r</sub> = 0.49 (Figure 4. 13).

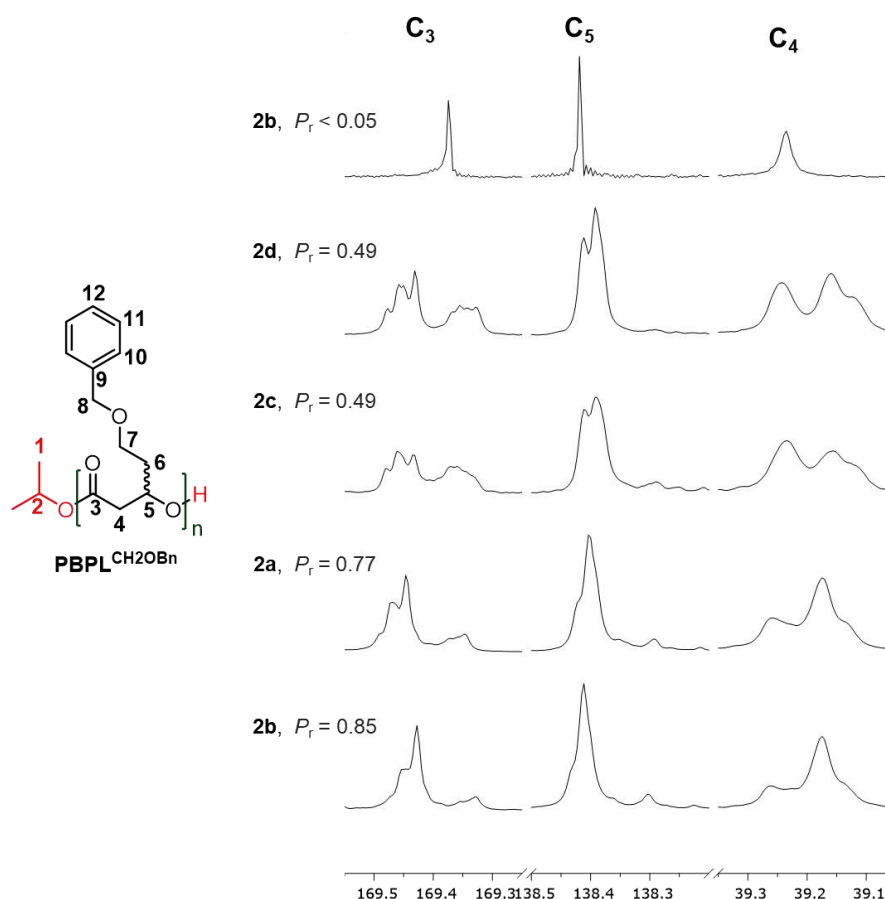


**Figure 4. 13** – Regions of the  $^{13}\text{C}\{^1\text{H}\}$  NMR spectra (125 MHz,  $\text{CDCl}_3$ , 23 °C) of  $\text{PBPL}^{\text{CH}_2\text{OBn}}$  prepared by ROP of  $\text{rac-BPL}^{\text{CH}_2\text{OBn}}$ , except for the top spectra: of enantiopure (*R*)- $\text{BPL}^{\text{CH}_2\text{OBn}}$  (Table 4. 3, entry 5), mediated by **2a**, **2b**, **2c**, or **2d**/ $i$ PrOH (Table 4. 3, entries 1–4).

It is worthy to mention that the  $T_g$  values enormously varies from  $\text{PBPL}^{\text{OPh}}$  to  $\text{PBPL}^{\text{CH}_2\text{OBn}}$ . Where  $\text{PBPL}^{\text{OPh}}$  has high positive  $T_g$ s (*vide supra*),  $\text{PBPL}^{\text{CH}_2\text{OBn}}$  has a negative value ( $T_g = -13$  to  $-11$ ) as was detected by DSC (Table 4. 3). This could be due the longer side chain of  $\text{PBPL}^{\text{CH}_2\text{OBn}}$ , hence leading to higher flexibility and then lower  $T_g$ s.<sup>[15]</sup>

### 2.1.3. ROP of $\text{rac-BPL}^{\text{SPh}}$

To further examine the effect of the exocyclic oxygen on the stereoselective ROP, oxygen was replaced by sulphur which is softer and bigger. As far as we are aware of, it is the first time a chemical synthetic polymerization of a PHA featuring a sulphur heteroatom within the exocyclic side-arm ( $\text{PBPL}^{\text{SPh}}$ ), was prepared. However, PHAs bearing taller sulphur side-chains (e.g.,  $\text{PBPL}^{\text{CH}_2\text{SPh}}$ ,  $\text{PBPL}^{(\text{CH}_2)_2\text{SPh}}$ ,<sup>[17]</sup>  $\text{PBPL}^{\text{CH}_2\text{S}(\text{CH}_2)_3}$ ,  $\text{PBPL}^{(\text{CH}_2)_2\text{S}(\text{CH}_2)_3}$ )<sup>[18]</sup> were reported to be produced from genetic engineering as atactic polymers. It has been reported that, polyesters containing sulphur have outstanding performances such as being responsiveness to oxidants, flame retardants, advanced optical (i.e. lenses and optical fibres) and electrical



characteristics, fuel cell materials and also in providing new possibilities for chemical modifications (oxidation to sulfonate promoting for more tuning in properties).<sup>[19]</sup>

The ROP of *rac*-BPL<sup>SPh</sup> was explored, at room temperature in toluene, using 1mol% of the diamino-bis(phenolate)yttrium catalytic systems Y{ONNO<sup>R1,R2</sup>}/(*i*PrOH) (**2a-d**/(*i*PrOH)) (Scheme 4. 4). All the characteristic data of the obtained PBPL<sup>SPh</sup>s from the latter polymerization are gathered in Table 4. 4. Once again, yttrium catalyst systems based on ligands with uncrowded methyl or chloro *ortho*-phenolate substituents (**2c-d**; Table 4. 4 – entries 1-5), in the presence of *i*PrOH, proved less active than the hindered cumyl and *tert*-butyl substituted ones (**2a-b**; Table 4. 2 – entries 6-13). The Me-substituted catalyst systems **2c**/(*i*PrOH) could achieve complete conversion of ca. 60 monomer equiv. in eight hours with TOF<sub>2c</sub> = 7.43 h<sup>-1</sup> (Table 4. 4 – entry 5), unlike the Cl-substituted one **2d** which hardly proceeded to complete monomer consumption reaching 48% conversion after 4 days with TOF<sub>2d</sub> = 0.03 h<sup>-1</sup> (Table 4. 4 – entry 5). Similar to *rac*-BPL<sup>OPh</sup>, yttrium catalyst systems with ancillary ligands bearing bulky substituents (*t*Bu, cumyl, **2a-b**/(*i*PrOH)) revealed quite active for the ROP of *rac*-BPL<sup>SPh</sup>. Nearly quantitative conversion of ca. 120 equivalents of *rac*-BPL<sup>SPh</sup> by **2a-b** was reached within 15 min with TOF<sub>2a-b</sub> > 480 h<sup>-1</sup> (Table 4. 4 – entries 8,13). The highest TOF values obtained for the ROP of *rac*-BPL<sup>SPh</sup> (TOF<sub>2b(ca. 500)</sub> > 225 h<sup>-1</sup>, Table 4. 4 – entry 10) is considerably lower than those reported for the *rac*-BPL<sup>OPh</sup> (TOF<sub>2a(ca. 500)</sub> > 2000 h<sup>-1</sup>, *vide supra*). This is most likely arising from the relative instability of BPL<sup>SPh</sup> at 20 °C, the secondary products formed (refer to Chapter 2, Figure 2. 12) presumably impeding the efficiency of the catalyst, hence altering the polymerization rate.

**Table 4. 4** – Characteristics of the PBPL<sup>SPh</sup> synthesized by ROP of *rac*-BPL<sup>SPh</sup> mediated by **2a-d**/(*i*PrOH) catalytic systems in toluene at room temperature.

Entry	Cat.	[BPL <sup>SPh</sup> ] <sub>0</sub> / [ <b>2</b> ] <sub>0</sub> /[ <i>i</i> PrOH] <sub>0</sub> <sup>a</sup>	Time <sup>b</sup> (min)	Conv. <sup>c</sup> (%)	<i>M</i> <sub>n,theo</sub> <sup>d</sup> (g.mol <sup>-1</sup> )	<i>M</i> <sub>n,NMR</sub> <sup>e</sup> (g.mol <sup>-1</sup> )	<i>M</i> <sub>n,SEC</sub> <sup>f</sup> (g.mol <sup>-1</sup> )	<i>D</i> <sub>M</sub> <sup>f</sup>	<i>P</i> <sub>r</sub> <sup>g</sup>	<i>T</i> <sub>g</sub> <sup>h</sup> (°C)
1	<b>2d</b>	20:1:1	240	38	1500	1400	1700	1.08	<i>nd</i> <sup>j</sup>	<i>nd</i> <sup>j</sup>
2	<b>2d</b>	30:1:1	60 h	57	3400	3400	3600	1.14	0.73	9
3 <sup>i</sup>	<b>2d</b>	60:1:1	96 h	48	5600	5100	6400	1.17	0.74	9
4	<b>2c</b>	30:1:1	240	100	5900	5800	6600	1.14	0.74	9
5	<b>2c</b>	60:1:1	480	99	11 600	11 300	13 900	1.21	0.76	8
6	<b>2b</b>	40:1:1	240	100	7800	7400	8900	1.19	0.83	<i>nd</i> <sup>j</sup>
7 <sup>i</sup>	<b>2b</b>	80:1:1	60	100	15 600	15 200	17 900	1.15	0.87	13
8	<b>2b</b>	120:1:1	15	100	23 200	23 300	25 700	1.07	0.86	14
9	<b>2b</b>	250:1:1	60	95	46 100	48 300	51 400	1.15	0.87	14
10	<b>2b</b>	500:1:1	120	90	87 400	86 400	96 700	1.17	0.86	12
11	<b>2a</b>	20:1:1	60	100	3900	3400	4400	1.19	0.85	<i>nd</i> <sup>j</sup>
12 <sup>i</sup>	<b>2a</b>	60:1:1	60	100	11 700	11 300	13 300	1.12	0.85	13

13	<b>2a</b>	120:1:1	15	95	22 200	23 200	24 600	1.14	0.84	12
14	<b>2b</b>	60:1:1	60	100	11 700	11 500	12 800	1.13	<0.05	13

<sup>a</sup> Reactions performed with  $[\text{BPL}^{\text{SPh}}]_0 = 1.0 \text{ M}$ . <sup>b</sup> Reaction time was not necessarily optimized. <sup>c</sup> Conversion of  $\text{BPL}^{\text{SPh}}$  as determined by  $^1\text{H}$  NMR analysis of the crude reaction mixture. <sup>d</sup> Molar mass calculated according to  $M_{n,\text{theo}} = ([\text{BPL}^{\text{SPh}}]_0/[\mathbf{2}]_0 \times \text{conv. BPL}^{\text{SPh}}) \times M_{\text{BPL}^{\text{SPh}}} + M_{i\text{PrOH}}$ , with  $M_{\text{BPL}^{\text{SPh}}} = 194 \text{ g.mol}^{-1}$ ,  $M_{i\text{PrOH}} = 60 \text{ g.mol}^{-1}$ . <sup>e</sup> Molar mass determined by  $^1\text{H}$  NMR analysis of the isolated polymer, from the resonances of the terminal O<sup>i</sup>Pr group (refer to Experimental section). <sup>f</sup> Number-average molar mass and dispersity ( $M_w/M_n$ ) determined by SEC analysis in THF at 30 °C vs. polystyrene standards. <sup>g</sup>  $P_r$  is the probability of *racemic* linkages between  $\text{BPL}^{\text{SPh}}$  units as determined by  $^{13}\text{C}\{^1\text{H}\}$  NMR analysis of the isolated  $\text{PBPL}^{\text{SPh}}$ s. <sup>h</sup> Glass transition temperature as determined by DSC. <sup>i</sup> Refer to the kinetic study (Figure 4. 20) <sup>j</sup> Not determined; <sup>k</sup> ROP of enantiopure (*S*)- $\text{BPL}^{\text{SPh}}$ .

The  $\text{PBPL}^{\text{SPh}}$  isolated showed, regardless of the catalytic system used, a quite good agreement between molar mass values ( $M_{n,\text{theo}}$ ,  $M_{n,\text{NMR}}$ ,  $M_{n,\text{SEC}}$ ), with narrow dispersities ( $\mathcal{D}_M = 1.07\text{--}1.21$ ). In fact, the experimental molar mass values of the  $\text{PBPL}^{\text{SPh}}$  increased linearly with the  $\text{BPL}^{\text{SPh}}$  monomer loading up to a degree of polymerization of ca. 500, as illustrated for the ROP of  $\text{BPL}^{\text{SPh}}$  mediated by **2b**/*i*PrOH) (1:1) catalytic system (Figure 4. 14), confirming the control feature of ROP.

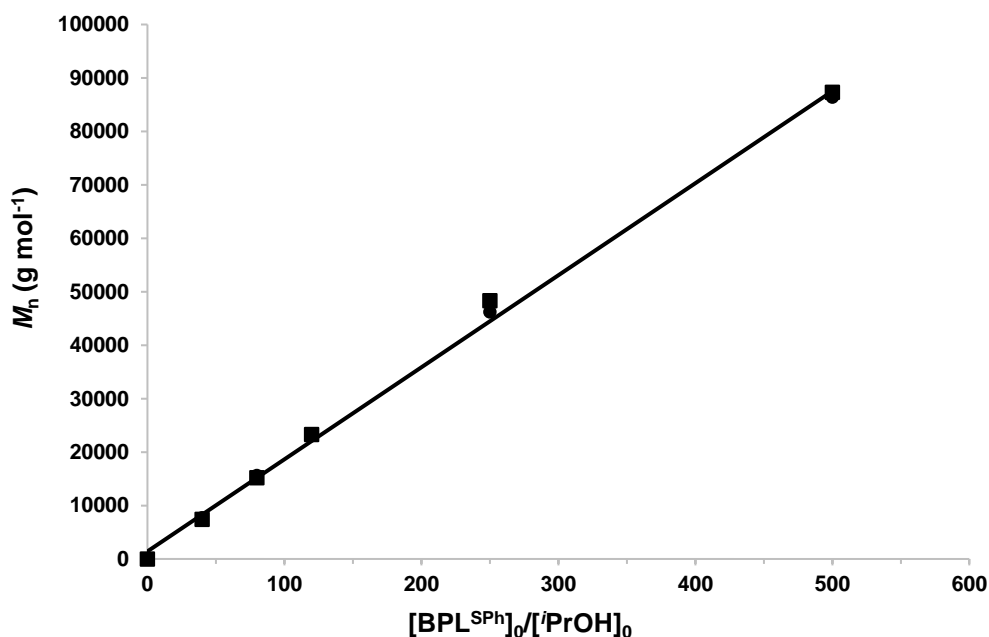


**Figure 4. 14** – Variation of  $M_{n,\text{NMR}}$  ■,  $M_{n,\text{SEC}}$  ●, and  $M_{n,\text{theo}}$  (solid line) values of  $\text{PBPL}^{\text{SPh}}$  synthesized from the ROP of *rac*- $\text{BPL}^{\text{SPh}}$  mediated by **2b**/*i*PrOH) (1:1) catalytic system as a function of the  $\text{BPL}^{\text{SPh}}$  monomer loading (Table 4. 4 – entries 6-10).

Alike  $\text{PBPL}^{\text{OPh}}$ ,  $^1\text{H}$  and J-MOD spectra of  $\text{PBPL}^{\text{SPh}}$  (Figure 4. 15) clearly showed the isopropoxycarbonyl chain-end group ( $\delta$  (ppm): ca. 4.95  $(\text{CH}_3)_2\text{CHO}$ –, ca. 1.19  $(\text{CH}_3)_2\text{CHO}$ –. Also, the signals for  $\text{BPL}^{\text{SPh}}$  repeating units including the methine and methylene, were both observed. For the corresponding 2D COSY and HMBC NMR spectra refer to Appendix 23 and Appendix 24.

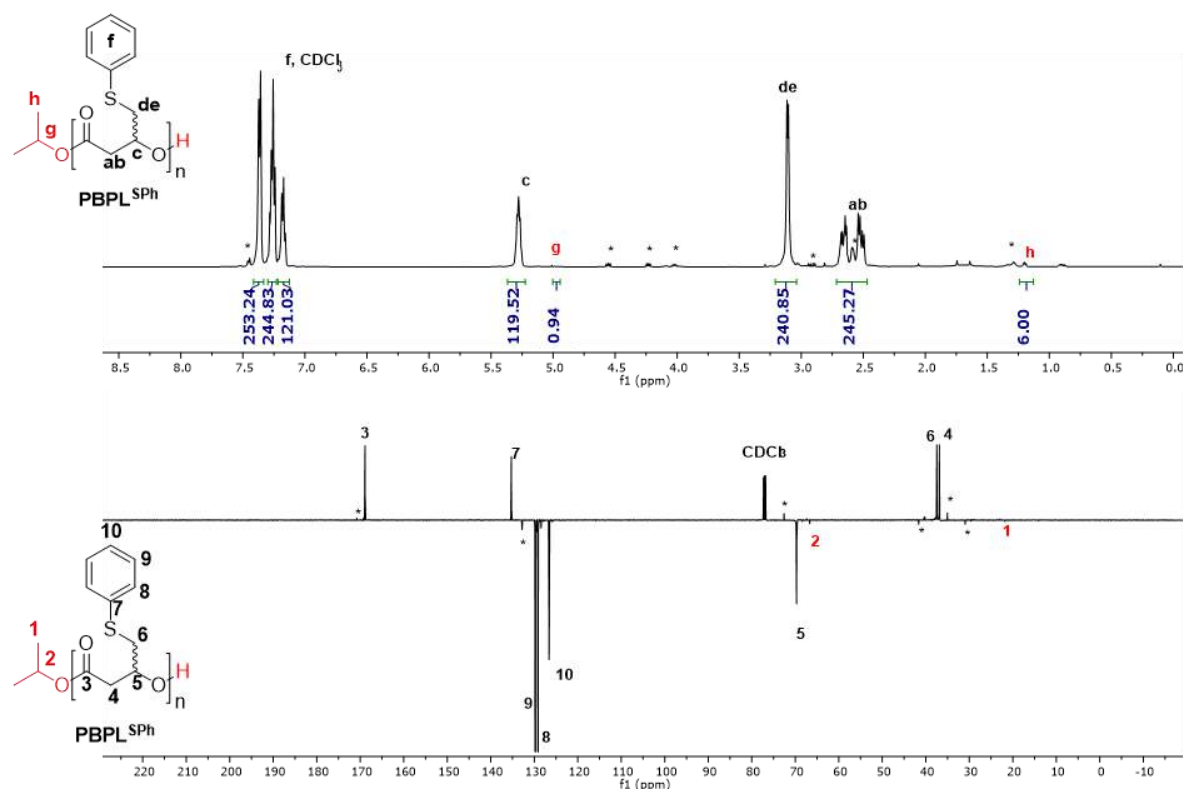


**Figure 4. 15** – <sup>1</sup>H NMR (500 MHz, CDCl<sub>3</sub>, 25 °C) (top) and J-MOD (125 MHz, CDCl<sub>3</sub>, 25 °C) (bottom) spectra of syndiotactic PBPL<sup>SPh</sup> prepared from the ROP of *rac*-BPL<sup>SPh</sup> mediated by complex **2a** in the presence of *i*PrOH and precipitated twice in cold pentane (Table 4. 4, entry 13); \* minor peaks correspond to the degradation product, the five membered ring, of BPL<sup>SPh</sup> (refer to Chapter 2 – Figure 2. 12).

Furthermore, the macromolecular structure of the PBPL<sup>SPh</sup> was detected by ESI mass spectrometry analyses (Figure 4. 16). The spectra recorded for low molar mass sample of PBPL<sup>SPh</sup> prepared from **2a**/*i*PrOH catalytic systems, showed a single population of macromolecules having a repeating unit of *m/z* 194, corresponding to  $\alpha$ -isopropoxy, $\omega$ -hydroxyl telechelic PBPL<sup>SPh</sup> chains ionized by Na<sup>+</sup>. This was confirmed by the close match with the corresponding isotopic simulations, as illustrated for [(CH<sub>3</sub>)<sub>2</sub>CHO(COCH<sub>2</sub>CH(CH<sub>2</sub>SC<sub>6</sub>H<sub>5</sub>)O)<sub>*n*</sub>H]·Na<sup>+</sup> with, for example, calculated *m/z* 1053.2475 versus found *m/z* 1053.2473 for *n* = 5.

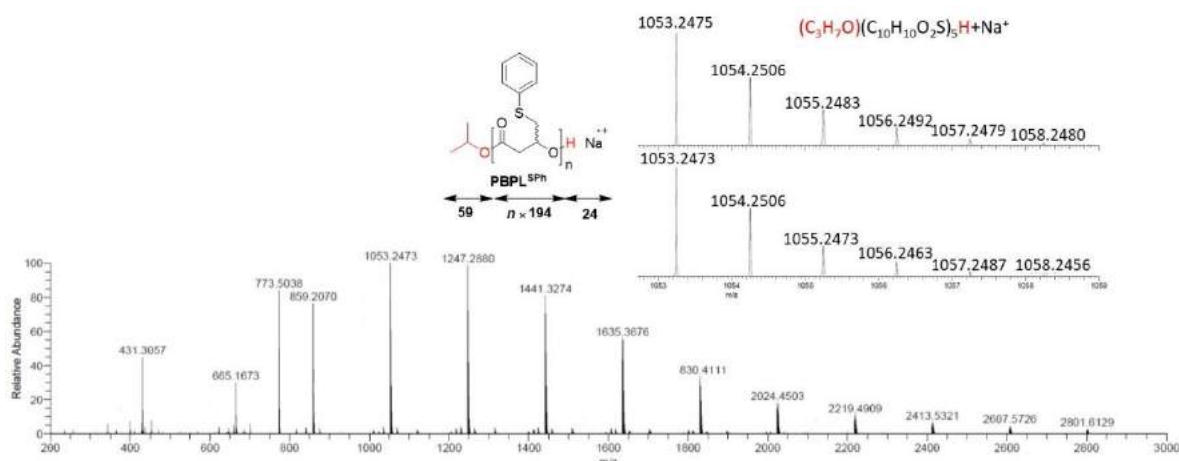


**Figure 4. 16** – ESI-MS (ionized by  $\text{Na}^+$ , solvent  $\text{CH}_3\text{OH}/\text{CH}_2\text{Cl}_2$  (90/10 v:v) of  $\text{PBPL}^{\text{SPh}}$  (Table 4. 4, entry 11) precipitated twice in cold pentane; right zoom spectra are theoretical data (top) vs. experimental (bottom).

Exchanging oxygen with sulphur in the side chain of the monomer ( $\text{BPL}^{\text{OPh}}$  vs.  $\text{BPL}^{\text{SPh}}$ ) did not affect the stereochemistry of the resulting  $\text{PBPL}^{\text{SPh}}$ s. Hence, the produced  $\text{PBPL}^{\text{SPh}}$ s were all found to be syndio-enriched, regardless of the catalyst system implemented (Figure 4. 17). Higher syndiotactic enrichment was obtained from bulky  $\text{R}^1$  substituents (cumyl and  $t\text{Bu}$ , **2a-b**;  $P_r = 0.85$ – $0.87$ ), rather than from small ones (Me and Cl, **2c-d**;  $P_r = 0.74$ – $0.76$ ).

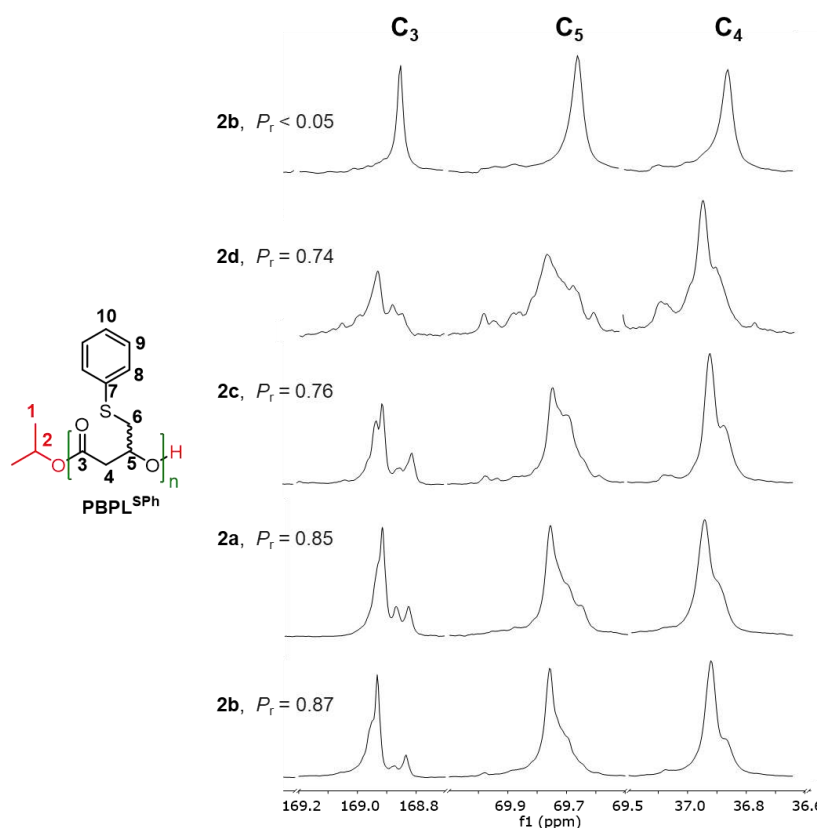


**Figure 4. 17** – Regions of the  $^{13}\text{C}\{^1\text{H}\}$  NMR spectra (125 MHz,  $\text{CDCl}_3$ ,  $23^\circ\text{C}$ ) of  $\text{PBPL}^{\text{SPh}}$  prepared by ROP of  $\text{rac-BPL}^{\text{SPh}}$ , except for the top spectra: of enantiopure ( $S$ )- $\text{BPL}^{\text{SPh}}$  (Table 4. 4, entry 14), mediated by **2a**, **2b**, **2c**, or **2d**/ $i\text{PrOH}$  (Table 4. 4, entries 3,5,7,12).

On the other hand, a remarkable change in the glass transition  $T_g$  was obtained depending on the type of the heteroatom in the pendent group ( $\text{BPL}^{\text{OPh}}$  vs.  $\text{BPL}^{\text{SPh}}$ ), unlike that of stereochemistry (no influence of S vs. O).  $\text{PBPL}^{\text{SPh}}$ s displayed  $T_g$  values varying from 8–14 °C (Table 4. 4, Figure 4. 18, Appendix 25,26), significantly lower than those of  $\text{PBPL}^{\text{OPh}}$ s (*vide supra*, Figure 4. 11). This is probably due to the higher electron negativity of the oxygen atom than sulphur, that leads to more electron deficient phenyl ring and more electronic rich oxygen lone pair. Hence O–Ph group can deliver more pronounced interactions between one monomeric unit and the other and between the different polymeric chains than S–Ph group, leading to a better packing of the polymer and thus to higher  $T_g$ s.<sup>[15, 20]</sup> Yet, the same trend obtained with  $\text{PBPL}^{\text{OPh}}$ s was observed with  $\text{PBPL}^{\text{SPh}}$ s, where the lower the stereoregularity, the lower the  $T_g$ s (for  $P_r = 0.74$ – $0.76$ ,  $T_g = 8$ – $9$  °C; Figure 4. 18 – left) and vice versa (for  $P_r = 0.85$ – $0.87$ ,  $T_g = 12$ – $14$  °C; Figure 4. 18 – right). Notably, these values are comparable to the similar atactic PHAs, namely  $\text{PBPL}^{\text{CH}_2\text{SPh}}$  and  $\text{PBPL}^{(\text{CH}_2)_2\text{SPh}}$  obtained with the genetic engineering method, that have slightly lower  $T_g$  (4 °C) for being more flexible.<sup>[17]</sup>

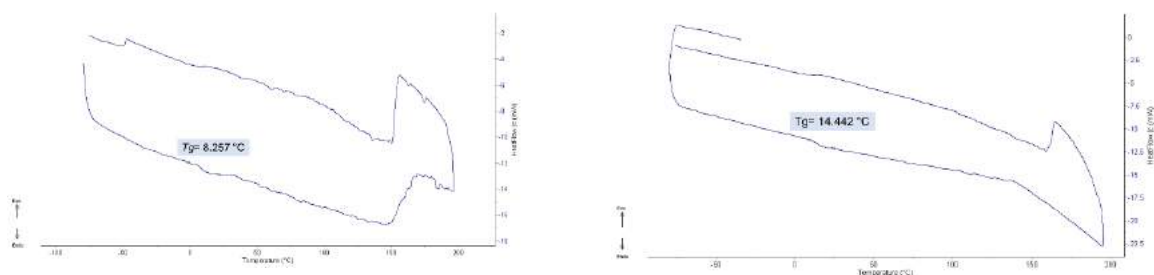


**Figure 4. 18** – DSC thermogram (heating rate of 10 °C min<sup>-1</sup>, second heating cycle –80 to 200 °C) of: (left) syndiotactic  $\text{PBPL}^{\text{SPh}}$  ( $P_r$  0.76) synthesized by ROP of *rac*- $\text{BPL}^{\text{SPh}}$  with **2c**/*i*PrOH (Table 4. 4, entry 5); (right) syndiotactic  $\text{PBPL}^{\text{SPh}}$  ( $P_r$  0.86) synthesized by ROP of *rac*- $\text{BPL}^{\text{SPh}}$  with **2b**/*i*PrOH (Table 4. 4, entry 8).

The  $\text{PBPL}^{\text{SPh}}$ s samples were found to thermally degrade at the same temperature as  $\text{PBPL}^{\text{OPh}}$  with  $T_d^{\text{onset}}_{\text{PBPL}(\text{SPh})} = 271$  °C (Figure 4. 19), that is significantly higher than the one measured for  $\text{PBPL}^{\text{Me}}$  ( $T_d^{\text{onset}} = 256$  °C) and  $\text{PBPL}^{\text{CH}_2\text{OBn}}$  ( $T_d^{\text{onset}}_{\text{PBPL}(\text{CH}_2\text{OBn})} = 226$  °C).<sup>[16]</sup>

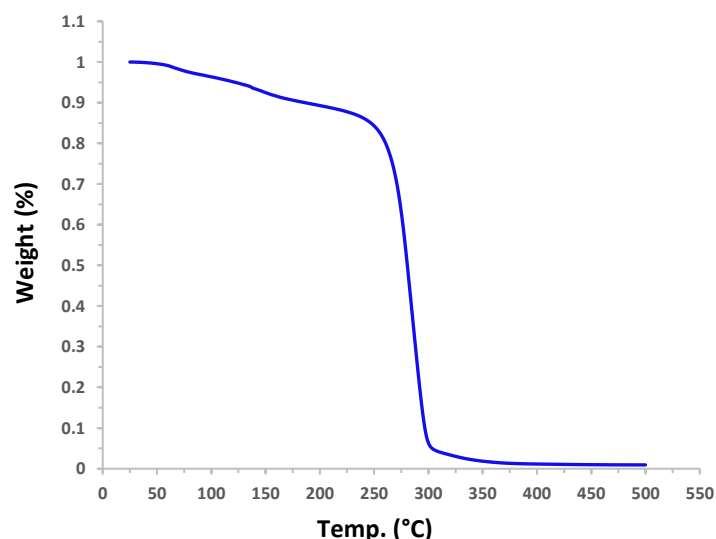


**Figure 4. 19** – TGA thermograms of syndiotactic PBPL<sup>SPh</sup> (Table 4. 4, entry 9).

#### 2.1.4. Insights into the kinetics and the catalyst activity

Monitoring of NMR-scale polymerizations of BPL<sup>OPh/CH<sub>2</sub>OBn/SPh</sup> performed with **2a-d** (*i*PrOH) confirmed the kinetics trend derived from batch experiments (Table 4. 2, Table 4. 3, Table 4. 4, Appendix 27), and linear semi-logarithmic plots established that all reactions were first order in monomer (apparent rate constant  $k_{app} = 67.3 \pm 3.1 \text{ min}^{-1}$ , BPL<sup>CH<sub>2</sub>OBn</sup>/**2b**;  $32.93 \pm 0.01 \text{ min}^{-1}$ , BPL<sup>OPh/SPh</sup>/**2a-b**;  $15.05 \pm 0.38 \text{ min}^{-1}$ , BPL<sup>CH<sub>2</sub>OBn</sup>/**2b**;  $0.76 \pm 0.07 \text{ min}^{-1}$ , BPL<sup>OPh</sup>/**2c**;  $0.58 \pm 0.11 \text{ min}^{-1}$ , BPL<sup>SPh</sup>/**2c**;  $9.05 \pm 0.06 \times 10^{-2} \text{ min}^{-1}$ , BPL<sup>OPh</sup>/**2d**;  $6.69 \pm 0.62 \times 10^{-2} \text{ min}^{-1}$ , BPL<sup>CH<sub>2</sub>OBn</sup>/**2c**;  $4.25 \pm 0.43 \times 10^{-2} \text{ min}^{-1}$ , BPL<sup>CH<sub>2</sub>OBn</sup>/**2d**;  $1.2 \pm 0.1 \times 10^{-2} \text{ min}^{-1}$ , BPL<sup>SPh</sup>/**2d** (Figure 4. 20). The major overall trend for the monomers' ROP ability is thus BPL<sup>OPh</sup>  $\approx$  BPL<sup>SPh</sup> > BPL<sup>CH<sub>2</sub>OBn</sup>, while the catalysts' activity thus generally followed the order **2a-b** >> **2c** >> **2d**, as previously reported for the previous ROP of various BPL<sup>FGs</sup>  $\beta$ -lactones (FG = OAll, OBn, OMe) and MLA<sup>FGs</sup> (All, Bn, Me) promoted by these catalyst systems.

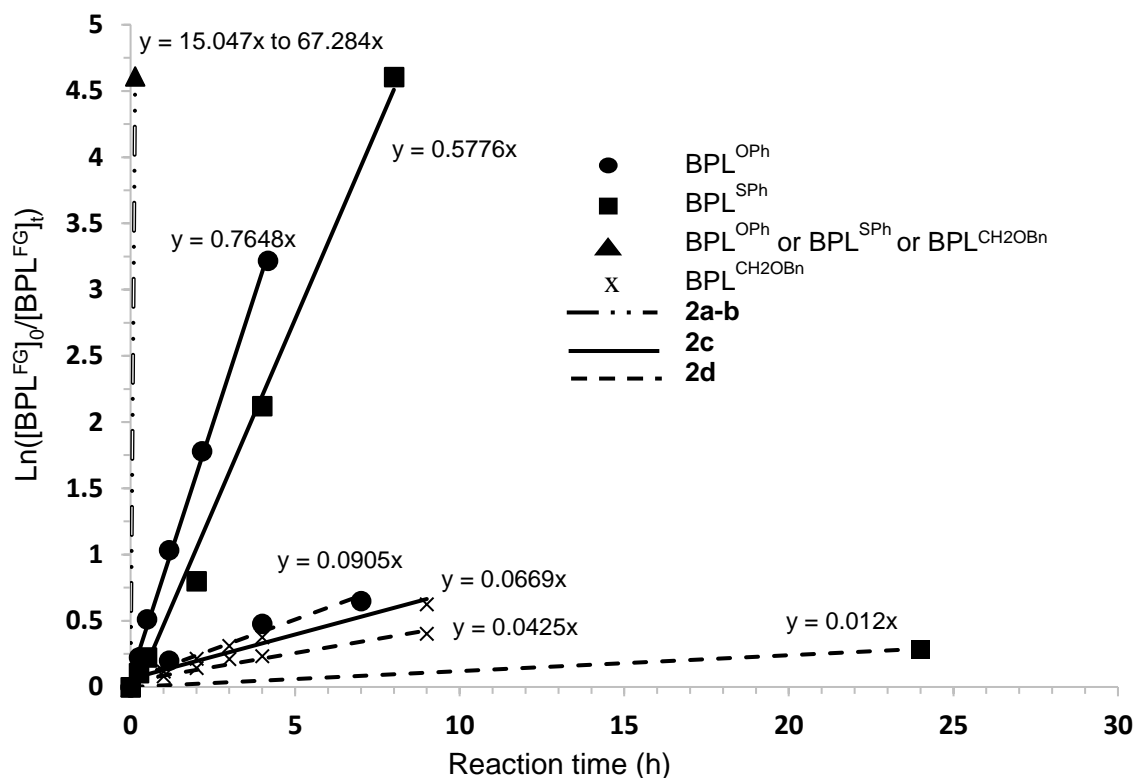


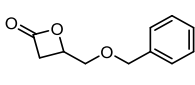
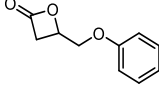
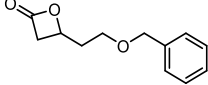
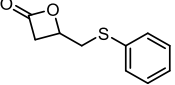
**Figure 4. 20** – Semi-logarithmic first-order plots for the ROP of *rac*-BPL<sup>FG</sup>s (FG = OPh, CH<sub>2</sub>OBn, SPh) mediated by **2a-d**/*i*PrOH (20 °C, toluene; [BPL<sup>FG</sup>]<sub>0</sub>/[[**2**]/[*i*PrOH]<sub>0</sub>] = 60:1:1): **2a** (Table 4. 2, entry 11; Table 4. 4, entry 12); **2b** (Table 4. 2, entry 6; Table 4. 4, entry 7); **2c** (Table 4. 2, entry 4; Table 4. 4, entry 5) and **2d** (Table 4. 2, entry 2; Table 4. 4, entry 3); plots from **2a-b** all overlap due to similar high activity of these catalysts regardless of the monomer functionality, and are represented as ▲.

### 2.1.5. Summery on the ROP of *rac*-BPL<sup>OPh/CH<sub>2</sub>OBn/SPh</sup>

Highly stereoregular and high molar masses PBPL<sup>OPh</sup> and PBPL<sup>SPh</sup> (reaching  $M_{n,SEC(OPh)} = 95,000$ ;  $D_M = 1.20$ ;  $P_r = 0.86$ ) were successfully synthesized by the stereoselective controlled ROP of the corresponding *rac*-BPL<sup>OPh</sup> and *rac*-BPL<sup>SPh</sup> promoted by achiral diamino-bis(phenolate) yttrium complexes bearing variable ligand substituents (Y{ONNO<sup>R1,R2</sup>}; **2a-d**). The impact of the monomer exocyclic chain on the thermal properties, and that of its relation with the ligand substituents on the tacticity of the produced polyesters, were considered by examining PBPL<sup>OPh</sup>, PBPL<sup>CH<sub>2</sub>OBn</sup> and the previously synthesized PBPL<sup>OBn</sup>, and are represented in (Table 4. 5). In fact, <sup>13</sup>C NMR spectra of the PBPL<sup>OPh/CH<sub>2</sub>OBn</sup> indicated that the length of the monomeric chain has no effect on the stereoregularity when the yttrium complex incorporated bulky substituents (cumyl or <sup>t</sup>Bu groups, **2a-b**), leading to highly syndio-enriched PBPL<sup>OPh/CH<sub>2</sub>OBn</sup> ( $P_r = 0.84$ – $0.90$ ) alike that of PBPL<sup>OBn</sup>. Nevertheless, removing or adding one methylene from *rac*-BPL<sup>OBn</sup> (to afford *rac*-BPL<sup>OPh</sup> and *rac*-BPL<sup>CH<sub>2</sub>OBn</sup>, respectively) had a significant impact on the stereochemistry when yttrium complex incorporated unbulky

substituents (Me or Cl groups, **2c-d**). When using uncrowded Me-substituents (**2c**), PBPL<sup>CH<sub>2</sub>OBn</sup> revealed atactic ( $P_r = 0.49$ ) similarly to PBPL<sup>OBn</sup> ( $P_r = 0.50$ ); however, *rac*-BPL<sup>O<sup>Ph</sup></sup> afforded syndio-enriched PBPL<sup>O<sup>Ph</sup></sup> ( $P_r = 0.76$ – $0.79$ ). The most striking was the use of Cl-substituents (**2d**) that afforded highly isotactic PBPL<sup>OBn</sup> ( $P_r = 0.10$  or  $P_m = 0.90$ ) and upon shortening the side-chain (PBPL<sup>O<sup>Ph</sup></sup>), it was switched to syndio-enriched ( $P_r = 0.75$ – $0.77$ ) while upon extending the side chain (PBPL<sup>CH<sub>2</sub>OBn</sup>), the lack of stereocontrol ( $P_r = 0.49$ ) was obtained. Furthermore, the exocyclic chain length showed to have a strong influence on the thermal properties of the produced polymers. The longer the chain (PBPL<sup>CH<sub>2</sub>OBn</sup> > PBPL<sup>OBn</sup> > PBPL<sup>O<sup>Ph</sup></sup>), the lower the observed  $T_g$  ( $-13$ – $-11$  <  $-6$ – $0$  <  $21$ – $40$  °C, respectively) (Table 4. 5). Finally, replacing oxygen with sulphur (PBPL<sup>O<sup>Ph</sup></sup> vs. PBPL<sup>S<sup>Ph</sup></sup>) presented no consequence on the stereochemistry affording highly syndiotactic PBPL<sup>O/S<sup>Ph</sup></sup>, yet it gave lower  $T_g$ s ( $8$ – $14$  °C).

**Table 4. 5** –  $P_r$  and  $T_g$  values for PBPL<sup>OBn</sup>, PBPL<sup>O<sup>Ph</sup></sup>, PBPL<sup>CH<sub>2</sub>OBn</sup>, and PBPL<sup>S<sup>Ph</sup></sup> produced from the stereoselective ROP of *rac*-BPL<sup>OBn</sup>, *rac*-BPL<sup>O<sup>Ph</sup></sup>, *rac*-BPL<sup>CH<sub>2</sub>OBn</sup>, and *rac*-BPL<sup>S<sup>Ph</sup></sup> mediated by **2a-d**.

<i>rac</i> -BPL <sup>FGs</sup>				
<b>R<sup>1</sup>, R<sup>2</sup></b>	<i>rac</i> -BPL <sup>OBn</sup> [11]	<i>rac</i> -BPL <sup>O<sup>Ph</sup></sup>	<i>rac</i> -BPL <sup>CH<sub>2</sub>OBn</sup>	<i>rac</i> -BPL <sup>S<sup>Ph</sup></sup>
<b>Crowded (2a-b)</b>	Syndiotactic $P_r = 0.85$ – $0.90$ $T_g = 0$ °C	Syndiotactic $P_r = 0.84$ – $0.87$ $T_g = 37$ – $40$ °C	Syndiotactic $P_r = 0.78$ – $0.90$ $T_g = -13$ – $-11$ °C	Syndiotactic $P_r = 0.83$ – $0.87$ $T_g = 12$ – $14$ °C
<b>Non-crowded 2c</b>	Atactic $P_r = 0.50$ $T_g = -6$ °C	Syndiotactic $P_r = 0.76$ – $0.79$ $T_g = 30$ °C	Atactic $P_r = 0.49$ $T_g = -11$ °C	Syndiotactic $P_r = 0.74$ – $0.76$ $T_g = 8$ – $9$ °C
<b>Halogenated non-crowded 2d</b>	Isotactic $P_r = 0.10$ $T_g = -1$ °C	Syndiotactic $P_r = 0.75$ – $0.77$ $T_g = 21$ – $22$ °C	Atactic $P_r = 0.49$ $T_g = -13$ °C	Syndiotactic $P_r = 0.73$ – $0.74$ $T_g = 9$ °C

## 2.2. ROP of BPL<sup>FGs</sup> with bulky exocyclic chains

As the chain length of the pendent group was examined first, the steric hindrance of the latter was studied secondly. *Rac*-BPL<sup>O<sup>Ph</sup></sup> is similar to BPL<sup>OBn</sup> but without a CH<sub>2</sub> (methylene C<sub>B</sub>H<sub>2</sub>R<sub>1</sub>; Figure 4. 5) and shows a different reactivity with the yttrium catalyst. Therefore, converting this methylene to methine (C<sub>B</sub>H<sub>2</sub>R<sub>1</sub> to C<sub>B</sub>H<sub>1</sub>R<sub>2</sub> (tertiary carbon)) was addressed here, upon using BPL<sup>O<sup>i</sup>Pr</sup> monomer, and was compared to the previously reported BPL<sup>O<sup>Me</sup></sup> (C<sub>B</sub>H<sub>3</sub> (primary carbon)) and BPL<sup>O<sup>All</sup></sup> (C<sub>B</sub>H<sub>2</sub>R<sub>1</sub> (secondary carbon)). In addition to BPL<sup>O<sup>i</sup>Pr</sup>, bulkier pendent group such as BPL<sup>O<sup>r</sup>Bu</sup> and BPL<sup>O<sup>TBDMS</sup></sup> (C<sub>B</sub>R<sub>4</sub> (quaternary carbon)) were investigated via ROP to comparatively study the architecture, molecular parameters and tacticity of the



generated PBPL<sup>O<sup>i</sup>Pr</sup>, PBPL<sup>O<sup>t</sup>Bu</sup> and PBPL<sup>OTBDMS</sup> (Figure 4. 21). Noteworthy, none of the latter polymers were synthesized and characterized before, except PBPL<sup>OTBDMS</sup> that was previously synthesized through organocatalyzed ROP in my work (refer to Chapter 3).

Moreover, PHAs featuring *iso*-propyl or *tert*-butyl arm chains can be used as bulky hydrophobic chains, PHA flanked with *tert*-butyldimethylsilyl can be used as a hydrophilic one (after converting OTBDMS groups into hydroxy ones via deprotection) of potential interest to elaborate amphiphilic drug delivery systems

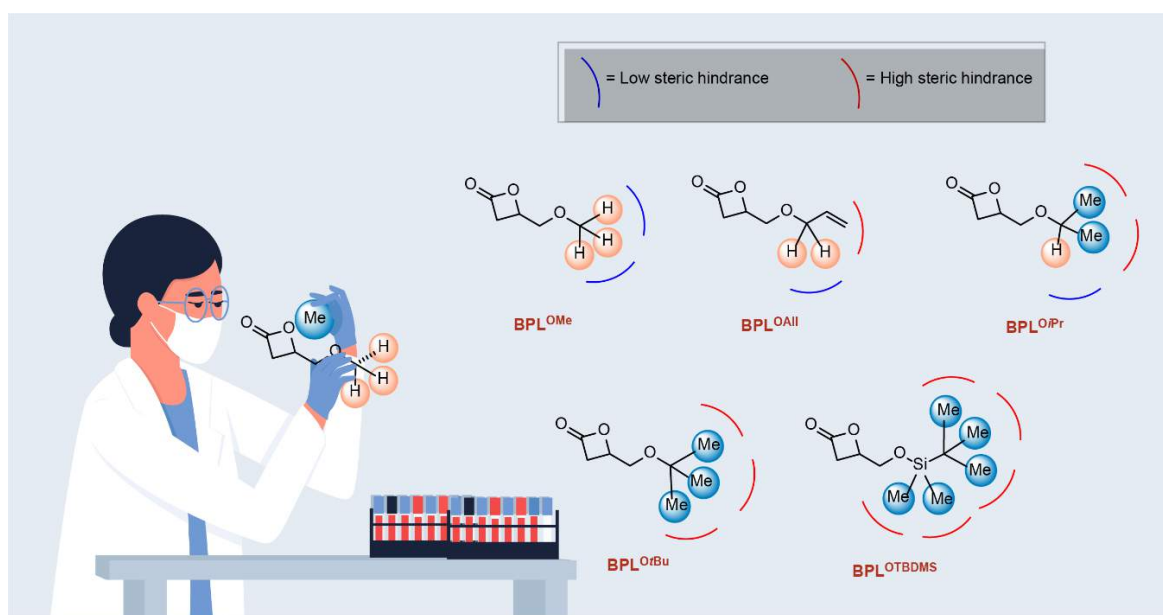


**Figure 4. 21** – Illustration on the steric hindrance of the BPL<sup>FG</sup>s (FG = O<sup>i</sup>Pr, O<sup>t</sup>Bu, OTBDMS) that were studied in my work.

### 2.2.1. ROP of *rac*-BPL<sup>O<sup>i</sup>Pr</sup>

The ROP of *rac*-BPL<sup>O<sup>i</sup>Pr</sup> was explored under the same general conditions as the above mentioned ROPs mediated by Y{ONNO<sup>R1,R2</sup>}/(*i*PrOH) catalysts (at room temperature in toluene, using 1mol% of (**2a-d**)/(*i*PrOH)) (Scheme 4. 4)). The characteristic data of the isolated PBPL<sup>O<sup>i</sup>Pr</sup>s generated from the latter polymerization are gathered in Table 4. 6. Typically, Cl-substituted yttrium catalyst (**2d**) revealed to be the least active (TOF<sub>(ca. 30)</sub> = 0.24 h<sup>-1</sup>; Table 4. 6, entry 1). The NMR control of the latter reaction showed that 15% monomer conversion was obtained after 25 min, and running the polymerization for 1 day increased the conversion by only 4% (Table 4. 6, entry 1). Another attempt over 2 days of reaction, without sampling the solution for NMR monitoring to avoid the risk of deactivating the catalyst by unadventitious traces oxygen, only gave 20% conversion (Table 4. 6, entry 2). Nevertheless, the Me-substituted yttrium catalyst (**2c**) could achieve nearly complete consumption of ca. 60 and 100 monomer

equiv. in 12 and 24 hours, respectively, with  $\text{TOF}_{2c} = 4.8 \text{ h}^{-1}$  (Table 4. 6, entry 3). High activity was observed with bulky substituents ligands (*t*Bu, cumyl, **2a-b**), and almost quantitative conversion of ca. 60–100 equivalents of *rac*-BPL<sup>O*i*Pr</sup> was reached within 5–15 min with  $\text{TOF}_{2a-b} > 720 \text{ h}^{-1}$  (Table 4. 6, entries 6,9).

**Table 4. 6** – Characteristics of the PBPL<sup>O*i*Pr</sup> synthesized by ROP of *rac*-BPL<sup>O*i*Pr</sup> mediated by **2a-d**/(*i*PrOH) catalytic systems in toluene at room temperature.

Entry	Cat.	[BPL <sup>O<i>i</i>Pr</sup> ] <sub>0</sub> / [ <b>2</b> ] <sub>0</sub> /[ <i>i</i> PrOH] <sub>0</sub> <sup>a</sup>	Time <sup>b</sup> (min)	Conv. <sup>c</sup> (%)	$M_{n,\text{theo}}$ <sup>d</sup> (g.mol <sup>-1</sup> )	$M_{n,\text{NMR}}$ <sup>e</sup> (g.mol <sup>-1</sup> )	$M_{n,\text{SEC}}$ <sup>f</sup> (g.mol <sup>-1</sup> )	$\bar{D}_M$ <sup>f</sup>	$P_r$ <sup>g</sup>	$T_g$ <sup>h</sup> (°C)
1 <sup>i</sup>	<b>2d</b>	30:1:1	24 h	19	850	1100	1400	1.15	0.70	<i>nd</i> <sup>j</sup>
2	<b>2d</b>	30:1:1	48 h	20	900	1150	1400	1.13	0.69	<i>nd</i> <sup>j</sup>
3 <sup>i</sup>	<b>2c</b>	60:1:1	12 h	96	8350	7550	9500	1.09	0.71	<i>nd</i> <sup>j</sup>
4	<b>2c</b>	100:1:1	24 h	90	13 000	15 000	15 900	1.18	0.72	1.8
5	<b>2b</b>	30:1:1	5	100	4400	3700	5400	1.09	0.84	<i>nd</i> <sup>j</sup>
6 <sup>i</sup>	<b>2b</b>	60:1:1	5	100	8700	9400	10 700	1.11	0.84	<i>nd</i> <sup>j</sup>
7	<b>2b</b>	100:1:1	15	100	14 450	14 400	15 300	1.13	0.85	2.1
8	<b>2b</b>	250:1:1	20	100	36 050	36 500	38 300	1.08	0.85	2.2
9 <sup>i</sup>	<b>2a</b>	60:1:1	5	100	8700	9000	10 050	1.10	0.82	<i>nd</i> <sup>j</sup>
10	<b>2a</b>	100:1:1	15	100	14 450	17 000	18 600	1.13	0.82	<i>nd</i> <sup>j</sup>
11 <sup>k</sup>	<b>2b</b>	30:1:1	60	94	4100	4600	5600	1.10	<0.05	<i>nd</i> <sup>j</sup>

<sup>a</sup> Reactions performed with [BPL<sup>O*i*Pr</sup>]<sub>0</sub> = 1.0 M. <sup>b</sup> Reaction time was not necessarily optimized. <sup>c</sup> Conversion of BPL<sup>O*i*Pr</sup> as determined by <sup>1</sup>H NMR analysis of the crude reaction mixture. <sup>d</sup> Molar mass calculated according to  $M_{n,\text{theo}} = ([\text{BPL}^{\text{O}i\text{Pr}}]_0/[2]_0 \times \text{conv. BPL}^{\text{O}i\text{Pr}} \times M_{\text{BPL}^{\text{O}i\text{Pr}}} + M_{i\text{PrOH}})$ , with  $M_{\text{BPL}^{\text{O}i\text{Pr}}} = 144 \text{ g.mol}^{-1}$ ,  $M_{i\text{PrOH}} = 60 \text{ g.mol}^{-1}$ . <sup>e</sup> Molar mass determined by <sup>1</sup>H NMR analysis of the isolated polymer, from the resonances of the terminal O*i*Pr group (refer to Experimental section). <sup>f</sup> Number-average molar mass and dispersity ( $M_w/M_n$ ) determined by SEC analysis in THF at 30 °C vs. polystyrene standards. <sup>g</sup>  $P_r$  is the probability of *racemic* linkages between BPL<sup>O*i*Pr</sup> units as determined by <sup>13</sup>C{<sup>1</sup>H} NMR analysis of the isolated PBPL<sup>O*i*Pr</sup>s. <sup>h</sup> Glass transition temperature as determined by DSC. <sup>i</sup> Refer to the kinetic study (Figure 4. 35) <sup>j</sup> Not determined; <sup>k</sup> ROP of enantiopure (*S*)-BPL<sup>O*i*Pr</sup>.

Again, the yttrium-based catalytic system (**2a-d**/(*i*PrOH)) proved to control the ROP of *rac*-BPL<sup>O*i*Pr</sup> in terms of molecular parameters ( $M_{n,\text{theo}}$ ,  $M_{n,\text{NMR}}$ ,  $M_{n,\text{SEC}}$  in good agreement), alongside ensuing in plainly narrow dispersities ( $\bar{D}_M = 1.09\text{--}1.18$ ). A linear plot of experimental molar mass values with respect to *rac*-BPL<sup>O*i*Pr</sup> monomer loading up to ca. 250 mediated by **2b**/(*i*PrOH) (1:1) catalytic system, was observed (Figure 4. 22). This confirms the scarcity or the absence of transfer or side reactions suggesting living polymerization features.

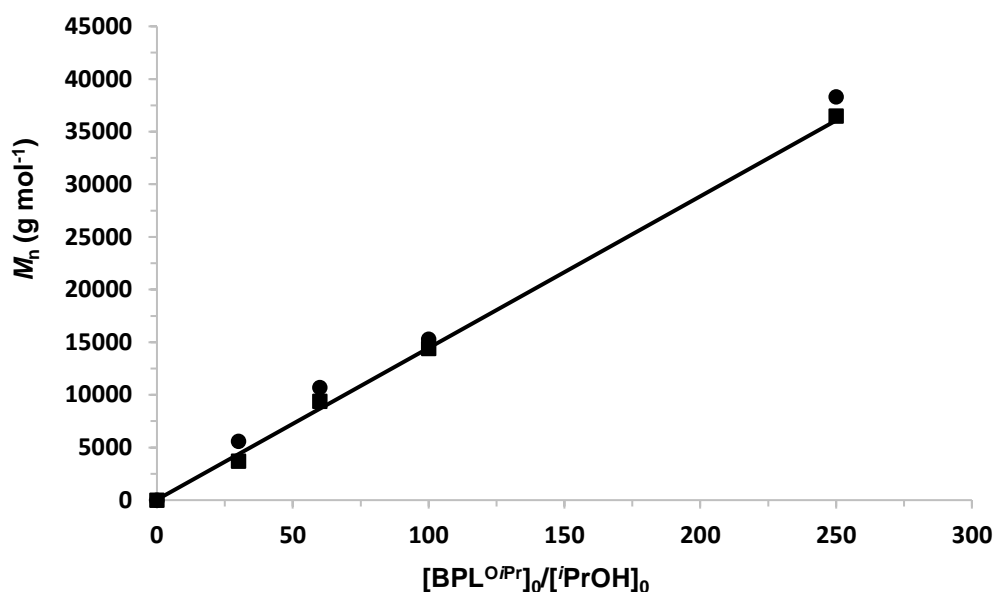


**Figure 4. 22** – Variation of  $M_{n,NMR}$  ■,  $M_{n,SEC}$  ●, and  $M_{n,theo}$  (solid line) values of PBPL<sup>ⁱᴾʳ</sup> synthesized from the ROP of *rac*-BPL<sup>ⁱᴾʳ</sup> mediated by **2b**/*i*PrOH (1:1) catalytic system as a function of the BPL<sup>ⁱᴾʳ</sup> monomer loading (Table 4. 6 – entries 5-8).

<sup>1</sup>H and J-MOD NMR spectra of the isolated PBPL<sup>ⁱᴾʳ</sup> (Figure 4. 23) evidenced the presence of the methine and methylene of the BPL<sup>ⁱᴾʳ</sup> repeating unit, as well as the isopropoxycarbonyl chain-end group ( $\delta$  (ppm): ca. 4.97 (CH<sub>3</sub>)<sub>2</sub>CHO–, ca. 1.25 (CH<sub>3</sub>)<sub>2</sub>CHO–), 2D COSY and HMBC NMR spectra are represented in Appendix 28,29).

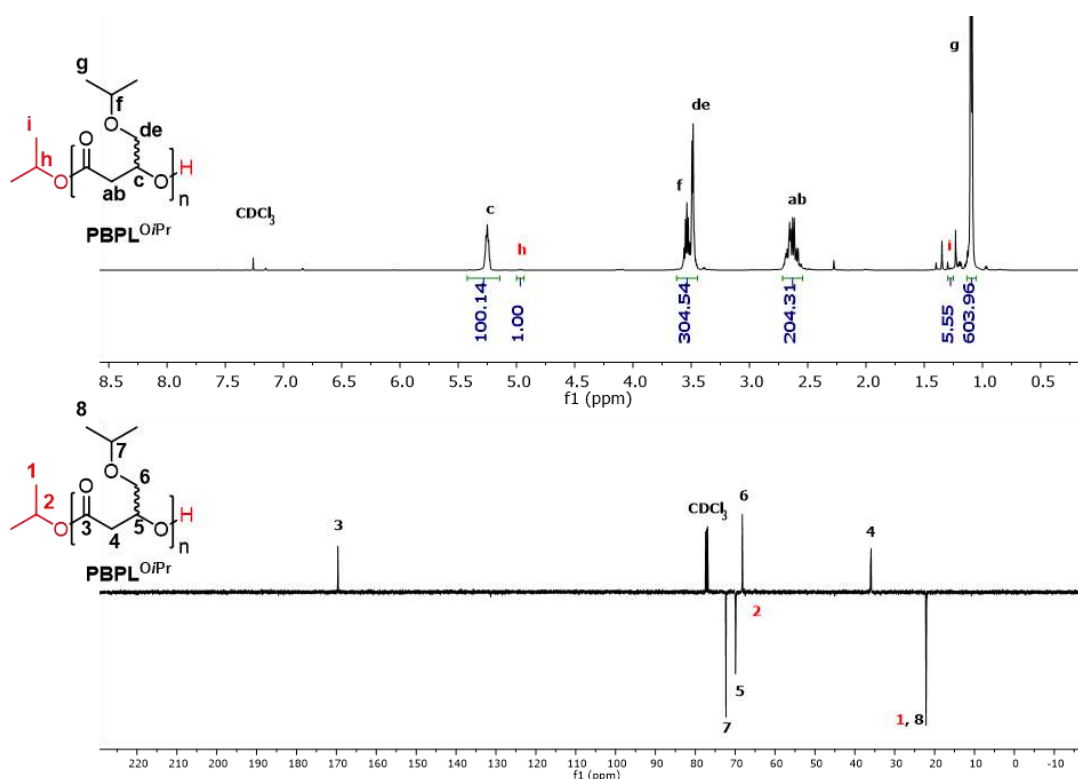


**Figure 4. 23** – <sup>1</sup>H NMR (500 MHz, CDCl<sub>3</sub>, 25 °C) (top) and J-MOD (125 MHz, CDCl<sub>3</sub>, 25 °C) (bottom) spectra of syndiotactic PBPL<sup>ⁱᴾʳ</sup> prepared from the ROP of *rac*-BPL<sup>ⁱᴾʳ</sup> mediated by complex **2b** in the presence of *i*PrOH and precipitated twice in cold pentane (Table 4. 6, entry 7).

The PBPL<sup>OiPr</sup> architecture was also studied by MALDI-Tof MS analysis (Figure 4. 24). The spectra recorded for a low molar mass sample of PBPL<sup>OiPr</sup> synthesized from **2d**/*i*PrOH catalytic system, showed two populations of macromolecules having a repeating unit of  $m/z$  144 corresponding to the BPL<sup>OiPr</sup> monomer unit. The major one corresponds to  $\alpha$ -isopropoxy, $\omega$ -hydroxyl telechelic PBPL<sup>OiPr</sup> chains ionized by Na<sup>+</sup> (Figure 4. 24 – top (I)). Population (I) was confirmed by the close match with the corresponding isotopic simulation of  $[(CH_3)_2CHO(COCH_2CH(CH_2OC_3H_7)O)_nH] \cdot Na^+$  with, for example, calculated  $m/z$  1379.7545 versus found  $m/z$  1379.746 for  $n = 9$ . The minor population corresponds to  $\alpha$ -carboxyl,  $\omega$ -hydroxy telechelic PBPL<sup>OiPr</sup> chains ionized by Na<sup>+</sup> (Figure 4. 24 – top (II)). Population (II) was confirmed by the close match with the corresponding isotopic simulations, as illustrated for  $[HO(C_7H_{12}O_3)_nH] \cdot Na^+$  with, for example, calculated  $m/z$  1337.7076 versus found  $m/z$  1337.709 for  $n = 9$ . Population (II) may result from traces of water within the polymerization medium or in the glove box or introduced during the MS sample preparation.

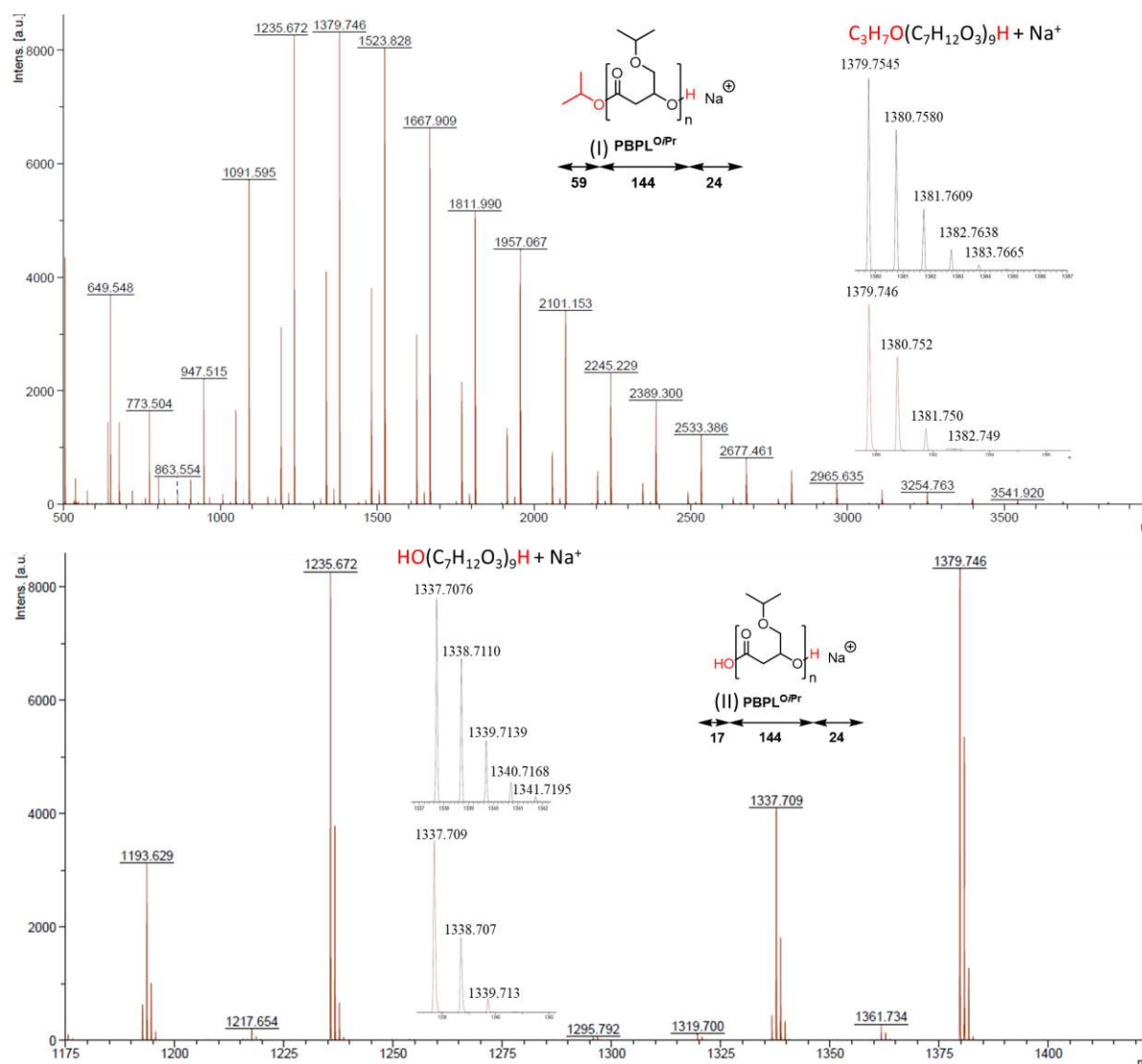


**Figure 4. 24** – MALDI-ToF MS (DCTB matrix, ionized by Na<sup>+</sup>) of PBPL<sup>O<sup>i</sup>Pr</sup> precipitated twice in cold pentane (Table 4. 6, entry 2), showing population (I) major (top) and (II) minor (bottom). Right and middle zoomed regions correspond to the simulated (top) and experimental (bottom) spectra for both population (I and II).

It turned out that the methine in *rac*-BPL<sup>O<sup>i</sup>Pr</sup> did not behave similarly to the methylene in *rac*-BPL<sup>OMe</sup> and *rac*-BPL<sup>OAll</sup>, with regard to the electronic attractive interactions with the Cl-substituents of **2d** that lead to isotactic PBPL<sup>OMe</sup> and PBPL<sup>OAll</sup> (Figure 4. 5). Instead, syndiotactic enriched PBPL<sup>O<sup>i</sup>Pr</sup>s were recovered ( $P_r = 0.69$ – $0.70$ ; Table 4. 6 – entries 1,2; **Figure 4. 25**), possibly arising from the steric hindrance of the isopropyl group that may prohibits the H...Cl interactions by repulsive forces. Moreover, **2c** catalyst (Me-substituents) gave approximately the same syndiotacticity ( $P_r = 0.71$ – $0.72$ ) as that of **2d** (Cl-substituents), thus suggesting the absence of any electronic effect in tuning the tacticity. Better syndiotactic enrichment was obtained from **2a-b** complexes (cumyl and <sup>t</sup>Bu) with  $P_r = 0.82$ – $0.85$ , close to those obtained for PBPL<sup>OMe</sup> and PBPL<sup>OAll</sup> ( $P_r = 0.78$ – $0.84$ ; Scheme 4. 3).

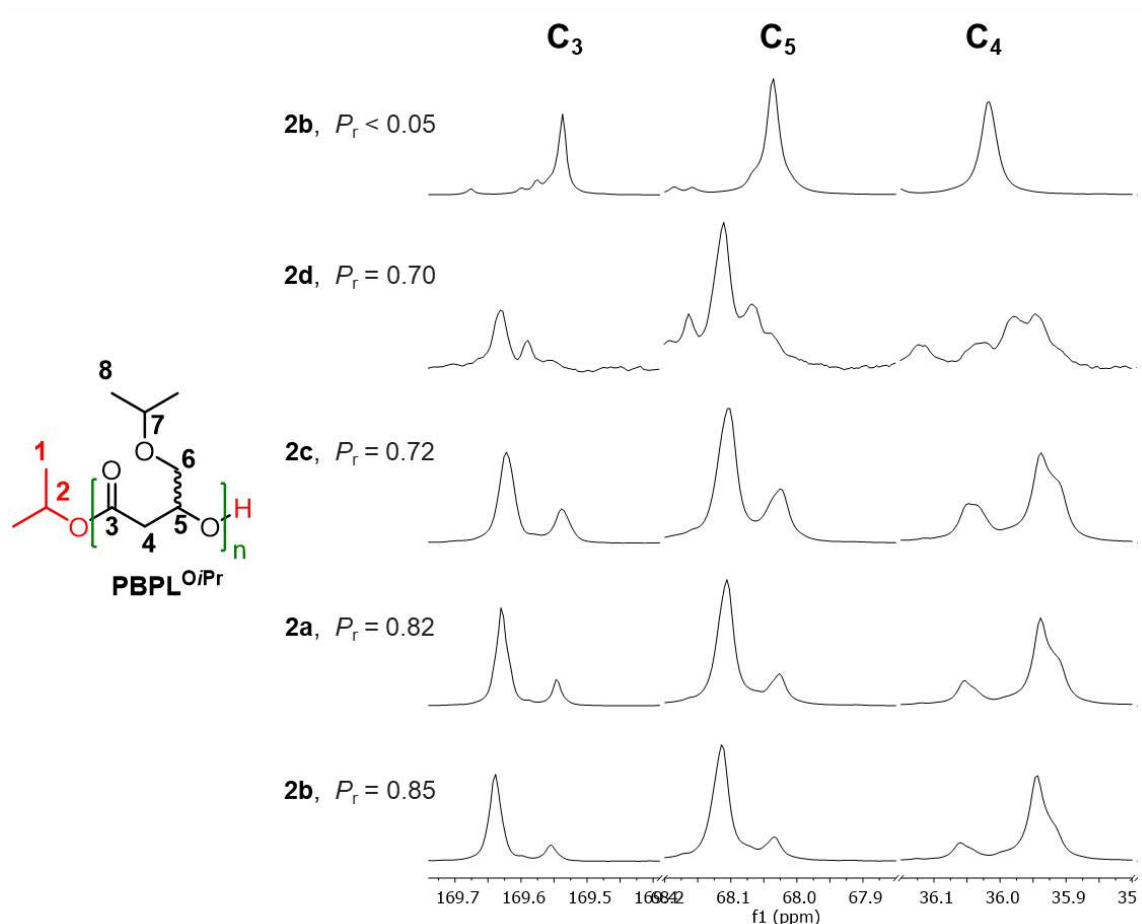


**Figure 4. 25** – Regions of the <sup>13</sup>C{<sup>1</sup>H} NMR spectra (125 MHz, CDCl<sub>3</sub>, 23 °C) of PBPL<sup>O<sup>i</sup>Pr</sup> prepared by ROP of *rac*-BPL<sup>O<sup>i</sup>Pr</sup>, except for the top spectra: of enantiopure (*S*)-BPL<sup>O<sup>i</sup>Pr</sup> (Table 4. 6, entry 11), mediated by **2a**, **2b**, **2c**, or **2d**/<sup>i</sup>PrOH (Table 4. 6, entries 1,4,7,10).

The isolated syndiotactic PBPL<sup>OrPr</sup>s analysed by DSC displayed  $T_g$  values of 1.8–2.2 °C (Table 4. 6; Figure 4. 26). Unlike the previously reported polymers with less steric branching chains (PBPL<sup>OAll</sup> and PBPL<sup>OMe</sup>; Figure 4. 21), the  $T_g$  values were negative ( $T_{g(\text{PBPL}(\text{OAll}))} = -36 - -40$  °C;  $T_{g(\text{PBPL}(\text{OMe}))} = -18 - -11$  °C).<sup>[11]</sup>

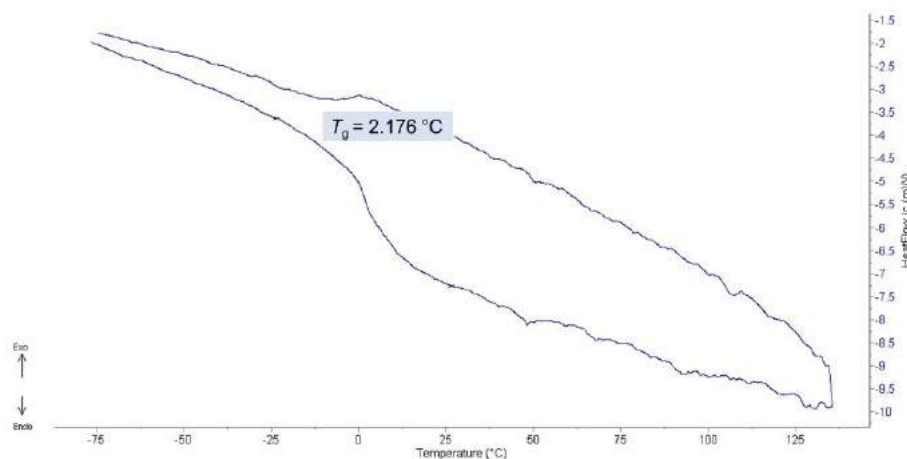


**Figure 4. 26** – DSC thermogram (heating rate of 10 °C min<sup>-1</sup>, second heating cycle –80 to 140 °C) of: syndiotactic PBPL<sup>OrPr</sup> ( $P_r$  0.85) synthesized by ROP of *rac*-BPL<sup>OrPr</sup> with **2b**/*i*PrOH (Table 4. 6, entry 8).

### 2.2.2. ROP of *rac*-BPL<sup>OrBu</sup>

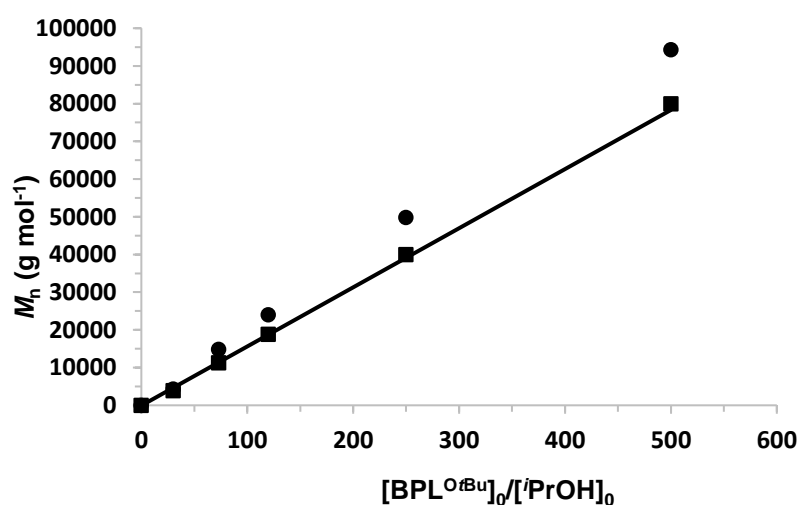
The stereoselective ROP of *rac*-BPL<sup>OrBu</sup> promoted by Y{ONNO<sup>R1,R2</sup>}/(*i*PrOH) catalysts was also examined at room temperature in toluene, using 1 mol% of (**2a-d**/*i*PrOH)), by targeting different monomer loadings as described in Table 4. 7. The corresponding PBPL<sup>OrBu</sup> characteristic data revealed to very similar to those of PBPL<sup>OrPr</sup>, even in the activity of the catalysts **2a-d** despite the steric difference of *iso*-propyl and *tert*-butyl. Catalyst **2d** (Cl-substituents) showed to be the least active among **2a-d**, and accordingly the monomer loading of ca. 25 and 75 did not afford complete *rac*-BPL<sup>OrBu</sup> conversions (67% and 28% in  $\geq 1$  day, respectively), with TOF<sub>2a</sub> = 0.70 h<sup>-1</sup> (Table 4. 7 – entry 1). The **2c** (Me-substituents) were more active reaching nearly complete conversions after  $\leq 7$  h for *rac*-BPL<sup>OrBu</sup> loadings of 25 and 75, with TOF<sub>2c</sub> = 9.64 h<sup>-1</sup> (Table 4. 7 – entry 4). As usual, a high activity was detected with **2a-b** complexes (*t*Bu- cumyl-substituents), allowing quantitative conversion of ca. 75 equivalents of *rac*-BPL<sup>OrBu</sup> in less than five minutes, with TOF<sub>2a-b</sub> > 900 h<sup>-1</sup> (Table 4. 7, entries 6,11).

**Table 4. 7** – Characteristics of the PBPL<sup>OrBu</sup> synthesized by ROP of *rac*-BPL<sup>OrBu</sup> mediated by **2a-d**/(*i*PrOH) catalytic systems in toluene at room temperature.

Entry	Cat.	[BPL <sup>OrBu</sup> ] <sub>0</sub> / [2] <sub>0</sub> /[ <i>i</i> PrOH] <sub>0</sub> <sup>a</sup>	Time <sup>b</sup> (min)	Conv. <sup>c</sup> (%)	$M_{n,theo}$ <sup>d</sup> (g.mol <sup>-1</sup> )	$M_{n,NMR}$ <sup>e</sup> (g.mol <sup>-1</sup> )	$M_{n,SEC}$ <sup>f</sup> (g.mol <sup>-1</sup> )	$\mathcal{D}_M$ <sup>f</sup>	$P_r$ <sup>g</sup>	$T_g$ <sup>h</sup> (°C)
1 <sup>i</sup>	<b>2d</b>	25:1:1	24 h	67	2600	2500	2400	1.12	0.70	<i>nd</i> <sup>j</sup>
2	<b>2d</b>	75:1:1	27 h	28	3300	3400	3000	1.06	0.71	3
3	<b>2c</b>	25:1:1	60	100	3600	3100	3200	1.09	0.74	<i>nd</i> <sup>j</sup>
4 <sup>i</sup>	<b>2c</b>	75:1:1	7 h	90	10 700	10 900	13 600	1.16	0.75	3
5	<b>2b</b>	30:1:1	30	100	4300	3900	4300	1.12	0.83	<i>nd</i> <sup>j</sup>
6 <sup>i</sup>	<b>2b</b>	73:1:1	5	100	11600	11300	14800	1.10	0.84	5
7	<b>2b</b>	120:1:1	10	100	18 800	18 800	24 000	1.14	0.83	<i>nd</i> <sup>j</sup>
8	<b>2b</b>	250:1:1	15	99	39 100	40 000	49 900	1.15	0.84	<i>nd</i> <sup>j</sup>
9	<b>2b</b>	500:1:1	15	99	78 300	80 000	94 300	1.18	0.84	5
10	<b>2a</b>	30:1:1	30	100	4300	4300	4000	1.12	0.78	<i>nd</i> <sup>j</sup>
11 <sup>i</sup>	<b>2a</b>	75:1:1	5	100	11 900	10 900	15 200	1.14	0.78	<i>nd</i> <sup>j</sup>
12 <sup>k</sup>	<b>2b</b>	70:1:1	30	100	11 100	10 300	14 300	1.09	<0.05	11

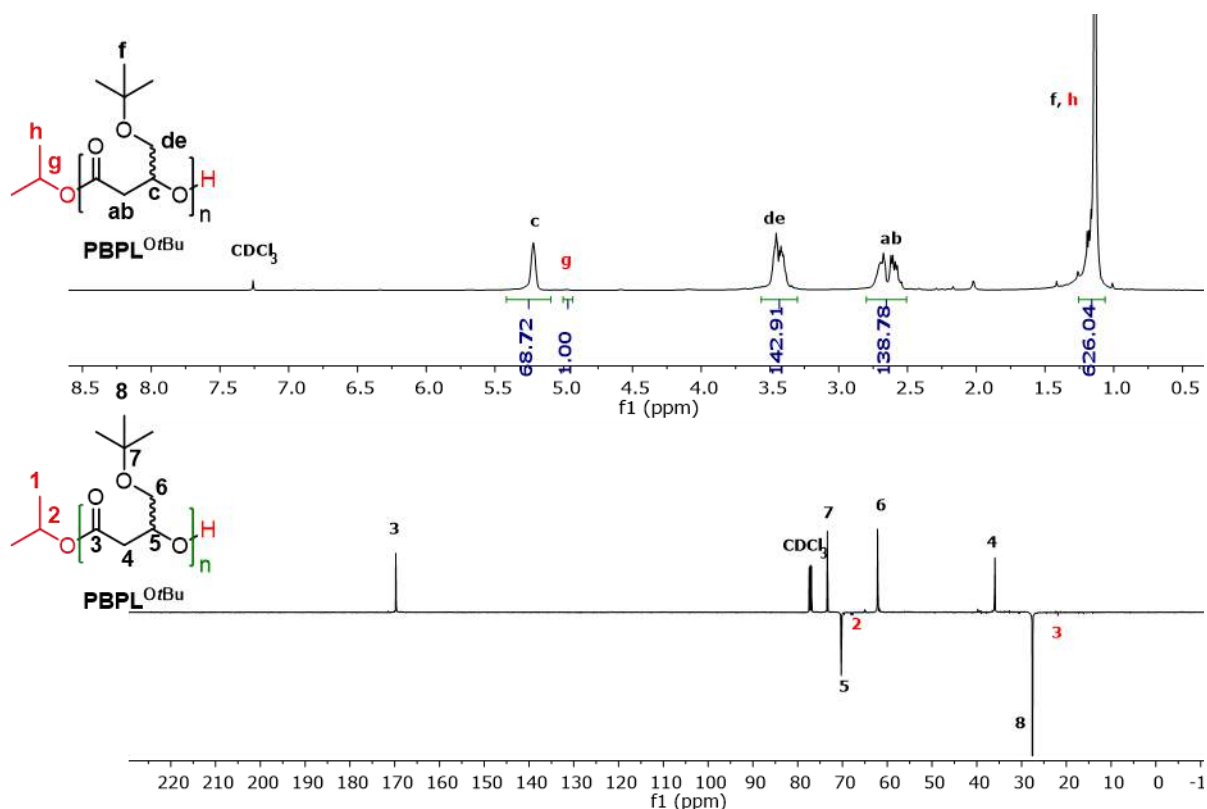
<sup>a</sup> Reactions performed with [BPL<sup>OrBu</sup>]<sub>0</sub> = 1.0 M. <sup>b</sup> Reaction time was not necessarily optimized. <sup>c</sup> Conversion of BPL<sup>OrBu</sup> as determined by <sup>1</sup>H NMR analysis of the crude reaction mixture. <sup>d</sup> Molar mass calculated according to  $M_{n,theo} = ([BPL^{OrBu}]_0/[2]_0 \times \text{CONV.BPL}^{OrBu}) \times M_{BPL^{OrBu}} + M_{iPrOH}$ , with  $M_{BPL^{OrBu}} = 158 \text{ g.mol}^{-1}$ ,  $M_{iPrOH} = 60 \text{ g.mol}^{-1}$ . <sup>e</sup> Molar mass determined by <sup>1</sup>H NMR analysis of the isolated polymer, from the resonances of the terminal O'Pr group (refer to Experimental section). <sup>f</sup> Number-average molar mass and dispersity ( $M_w/M_n$ ) determined by SEC analysis in THF at 30 °C vs. polystyrene standards. <sup>g</sup>  $P_r$  is the probability of *racemic* linkages between BPL<sup>OrBu</sup> units as determined by <sup>13</sup>C{<sup>1</sup>H} NMR analysis of the isolated PBPL<sup>OrBu</sup>s. <sup>h</sup> Glass transition temperature as determined by DSC. <sup>i</sup> Refer to the kinetic study (Figure 4. 35) <sup>j</sup> Not determined; <sup>k</sup> ROP of enantiopure (*S*)-BPL<sup>OrBu</sup>.

Generally, all the ROPs of *rac*-BPL<sup>OrBu</sup> in the presence of the catalytic system **2a-d**/(*i*PrOH) proved to display a control polymerization in term of molar masses ( $M_{n,theo}$ ,  $M_{n,NMR}$ ,  $M_{n,SEC}$ ), and dispersities ( $\mathcal{D}_M = 1.069$ –1.18). Furthermore, a linear plot was detected for experimental molar mass values with respect to *rac*-BPL<sup>OrBu</sup> monomer loading up to ca. 500 promoted by **2b**/(*i*PrOH) (1:1) catalytic system (Figure 4. 27).

**Figure 4. 27** – Variation of  $M_{n,NMR}$  ■,  $M_{n,SEC}$  ●, and  $M_{n,theo}$  (solid line) values of PBPL<sup>OrBu</sup> synthesized from the ROP of *rac*-BPL<sup>OrBu</sup> mediated by **2b**/(*i*PrOH) (1:1) catalytic system as a function of the BPL<sup>OrBu</sup> monomer loading (Table 4. 7 – entries 5-9).



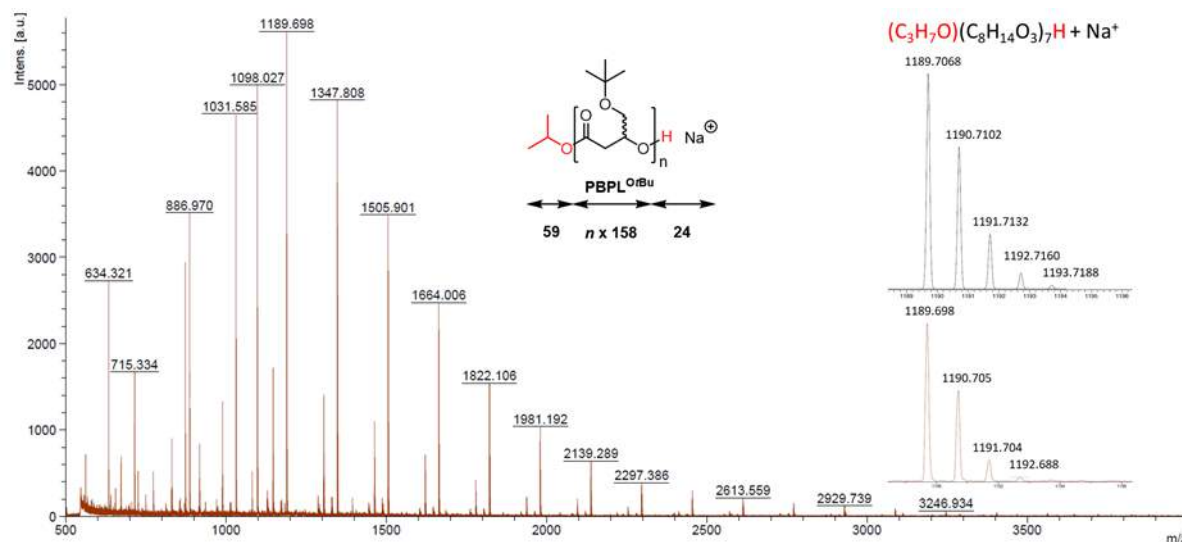
PBPL<sup>OrBu</sup> architectures were analysed by <sup>1</sup>H, J-MOD NMR (Figure 4. 28) and 2D COSY and HMBC NMR (Appendix 30,31). The spectra presented in Figure 4. 28, evidenced the formation of PBPL<sup>OrBu</sup> by the presence of methine and methylene signals of the BPL<sup>OrBu</sup> repeating unit with the isopropoxycarbonyl end-capped group ( $\delta$  (ppm): ca. 4.98 (CH<sub>3</sub>)<sub>2</sub>CHO–, ca. 1.19 (CH<sub>3</sub>)<sub>2</sub>CHO–).



**Figure 4. 28** – <sup>1</sup>H NMR (500 MHz, CDCl<sub>3</sub>, 25 °C) (top) and J-MOD (125 MHz, CDCl<sub>3</sub>, 25 °C) (bottom) spectra of syndiotactic PBPL<sup>OrBu</sup> prepared from the ROP of *rac*-BPL<sup>OrBu</sup> mediated by complex **2a** in the presence of *i*PrOH and precipitated twice in cold pentane (Table 4. 7, entry 11).

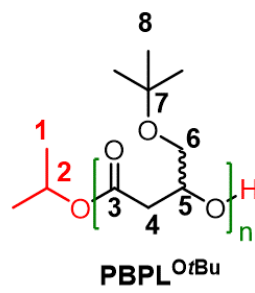
The MALDI-Tof mass spectrum of PBPL<sup>OrBu</sup> sample synthesized from the **2b**/*i*PrOH catalytic system (Table 4. 7, entry 5), showed the expected population of macromolecules having a repeating unit of  $m/z$  158, corresponding to  $\alpha$ -isopropoxy, $\omega$ -hydroxyl telechelic PBPL<sup>OrBu</sup> chains ionized by Na<sup>+</sup>. This was confirmed by the close match with the corresponding isotopic simulations, as illustrated for [(CH<sub>3</sub>)<sub>2</sub>CHO(COCH<sub>2</sub>CH(CH<sub>2</sub>OC<sub>4</sub>H<sub>9</sub>)O)<sub>*n*</sub>H]·Na<sup>+</sup> with, for example, calculated  $m/z$  1189.7068 versus found  $m/z$  1189.698 for  $n = 7$  (Figure 4. 29).





**Figure 4. 29** – MALDI-ToF MS (DCTB matrix, ionized by  $\text{Na}^+$ ) of  $\text{PBPL}^{\text{OrBu}}$  precipitated twice in cold pentane (Table 4. 7, entry 5). Right zoomed regions correspond to the simulated (top) and experimental (bottom) spectra.

The stereochemistry of  $\text{PBPL}^{\text{OrBu}}$  prepared by ROP of  $\text{rac-BPL}^{\text{OrBu}}$  through **2a-d**(*i*PrOH) catalytic system closely resembles that of  $\text{PBPL}^{\text{OiPr}}$ . All the isolated  $\text{PBPL}^{\text{OrBu}}$  samples revealed stereoregular with a syndiotactic enrichment whichever the complex used (**2a-d**) (Figure 4. 30). While **2d** (Cl-substituent) afforded almost the same enrichment of  $\text{PBPL}^{\text{OrBu}}$  as in  $\text{PBPL}^{\text{OiPr}}$  ( $P_r = 0.71$  and  $0.70$ , respectively), **2c** (Me-substituent) contributed to a slightly higher syndio-enrichment ( $P_r = 0.75$  vs.  $0.72$ ), and that of **2a** (cumyl-substituent) provided slightly inferior syndio-enrichment ( $P_r = 0.78$  vs.  $0.82$ ). Last, **2b** (*t*Bu-substituent) engendered the highest syndiotactic enrichment  $\text{PBPL}^{\text{OrBu}}$  ( $P_r = 0.84$ ), that matches with that of  $\text{PBPL}^{\text{OiPr}}$  ( $P_r = 0.85$ ). Hence, the general trend of **2a-d** catalysts to yield syndio-enriched  $\text{PBPL}^{\text{OrBu}}$  is the same as observed for  $\text{PBPL}^{\text{OiPr}}$ , but with minor differences in the enrichment in case of **2a,c**.



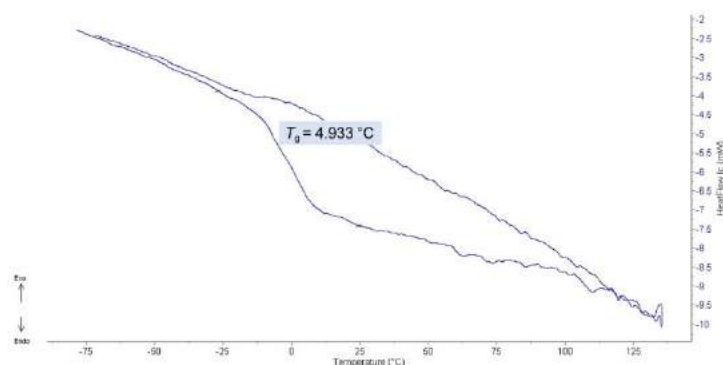


**Figure 4. 31** – DSC thermogram (heating rate of 10 °C min<sup>-1</sup>, second heating cycle –80 to 140 °C) of: syndiotactic PBPL<sup>OrBu</sup> ( $P_r$  0.84) synthesized by ROP of *rac*-BPL<sup>OrBu</sup> with **2b**/*i*PrOH (Table 4. 7, entry 6).

### 2.2.3. ROP of *rac*-BPL<sup>OTBDMS</sup>

The investigation of the ROP of *rac*-BPL<sup>OTBDMS</sup> in toluene at room temperature mediated by **2a-d**/*i*PrOH catalysts is represented in Table 4. 8. In the case of both **2c-d** (Me-, Cl-substituents), uncomplete or low conversions were obtained for *rac*-BPL<sup>OTBDMS</sup> loadings of ca. 30 and 60 after 2-3 days (Table 4. 8 – entries 1-3), with very low TOF<sub>2c</sub> = 0.1 h<sup>-1</sup> and TOF<sub>2d</sub> = 0.21 h<sup>-1</sup> (Table 4. 8 – entries 1,3; respectively). In the case of **2a-b** (*t*Bu- and cumyl-substituents), almost complete conversions were reached for *rac*-BPL<sup>OTBDMS</sup> loadings of 30–120 after 1–8 hours (Table 4. 8 – entries 4-7), with significantly higher TOF<sub>2a-b</sub> > 14.40–14.85 h<sup>-1</sup> (Table 4. 8 – entries 4,7). Nevertheless, the activity of **2a-d**/*i*PrOH catalysts in the presence of *rac*-BPL<sup>OTBDMS</sup> remained inferior to that in the presence of *rac*-BPL<sup>OrPr</sup> and *rac*-BPL<sup>OrBu</sup> (*vide supra*).

The catalytic system **2a-d**/*i*PrOH proved to display a control polymerization in term of molar masses ( $M_{n,theo}$ ,  $M_{n,NMR}$ ,  $M_{n,SEC}$ ), and dispersities ( $\mathcal{D}_M$  = 1.07–1.15), upon ring-opening *rac*-BPL<sup>OTBDMS</sup> (Table 4. 8).

**Table 4. 8** – Characteristics of the PBPL<sup>OTBDMS</sup> synthesized by ROP of *rac*-BPL<sup>OTBDMS</sup> mediated by **2a-d**/*i*PrOH catalytic systems in toluene at room temperature.

Entry	Cat.	[BPL <sup>OTBDMS</sup> ] <sub>0</sub> / [ <b>2</b> ] <sub>0</sub> / <i>i</i> PrOH] <sub>0</sub> <sup>a</sup>	Time <sup>b</sup> (h)	Conv. <sup>c</sup> (%)	$M_{n,theo}$ <sup>d</sup> (g.mol <sup>-1</sup> )	$M_{n,NMR}$ <sup>e</sup> (g.mol <sup>-1</sup> )	$M_{n,SEC}$ <sup>f</sup> (g.mol <sup>-1</sup> )	$\mathcal{D}_M$ <sup>f</sup>	$P_r$ <sup>g</sup>	$T_g$ <sup>h</sup> (°C)
1	<b>2d</b>	30:1:1	48	16	1800	2500	1000	1.07	0.69	<i>nd</i> <sup>j</sup>
2	<b>2c</b>	30:1:1	8	30	2000	1600	2500	1.14	<i>nd</i> <sup>j</sup>	<i>nd</i> <sup>j</sup>
3 <sup>i</sup>	<b>2c</b>	60:1:1	72	25	3300	3750	3000	1.12	0.77	<i>nd</i> <sup>j</sup>
4 <sup>i</sup>	<b>2b</b>	60:1:1	4	96	12500	13500	9000	1.13	0.83	0.7
5	<b>2b</b>	120:1:1	8	95	24 700	23 400	19 200	1.12	0.84	<i>nd</i> <sup>j</sup>
6	<b>2a</b>	30:1:1	1	98	6400	7600	8000	1.11	0.87	<i>nd</i> <sup>j</sup>
7 <sup>i</sup>	<b>2a</b>	60:1:1	4	99	12 900	12 350	10 000	1.10	0.87	1
8 <sup>k</sup>	<b>2a</b>	50:1:1	4	99	10300	9100	8400	1.15	<0.05	<i>nd</i> <sup>j</sup>

<sup>a</sup> Reactions performed with  $[\text{BPL}^{\text{OTBDMS}}]_0 = 1.0 \text{ M}$ . <sup>b</sup> Reaction time was not necessarily optimized. <sup>c</sup> Conversion of  $\text{BPL}^{\text{OTBDMS}}$  as determined by  $^1\text{H}$  NMR analysis of the crude reaction mixture. <sup>d</sup> Molar mass calculated according to  $M_{n,\text{theo}} = ([\text{BPL}^{\text{OTBDMS}}]_0/[2]_0 \times \text{conv.}_{\text{BPL}^{\text{OTBDMS}}} \times M_{\text{BPL}^{\text{OTBDMS}}}) + M_{i\text{PrOH}}$ , with  $M_{\text{BPL}^{\text{OTBDMS}}} = 216 \text{ g}\cdot\text{mol}^{-1}$ ,  $M_{i\text{PrOH}} = 60 \text{ g}\cdot\text{mol}^{-1}$ . <sup>e</sup> Molar mass determined by  $^1\text{H}$  NMR analysis of the isolated polymer, from the resonances of the terminal O<sup>i</sup>Pr group (refer to Experimental section). <sup>f</sup> Number-average molar mass and dispersity ( $M_w/M_n$ ) determined by SEC analysis in THF at 30 °C vs. polystyrene standards. <sup>g</sup>  $P_r$  is the probability of *racemic* linkages between  $\text{BPL}^{\text{OTBDMS}}$  units as determined by  $^{13}\text{C}\{^1\text{H}\}$  NMR analysis of the isolated  $\text{PBPL}^{\text{OTBDMS}}$ s. <sup>h</sup> Glass transition temperature as determined by DSC. <sup>i</sup> Refer to the kinetic study (Figure 4. 35) <sup>j</sup> Not determined; <sup>k</sup> ROP of enantiopure (*S*)- $\text{BPL}^{\text{OTBDMS}}$ .

$^1\text{H}$  and J-MOD NMR spectra of the isolated  $\text{PBPL}^{\text{OTBDMS}}$ s demonstrated the presence of the methine and methylene of the  $\text{BPL}^{\text{OTBDMS}}$  repeating unit, as well as the isopropoxycarbonyl chain-end group ( $\delta$  (ppm): ca. 4.98 ( $\text{CH}_3$ )<sub>2</sub>CHO–, ca. 1.21 ( $\text{CH}_3$ )<sub>2</sub>CHO–) (Figure 4. 32). 2D COSY and HMBC NMR also confirm the  $\text{PBPL}^{\text{OTBDMS}}$  architecture (Appendix 33,34).

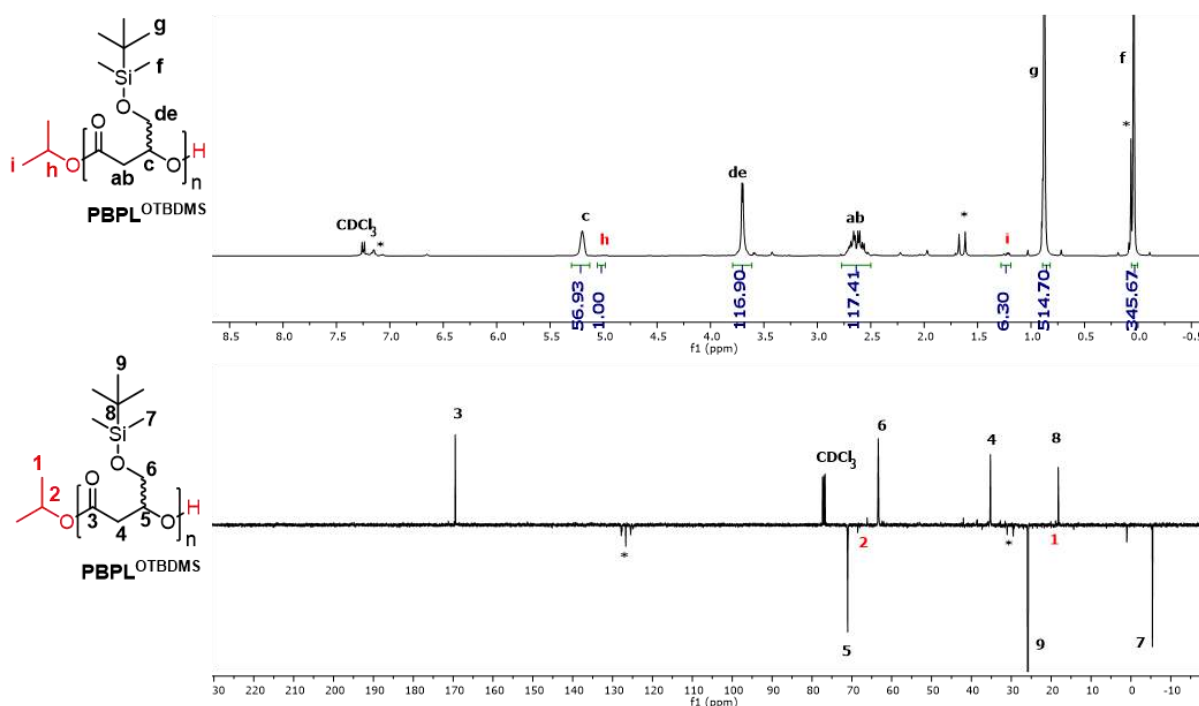


**Figure 4. 32** –  $^1\text{H}$  NMR (500 MHz,  $\text{CDCl}_3$ , 25 °C) (top) and J-MOD (125 MHz,  $\text{CDCl}_3$ , 25 °C) (bottom) spectra of syndiotactic  $\text{PBPL}^{\text{OTBDMS}}$  prepared from the ROP of *rac*- $\text{BPL}^{\text{OTBDMS}}$  mediated by complex **2a** in the presence of *i*PrOH and precipitated twice in cold pentane (Table 4. 8, entry 7); \* residual monomer, toluene, and water.

Similarly, to other bulky functional  $\beta$ -lactones ( $\text{PBPL}^{\text{OiPr}}$  and  $\text{PBPL}^{\text{OiBu}}$ ), all  $\text{PBPL}^{\text{OTBDMS}}$  macromolecules analysed by  $^{13}\text{C}$  NMR also revealed to be syndioenriched ( $P_r = 0.69$ – $0.87$ ; Figure 4. 33). Obviously, the stereochemistry is controlled by steric components only, where the ascending trend is as follow: **2d** (Cl-substituent);  $P_r = 0.69 < \mathbf{2c}$  (Me-substituent);  $P_r = 0.77 < \mathbf{2b}$  (*t*Bu-substituent);  $P_r = 0.84 < \mathbf{2a}$  (cumyl-substituent);  $P_r = 0.87$ .

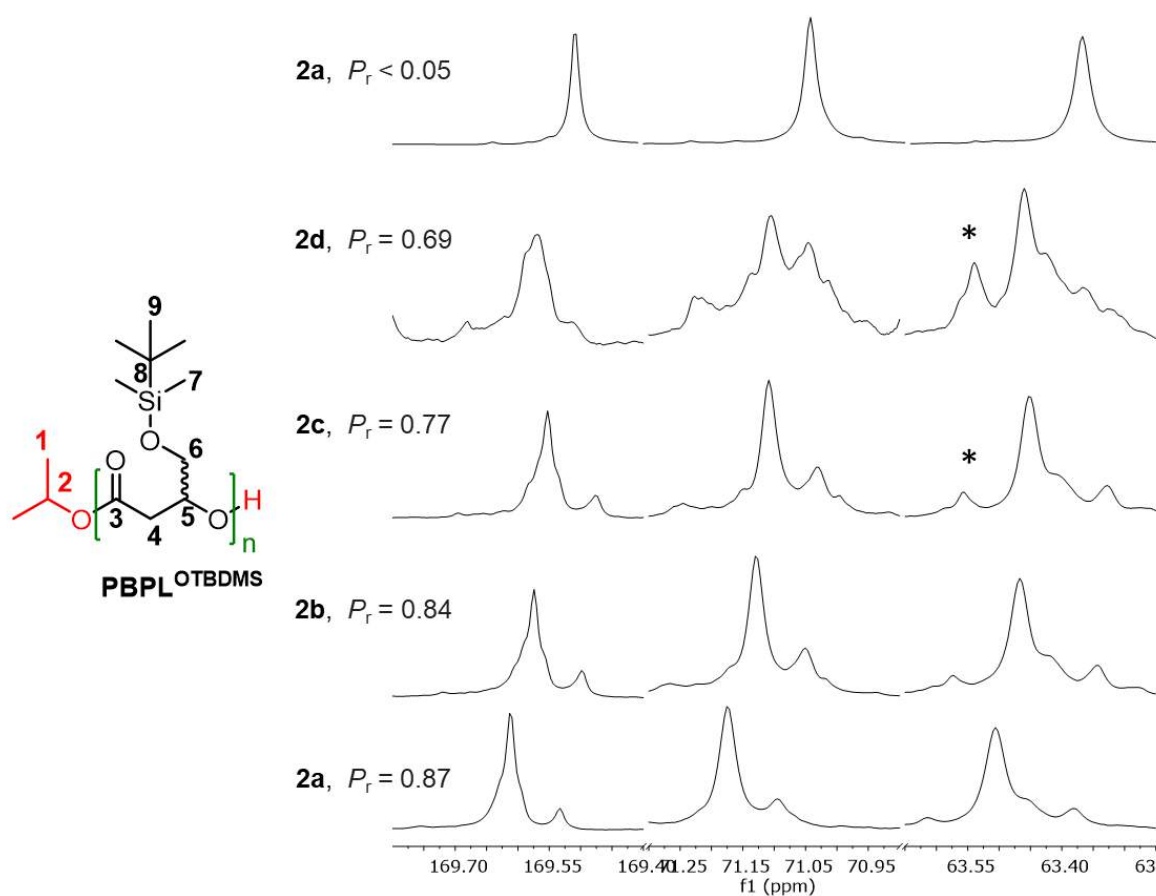


**Figure 4.33** – Regions of the  $^{13}\text{C}\{^1\text{H}\}$  NMR spectra (125 MHz,  $\text{CDCl}_3$ , 23 °C) of PBPL<sup>OTBDMS</sup> prepared by ROP of *rac*-BPL<sup>OTBDMS</sup>, except for the top spectra: of enantiopure (*S*)-BPL<sup>OTBDMS</sup> (Table 4. 8, entry 8), mediated by **2a**, **2b**, **2c**, or **2d**/*i*PrOH (Table 4. 8, entries 1,3,5,7); \* residual monomer.

The measured  $T_g$  for the isolated syndiotactic PBPL<sup>OTBDMS</sup> samples is nearly 1 °C (Figure 4.34). This value is also close to that obtained with syndiotactic PBPL<sup>O*i*Pr</sup> and PBPL<sup>O*t*Bu</sup> (*vide supra*). Moreover, the  $T_d^{\text{onset}}$ <sub>PBPL(OTBDMS)</sub> was measured by TgA to be 273 °C (Appendix 35), which is similar to that of  $T_d^{\text{onset}}$ <sub>PBPL(OPh/Sph)</sub> (*vide supra*).

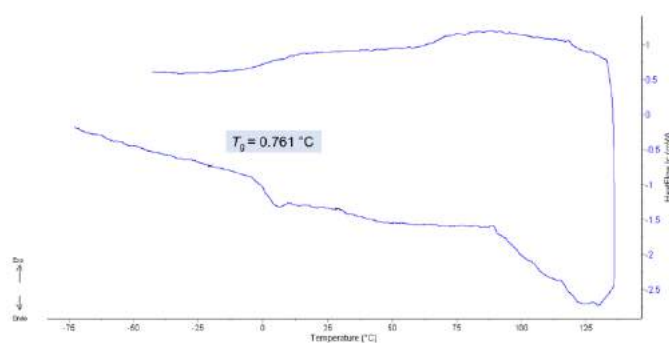


**Figure 4.34** – DSC thermogram (heating rate of 10 °C min<sup>-1</sup>, second heating cycle –80 to 140 °C) of: syndiotactic PBPL<sup>OTBDMS</sup> ( $P_r$  0.83) synthesized by ROP of *rac*-BPL<sup>OTBDMS</sup> with **2b**/*i*PrOH (Table 4. 8; entry 4).

### 2.2.1. Summary of the kinetics and the activity of the catalyst

Monitoring of NMR-scale polymerizations of  $\text{BPL}^{\text{O}i\text{Pr}/\text{O}t\text{Bu}/\text{OTBDMS}}$  performed with **2a-d** (*i*PrOH) confirmed the kinetics trend derived from batch experiments (Table 4. 6, Table 4. 7, Table 4. 8), and linear semi-logarithmic plots established that all reactions were first order in monomer (apparent rate constant  $k_{\text{app}} = 55.264\text{--}55.284$ ,  $\text{BPL}^{\text{O}i\text{Pr}/\text{O}t\text{Bu}}/\mathbf{2a-b}$ ;  $1.1427 \pm 0.072 \text{ min}^{-1}$ ,  $\text{BPL}^{\text{OTBDMS}}/\mathbf{2a}$ ;  $0.7972 \pm 0.0312 \text{ min}^{-1}$ ,  $\text{BPL}^{\text{OTBDMS}}/\mathbf{2b}$ ;  $0.3236 \pm 0.0331 \text{ min}^{-1}$ ,  $\text{BPL}^{\text{O}t\text{Bu}}/\mathbf{2c}$ ;  $0.2651 \pm 0.0321 \text{ min}^{-1}$ ,  $\text{BPL}^{\text{O}i\text{Pr}}/\mathbf{2c}$ ;  $0.0462 \pm 0.0412 \text{ min}^{-1}$ ,  $\text{BPL}^{\text{O}t\text{Bu}}/\mathbf{2d}$ ;  $0.0088 \text{ min}^{-1}$ ,  $\text{BPL}^{\text{O}i\text{Pr}}/\mathbf{2d}$ ;  $0.0037 \pm 0.0033 \text{ min}^{-1}$ ,  $\text{BPL}^{\text{OTBDMS}}/\mathbf{2c}$  (Figure 4. 35). The major overall trend for the monomers' ROP ability is thus  $\text{BPL}^{\text{O}t\text{Bu}} \geq \text{BPL}^{\text{O}i\text{Pr}} \gg \text{BPL}^{\text{OTBDMS}}$ , while the catalysts' activity thus generally followed the order **2a-b**  $\gg$  **2c**  $\gg$  **2d**, as previously obtained for the previous ROP of various  $\text{BPL}^{\text{FG}}$ s  $\beta$ -lactones (FG = OAll, OBn, OMe, OPh,  $\text{CH}_2\text{OBn}$ , SPh) promoted by these catalyst systems (*vide supra*).

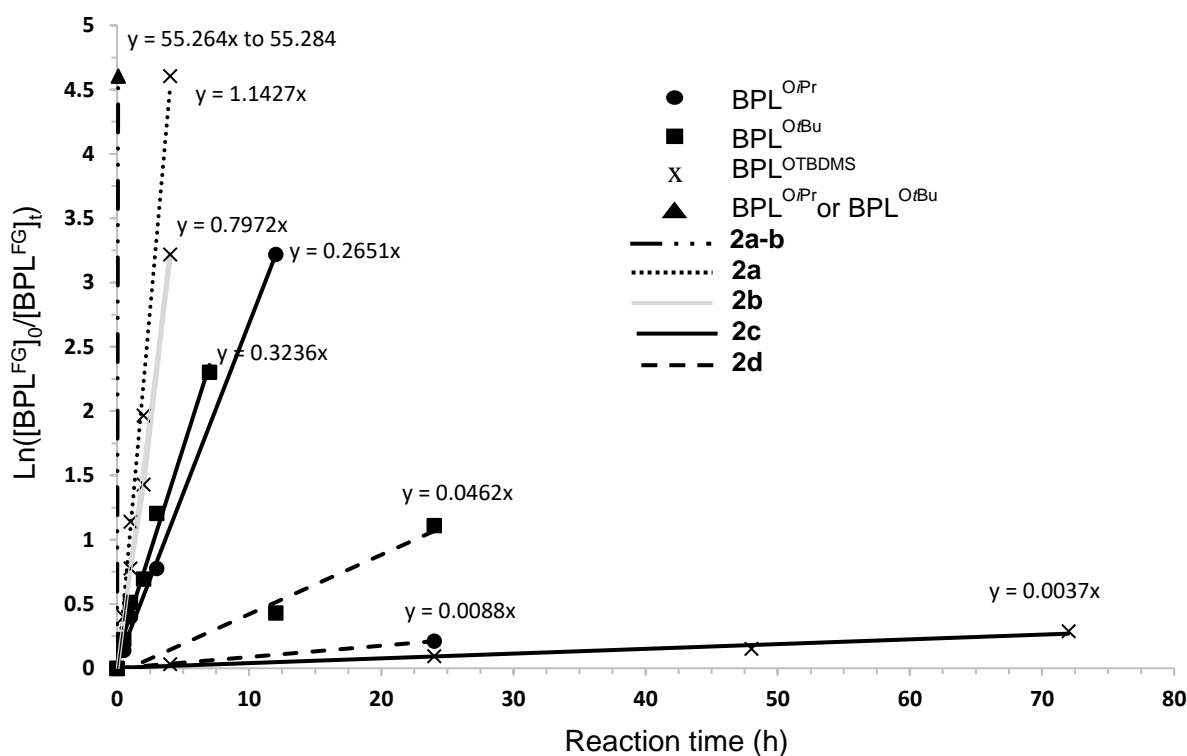


**Figure 4. 35** – Semi-logarithmic first-order plots for the ROP of *rac*- $\text{BPL}^{\text{FG}}$ s (FG = *O*<sup>*i*</sup>Pr, *O*<sup>*t*</sup>Bu, OTBDMS) mediated by **2a-d** (*i*PrOH) (20 °C, toluene;  $[\text{BPL}^{\text{FG}}]_0/[\mathbf{2a-c}]_0/[i\text{PrOH}]_0 = 60/75:1:1$  and  $[\text{BPL}^{\text{FG}}]_0/[\mathbf{2d}]_0/[i\text{PrOH}]_0 = 25/30:1:1$ ): **2a** (Table 4. 6, entry 9; Table 4. 7, entry 11; Table 4. 8, entry 7); **2b** (Table 4. 6, entry 6; Table 4. 7, entry 6; Table 4. 8, entry 4); **2c** (Table 4. 6, entry 3; Table 4. 7, entry 4; Table 4. 8, entry 3) and **2d** (Table 4. 6, entry 1; Table 4. 7, entry 1); plots from **2a-b** all overlap due to similar high activity of these catalysts regardless of the monomer functionality, and are represented as ▲.

### 2.2.2. Recapitulation on PBPL<sup>O<sub>i</sub>Pr/O<sub>t</sub>Bn/OTBDMS</sup>

Highly stereoregular and high molar masses PBPL<sup>O<sub>i</sub>Pr</sup>, PBPL<sup>O<sub>t</sub>Bu</sup> and PBPL<sup>OTBDMS</sup> (reaching  $M_{n,SEC(OtBu)} = 94,300$ ;  $\bar{D}_M = 1.18$ ;  $P_r = 0.84$ ) were successfully synthesized by stereoselective controlled ROP of the corresponding *rac*-BPL<sup>O<sub>i</sub>Pr</sup>, *rac*-BPL<sup>O<sub>t</sub>Bu</sup> and *rac*-BPL<sup>OTBDMS</sup>, respectively, promoted by diverse achiral diamino-bis(phenolate) yttrium complexes (Y{ONNO<sup>R<sub>1</sub>,R<sub>2</sub></sup>}), **2a-d**). The influence of the BPL<sup>FG</sup> monomers with various steric hindrance of their functionality (FG = O<sup>i</sup>Pr, O<sup>t</sup>Bu, OTBDMS), on the thermal properties and the stereoselectivity of **2a-d** catalysts were regarded with respect to the previously reported similar but less hindered BPL<sup>FGs</sup> (FG = OMe, OAll; with extra methylene hydrogens) and are gathered in Table 4. 9.

Highly syndiotactic PBPL<sup>O<sub>i</sub>Pr/O<sub>t</sub>Bu/OTBDMS</sup> were obtained by **2a-b**, alike PBPL<sup>OMe/OAll</sup> ( $P_r = 0.78$ – $0.87$  vs.  $0.78$ – $0.84$ ; respectively). Nonetheless, trading 1H or 2H (of *rac*-BPL<sup>OMe/OAll</sup> on C<sub>B</sub>; Figure 4. 5) by 1Me, 2Me or completely removing the methylene (*rac*-BPL<sup>O<sub>i</sub>Pr/O<sub>t</sub>Bu/OTBDMS</sup>; Figure 4. 21), resulted in changing the stereoregularity from atactic to syndio-enriched polyesters with catalyst **2c** ( $P_r = 0.49$  vs.  $0.71$ – $0.77$ , respectively). In addition, it induced the switch from isotactic to syndio-enriched polymers in the case of catalyst **2d** ( $P_r = 0.09$ – $0.10$  vs.  $0.69$ – $0.71$ , respectively). The  $T_g$  values detected for crowded functional PHAs (PBPL<sup>O<sub>i</sub>Pr/O<sub>t</sub>Bu/OTBDMS</sup>) hardly changed from one to another, whichever the functionality, and ranged from 0–5 °C. However, the latter values are much higher than those detected for uncrowded functional PHAs (PBPL<sup>OMe/OAll</sup>), that have negative  $T_g$  values (–40– –12 °C). This is probably because bulkier groups are less flexible leading to decrease the mobility of the polymeric chains and hence affording higher  $T_g$  values.

**Table 4. 9** –  $P_r$  and  $T_g$  values of PBPL<sup>OMe</sup>, PBPL<sup>OAll</sup>, PBPL<sup>OiPr</sup>, PBPL<sup>OBu</sup> and PBPL<sup>OTBDMS</sup> prepared from the stereoselective ROP of *rac*-BPL<sup>OMe</sup>, *rac*-BPL<sup>OAll</sup>, *rac*-BPL<sup>OiPr</sup>, *rac*-BPL<sup>OBu</sup> and *rac*-BPL<sup>OTBDMS</sup> mediated by **2a-d**.

<i>rac</i> -BPL <sup>FGs</sup>					
$R^1, R^2$	<i>rac</i> -BPL <sup>OMe</sup> [11]	<i>rac</i> -BPL <sup>OAll</sup> [11]	<i>rac</i> -BPL <sup>OiPr</sup>	<i>rac</i> -BPL <sup>OBu</sup>	<i>rac</i> -BPL <sup>OTBDMS</sup>
<b>Crowded (2a-b)</b>	Syndiotactic $P_r = 0.78\text{--}0.81$ $T_g = -12\text{ }^\circ\text{C}$	Syndiotactic $P_r = 0.81\text{--}0.84$ $T_g = -38\text{ }^\circ\text{C}$	Syndiotactic $P_r = 0.82\text{--}0.85$ $T_g = 2.1\text{--}2.2\text{ }^\circ\text{C}$	Syndiotactic $P_r = 0.78\text{--}0.84$ $T_g = 5\text{ }^\circ\text{C}$	Syndiotactic $P_r = 0.83\text{--}0.87$ $T_g = 0.7\text{--}1\text{ }^\circ\text{C}$
<b>Non-crowded 2c</b>	Atactic $P_r = 0.49$ $T_g = -18\text{ }^\circ\text{C}$	Atactic $P_r = 0.49$ $T_g = -40\text{ }^\circ\text{C}$	Syndiotactic $P_r = 0.71\text{--}0.72$ $T_g = 1.8\text{ }^\circ\text{C}$	Syndiotactic $P_r = 0.74\text{--}0.75$ $T_g = 3\text{ }^\circ\text{C}$	Syndiotactic $P_r = 0.77$ $T_g = nd^a$
<b>Halogenated non-crowded 2d</b>	Isotactic $P_r = 0.10$ $T_g = -12\text{ }^\circ\text{C}$	Isotactic $P_r = 0.09$ $T_g = nd^a$	Syndiotactic $P_r = 0.69\text{--}0.70$ $T_g = nd^a$	Syndiotactic $P_r = 0.70\text{--}0.71$ $T_g = 3\text{ }^\circ\text{C}$	Syndiotactic $P_r = 0.69$ $T_g = nd^a$

<sup>a</sup> not determined

### 2.3. Preliminary investigations of the ROP of *rac*-BPL<sup>OP(O)Ph2</sup>

In the first place, the ROP of *rac*-BPL<sup>OP(O)Ph2</sup> was investigated mainly with **2b** yttrium complex (for its high activity with  $\beta$ -lactones (*vide supra*); Y{ONNO<sup>tBu</sup>2}/[*i*PrOH]) in toluene at room temperature. Different monomer loadings and different conditions (temperature, homopolymerization, copolymerization with *rac*-BPL<sup>OAll</sup> and *rac*-BL<sup>Me</sup>) were also tested and data are all collected in Table 4. 10. Despite that monomer loadings as low as 10 and 30 were first used, the ROP proceeded very slowly giving only 38% and 66% *rac*-BPL<sup>OP(O)Ph2</sup> conversion after 3 h and 6 days (42% after 42 h), respectively (Table 4. 10 – entries 1,2). An attempt to promote the propagation by raising the temperature from 23 to 60 °C with 30 monomer units, only resulted in an insignificant increase in conversion (38% to 42% conversion in 3 h, Table 4. 10 – entries 2,3). Furthermore, the control observed in the homopolymerization of *rac*-BPL<sup>OP(O)Ph2</sup> in terms of molar masses and dispersities (Table 4. 10 – entries 1-3;  $\bar{M}_n = 1.09\text{--}135$ ) remained poorer than those recorded for the ROP of all other BPL<sup>FGs</sup> mediated by the same catalytic system (**2b**/*i*PrOH) (*vide supra*). Possible causes for the slow or incomplete propagation include either the diphenylphosphinate functionality that may coordinate the yttrium through its P(O) group and thus impeded/inhibit its reactivity, or the presence of undesirable transfer/termination reactions ultimately hampering the polymerization.

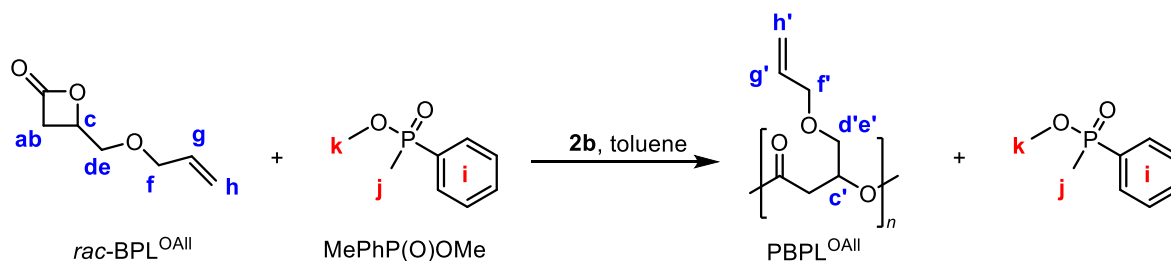


**Table 4. 10** – Characteristics of the PBPL<sup>OP(O)Ph2</sup>, PBPL<sup>OP(O)Ph2-co-PBPL<sup>OAll</sup></sup>, PBPL<sup>OP(O)Ph2-co-PBL<sup>Me</sup></sup> synthesized by ROP of *rac*-BPL<sup>OP(O)Ph2</sup> and ROP of *rac*-BPL<sup>OP(O)Ph2</sup> with *rac*-BPL<sup>OAll</sup> or *rac*-BL<sup>Me</sup>, mediated by **2b**/(*i*PrOH) catalytic systems in toluene at room temperature.

Entry	[BPL <sup>OP(O)Ph2</sup> ] <sub>0</sub> /[BPL <sup>OAll</sup> ] <sub>0</sub> /[ <b>2b</b> ] <sub>0</sub> /[ <i>i</i> PrOH] <sub>0</sub> <sup>a</sup>	Time <sup>b</sup> (h)	Conv. [BPL <sup>OP(O)Ph2</sup> ] <sub>0</sub> /[BPL <sup>OAll</sup> ] <sub>0</sub> <sup>c</sup> (%)	<i>M</i> <sub>n,theo</sub> <sup>d</sup> (g.mol <sup>-1</sup> )	<i>M</i> <sub>n,NMR</sub> <sup>e</sup> (g.mol <sup>-1</sup> )	<i>M</i> <sub>n,SEC</sub> <sup>f</sup> (g.mol <sup>-1</sup> )	<i>D</i> <sub>M</sub> <sup>f</sup>
1	10:0:1:1	42 144	42/0 66/0	1350 2050	1100 1750	<i>nd</i> <sup>g</sup> 1800	<i>nd</i> <sup>g</sup> 1.09
2	30:0:1:1	3	38/0	3500	2200	7000	1.32
3 <sup>h</sup>	30:0:1:1	3	42/0	3900	4300	6600	1.35
4	0:25:1:1	1	100	3600	3500	4100	1.12
5 <sup>i</sup>	25:25:1:1	24 72	19 40	1000 1850	1050 2000	<i>nd</i> <sup>g</sup> <i>nd</i> <sup>g</sup>	<i>nd</i> <sup>g</sup> <i>nd</i> <sup>g</sup>
6	1:0:1:0	12	90	<i>nd</i> <sup>g</sup>	<i>nd</i> <sup>g</sup>	<i>nd</i> <sup>g</sup>	<i>nd</i> <sup>g</sup>
7	25:25:1:1	4	55/48	5900	3350	6700	1.40
8	25:55:1:1	4 144	50/25 63/41	5750 8000	5400 6650	<i>nd</i> <sup>g</sup> 8000	<i>nd</i> <sup>g</sup> 1.39
9 <sup>j</sup>	25:25:1:1	24	47/33	4350	3100	8100	1.38

<sup>a</sup> Reactions performed with [BPL<sup>OP(O)Ph2</sup>]<sub>0</sub> = 1.0 M or [BPL<sup>OP(O)Ph2</sup>]<sub>0</sub>/[BPL<sup>OAll</sup>]<sub>0</sub> = 1.0 M <sup>b</sup> Reaction time was not necessarily optimized. <sup>c</sup> Conversion of BPL<sup>OP(O)Ph2</sup> and BPL<sup>OAll</sup> as determined by <sup>1</sup>H NMR analysis of the crude reaction mixture. <sup>d</sup> Molar mass calculated for homopolymers according to *M*<sub>n,theo</sub> = [BPL<sup>OP(O)Ph2/OAll</sup>]<sub>0</sub>/[**2b**]<sub>0</sub> × conv.BPL(OP(O)Ph2/OAll) × *M*<sub>BPL(OP(O)Ph2/OAll)</sub> + *M*<sub>*i*PrOH</sub>, and molar mass calculated for copolymers according to *M*<sub>n,theo</sub>(PBPL(OP(O)Ph2)-co-PBPL(OAll)) = ([BPL<sup>OP(O)Ph2</sup>]<sub>0</sub>/[**2b**]<sub>0</sub> × conv.BPL(OP(O)Ph2) × *M*<sub>BPL(OP(O)Ph2)</sub>) + ([BPL<sup>OAll</sup>]<sub>0</sub>/[**2b**]<sub>0</sub> × conv.BPL(OAll) × *M*<sub>BPL(OAll)</sub>) + *M*<sub>*i*PrOH</sub>, with *M*<sub>BPL(OP(O)Ph2)</sub> = 302 g.mol<sup>-1</sup>, *M*<sub>BPL(OAll)</sub> = 142 g.mol<sup>-1</sup>, *M*<sub>*i*PrOH</sub> = 60 g.mol<sup>-1</sup>. <sup>e</sup> Molar mass determined by <sup>1</sup>H NMR analysis of the isolated polymer, from the resonances of the terminal O<sup>*i*</sup>Pr group (refer to Experimental section). <sup>f</sup> Number-average molar mass and dispersity (*M*<sub>w</sub>/*M*<sub>n</sub>) determined by SEC analysis in THF at 30 °C vs. polystyrene standards; <sup>g</sup> Not determined; <sup>h</sup> ROP performed at 60 °C; <sup>i</sup> methoxy methyl(phenyl)phosphinate (MePhP(O)OMe) was used in place of *rac*-BPL<sup>OP(O)Ph2</sup>; <sup>j</sup> *rac*-BL<sup>Me</sup> is used instead of *rac*-BPL<sup>OAll</sup>, with *M*<sub>BL(Me)</sub> = 86 g.mol<sup>-1</sup>.

To investigate the first above-mentioned hypothesis, methoxy methyl(phenyl)phosphinate (MePhP(O)OMe) was added to the catalytic system to mimic the effect of the possible O–P=O... Y-**2b** coordination onto the ROP of the high reactive *rac*-BPL<sup>OAll</sup> β-lactone (Scheme 4. 5).



**Scheme 4. 5** – ROP of *rac*-BPL<sup>OAll</sup> via **2b** in the presence of MePhP(O)OMe (Table 4. 10, entry 5); the labelling alphabetic (blue and red) are for the <sup>1</sup>H NMR (*vide infra*).

While that the ROP of 25 monomer units of *rac*-BPL<sup>OAll</sup> mediated by **2b** in toluene at room temperature leads to its complete conversion in less than 1 h (Table 4. 10 – entry 4), the ROP of *rac*-BPL<sup>OAll</sup> under the same conditions but in the presence of 25 equivalent of

MePhP(O)OMe, only reached 19% conversion in 1 day and 40% in 3 days, as determined by  $^1\text{H}$  NMR analysis (Table 4. 10 – entry 5; Figure 4. 36).

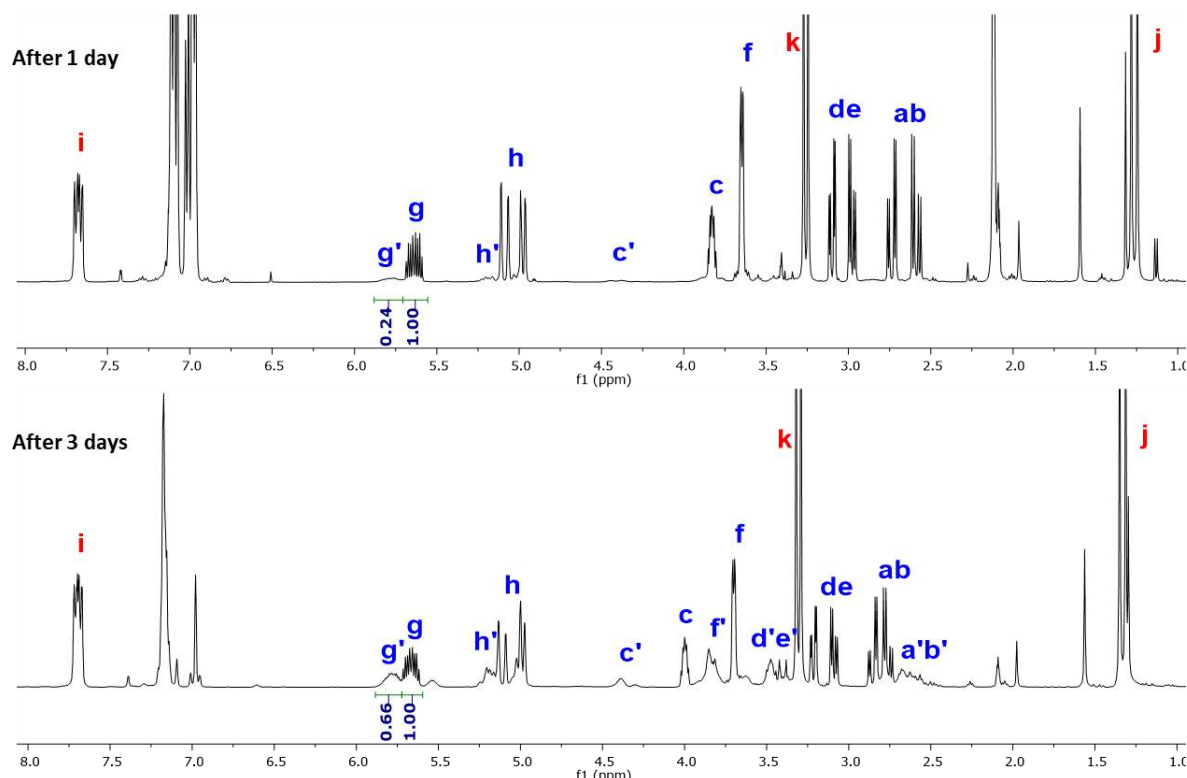


**Figure 4. 36** –  $^1\text{H}$  NMR (400 MHz,  $\text{CDCl}_3$ , 25 °C) spectra of crude PBPL<sup>OAll</sup> prepared from the ROP of *rac*-BPL<sup>OAll</sup> mediated by complex **2b** in the presence of *i*PrOH and MePhP(O)OMe after 1 day (top) and 3 days (bottom) (Table 4. 10, entry 5).

In addition, the  $^{31}\text{P}$  NMR spectra of the polymerization displayed a small shift of the signal from free MePhP(O)OMe ( $\Delta\delta = 0.42$  ppm) suggesting its (partial) coordination to the yttrium metal center (Figure 4. 37), thereby somewhat inhibiting the catalyst.

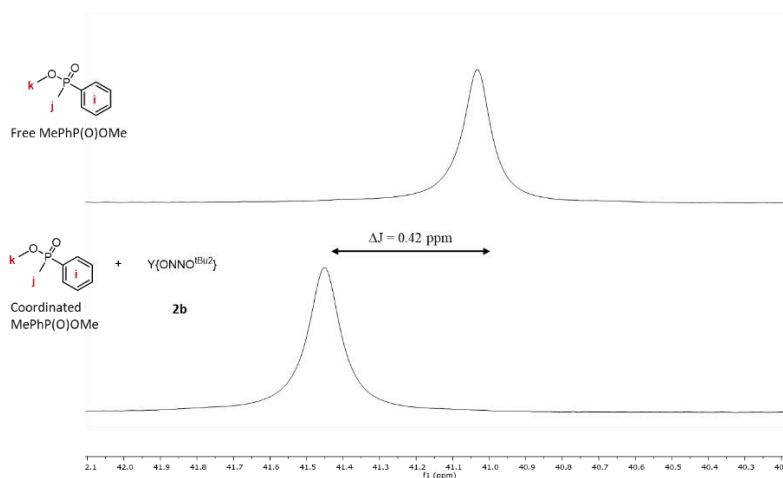


**Figure 4. 37** –  $^{31}\text{P}$  NMR (125 MHz,  $\text{CDCl}_3$ , 25 °C) spectra of free MePhP(O)OMe (top) and in the polymerization medium of *rac*-BPL<sup>OAll</sup> with **2b**, possibly coordinated (bottom) (Table 4. 10, entry 5).

Since  $rac\text{-BPL}^{\text{OP(O)Ph}_2}$  was anticipated to behave as its  $\text{MePhP(O)OMe}$  analogue, an equimolar reaction between  $rac\text{-BPL}^{\text{OP(O)Ph}_2}$  and  $\text{Y}\{\text{ONNO}^{\text{tBu}_2}\}$  (**2b**) was performed in the absence of  $i\text{PrOH}$  in deuterated toluene at room temperature in a Young NMR tube, aiming to crystallize a product that could manifest the coordination of  $rac\text{-BPL}^{\text{OP(O)Ph}_2}$  to  $\text{Y}\{\text{ONNO}^{\text{tBu}_2}\}$ . However, after 12 h, 90% of the monomer was converted to  $\text{PBPL}^{\text{OP(O)Ph}_2}$  (Table 4. 10 – entry 6) as detected by  $^1\text{H}$  and  $^{31}\text{P}$  NMR ( $\delta$  20.91 ppm) spectra (Figure 4. 38). Noteworthy, the signals in  $^{31}\text{P}$  NMR at  $\delta$  38.00 and 37.93 ppm may be the remaining (10%) monomer coordinating to **2b** (Figure 4. 38 – bottom).

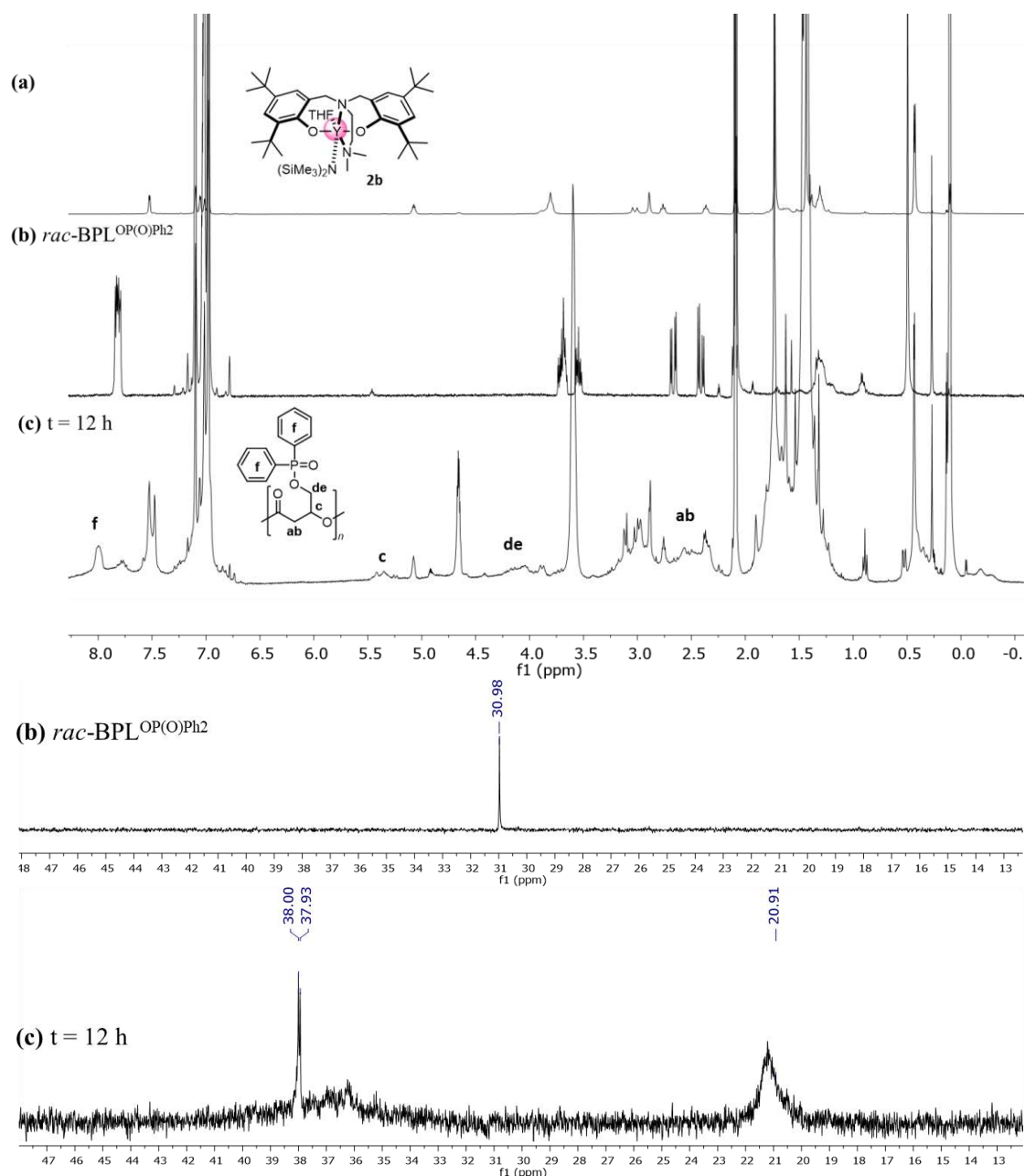


**Figure 4. 38** – Equimolar reaction between  $rac\text{-BPL}^{\text{OP(O)Ph}_2}$  and  $\text{Y}\{\text{ONNO}^{\text{tBu}_2}\}$ ;  $^1\text{H}$  NMR (400 MHz,  $\text{tol-}d_8$ , 25 °C) (up) and  $^{31}\text{P}$  (162 MHz,  $\text{CDCl}_3$ , 25 °C) (bottom) spectra of catalyst **2b** (a);  $rac\text{-BPL}^{\text{OP(O)Ph}_2}$  (b); crude  $\text{PBPL}^{\text{OP(O)Ph}_2}$  obtained after 12 h presented (c) (Table 4. 10, entry 6).

While the latter experiments may hint at the presence of some  $P(O)\dots$ yttrium coordination that can obstruct the propagation, it may be overcome by a high catalyst (**2b**) loading or by a low  $rac\text{-BPL}^{OP(O)Ph_2}$  feed. Therefore, the simultaneous copolymerization of  $rac\text{-BPL}^{OP(O)Ph_2}$  with  $rac\text{-BPL}^{OAll}$  or  $rac\text{-BL}^{Me}$  were performed, expecting to enhance the propagation of  $PBPL^{OP(O)Ph_2}$  active chains (Table 4. 10 – entries 7-9). However, the conversion of  $rac\text{-BPL}^{OP(O)Ph_2}$  remained around 50% after 4 h, only further increasing up to 63% after 6 days (Table 4. 10 – entry 8). The copolymerization afforded oligomers of  $P(BPL^{OP(O)Ph_2}\text{-}co\text{-}BPL^{OAll})$  ( $M_{n,sec} = 8000 \text{ g mol}^{-1}$ ,  $D_M = 1.39$ ) and  $P(BPL^{OP(O)Ph_2}\text{-}co\text{-}BL^{Me})$  ( $M_{n,sec} = 8100 \text{ g mol}^{-1}$ ,  $D_M = 1.38$ ) (Table 4. 10 – entries 7,9). The corresponding  $^1H$  NMR and  $^{31}P$  NMR are depicted in Figure 4. 39 and Figure 4. 40, presenting the methine and methylene signals of the copolymers and  $PBPL^{OP(O)Ph_2}$  signals in  $^{31}P$  NMR ( $\delta$  32.23–33.36 ppm; *vide infra*). Noteworthy, the conversions were calculated from  $BPL^{OAll}$  signal ( $\delta$  4.66 ppm) and  $PBPL^{OAll}$  methine hydrogen ( $\delta$  5.79 ppm), and that of  $BPL^{OP(O)Ph_2}$  ( $\delta$  4.77 ppm) and  $PBPL^{OP(O)Ph_2}$  aromatic hydrogens signal ( $\delta$  7.82 ppm), for  $P(BPL^{OP(O)Ph_2}\text{-}co\text{-}BPL^{OAll})$ . For  $P(BPL^{OP(O)Ph_2}\text{-}co\text{-}BL^{Me})$ , they were calculated from  $BL^{Me}$  signal ( $\delta$  4.69 ppm) and  $PBL^{Me}$  methine hydrogen ( $\delta$  5.17 ppm), and that of  $BPL^{OP(O)Ph_2}$  ( $\delta$  4.79 ppm) and  $PBPL^{OP(O)Ph_2}$  methine hydrogen signal ( $\delta$  5.41 ppm).

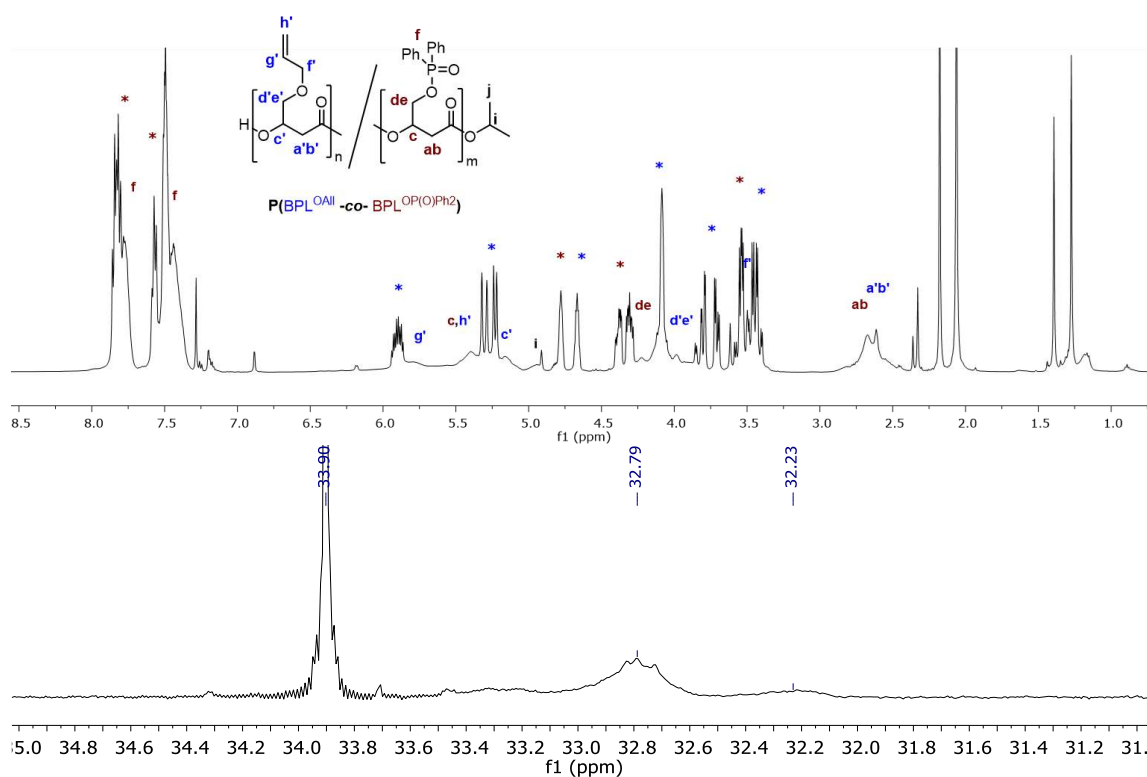


**Figure 4. 39** –  $^1H$  NMR (400 MHz,  $CDCl_3$ , 25 °C) (top) and  $^{31}P$  (162 MHz,  $CDCl_3$ , 25 °C) (bottom) spectra of  $P(BPL^{OP(O)Ph_2}\text{-}co\text{-}BPL^{OAll})$  prepared from the ROP of  $rac\text{-BPL}^{OP(O)Ph_2}$  and  $rac\text{-BPL}^{OAll}$  mediated by complex **2b** in the presence of  $iPrOH$  (Table 4. 10, entry 7); \* : unreacted monomer (blue\* for  $rac\text{-BPL}^{OAll}$  and red\* for  $rac\text{-BPL}^{OP(O)Ph_2}$  in  $^1H$  NMR); and  $\delta$  33.90 in  $^{31}P$  NMR is for the unreacted  $rac\text{-BPL}^{OP(O)Ph_2}$ .

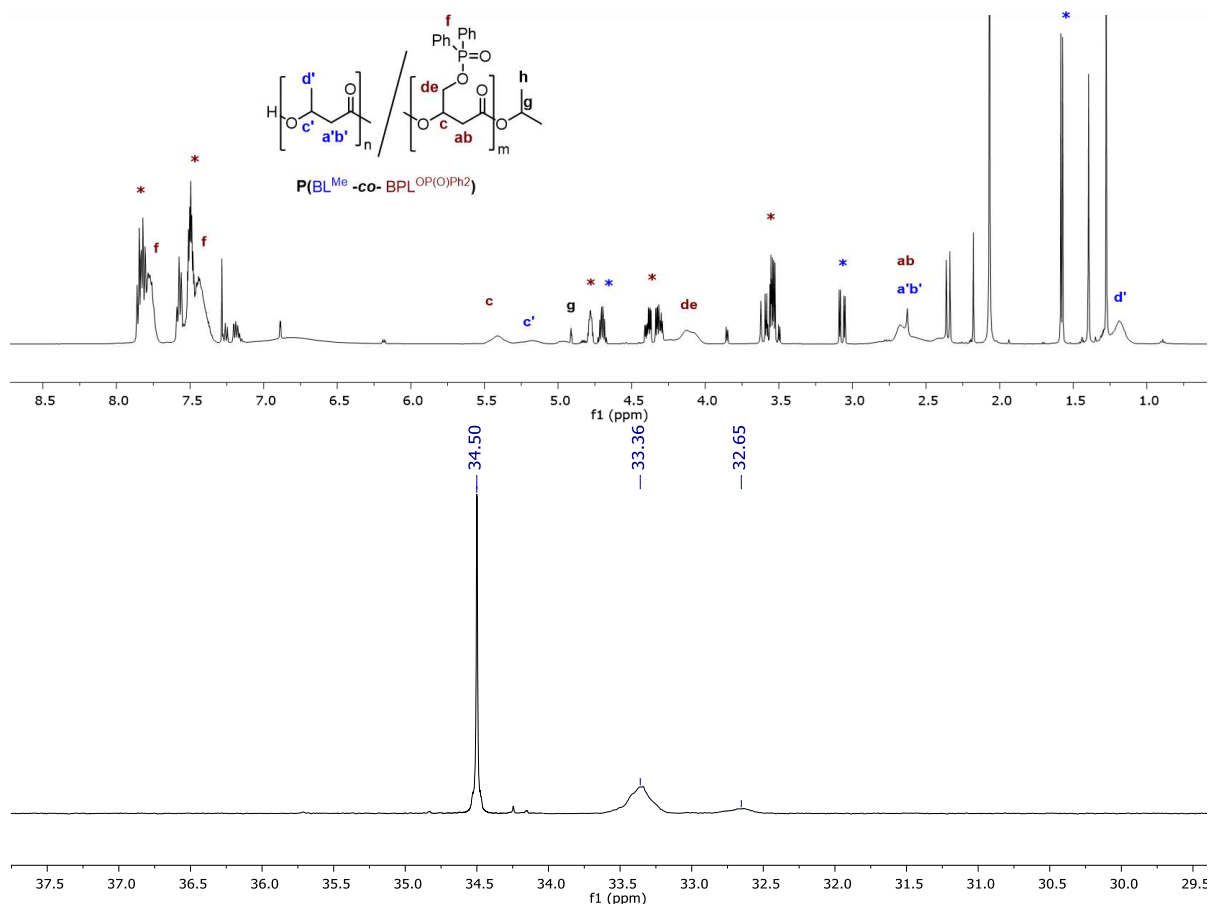


**Figure 4. 40** –  $^1\text{H}$  NMR (400 MHz,  $\text{CDCl}_3$ , 25  $^\circ\text{C}$ ) (top) and  $^{31}\text{P}$  (162 MHz,  $\text{CDCl}_3$ , 25  $^\circ\text{C}$ ) (bottom) spectra of  $\text{P}(\text{BPL}^{\text{OP}(\text{O})\text{Ph}_2}\text{-co-BL}^{\text{Me}})$  prepared from the ROP of  $\text{rac-BPL}^{\text{OP}(\text{O})\text{Ph}_2}$  and  $\text{rac-BPL}^{\text{OAll}}$  mediated by complex **2b** in the presence of  $i\text{PrOH}$  (Table 4. 10, entry 10); \*: unreacted monomer (blue\* for  $\text{rac-BL}^{\text{Me}}$  and red\* for  $\text{rac-BPL}^{\text{OP}(\text{O})\text{Ph}_2}$  in  $^1\text{H}$  NMR); and  $\delta$  34.50 in  $^{31}\text{P}$  NMR is for the unreacted  $\text{rac-BPL}^{\text{OP}(\text{O})\text{Ph}_2}$ .

The second hypothesis (presence of transfer or termination reactions) was checked by analysing the  $^1\text{H}$  NMR,  $^{31}\text{P}$  NMR and 2D COSY of the homopolymers of  $\text{PBPL}^{\text{OP}(\text{O})\text{Ph}_2}$  produced at room temperature and at 60  $^\circ\text{C}$  through **2b**/ $i\text{PrOH}$  (Table 4. 10 – entries 2,3), that are displayed in Figure 4. 41 and Figure 4. 42, respectively. Unexpectedly, the NMR spectra demonstrate the presence of two distinct  $\text{PBPL}^{\text{OP}(\text{O})\text{Ph}_2}$  populations, a major one end-capped with an isopropoxycarbonyl and a hydroxy group (**3**), and a minor one with isopropoxycarbonyl and an  $\alpha,\beta$ -unsaturated system (or crotonate) (**4**). Unfortunately, the latter population (**4**) corresponds to dead chains (unable to propagate), hence converting all the active alkoxide anionic species (**3**) to (**4**) through an elimination reaction ( $\text{E}_2$ ) may prevent the monomer consumption. This transformation ( $\text{E}_2$ ) can be considered as termination reaction, which can elucidate the slow propagation or the uncomplete monomer conversions. Moreover, it was detected that the reaction was enhanced (revealed by higher signal intensity in  $^1\text{H}$  NMR) at higher temperature (60  $^\circ\text{C}$ ), which is related to elimination reactions. In addition to that,  $\text{E}_2$  reactions also occurred during the copolymerization reaction as revealed by  $^1\text{H}$  NMR ( $\delta$  6.18

ppm; Figure 4. 39, Figure 4. 40 – top) and  $^{31}\text{P}$  NMR ( $\delta$  32.23, 32.65 ppm; Figure 4. 39, Figure 4. 40 – bottom) the corresponding signals of the crotonate, but in lower intensity than in the case of the homopolymerization. 2D COSY confirmed the presence of crotonate as chain-end of  $\text{PBPL}^{\text{OP}(\text{O})\text{Ph}_2}$  by the correlation between the vinylic hydrogens (g,h in blue) and the end-group methylene hydrogens (i in black) (Figure 4. 41 and Figure 4. 42 – bottom).

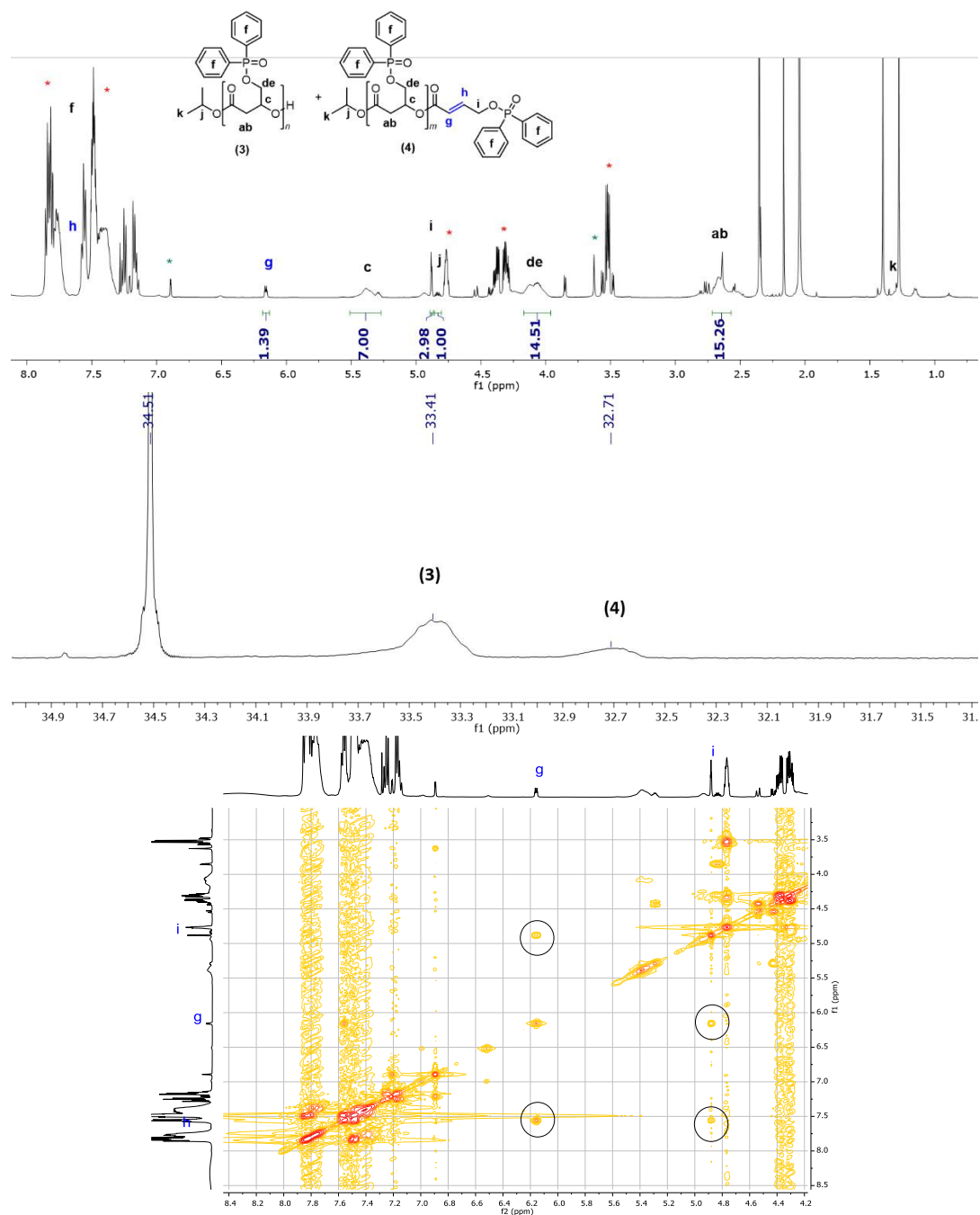


**Figure 4. 41** –  $^1\text{H}$  NMR (400 MHz,  $\text{CDCl}_3$ , 25 °C) (top),  $^{31}\text{P}$  (162 MHz,  $\text{CDCl}_3$ , 25 °C) (middle), and  $^1\text{H}$ - $^1\text{H}$  COSY (400 MHz,  $\text{CDCl}_3$ , 25 °C) (bottom) spectra of crude  $\text{PBPL}^{\text{OP}(\text{O})\text{Ph}_2}$  prepared from the ROP of  $\text{rac-BPL}^{\text{OP}(\text{O})\text{Ph}_2}$  mediated by complex **2b** in the presence of  $i\text{PrOH}$  at room temperature revealing two polymer populations (3) and (4) (Table 4. 10, entry 2); \* (red and green) unreacted  $\text{rac-BPL}^{\text{OP}(\text{O})\text{Ph}_2}$  and residual **2b** catalyst; respectively.

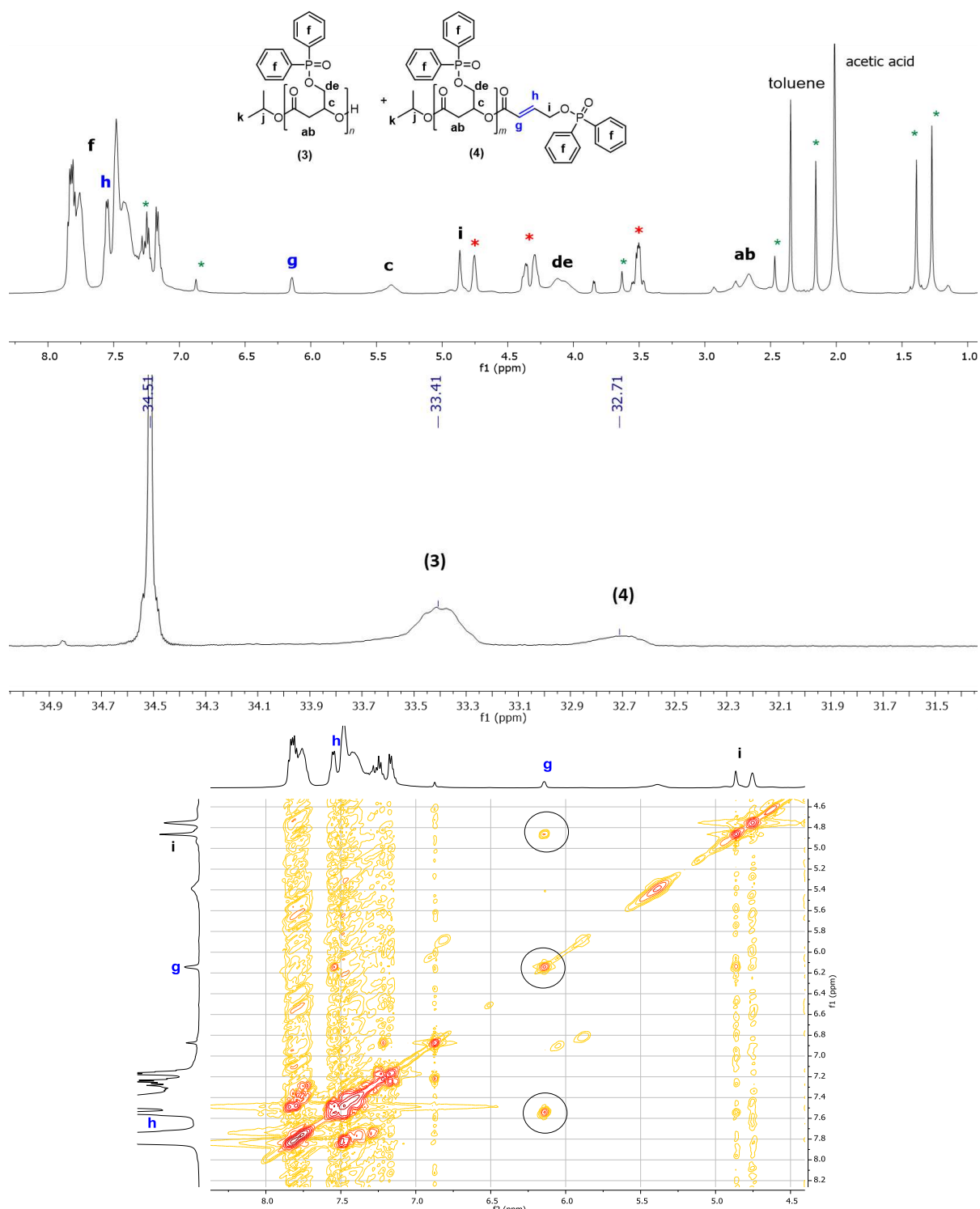


**Figure 4. 42** – <sup>1</sup>H NMR (400 MHz, CDCl<sub>3</sub>, 25 °C) (top), <sup>31</sup>P (162 MHz, CDCl<sub>3</sub>, 25 °C) (middle), and <sup>1</sup>H-<sup>1</sup>H COSY (400 MHz, CDCl<sub>3</sub>, 25 °C) (bottom) spectra of crude PBPL<sup>OP(O)Ph<sub>2</sub></sup> prepared from the ROP of *rac*-BPL<sup>OP(O)Ph<sub>2</sub></sup> mediated by complex **2b** in the presence of *i*PrOH at 60 °C temperature revealing two polymer populations (3) and (4) (Table 4. 10, entry 3); \* (red and green) unreacted *rac*-BPL<sup>OP(O)Ph<sub>2</sub></sup> and **2b** catalyst; respectively.

These preliminary experimental data on the ROP of *rac*-BPL<sup>OP(O)Ph<sub>2</sub></sup> mediated by **2b** catalysts, thus support that both the P=O group of *rac*-BPL<sup>OP(O)Ph<sub>2</sub></sup> and the presence of unsought



termination, side reactions could impact the propagation and thus result in inadequate monomer conversions. Nonetheless, further investigations are needed to confirm these latter results. Besides, operating the ROP of *rac*-BPL<sup>OP(O)Ph<sup>2</sup></sup> with high **2b** catalyst loading, in the absence of a co-initiator, depending on the choice of solvent (does provide high solubility for the monomer), choice of catalyst **1,2a-d**, sequentially copolymerization, and other alternatives would be examined.

### 3. Conclusion : achievements and perspectives

In this work, the synthesis of a variety of unprecedented functional PHAs, namely PBPL<sup>FG</sup>s with FG = OPh, SPh, O<sup>i</sup>Pr, O<sup>t</sup>Bu, OTBDMS, having high experimental molar masses ( $M_{n,SEC(max)} = 96,700 \text{ g mol}^{-1}$ ), narrow dispersities ( $1.06 < D_M < 1.21$ ), and high stereoregularity with syndiotactic enrichment ( $0.69 < P_r < 0.87$ ), was successfully achieved. PBPL<sup>FG</sup>s have been prepared from the stereoselective controlled ROP of the corresponding *racemic* 4-substituted- $\beta$ -propiolactones *rac*-BPL<sup>FG</sup>s, mediated by achiral rare earth catalysts diamino-bis(phenolate) yttrium amido complexes **2a-d** ( $Y\{ONNO\}^{R^1R^2}$ ;  $R^1 = R^2 = \text{Cumyl, } ^t\text{Bu, Me, Cl}$ ) in the presence of isopropanol as co-initiator, through a controlled coordination-insertion and chain end mechanism (CEM) mechanisms. The prevailing tendency of the *rac*-BPL<sup>FG</sup>s to undergo ROP efficiently, as perceived from the kinetic studies, in descending order: (less crowded > moderately crowded > highly crowded): *rac*-BPL<sup>OPh</sup> > *rac*-BPL<sup>SPh</sup> > *rac*-BPL<sup>O<sup>i</sup>Pr</sup>  $\approx$  *rac*-BPL<sup>O<sup>t</sup>Bu</sup> > *rac*-BPL<sup>OTBDMS</sup>. The prevailing catalyst activity (**2a-d**) trend in the ROP of *rac*-BPL<sup>FG</sup>s is, by descending: (crowded > uncrowded): **2a-b** > **2c** > **2d**. Whilst the impact of the functionality (FG) of the  $\beta$ -lactones (e.g., alkyl: *rac*-BL<sup>Me</sup>; ester: *rac*-MLA<sup>FG</sup>s, ether: *rac*-BPL<sup>FG</sup>s) on the resulting polyesters stereochemistry was already investigated by our group, and revealed to switch between highly syndiotactic and highly isotactic or atactic depending on steric and electronic secondary interactions present during the polymerization. Herein, the impact of the functionality of the  $\beta$ -lactone was further investigated within new BPL<sup>FG</sup>s, with different exocyclic chain length and/or steric hindrance. Indeed, it was noticed that any minor modification in the ether functionality, such as removing or adding a methylene ( $\pm \text{CH}_2$ ) or replacing  $\text{CH}_3$  group with  $\text{CHMe}_2/\text{CMe}_3$  group, will influence the stereochemistry of the produced polyesters especially when using a catalyst bearing ancillary ligand with uncrowded substituents ( $R^1 = R^2 = \text{Me, Cl}$ ). Moreover, the modulation of the exocyclic ether (thioether) chains revealed to have an intriguing influence on the glass transition temperature with overall ascending trend: tall, flexible, uncrowded chains (PBPL<sup>OAll/OMe</sup>:  $T_g = -40^\circ\text{C} - 12^\circ\text{C}$ ) < tall,



flexible aromatic (PBPL<sup>CH<sub>2</sub>OBn/OBn</sup>;  $T_g = -12\text{ }^{\circ}\text{C} - 0\text{ }^{\circ}\text{C}$ ); short and crowded chains (PBPL<sup>O<sub>i</sub>Pr/O<sub>r</sub>Bu/OTBDMS</sup>;  $T_g = 0\text{ }^{\circ}\text{C} - 5\text{ }^{\circ}\text{C}$ ) < short and aromatic chains (PBPL<sup>SPh/OPh</sup>;  $T_g = 7\text{ }^{\circ}\text{C} - 40\text{ }^{\circ}\text{C}$ ). Last of all, an incipient study for the ROP of the novel monomer *rac*-BPL<sup>OP(O)Ph<sub>2</sub></sup> promoted by **2b** catalyst was initiated. Even though, its ROP appeared to be more challenging than other BPL<sup>FG</sup>s, it will be further explored in our group.

Furthermore, inspired by the experimental and theoretical results gathered in this Chapter, one can think about perusing the ROP of appealing functionalities on the pendent chain of the  $\beta$ -lactones. Fluorinated ether chains where the methylene is exchanged with fluorine (BPL<sup>OCF<sub>2</sub>CHF<sub>2</sub></sup>) or amines functionality (BPL<sup>NBn<sub>2</sub>/NPh<sub>2</sub></sup>), are impressive examples. An attempt to operate ROP of *rac*-BPL<sup>FG</sup>s by chiral yttrium complexes (that were used with *rac*-DL<sup>R</sup>; refer to Chapter 1; Scheme 1. 15) is also interesting, to perceive its impact on the stereochemistry of PBPL<sup>FG</sup>s (enhancement or deterioration or switching; CEM vs. ESM stereoselective mechanism). Needless to mention the almost interminable copolymerization of *rac*-BPL<sup>FG</sup>s in the presence of **2a-d**, such as, with other  $\beta$ -lactones or/and other heterocyclic cyclic monomers.

## 4. Experimental section

### Material and methods

All manipulations involving organometallic catalysts were performed under inert atmosphere (argon, < 3 ppm O<sub>2</sub>) using standard Schlenk, vacuum line, and glovebox techniques. Toluene was freshly distilled from Na/benzophenone under argon and degassed thoroughly by freeze-thaw-vacuum cycles prior to use. Isopropyl alcohol (Acros) was distilled over Mg turnings under argon atmosphere and kept over activated 3–4 Å molecular sieves. 2,4-dichlorophenol, 2,4-dimethylphenol, 2,4-di-*tert*-butylphenol, 2,4-dicumylphenol, *N,N*-dimethylethylenediamine, formaldehyde, were purchased from Sigma, Across or TCI and were used as received. 6,6'-(*N,N*-dimethylethylenediamine) bis(methylene) bis(2,4-dichlorophenol) ({ONNO<sup>Cl<sub>2</sub></sup>}H<sub>2</sub>), 6,6'-(((2-(dimethylamino)ethyl)azanediyl) bis(methylene)) bis(2,4-dimethylphenol) ({ONNO<sup>Me<sub>2</sub></sup>}H<sub>2</sub>), 6,6'-(*N,N*-dimethylethylenediamine) bis(methylene) bis(2,4-di-*tert*-butylphenol) ({ONNO<sup>*t*Bu<sub>2</sub></sup>}H<sub>2</sub>), 6,6'-(*N,N*-dimethylethylenediamine) bis(methylene) bis(2,4-dicumylphenol) {ONNO<sup>cumyl<sub>2</sub></sup>}H<sub>2</sub>},<sup>[9c]</sup> bis(dimethylsilyl)amido lithium (Li(N(SiHMe<sub>2</sub>)<sub>2</sub>),<sup>[21]</sup> Y[N(SiHMe<sub>2</sub>)<sub>2</sub>]<sub>3</sub>(THF)<sub>1.5</sub> (Appendix 36),<sup>[22]</sup> were synthesized according to the reported procedures.

## Instrumentation and measurements

$^1\text{H}$  (500 and 400 MHz),  $^{13}\text{C}\{^1\text{H}\}$  (125 MHz and 100 MHz) and  $^{31}\text{P}$  (162 MHz and 202 MHz) NMR spectra were recorded on Bruker Avance AM 500 and Ascend 400 spectrometers at 25 °C.  $^1\text{H}$ ,  $^{13}\text{C}\{^1\text{H}\}$  and  $^{31}\text{P}$  NMR spectra were referenced internally relative to  $\text{SiMe}_4$  ( $\delta = 0$  ppm) using the residual solvent resonances.

Number-average molar mass ( $M_{n,\text{SEC}}$ ) and dispersity ( $D_M = M_w/M_n$ ) values of the PBPL<sup>FG</sup>s were determined by size-exclusion chromatography (SEC) in THF at 30 °C (flow rate = 1.0 mL.min<sup>-1</sup>) on a Polymer Laboratories PL50 apparatus equipped with a refractive index detector and a set of two ResiPore PLgel 3  $\mu\text{m}$  MIXED-D 300  $\times$  7.5 mm columns. The polymer samples were dissolved in THF (2 mg.mL<sup>-1</sup>). All elution curves were calibrated with polystyrene standards;  $M_{n,\text{SEC}}$  values of the PBPL<sup>FG</sup>s were uncorrected for the possible difference in hydrodynamic radius *vs.* that of polystyrene.

The molar mass of PBPL<sup>FG</sup> samples was also determined by  $^1\text{H}$  NMR analysis in  $\text{CDCl}_3$  from the relative intensities of the signals of the PBPL<sup>FG</sup> repeating unit methine hydrogen ( $\delta$  (ppm): 5.48  $-\text{OCH}(\text{CH}_2\text{OPh})\text{CH}_2$ , PBPL<sup>O<sup>Ph</sup></sup>; 5.26  $-\text{OCH}(\text{CH}_2\text{SPh})\text{CH}_2$ , PBPL<sup>S<sup>Ph</sup></sup>; 5.25  $-\text{OCH}(\text{CH}_2\text{OCH}(\text{CH}_3)_2)$ , PBPL<sup>O<sup>i</sup>Pr</sup>; 5.22  $-\text{OCH}(\text{CH}_2\text{OC}(\text{CH}_3)_3)$ , PBPL<sup>O<sup>t</sup>Bu</sup>; 5.20  $-\text{OCH}(\text{CH}_2\text{OSi}(\text{CH}_3)_2\text{C}(\text{CH}_3)_3)$ , PBPL<sup>OTBDMS</sup>; and of the isopropyl chain-end ( $\delta$  (ppm): 4.94–4.98  $(\text{CH}_3)_2\text{CHO}-$ , 1.19–1.25  $(\text{CH}_3)_2\text{CHO}-$ ).

Monomer conversions were calculated from  $^1\text{H}$  NMR spectra of the crude polymer samples in  $\text{CDCl}_3$  by using the integration (Int.) ratios  $[\text{Int. PBPL}(\text{OPh})/\text{PBPL}(\text{O}^i\text{Pr})/\text{PBPL}(\text{O}^t\text{Bu})/\text{PBPL}(\text{OTBDMS})] / (\text{Int. PBPL}(\text{OPh})/\text{PBPL}(\text{O}^i\text{Pr})/\text{PBPL}(\text{O}^t\text{Bu})/\text{PBPL}(\text{OTBDMS}) + \text{Int. BPL}(\text{OPh})/\text{PBPL}(\text{O}^i\text{Pr})/\text{PBPL}(\text{O}^t\text{Bu})/\text{PBPL}(\text{OTBDMS}))$  and  $[\text{Int. PBPL}(\text{SPh}) + \text{Int.}(\text{SPh}') + \text{Int.}(\text{SPh}'')] / [\text{Int. PBPL}(\text{SPh}) + \text{Int. BPL}(\text{SPh}) + \text{Int.}(\text{SPh}') + \text{Int.}(\text{SPh}'')]$  (compounds **SPh'** and **SPh''** correspond to the decomposed and rearrangement products of *rac*-BPL<sup>S<sup>Ph</sup></sup>, respectively; refer to Chapter 2, Figure 2. 12) of the methine hydrogens of BPL<sup>FG</sup>s and PBPL<sup>FG</sup>s (corresponding methine hydrogen signal of the polymers (see above), and of the monomers:  $\delta$  (ppm) 4.85 BPL<sup>O<sup>Ph</sup></sup>, 4.62 BPL<sup>S<sup>Ph</sup></sup>, 4.60 BPL<sup>O<sup>i</sup>Pr</sup>, 4.55 BPL<sup>O<sup>t</sup>Bu</sup>, and 4.65 BPL<sup>OTBDMS</sup>.

Mass spectra were recorded at CRMPO-ScanMAT (Rennes, France). ESI mass spectra were recorded on an orbitrap type Thermofisher Scientific Q-Exactive instrument with an ESI source in positive mode by direct introduction with a flow rate of 5–10  $\mu\text{L min}^{-1}$ . Samples were prepared in  $\text{CH}_2\text{Cl}_2$  at 10  $\mu\text{g mL}^{-1}$ . High resolution Matrix Assisted Laser Desorption Ionization

- Time of Flight, MALDI-ToF, mass spectra were recorded using an ULTRAFLEX III TOF/TOF spectrometer (Bruker Daltonik GmbH, Bremen, Germany) in positive ionization mode. Spectra were recorded using reflectron mode and an accelerating voltage of 25 kV. A mixture of a freshly prepared solution of the polymer in THF or CH<sub>2</sub>Cl<sub>2</sub> (HPLC grade, 10 mg mL<sup>-1</sup>) and DCTB (*trans*-2-(3-(4-*tert*-butylphenyl)-2methyl-2-propenylidene) malononitrile, and a MeOH solution of the cationizing agent (NaI, 10 mg mL<sup>-1</sup>) were prepared. The solutions were combined in a 1:1:1 v/v/v ratio of matrix-to-sample-to-cationizing agent. The resulting solution (0.25–0.5 µL) was deposited onto the sample target (Prespotted AnchorChip PAC II 384 / 96 HCCA) and air or vacuum dried.

Differential scanning calorimetry (DSC) analyses were performed with a Setaram DSC 131 apparatus calibrated with indium, at a rate of 10 °C min<sup>-1</sup>, under a continuous flow of helium (25 mL.min<sup>-1</sup>), using aluminum capsules. The thermograms were recorded according to the following cycles: –80 to 140/200 °C at 10 °C min<sup>-1</sup>; 200/140 to –80 °C at 10 °C min<sup>-1</sup>; –80 °C for 5 min; –80 to 140/200 °C at 10 °C min<sup>-1</sup>; 140/200 to –80 °C at 10 °C min<sup>-1</sup>.

Thermal gravimetry analyses (TGA) were performed on a Metler Toledo TGA/DSC1 by heating the polymer samples at a rate of 10 °C min<sup>-1</sup> from +25 to +600 °C in a dynamic nitrogen atmosphere (flow rate = 50 mL min<sup>-1</sup>).

## Synthesis of the yttrium complexes pro-ligands {ONNO<sup>R</sup>} H<sub>2</sub>

### Synthesis of {ONNO<sup>Cl2</sup>}H<sub>2</sub>[<sup>9c</sup>]

In a round bottom flask, a solution of 2,4-dichlorophenol (14.96 g, 91.76 mmol), *N,N*-dimethylethylenediamine (5.04 mL, 46.90 mmol) and formaldehyde (10.8 mL of a 36% solution, 129.60 mmol) in methanol (30 mL) was refluxed for 24 h. The mixture was next cooled and decanted. Following removal of the supernatant solution, the remaining oil was dissolved in methanol and heated to reflux for 4 h. Cooling the mixture gave a white precipitate which was filtered and washed with cold ethanol to afford 6,6'-(*N,N*-dimethylethylenediamine) bis(methylene) bis(2,4-dichlorophenol) {ONNO<sup>Cl2</sup>}H<sub>2</sub> as a white powder (39% yield, 18.07 mmol).

<sup>1</sup>H NMR (400 MHz, CDCl<sub>3</sub>, 25 °C) δ (ppm): 2.37 (s, 6H, NMe<sub>2</sub>), 2.63 (s, 4H, N(CH<sub>2</sub>)<sub>2</sub>N), 3.67 (s, 4H, NCH<sub>2</sub>Ph), 6.91 (d, 2H, *J* = 2.5 Hz, NCH<sub>2</sub>CCH), 7.27 (d, 2H, *J* = 2.5 Hz, CClCHCCl) (Appendix 37).

**$^{13}\text{C}\{\text{H}\}$  NMR** (100 MHz,  $\text{CDCl}_3$ , 25 °C)  $\delta$  (ppm): 45.0 ( $\text{NMe}_2$ ), 49.3 ( $\text{N}(\text{CH}_2)_2\text{N}$ ), 55.9 ( $\text{NCH}_2\text{Ph}$ ), 56.3 ( $\text{N}(\text{CH}_2)_2\text{N}$ ), 122.8 (*Ar*), 123.6 (*Ar*), 124.5 (*Ar*), 128.4 (*Ar*), 129.8 ( $\text{CClCHCCl}$ ), 151.9 (*COH*).

### Synthesis of $\{\text{ONNO}^{\text{Me}_2}\} \text{H}_2$ [9c]

In a round bottom flask, a solution of 2,4-dimethylphenol (15.85 g, 129.95 mmol), *N,N*-dimethylethylenediamine (5.45 mL, 49.98 mmol) and formaldehyde (9.5 mL of a 36% solution, 131.59 mmol) in methanol (34 mL) was heated at reflux for 2 days. Cooling of the mixture gave a white precipitate which was filtered and washed with cold EtOH to give 6,6'-(((2-(dimethylamino)ethyl)azanediyl) bis(methylene)) bis(2,4-dimethylphenol)  $\{\text{ONNO}^{\text{Me}_2}\} \text{H}_2$  as a white powder (84% yield, 42.20 mmol).

**$^1\text{H}$  NMR** (400 MHz,  $\text{CDCl}_3$ , 25 °C)  $\delta$  (ppm): 2.19 (s, 12H, *Me*), 2.30 (s, 6H,  $\text{NMe}_2$ ), 2.55 (s, 4H,  $\text{N}(\text{CH}_2)_2\text{N}$ ), 3.57 (s, 4H,  $\text{NCH}_2\text{Ph}$ ), 6.66 (br s, 2H,  $\text{NCH}_2\text{CCH}$ ), 6.84 (br s, 2H,  $\text{C}(\text{Me})\text{CHC}(\text{Me})$ ), 9.42 (bs, 2H, *COH*) (Appendix 38).

**$^{13}\text{C}\{\text{H}\}$  NMR** (100 MHz,  $\text{CDCl}_3$ , 25 °C)  $\delta$  (ppm): 16.3 ( $\text{CH}_3$ ), 20.5 ( $\text{CH}_3$ ), 45.0 ( $\text{NMe}_2$ ), 49.1 ( $\text{N}(\text{CH}_2)_2\text{N}$ ), 56.1 ( $\text{NCH}_2\text{Ph}$ ), 56.5 ( $\text{N}(\text{CH}_2)_2\text{N}$ ), 121.7 (*Ar*), 125.5 (*Ar*), 127.5 (*Ar*), 128.4 (*Ar*), 131.3 (*Ar*), 152.7 (*COH*).

### Synthesis of $\{\text{ONNO}^{t\text{Bu}_2}\} \text{H}_2$ [9c]

In a round bottom flask, a solution of 2,4-di-*tert*-butylphenol (15.02 g, 72.89 mmol), *N,N*-dimethylethylenediamine (3.12 mL, 29.03 mmol) and formaldehyde (5.25 mL of a 36% solution, 72.82 mmol) in of methanol (30 mL) was heated at reflux for 6 days. Cooling of the mixture gave a white precipitate which was filtered and washed with cold EtOH to give 6,6'-(*N,N*-dimethylethylenediamine) bis(methylene) bis(2,4-di-*tert*-butylphenol)  $\{\text{ONNO}^{t\text{Bu}_2}\} \text{H}_2$  as a white powder (86% yield, 25.00 mmol).

**$^1\text{H}$  NMR** (400 MHz,  $\text{CDCl}_3$ , 25 °C)  $\delta$  (ppm): 1.26 (s, 18H, *tBu*), 1.38 (s, 18H, *tBu*), 2.31 (s, 6H,  $\text{NMe}_2$ ), 2.58 (m, 4H,  $\text{N}(\text{CH}_2)_2\text{N}$ ), 3.60 (s, 4H,  $\text{NCH}_2\text{Ph}$ ), 6.87 (d, 2H,  $J = 2.5$  Hz,  $\text{NCH}_2\text{CCH}$ ), 7.19 (d, 2H,  $J = 2.5$  Hz,  $\text{C}(t\text{Bu})\text{CHC}(t\text{Bu})$ ), 9.78 (br s, 2H, *COH*) (Appendix 39).

**$^{13}\text{C}\{\text{H}\}$  NMR** (100 MHz,  $\text{CDCl}_3$ , 25 °C)  $\delta$  (ppm): 29.7 (*tBu*), 31.9 (*tBu*), 34.2 (*tBu*), 35.2 (*tBu*), 45.0 ( $\text{NMe}_2$ ), 49.2 ( $\text{N}(\text{CH}_2)_2\text{N}$ ), 56.1 ( $\text{NCH}_2\text{Ph}$ ), 56.7 ( $\text{N}(\text{CH}_2)_2\text{N}$ ), 121.8 (*Ar*), 123.5 (*Ar*), 125.0 (*Ar*), 136.2 (*Ar*), 140.3 ( $\text{C}(t\text{Bu})$ ), 153.4 (*COH*).

### Synthesis of {ONNO<sup>cumyl</sup>2} H<sub>2</sub>[<sup>9</sup>Cl]

In a 25 mL round bottom flask, a solution of 2,4-dicumylphenol (15.11 g, 45.78 mmol), *N,N*-dimethylethylenediamine (1.95 mL, 18.15 mmol) and formaldehyde (3.3 mL of a 36% solution, 45.77 mmol) in methanol (30 mL) was refluxed for 6 days during which a white precipitate was formed. Filtration and washing of the solid with cold ethanol afforded 6,6'-(*N,N*-dimethylethylenediamine) bis(methylene) bis(2,4-dicumylphenol) {ONNO<sup>cumyl</sup>2} H<sub>2</sub> as a white powder in 99% yield (17.96 mmol).

<sup>1</sup>H NMR (400 MHz, CDCl<sub>3</sub>, 25 °C) δ (ppm): 1.63–1.68 (m, 24H, CMe<sub>2</sub>Ph), 2.09 (m, 2H, NCH<sub>2</sub>CH<sub>2</sub>NMe<sub>2</sub>), 2.27 (m, 2H, NCH<sub>2</sub>CH<sub>2</sub>NMe<sub>2</sub>), 3.36 (s, 4H, NCH<sub>2</sub>Ph), 6.69 (d, 2H, *J* = 2.5 Hz, NCH<sub>2</sub>CCH), 7.06 (d, 2H, *J* = 2.5 Hz, C(cumyl)CHC(cumyl)), 7.10–7.24 (m, 20H, CH<sub>ar</sub>o), 9.44 (br s, 2H, COH) (Appendix 40).

<sup>13</sup>C{<sup>1</sup>H} NMR (100 MHz, CDCl<sub>3</sub>, 25 °C) δ (ppm): 29.4 (CMe<sub>2</sub>Ph), 31.2 (CMe<sub>2</sub>Ph), 42.2 (CMe<sub>2</sub>Ph), 42.5 (CMe<sub>2</sub>Ph), 44.4 (NMe<sub>2</sub>), 48.8 (N(CH<sub>2</sub>)<sub>2</sub>N), 56.2 (NCH<sub>2</sub>Ph), 56.6 (N(CH<sub>2</sub>)<sub>2</sub>N), 122.1 (Ar), 124.6 (Ar), 125.3 (Ar), 125.5 (Ar), 126.1 (Ar), 126.1 (Ar), 126.9 (Ar), 127.0 (Ar), 127.5 (Ar), 128.0 (Ar), 135.9 (Ar), 139.5 (Ar), 151.6 (COH), 153.1(COH).

### Typical polymerization procedure<sup>[11]</sup>

In a typical experiment (Table 1, entry 6), in the glovebox, a Schlenk flask was charged with [Y(N(SiHMe<sub>2</sub>)<sub>2</sub>)<sub>3</sub>](THF)<sub>2</sub> (8.8 mg, 14 μmol) and {ONNO<sup>tBu</sup>2}(2b, 7.4 mg, 14 μmol), and toluene (0.25 mL) was next added. To this solution, <sup>i</sup>PrOH (107 μL of a 1% (v/v) solution in toluene, 1 equiv vs. Y) was added under stirring at room temperature (ca. 20 °C). After 5 min of stirring, a solution of *rac*-BPL<sup>O<sup>Ph</sup></sup>, for example, (150 mg, 0.84 mmol, 60 equiv) in toluene (0.5 mL) was added rapidly and the mixture was stirred at 20 °C for 1 h. The reaction was quenched by addition of acetic acid (ca. 0.5 mL of a 1.6 mol·L<sup>-1</sup> solution in toluene). The resulting mixture was concentrated to dryness under vacuum and the conversion was determined by <sup>1</sup>H NMR analysis of the residue in CDCl<sub>3</sub>. The crude polymer was then dissolved in CH<sub>2</sub>Cl<sub>2</sub> (ca. 1 mL) and precipitated in cold pentane (ca. 5 mL), filtered and dried in vacuum oven at 60 °C. The PBPL<sup>FG</sup>s were recovered as white solid (FG = OPh), yellow oil (FG = SPh), and colorless oil (FG = *Or*Pr, *Or*Bu, OTBDMS). All recovered polymers were then analyzed by NMR spectroscopy, mass spectrometry, SEC, TGA and DSC analyses.

### Kinetic study procedure

Following the typical polymerization procedure reported above, an aliquot of the reaction mixture was taken and quenched in acetic acid (ca. 0.1 mL of a 1.6 mol·L<sup>-1</sup> solution in toluene), at different reaction times. The resulting mixture was concentrated to dryness under vacuum and the conversion was determined by <sup>1</sup>H NMR analysis.

## 5. References

- [1] Z. Li, J. Yang, X. J. Loh, *NPG Asia Materials* **2016**, 8, e265-e265.
- [2] a) D. M. Lyubov, A. O. Tolpygin, A. A. Trifonov, *Coord. Chem. Rev.* **2019**, 392, 83-145; b) R. M. Shakaroun, H. Li, S. M. Guillaume, J. F. Carpentier, *Chem. Eur. J.* **2020**, 26, 128-138; c) J.-F. o. Carpentier, *Organometallics* **2015**, 34, 4175-4189.
- [3] a) A. Hamitou, R. Jerome, A. Hubert, P. Teyssie, *Macromolecules* **1973**, 6, 651-652; b) T. Ouhadi, A. Hamitou, R. Jérôme, P. Teyssié, *Macromolecules* **1976**, 9, 927-931.
- [4] a) K. M. Stridsberg, M. Ryner, A.-C. Albertsson, *Degradable aliphatic polyesters* **2002**, 41-65; b) R. Jianming, X. Anguo, W. Hongwei, Y. Hailin, *Designed Monomers and Polymers* **2014**, 17, 345-355; c) M. Labet, W. Thielemans, *Chem. Soc. Rev.* **2009**, 38, 3484-3504; d) C. M. Thomas, *Chem. Soc. Rev.* **2010**, 39, 165-173; e) K. E. Washington, R. N. Kularatne, V. Karmegam, M. C. Biewer, M. C. Stefan, *Wiley Interdisciplinary Reviews: Nanomedicine and Nanobiotechnology* **2017**, 9, e1446.
- [5] J. C. Worch, H. Prydderch, S. Jimaja, P. Bexis, M. L. Becker, A. P. Dove, *Nature Reviews Chemistry* **2019**, 3, 514-535.
- [6] L. R. Rieth, D. R. Moore, E. B. Lobkovsky, G. W. Coates, *J. Am. Chem. Soc.* **2002**, 124, 15239-15248.
- [7] G.-Q. Chen, *Chem. Soc. Rev.* **2009**, 38, 2434-2446.
- [8] a) F. Bovey, *Pure Appl. Chem.* **1967**, 15, 349-368; b) M. Sepulchre, *Macromol. Chem. Phys.* **1988**, 189, 1117-1131.
- [9] a) A. Amgoune, C. M. Thomas, S. Ilinca, T. Roisnel, J. F. Carpentier, *Angew. Chem. Int. Ed.* **2006**, 45, 2782-2784; b) N. Ajellal, M. Bouyahyi, A. Amgoune, C. M. Thomas, A. Bondon, I. Pillin, Y. Grohens, J.-F. Carpentier, *Macromolecules* **2009**, 42, 987-993; c) M. Bouyahyi, N. Ajellal, E. Kirillov, C. M. Thomas, J. F. Carpentier, *Chem. Eur. J.* **2011**, 17, 1872-1883; d) Y. Chapurina, J. Klitzke, O. d. L. Casagrande Jr, M. Awada, V. Dorcet, E. Kirillov, J.-F. Carpentier, *Dalton Transactions* **2014**, 43, 14322-14333; e) J. Fang, M. J.-L. Tschan, T. Roisnel, X. Trivelli, R. M. Gauvin, C. M. Thomas, L. Maron, *Poly. Chem.* **2013**, 4, 360-367; f) P. T. Altenbuchner, A. Kronast, S. Kissling, S. I. Vagin, E. Herdtweck, A. Pöthig, P. Deglmann, R. Loos, B. Rieger, *Chem. Eur. J.* **2015**, 21, 13609-13617.
- [10] a) C. G. Jaffredo, Y. Chapurina, S. M. Guillaume, J. F. Carpentier, *Angew. Chem. Int. Ed.* **2014**, 53, 2687-2691; b) C. G. Jaffredo, Y. Chapurina, E. Kirillov, J. F. Carpentier, S. M. Guillaume, *Chem. Eur. J.* **2016**, 22, 7629-7641; c) R. Ligny, M. M. Hänninen, S. M. Guillaume, J.-F. Carpentier, *Chem. Commun.* **2018**, 54, 8024-8031.
- [11] R. Ligny, M. M. Hänninen, S. M. Guillaume, J. F. Carpentier, *Angew. Chem.* **2017**, 129, 10524-10529.
- [12] G. Adamus, I. Kwiecień, M. Maksymiak, T. Bałakier, J. Jurczak, M. Kowalczyk, *Anal. Chim. Acta* **2014**, 808, 104-114.
- [13] F. Ouhib, S. Randriamahefa, P. Guérin, C. Barbaud, *Designed monomers and polymers* **2005**, 8, 25-35.
- [14] A. H. Westlie, E. Y.-X. Chen, *Macromolecules* **2020**, 53, 9906-9915.
- [15] J. M. G. Cowie, V. Arrighi, *Polymers: chemistry and physics of modern materials*, CRC press, **2007**.

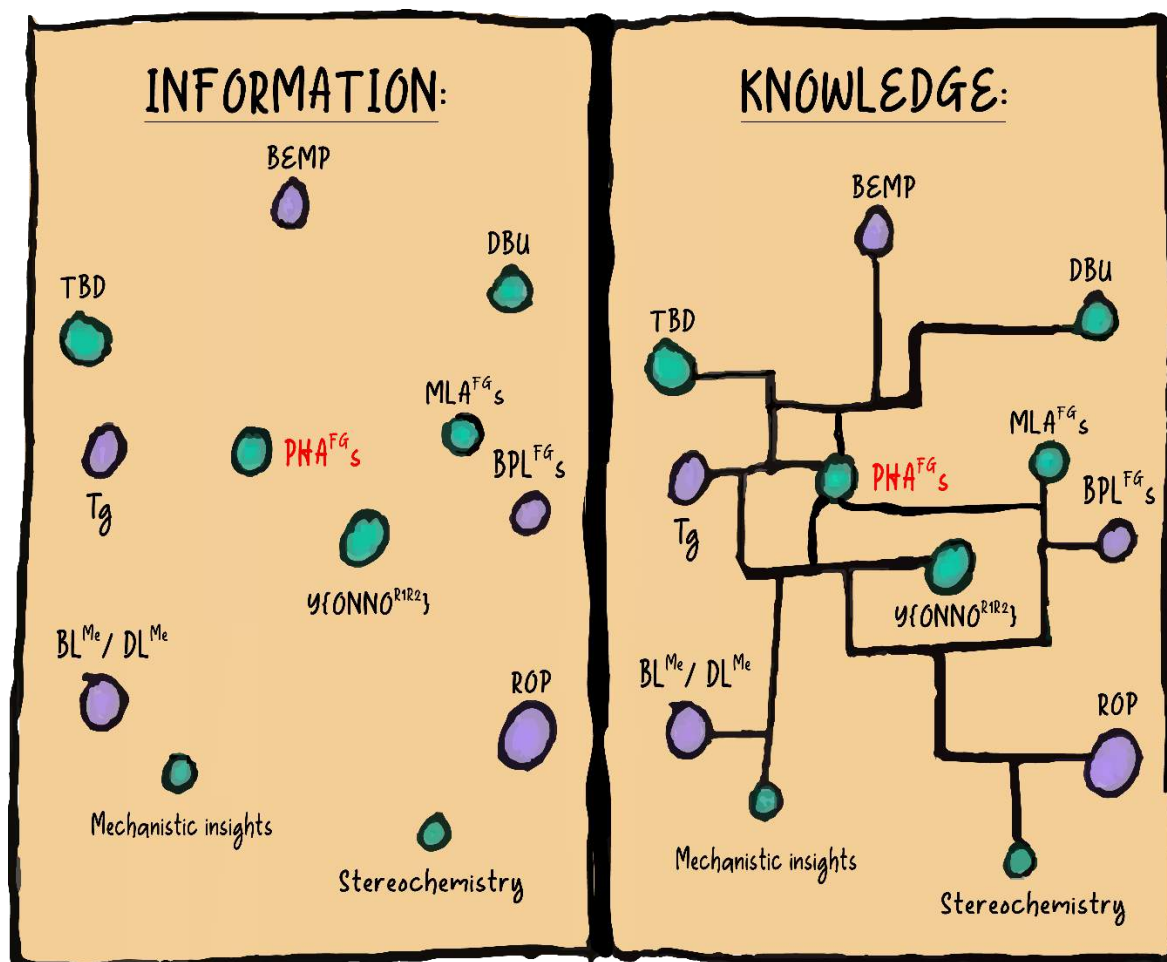
- [16] R. Shakaroun, H. Li, P. Jéhan, M. Blot, A. Alaaeddine, J.-F. Carpentier, S. M. Guillaume, *Poly. Chem.* **2021**.
- [17] Y. Takagi, M. Hashii, A. Maehara, T. Yamane, *Macromolecules* **1999**, *32*, 8315-8318.
- [18] C. Ewering, T. Lütke-Eversloh, H. Luftmann, A. Steinbüchel, *Microbiology* **2002**, *148*, 1397-1406.
- [19] a) A. Kausar, S. Zulfiqar, M. I. Sarwar, *Polymer Reviews* **2014**, *54*, 185-267; b) C. D. Vo, G. Kilcher, N. Tirelli, *Macromol. Rapid Commun.* **2009**, *30*, 299-315; c) E. Marianucci, C. Berti, F. Pilati, P. Manaresi, M. Guaita, O. Chiantore, *Polymer* **1994**, *35*, 1564-1566; d) R. Sadhir, K. Schoch, *Chem. Mater.* **1996**, *8*, 1281-1286.
- [20] a) N. Mohan, C. H. Suresh, A. Kumar, S. R. Gadre, *PCCP* **2013**, *15*, 18401-18409; b) J. Kawada, T. Lütke-Eversloh, A. Steinbüchel, R. H. Marchessault, *Biomacromolecules* **2003**, *4*, 1698-1702.
- [21] J. Eppinger, E. Herdtweck, R. Anwender, *Polyhedron* **1998**, *17*, 1195-1201.
- [22] a) K. C. Hultsch, P. Voth, K. Beckerle, T. P. Spaniol, J. Okuda, *Organometallics* **2000**, *19*, 228-243; b) R. Anwender, O. Runte, J. Eppinger, G. Gerstberger, E. Herdtweck, M. Spiegler, *J. Chem. Soc., Dalton Trans.* **1998**, 847-858.







## General Conclusion





## 1. General conclusion

Petroleum-derived plastics that have fuelled modern economies are the most widely used man-made substances in modern life; they have now become indispensable to our daily life and to the global economy. However, when disposed of or leaked into the environment, their durability and resistance to degradation in ambient environments result in severe plastics pollution to landfills and oceans as well as other environmental consequences. Thus, the development plastics should focus on materials that can be recycled or disposed of in ways that are environmentally less damaging. In this context, polyhydroxyalkanoates (PHAs), a unique class of biorenewable aliphatic polyesters that are biodegradable in ambient environments, have shown great potential as a replacement for petroleum-based plastics. Natural PHAs, produced by bacteria and other living microorganisms from biorenewable resources, are purely isotactic polymers, and their thermal and mechanical properties span a varied range depending on the length of the pendant alkyl group on the  $\beta$ -carbon. Nevertheless, natural PHAs are hard to process due to their physio-mechanical properties (e.g., melting temperature ( $T_m$ ) close to degradation temperature ( $T_d$ )). Inserting original functionalities along the PHA backbone with syndiotacticity is an important approach to tune the properties of the natural PHAs, expecting to facilitate their processability and to broaden their commercial applications. Consequently, the chemical synthesis of PHAs via the catalysed ring-opening polymerization (ROP) of  $\beta$ -lactones (mainly *rac*-BL<sup>Me</sup>) has been developed since 1960s, and proved to be a versatile strategy for the latter purpose.

With my work, we have contributed to the production of original and novel (thio)ether functional PHA homopolymers, represented as PBPL<sup>FG</sup>s (FG = OAlI, O<sup>n</sup>Bu, OBn, OTBDMS, OPh, SPh, O<sup>i</sup>Pr, O<sup>t</sup>Bu, OP(O)Ph<sub>2</sub>), having varied thermal properties, molar masses and stereochemistry, through the ROP of the functional cyclic  $\beta$ -propiolactones BPL<sup>FG</sup>s in the presence of organic activators (BEMP, TBD, DBU) or yttrium complexes/<sup>i</sup>PrOH (Y{ONNO<sup>R1R2</sup>}). All *racemic* and enantiopure BPL<sup>FG</sup>s were successfully synthesized by the carbonylation reaction of their corresponding epoxides (G<sup>FG</sup>s), in the presence of [Lewis acid]<sup>+</sup>[CoCO<sub>4</sub>]<sup>-</sup> catalysis, in good to high isolated yields (51%–82%).

Even though, the organic activators BEMP, TBD, and DBU are commercially available, generally non-toxic and stable to air, their usage in the ROP of  $\beta$ -lactones (*rac*-BL<sup>Me</sup> and *rac*-MLA<sup>FG</sup>s) was barely studied. Most likely because their mechanism at play during ROP was not discovered or remained obscured, and their activity enormously depends on the operating

conditions. In my work, investment in their usage in the bulk ROP of *rac*-BPL<sup>FG</sup>s (FG = OAll, O<sup>n</sup>Bu, OBn, OTBDMS, OP(O)Ph<sub>2</sub>) to produce atactic PBPL<sup>FG</sup>s, was managed. Most importantly, the complete mechanisms of the corresponding BEMP and DBU mediated ROP were proposed for the first time, and TBD mechanism was reinvestigated leading to deeper insights and modification in the previously proposed mechanism, as based on thorough <sup>1</sup>H and <sup>13</sup>C NMR and MALDI-ToF MS analyses. Investigating the mechanisms revealed the presence of unavoidable transfer reactions, resulting from the intrinsic nature of the β-lactones (the presence of an α-acidic hydrogen), that causes a decrease in the control of the polymerization in term of molar masses. Accordingly, it was proposed to utilize BEMP, TBD, and DBU in ROP of *rac*-DL<sup>R</sup> (R = Me, Et, Bn, ...), which could assist in bypassing the undesirable side reactions.

On the other hand, the ROP of *rac*-BPL<sup>FG</sup>s (FG = OPh, SPh, O<sup>i</sup>Pr, O<sup>t</sup>Bu, OTBDMS, OP(O)Ph<sub>2</sub>), mediated by yttrium-based complexes revealed to be highly active, regio- and stereo-selective, affording high molar mass polyesters ( $M_{n,SEC} = 96,000 \text{ g mol}^{-1}$ ) with narrow dispersities ( $D_M = 1.18$ ) and highly syndiotactic-enriched ( $P_{r(max)} = 0.87$ ) functional PHAs with unique and diverse thermal properties. This paves the way to investigate in their copolymerization to unveil unprecedented polymers.

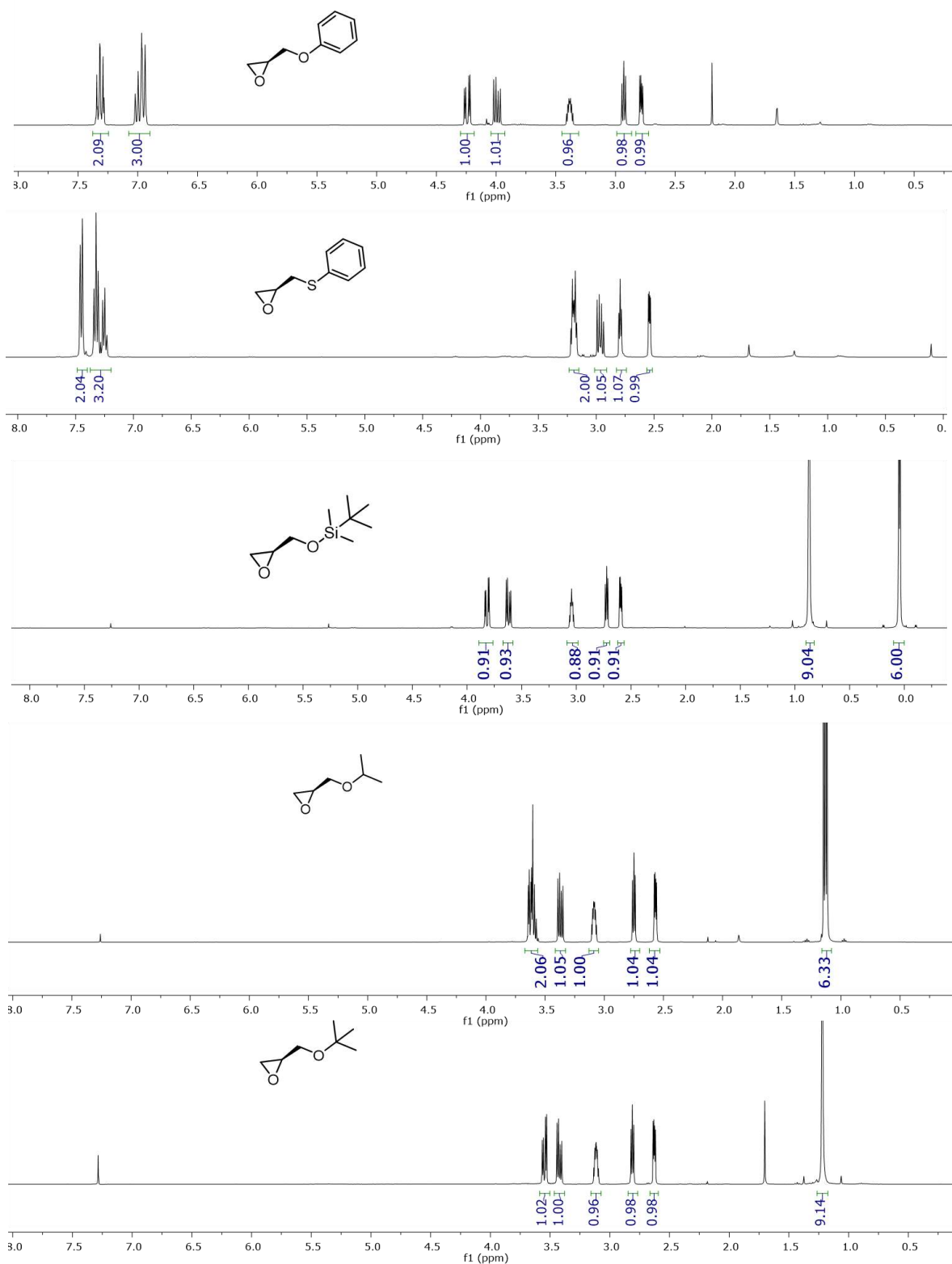




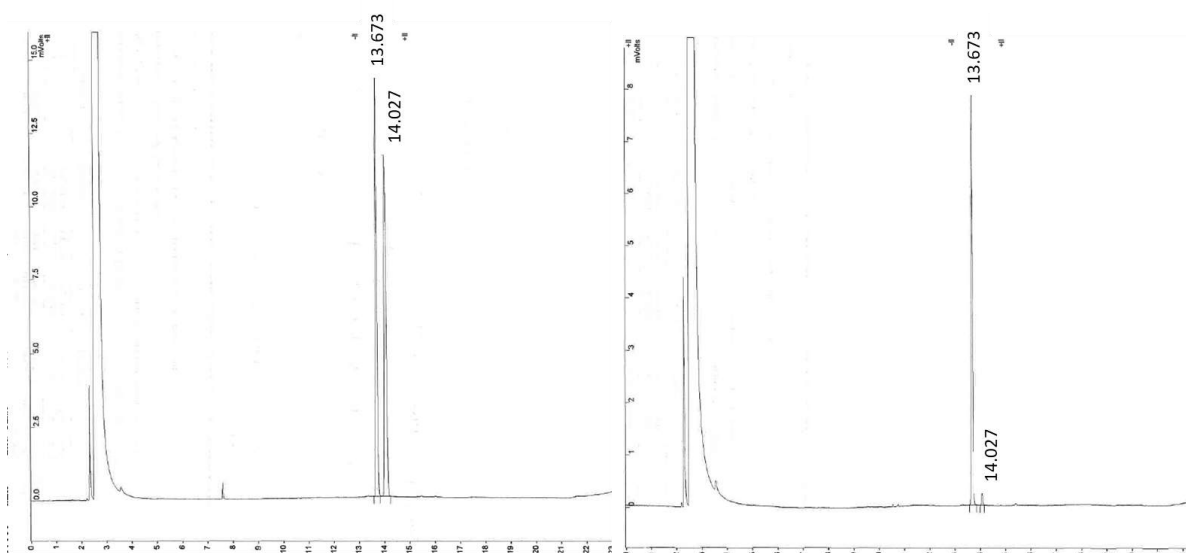
# Appendices



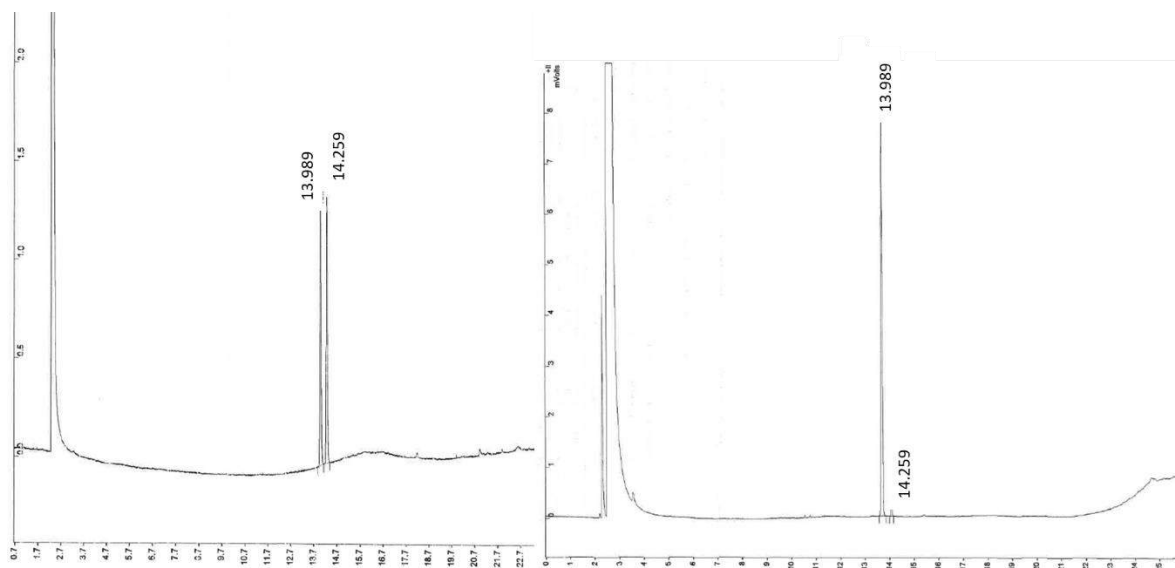




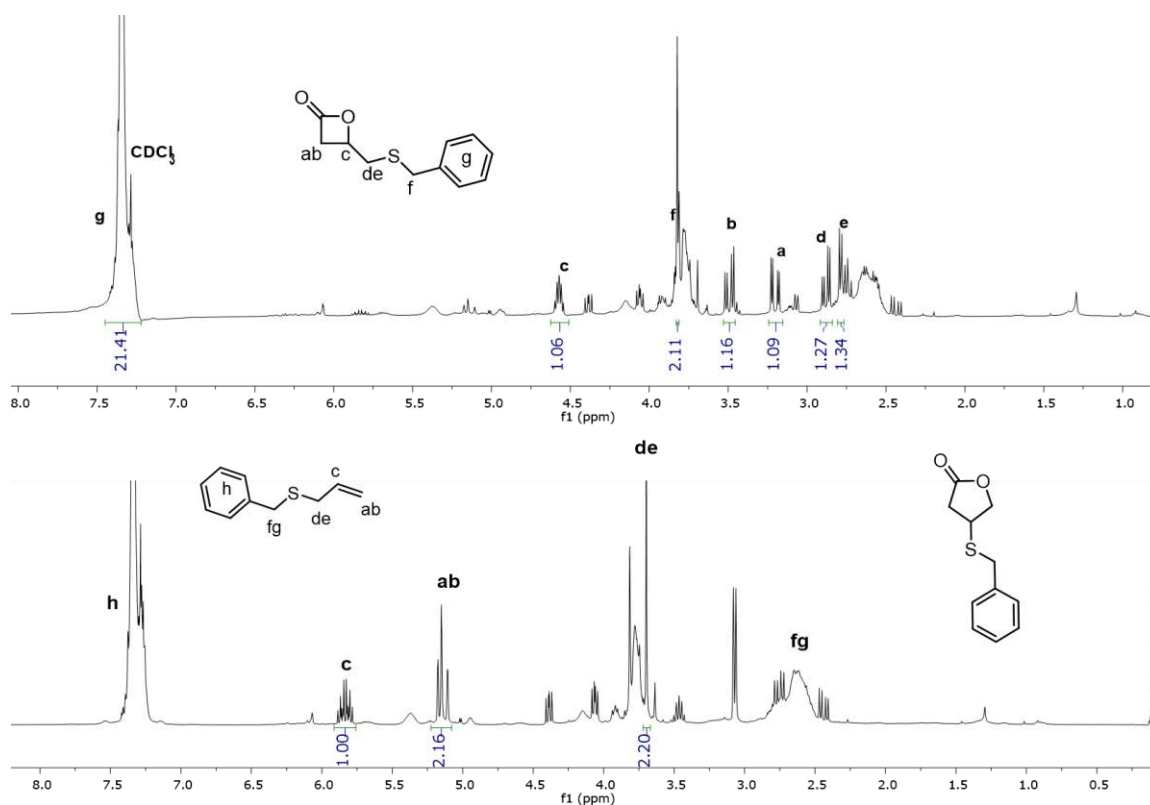
**Appendix 1** –  $^1\text{H}$  NMR spectra (400 MHz,  $\text{CDCl}_3$ , 23  $^\circ\text{C}$ ) of  $(S)\text{-G}^{\text{FG}}\text{s}$ ; FG = OPh, SPh, OTBDMS, O $i$ Pr, O $t$ Bu.



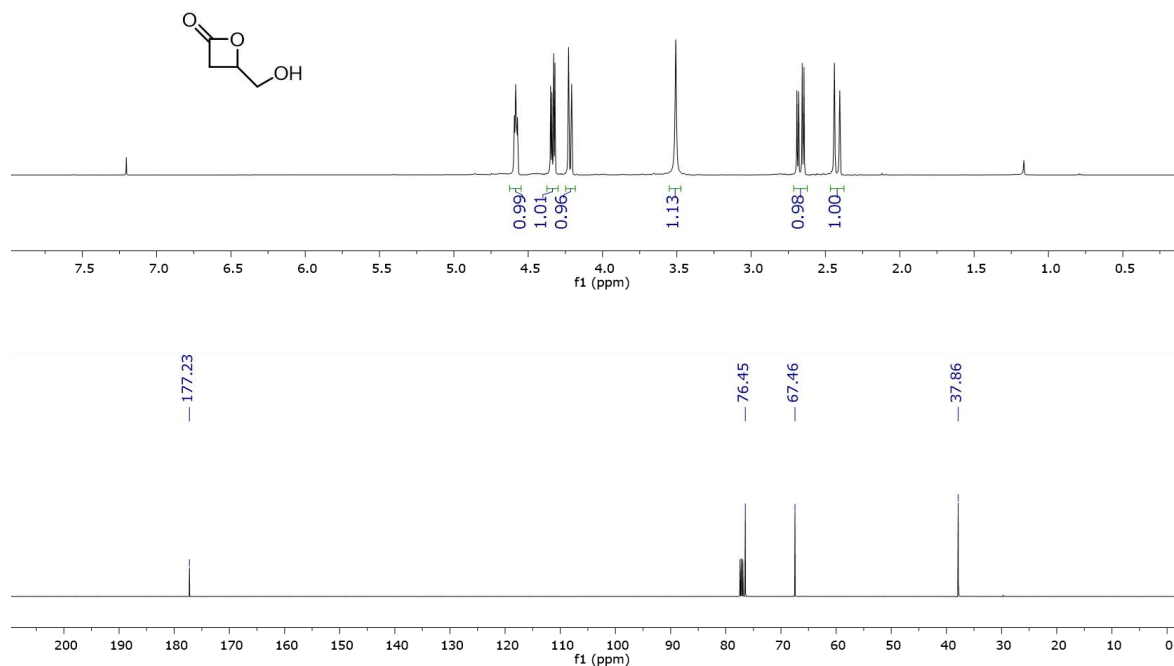
**Appendix 2** – Chiral gas chromatography analysis (GC); (left) *rac*-BPL<sup>O<sup>i</sup>Pr</sup>; (right) (*S*)-BPL<sup>O<sup>i</sup>Pr</sup>.



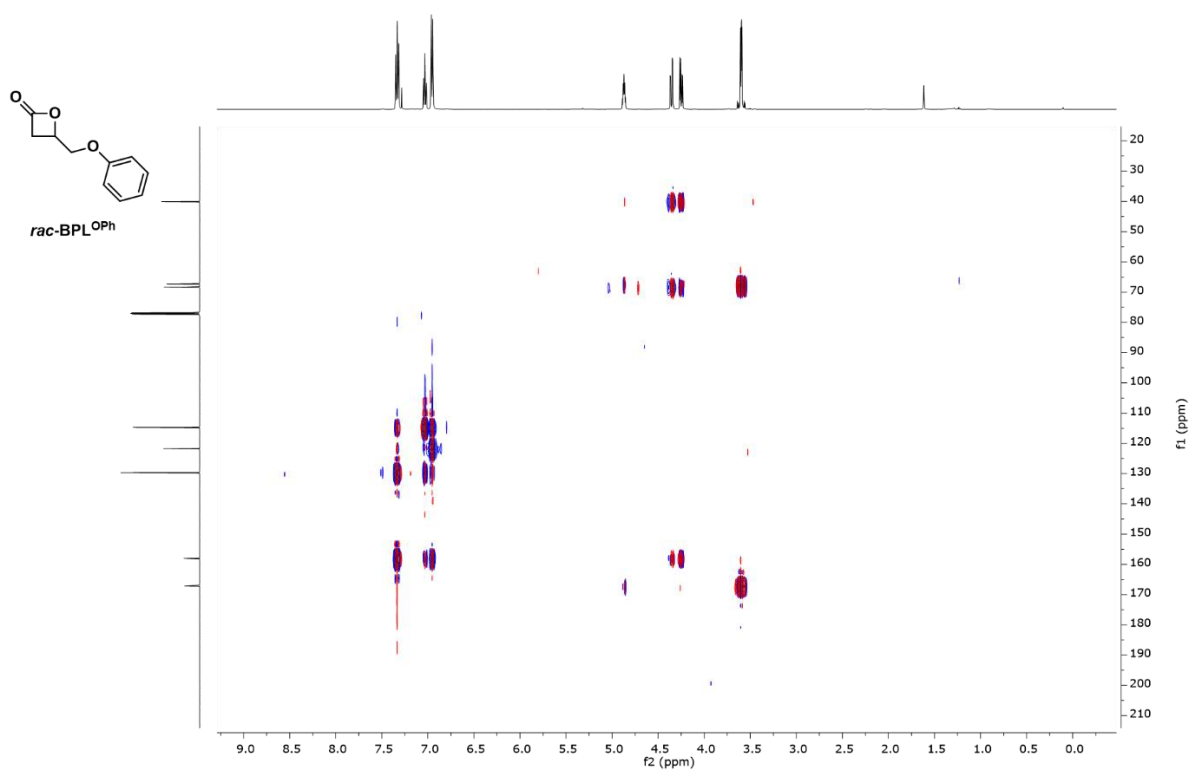
**Appendix 3** – Chiral gas chromatography analysis (GC); (left) *rac*-BPL<sup>O<sup>t</sup>Bu</sup>; (right) (*S*)-BPL<sup>O<sup>t</sup>Bu</sup>.



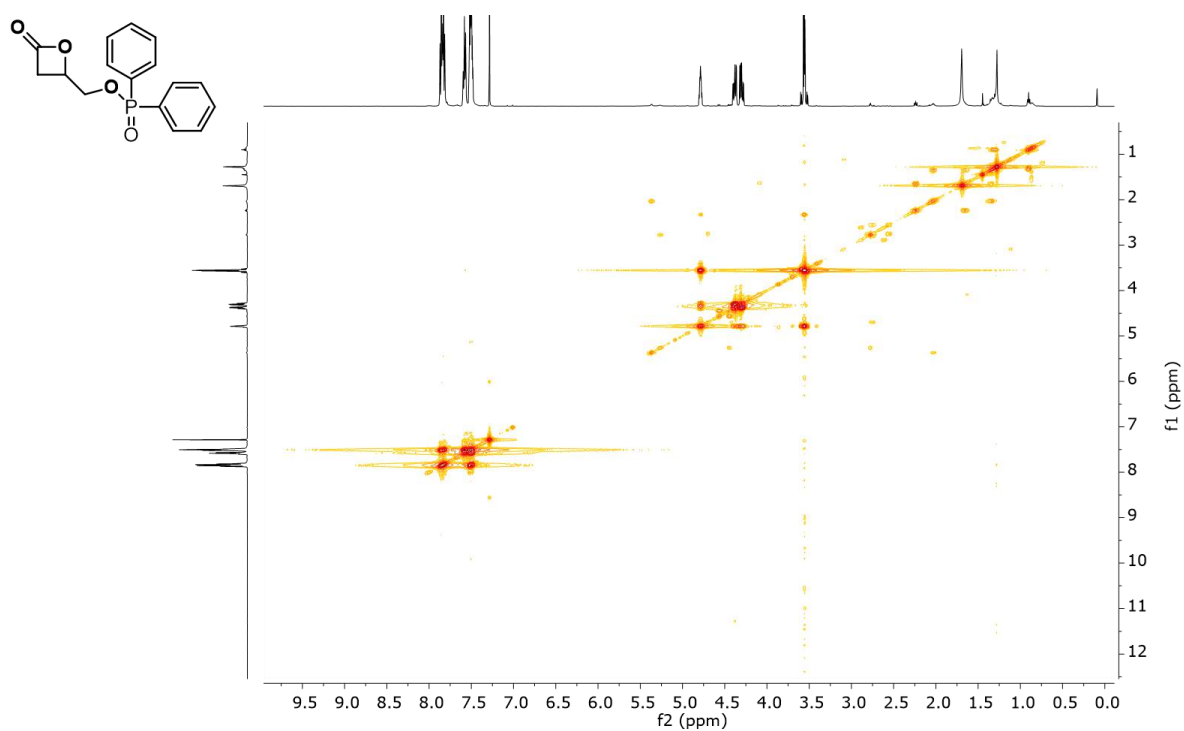
**Appendix 4** –  $^1\text{H}$  NMR spectra (400 MHz,  $\text{CDCl}_3$ , 25  $^\circ\text{C}$ ); crude  $\text{rac-BPL}^{\text{SBn}}$  obtained from carbonylation of  $\text{rac-G}^{\text{SBn}}$  accompanied with byproducts (top); decomposed and rearrangement products of  $\text{rac-BPL}^{\text{SBn}}$  to alkene and  $\gamma$ -lactone, respectively, after column and distillation at 120  $^\circ\text{C}$ .



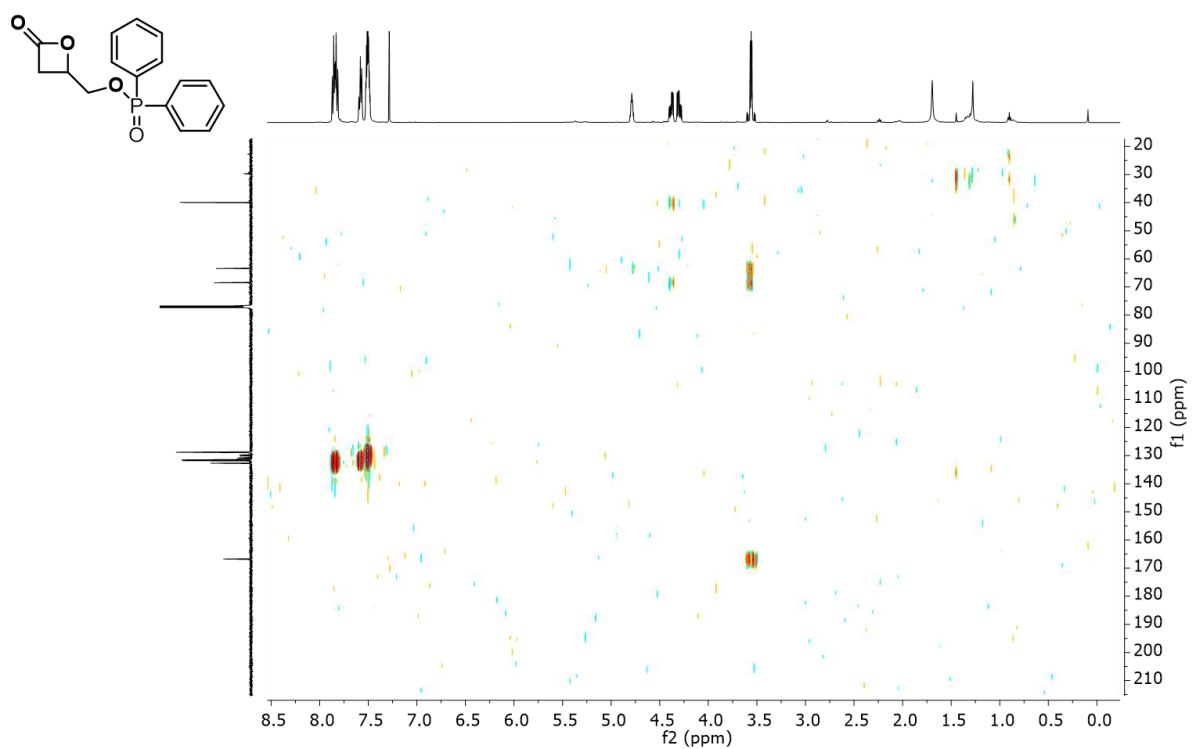
**Appendix 5** –  $^1\text{H}$  NMR (500 MHz,  $\text{CDCl}_3$ , 25  $^\circ\text{C}$ ) (top) and  $^{13}\text{C}$  (125 MHz,  $\text{CDCl}_3$ , 25  $^\circ\text{C}$ ) (bottom) spectra; for  $\text{rac-BPL}^{\text{OH}}$  obtained from carbonylation of  $\text{rac-G}^{\text{OH}}$  after purification.



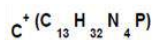
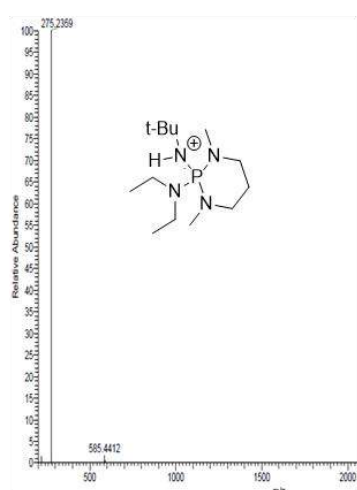
**Appendix 6** – <sup>1</sup>H-<sup>1</sup>H COSY (500 MHz, CDCl<sub>3</sub>, 25 °C) NMR spectrum of *rac*-BPL<sup>OPh</sup>.



**Appendix 7** – <sup>1</sup>H-<sup>1</sup>H COSY (500 MHz, CDCl<sub>3</sub>, 25 °C) NMR spectrum of *rac*-BPL<sup>OP(O)Ph<sub>2</sub></sup>.



**Appendix 8** –  $^1\text{H}$ - $^{13}\text{C}$  HMBC (500 MHz, 125 MHz,  $\text{CDCl}_3$ , 25 °C) spectrum of *rac*-BPL  $\text{OP(O)Ph}_2$ .

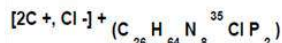


Theoretical mass: 275.23646

z = 1

m / z Theoretical: 275.23591

m / z Found: 275.2359 (0 ppm)

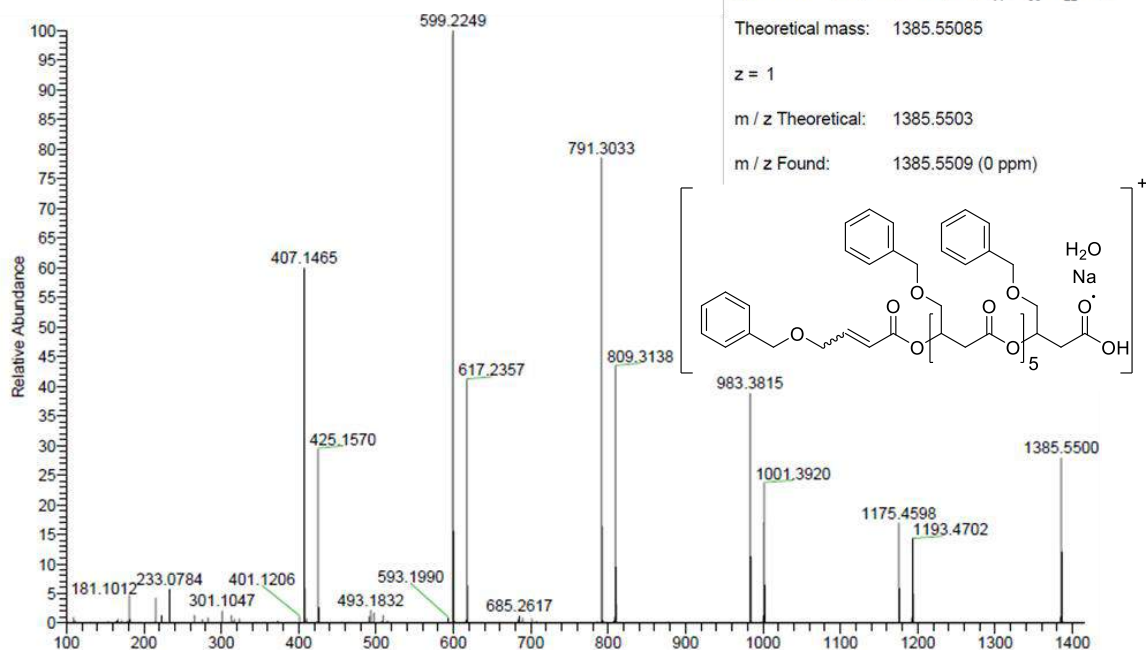


Theoretical mass: 585.44177

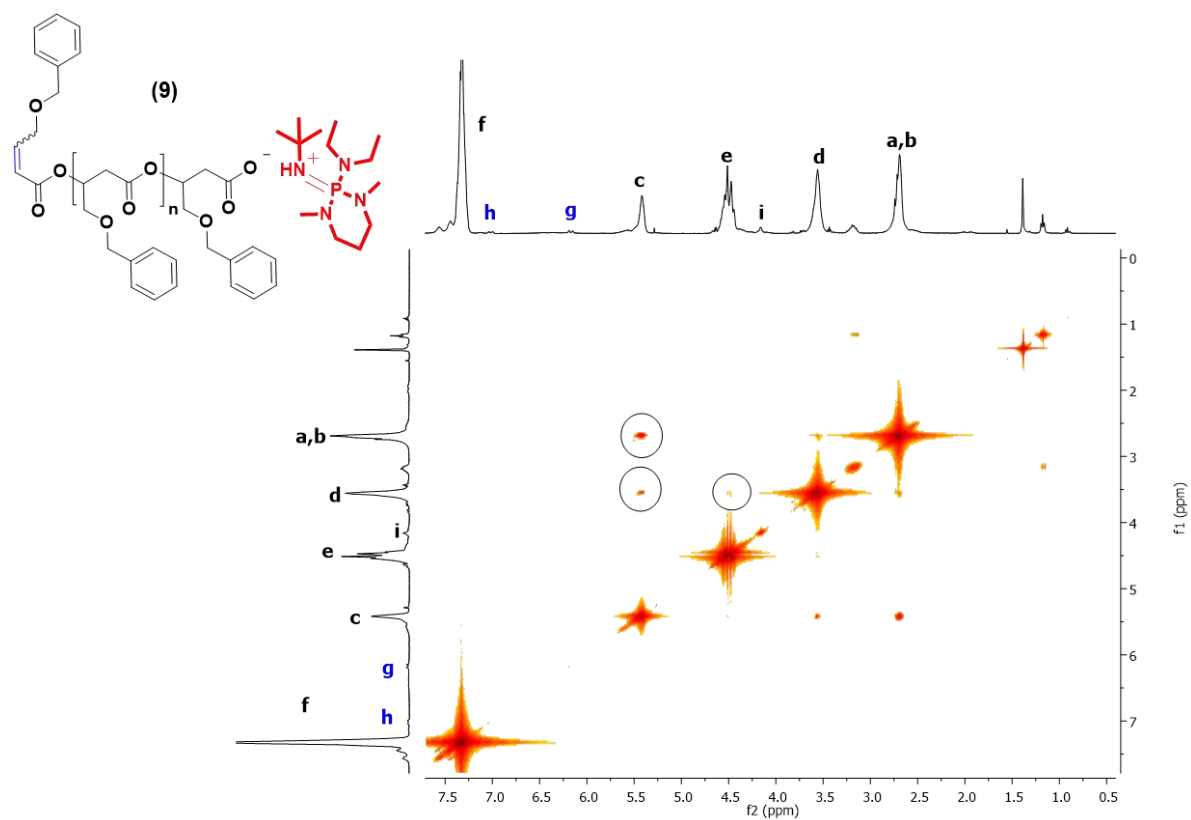
z = 1

m / z Theoretical: 585.44122

m / z Found: 585.4412 (0 ppm)

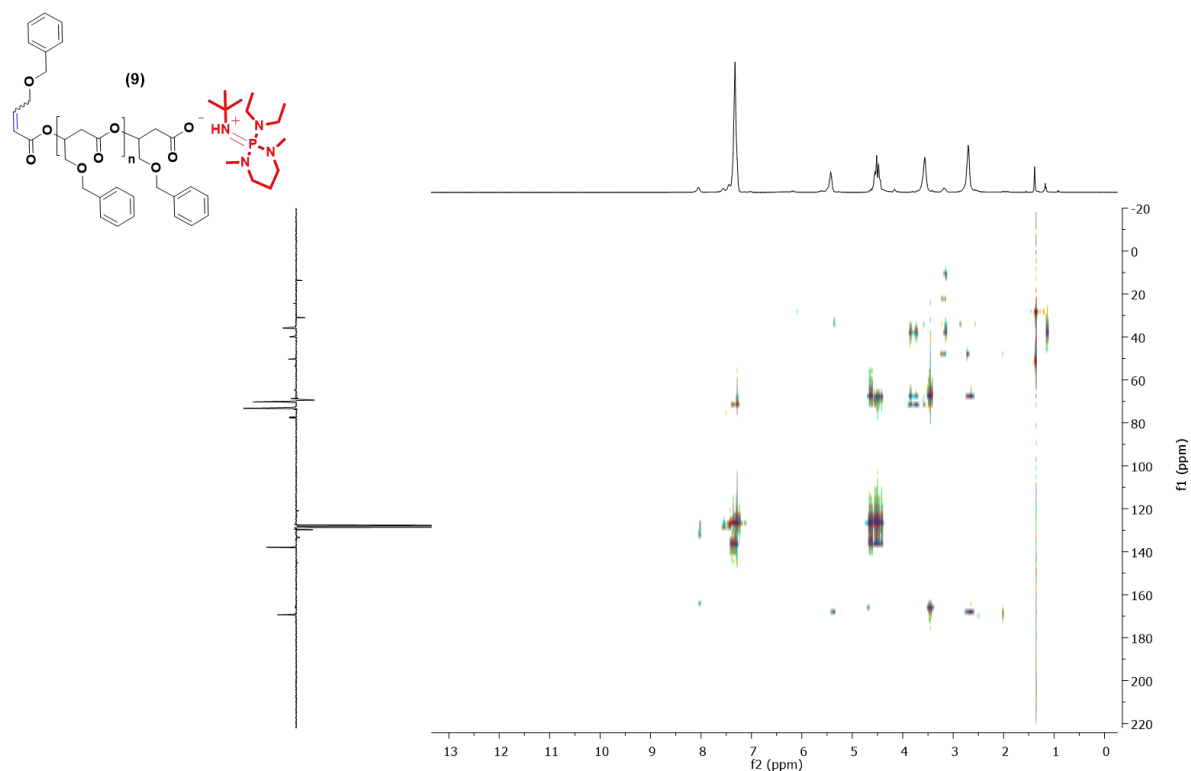


**Appendix 9** – ESI mass spectrum of PBPL<sup>OBn</sup> (CH<sub>2</sub>Cl<sub>2</sub>, NaCl) sample freshly synthesized from the ROP of *rac*-BPL<sup>OBn</sup> mediated by BEMP (Table 3.3, entry 7); showing BEMP<sup>H+</sup> and PBPL<sup>OBn</sup> macromolecules end-capped with both an α-crotonate and an ω-carboxylic acid end-groups; ionized by Na<sup>+</sup> in presence of adventitious H<sub>2</sub>O.

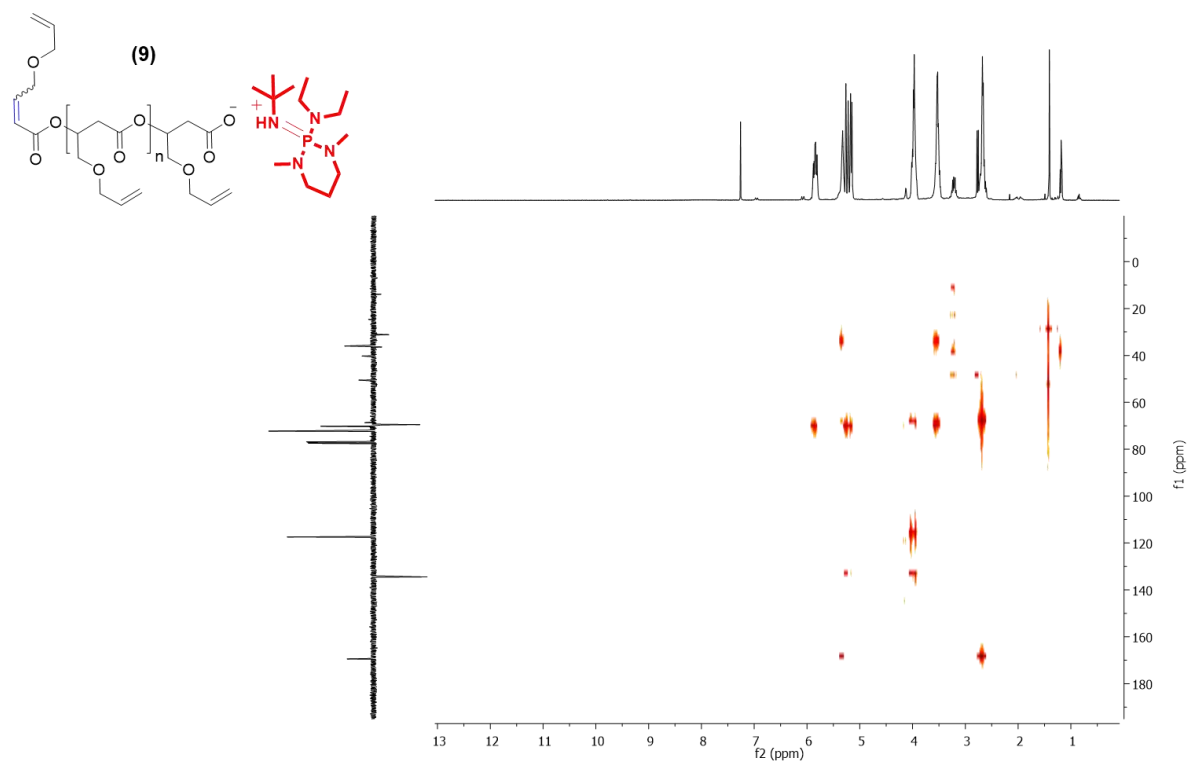


**Appendix 10** – <sup>1</sup>H-<sup>1</sup>H COSY (500 MHz, CDCl<sub>3</sub>, 25 °C) NMR spectrum of PBPL<sup>OBn</sup> recovered from the ROP of *rac*-BPL<sup>OBn</sup> mediated by BEMP (Table 3.3, entry 12).

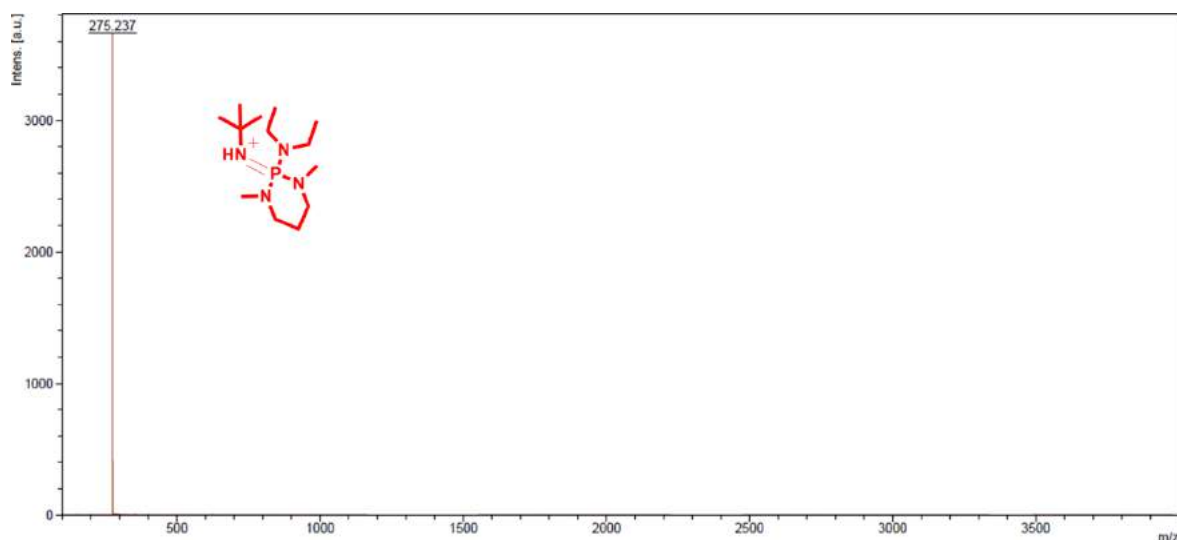




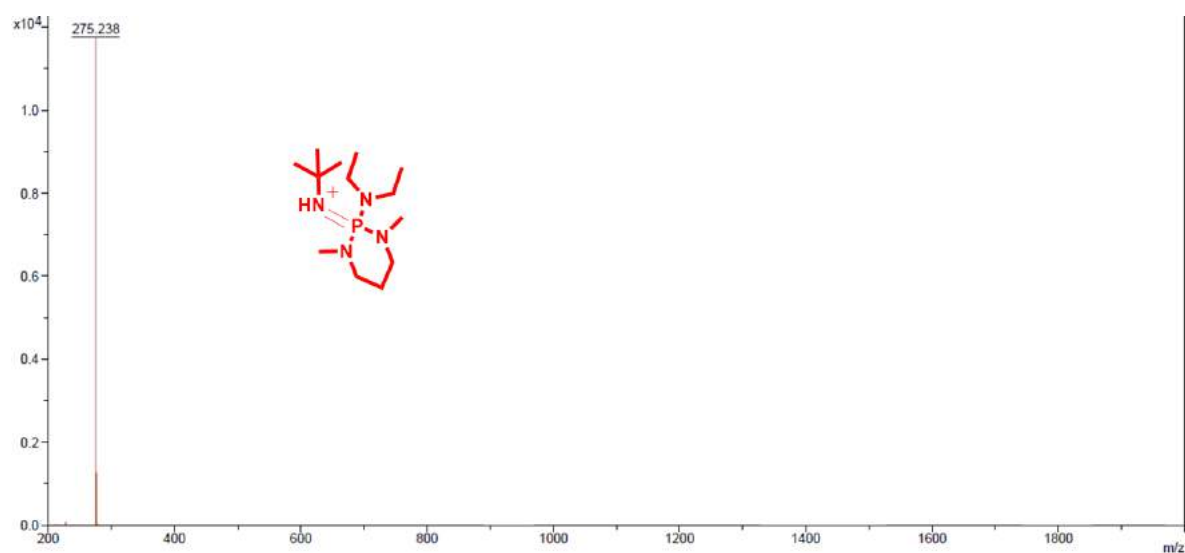
**Appendix 11** –  $^1\text{H}$ - $^{13}\text{C}$  HMBC (500 MHz,  $\text{CDCl}_3$ , 25 °C) NMR spectra of PBPL<sup>OBn</sup> recovered from the ROP of *rac*-BPL<sup>OBn</sup> mediated by BEMP (Table 3.3, entries 12).



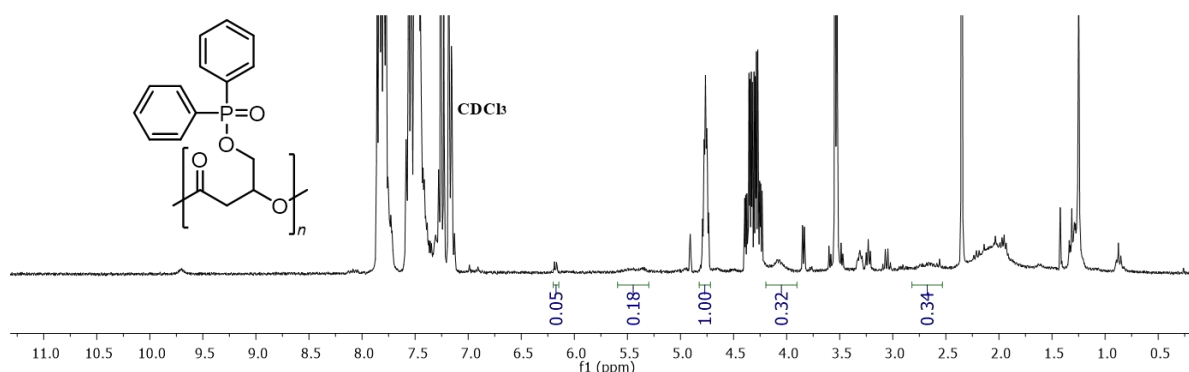
**Appendix 12** –  $^1\text{H}$ - $^{13}\text{C}$  HMBC (500 MHz,  $\text{CDCl}_3$ , 25 °C) NMR spectra of PBPL<sup>OAll</sup> recovered from the ROP of *rac*-BPL<sup>OAll</sup> mediated by BEMP (Table 3.3, entries 3).



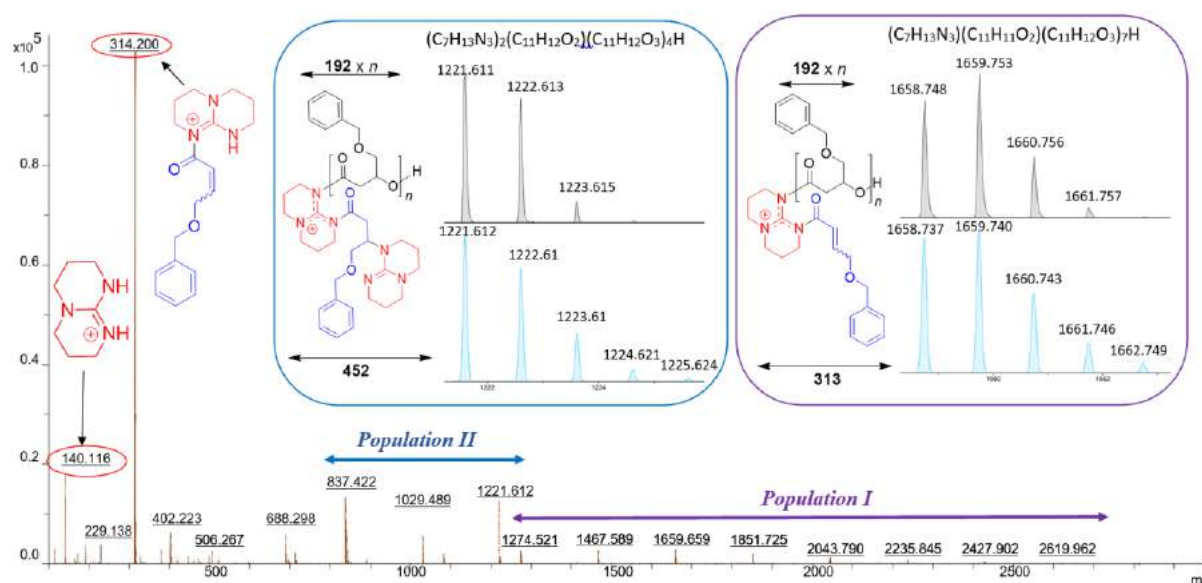
**Appendix 13** – MALDI-ToF mass spectrum (positive mode, DCTB matrix, without any cationizing salt) of a sample freshly synthesized from the ROP of *rac*-BPL<sup>OBn</sup> mediated by BEMP (**Error! Reference source not found.**, entry 11) showing only [BEMPH]<sup>+</sup>.



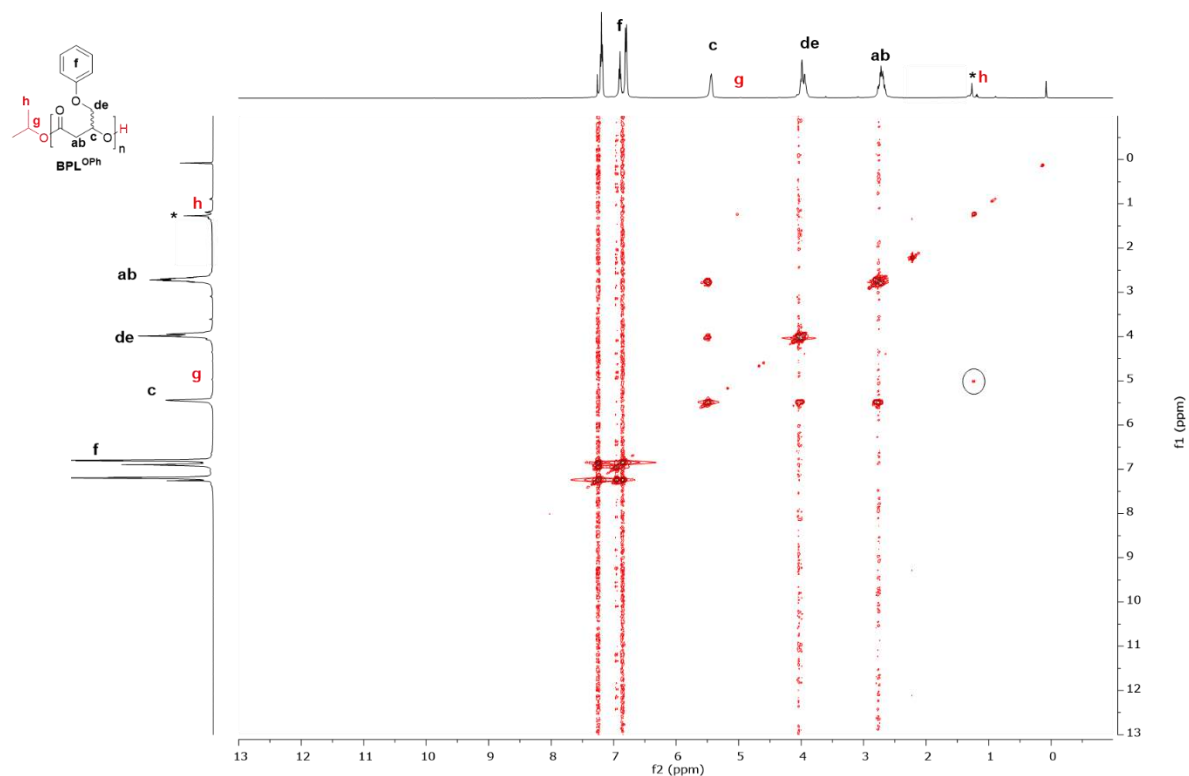
**Appendix 14** – MALDI-ToF mass spectrum (positive mode, HCCA matrix, without any cationizing salt) of a sample freshly synthesized from the ROP of *rac*-BPL<sup>OBn</sup> mediated by BEMP (**Error! Reference source not found.**, entry 16) showing only [BEMPH]<sup>+</sup>.



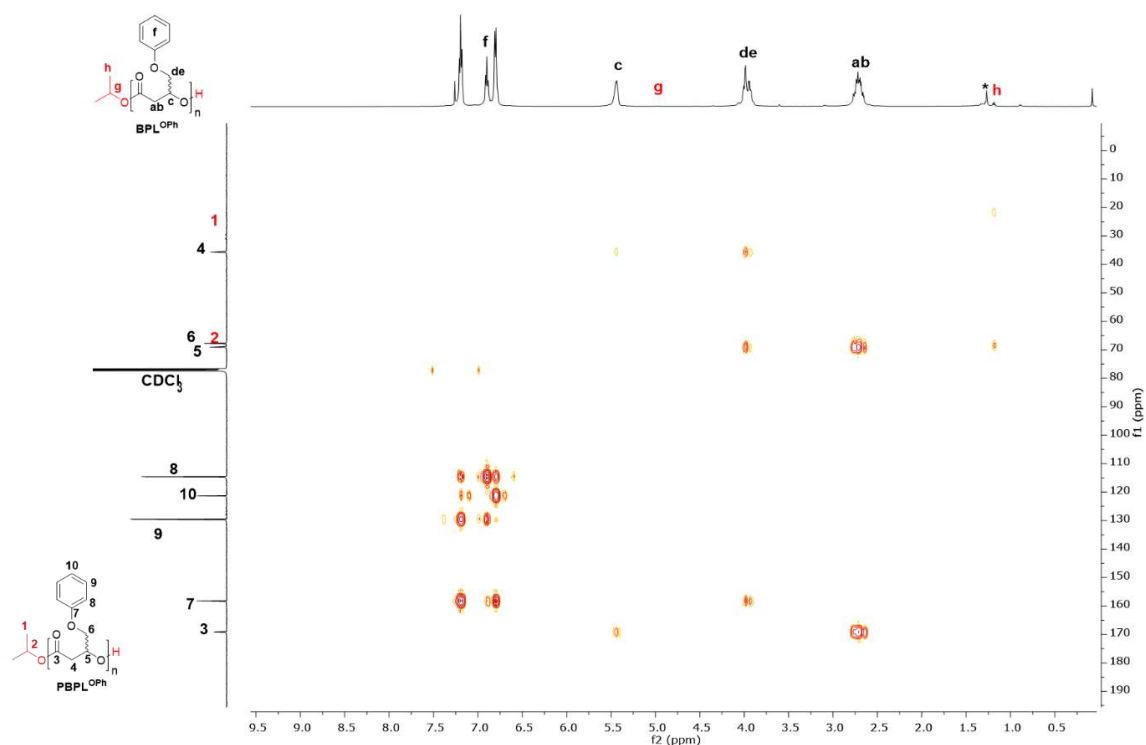
**Appendix 15** – <sup>1</sup>H NMR (400 MHz, CDCl<sub>3</sub>, 25 °C) spectrum for ROP of *rac*-BPL<sup>OP(O)Ph<sub>2</sub></sup> mediated by TBD; giving 15% monomer conversion, and a crotonate peak is observed at δ 6.21 ppm (Table 3.4 – entry 9).



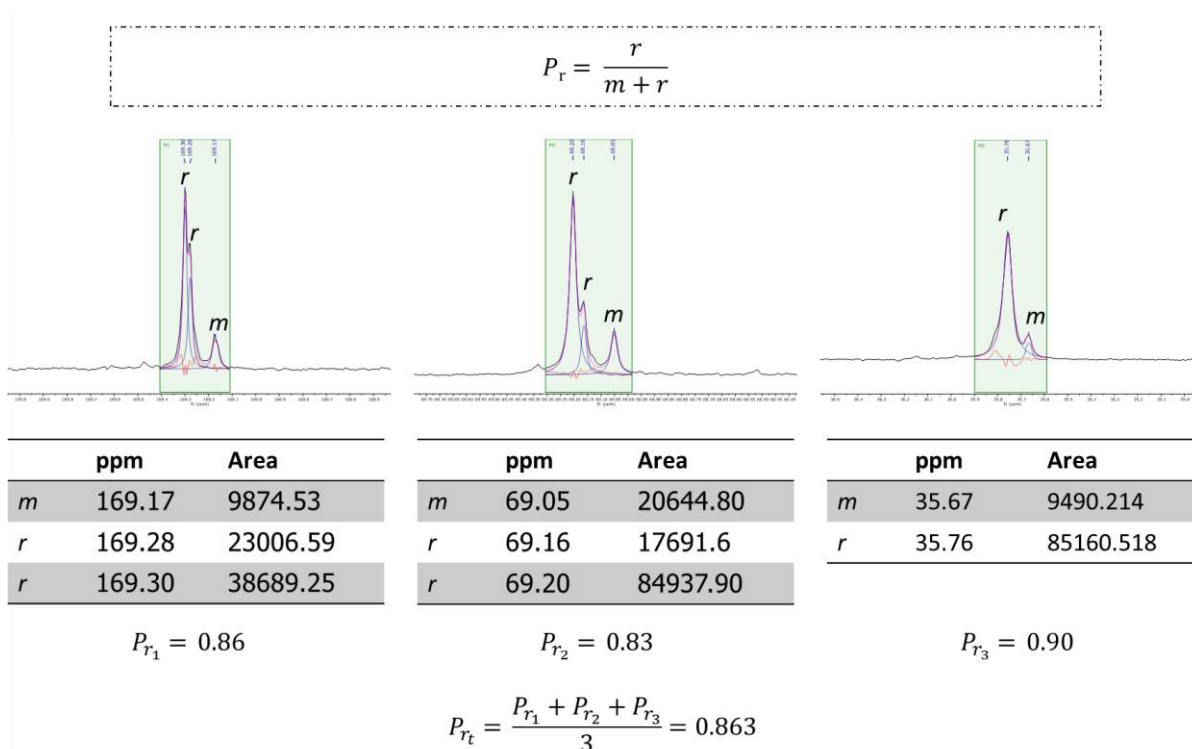
**Appendix 16** – MALDI-ToF mass spectrum (positive mode, DCTB matrix, absence of cationizing salt) of a sample freshly synthesized from the ROP of *rac*-BPL<sup>OBn</sup> mediated by TBD (Table 3.4 **Error! Reference source not found.**, entry 6) showing populations I and II.



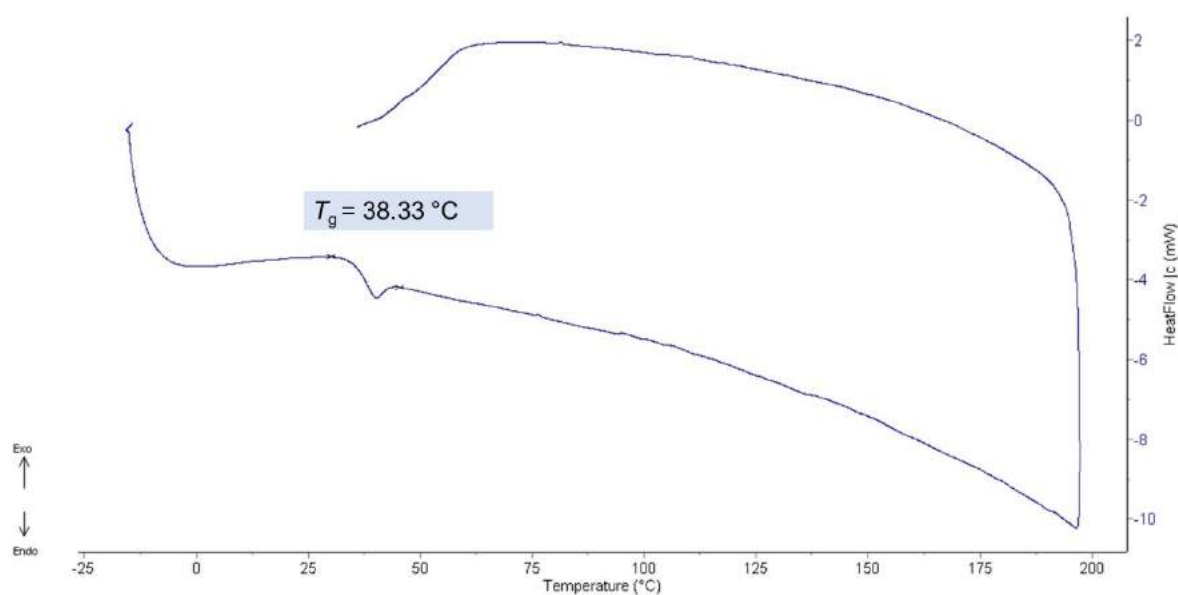
**Appendix 17** –  $^1\text{H}$ - $^1\text{H}$  COSY NMR spectrum (500 MHz,  $\text{CDCl}_3$ , 25 °C) of syndiotactic PBPL<sup>OPh</sup> precipitated twice in cold pentane (Table 4. 2, entry 6) (\*: residual H-grease).



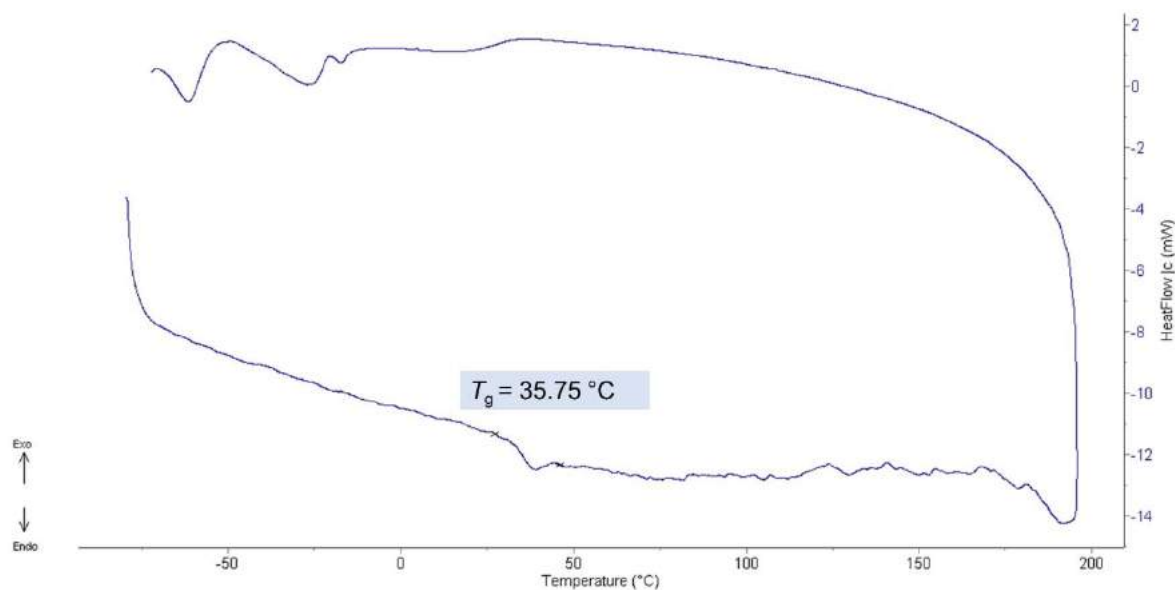
**Appendix 18** –  $^1\text{H}$ - $^{13}\text{C}$  HMBC (500 MHz, 125 MHz,  $\text{CDCl}_3$ , 25 °C) of syndiotactic PBPL<sup>OPh</sup> precipitated twice in cold pentane (Table 4. 2, entry 6) (\*: residual H-grease).



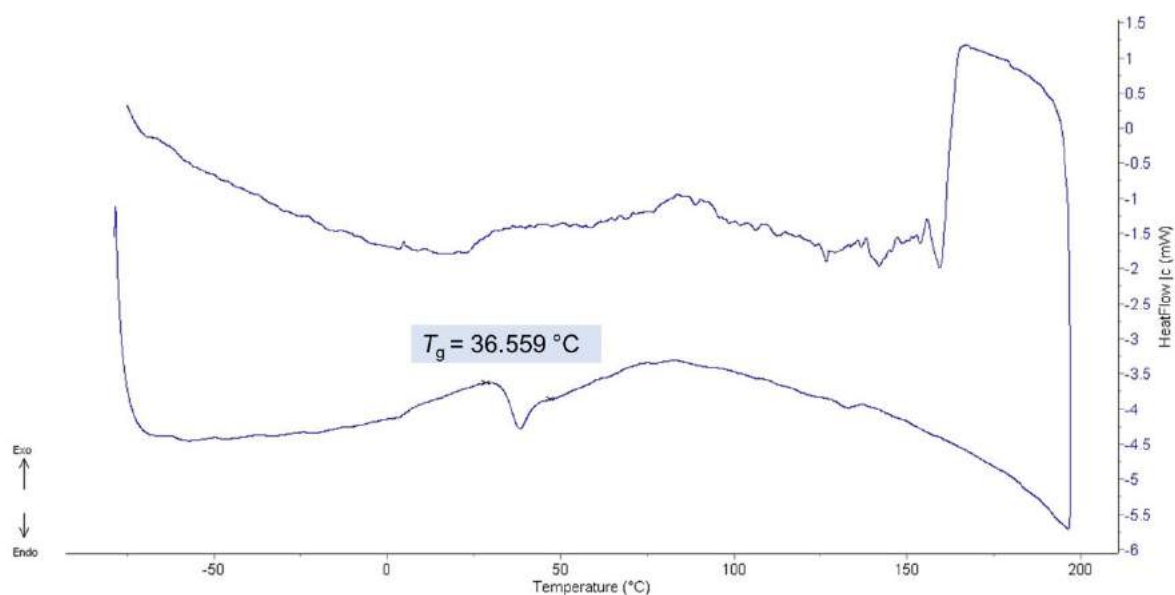
**Appendix 19** –  $P_r$  calculation by using Mestrenova Fitting Region of  $^{13}\text{C}$  NMR for PBPL<sup>OPh</sup> (Table 4. 2, entry 6).



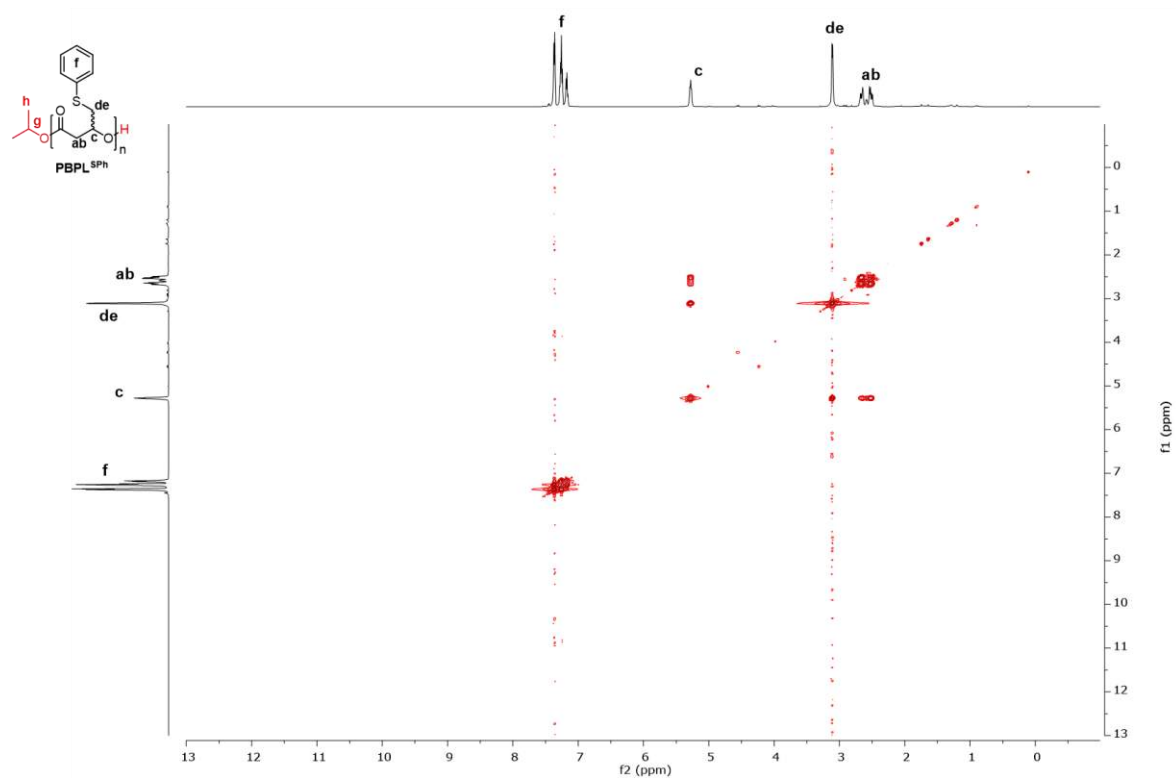
**Appendix 20** – DSC thermogram (heating rate of  $10\text{ }^{\circ}\text{C min}^{-1}$ , second heating cycle, from  $-80$  to  $200\text{ }^{\circ}\text{C}$ ) of syndiotactic PBPL<sup>OPh</sup> ( $P_r = 0.87$ ) synthesized by ROP of *rac*-BPL<sup>OPh</sup> with **2b**/*i*PrOH (Table 4. 2, entry 8).



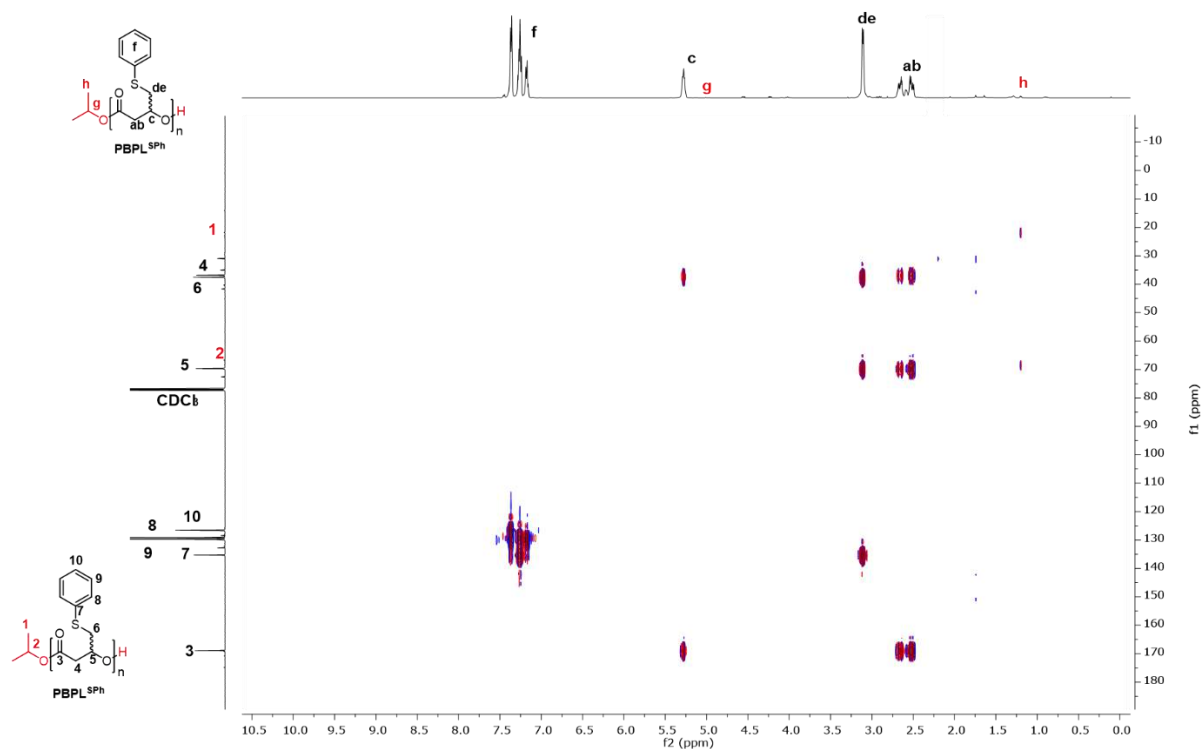
**Appendix 21** – DSC thermogram (heating rate of  $10\text{ °C min}^{-1}$ , second heating cycle, from  $-80$  to  $200\text{ °C}$ ) of isotactic PBPL<sup>OPh</sup> ( $P_r < 0.05$ ) synthesized by ROP of (*S*)-BPL<sup>OPh</sup> with **2b**/*i*PrOH) (Table 4. 2, entry 13).



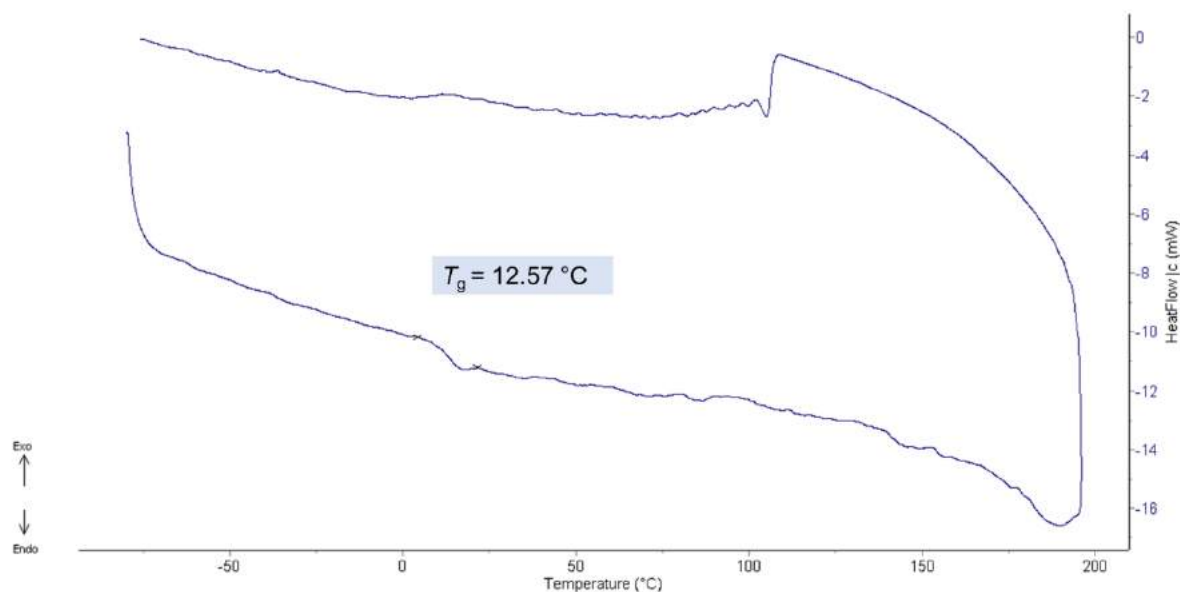
**Appendix 22** – DSC thermogram (heating rate of  $10\text{ °C min}^{-1}$ , second heating cycle, from  $-80$  to  $200\text{ °C}$ ) of syndiotactic PBPL<sup>OPh</sup> ( $P_r = 0.86$ ) synthesized by ROP of *rac*-BPL<sup>OPh</sup> with **2b**/*i*PrOH) (Table 4. 2, entry 7).



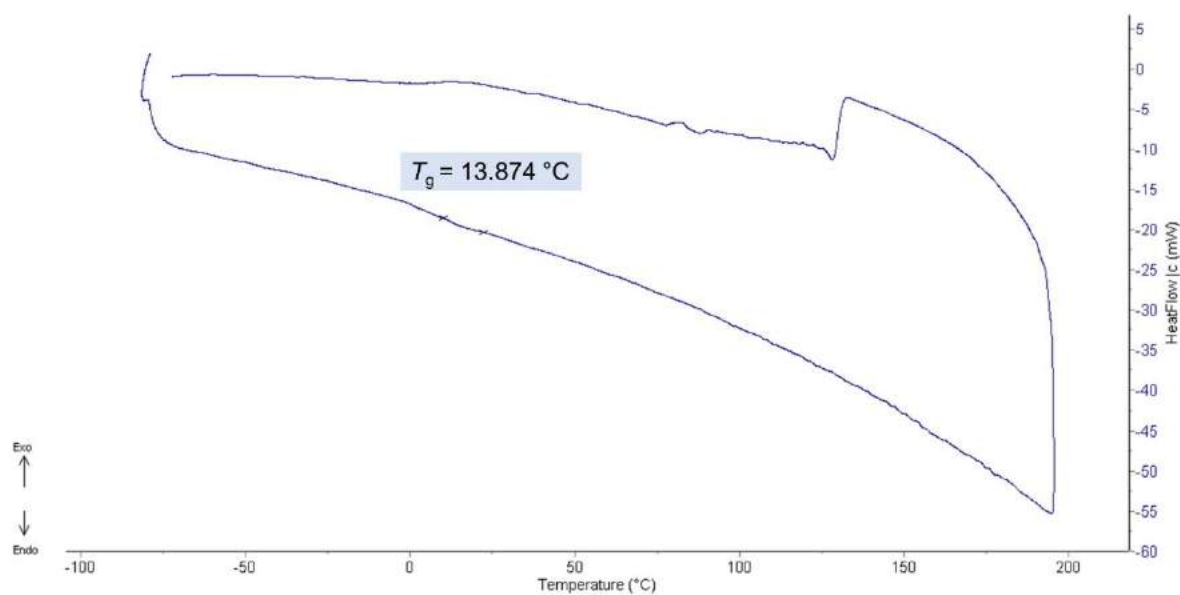
**Appendix 23** –  $^1\text{H}$ - $^1\text{H}$  COSY NMR spectrum (500 MHz,  $\text{CDCl}_3$ , 25 °C) of syndiotactic PBPL<sup>SPh</sup> precipitated twice in cold pentane (Table 4. 3, entry 13).



**Appendix 24** –  $^1\text{H}$ - $^{13}\text{C}$  HMBC (500 MHz, 125 MHz,  $\text{CDCl}_3$ , 25 °C) of syndiotactic PBPL<sup>SPh</sup> precipitated twice in cold pentane (Table 4. 3, entry 13).



**Appendix 25** – DSC thermogram (heating rate of  $10\text{ °C min}^{-1}$ , second heating cycle, from  $-80$  to  $200\text{ °C}$ ) of isotactic PBPL<sup>SPh</sup> ( $Pr < 0.05$ ) synthesized by ROP of (*S*)-BPL<sup>SPh</sup> with **2b**/*i*PrOH) (Table 4. 2, entry 14).



**Appendix 26** – DSC thermogram (heating rate of  $10\text{ °C min}^{-1}$ , second heating cycle, from  $-80$  to  $200\text{ °C}$ ) of syndiotactic PBPL<sup>SPh</sup> ( $Pr = 0.86$ ) synthesized by ROP of *rac*-BPL<sup>SPh</sup> with **2b**/*i*PrOH) (Table 4. 2, entry 8).

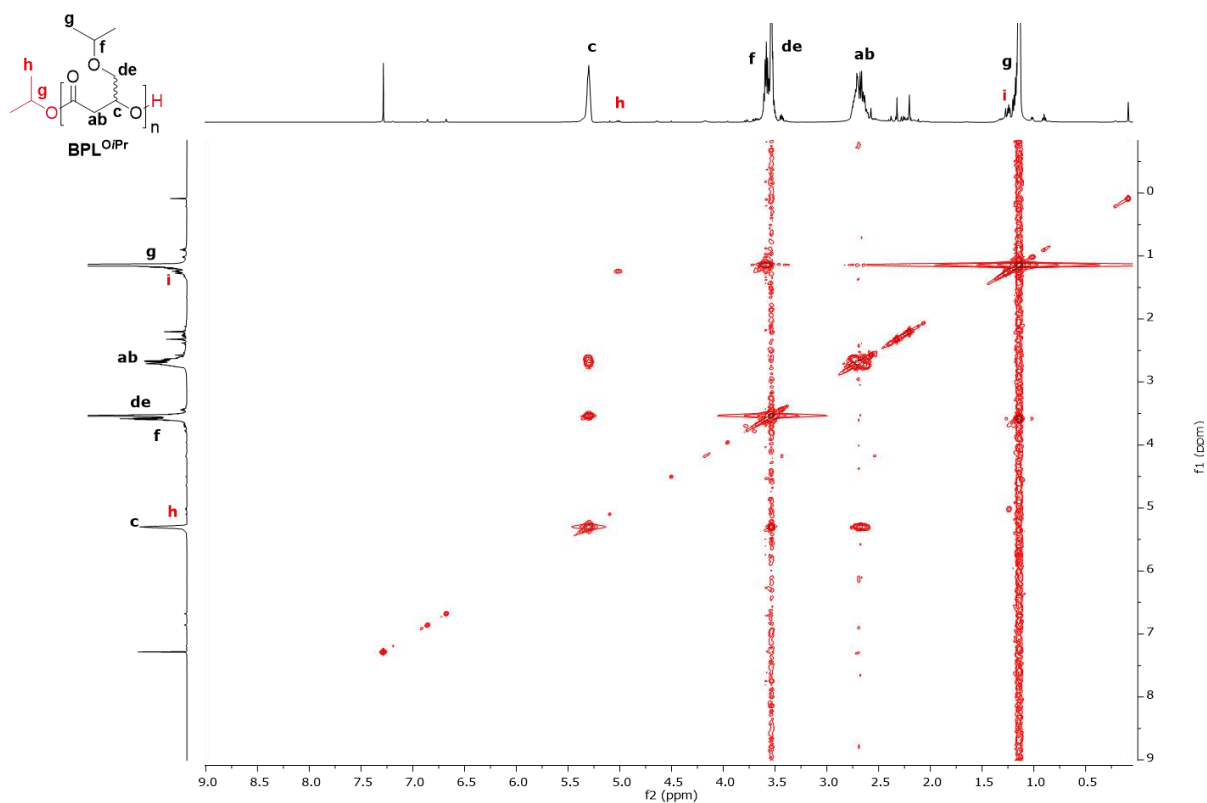


**Appendix 27** – Kinetic data for the monitoring of the ROP of *rac*-BPL<sup>FG</sup>s with various 2/<sup>i</sup>PrOH (1:1) catalytic systems ([BPL<sup>FG</sup>]<sub>0</sub>/[2]<sub>0</sub>/[<sup>i</sup>PrOH]<sub>0</sub> = 60:1:1; Figure 1. 20).

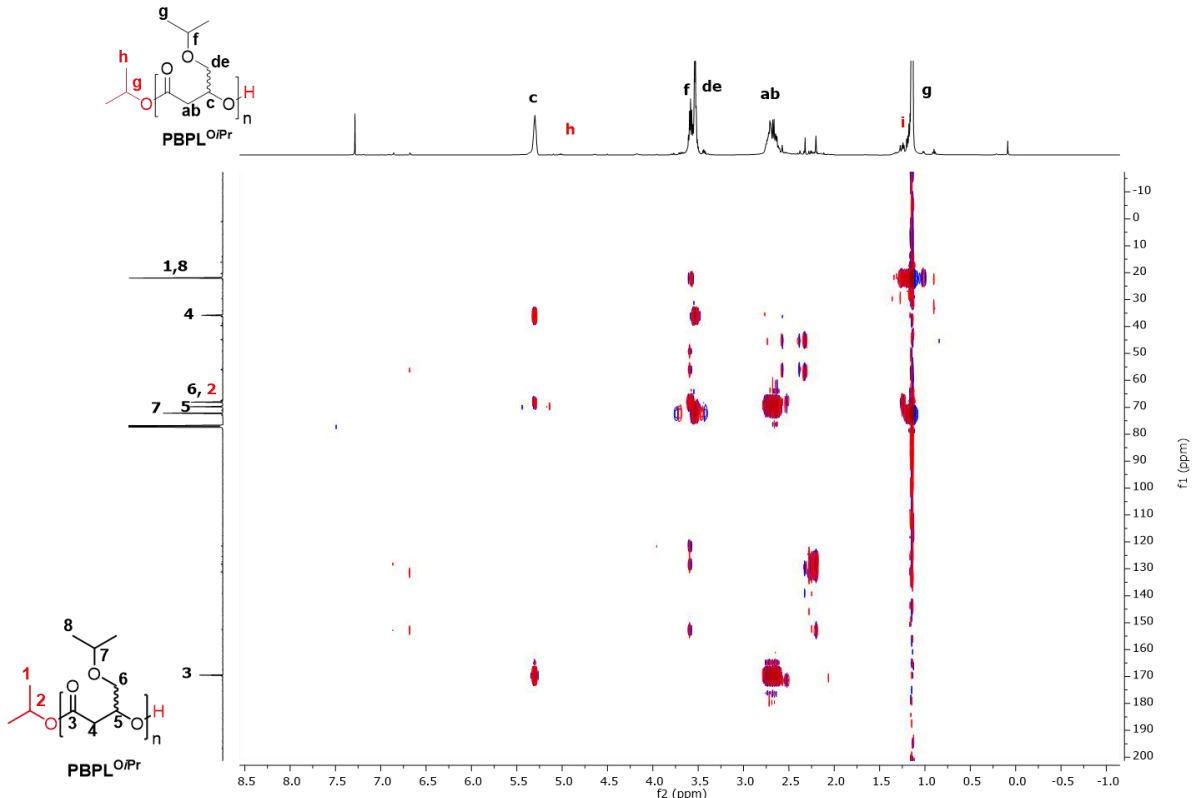
BPL <sup>FG</sup> /2	Time (h)	Conv. (%)	ln([BPL <sup>CH2ZPh</sup> ] <sub>0</sub> / [BPL <sup>CH2ZPh</sup> ] <sub>t</sub> )	<i>M</i> <sub>n,theo</sub> (g mol <sup>-1</sup> )	<i>M</i> <sub>n,NMR</sub> (g mol <sup>-1</sup> )	<i>M</i> <sub>n,SEC</sub> (g mol <sup>-1</sup> )	<i>Đ</i> <sub>M</sub>
Table 2. 2, entry 2 BPL <sup>OPh</sup> {ONNO <sup>Cl2</sup> } <b>2d</b>	0	0	0	0	0	0	-
	1.17	19	0.21	3 000	2 500	3 500	1.09
	4	38	0.48	4 100	3 900	4 300	1.10
	7	48	0.65	5 100	5 000	5 200	1.13
	50	54	-	5 800	5 400	6 200	1.15
Table 2.2, entry 4 BPL <sup>OPh</sup> {ONNO <sup>Me2</sup> } <b>2c</b>	0	0	0	0	0	0	-
	0.25	20	0.22	2 200	2 000	2 600	1.11
	0.50	40	0.51	4 300	5 700	5 100	1.11
	1.17	64	1.03	6 900	6 900	8 200	1.13
	2.17	83	1.78	8 900	8 000	10 400	1.13
	4.17	95	3.22	10 200	10 000	11 100	1.13
Table 2. 2, entry 11 BPL <sup>OPh</sup> {ONNO <sup>Cumyl2</sup> } <b>2a</b>	0	0	0	0	0	0	-
	0.14	100	4.61	10 700	10 000	12 200	1.12
	0.5	100	-	10 700	10 000	12 200	1.15
Table 2. 2, entry 6 BPL <sup>OPh</sup> {ONNO <sup>tBu2</sup> } <b>2b</b>	0	0	0	0	0	0	-
	0.14	100	4.61	10 700	10 600	12 200	1.11
	0.25	100	-	10 700	10 600	12 200	1.14
Table 2. 4, entry 3 BPL <sup>SPh</sup> {ONNO <sup>Cl2</sup> } <b>2d</b>	0	0	0	0	0	0	-
	24	12	0.13	1 500	1 300	1 600	1.08
	48	21	0.24	2 500	2 400	2 600	1.12
	60	28	0.33	3 300	3 200	3 600	1.14
	96	48	-	5 700	5 100	6 400	1.17
Table 2. 4, entry 5 BPL <sup>SPh</sup> {ONNO <sup>Me2</sup> } <b>2c</b>	0	0	0	0	0	0	-
	0.25	10	0.11	1 200	1 100	1 500	1.13
	0.5	20	0.22	2 400	2 400	3 200	1.14
	2	55	0.80	6 400	6 300	8 900	1.16
	4	88	2.12	10 400	10 200	12 500	1.18
	8	99	4.61	11 600	11 300	13 900	1.21
Table 2. 4, entry 12 BPL <sup>SPh</sup> {ONNO <sup>Cumyl2</sup> } <b>2a</b>	0	0	0	0	0	0	-
	0.17	100	4.61	11 700	11 300	12 700	1.08
	1	100	-	11 700	11 300	13 300	1.12
Table 2. 4, entry 7	0	0	0	0	0	0	-
	0.17	100	4.61	15 600	15 200	16 200	1.07

BPL<sup>SPh</sup>  
{ONNO<sup>tBu2</sup>}  
**2b**

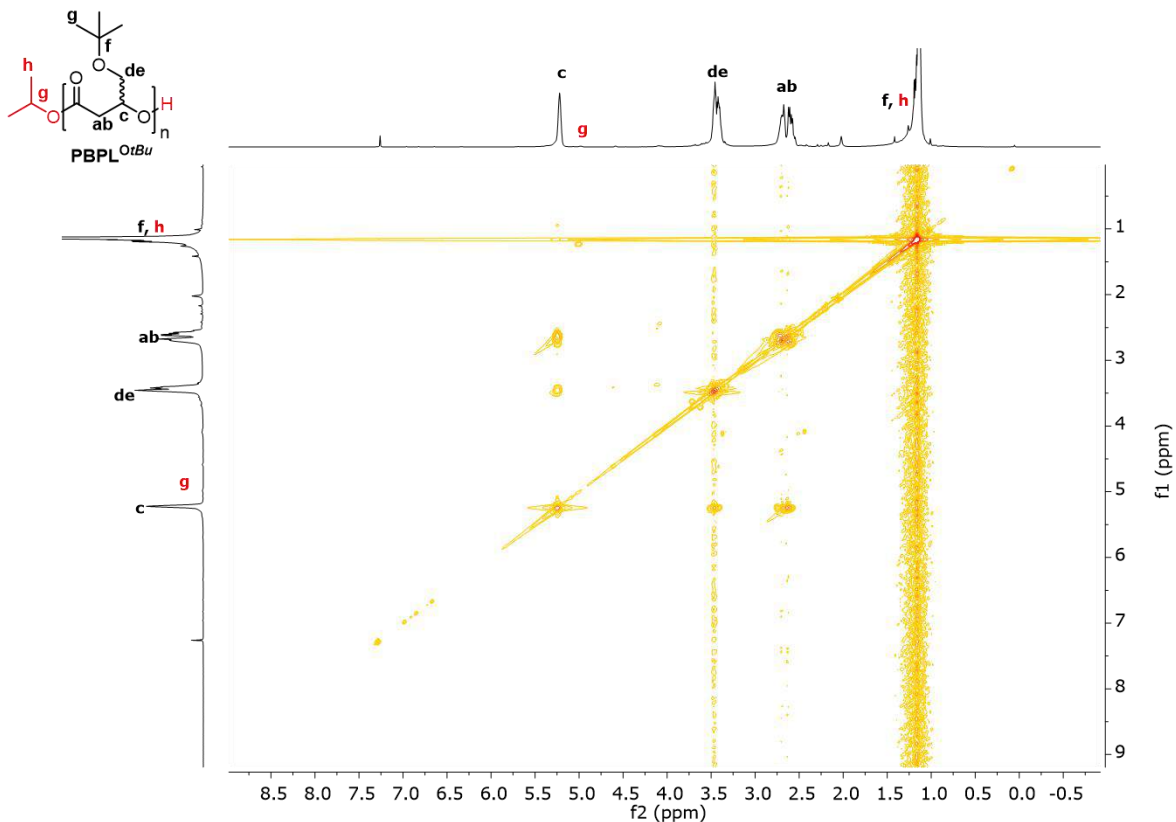
1      100      4.61      15 600      15 200      17 900      1.15



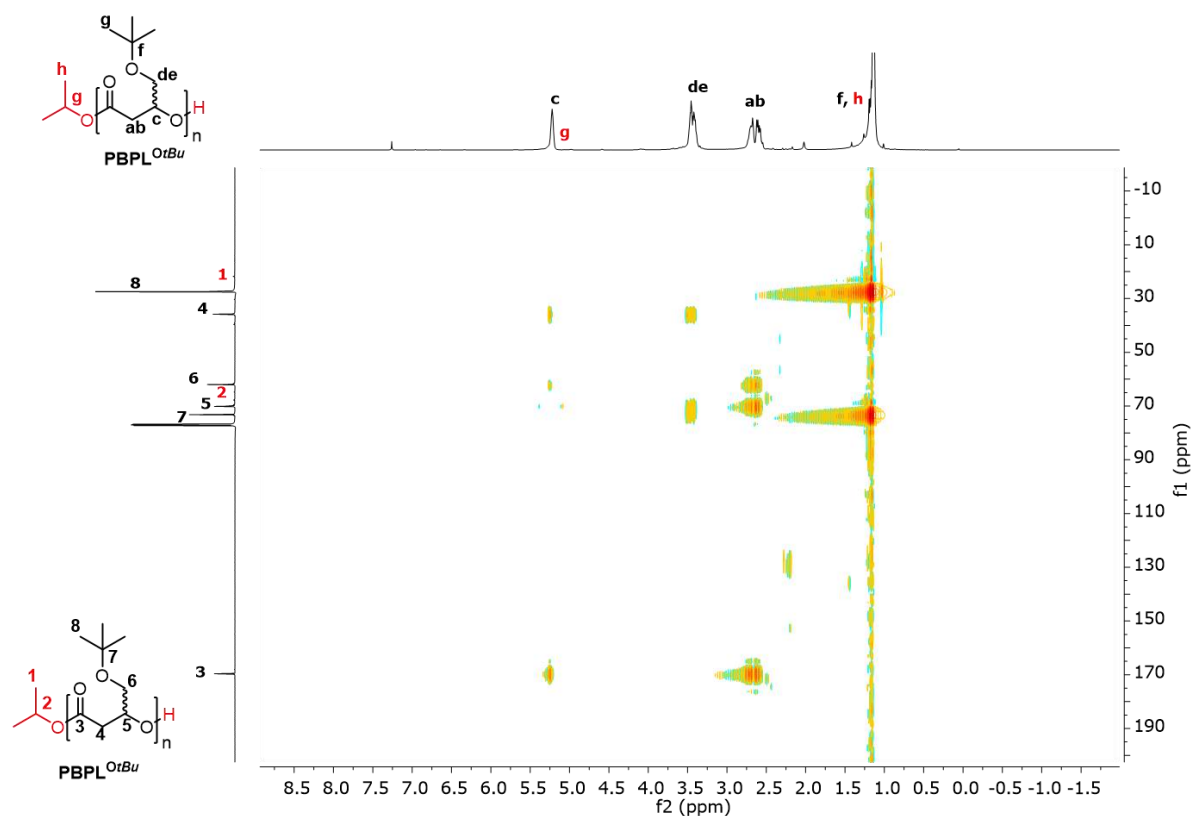
**Appendix 28** –  $^1\text{H}$ - $^1\text{H}$  COSY NMR spectrum (500 MHz,  $\text{CDCl}_3$ , 25 °C) of syndiotactic PBPL<sup>OiPr</sup> precipitated twice in cold pentane (Table 4. 6, entry 7).



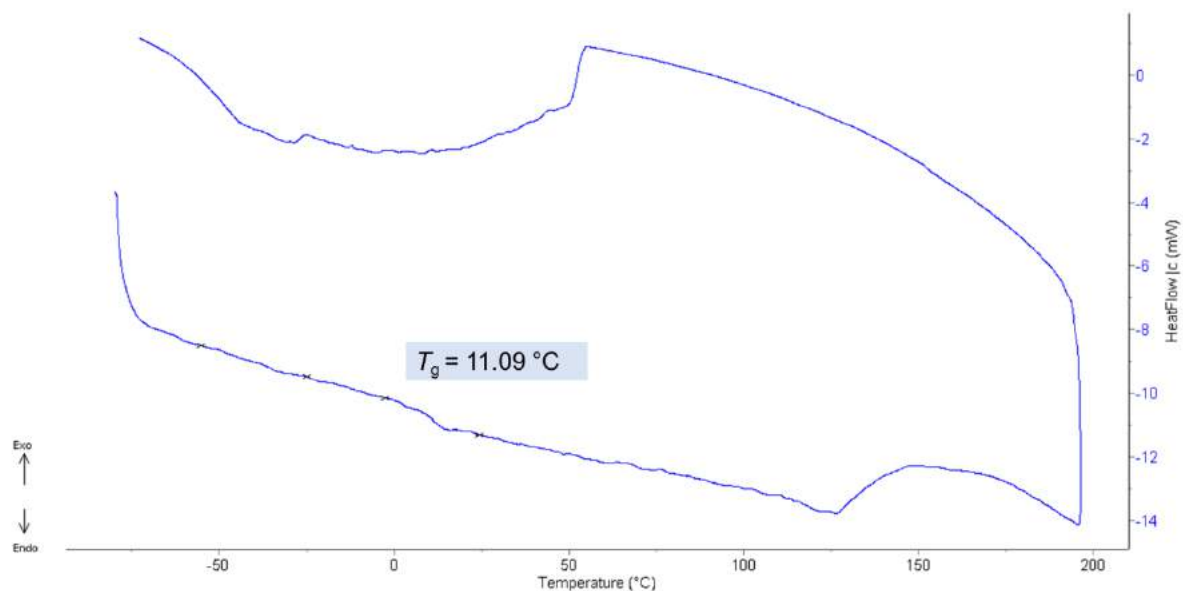
**Appendix 29** –  $^1\text{H}$ - $^{13}\text{C}$  HMBC (500 MHz, 125 MHz,  $\text{CDCl}_3$ , 25 °C) of syndiotactic PBPL<sup>OiPr</sup> precipitated twice in cold pentane (Table 4. 6, entry 7).



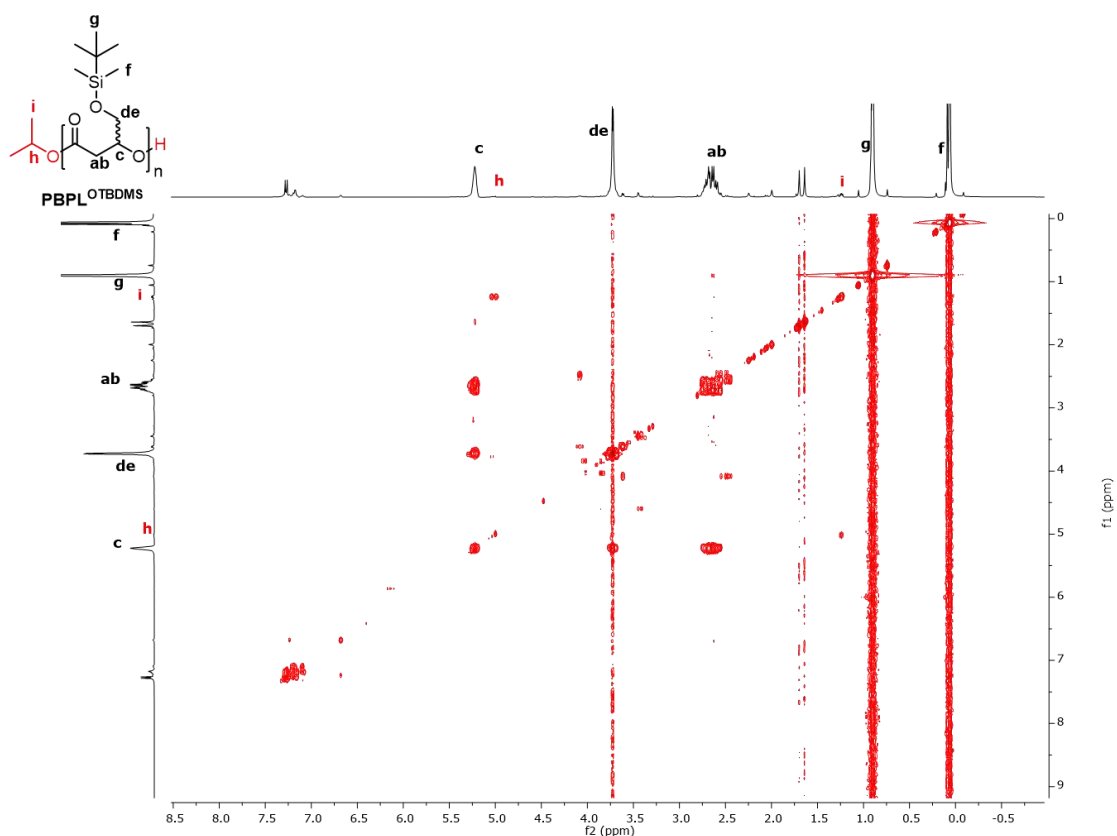
**Appendix 30** –  $^1\text{H}$ - $^1\text{H}$  COSY NMR spectrum (500 MHz,  $\text{CDCl}_3$ , 25 °C) of syndiotactic PBPL<sup>OrBu</sup> precipitated twice in cold pentane (Table 4. 7, entry 11).



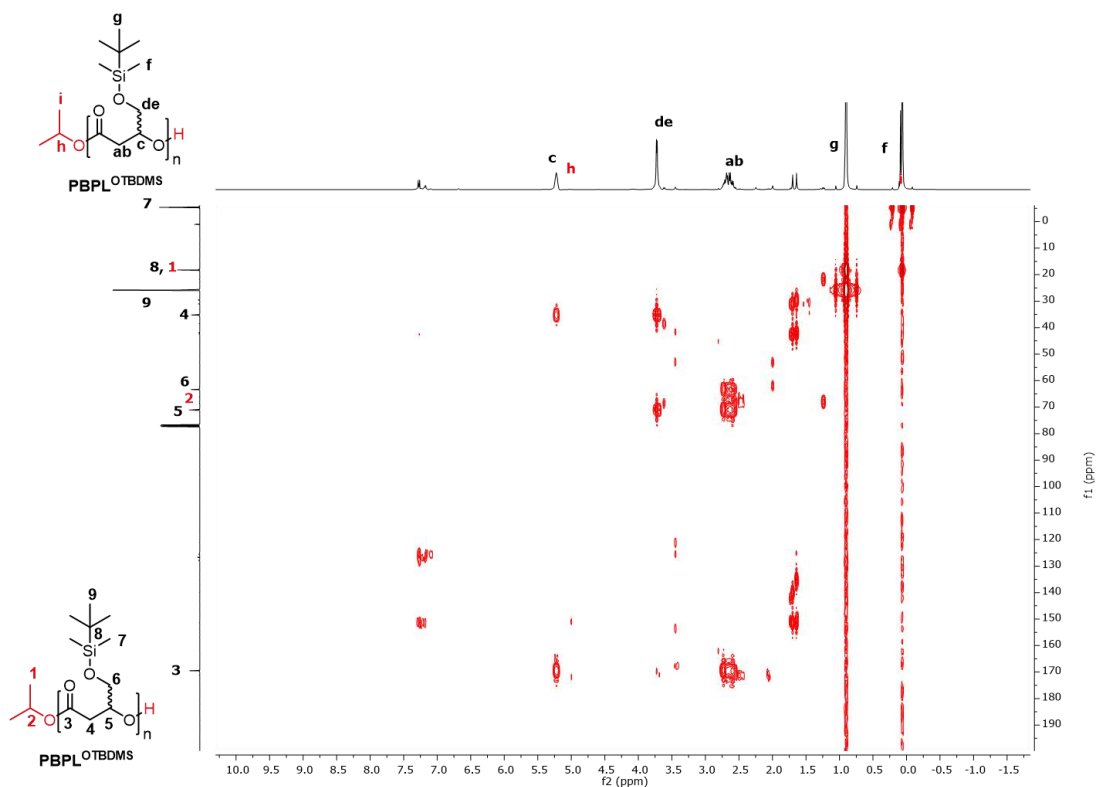
**Appendix 31** –  $^1\text{H}$ - $^{13}\text{C}$  HMBC (500 MHz, 125 MHz,  $\text{CDCl}_3$ , 25  $^\circ\text{C}$ ) of syndiotactic  $\text{PBPL}^{\text{OrBu}}$  precipitated twice in cold pentane (Table 4. 7, entry 11).



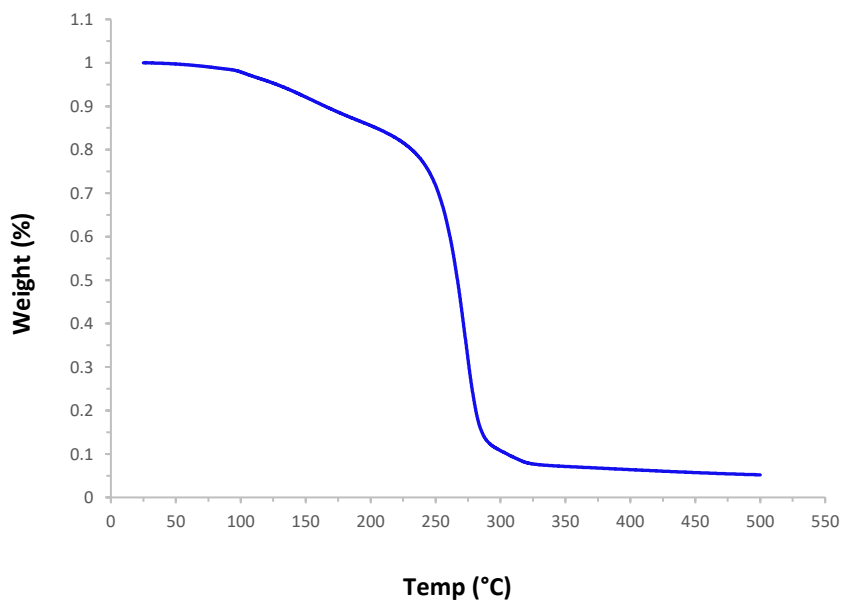
**Appendix 32** – DSC thermogram (heating rate of 10  $^\circ\text{C min}^{-1}$ , second heating cycle  $-80$  to  $140$   $^\circ\text{C}$ ) of isotactic  $\text{PBPL}^{\text{OrBu}}$  ( $P_r < 0.05$ ) synthesized by ROP of (*S*)- $\text{BPL}^{\text{OrBu}}$  with **2b**/*i*PrOH) (Table 4. 7, entry 12).



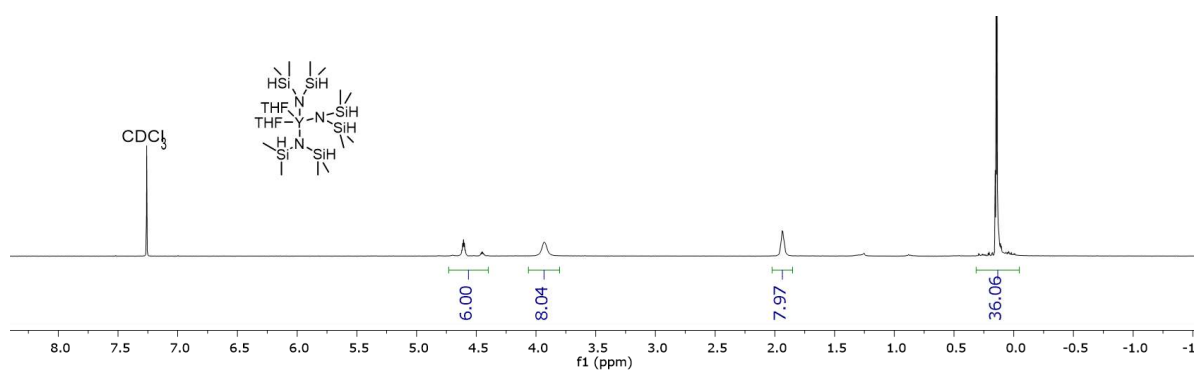
**Appendix 33** –  $^1\text{H}$ - $^1\text{H}$  COSY NMR spectrum (500 MHz,  $\text{CDCl}_3$ , 25 °C) of syndiotactic PBPL<sup>OTBDMS</sup> precipitated twice in cold pentane (Table 4. 8, entry 11).



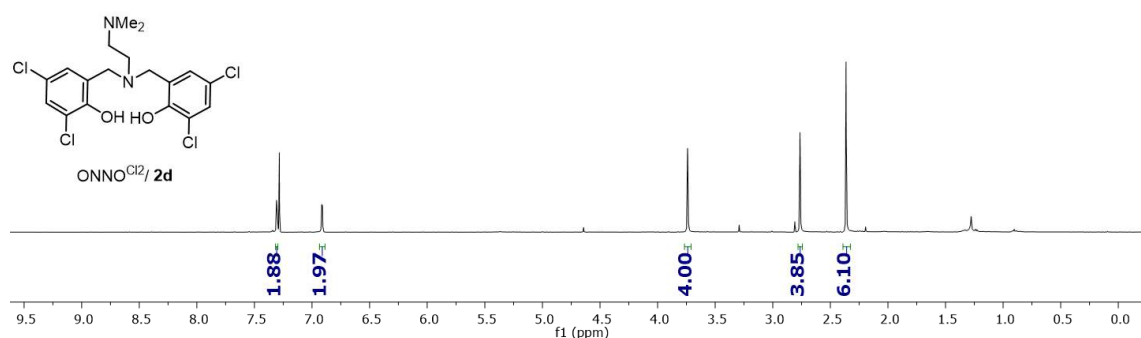
**Appendix 34** –  $^1\text{H}$ - $^{13}\text{C}$  HMBC (500 MHz, 125 MHz,  $\text{CDCl}_3$ , 25 °C) of syndiotactic PBPL<sup>OTBDMS</sup> precipitated twice in cold pentane (Table 4. 8, entry 11).



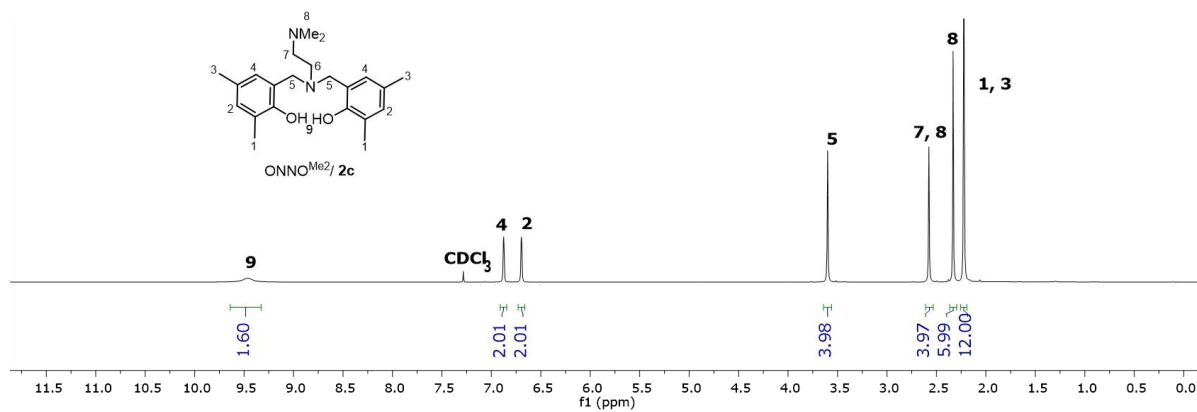
**Appendix 35** – TGA thermograms of syndiotactic PBPL<sup>OTBDMS</sup> (Table 4. 4, entry 11).



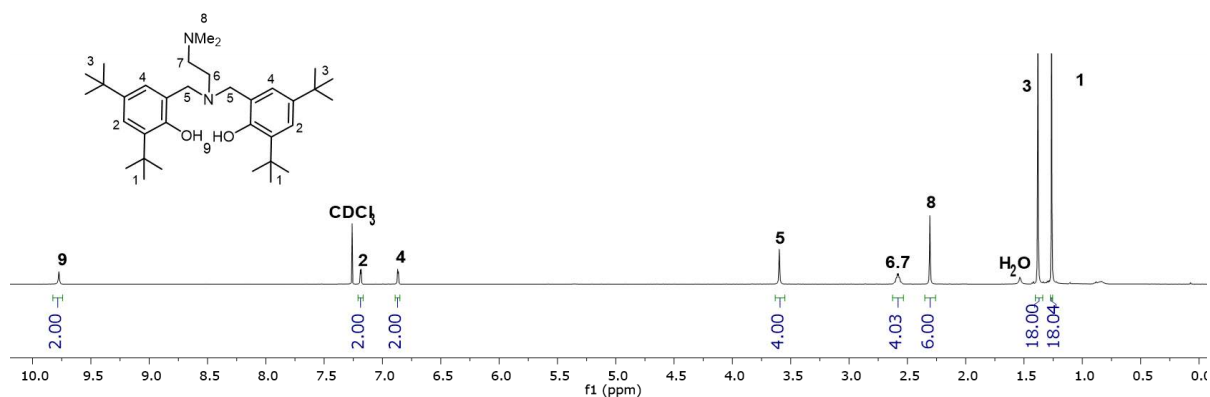
**Appendix 36** – <sup>1</sup>H NMR (500 MHz, CDCl<sub>3</sub>, 25 °C) spectrum for catalyst **2** precursor, Y{(N(SiHMe<sub>2</sub>)<sub>2</sub>)<sub>3</sub>}THF<sub>2</sub>.



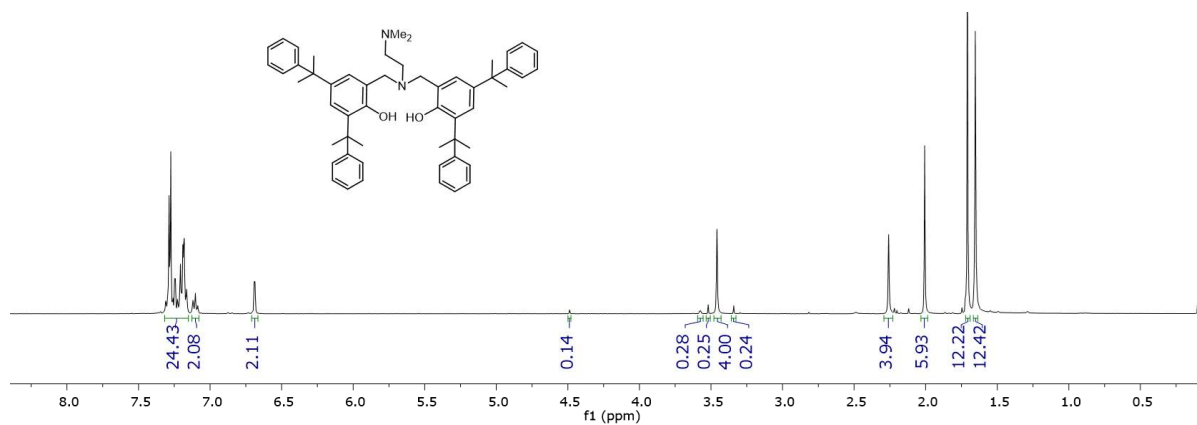
**Appendix 37** – <sup>1</sup>H NMR (400 MHz, CDCl<sub>3</sub>, 25 °C) spectrum for catalyst **2d** proligand ONNO<sup>Cl2</sup>.



**Appendix 38** –  $^1\text{H}$  NMR (400 MHz,  $\text{CDCl}_3$ , 25 °C) spectrum for catalyst **2c** proligand  $\text{ONNO}^{\text{Me}2}$ .



**Appendix 39** –  $^1\text{H}$  NMR (400 MHz,  $\text{CDCl}_3$ , 25 °C) spectrum for catalyst **2b** proligand  $\text{ONNO}^{\text{tBu}2}$ .



**Appendix 40** –  $^1\text{H}$  NMR (400 MHz,  $\text{CDCl}_3$ , 25 °C) spectrum for catalyst **2a** proligand  $\text{ONNO}^{\text{cumyl}2}$ .

# Resumé

*“If you can’t explain it simply, you don’t understand it well enough.”*

– **Albert Einstein**





## 1. Introduction

Les plastiques dérivés du pétrole qui ont alimenté les économies modernes sont les substances artificielles les plus largement utilisées dans la vie moderne, ils sont maintenant devenus indispensables à la vie quotidienne et à l'économie mondiale. Cependant, lorsqu'ils sont éliminés ou rejetés dans l'environnement, leur durabilité et leur résistance à la dégradation dans les environnements ambiants entraînent une grave pollution par les plastiques des décharges et des océans, ainsi que d'autres conséquences environnementales.<sup>[1]</sup> Ainsi, le développement des polymères, y compris les plastiques, devrait se concentrer sur des matériaux qui peuvent être recyclés ou éliminés de manière moins dommageable pour l'environnement (Figure 1).

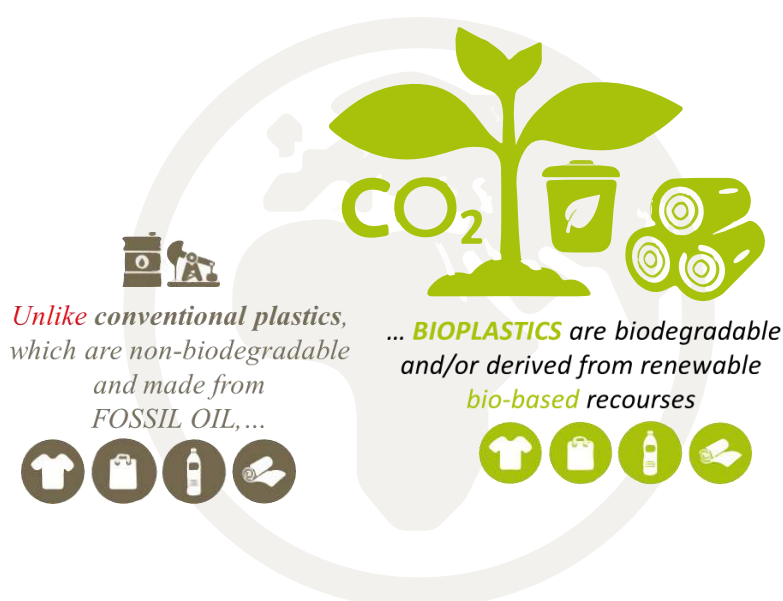


**Figure 1** – Le diagramme montre la différence entre les plastiques conventionnels et les bioplastiques; les bioplastiques peuvent aider à réduire l'impact environnemental dangereux.<sup>[1]</sup>

Dans ce contexte, les polyhydroxyalcanoates (PHA), une classe unique de polyesters aliphatiques biorenouvelables et biodégradables dans les environnements ambiants, ont montré un grand potentiel en remplacement des plastiques à base de pétrole, principalement pour les applications biomédicales, pharmaceutiques et d'emballage.<sup>[2]</sup> Les PHA naturels (ou bactériens), produits par des bactéries et d'autres micro-organismes vivants à partir de ressources biorenouvelables, sont des polymères purement isotactiques, et leurs propriétés thermiques et mécaniques couvrent une gamme variée en fonction de la longueur du groupe alkyle pendant sur le carbone  $\beta$  (Figure 2 ).<sup>[3]</sup> Le PHA le plus populaire est le poly(3-hydroxybutyrate) (P3HB ou PHB), qui est un matériau possédant des propriétés adaptées pour

remplacer les plastiques pétroliers. Néanmoins, ils sont difficiles à traiter en raison de leurs propriétés physico-mécaniques (par exemple, température de fusion ( $T_m$ ) proche de la température de dégradation ( $T_d$ )), ainsi que les coûts élevés et les faibles volumes de sa production ne sont pas pratiques pour les applications de produits de base.

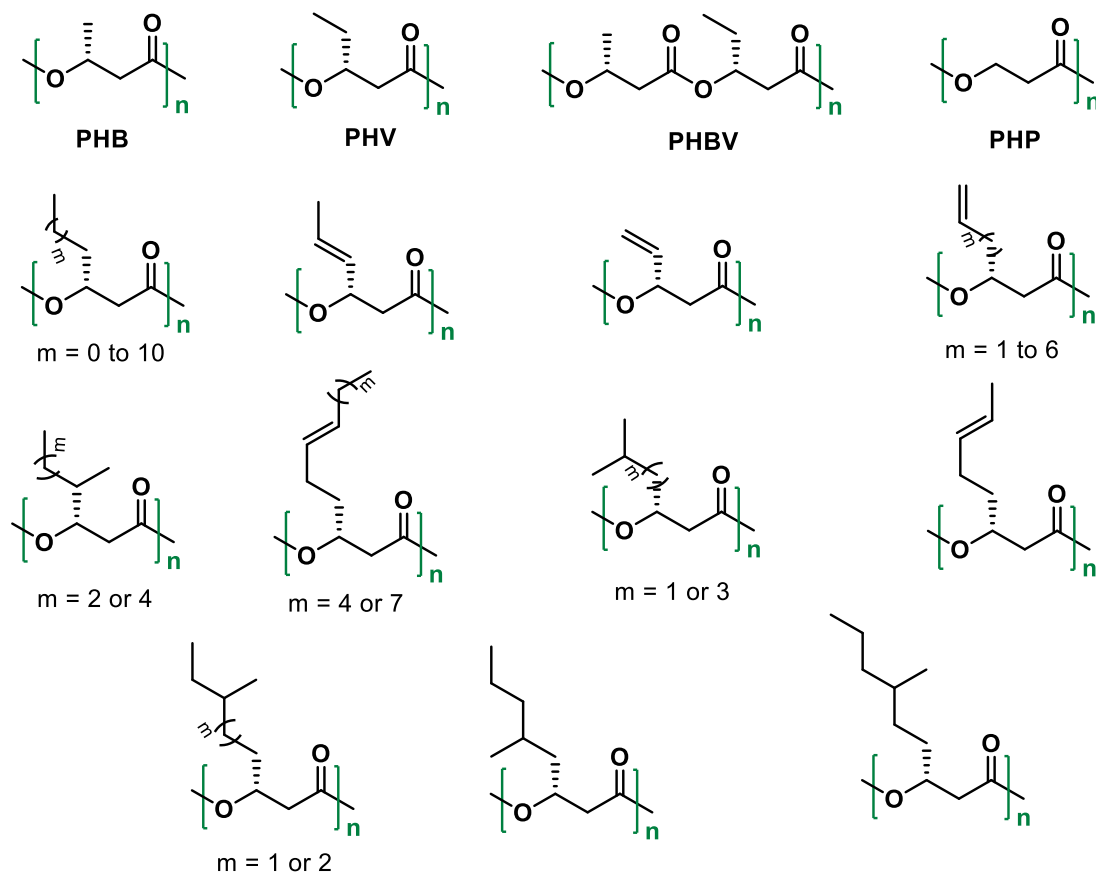
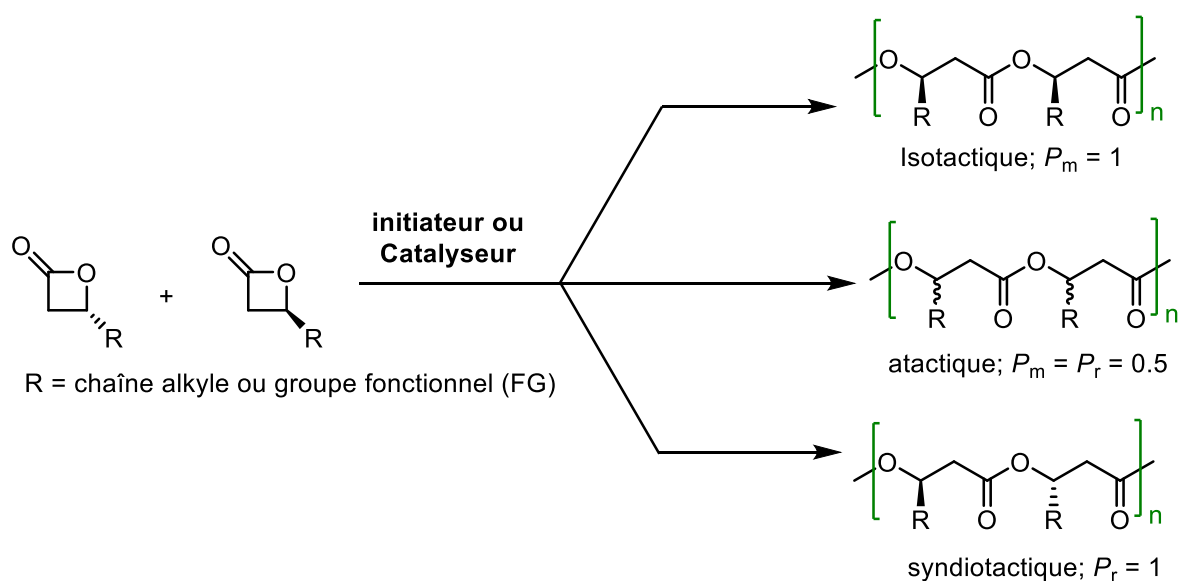


**Figure 2** – Structure chimique de divers types de (R)-PHA isotactiques naturels, extraits de micro-organismes.

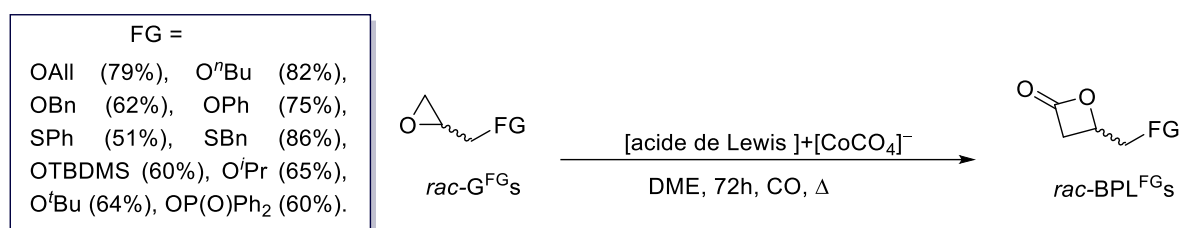
L'insertion de fonctionnalités originales sur le squelette des PHA avec une tacticité syndiotactique est une approche importante pour ajuster les propriétés des PHA naturels, dans l'espoir de faciliter leur processabilité et d'élargir leurs applications commerciales. Par conséquent, la synthèse chimique des PHA via la polymérisation catalysée par ouverture de cycle (ROP) des  $\beta$ -lactones (principalement *rac*-BL<sup>Me</sup>) a été développée depuis les années 1960 et s'est avérée être une stratégie polyvalente à cette dernière fin (Schème 1).<sup>[4]</sup>



**Schème 1** – ROP catalysée de la  $\beta$ -lactone racémique aux PHA isotactiques, atactiques ou syndiotactiques ;  $P_m$  et  $P_r$  sont respectivement la probabilité d'enrichissement isotactique et syndiotactique.

## 2. Partie expérimentale

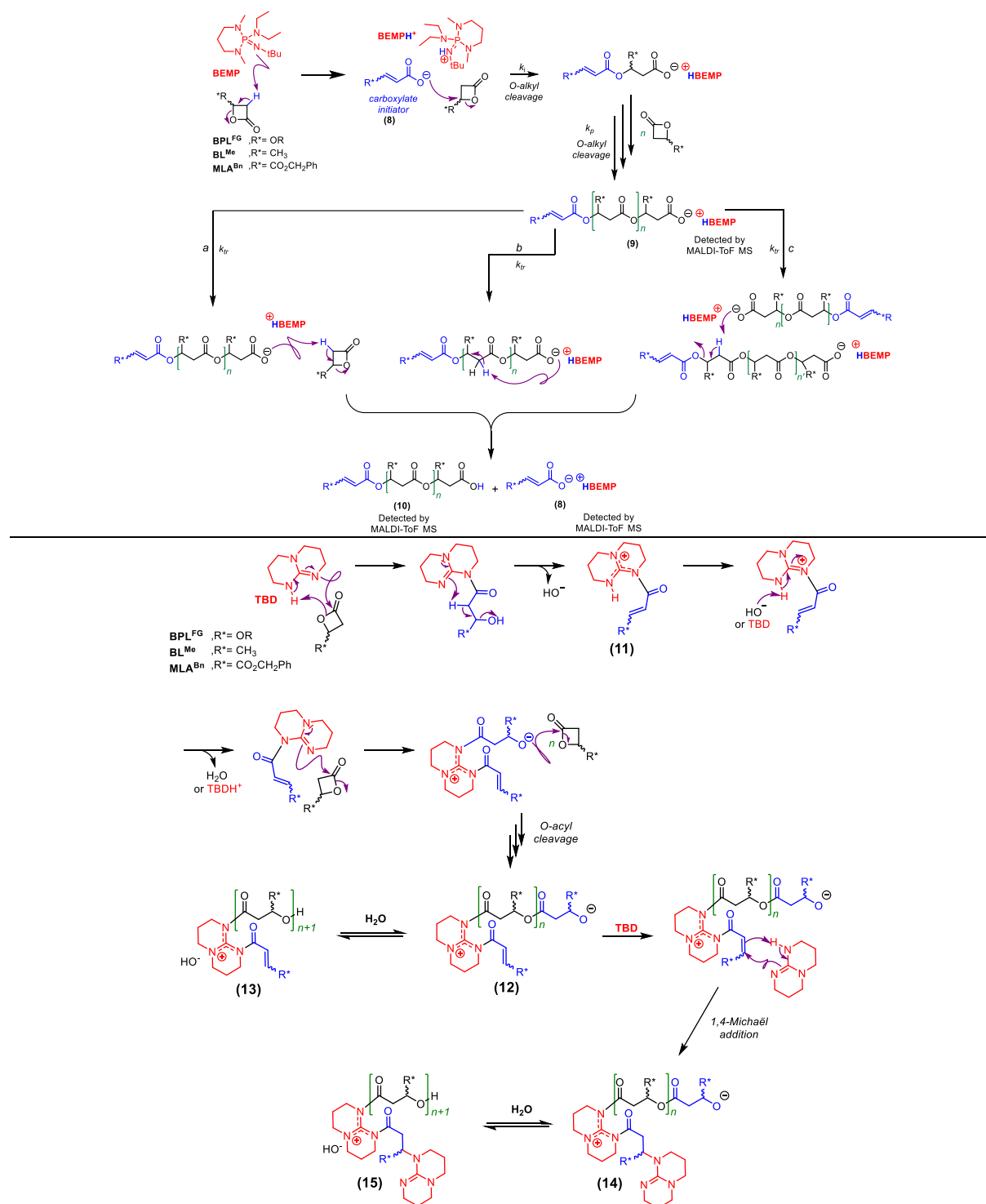
Ici, nous avons d'abord réussi à synthétiser diverses  $\beta$ -lactones fonctionnelles (BPL<sup>FG</sup>s), qui sont la pierre angulaire de nos PHA fonctionnels ciblés (BPL<sup>FG</sup>s). Tous les BPL<sup>FG</sup> racémiques et énantiopurs ont été synthétisés avec succès par réaction de carbonylation de leurs époxydes correspondants (G<sup>FG</sup>s), en présence de [acide de Lewis]<sup>+</sup>[CoCO<sub>4</sub>]<sup>-</sup> catalyse, avec des rendements bons à élevés ca. 51%–82% (Schème 2).

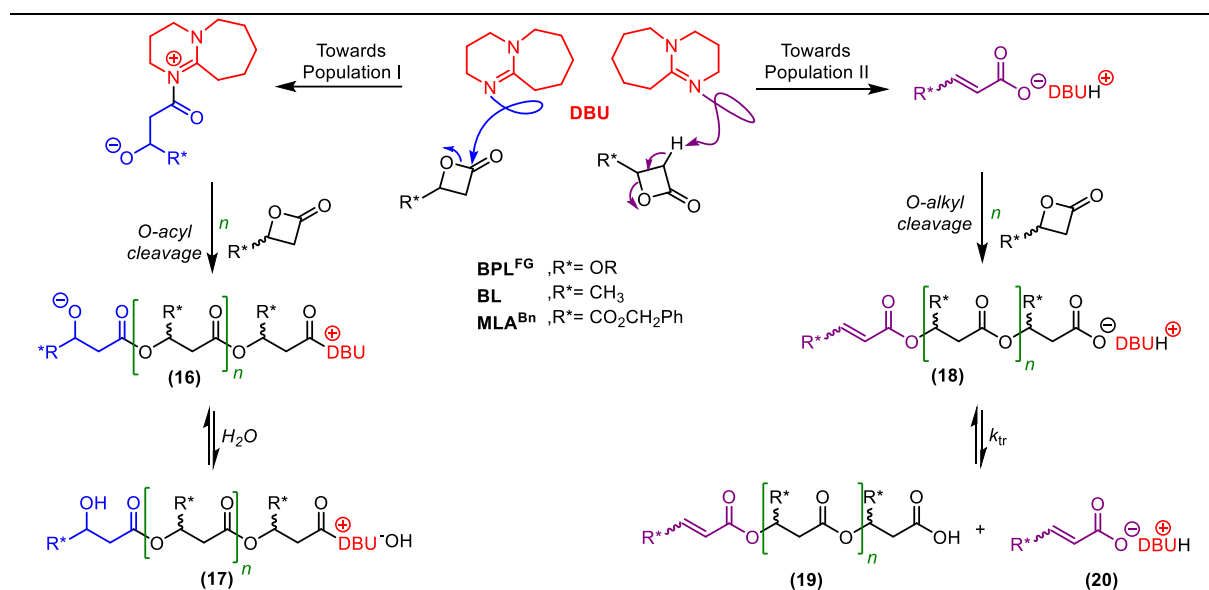


**Schème 2** – Synthèse des BPL<sup>FG</sup>s par carbonylation des G<sup>FG</sup>s correspondants favorisée par le [acide de Lewis]<sup>+</sup>[CoCO<sub>4</sub>]<sup>-</sup> catalyseur.

Même si les activateurs organiques BEMP, TBD et DBU sont disponibles dans le commerce, généralement non toxiques et stables à l'air, leur utilisation dans la ROP des  $\beta$ -lactones ( $rac-BL^{Me}$  et  $rac-MLA^{FG}$ ) a été à peine étudiée. Probablement parce que leur mécanisme en jeu lors de la ROP n'a pas été découvert et que leur activité dépend énormément des conditions du milieu. Dans ce travail, l'investissement dans leur utilisation en vrac de  $rac-BPL^{FG}$  (FG = OAll, O<sup>n</sup>Bu, OBn, OTBDMS, OP(O)Ph<sub>2</sub>) pour produire des PBPL<sup>FG</sup> atactiques a été géré. Plus important encore, les mécanismes complets de BEMP et de DBU ont été proposés pour la première fois, et le mécanisme TBD a été réexaminé, ce qui a entraîné une modification

du mécanisme déjà proposé, basé sur l'analyse RMN  $^1\text{H}$  et  $^{13}\text{C}$  et MALDI-ToF MS (Schéma 3). La perception des mécanismes a révélé la présence d'inévitables réactions de transfert, résultant de la particularité des  $\beta$ -lactones (hydrogène  $\alpha$ -acide), qui provoquent une diminution du contrôle de la polymérisation en termes de masses molaires. En conséquence, il a été proposé d'utiliser BEMP, TBD et DBU dans la ROP du *rac*-DL<sup>R</sup> ( $R = \text{Me, Eth, Bn, ...}$ ), ce qui pourrait aider à contourner les réactions secondaires indésirables.





D'autre part, la ROP des *rac*-BPL<sup>FG</sup> (FG = OPh, SPh, OiPr, OtBu, OTBDMS, OP(O)Ph<sub>2</sub>), médiée par des complexes à base d'yttrium avérés hautement actifs, régio- et stéréosélectifs, permettant masses molaires élevées ( $M_n$ , SEC = 96 000 g mol<sup>-1</sup>) avec des dispersités étroites ( $\mathcal{D}_M = 1,18$ ) et des PHA fonctionnels enrichis en syndiotactique ( $P_r(\text{max}) = 0,87$  ; exemple sur PBL<sup>SPh</sup> (Figure 3)) avec des propriétés thermiques uniques et diverses. Cela ouvre la porte à l'avenir pour investir dans leur copolymérisation.

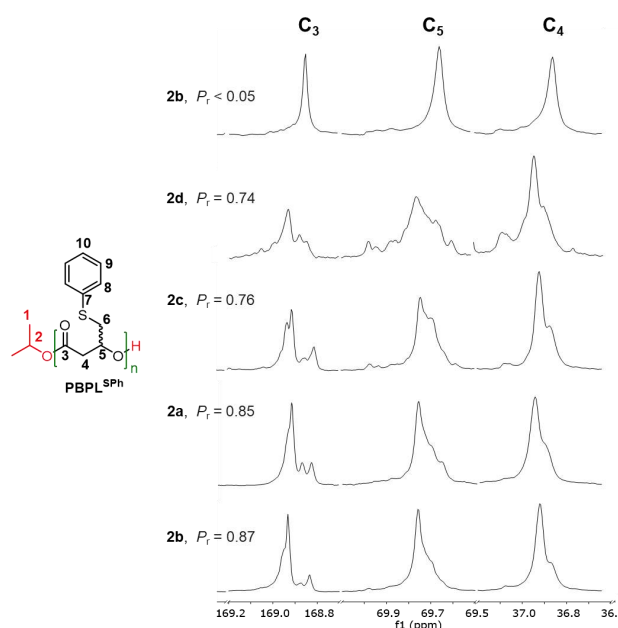


**Figure 3** – Regions of the  $^{13}\text{C}\{^1\text{H}\}$  NMR spectra (125 MHz,  $\text{CDCl}_3$ , 23 °C) of PBPL<sup>SPh</sup> prepared by ROP of *rac*-BPL<sup>SPh</sup>, except for the top spectra: of enantiopure (*S*)-BPL<sup>SPh</sup> (Table 4. 4, entry 14), mediated by **2a**, **2b**, **2c**, or **2d**/iPrOH (Table 4. 4, entries 3,5,7,12).

### 3. Conclusion et perspective

Les plastiques dérivés du pétrole qui ont alimenté les économies modernes sont les substances artificielles les plus largement utilisées dans la vie moderne ; ils sont désormais devenus indispensables à notre quotidien et à l'économie mondiale. Cependant, lorsqu'ils sont éliminés ou rejetés dans l'environnement, leur durabilité et leur résistance à la dégradation dans les environnements ambiants entraînent une grave pollution par les plastiques des décharges et des océans, ainsi que d'autres conséquences environnementales. Ainsi, le développement des plastiques devrait se concentrer sur des matériaux qui peuvent être recyclés ou éliminés de manière moins dommageable pour l'environnement. Dans ce contexte, les polyhydroxyalcanoates (PHA), une classe unique de polyesters aliphatiques biorenouvelables et biodégradables dans les environnements ambiants, ont montré un grand potentiel en remplacement des plastiques à base de pétrole. Les PHA naturels, produits par des bactéries et d'autres micro-organismes vivants à partir de ressources biorenouvelables, sont des polymères purement isotactiques, et leurs propriétés thermiques et mécaniques couvrent une gamme variée en fonction de la longueur du groupe alkyle pendant sur le carbone  $\beta$ . Néanmoins, les PHA naturels sont difficiles à traiter en raison de leurs propriétés physico-mécaniques (par exemple, température de fusion ( $T_m$ ) proche de la température de dégradation ( $T_d$ )). L'insertion de fonctionnalités originales le long du squelette PHA avec la syndiotacticité est une approche importante pour ajuster les propriétés des PHA naturels, dans l'espoir de faciliter leur processabilité et d'élargir leurs applications commerciales. Par conséquent, la synthèse chimique des PHA via la polymérisation catalysée par ouverture de cycle (ROP) des  $\beta$ -lactones (principalement *rac*-BL<sup>Me</sup>) a été développée depuis les années 1960 et s'est avérée être une stratégie polyvalente à cette dernière fin. Avec ce travail, nous avons contribué à la production d'homopolymères PHA originaux et nouveaux à fonction (thio)éther, représentés par des PBPL<sup>FG</sup> (FG = OAll, O<sup>n</sup>Bu, OBn, OTBDMS, OPh, SPh, O<sup>i</sup>Pr, O<sup>t</sup>Bu, OP(O)Ph<sub>2</sub>), ayant des propriétés thermiques, des masses molaires et une stéréochimie variées, par le ROP des  $\beta$ -propiolactones cycliques fonctionnelles BPLFG en présence d'activateurs organiques (BEMP, TBD, DBU) ou de complexes yttrium/<sup>i</sup>PrOH (Y{ONNOR1R2} ; R1 = R2 = Cumyl, <sup>t</sup>Bu, Me, Cl).

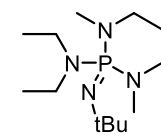
## 4. Référence

- [1] <https://www.european-bioplastics.org/bioplastics/>, **2019**.
- [2] aA. Anjum, M. Zuber, K. M. Zia, A. Noreen, M. N. Anjum, S. Tabasum, *Int. J. Biol. Macromol.* **2016**, 89, 161-174; bMuhammadi, Shabina, M. Afzal, S. Hameed, *Green Chemistry Letters and Reviews* **2015**, 8, 56-77; cG.-Q. Chen, in *Plastics from bacteria*, Springer, **2010**, pp. 17-37.
- [3] B. Laycock, P. Halley, S. Pratt, A. Werker, P. Lant, *Prog. Polym. Sci.* **2013**, 38, 536-583.
- [4] aC. M. Thomas, *Chem. Soc. Rev.* **2010**, 39, 165-173; bJ. F. Carpentier, *Macromol. Rapid Commun.* **2010**, 31, 1696-1705; cJ.-F. o. Carpentier, *Organometallics* **2015**, 34, 4175-4189; dR. M. Shakaroun, H. Li, S. M. Guillaume, J. F. Carpentier, *Chem. Eur. J.* **2020**, 26, 128-138; eA. Domiński, T. Konieczny, M. Zięba, M. Klim, P. Kurcok, *Polymers* 2019, 11, 1221; fO. Santoro, X. Zhang, C. Redshaw, *Catalysts* 2020, 10, 800; gR. Tong, *Ind. Eng. Chem. Res.* 2017, 56, 4207-4219.

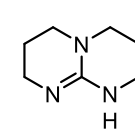




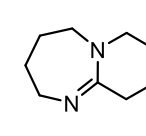
### Organic Activators



**BEMP**

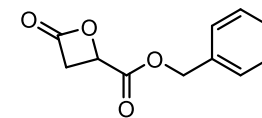


**TBD**

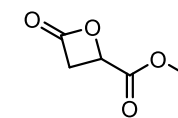


**DBU**

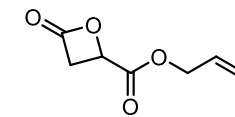
### MLA<sup>FGs</sup>



**MLA<sup>Bn</sup>**

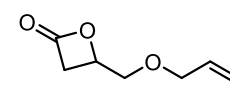


**MLA<sup>Me</sup>**

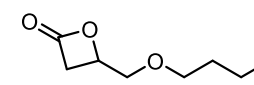


**MLA<sup>All</sup>**

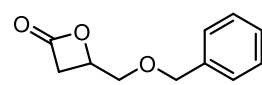
### BPL<sup>FGs</sup>



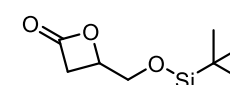
**BPL<sup>OAII</sup>**



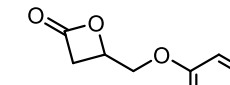
**BPL<sup>OnBu</sup>**



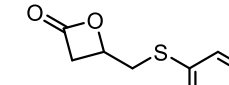
**BPL<sup>OBn</sup>**



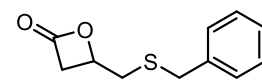
**BPL<sup>OTBDMS</sup>**



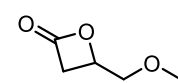
**BPL<sup>OPh</sup>**



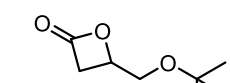
**BPL<sup>SPh</sup>**



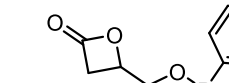
**BPL<sup>SBn</sup>**



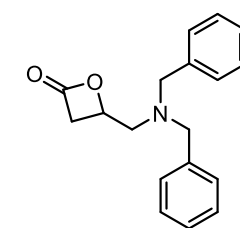
**BPL<sup>O<sup>i</sup>Pr</sup>**



**BPL<sup>O<sup>t</sup>Bu</sup>**

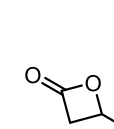


**BPL<sup>OP(O)Ph<sub>2</sub></sup>**

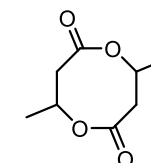


**BPL<sup>NBn<sub>2</sub></sup>**

### Others

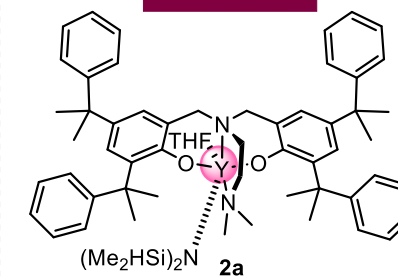


**BL<sup>Me</sup>**

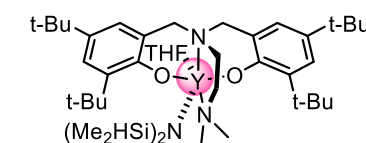


**DL<sup>Me</sup>**

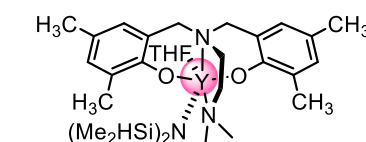
### Y{ONNO<sup>R1,R2</sup>}



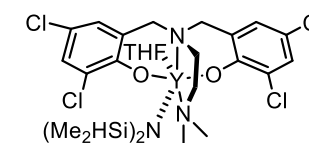
**2a**



**2b**



**2c**



**2d**





**Titre :** Synthèse de PHAs fonctionnels par ROP de  $\beta$ -lactones: approche mécanistique et catalyse stéréosélective

**Mots clés :** Poly(hydroxyalkanoate)s (PHAs), polymérisation par ouverture de cycle (ROP),  $\beta$ -lactones, catalyse organique, catalyseur d'yttrium, Stéréochimie

**Résumé :** Les stratégies actuelles de gestion des déchets plastiques se concentrent principalement sur la prévention et la réduction des déchets, et sur l'utilisation de polymères biodégradables tels que les poly(hydroxyalkanoates) (PHAs). Les PHAs sont biosourcés, biodégradables, biocompatibles et non toxiques, ce qui leur confère un rôle important dans l'emballage et dans une moindre mesure dans les applications médicales. Ils peuvent être naturels dérivés de bactéries, ou formés synthétiquement par polymérisation par ouverture de cycle (ROP) catalysée de  $\beta$ -lactones. Les PHAs naturels se trouvent que sous forme stéréorégulière isotactique principalement cristalline (configuration *R*) ce qui les rend cassants. Ils ont également des masses molaires limitées et une fonctionnalité restreinte sur le groupe exocyclique -principalement une chaîne alkyle-, ce qui limite leurs propriétés mécaniques et donc leur domaine d'application. Par conséquent, afin de dépasser ces inconvénients, les chimistes des polymères ont recouru à la synthèse chimique par ROP.

La ROP des  $\beta$ -lactones conduit à des PHAs bien définis d'une manière stérocontrôlée (isotactique ou syndiotactique).

La synthèse de  $\beta$ -lactones fonctionnelles, nommément BPL<sup>FG</sup>s (FG = OAlI, OnBu, OBn, OTBDMS, OPh, SPh, OiPr, OtBu, OP(O)Ph<sub>2</sub>), a été réalisée par carbonylation de leurs époxydes correspondants. Certains de ces derniers BPL<sup>FG</sup>s ont été polymérisés par ROP par une approche exempte de solvant et de métal (par des activateurs organiques : BEMP, TBD et DBU), où les mécanismes mis en jeu pour produire les PHAs ont été examinés. D'autres BPL<sup>FG</sup>s ont été polymérisés par ROP par des catalyseurs stéréosélectifs achiraux diamino-bis(phénolate) de yttrium pour produire des PHAs fonctionnels avec un enrichissement syndiotactique élevé et des masses molaires élevées. L'accent a été mis sur la relation entre la fonctionnalité du monomère et les substituants des catalyseurs.

**Title :** Synthesis of functional PHAs by ROP of  $\beta$ -lactones : Mechanistic insights and stereoselective catalysis

**Keywords :** Poly(hydroxyalkanoate)s (PHAs), Ring-opening polymerization (ROP), Functional  $\beta$ -lactone, Organocatalyst, Yttrium catalyst, Stereochemistry

**Abstract :** The recent plastic waste management strategies focus mainly on the prevention and reduction of waste, and on the use of biodegradable counterparts such as poly(hydroxyalkanoates) (PHAs). PHAs are biobased, biodegradable, biocompatible, and non-toxic which endowed them a significant role in packaging and to a lesser extent in medical applications. They can be either natural derived from bacteria or synthetically produced through catalysed ring-opening polymerization (ROP) of  $\beta$ -lactones. Natural PHAs are only found as stereoregular isotactic mainly crystalline (*R* configuration) which makes them brittle. They also have limited molar masses and restricted functionality on the exocyclic group mainly alkyl chain, which limit their mechanical properties and hence their range of application. Therefore, in order to exceed these drawbacks, polymer chemists tend to resort to chemical synthesis via

ROP. ROP of  $\beta$ -lactones can provide well-defined PHAs in a stereocontrol manner (isotactic or syndiotactic).

The synthesis of assorted functional  $\beta$ -lactones, namely BPL<sup>FG</sup>s (FG = OAlI, O<sup>n</sup>Bu, OBn, OTBDMS, OPh, SPh, O<sup>i</sup>Pr, O<sup>t</sup>Bu, OP(O)Ph<sub>2</sub>), was achieved successfully by carbonylation of their corresponding epoxides. Some of the latter BPL<sup>FG</sup>s were ring-open polymerized by solvent- and metal-free approach (by organic activators: BEMP, TBD and DBU neatly), where the mechanisms at play to produce PHAs were investigated. Other BPL<sup>FG</sup>s were ring-open polymerized by stereoselective achiral diamino-bis(phenolate) yttrium catalysts to produce functional PHAs with high syndiotactic enrichment and high molar masses. An emphasize was done on the relation between the monomer functionality and the catalysts substituents.